LBL-16281
UC-34C
CONF-830675

PROCEEDINGS OF THE
6th HIGH ENERGY HEAVY ION STUDY
AND
2nd WORKSHOP ON ANOMALONS

Lawrence Berkeley Laboratory, University of California
June 28 - July 1, 1983

RECEIVED
LAWRENCE
BERKELEY LABORATORY
FEB 3 1984
LIBRARY AND
DOCUMENTS SECTION

December 1983

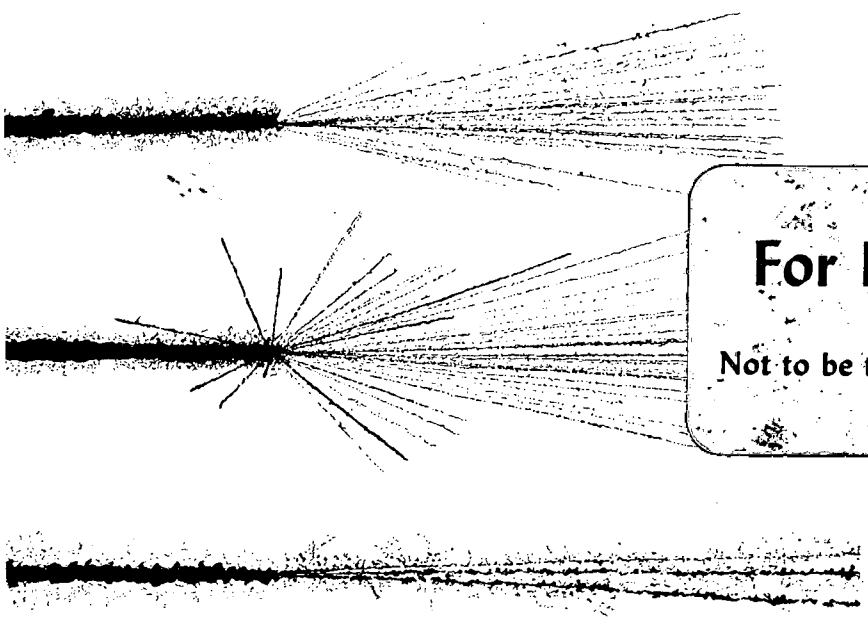

For Reference
Not to be taken from this room

Lawrence Berkeley Laboratory
University of California
Berkeley, CA 94720

LBL-16281

Prepared for the U.S. Department of Energy under Contract DE-AC03-76SF00098

DISCLAIMER

This document was prepared as an account of work sponsored by the United States Government. While this document is believed to contain correct information, neither the United States Government nor any agency thereof, nor the Regents of the University of California, nor any of their employees, makes any warranty, express or implied, or assumes any legal responsibility for the accuracy, completeness, or usefulness of any information, apparatus, product, or process disclosed, or represents that its use would not infringe privately owned rights. Reference herein to any specific commercial product, process, or service by its trade name, trademark, manufacturer, or otherwise, does not necessarily constitute or imply its endorsement, recommendation, or favoring by the United States Government or any agency thereof, or the Regents of the University of California. The views and opinions of authors expressed herein do not necessarily state or reflect those of the United States Government or any agency thereof or the Regents of the University of California.

LBL-16281

PROCEEDINGS OF THE
6th HIGH ENERGY HEAVY ION STUDY
AND
2nd WORKSHOP ON ANOMALONS

Lawrence Berkeley Laboratory, University of California
June 28 - July 1, 1983

Lawrence Berkeley Laboratory
University of California
Berkeley, California 94720

International Advisory Committee

G.F. Bertsch, Michigan State University
R. Bock, GSI Darmstadt
G.E. Brown, SUNY, Stony Brook and Nordita
A.S. Goldhaber, SUNY, Stony Brook
K. Nakai, University of Tokyo

Organizing Committee

H.H. Gutbrod
M. Gyulassy
H.H. Heckman
W.D. Myers
L.S. Schroeder
H.G. Pugh, Chairman

This work was supported by the U.S. Department of Energy
under Contract No. DE-AC03-76SF00098.

Foreword

This was the sixth in a series of summer studies held at LBL to discuss high energy heavy ion collisions. Because of the special current interest in anomalous projectile fragments, we combined it with the second workshop on anomalons, the previous one having been held at LBL on February 8–10, 1982. On previous occasions we have often chosen special topics for emphasis: for example, in 1979, the meeting was devoted entirely to ultra-relativistic nuclear collisions. Similar workshops have also been held in the alternate years at GSI, Darmstadt, in 1978 and 1980. The 1985 Berkeley meeting is already planned to be the international workshop on Quark Matter Formation and Heavy Ion Collisions, in the sequence previously held in Bielefeld (1982), Brookhaven (1983) and Helsinki (1984).

In the present meeting, apart from a special focus on anomalons, we attempted to cover the entire energy range of relativistic nuclear collisions, from the lowest end of the Bevalac energy range up to the SPS $\bar{p}p$ collider and cosmic rays. The result was very exciting, with the largest participation of any in the series and a real feeling of unity between various aspects of the research, from deep inelastic electron scattering to speculations on the quark-gluon plasma. It is remarkable how rapidly this field has advanced, particularly since the 1979 meeting at LBL and the 1979 VENUS proposal for a heavy ion collider: in 1983 it is taken for granted that the next facility to be constructed will be a device of the VENUS type, with three laboratories (at least) in the U.S. competing to build it.

This year, for the first time, we were aided by a distinguished international advisory committee. The organizing committee is grateful to them for their help. Extraordinary help was given by Linda Davis and Zoe Moody, while many others, especially Wanda Smith-Burnette, Kathy Williams and Maudie Noyd provided essential services at various stages of the meeting and preparation for it. Peggy Little and Pat Marlin, the Conference Coordinators, provided expertise that saved us in the Nuclear Science Division a great deal of time and worry. The Technical Information Department of LBL deserves our unstinted praise for its willingness to meet the unreasonable schedules we requested, and for doing highly professional work nonetheless. Heather Thomson/Freeman did an excellent job of preparing the printed program and book of contributed papers which was provided to each participant on arrival and of assembling the material for the proceedings. Loretta Lizama has done an excellent job of editing the Proceedings and getting them out on schedule. Finally we are grateful to the Director of LBL for providing support which made it possible to reduce the conference fee to a nominal value. Such support is well rewarded not only in benefits to the Laboratory, but in scientific progress.

Howel G. Pugh
Chairman, Organizing Committee

Table of Contents

SESSION I: ANOMALONS — EXPERIMENTAL

* Mean Free Path of ^{40}Ar Projectile Fragments in CR39 Track Detectors
W. Heinrich, H. Drechsel, W. Trakowski, J. Beer, C. Brechtmann, J. Dreute, and S. Sonntag 3

Study of Anomalous Nuclear Projectile Fragments in Reactions of 1.85 A GeV ^{40}Ar in CR-39 Etched Track Detector
M.L. Tincknell and P.B. Price 19

First Results From a Repeat Experiment on the Mean Free Path of Projectile Fragments From 1.88 A GeV ^{56}Fe—Emulsion Interactions
Y.J. Karant, H.H. Heckman, and E.M. Friedlander 23

The Mean Free Path of Relativistic Fragments From Heavy Ion Reactions Induced by 1.8 A GeV ^{40}Ar in Low Sensitive Nuclear Emulsions
Banaras-Chandigarh-Jaipur-Jammu-Lund Collaboration 27

Anomalous Mean Free Path for Z=2 Relativistic Projectile Fragments in Emulsion
M. El-Nadi, O.E. Badawy, M.N. El-Bakry, A. Abdel-Salam, A.A. El-Hamalawy, E.I. Kaalil, A.M. Mousa, and M. El-Nagdy 43

Are There Anomalons at Charge Two?—A Comparison of Helium Induced Primary and Secondary Interactions in Nuclear Research Emulsion at About 2 GeV/Nucleon
N. Klein, E. Ganβauge, M. Bàagil, U. Bieschke, F. Killinger, R. Kretschmer, A. Laschek, and W. Weidner 47

Behavior of Secondary Particles of Charge Two, Three and Four Produced From Relativistic Heavy-Ion Collisions
P.L. Jain, M.M. Aggarwal, M.S. El-Nagdy, A.Z.M. Ismail, and K.L. Gomber 51

Search for Anomalons Among Singly Charged Relativistic Particles From ^{16}O Interactions at 2 GeV/Nucleon
B. Judek 53

A Search for Short-Lived Anomalons in Projectile Fragmentation
H.A. Gustafsson, H.H. Gutbrod, B. Kolb, B. Ludewigt, A.M. Poskanzer, T. Renner, H. Riedesel, H.G. Ritter, A.I. Warwick, and H.H. Wieman 59

A Search For Anomalon Decay by Radiochemical Methods
G. Dersch, K. Aleklett, R. Beckmann, R. Brandt, E.M. Friedlander, W. Loveland, T. Lund, P. McGaughey, N. Porile, G.T. Seaborg, and R. Weiner 63

About a Possible Energy Dependence of the Anomalon Effect at Charge Two
F. Killinger, E. Ganβauge, U. Bieschke, N. Klein, R. Kretschmer, A. Laschek, and W. Weidner 65

A Search for Topological Correlations in the Interactions of Relativistic Projectile Fragments From Relativistic Heavy Ion Collisions
E.M. Friedlander, H.H. Heckman, and Y.J. Karant 69

*Invited Talk.

Particle-Gamma Coincidence Measurements in $^{12}C + ^{12}C$ and $^{12}C + Pb$ Collisions at 2.1 GeV/A Incident Energy, First Results—γ-Ray Spectrum
G. Roche, J. Carroll, C.C. Chang, T. Hallman, P.N. Kirk, R. Koontz, G. Krebs, L. Madansky, T. Mulera, H. Pugh, L. Schroeder, and J. Vicente 73

Studies of Anomalous Projectile Fragments with Lead-Glass, Plastic-Track Detectors, and Cerenkov Detectors
P.B. Price 77

A Detector for the Measurement of Projectile Fragment Interaction Cross Sections
J.P. Dufour, J.G. Girard, P.J. Lindstrom, D.E. Greiner, D.L. Olson, T.J.M. Symons, and H.J. Crawford 81

Development of a Segmented Cerenkov Detector for Study of the "Anomalon" Phenomenon
J.D. Stevenson, J.A. Musser, and S. W. Barwick 83

Active Multitarget Experiment for Anomalons
M. Enorini, F.L. Fabbri, and A. Zallo 87

χ^2 Analyses of Nuclear Emulsion Anomalous Projectile Fragment Data
M.H. Mac Gregor 91

SESSION II: ANOMALONS—THEORETICAL

* Is the Anomalon a Dinotor?
L. Castillejo, A.S. Goldhaber, A.D. Jackson, and M.B. Johnson 97

* Spontaneously Broken Symmetries in Nuclear Physics
J. Boguta 111

* Quasi-Molecular Structures in Nuclear Systems
Y.C. Tang 149

Anomalous Nuclei and a Nonstatic Metastable σ-τ Phase
F. Palumbo 167

Pion Condensates as Anomalons
G.N. Fowler, S. Raha, and R.M. Weiner 169

Nuclear Chromodynamics and "Anomalons"
Y.E. Kim and M. Orlowski 173

Some Anomalon Phenomenology
P.J.S. Watson 177

Limits on Anomalon Production in Deuterium-Deuterium Collisions at 7.9 GeV/c
R.L. Clarke, D.N. Fernandes, J.E. Hardy, R.J. Hemingway, D. Kessler, A.H. Lefcoe, C. Loken, A.C. McPherson, J.L. Pinfold, W.J. Romo, R. Saly, M.K. Sundaresan, P.J.S. Watson, J.L. Wolfson, B. Judek, and M. Losty 181

Are "Anomalons" a Bag Ful'o Colorful Nucleons?
F. Kruse and C.C. Noack 185

*Invited Talk.

SESSIONS III AND IV: HEAVY ION COLLISIONS AT BEVALAC ENERGIES

* Results Obtained Using the Plastic Ball
H.G. Ritter, H.A. Gustafsson, H.H. Gutbrod, B. Kolb, H. Löhner, B. Ludewigt, A.M. Poskanzer, T.R. Renner, H. Riedesel, A. Warwick, F. Weik, and H. Wieman 191

Search for Flow in the Reaction Ar + Pb
R.E. Renfordt, R. Brockmann, J.W. Harris, M. Maier, F. Riess, A. Sandoval, R. Stock, H. Ströbele, K.L. Wolf, H.G. Pugh, L.S. Schroeder, D. Schall, and K. Tittel 203

* Evidence on the Equation of State of Nuclear Matter at High Densities
J.W. Harris, D. Bangert, R. Bock, R. Brockmann, A. Dacal, M. Maier, G. Odyniec, M.E. Ortiz, H.G. Pugh, W. Rauch, R.E. Renfordt, A. Sandoval, L.S. Schroeder, R. Stock, H. Ströbele, and K.L. Wolf 209

* Collective Effects in Subthreshold Pion Production
E. Grosse 225

Coincidence Experiments Between Pions ($\pi^{\pm}$ and Forward Charged Particles From Intermediate Energy Heavy Ion Collisions
J. Julien, M. Bolore, X. Charlot, J-M. Hisleur, R. Legrain, G.S. Pappalardo, J. Poitou, T. Johansson, C. Guet, M. Maurel, B. Million, C. Ristori, V. Bellini, G. Lanzano, and A. Palmeri 237

* Current Status of High Energy Cascade Models
E.A. Remler 241

Scaling Properties in the Hydrodynamical Description of Nucleus Nucleus Collisions at Intermediate Energies
N.L. Balazs, B. Schürmann, K. Dietrich, and L.P. Csernai 251

Inclusive Measurements of Pions and Light Fragments in 800 MeV/nucleon $^{139}_{57}$La + $^{139}_{57}$La Collisions
X.Bai, H. Hamagaki, O. Hashimoto, K. Kimura, T. Kobayashi, Y. Miake, S. Nagamiya, G. Shapiro, Y. Shida, and I. Tanihata 255

Production of Light Fragments with High P_T at CM 90 Degrees in 800 MeV/Nucleon ^{12}C + ^{12}C Collisions
X. Bai, H. Hamagaki, O. Hashimoto, S. Kadota, K. Kimura, Y. Miake, S. Nagamiya, K. Omata, Y. Shida, I. Tanihata, and N. Yoshikawa 259

* Critical Phenomena at Low Temperature
D.K. Scott 263

High Energy (30–350 GeV) Proton-Nucleus Collisions and the Description of Fragmentation as a Critical Phenomenon
A.S. Hirsch, A. Bujak, J.E. Finn, L.J. Gutay, R.W. Minich, N.T. Porile, R.P. Scharenberg, B.C. Stringfellow, and F. Turkot 291

Aspects of Data on the Breakup of Highly Excited Nuclei
A.I. Warwick, H.H. Wieman, H.H. Gutbrod, H.G. Ritter, H. Stelzer, F. Weik, S.B. Kaufman, E.P. Steinberg, and B.D. Wilkins 295

The Asymmetric Fission of Relativistic Gold Nuclei
P.S. Freier and C.J. Waddington 301

*Invited Talk.

Angular Correlations Between Target and Projectile Fragments Emitted From ^{238}U + Ag(Br) Collisions at 0.85 A GeV
H.H. Heckman, E.M. Friedlander, and Y.J. Karant 305

Azimuthal Angular Correlations Between Heavy Projectile Fragments and Light Particles in the Reaction ^{18}O + Ni at 84 MeV/u
W.F.J. Müller, A. Gobbi, K.D. Hildenbrand, A. Olmi, H. Sann, H. Stelzer, I. Bock, U. Lynen, D. Pelte, U. Winkler, R. Glasow, K.H. Kampert, and R. Santo 309

Subthreshold K^- Production in Nucleus-Nucleus Collisions
A. Shor, J. Carroll, E. Barasch, S. Abachi, V. Perez-Mendez, T. Mulera, P. Fisher, G. Igo, S. Trentalange, K. Ganezer, and F. Kazeminzhad 313

Neutron Emission From Collisions of 390 MeV/u Neon Ions on Lead
R. Madey, J.C. Varga, B.D. Anderson, A.R. Baldwin, R. Cecil, J.W. Watson, and G.D. Westfall 317

Two-Pion Correlations for 1.2 GeV/Nucleon Ar on KCl
D. Beavis, S.Y. Chu, S.Y. Fung, W. Gorn, A. Huie, D. Keane, J.J. Lu, R.T. Poe, G. VanDalen, and M. Vient 321

Two Particle Correlations Observed with the Plastic Ball Detector
H. Wieman, H.H. Gutbrod, H.A. Gustafsson, B. Kolb, H. Löhner, B. Ludewigt, A.M. Poskanzer, T. Renner, H. Riedesel, H.G. Ritter, A. Warwick, and F. Weik 325

Composite Particle Production Measured with the Plastic Ball
T.R. Renner, H.A. Gustafsson, H.H. Gutbrod, B. Kolb, H. Löhner, B. Ludewigt, A.M. Poskanzer, H. Riedesel, H.G. Ritter, A. Warwick, F. Weik, and H. Wieman 329

Pion Spectra in the Reaction Ar + KCl at 1.8 GeV/Nucleon
R. Brockmann, J.W. Harris, M. Maier, A. Sandoval, R. Stock, H. Ströbele, K.L. Wolf, H.G. Pugh, L.S. Schroeder, and R.E. Renfordt 333

Au Target Fragmentation at Intermediate Energies
K. Aleklett, W. Loveland, P.L. McGaughey, K.J. Moody, R.M. McFarland, R.H. Kraus, Jr., and G.T. Seaborg 337

Phase-Space Constraints on the Momenta of Projectile Fragments
M.J. Murphy 341

Inclusive K^+-Production in the Model of Transport Theory for High-Energy Nucleus-Nucleus Collisions
W. Zwermann, B. Schürmann, K. Dietrich, and E. Martschew 345

Subthreshold Pion Production in Nucleus-Nucleus Collisions—A Co-Operative Process!
R. Shyam and J. Knoll 349

Pion Production From Peripheral Heavy-Ion Collisions Through Coherent Isobar and Isobaric Analog Giant Resonance Formation
P.A. Deutchman, R.L. Madigan, J.W. Norbury, and L.W. Townsend 353

Complex WKB Solutions for ^{12}C + ^{12}C Scattering
L.W. Townsend, H.B. Bidasaria, and J.W. Wilson 357

SESSIONS V AND VI: HIGH ENERGY REACTIONS

* Search for a Possible Deconfinement Phase Transition in Nuclear Matter by Proton and Anti-Proton Interactions with Nuclei at 200 GeV
I. Derado 363

* $\alpha\alpha$ and αp Interactions at the CERN ISR
E. Stenlund 373

Particle Densities in Ultrarelativistic Heavy Ion Reactions Extrapolated From Proton-Nucleus Collisions
I. Otterlund, S. Garpman, I. Lund, and E. Stenlund 385

Analysis of the High Multiplicity Events in Ultra-Relativistic Heavy Ion Collisions
H. Sumiyoshi 389

* † Study of $\bar{p}$p Collisions at the CERN SPS Using a Streamer Chamber
J.G. Rushbrooke ..... —

* Lepton Scattering From Nuclear Targets
A. Bodek 393

Deep Inelastic Lepton Scattering and the Quark Structure of Nuclei
J.P. Vary and H.J. Pirner 405

Anomalous Behavior of Nuclear Structure Functions Revisited
W. Furmanski and A. Krzywicki 409

* Stopping Process of GeV Particles in Target Nuclei
K. Nakai 413

* First Performance Tests of the Diogene Detector, With Alpha Particles
J. Gosset 427

* Hydrodynamical Aspects of Ultrarelativistic Heavy Ion Collisions
P.V. Ruuskanen 433

* Transverse Expansion at Central Rapidities in Ultra-Relativistic Heavy Ion Collisions
G. Baym 447

Shock Fronts Without Thermalization in Ultrarelativistic Heavy-Ion Reactions
L.P. Csernai 455

Entropy Production by Nonquasistatic Phase Transitions in High-Energy Heavy-Ion Reactions
L.P. Csernai and B. Lukács 459

* Partons in Nuclear Collisions Before Recombination
R.C. Hwa 463

* † Quark-Nucleus Collisions: Implications for Heavy Ion Collisions
N.N. Nikolaev ..... —

Central Collisions of Heavy Ions in the Dual Parton Model
A. Capella, C. Pajares, and A.V. Ramallo 479

Thermalization of Central Products in Ultra-Relativistic Heavy Ion Collisions
S. Date, O. Miyamura, T. Ochiai, H. Sumiyoshi, and N. Suzuki 483

SESSION VII: MORE OR LESS EXOTICA

* Strangeness and Phase Changes in Hot Hadronic Matter
J. Rafelski 489

*Invited Talk.

†Manuscript not received.

Meson Emissions From Quark-Gluon Plasma Through Formation and Fission of Chromoelectric Flux Tubes
T. Matsui, B. Banerjee, and N.K. Glendenning 511

Pion Radiation by Hot Quark-Gluon Plasma
J. Rafelski and M. Danos 515

Do Light Fermions Destroy the Confinement/Deconfinement Phase Transition?
T.A. DeGrand and C.E. DeTar 519

* Normalons, Anomalons and Anomalies in High Energy Cosmic Rays
A. Dar 523

Possible Candidates for Quark-Gluon Plasma in the JACEE Emulsion Chamber
The JACEE Collaboration 563

* Fractional Charge Search at the Bevalac
G.L. Shaw 567

* Recent Atomic Physics Experiments at the Bevalac
H. Gould 575

Evidence for the Non-Existence of Anomalous Projectile Fragments with $Z^* = 1.33, 1.67, 2.33$ and 2.67
M.A. Bloomer, E.M. Friedlander, H.H. Heckman, and Y.J. Karant 579

Equilibrium Charge States of Uranium at Relativistic Energies
H. Crawford, H. Gould, D. Greiner, P. Lindstrom, and J. Symons 583

The Stopping of 200 GeV Gold Nuclei in Nuclear Emulsions
C.J. Waddington, P.S. Freier, and D.J. Fixsen 585

Search for Unstable Superdense Nuclei at the Dubna Synchrophasotron
A.A. Kuznetsov 589

SESSION VIII: FINAL SESSION

* Multiquark Exotics
H.J. Lipkin 595

* Are Anomalons Still Provocative?—A Summary of the Present Experimental Situation
I. Otterlund 607

* Impressions of the Meeting
A.S. Goldhaber 627

List of Participants 631

*Invited Talk.

SESSION I: ANOMALONS—EXPERIMENTAL

MEAN FREE PATH OF ^{40}AR PROJECTILE FRAGMENTS IN CR39 TRACK DETECTORS

W.Heinrich, H.Drechsel, W.Trakowski, J. Beer, C.Brechtmann, J.Dreute and S.Sonntag

Department of Physics, University of Siegen, 59 Siegen, W.Germany

Abstract:

This paper describes an experiment investigating the effect of anomalous short interaction mean free paths for fragments of relativistic heavy ions. We use a stack of CR39 plastic nuclear track detectors that was irradiated with 1.8 GeV/nucleon ^{40}AR ions at the Berkeley Bevalac. About $1.5 \cdot 10^7$ etch cones were measured in this experiment using an automatic measuring system. For 6444 nuclear collisions of fragments with charges 9-15 the interaction mean free path in the plastic was determined. This analysis cannot rule out the observations of enlarged cross sections for relativistic projectile fragments in the first centimeters after emission [1-3], but in contradiction to the experiments in nuclear emulsion [1] the effect observed in our experiment is weaker and detectable only within the first centimeter.

Introduction:

The most significant hint on the anomalous mean free path effect is the considerable smaller mean free path of fragments of relativistic heavy ions within the first few centimeters after their production. Behind this distance the mean free path approaches the value observed for beam nuclei. The first observations [1] were consistent with an admixture of 6% of all projectile fragments having a mean free path of λ_a = 2.5cm in nuclear emulsions. These experimental results have been confirmed by P.L.Jain and G.Das [2] and H.B.Barber et al. [3] . All these experiments used nuclear emulsion as detector material. The aim of our experiment was on the one hand to confirm the anomalous mean free path effect using another experimental method and on the other hand to improve the underlying statistics.

Experimental technique and track measurements:

We use CR39 plastic nuclear track detectors ($C_{12}H_{18}O_7$) as a target and simultaneously to record the tracks of beam particles and their fragments. A stack of 300 foils each 0.6 mm thick with an effective area of 6.0 cm x 4.5 cm was exposed

at the Bevalac to a 1.8 GeV/nucleon ^{40}Ar beam incident perpendicular to the foil surface with 1500 particles/cm^2. The plastic foils were etched in NaOH-solution to develop the particle tracks to etch cones. The size of an etch cone depends on the radiation damage which is proportional to the energy loss of the particle. After a calibration of the detector the charge of the ion can directly be determined from the measured dE/dx signal. This is possible, because the projectiles lose only energy of about 400 MeV/nucleon in the stack and therefore beam nuclei and fragments are near the regime of minimum ionization for all measured tracks. Based on our experimental technique we can only detect charge changing interactions. Projectile fragments with charges smaller than 7 cannot be registrated due to the detection threshold of the CR39. Additionally a cut for a minimum size of etch cones that corresponds to a detectable charge between 8 and 7 was made by the track measuring system.

The scanning and measuring of $1.5 \cdot 10^7$ etch cones all together on the top and rear side of the foils was done with the help of an automatic measuring system (figure 1), developed at the Physics Department of the University of Siegen [4] . This technique is based on the method of picture analysis.

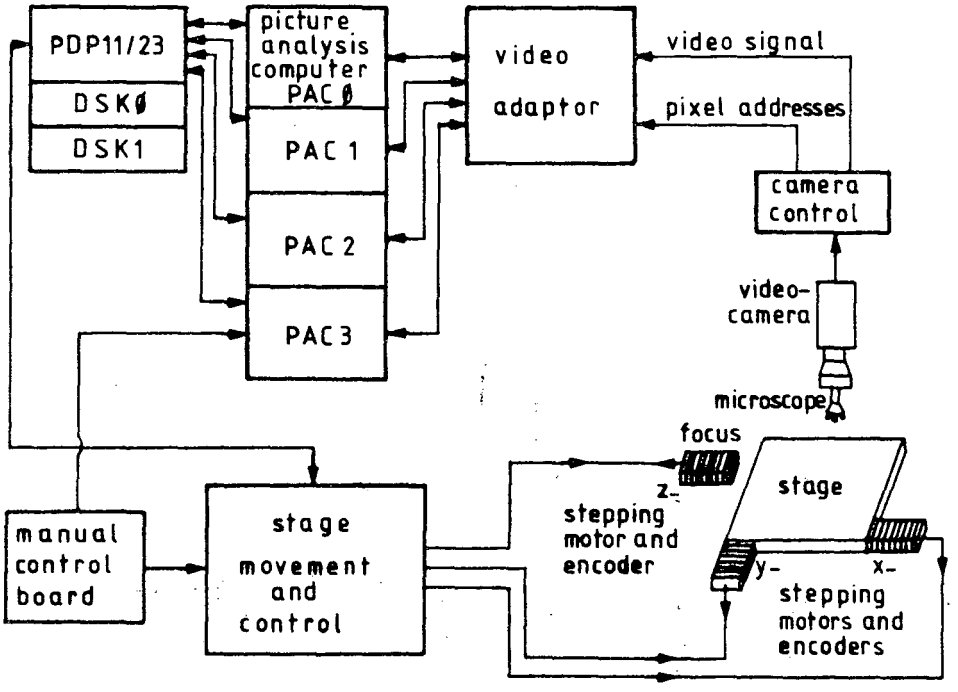

Figure 1: The automatic measuring system for plastic nuclear track detectors.

The plastic foils are mounted on a microscope stage which can be moved by stepping motors. A video camera is looking through

the microscope and the video pictures are digitized in real time by a video adaptor. The grey levels of 512 x 512 picture points are written into the memory of one of the picture analysis computers (MOTOROLA MC 68000). The etch cones, which appear as dark areas on a brighter background, are detected by a special software and their areas, perimeters and center of mass coordinates are determined. A detailed description of this automatic measuring system will be published elsewhere. For the experiment described here an early version of this system containing only one picture analysis computer was used.

The area of the etch cones measured by the automatic system is dependent on the focus of the microscope. We minimized this dependence by using a low magnification objective (4x). The surface of the plastic foil was approximated by a plane. A stepping motor for the z-coordinate kept the distance between this plane and the objective constant.

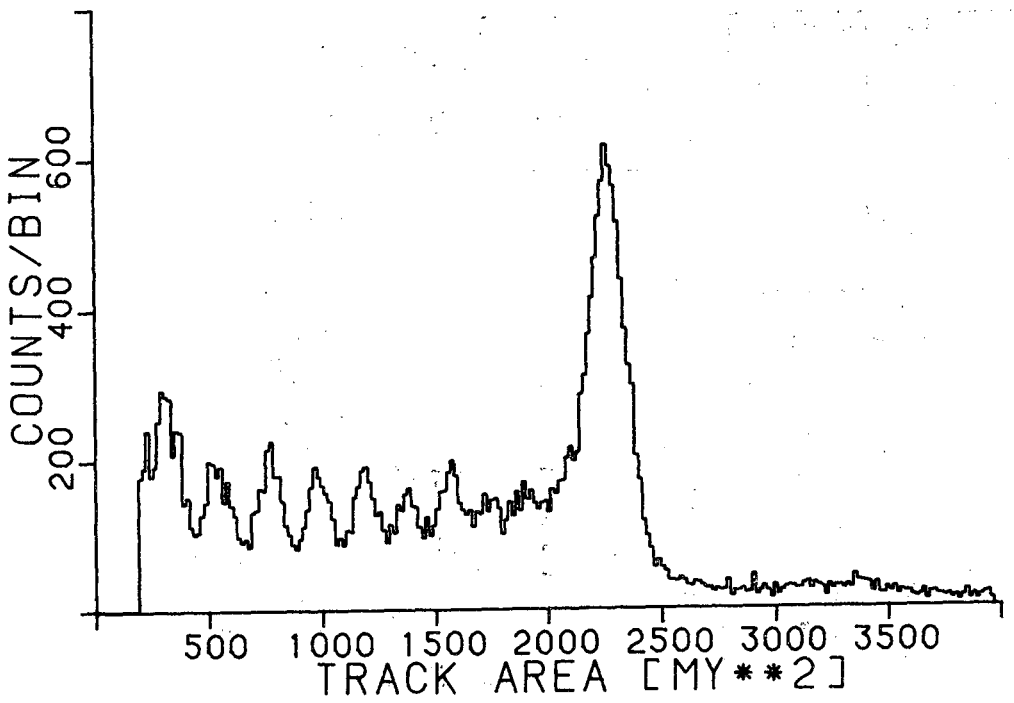

Figure 2: Distribution of track areas (μm^2) measured for one layer of plastic at a depth of approximately 14cm in the stack.

Figure 2 shows the distribution of the measured areas for one detector foil. Clearly detectable peaks for the ^{40}Ar beam particles and the fragments of distinct charges can be seen. The mean areas differ for the same charge on different foils. Reasons for this are non constant conditions for the automatic track measurements and a non constant sensitivity of the foils due to inhomogenities of the plastic material. Based on a linear dependence of the mean area for fragment tracks on the mean areas for beam tracks a local calibration of the detectors was possible. We determined the charge of a particle from the area of its etch cone and from the mean cone size of projectile tracks in the vicinity. The charge resolution for a single etch cone is $\Delta Z = 0.2$ for charge 8 fragments and decreases to about $\Delta Z = 0.7$ for charge 17 fragments.

Data Analysis:

The first step in the data analysis procedure was the reconstruction of the trajectories of individual projectile fragments in the stack. Due to limitations in computer power this tracing had to be done within a charge interval for each fragment separately. Each single measured etch cone, having a charge within the choosen interval and not belonging to an already defined trajectory, established a new one. Tracks were reconstructed throughout the stack by extrapolation of all trajectories into the following foil layers and looking for coincidences between the extrapolated positions and measured etch cones. If during the tracing procedure no etch cones were found within three consecutive layers, the end of the track was defined. Tracks shorter than a minimum of three measured etch cones were rejected to avoid confusion by randomly tracing background objects.

A problem for the tracing procedure arises, if the tracks of two particles cross. In the crossing over region the charge measured by the automatic system for two overlapping etch cones lies outside the charge interval for which tracing is performed. For this reason the tracing will be interrupted at this point and in a deeper layer where the two overlapping tracks separate again, a new trajectory may be defined. In this case two segments belonging to the same trajectory are constructed. Therefore in a second step we matched incompletely traced trajectory segments together.

To get information about the nuclear interactions in which the fragments were produced and destroyed, we traced in a third step for each trajectory ten foil layers from the starting point into upstream direction and also ten foil layers from the end point into downstream direction without restriction of the charge. From these data we determined for each individual fragment trajectory the charge of the parent nucleus and the charge of the fragment of the next generation, if it was visible in our detector ($Z \geq 8$).

Overlapping etch cones or etch cones with a small separation distance cause problems for the trajectory reconstruction software. Interactions might be defined by mistake. To overcome this problem we analyzed adjacent tracks in more detail at the beginning and endpoint of each trajectory.

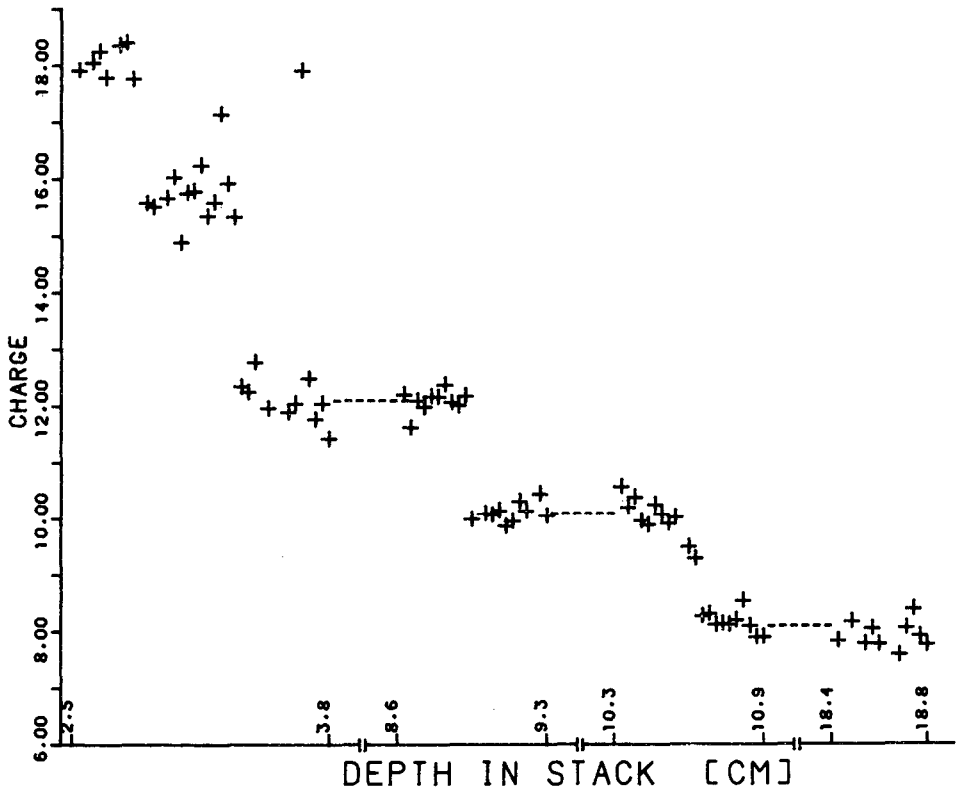

Figure 3: Event with four charge changing nuclear collisions. From the incoming ^{40}Ar beam particle successively fragments of charges Z=16, Z=12, Z=10 and Z=8 are produced.

For fragments of higher generations, that means fragments that originiate from collisions of other fragments but not from beam nuclei, the trajectory was completey reconstructed upstream up to the first interaction of the beam nucleus. Figure 3 shows an example of a chain of 4 nuclear fragmentations.

Systematic errors in the reconstructed trajectories arise if these are short and contain only a few data points. For this reason we excluded trajectories shorter than 2 mm (6 foil layers) from the later analysis. The trajectories of oxygen (Z=8) fragments have been excluded because the areas of etch

cones for these tracks have a value close to the minimum area accepted by the automatic measuring system. Therefore datapoints along a Z=8 trajectory may be lost. Not analysed were also the fragments of charge 16 and 17. For these higher charges due to the poorer charge resolution the detection of $\Delta Z=1$ interactions is slightly biased, especially for short trajectories.

Results:

Figure 4 shows the charge spectrum of 14185 traced fragment trajectories longer than 2 mm. The charge values for short tracks are averaged over a smaller number of individual measurements and therefore these events contribute with a larger variance to the distribution. An asymmetric tail of the distributions for charges greater than the integer value is observable. This originates from trajectories containing measured etch cones, where a surface structure of the plastic overlaps with an etch cone. In these cases the automatic system measures an area which is too large, giving also a too large charge value. But beside this the overall charge resolution of our experiment is below $\Delta Z = 0.1$.

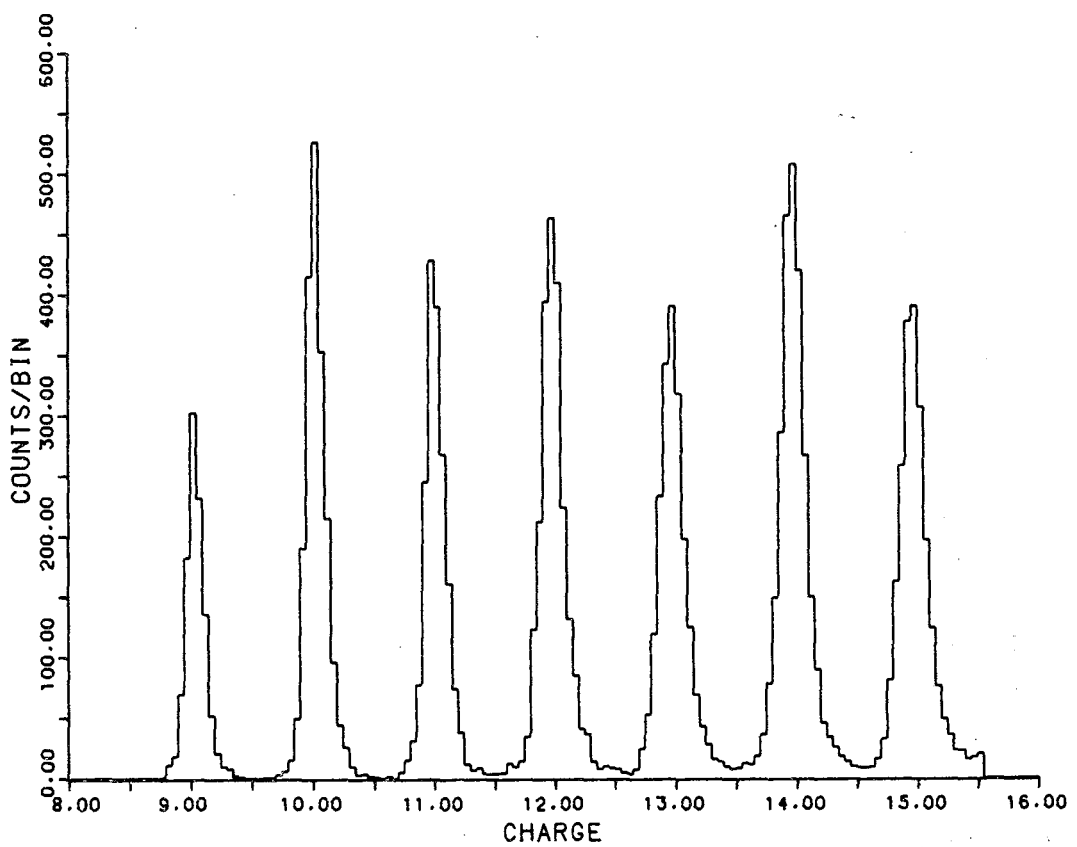

Figure 4: Distribution of charges measured for fragment trajectories of a length > 2 mm.

To determine the interaction mean free path the total number n_Z of interactions of nuclei with charge Z was counted. Then for each particle i with charge Z the path length l_i^Z along which an interaction could possibly be detected was determined. If a trajectory leaves the scanned area on the detector foils or leaves the stack on the rear side, or if the trajectory overlaps with another particle's trajectory without a detectable separation deeper in the stack, the length down to the point where the trajectory was lost is included in the analysis. For each individual fragment charge we determined

$$\lambda_z = \sum_i l_i^Z / n_Z \ .$$

The measured value of λ_Z was then normalized to a calculated interaction mean free path λ_Z^C for charge changing interactions. This was determined using the empirical overlap formula of P.J.Lindstrom et al. [5] for total interaction cross sections of nuclear collisions with carbon and oxygen in the CR39. For collisions with hydrogen the empirical formula of R.Silberberg and C.H.Tsao was used [6]. A correction for non charge changing interactions was included. This was derived from the semiempirical formula for partial fragmentation cross sections of R.Silberberg and C.H.Tsao [7] and assuming a factorisation of the cross sections for heavier targets. For the fragments of different charges the mass of the most abundant isotope was used in the calculation. This mass was determined from mass yields calculated after R.Silberberg and C.H.Tsao [7] .

Based on this normalization we can pool the information from the different fragment charges and determine

$$\lambda^* = \sum_i (l_i^Z / \lambda_Z^C) / \Sigma\, n_Z \ .$$

This normalized interaction mean free path is shown in figure 5 for different intervals of depth in the plastic stack. Data from fragment charges 9 to 15 and all fragment generations are included. A total number of 14501 fragments with 7120 detected interactions is involved in this picture. The line shown in figure 6 represents the value of λ^* averaged over the whole stack. This value of $\lambda^* = 0.96 \pm 0.01$ is below the normalized value of 1.

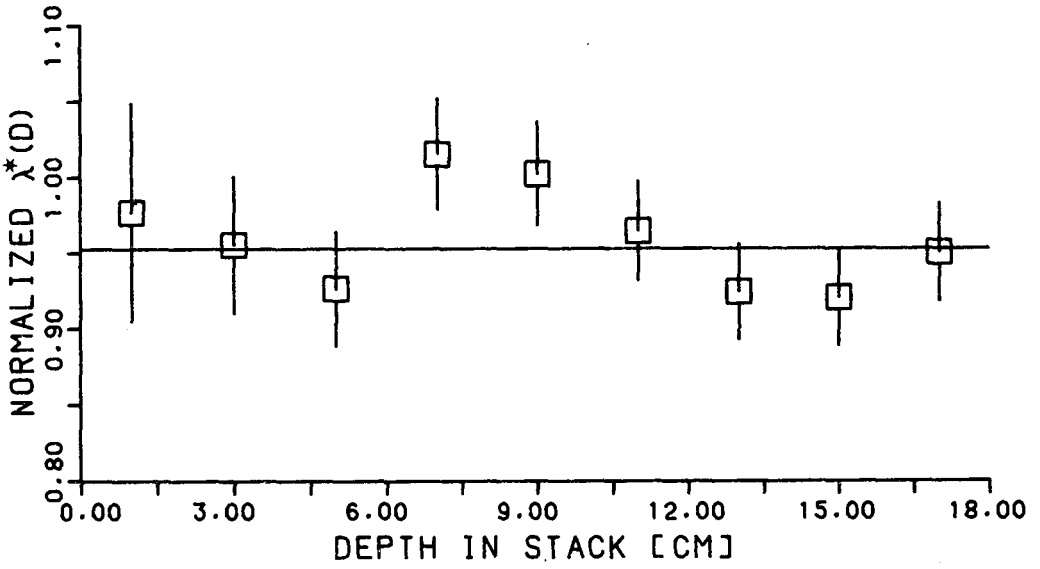

Figure 5: The normalized interaction mean free path as a function of depth D in the stack for fragments of $9 \leq Z \leq 15$.

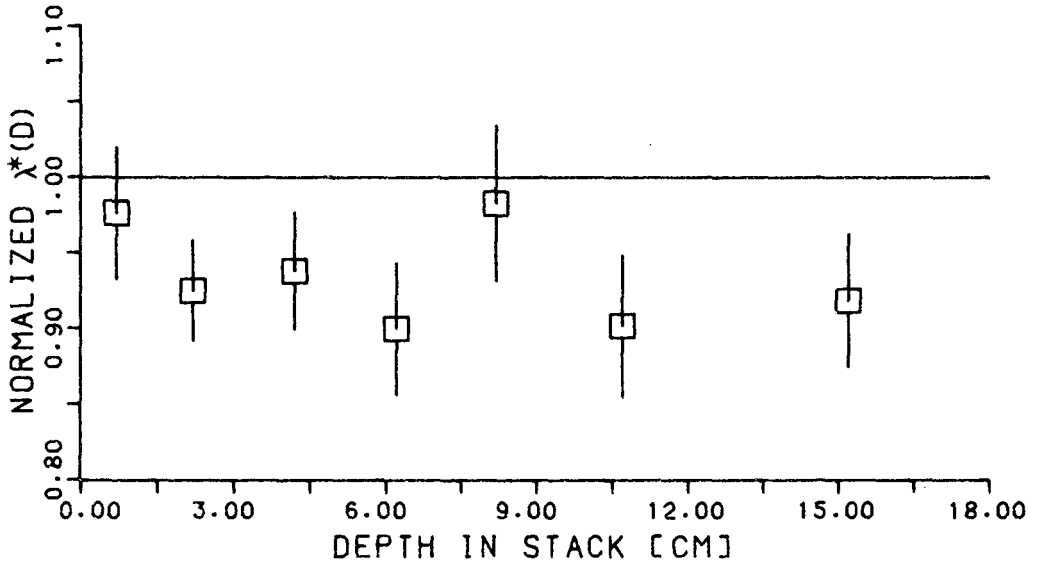

Figure 6: The normalized interaction mean free path of Z=18 beam particles as a function of depth D in the stack.

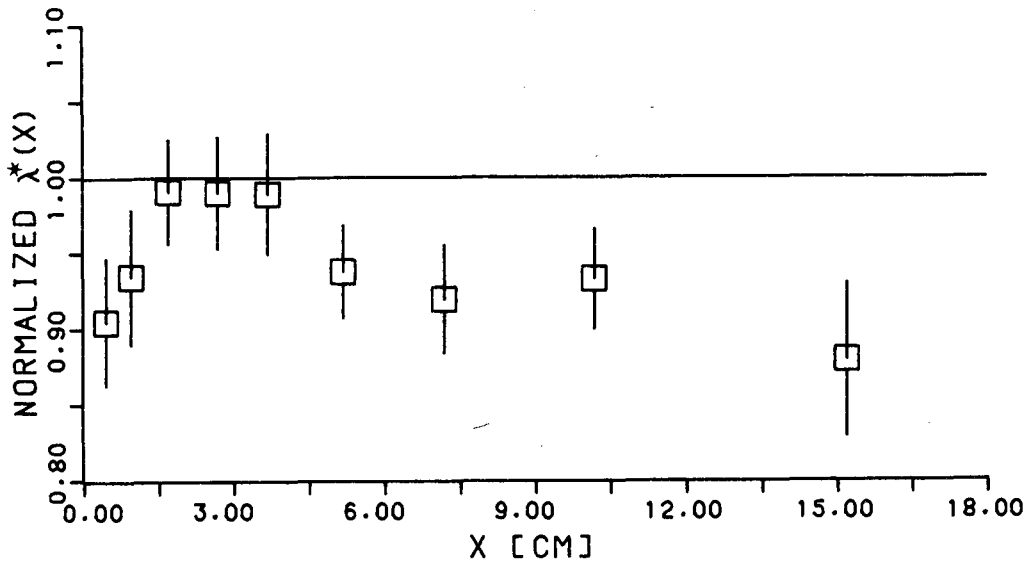

Figure 7: The normalized interaction mean free path as a function of distance x from the point of emission for fragments of charges $9 \leq Z \leq 15$ for all generations of fragments. The data are corrected for the systematic bias

The error bars in figure 5 and the following figures 6 and 7 indicate statistical errors only. Because of our high statistics we can assume the probability distribution of the λ^* for each interval of depth to be gaussian. The errors are calculated for $\lambda^* = 1$, assuming that the deviations of the measured λ^* from 1 are statistical fluctuations.

Figure 6 shows the results of the normalized mean free path λ^* (D) for the beam particles as a function of depth in the stack. The mean value over all data points is $\lambda^* = 0.93 \pm 0.02$. For Z=18 projectiles the detection of $\Delta Z=1$ interactions is biased, causing a too small value of λ_{18} in comparison to λ^c_{18}. Here 5795 particles with 3968 interactions are involved. That is only a part of the beam nuclei.

To investigate the anomalous mean free path effect, $\lambda^*(x)$ was determined for intervals of distance x from the point of emission of the fragments. Figure 7 shows the result for fragments of charge $9 \leq Z \leq 15$ with 6444 charge changing interactions. These data show a reduced interaction mean free path within distances $x \leq 1.2$ cm and surprisingly above $x > 4.2$ cm. The short mean free path effect observable in our experiment is restricted to small values of x. This was already indicated in a preliminary analysis for Z=14 fragments [8] .

Analysis of Systematic Errors:

Various systematic errors can in principle influence the result of figure 7. A specific problem causing systematic errors in our experiment arises from a small fraction of particle trajectories that are artefacts constructed by the computer programs. These trajectories are typically short and originate from data measured for overlapping etch cones and etch cones flawed by a surface structure of the plastic foils. A small number of faulty events has a significant influence in an experiment looking for a few percent of anomalous particles. This problem of our experimentl technique can in principle be solved by an improved software for the picture analysis system. The development of this software is in progress. For the experiment described here the only possibility was a reanalysis of all events with interacting or ending trajectories shorter than 1.2 cm. In a reanalysis by eyeball of more than 2000 fragment trajectories the artefacts constructed by the automatic measurement and trajectory reconstruction were detected and eliminated. The results shown in figure 7 are free of this systematic error.

To ensure that for the data with $x > 1.2$ cm this systematic error has no influence, we determined the difference of $\lambda^*(x)$ before reanalysis by eyeball and after this reanalysis as a function of x. The systematic bias determined by this difference is shown in figure 8. It can be seen. that for x approaching 1 cm this bias vanishes.

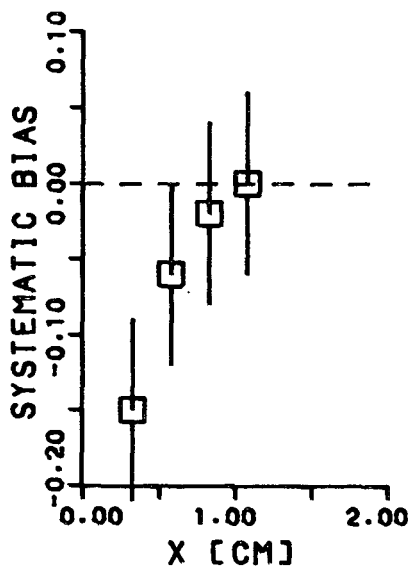

Figure 8: Systematic bias as a function of distance x from the point of emission of the fragments. The bias gives the difference of $\lambda^*(x)$ before reanalysis by eyeball and $\lambda^*(x)$ after reanalysis by eyeball.

If the probability to detect interactions of fragments depends on the distance from the point of production this would of course influence the measured value of $\lambda^*(x)$. Since our

data are taken by a computerized device, a possible bias of scanners knowing the value of x can be excluded. As the point of interaction (x=0) is distributed randomly over the plastic stack fluctuations of the conditions for data measurement should be smeared out over all events and all values of x. Major influence of such fluctuations should be visible in the presentation of $\lambda^*(D)$ in dependence of depth D in the stack shown in figure 6. These data and also the data of figure 7 show no significant deviation of λ^* from the average. We re-examined the experimental conditions for depths 6cm to 9cm but found no reason for the slight increase of $\lambda^*(D)$ in this interval, so that we have to interpret this as a statistical fluctuation. If we exclude this part of the stack from the analysis of $\lambda^*(x)$ shown in figure 7 the difference between the interaction mean free path within the first centimeter and the next few centimeters is not influenced.

We now discuss a systematic error that could in principle hide an anomalous mean free path effect. The dataset presented in figure 7 might contain events for which the point of emission (x=0) of the fragment is not correct. That means that an arbitrary point $x>0$ is assumed as x=0, where the probability of contributions by anomalous fragments has already decreased. In our data we included only fragments of charge $Z\leq 15$ to ensure the correct recognition of the production of a fragment from the primary beam nuclei of Z=18 by a charge changing interaction of $\Delta Z\geq 3$. However, the data of figure 7 include also higher generation fragments that were produced in interactions with $\Delta Z\leq 3$. By excluding these higher generation fragments from the analysis the plot equivalent to figure 7 shows with slightly decreased statistic no significant enhancement of the anomalous mean free path effect.

As tests for systematic effects of the experiment and to investigate a dependence of the result on different parameters, we divided the data in subsets looking for significant differences from the presentations of figure 6 and figure 7. This was done

1. as mentioned for fragments of the first generation and higher generations,
2. by excluding higher generation fragments produced in $\Delta Z = 1$ interactions,
3. for interactions in which the fragments undergo a nuclear interaction with $\Delta Z = 1$,
4. for interactions in which a fragment of charge $Z\geq 8$ is produced in a collision of a fragment,
5. for the same conditions described in 4) but $Z<8$ that means not detectable in CR39,
6. for the data in an upstream and downstream part of the stack,

7. by dividing the data with respect to coordinates in the plastic detectors.
8. by dividing the data with respect to odd and even fragment charges,
9. by dividing the data with respect to small and large fragment charge ($9 \leq Z \leq 12$ and $13 \leq Z \leq 15$).

In none of these cases results with statistically significant difference to those of figure 6 and 7 were observed. That means that after all these tests no systematic effect was detected explaining the difference of $\lambda^*(x)$ between the first centimeter and the next three centimeters. Also no explanation of the decrease of $\lambda^*(x)$, for $x>4$cm was found. Fragments interacting after large distances x from their point of emission necessarily interact in the downstream part of the stack. As indicated by figure 6 the probability for defining interactions might be slightly enlarged in this part of the stack and as a result $\lambda^*(x)$ might be reduced in figure 7 for large values of x. But this explanation is ruled out by test number 4. Interactions, in which an outcoming fragment with a charge $Z \geq 8$ is seen are very unlikely to be simulated by systematic errors.

Discussion:

To answer the question whether we see an anomalous mean free path effect at all the problem of the normalization has to be discussed. The values of λ_z measured for interactions in the interval $1.2\text{xm} \leq x \leq 4.2$cm of distance from the point of emission are compared with the calculated values of λ_z^c shown as lines in figure 9. A comparison of the seven data points with the calculated values based on a χ^2-test gives $\chi^2=5.87$ for 7 degrees of freedom. That means that the measured and calculated values of λ_z agree for $1.2\text{cm} \leq x \leq 4.2$cm. The most crucial point is the decrease of $\lambda^*(x)$ for $\bar{x} \geq 4.2$cm. We presently reanalyse the data for $4.2\text{cm} \leq x \leq 6.2$cm by eyeball to be sure, whether this is due to a systematic effect. It should be mentioned however that an increase of the cross section behind large distances was observed earlier for fragments of ^{12}C projectiles in the Dubna bubble chamber 10cm behind the point of emission [10].

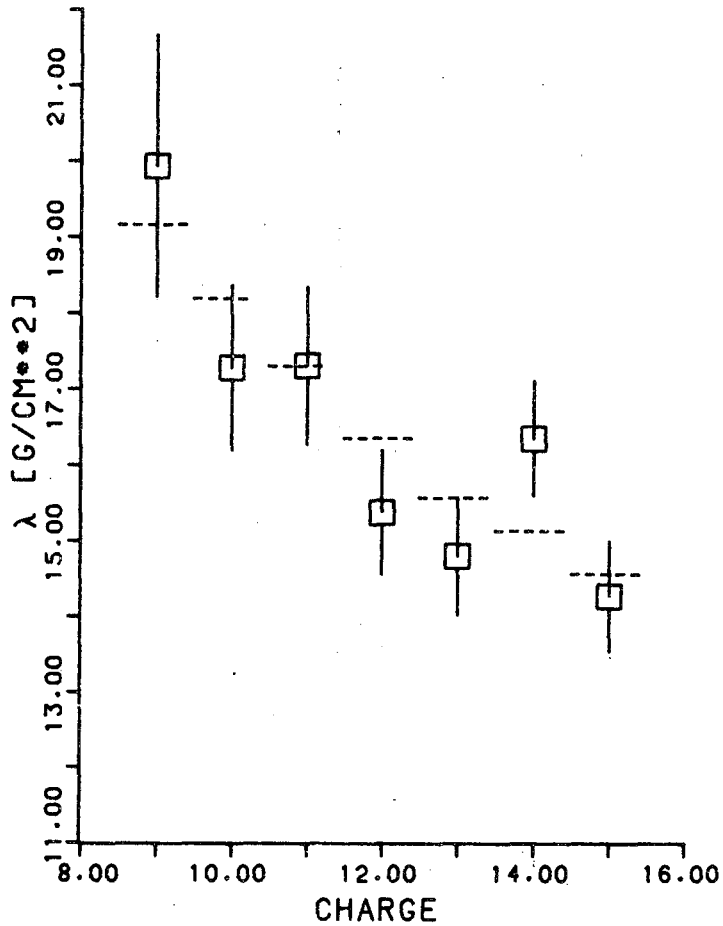

Figure 9: Comparison between the interaction mean free path measured for 1.2cm $\leq x \leq$ 4.2cm (points with error bars) and the calculated values (dotted lines).

If we restrict our discussion to the results for $x \leq 4.2$cm, tha data in the first 1.2cm are 2.8 standard deviations away from the normalization value of 1. A parameterization of our data ignoring $\lambda^*(x)$ for $x \geq 4.2$cm based on the model of E.M.Friedlaender et al. [1] shows that an admixture of 1.2% fragments having an interaction mean free path of λ_a=0.65cm can explain the observations. The normalized likelihood to observe our result under the assumption of an admixture of 6% with λ_a=2.5cm is $2 \cdot 10^{-6}$ if we compare the raw data. Such a comparison of course has to consider the influence of the different targets on the anomalous mean free path effect. This is unknown. But for a model where anomalous fragments disappear due to collisions only - based on a very large cross section - we can assume, that instead of measuring the distance x from the point of emission of the anomalous fragments, this should be done with respect to the number of collisions. Following this idea we can estimate that 1cm of CR39 corresponds to 1.37cm of emulsion. The norma-

lized likelihood to observe our results under this assumption for the parameters 6% and λ_a=2.5/1.37cm is $2 \cdot 10^{-3}$.

Our experiment looking for an anomalous short mean free path of fragments from relativistic heavy nuclei was performed under conditions slightly different to the experiments using nuclear emulsions.

1. In CR39 (C_{12} H_{18} O_7) as a target all nuclear collisions take place with light target nuclei. For a considerable number of the collisions hydrogen is the target. This is different to an experiment using nuclear emulsions, where additionally to light target nuclei the heavy nuclei like Ag and Br are present.

2. Our analysis was restricted only to heavy fragments, light fragments are not detectable due to a threshold of the CR39. Additionally fragments of charge Z=17 and Z=16 produced from the primary Ar-beam nuclei are not included. That means our data include only a small number of interactions where the fragment is produced in a $\Delta Z \leq 2$ charge changing fragmentation for fragments of higher generations.

3. Furthermore only the results of one experiment using nuclear emulsions were based on a considerable number of primary ^{40}Ar projectiles [2]. The other experiments used ^{16}O or ^{56}Fe beams.

Our data cannot rule out the existence of an anomalous component showing a reduced mean free path. But this is present only within the first 1.2cm after emission with a small abundance of 1.2%. Due to this the statistical significance for the existence of this component is still below 3 standard deviations in our experiment although based on our technique we have been able to investigate a large number of interactions. We will perform further experiments with different beam nuclei and heavy target foils between the plastic detectors to look for an enlarged signal from anomalous fragments under different experimental conditions.

Work supported by the Bundesminister für Forschung und Technologie, No 06 SI 159.

References:

[1] E.M.Friedlaender, R.W.Gimpel, H.H.Heckman, Y.J.Karant, B.Judeck and E.Ganssauge, Phys.Rev.Lett.45, 1084 (1980)

[2] P.L.Jain and G.Das, Phys.Rev.Lett. 48, 305 (1982)

[3] H.B.Barber, P.S.Freier and C.J.Waddington, Phys.Rev.Lett. 48, 856 (1982)

[4] J.Beer, J.Pipper, W.Heinrich, J Phys. E: Sci.Instrum. 15, 439 (1982)

[5] P.J.Lindstrom, D.E.Greiner, H.H.Heckman, B.Cork, F.S.Bieser, 14th Int.Conf.Cosmic Rays, München, page 2315 (1975)

[6] R.Silberberg, C.H.Tsao and M.M.Shapiro, eds. Shen and Merker (D.Reidel Publishing Co.,Dordrecht,Holland, 1975) p.49

[7] R.Silberberg, C.H.Tsao, Astrophys.Journ.Suppl.25, 315(1973)

[8] W.Heinrich, H.Drechsel, W.Trakoswki, J.Beer, C.Brechtmann, Jreute, R.Rudat, S.Sonntag, E.V.Benton, R.M.Cassou and R.P.Henke, Nucl.Phys. A400, 315c (1973)

[9] E.M.Friedländer, R.W.Gimpel, H.H.Heckman, Y.J.Karant, B.Judek and E.Ganssauge, Phys.Rev. C27, 1489 (1983)

[10] Alma-Ata, et al. collaboration, Joint Institute of Nuclear Research report JINR E1-82-510 (1982)

Study of Anomalous Nuclear Projectile Fragments in Reactions of 1.85A GeV ^{40}Ar in CR-39 Etched Track Detector

M.L. Tincknell and P.B. Price
University of California, Berkeley

Anomalous nuclear projectile fragments, or "anomalons," were first observed in cosmic rays by nuclear emulsion as a rapid series of nuclear interactions in a short distance. They were later seen as a statistical anomaly in secondary mean-free-paths (mfp's) in cosmic rays, and most recently and convincingly observed in high-statistics experiments using Bevalac beams which showed short mfp's for secondary fragments measured within the first few centimeters after the primary interactions. Because of the controversial and provocative nature of these reports, an alternative technique with different systematic errors and methodology is essential to confirm and illuminate the anomalon phenomenon. CR-39 etched track detector provides this alternative. It allows sampling of the electric charge with high resolution at approximately 600 μm intervals along a nuclear track, and thus successive nuclear charge-changing interactions in short distances can be observed. We report here the observation of depressed secondary mfp's in the first centimeter or so beyond the primary interactions in CR-39, in agreement with the previous emulsion work.

CR-39 is a visual detector like emulsion, and the use of human observers to record data for individual tracks necessitates slow data acquisition and limited statistics. In our experiment a beam of 1.85A GeV ^{40}Ar ions enters a stack of 640 μm CR-39 sheets perpendicularly, and the etched tracks appear as conical pits on the top and bottom surfaces of the plastic. The pit diameter is a monotonically increasing function of (Z/β), and for our etching conditions, the diameters of the Ar tracks are about 35 μm. The modest energy loss in plastic, and persistence of beam velocity by nuclear fragments, allows the nuclear charge to be extracted from a measurement of a single diameter with charge resolution $\leq 0.25e$ for nuclei $10 \leq Z \leq 18$. The following are important differences between tracks observed in CR-39 and nuclear emulsion:

1) only charge-changing nuclear interactions can be seen;
2) in CR-39(DOP), only particles with $Z \geq 10$ at relativistic velocity record tracks;
3) no target fragmentation is observed;
4) there is a finite sampling thickness, fundamentally limited by the sheet thickness.

Our measurement technique is semi-automated, with a human observer participating in the acquisition of each individual track diameter. We have a computer-driven precision stage which can index to prerecorded track positions, and a Compumetric Automatic Measuring System which automatically finds the track diameter by detecting the edges of the track's video image. The human must distinguish the track being followed from neighbors, center it, and ensure that the track diameter is not flawed. The diameter and position for each observed track are recorded directly on a computer file. This system has been previously successful in measuring the interaction mfp's of primary Ne, Ar, Fe, and U, and was used in our recent negative search of over 1000 projectile fragments for nonintegral charge (Price et al., Phys. Rev. Lett. 50, 566 (1983)).

We use a "find and follow" technique which isolates secondaries immediately and propagates them into the stack in centimeter jumps. Secondary interactions are further localized to 0.25 cm intervals by a binary cut process. CR-39(DOP) is quite transparent after etching, and the physical superimposure of sheets on the stage is essential to our method. We find the secondaries initially by superimposing and aligning two sheets which were four sheets apart in the original stack. We then focus through to the interface between the two sheets and scan a large area at 160X magnification. The associated pairs of tracks are observed and the positions of any new, observable secondaries produced in the 0.32 cm interval are recorded. In five such intervals that we scanned near the front of the stack, we observed 1615 secondaries with $11 \leq Z \leq 17$. The centimeter jumps were done by superimposing a new sheet on one taken from a location 1 cm upstream, so all tracks in a field of view could be matched, and ambiguities and interactions simply resolved. Diameter measurements were taken from the topmost surface at 200X magnification. With our exposure density of about 500 tracks/cm^2, the crossing of tracks and the lateral displacement of tracks of nuclei with large transverse momentum were only minor problems. About 18000 diameters were recorded, not including verifications. Almost all measurements were done by a single individual (Tincknell).

Several pitfalls and potential systematic errors were encountered, as follows:

1) there were significant variations in track response from sheet to sheet, necessitating two-parameter normalizations of the data in each sheet;
2) there were minor variations of response within a single sheet which broadened the charge peaks;
3) crossing tracks of similar diameter were sometimes difficult to identify;
4) an interacting fragment near another small track could sometimes be misinterpreted as no interaction, or an interaction to the wrong daughter;
5) there were rare, very small, insensitive patches on some sheets where the tracks did not record;
6) occasionally a secondary track would cross an unrelated primary over a 0.5 cm interval and be temporarily eclipsed;
7) interactions which occurred in the small volume of plastic which was subsequently removed by etching sometimes produced a single track apparently intermediate in charge between the previous and following particle, mimicking a fragment of short pathlength.

The latter three potential problems were mitigated by requiring two observations of a track with the same charge in order to confirm its existence. Problems 3) and 4) were mostly resolved by reference to the underlying sheet where tracks could be matched up.

The data were analyzed by standard techniques first outlined by Friedlander et al. 610 secondary interactions in the charge range $11 \leq Z \leq 17$ were observed within the first 6 cm after the primary interactions. The data for individual charges were pooled in two different ways to increase statistical significance. A charge-weighting derived from the empirical relation $\lambda = \Lambda Z^{-b}$ was used to define a parameter Λ for various

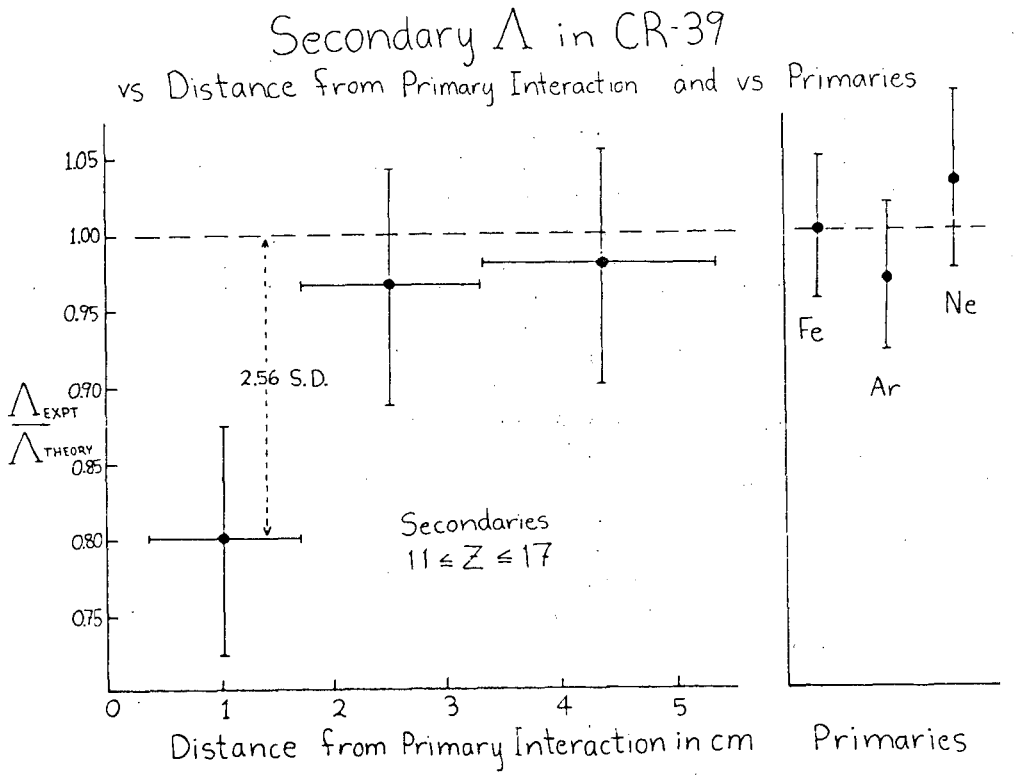

distance bins beyond the primary interaction, as shown in Fig. 1. The data are binned so that there are about 175 interactions in each of the three bins. A 2.5 Standard Error depression in Λ is obtained in the first bin of 0.38 to 1.54 cm from the primary interaction. The latter two bins from 1.54 to 3.1 cm and from 3.1 to 5.0 cm and the primary mfp's for Ne, Ar, and Fe agree well with values calculated from the Bradt-Peters expression for geometrical cross section, using the constants obtained by Westfall et al. (Phys. Rev. C 19, 1309 (1979)). A second method of pooling charges, using F ratios of the upstream to downstream mfp's of individual charges, and adding the logarithms of the F probabilities as a Chi-squared sum, gives a statistical probability of $<3 \times 10^{-2}$ for observing our result under the null hypothesis of no anomalous behavior. A two-parameter fit to the data in Fig. 1 leads to a fraction of anomalons of about 0.05 and anomalous mfp slightly greater than 1 cm. Figs. 2 and 3 show a breakdown of the Λ parameter for subsets of the data, first for even vs. odd charges, and then for low, medium, and high charge groups. Within the weak statistics of individual charges, all in the range $11 \leq Z \leq 17$ except 15 and 16 show anomalous behavior.

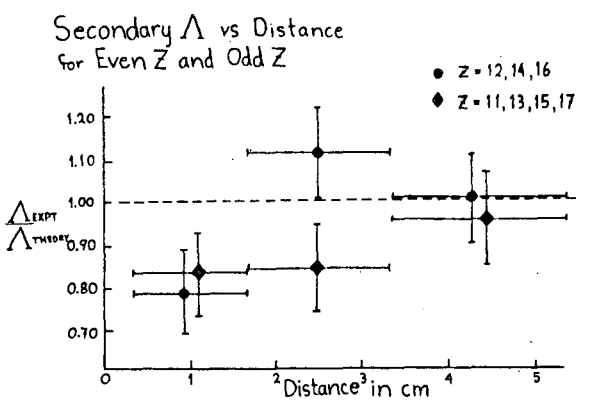

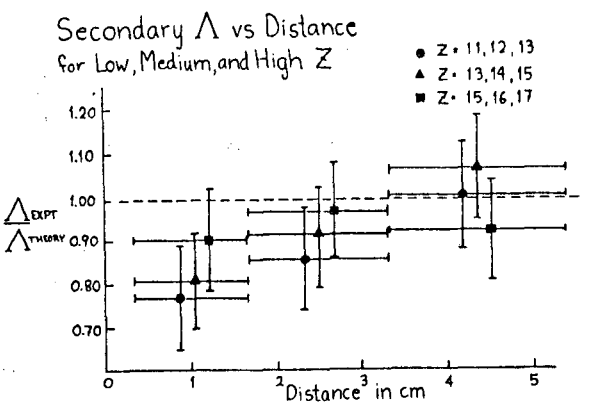

The main conclusions of our work are as follows:

1) anomalons are observed at ~2.5 S.D. in CR-39 for $11 \leq Z \leq 17$ in projectile fragmentation of 1.85A GeV ^{40}Ar;
2) both even and odd charge secondaries show anomalous behavior;
3) the anomalon mfp of ~1 cm is shorter than the 2.5 cm value usually reported in nuclear emulsion, whereas the primary mfp's are closely similar in the two media when measured in centimeters.

These observations confirm the emulsion results with a very different technique and validate CR-39 as a useful detector for anomalon investigation. We cast doubt on theories of anomalons where just a few "magic number" charges may be anomalous, or which predict an even-odd charge dependence. The apparent shorter anomalous mfp in CR-39 than in emulsion may result from the different target composition of CR-39 ($C_{12}H_{18}O_7$), or may support Mac Gregor's hypothesis that anomalous mfp's are a decreasing function of charge. (Our average Z is ~14, whereas the average charge in the emulsion measurement of Friedlander et al. is ~10.)

Future uses of CR-39 in our group for anomalon research will include investigation of more heavily charged primaries (Z = 26 and 36), an experiment to observe an anomalon lifetime in a dilute stack, and a project to find a primary energy threshold for anomalon production.

First Results from a Repeat Experiment on the Mean Free Path of Projectile Fragments from 1.88 A GeV ^{56}Fe--Emulsion Interactions

Y.J. Karant, H.H. Heckman, and E.M. Friedlander

Nuclear Science Division, Lawrence Berkeley Laboratory
University of California, Berkeley, CA 94720

In previous papers [1,2], we reported on results we had obtained on the mean free path (MFP) of secondary and later generation projectile fragments (PFs) from 1.88 A GeV ^{56}Fe primary nuclei incident on emulsion. We have repeated the experiment with careful systematic controls and report here our first results on the PF MFP.

In this experiment, we used three different stacks denoted symbolically by 2 Fe, Long Fe, and 3 Fe; each stack was made of 600 μm thick pellicles of Ilford G-5 research emulsion. The number of pellicles and dimensions of these stacks are, respectively, 42 pellicles of size 7.5 x 12 cm^2, 63 pellicles of size 10 x 23 cm^2, and 50 pellicles of size 7.5 x 25.5 cm^2, where the dimensions have been rounded to the nearest 0.5 cm. In all cases the primary particles entered the stacks normal to one end and parallel to the long dimension. Stack 2 Fe was the stack used for our previous investigation. We have done further scanning in stack 2 Fe, as well as in stacks Long Fe and 3 Fe. The MFP of PFs of charge $\geq$3 are reported from stack 3 Fe only, while He PFs are reported from all three stacks.

The reason for this charge selection is that for stack 3 Fe we had calibration beams of C and Ar present in the same emulsion batch, exposed at essentially the same time, and processed with the emulsion that we used for track following. Hence, we can verify with known charges our charge measurement methods that depend on delta-ray parameters of the track structure over a wide range of charge. By comparison, our published results for the 2 Fe stack were dependent on the known primary Fe tracks and one very good candidate for the track of an O PF, where the O was identified by its own interaction topology into four He PFs. For charges from He to C, we have an alternative method using lacunarity [3], which can be internally self calibrated; however, as we have not yet calibrated charges from Li to B in stack Long Fe, nor have we charge measured our new data in stack 2 Fe, we only analyzed He PFs from these stacks. Direct measurements under several conditions have shown that visual identification of He PFs is better than 99% reliable.

In this scan, as in our previous experiment, we followed Fe primaries until they either interacted or left the pellicle in which they entered the stack; no primaries were followed from pellicle to pellicle within the stack. When a primary interacted and gave rise to PFs of charge greater than or equal to He within the forward 6° cone, such PFs were followed throughout the stack (from pellicle to pellicle, if needed) until they interacted, left the stack, or stopped in the stack due to ionization energy loss. Unlike stack 2 Fe, stacks Long Fe and 3 Fe were long enough to actually stop PFs of charge near to Fe by ionization losses even if they had the beam velocity. Hence, if we wish to compare our present data with our published results, we must make them systematically compatible, i.e., provide the same energy spectra and the same potential paths.

The simplest first step to compare the two experiments is to change the actual stack length in all cases to that of stack 2 Fe, i.e., 12 cm; this can be easily accomplished in the data analysis programs by ignoring all tracks that have a starting coordinate beyond 12 cm and by terminating all other tracks at 12 cm, so that interactions beyond 12 cm are ignored. This is what we have actually done. Under this cut, we have a total of 754 PF interactions to use, as compared to the 730 that we previously had from Fe initiated processes in [2].

While there are many ways to examine the MFP data for the presence of an anomalously short component, one of the most direct is to plot the MFP parameter Λ^* as a function of the distance after emission of a PF and thereby determine if the data agree with our previous observations. In this analysis we assume the same scaling law for the MFP as a function of charge as we used in the previous analysis of the LBL data:

$$\lambda(Z) = \Lambda Z^{-b}$$

where we assign $\Lambda = 32$ cm and $b = 0.43$.

A basic quantity to plot is the ratio R of the measured Λ^* to its expectation Λ; this permits experiments with different scanning efficiencies, interaction definitions, or other systematic differences to be compared. To compute Λ^* one sums all the measured path length $S_N(Z)$ of particles of charge Z, multiplies it by Z^b, adds this to the charge weighted path length of the other charges, and divides the whole by the number N of interactions observed, i.e.,

$$\Lambda^* = \frac{\sum_Z S_N(Z) Z^b}{\sum_Z N(Z)}$$

Computed in this fashion, the ratio R has the expectation value of 1 in the absence of anomalons. We have plotted in fig. 1 the published results of three different experiments [1,4,5] including the NRC-LBL result of ref. [1]. Superimposed on this plot is a curve that represents the alternate hypothesis that 6% of PFs are anomalons with a fixed MFP of 2.5 cm independent of Z. We also plot here our new results under the systematic cuts mentioned above. As can be seen by direct inspection, our new data deviate from a value of R = 1 and are fully consistent with the other experiments and with the anomalon hypothesis.

Unlike our previous experiment, a systematic scan was also done on all He PFs from extranuclear cascades initiated by Fe primaries. To keep consistency with the 12 cm stack cut used for PFs of charge ≥ 3, we present here our first results for He PFs under the same cut. Under this cut, we have 1161 He PF interactions. We compute the observed MFP λ^* unscaled by any charge weight factor, i.e.,

$$\lambda^* = \frac{S_N}{N}$$

where S_N is the total path length within the bin of both interacting and noninteracting He PF tracks, and N is the number of observed interactions

within the bin. We have already measured the MFP at 2 AGeV of primary ^{4}He and primary ^{3}He, the only isotopes expected to have any reasonable population in He PFs. We observed 1010 ^{4}He interactions with a MFP of 21.85 cm and 445 interactions of ^{3}He with a MFP of 19.50 cm. Based on PF cross sections [6], we expect 75% of the He PFs to be ^{4}He and 25% to be ^{3}He. Using this mix, we would expect a He MFP of 21.26 cm; to be on the conservative side, we take the expected value of the He PF MFP to be 21 cm. Even though there is a slight difference between the measured MFPs of the two He isotopes, over a 10 cm interval the MFP of the mix should stay essentially constant at its expectation value.

We plot in Fig. 2 the ratio R of our measured He PF MFP, λ^*, to its expectation value of 21 cm, against the distance D after emission of a He PF, along with a curve representing a 2.5% 2.5 cm component. As is evident by visual inspection, the data agree rather well with such a curve. By combining the first three cm distance bins, we observe a MFP of 18.9 cm with 513 interactions, which is 2.3 SD away from the expected value of 21 cm.

In conclusion, our new data on PFs in the charge interval from Li to Fe from 1.88 AGeV ^{56}Fe primaries agree with our previous results. In addition, we have made a systematic examination of the MFP of He PFs as a function of distance after emission and find that these too appear to have anomalons present. However, the inclusive effect in He PFs is weaker and will require further analysis and data for elucidation.

This work was supported by the Director, Office of Energy Research, Division of Nuclear Physics of the Office of High Energy and Nuclear Physics of the U.S. Department of Energy under Contract DE-AC03-76SF00098.

References

[1] E.M. Friedlander, R.W. Gimpel, H.H. Heckman, Y.J. Karant, B. Judek, and E. Ganssauge, Phys. Rev. Lett. 45, 1084 (1980).
[2] E.M. Friedlander, R.W. Gimpel, H.H. Heckman, and Y.J. Karant, Phys. Rev. C27, 1489 (1983).
[3] M.A. Bloomer, H.H. Heckman, and Y.J. Karant, Lawrence Berkeley Laboratory Report LBL-15246 (to be published in Nuclear Instruments and Methods).
[4] H.B. Barber, P.S. Freier, and C.J. Waddington, Phys. Rev. Lett. 48, 856 (1982).
[5] P.L. Jain and G. Das, Phys. Rev. Lett. 48, 305 (1982).
[6] D.E. Greiner, P.J. Lindstrom, H.H. Heckman, B. Cork, and F.S. Bieser, Lawrence Berkeley Laboratory Report LBL-3650.

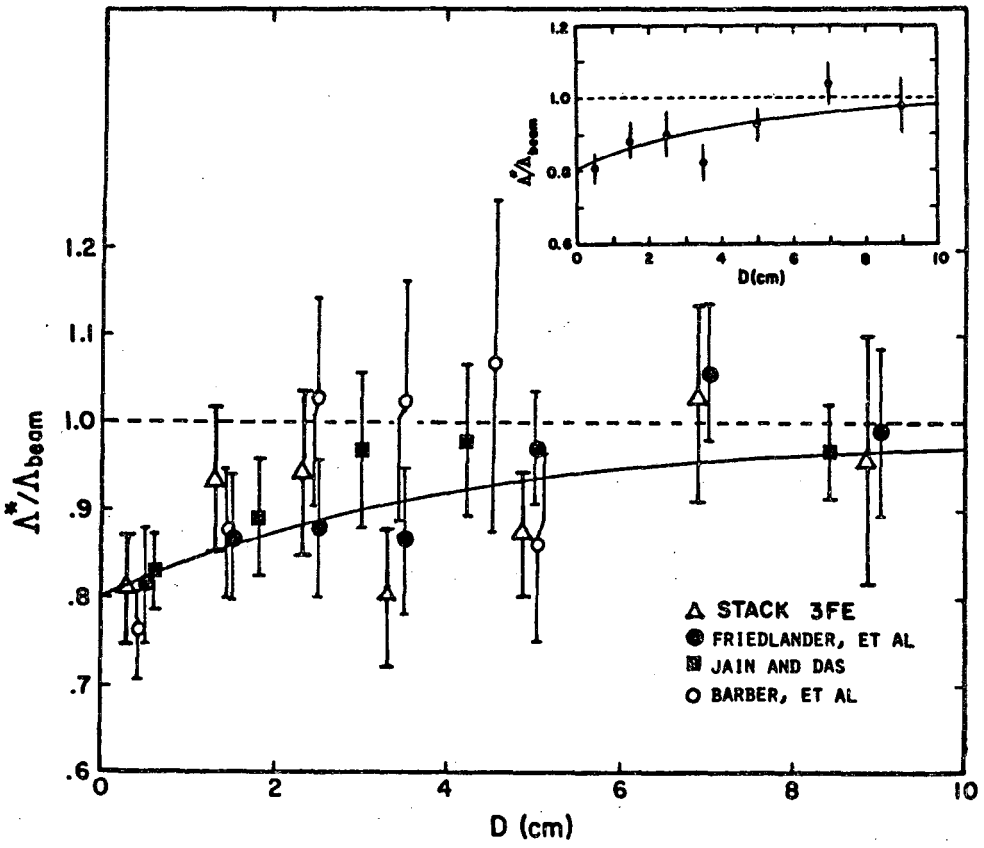

Fig. 1: A comparison of the data of Refs. [1,4,5] with the data of this report. The ratio of Λ^*/Λ is plotted as a function of distance after emission. The straight line at 1 represents the null hypothesis of a normal PF MFP, while the curve represents the hypothesis of 6% anomalons with a fixed MFP of 2.5 cm independent of PF charge. Insert: the points are the result of combining the data of Ref. [1] with the data of this report, while the straight line and curve are the same as in the main figure.

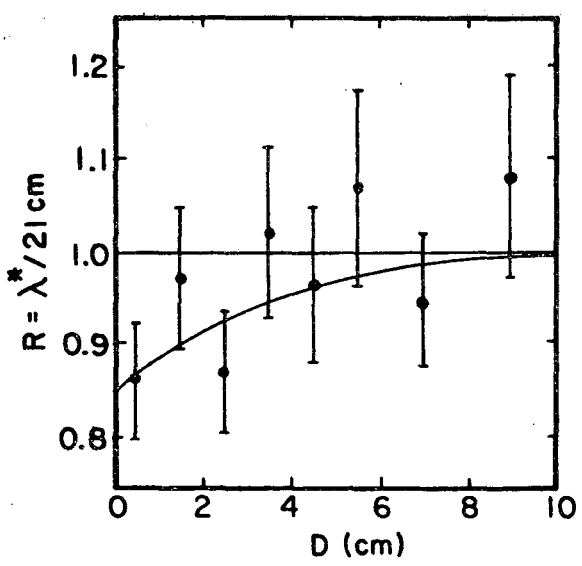

Fig. 2: A plot of the ratio of the observed He PF MFP from this experiment to its expectation value of 21 cm; the ratio is plotted against the distance after emission of the PFs; straight line, the expected dependence under the null hypothesis of normal PFs; curve, the expected dependence under the hypothesis that 2.5% of the He PFs are anomalons with a 2.5 cm MFP.

THE MEAN FREE PATH OF RELATIVISTIC FRAGMENTS FROM HEAVY ION REACTIONS INDUCED BY 1.8A GeV ^{40}Ar IN LOW SENSITIVE NUCLEAR EMULSIONS*

BANARAS[1] - CHANDIGARH[2] - JAIPUR[3] - JAMMU[4] - LUND[5] collaboration

S.B.Beri[2], K.B.Bhalla[3], R.Bhanja[1], A.Bharti[3], V.S.Bhatia[2], G.Claesson[5], S.Garpman[5], S.K.Gupta[4], V.K.Gupta[4], N-Y.Herrström[5], B.Jakobsson[5], R.Joseph[1], G.L.Kaul[4], G.Kaur[2], M.Kaur[2], S.Kumar[4], V.Kumar[4], S.Lokanathan[3], I.Lund[5], L.K.Mangotra[4], I.S.Mittra[2], B.Norén[5], A.Oskarsson[5], I.Otterlund[5], Y.Prakash[4], N.K.Rao[4], S.Sankhyadhar[4], S.Satti[4], M.M.Sherif[5**], K.Söderström[5], S.K.Tuli[1].

Preliminary data is given for the mean free path of projectile-like fragments, $2 \leq Z \leq 18$, emitted in ^{40}Ar induced heavy ion reactions in nuclear emulsions at 1.8A GeV as well as in later generations of fragmentation chains.
Only within a distance of one cm or less from the interaction point do we observe an enhanced collision frequency. If this observation is a signal of an anomalous fragmentation component this must have a very short mean free path or a lifetime less than 10^{-11}s. Some suggestions are given for systematic or statistical effects which could also possibly explain our results.

*Presented at the 2:nd Workshop on Anomalons, Lawrence Berkeley Lab., June 28 - July 1, 1983, by B.Jakobsson, Univ. of Lund, Lund, Sweden.

**On leave from Phys.Dep., Fac. of Science, Cairo Univ., Egypt.

INTRODUCTION

Cosmic ray based-[1] and recent accelerator based heavy ion fragmentation experiments[2-4] have given some indications of an anomalous component which has an extremely large reaction probability and a long enough lifetime to produce collisions separated in space from the primary interaction. Speculations about the origin of this component range from quark-gluon effects[5-6] via normal nuclear physics effects[7-8] to quasi-molecular effects[9].

In this paper we give a status report from a proceeding nuclear emulsion experiment where particular attention is paid to;

i) The charge identification of the fragments from all generations of collisions.

ii) Estimations of statistical fluctuations by means of Monte-Carlo simulations of the experiment.

iii) A test of possible sources of background which may simulate the observed "anomalous" effect.

EXPERIMENTAL DETAILS

Three stacks, containing 1.1 litre of Ilford G5 emulsions have been exposed horisontally to the 1.8A GeV ^{40}Ar beam of the Bevalac with a flux of $2 \cdot 10^3$ ions/cm^2. The sensitivity of the emulsions is low (7 grains per 100μm for minimum-ionizing particles) which means that only projectile fragments with a charge $Z \geq 2$ can be observed normally. This has the advantage of giving a relatively clean registration of the projectile-like fragments close to the interaction point. Almost 5300 primary ^{40}Ar tracks have so far been followed (along-the-track) under 250^x magnifi-

1) B.Judek, Can.J.Phys. 46 (1968)343, 50 (1974)2082 and references therein.

2) E.M.Friedlander et al., Phys.Rev.Lett. 45 (1980)1084

3) P.L.Jain and G.Das, Phys.Rev.Lett. 48 (1982)305.

cation and the mean free path is found to be 9.21±0.16 cm. This value is surprisingly close to the expected mean free path (9.08 cm) determined from the overlap reaction cross-section expression,

$$\sigma_R = \pi r_o^2 (A_1^{1/3} + A_2^{1/3} - b)^2 , \qquad (1)$$

fitted to all available data (r_o = 1.5 fm , b = 1.3 fm) as we know it. This indicates that we lose only a few interactions in spite of the low sensitivity. Normal scanning efficiency tests by double-scanning agree well with this statement since the efficiency was found to be ≥ 95%.

The mean free paths of ^{40}Ar reported from the five different laboratories which contributed to the data collection have only normal statistical fluctuations as shown in table 1. The natural guess that those collisions which are lost in the scanning, have a small charge difference between primary and secondary fragment is confirmed in the next section.

About 700m of ^{40}Ar and $2 \leq Z \leq 18$ fragment tracks has been followed so far, resulting in the number of collisions in the different generations given in table 2. Up to five generations of fragments have been observed and in one single case a fifth generation fragment collided within the stack. The notations which are used subsequently in this paper for various fragments and collisions are given in table 2.

CHARGE DETERMINATION

The preliminary classification of the fragments into the charge groups α (Z=2), L ($3 \leq Z \leq 5$), M ($6 \leq Z \leq 9$) and H ($Z \geq 10$), based mainly on the scanners visual inspection of the track, is followed

---

4) W.Heinrich et al., Univ. of Siegen Preprint SI-82-15 (1982).
5) Y.Karant, Lawrence Berkeley Lab. Preprint LBL-9179 (1979).
6) S.Fredriksson and M.Jandel, Phys.Rev.Lett. 48 (1982)14.

up by accurate charge measurements. Two methods were followed independently. One group (Lund) measured the gap densities of light fragments ($Z \leq 4$) and the track width from light absorption with a photometer for higher charges. The charge spectrum based on fragments from 1350 primary nuclei (only F_1) is given in fig.1. Here the proper gap density-charge and width-charge relations, based mainly on calibration tracks of He,Li,C(calibration exposure) and Ar, have been introduced. The charge resolution (σ_z) is 0.2 units for light fragments, 0.3 units for ^{12}C and 0.5 units for ^{40}Ar (see fig.1). Because of this resolution and the low statistics of medium- and heavy fragments we can of course not expect to see separated charge peaks for $Z \geq 7$.

The other experimental groups measured the gap density and gap-length distribution with eyepiece micrometers for each fragment track. The correlation between the gap density and the (inverse) mean gap length (the gap length coefficient) gives the charge determination within 0.5, 1.0 and 1.5 units for the L, M and H groups respectively. The mutual normalization between the different pellicles and the different scanners was checked continously by measurements on tracks with known charges (i.e. Z = 2,3,6 and 18).

The two methods give charge distributions in good qualitative agreement. Therefore the charge distribution of the entire sample of F_1 fragments is shown in fig.2 (histogram) compared to a distribution which is obtained from existing spectrometer data[10-11] and the assumption of factorization of fragmentation cross-sections[10]. This comparison indicates that we are underestimating the number of fragments with $Z \geq 13$. Because of the poor information on the He-production cross-sections one may leave out this dominating contribution and renormalize the distributions in the interval $3 \leq Z \leq 18$ in order to make a reaso-

---

7) J.Boguta, Lawrence Berkeley Lab. Preprint LBL-13885 (1982).

8) W.C.Harris and J.O.Rasmussen, Lawrence Berkeley Lab. Preprint LBL-14075 (1982).

nable efficiency estimation. When doing so, we find that only about 20% of the events producing a fragment with $Z \geq 13$ is left out. This corresponds well to a total scanning loss of ~5% as observed in the efficiency tests.

EXPERIMENTAL RESULTS

It has been suggested[2)] that the charge dependence of the mean free path can be represented by the formula,

$$\lambda_Z = \lambda_o Z^{-\beta} \qquad (2)$$

The overlap formula (1) together with information about isotope production cross-sections[10)] (or a parabolic mass distribution centered around the most stable isotope) leads to λ_Z values giving the best fit to (2) for λ_o=26.0cm and β = 0.38. Since we have not yet completed our charge determination we use the α, L, M, H classification and assume from the preliminary charge distribution (fig.2) that the average charge within each group ($\bar{Z}$) is 2, 3.65, 7.41 and 14.45 respectively. The experimental mean free path within each group ($\lambda_i = L_i/N_i$ where L_i is the followed track length and N_i the number of collisions) is now multiplied by $\bar{Z}^\beta$ and a weighted Z-independent mean free path,

$$\lambda_o^* = \Sigma L_i \bar{Z}^\beta / \Sigma N_i \qquad (3)$$

can be obtained. The α-group should contain a negligible amount of $Z \neq 2$ fragments and we have therefore first separated the fragment sample into this group and the $3 \leq Z \leq 18$ group. All generations are included since we did not observe any significant differences between them with respect to λ_o^*.

---

9) B.F.Bayman, J.S.Ellis and Y.C.Tang, Phys.Rev.Lett. 49 (1982) 532

10) P.J.Lindstrom et al., Lawrence Berkeley Lab. Preprint LBL-3650 (1975).

In fig.3 where λ_o^* is presented as a function of the distance from the interaction point we observe that neither the α distribution nor the $3 \leq Z \leq 18$ distribution is significantly different from a hypothesis of a normal constant λ_o^*. Possibly there is in both cases a deviation in the first cm. When the two distributions are combined (fig.4) the fluctuations become small enough to draw significant conclusions. We see now, that the point representing the first cm is about three s.d. below the normal λ_o^*, while the other points are statistically distributed around this value. It should be noticed that λ_o was not obtained from our data which (excluding the first cm) give a slightly higher value (λ_o=26.7 cm).

A separation into smaller d-bins (fig.4) shows that it is mainly in the first few mm from the interaction point where a substantially enhanced reaction probability is observed.

From the detailed information about the generation number, the charge of the fragments, the number of "target associated" particles (N_h) etc., we have observed the following tendencies;

i) The tendency of a short mean free path in the first cm is more clearly observable for light fragments (i.e. α and L) than for heavy.

ii) No differences are observed between the primary fragments and those coming from later generations of collisions (no memory).

iii) A tendency towards a more clear short mean free path effect after N_h=0 - than after $N_h \geq 1$ events is observed. The main contribution to the N_h=0 sample comes from reactions induced in the H-target component (can also contain decays).

The generation distribution is given in table 2. From this we can obtain the probability that N collisions in a chain from an F_1 fragment will appear (P(N)). For P(3), P(4) and P(5) we

---

11) G.D.Westfall et al., Phys.Rev. C19 (1979)1309.

get $(1.6\pm0.2)\cdot10^{-2}$, $(2.0\pm0.7)\cdot10^{-3}$ and $(2.4\pm2.4)\cdot10^{-4}$ respectively. A complete simulation of the experiment (in progress) is in our opinion the only way to make a good comparison to the null hypothesis (normal fragmentation). However we can meanwhile compare the experimental distribution to those obtained from a) an assumption of independent reaction probabilities (except for an increasing λ with increasing generation number) along the track and b) a Poisson distribution with the average N ($\bar{N}$) taken from the experimental P(N) distribution (for justification see ref.[12]). Hypothesis a) gives,

$$P(N) = f_P \prod_1^N (1-e^{-x_i/\lambda_i}) \quad . \qquad (4)$$

The frequency of potential F_5 collision candidates at the end of the stack (f_P;decreases due to escaping fragments and collisions without a $Z\geq2$ fragment and increases due to multi-fragmentation) was found to be 0.5 in preliminary Monte Carlo simulations. x_i can be taken as the potential path length (15cm) divided by N and λ_i as λ_H, λ_M, λ_L, and λ_α for i= 1, 2, 3 and ≥4 respectively. Hypothesis b) gives,

$$P(N) = (\bar{N}^N/N!)e^{-\bar{N}} \quad , \qquad (5)$$

where $\bar{N}$ is 0.46136. The values for P(3), P(4) and P(5) obtained from these assumptions are (hypothesis b) within brackets); $1.9\cdot10^{-2}$ $(1.0\cdot10^{-2})$, $1.6\cdot10^{-3}$ $(1.2\cdot10^{-3})$ and $9.9\cdot10^{-5}$ $(1.1\cdot10^{-4})$ respectively. Since none of the experimental frequencies for 3, 4 or 5 collisions is significantly above the estimated null hypothesis, we can not claim to see any anomalous fragmentation component with memory from the generation distribution. More elaborated tests are discussed in [12].

---

12) E.M.Friedlander et al., Phys.Rev. C27 (1983)1489.

INTERPRETATION OF THE RESULTS

If we take the viewpoint that the short mean free path we observe in the first few mm after an interaction is a signal of an anomalous fragmentation component, then we can make the following statements;

i) A pure stable anomalon contribution is of the order of 1% and its characteristic mean free path is about 0.5cm. These values are obtained from a least squares fit of the inverse observed mean free path, $1/\lambda(x) = (1/N_c(x))\Delta N_c(x)/\Delta x$, ($N_c$ is the number of collisions) to the function,

$$1/\lambda(x) = \frac{(f_N/\lambda_N)e^{-x/\lambda_N} + ([1-f_N]/\lambda_A)e^{-x/\lambda_A}}{f_N e^{-x/\lambda_N} + (1-f_N)e^{-x/\lambda_A}} \qquad (6)$$

where f_N is the frequency of normal fragments and $\lambda_{N(A)}$ is the mean free path of the normal(anomalous) component. The contribution we find is smaller and the mean free path shorter than previous reported values[2-4].

ii) A pure decaying anomalous component must have a decay length ($D = \beta c\gamma\tau$) shorter than 1cm and thus a lifetime $\tau<10^{-11}$s. The unstable component may of course also have an enhanced reaction probability but this situation will hardly increase the upper limit of the lifetime.

Since we have found an enhanced reaction probability only within a short distance from the collision point it is very important to study whether statistical fluctuations or systematic ambiguities in the detection technique can introduce a simulation of this effect. The Monte Carlo simulation procedure, which we develop, includes an initial generation of the Ar entrance coordinates (from the beam profile) and the depth (from the differential reaction probability distribution) as well as the kind

of target nucleus for an eventual first collision. Once a collision is appearing we generate the charge(s) of the produced fragment(s) (from topological cross-section weights) as well as its(their) angular distribution (Fermi gas breakup). Generation for generation these fragments are followed until they leave the stack or produce a collision without any $Z \geq 2$ fragment.

In fig.5 we present a preliminary normal fragmentation simulation of the first cm λ_o^* distribution in 66 events with 3500 primaries in each. This distribution should be asymmetric but for simplicity we have here fitted a Gaussian (not normal) distribution. The experimental points of fig.4(lower) are indicated. A normal distribution of random errors (σ=1.24cm) places the 0-1cm point 2.7σ (0.7%) from the average λ_o^*. In view of the fact that several other experiments[2-4] have reported a short mean free path in this interval we find it unlikely that this point is created by statistical fluctuations alone.

Let us now turn to the possible systematic ambiguities.

In fact most of the possible systematic errors have been discussed and ruled out as explanations for the anomalous effect in ref.[12]. The discussion about possible errors in measurements of distances, inhomogeneities in the emulsion, spread in the fragment energy and variable scanning efficiency is valid also for our experiment.

Because of the short distance of enhanced reaction frequency in our experiment, both systematic and statistical errors in the final charge determination should be carefully considered. However, as long as the visual inspection of a few hundreds of μm is the base for our α, L, M, H classification, there should be no differences in the systematic errors between the first cm and the rest of the track. Naturally, a decrease of $\bar{Z}$ with increasing distance from the interaction point is to be expected.

Very few He-nuclei are misidentified and for the other groups the estimated maximum systematic error is 0.5 charge units which for the L group means that λ_o^* has an error of < 5%. This is too small an effect to account for the point of short mean free path. The strongest candidate for a simulating systematic error is in our opinion the possible background of n, p, d, t and π induced reactions within a cylinder around the fragment track where confusion is possible. We have tried to estimate the possible number of confusing interactions within a cylinder of 1μm radius, under the assumption that all nucleons which are not bound in $Z \geq 2$ fragments come out as free protons and neutrons with an angular distribution of,

$$dN/d\cos\theta = C_o + C_1 p_{beam}^2 \cos\theta \cdot e^{-p_{beam}^2(1-\cos^2\theta)/2\sigma^2} \quad .(7)$$

p_{beam} is here the momentum per nucleon of the projectile. The distribution is a consequence of a Fermi-gas breakup + an isotropic (direct) scattering process. The constants C_o, C_1 and σ are taken (after renormalization) from ref.[13]. The $Z \geq 2$ fragments are in a first approximation all given an emission angle of $\theta = 0^o$ - all except the He-nuclei which have a correction due to their rather wide angular distribution. A correct angular distribution of the heavy fragments, inclusion of nucleons bound in d and t fragments and track divergence due to multiple Coulomb scattering are all effects which may decrease the frequency of confusing collisions substantially. However, the radius of the cylinder may well be 2μm and that would compensate the decrease.

Because of all uncertainties, the graph shown in fig.6, which presents the number of confusing interactions per true fragment interaction as a function of the distance from the collision point, has an error of ~50%. Anyhow, it is obvious that if only

---

13) G.M.Chernov et al., to be published in Nucl.Phys A.

the first 2.5mm after a collision gives a significant lower λ_o^* (see fig.4) then the introduced false anomalous behaviour due to the disturbing background cannot be ruled out (without further investigations) as a source of this effect.

CONCLUDING REMARKS

From our present data we cannot decide if the observed anomalous component (frequency 1%, mean free path 0.5cm) is a reality which must be given a physical interpretation or if it is introduced due to a confusing background of interactions (possibly combined with other effects of systematic and/or statistical nature). Increased statistics of collisions within the first two cm from the interaction point, careful vertex measurements and complete charge determinations are ingredients in the final state of our experiment. We hope thereby to be able to make a final conclusion about the observed short mean free path very soon.

One of us (B.J.), who presented the status report, wishes to thank V.Kopljar and S.Persson for valuable contributions to the presentation and to the experimental work.

TABLES

LABORATORY	λ_{Ar} (cm)
Banaras	9.67±0.38
Chandigarh	8.95±0.45
Jaipur	8.76±0.38
Jammu	9.01±0.37
Lund	9.34±0.26
Totally	9.21±0.16

Table 1. The primary ^{40}Ar mean free path in emulsion reported from the different laboratories.

KIND OF PARTICLE OR COLLISION	NOTATION	NUMBER OF EVENTS total	α(2)	L(3-5)	M(6-9)	H(≥10)
Primary	P	5293				
Primary collision	P_*	3494				
1:st gen.fragment	F_1	5603+	3442+	539	551	1071
1:st gen.coll.	F_{1*}	2141+				
2:nd gen.fragment	F_2	1395	851	191	194	159
2:nd gen.coll.	F_{2*}	371				
3:rd gen.fragment	F_3	229	159	28	25	17
3:rd gen.coll.	F_{3*}	64				
4:th gen.fragment	F_4	30	22	3	2	3
4:th gen.coll.	F_{4*}	8				
5:th gen.fragment	F_5	4	3	1	0	0
5:th gen.coll.	F_{5*}	1				

Table 2. The total number of fragments and colliding fragments(*) in all generations of the followed Ar projectiles. It should be noticed that two stacks with different length (15 and 20 cm) have been scanned. +means that the number has been corrected for some F_1-He nuclei which were left out in a part (25%) of the scanning.

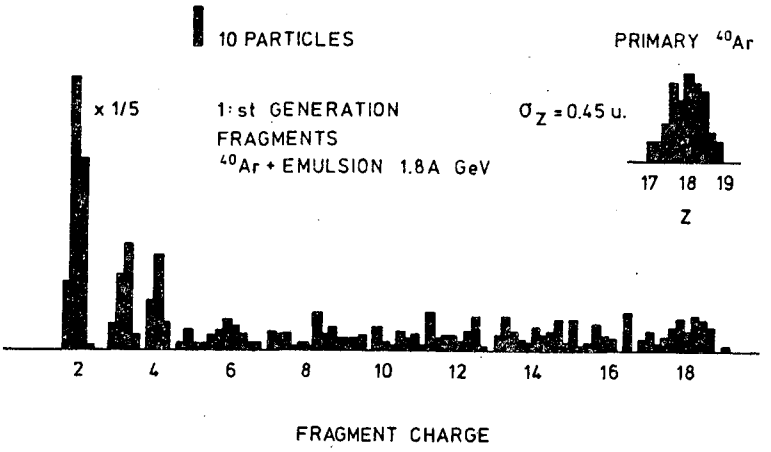

Fig.1. The charge spectrum from gap **density**($Z \leq 4$) and photometric($Z \geq 5$) measurements on F_1 fragments.

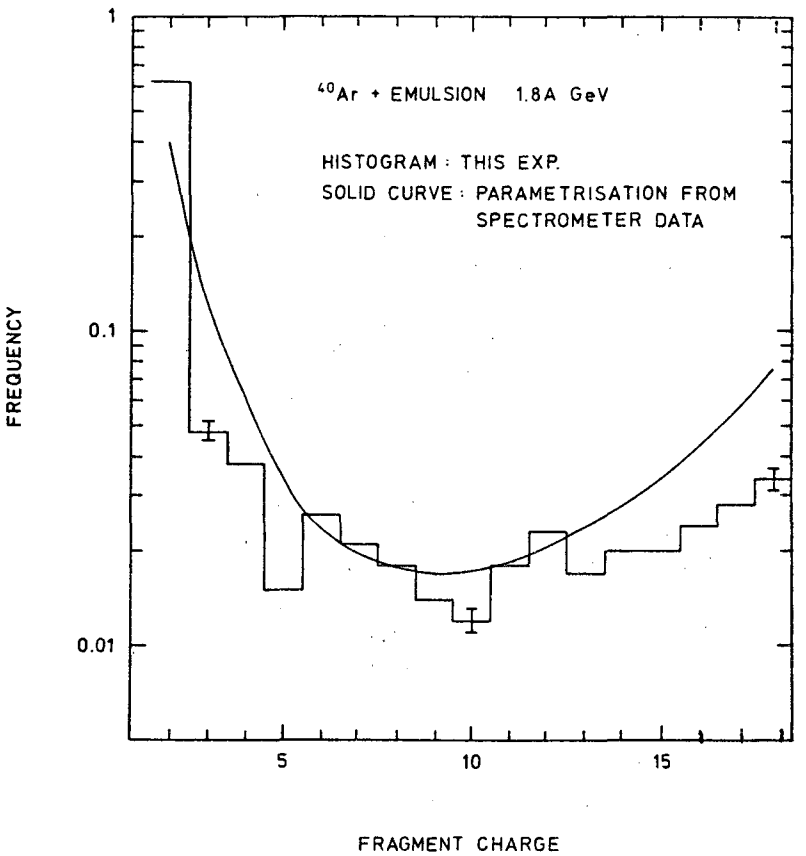

Fig.2. The charge distribution of all F_1 fragments in ^{40}Ar+emulsion collisions at 1.8A GeV. The solid curve is obtained from data in ref[10-11].

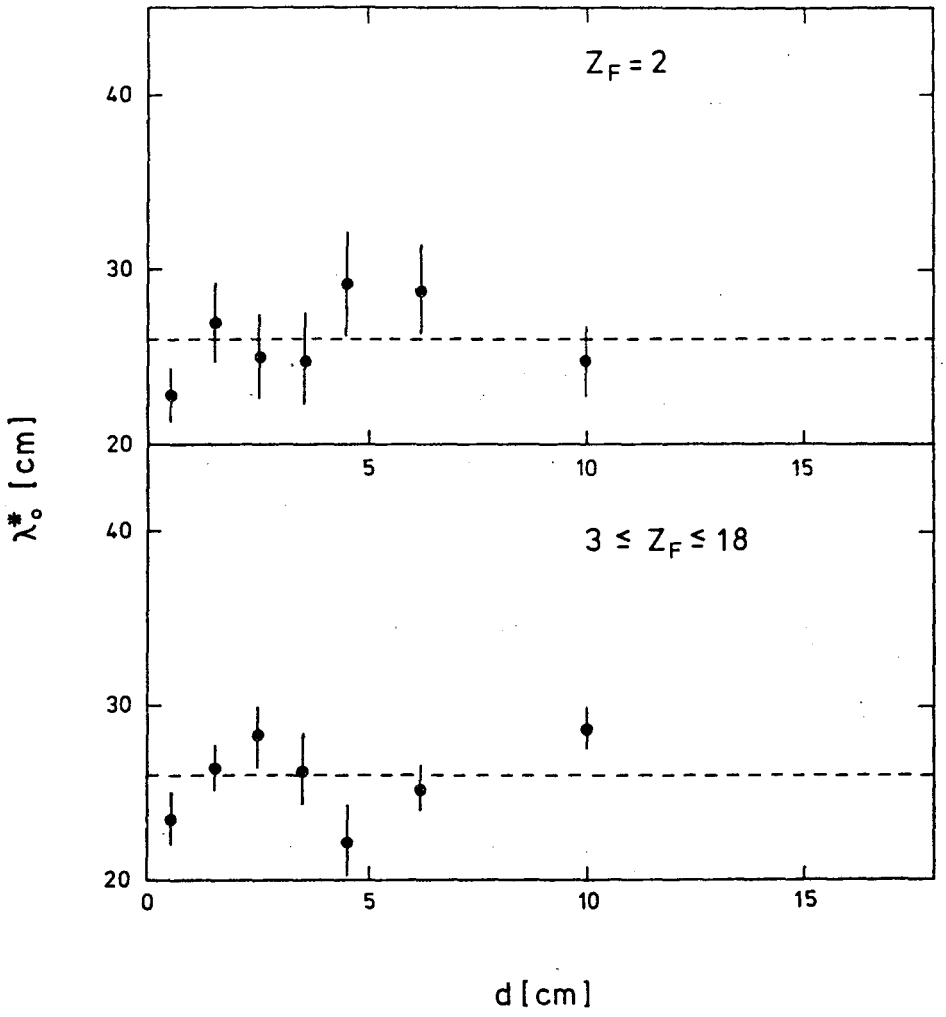

Fig.3. The charge independent mean free path (λ_o^*) as a function of the distance from the interaction point. Upper figure: He fragments from generations 1-5. Lower figure: $3 \leq Z \leq 18$ fragments from generations 1-5. The dashed line represents λ_o (see (2))

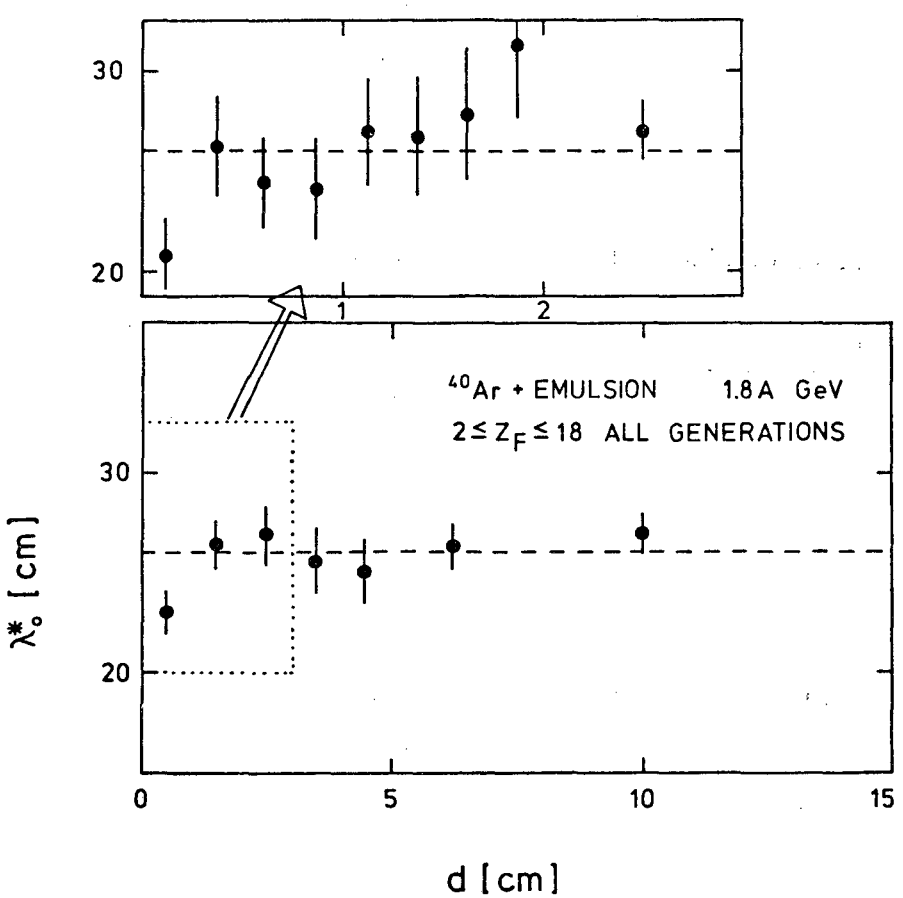

Fig.4. The charge independent mean free path (λ_o^*) as a function of the distance from the interaction point. All fragments with $2 \leq Z \leq 18$ from generation 1-5 are included. The upper figure gives the $0 \leq d \leq 2$cm interval in 2.5mm bins.

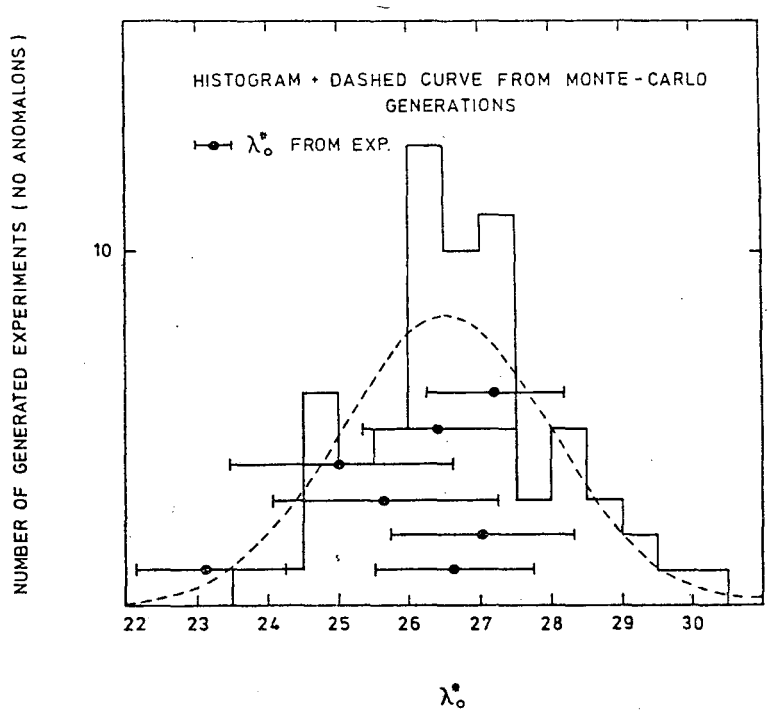

Fig.5. The λ_o^* value in the first cm from the interaction point obtained in 66 Monte Carlo generations of our experiment (normal fragmentation). The points represent the measured λ_o^* values from fig.4. The curve is a Gaussian fit.

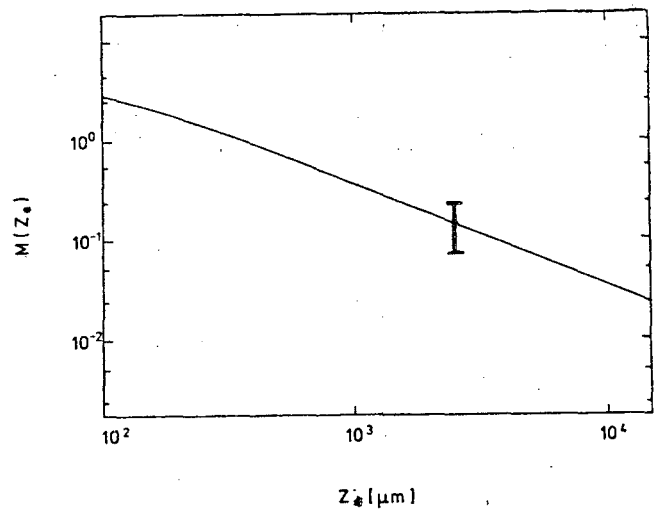

Fig.6. The number of confusing p- and n induced collisions per Z≥2 fragment collision ($M(z_*)$) as a function of the distance from the interaction point (z_*). The error bar is placed at a distance of 2.5mm from the int. point. For details see text.

Anomalous Mean Free Path For Z=2 Relativistic Projectile Fragments In Emulsion

M. EL-NADI, O.E. BADAWY, M.N. EL-BAKRY, A.ABDEL-SALAM, A.A. EL-HAMALAWY, E.I. KAALIL, A.M. MOUSA and M. EL-NAGDY.

Physics Department, Faculty of Science, Cairo University.

The anomalous short mean free path (m.f.p.) of projectile fragments (p.f.) at small distances from emission vertix has been detected for fragments of $Z \geq 3$ from different projectiles at energies up to ≈ 2.0 AGeV. (ref. 1 and references therein). For Z=2 fragments no clear cut conclusion is present (ref. 2,3).

Here we report on some measurements of m.f.p. of Z=2 ^{12}C p.f. at 4.5 GeV/C/N (the highest available momentum now). Two NIKFI-BR-2 nuclear emulsion stacks (10cm X 20cm X 600μm pellicles dmensions), were tangentially irradiated with 4.5 GeV/C/N ^{12}C- ions and α- particles at the Synchrophasatron of the JINR, Dubna, USSR. 636, Z=2 p.f.s. emitted in a 3° cone were collected by along the track scanning for the primary ^{12}C interactions. These p.f. were classified according to the number N_h(N_h = number of heavily ionizing particles tracks) of the primary ^{12}C interaction events. Each p.f. was followed untill it interacted or left the stack. The maximum path length detected for these p.f. amounts to $\approx$150mm. About 280 secondary interactions were collected.

Fig. (1) shows the exponential absorption curve of Z=2 p.f. as a function of the distance D from the primary vertix. This fig. shows the presence of a component of an anomalously short m.f.p. λa=2.5.cm and another one of an anomalously long m.f.p. of value $>$ 20cm for the Z=2 p.f.s. produced in N_h=0(A) and N_h=1-5 (B) ^{12}C primary interactions. Fig. (2) shows the m.f.p. of the Z=2 p.f.s. at distances $D<2.5$cm. and $D>2.5$cm. from the primary vertix as well as its average value in different groups of N_h of the ^{12}C interactions. The observations seen in fig. (1) are also clear here. Table (1) summarizes all these results. In fig. (3) we present the distribution of the m.f.p. of the Z=2 p.f. at distances D from the primary vertix for all N_h, N_h= 0 , and all N_h except N_h=1-5 groups of ^{12}C primary interactions. (A, B, and C curves respectively). The contineous curves are calculated according to the interaction model (ref. 1). These contineous curves in fig.(3) correspond to a value of the λa=2.5cm. and a fraction α of the anomalon compoment = 6%, 17% and 13% in the groups of N_h

mentioned above respectively. The straight lines shown in fig. (3) indicate the value of the average mean path of the 4.5 GeV/C/N α- particle beam λ(normal) = λ(beam) = 19.9±0.6 cm. determined from 1307 -inelastic interactions collected by along the track scanning of the stack irradiated by α - beam.

From our results we can conclude that:

1. The presence of an anomalon component with short m.f.p. λ_a=2.5cm. associated with the Z=2 ^{12}C fragments at 4.5 GeV/C/N is enhanced to a fraction of α = 17.4% for N_h = 0 interactions of ^{12}C. The average m.f.p. of Z=2 p.f. here is λ = 12.7±1.3cm. which is $\simeq$ 4 S.D. lower than normal.

2. A new component having an anomalously low cross-section or a m.f.p. much higher than normal λ(normal), is detected in case of N_h= 1-5 events of ^{12}C interactions at distances D$\lesssim$2.5cm. from the primary vertix. The average m.f.p. of the Z=2 p.f. in this regions λ =29.5±6.4cm. which is $\simeq$ 2 S.D. higher than normal.

3. It was also observed that the probability for production of N_h=0 events (white starts) in interactions of Z=2 fragments produced in ^{12}C N_h=0 interactions is about three times higher than that for fragments produced in ^{12}C $N_h \neq 0$ interactions. The difference between these probabilities is about -3.0 S.D. with a probability =1.1 X 10^{-3}. According to the 2 x 2 Fisher test we get -3.42 S.D. with 3.10 x 10^{-4} probability, a matter which cannot be normal.

The authors are grateful to Prof. K.D.Tolstov of the JINR, Dubna, USSR for supplying the irradiated emulsions.

Thanks also to Z.M. Abo-Gabal, Z. Abo-Mosa, and Z.A. Motawei for helping in scanning of primary interactions.

References:

1. E. M.Friedlander, R.W. Gimpel, H.H. Heckman, Y.J. Karant, B. Judek, and E. Ganssauge, Lawrence Berkeley Laboratory Report No. LBL - 10573, 1982.

2. P.L. Jain, M.M. Aggrawal, G. Das and K.B. Bhalla, Phys. Rev. C25, 3216 (1982).

3. E. Ganssauge et al., GSI-82-ISSN 0714-081.

Table 1. **Detailed experimental information used for the comparison of estimated mean free path at D≤2.5cm. and D>2.5cm from the origin of the projectile fragment for different values of N_h(interaction size of ^{12}C with emulsion)**

	$D \leq 2.5$ cm.			$D > 2.5$ cm.			Average Value		
N_h	Tracks	Stars	λ cm.	Tracks	Stars	λ cm.	Tracks	Stars	λ cm.
0	203	36	12.5±2.1	167	60	12.8±1.7	203	96	12.7±1.3
1-5	262	21	29.5±6.4	241	82	18.3±2.2	262	103	20.6±2.0
≥6	171	27	14.4±2.8	144	54	15.6±2.1	171	81	15.2±1.0
All	636	84	17.3±1.9	552	196	15.9±1.1	636	280	16.3±1.0

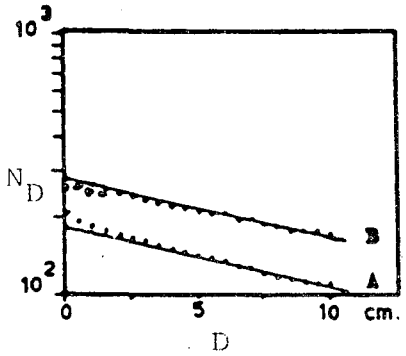

Fig.(1): Dependence of the number of noninteracting carbon projectile fragments on the distance D from the primary vertex.

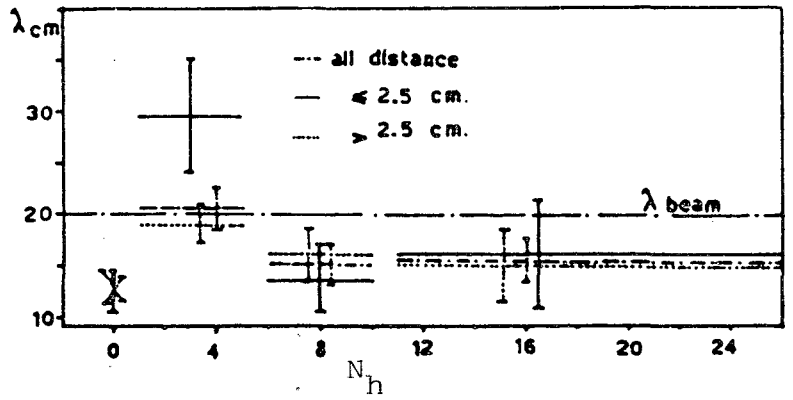

Fig.(2): Distributions of the observed mean free path of Z=2 fragments emitted from 4.5 GeV/C/N ^{12}C interacting in emulsion for different values of the range of N_h considered (horizontal bars). Vertical lines represent the expected error in λ.

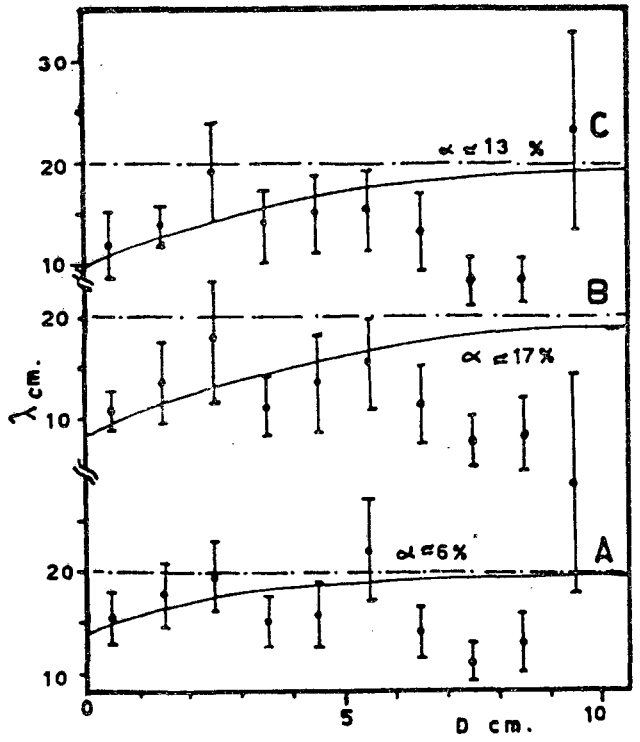

Fig.(3): Values of the mean free path of Z=2 fragments from 4.5 GeV/C/N ^{12}C (of different interactions size i.e. ranges of N_h defined in the text) at different distances D from the origin of projectile fragments.

Are there Anomalons at Charge Two? A Comparison of Helium Induced Primary and Secondary Interactions in Nuclear Research Emulsion at about 2 GeV/Nucleon.

N.Klein, E.Ganßauge, M.Bàagil, U.Bieschke, F.Killinger, R.Kretschmer, A.Laschek, and W.Weidner
Philipps-University Marburg, West-Germany

Abstract:

A Comparison of secondary α stars induced in emulsion by ^{56}Fe-primary beams at Bevalac energies of around 2 GeV/nucleon with primary stars of ^{3}He and ^{4}He of the same energy shows a clear difference in the asymmetry distribution of the target fragments as well as in the multiplicity distribution. Besides this a cut in the data set of the secondaries at the distance D = 3 cm downstream from the emission point exhibits a special behaviour of the α -stars which are produced near to the primary star ($D \leq 3$ cm) A connection with the anomalon effect seems to be obvious.

At projectiles of charge $Z \geq 3$ three independent experiments[1-3] have shown evidence for anomalons. Only one group[4] reported about research on Z=2 particles, and the effect was not found. At Marburg we compared three different Z=2 particles:

1) A stack of Ilford G 5 nuclear research emulsion pellicles, 600 μm thick, was exposed to a relativistic heavy-ion beam parallel to the emulsion surface at the Berkeley Bevalac (1.88 A GeV ^{56}Fe). The pellicle size was 7.5 x 25 cm^2.
2) A stack of smaller size, 7 x 12.5 cm^2, was exposed like 1)
3) Another stack was irradiated at Berkeley with ^{3}He at the same energy, the size being 6 x 7.5 cm^2, and
4) A fourth stack was exposed to ^{4}He at a slightly higher energy (2.1 A GeV) with size 10x20 cm^2.

Out of these four stacks we have three categories of beam particles to be compared: ^{3}He, ^{4}He primaries and secondary α's produced by ^{56}Fe. The difference in the beam energy is so small that we can neglect it. From counter measurements we know that in nature the mixture of ^{3}He and ^{4}He is about 1:3. Therefore we took this ratio into account handling the two primary He-beams. If we speak about He, we mean the proportion 1:3 of ^{3}He and ^{4}He respectively.
The tracks of the primary beams were followed along the first 6 cm while the beam looses up to 350 MeV/nucleon. This means, the energy of the secondary α's are spread over an energy range of 1.9 to about 1.5 GeV/nucleon. Because of the low charge the energy loss of the relativistic α's can be neglected, and there is no difference between the mean energy of α tracks which originate a star "near" to the emission point ($\alpha_{\leq}$; $D \leq 3$ cm) and the mean energy of such α tracks which go further through the stack ($\alpha_{>}$; $D > 3$ cm).

Unlike the methods used in the experiments mentioned above[1-3], we did not measure the mean-free pathes of the projectile fragments but analysed the target fragmentation. For each star the asymmetry A, defined by $A \equiv (F-B)/(F+B)$ was calculated and the distribution of A for the different groups was compared. F,B are the numbers of heavy tracks in the forward and backward cone respectively. Moreover the number N_h of heavy tracks was counted their scattering angle ϑ versus the primary direction was measured, and also the projectile fragmentation frame was completely analysed. To make sure that no single track would be missed, by means of a special device the projection of each star into the x-y plane of the view field of the microscope was drawn on paper, and the hight (z-coordinate) was measured with a precision of $\pm$ 1 μm and noted on each track. From these data we can reconstruct the full geometry of the individual star.

Normally it is obvious which track corresponds to an α-particle, because the structure of the α-tracks is very typical in emulsion. Nevertheless there is a danger of mixing the α-tracks with tracks of slow protons from the target fragmentation.

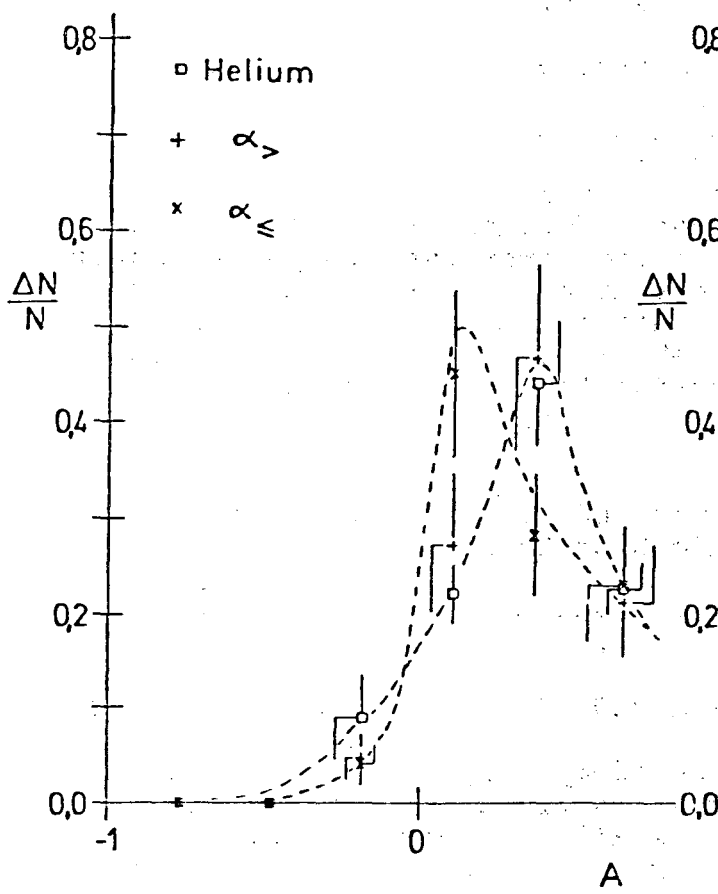

Fig.1: Normalized distribution of anisotropy A=(F-B)/(F+B). See text

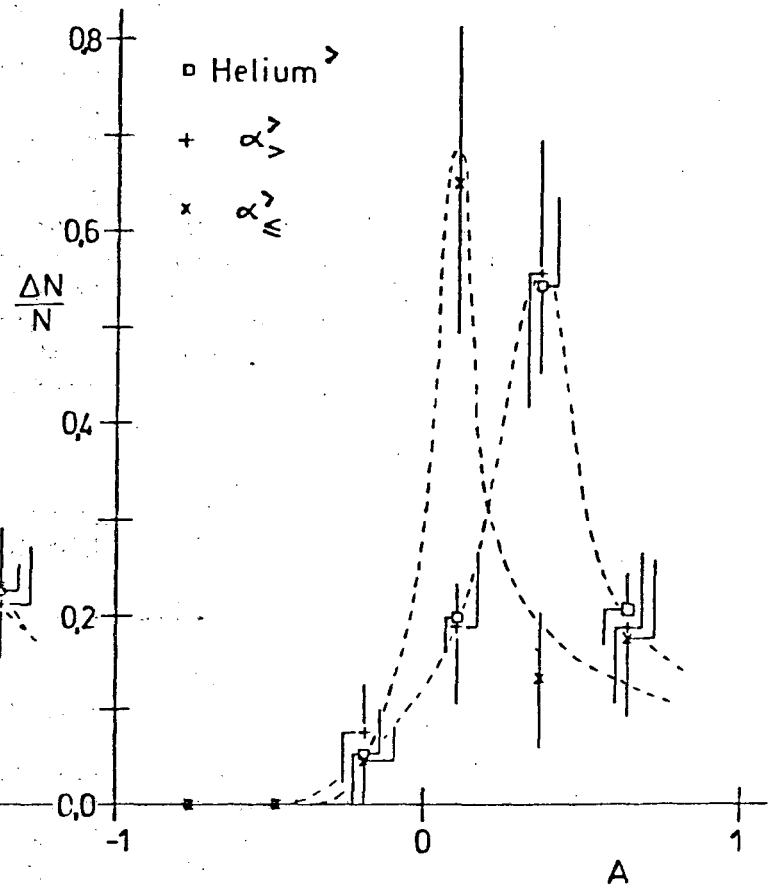

Fig.2: Like Fig.1, but only for "large" stars ($N_h \geq 9$)

But this danger is easy to overcome in the case of $\alpha_>$ because of the slow protons changing their track structure considerably after about 3 cm. In the case of $\alpha_\leq$ on the other hand the probability for a slow proton to produce a star into the 6° forward cone is negligibly small ($< 3 \cdot 10^{-5}$).

A total number of 508 stars was analysed, 144 ^{3}He stars, 211 ^{4}He stars, and 153 α-stars. While the stars belonging to $\alpha_>$ and the He stars look very much the same, the behaviour of the "near" α group, $\alpha_\leq$, is a special one. This group shows a significant shift of the mean asymmetry $\bar{A}$ towards isotropy (A=o) which implies that the α's seem to transfer less momentum to the target nucleus. The angular distributions show the same tendency albeit not so expressively.
With the asymmetry distribution of the "normal" stars, He-stars as reference, a χ^2 - test of the two distributions leads with 2 degrees of freedom to χ^2=15.8. This corresponds to a probability for the deviation being caused by just a statistical fluctuation of less than 1 ‰. Fig.1 shows the normalized anisotropy distribution of the two groups of stars.

If the data is subdivided, corresponding to the complexity of the target, into three groups

1) small stars $N_h = 1$
2) medium stars $2 \leq N_h \leq 8$
3) large stars $N_h \geq 9$

one finds that the above mentioned effect is strongest in the third group (see fig.2), while in the first two groups we cannot find any significant shift. From this one feels tempted to conclude that only the large stars near the emission point are those which show the anomalous behaviour. That this is not the case we see immediately by inspecting table I which shows the probability P of "medium" and "large" stars of both groups and the ratio R=P $(2 \nearrow 8)$/P(≥ 9).

Table I: Probability P of "medium" and "large" stars induced by He and $\alpha_\leq$, and the ratio R of both.

	He	$\alpha_\leq$
medium	0.33 ± 0.04	0.51 ± 0.10
large	0.42 ± 0.04	0.28 ± 0.07
R=med./large	0.80 ± 0.13	1.78 ± 0.40

Table I tells us that in the case of $\alpha_\leq$ being the projectile there are almost twice as many medium stars produced than in the case of "normal" projectiles (He). We shall consider the $\alpha_\leq$ group as being enriched with anomalons as we would expect it to be from earlier work[6]. They originate medium stars as well as large ones. But we find the fraction of "medium" stars to be shifted towards normal asymmetry. Only the "large" ones show the typical behaviour of target explosion, they exhibit a large number of fragments distributed rather isotropically.

May be the anomalons are produced with a high amount of inner energy. In a more central collision this could give rise to an explosion while in a more peripheral collision the anomalon may survive. It would have been interesting to check this idea by following the fate of the α_6 projectiles. Unfortunately we had only 12 events of the so called α, α'-type. But from B. Judek's work[7] one can see that infact the mean-free path of her 55 α, α'-events is extraordinarily short, namely $\lambda^*(\alpha, \alpha') = 12.5 \pm 1.7$ cm.

Work supported by the Bundesminister für Forschung und Technologie, No.06 MR 136 and 158.

References

1) E.M.Friedlander, R.W.Gimpel, H.H.Heckman, Y.J.Karant, B.Judek, and E.Ganßauge
Phys.Rev.Lett.45 (1980),1084 and Phys.Rev.C,27 (1983),1489
2) P.L.Jain and G.Das, Phys.Rev.Lett.48 (1982), 305
3) H.B.Barber, P.S.Freier, and C.J.Waddington
Phys.Rev.Lett.48 (1982), 856
4) P.L.Jain, M.M.Aggarwal, G.Das, and K.B.Bhalla
Phys.Rev.C,25 (1982), 3216
5) C.F.Powell, P.H.Fowler, and D.M.Perkins
"The Study of Elementary Particles by the Photographic Method", Pergamon Press 1959, page 440 ff.
6) E.Ganßauge, N.Klein, M.Bàagil, U.Bieschke, F.Killinger, R.Kretschmer, A.Laschek, and W.Weidner
GSI-Scientific report 1981, p.43
7) B.Judek (1977) NRC-report

Behavior of Secondary Particles of Charge two, three and four produced from Relativistic heavy-ion collisions.

P.L. Jain, M.M. Aggarwal, M.S. El-Nagdy, A.Z.M. Ismail and K.L. Gomber, High Energy Experimental Laboratory, Department of Physics, State University of New York at Buffalo, Buffalo, New York 14260

ABSTRACT

We have used two small stacks of Ilford G-5 emulsion exposed to ^{56}Fe and ^{40}Ar beams at about 2 GeV parallel to the pellicles surfaces. Each pellicle was scanned by along-the-track method. We thus found about 6000 primary interactions from which about 6000 relativistic tracks of Z=2 and about 800 tracks of Z=3 and 4 emitted from the primary interactions within 0.2 rad forward cone were followed until they either interacted or left the stack. We observed about 850 secondary H_e interactions. The H_e fragments are easily identified by their distinct grain intensities (~4g min and for relativistic tracks it should not change within 2cm of its path length followed from its production point) or by their δ-ray density measurements for Z=2,3 and 4. From the production points of Z=2,3 and 4 fragments, the distance T available for its interaction in emulsion (the potential length) or if it interacted, the distance S to the interaction point was recorded. The mfp of interaction is given by $\lambda=(\Sigma_i d_i)/N$ where $\Sigma_i d_i$ and N are the total path length of both interacting and noninteracting tracks and the number of interactions of the i particles within that path length interval, respectively. We shall discuss the mfp of H_e as a function of distances for different production angles and for Li and Be, we shall discuss mfp as a function of distance.

Search for Anomalons Among Singly Charged Relativistic Particles from ^{16}O Interactions at 2 Gev/Nucleon

B. Judek
Division of Physics, National Research Council of Canada

Abstract. Mean free paths of singly charged relativistic secondary particles from ^{16}O interactions in emulsions have been measured. The results based on 1087 observed interactions indicate the presence of an anomalous component with a mean free path of about 5 cm, among the particles emitted in the angular interval corresponding to P tan θ[1] between 200 and 400 MeV/c.

Observations. A sample of 734 primary interactions with various fragmentation topologies, produced by 2.1 AGev ^{16}O ions in a large emulsion stack[2] have been selected. In each event the emission angles (both the horizontal and vertical components) of the relativistic secondary particles have been measured. Tracks of 2385 particles were followed through the emulsions until they interacted or left the stack. They were selected on the basis of their grain densities (<1.5 minimum ionization) and length per plate ($\gtrsim$5 mm). Altogether 1087 secondary stars have been observed. The multiplicities of the singly charged relativistic particles (n_s) and of the nonrelativistic target fragments (n_h) have been examined in both the primary and secondary interactions.

Results. The secondary particles should mainly consist of projectile fragments including ^1H, ^2H and ^3H nuclei emitted at small angles to the primary direction, and pions spread over much wider angles. The transverse momenta per nucleon of the projectile fragments are approximately equal to P tan θ[1] and therefore this parameter was chosen for the presentation of the angular distributions in Fig. 1. The proportion of pions present has been estimated by evaluating the ratio of the average excess absolute charge carried by the secondary particles Δz_s[3] to the average n_s multiplicity.

The observations on primary stars from which at least one projectile fragment with $Z \gtrsim 2$ was emitted are shown in Fig. 1(a). The shape of this distribution is consistent with the assumption of a mixture of projectile fragments producing a peak at about 60 Mev/c and pions ($\sim$30%), contributing to the wide spread of the distribution. The sample of the more central primary collisions from which only singly charged relativistic secondaries

(1) P-primary momentum per nucleon at the interaction, θ-lab. emission angle of the particle.

(2) E.M. Friedlander et al Phys. Rev. Lett. 45, 1084 (1980).

(3) $\Delta Z_s = \Sigma Z(\text{fragments}) + n_s - Z(\text{primary})$.

are emitted gives rise to the distribution in Fig. 1(b). It is very flat and the proportion of pions among the particles is estimated at about 50%.

The particles have been grouped into three distinct P tan Θ intervals and the variations of their mean free paths (mfp) with distance (D) from the primary interactions are presented in Fig. 2. The observations shown in Figs. 2(a) & (c) are consistent with their respective average values over the whole range of distances. On the other hand, for $200 < P \tan \Theta \leq 400$ Mev/c (Fig. 2(b)) the mfp's appear to be shorter at $D \leq 5$ cm than at $D > 5$ cm.

Table I shows the average mfp's (λ), their values for $D \leq 5$ cm (λ_1) and $D > 5$ cm (λ_2), as well as the ratios $F = \lambda_1/\lambda_2$, evaluated for smaller P tan Θ intervals. The mfp's of protons[4], deutrons[5] and pions[6] determined by measurements on primary beams are 35.3 ± 1 cm, 25.6 ± 1.1 cm and about 40 cm respectively. Thus, for example, a beam of particles consisting of 70% protons and 30% deutrons would have an average mfp of 31.7 cm at D = 0 cm and 32.9 cm at D = 10 cm, i.e. its variation with distance would be rather slow. The present measurements for the secondary particles with $P \tan \Theta \leq 200$ Mev/c give an average mfp of 31.1 ± 1.3 cm which is consistent with a mixture of protons and deutrons, while the higher value of 36.3 ± 2.3 cm obtained for $P \tan \Theta > 400$ Mev/c suggests that the particles there are mainly protons and/or pions.

The particles emitted with $200 < P \tan \Theta \leq 400$ Mev/c exhibit an anomalously short mfp of 24.7 ± 2.2 cm for $D \leq 5$ cm and 38.9 ± 3.0 cm for $D > 5$ cm. The corresponding F-ratio is .64 ± .12, i.e. it differs from unity by about 3 standard deviations. Similar calculations have also been carried out using different subdivisions of the data with P tan Θ intervals of 250-350, 200-400, 150-500 Mev/c and values of D of 4, 5 and 6 cm. In all cases the F-ratio's were found to be less than unity by 2 standard deviations or more. These results cannot be adequately explained by the presence of deutrons or some other particles interacting with a moderately short mean free paths ($\geq$ 20 cm). On the other hand they are consistent with the assumption of an anomalous component with a mfp of the order of 5 cm and relative intensity of about 7%.

(4) N. Meyer & M.W. Teucher, Nuovo Cim. 28, 1399 (1963).

(5) A.O. Vaisenberg et al, Sov. J. Phys. 18, 636 (1974).

(6) J.E. Allen et al, Phil. Mag. 6, 833 (1961) and P.J. Finney et al, Phil. Mag. 7, 237 (1961)

Conclusions

(1) Singly charged secondary particles from ^{16}O interactions emitted with $200 < P \tan\Theta \leq 400$ Mev/c exhibit shorter mean free paths at distances $D \leq 5$ cm, than for $D > 5$ cm from the primary interactions. This effect cannot be explained adequately by the presence of particles interacting with moderately short mean free path (≥ 20 cm), including deutrons while it is consistent with the assumption of an anomalous component with a mean free path of order of 5 cm and relative frequency about 7%.

(2) The particles measured in this experiment should mainly consist of projectile fragments including ^1H, ^2H & ^3H nuclei and pions. Using the nuclear emulsions technique it is not possible to identify them individually, nor to measure their momenta with any precision. However, using the available information on the transferse momentum distributions of projectile fragments[7] it is possible to analyse the situation as follows:

(i) The "anomalous effect" is not observed at $P \tan\Theta \leq 200$ Mev/c. The main Gaussian portions of the distributions of the projectile fragments should be contained in this interval.

(ii) The "anomalons" seem to appear among the particles emitted with $200 < P \tan\Theta \leq 400$ Mev/c. This region corresponds to the "tail" portion of the projectile fragments distribution and which is attributed to the hadronic scattering processes[7]. One expects that the proportion of pions among the particles is rather small.

(iii) At $P \tan\Theta > 400$ Mev/c no effect is observed. The measured particles should contain a large proportion of pions as well as the projectile fragments scattered through large angles.

(3) The examination of the n_s and n_h multiplicities of the secondary stars have not revealed any distinct features of the anomalon interactions.

(4) The present results confirm our previous observations on the secondary particles emitted from interaction of relativistic cosmic ray nuclei[8].

(7) E.M. Friedlander & H.H. Heckman, LBL-13864 (1982).

(8) B. Judek, Can. J. Phys. 46, 343 (1968) and 50, 2082 (1972).

TABLE 1

P tan θ Mev/c	No. of Tracks	Mean Free Path (cm) λ	λ_1 (D≤5cm)	λ_2 (D>5cm)	$F = \lambda_1/\lambda_2$
≤50	217	33.9(110)*	39.2 (26)	32.2 (84)	1.22±.22
50-100	357	27.9(205)	32.5 (51)	26.4(154)	1.23±.16
100-150	277	31.0(147)	31.3 (41)	30.8(106)	1.02±.18
150-200	203	34.7 (95)	36.0 (26)	34.1 (69)	1.06±.23
≤ 200	1054	31.1(557)	34.0(144)	30.0(413)	1.13±.10
200-250	171	40.8 (66)	34.4 (23)	44.2 (43)	0.78±.26
250-300	163	29.2 (73)	21.9 (32)	34.8 (41)	0.63±.24
300-350	197	31.7 (87)	22.4 (40)	39.7 (47)	0.56±.22
350-400	149	30.3 (65)	23.2 (29)	36.0 (36)	0.64±.25
200-400	680	32.8(291)	24.7(124)	38.9(167)	0.64±.12
400-500	184	35.7 (70)	35.9 (24)	35.7 (46)	1.01±.25
500-700	178	37.4 (65)	39.6 (21)	36.3 (44)	1.09±.27
700-1000	146	34.1 (61)	28.9 (23)	37.4 (38)	0.77±.26
>1000	143	39.0 (43)	37.2 (18)	40.3 (25)	0.92±.31
> 400	651	36.3(239)	35.2 (86)	37.0(153)	0.95±.13
Total	2385	32.7(1087)	32.0(354)	33.5(733)	0.96±.06

* Number of interactions.

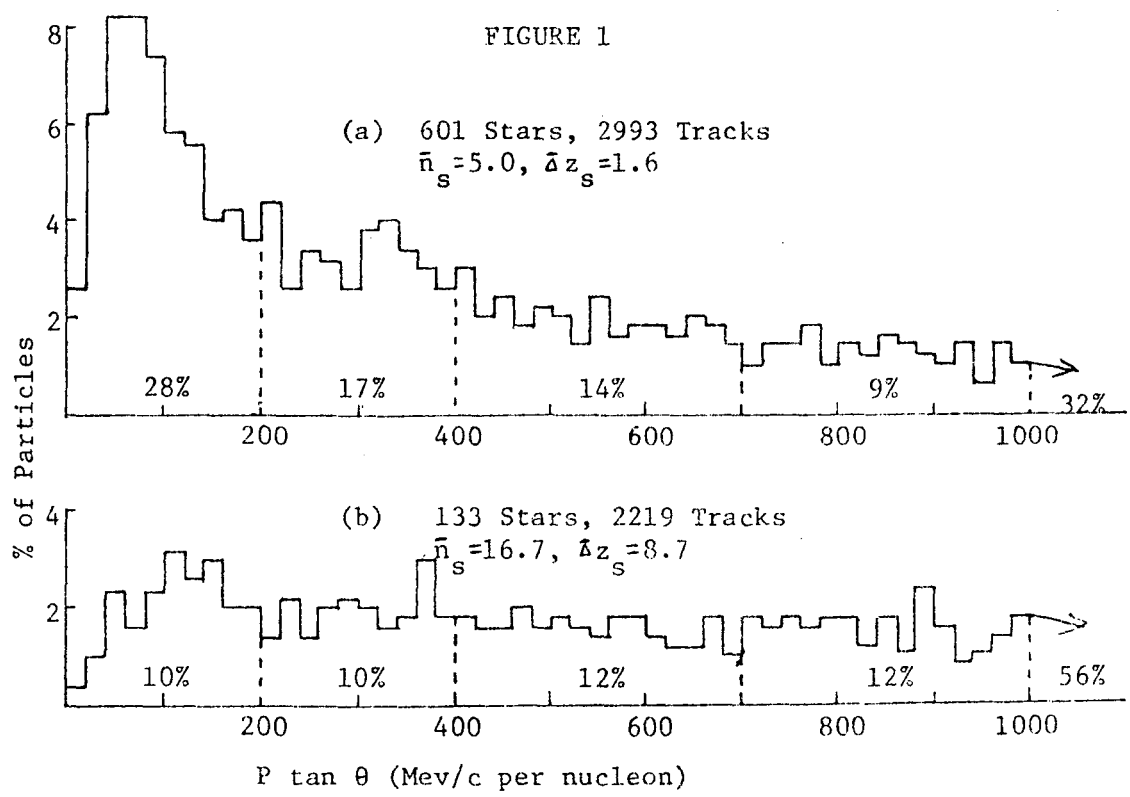

FIGURE 2

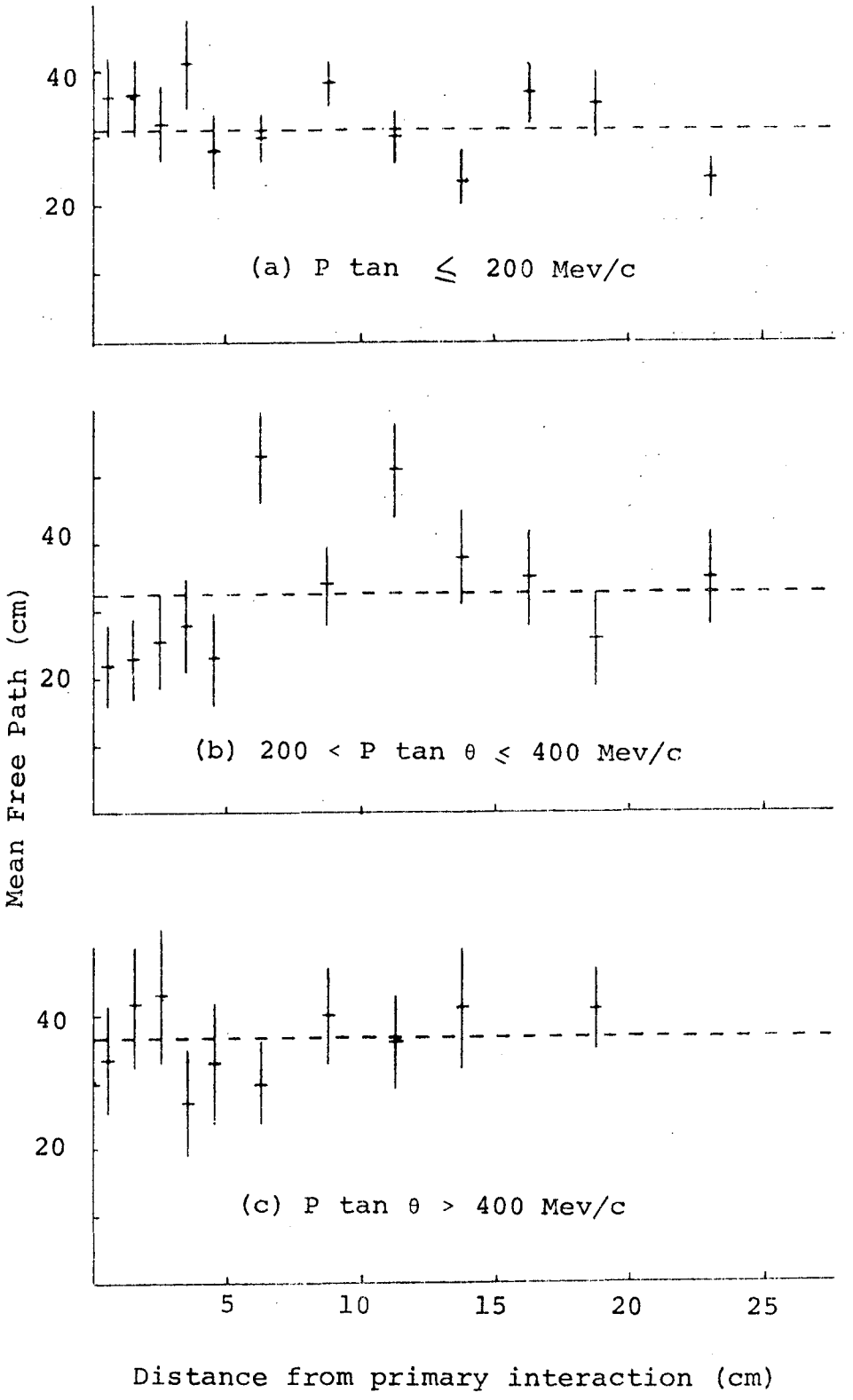
40
20
(a) P tan ≤ 200 Mev/c
40
20
(b) 200 < P tan θ ≤ 400 Mev/c
Mean Free Path (cm)
40
20
(c) P tan θ > 400 Mev/c
5
10
15
20
25
Distance from primary interaction (cm)

A Search for Short-lived Anomalons in Projectile Fragmentation

H.A. Gustafsson, H.H. Gutbrod, B. Kolb, B. Ludewigt, A.M. Poskanzer, T. Renner, H. Riedesel, H.G. Ritter, A.I. Warwick, H.H. Wieman

Gesellschaft für Schwerionenforschung
D-1600 Darmstadt, West Germany and
Nuclear Science Division, Lawrence Berkeley Laboratory
University of California, Berkeley, CA 94720

Nuclear emulsion studies[1,2] suggest that fragmentation products from relativistic heavy ion collisions have anomalously large reaction cross sections and that these anomalons disappear over the first few centimeters of their track in emulsions. If these "anomalons" exist, their disappearance could be due to either depletion by a very large reaction cross section, or decay with a mean lifetime of about 10^{-11} seconds and with only somewhat enhanced cross section. The counter experiment described here was designed to test the decay model proposed by Barber et al.[2] that explains the emulsion data by assuming that all produced fragments are anomalons with 1.6 times the cross section of normal fragments and that the anomalons have a mean lifetime (τ) of about 10^{-11} s corresponding to a mean decay length ($c\beta\gamma\tau$) of 9 mm. If the disappearance in emulsions is due to decay, one should observe a decreased number of secondary interactions in a low-density target, compared to the number observed in a solid target.

We have conducted an experiment based on this density effect. Figure 1 shows a schematic view of the experiment that was performed by bombarding alternatively a solid (20 mm thick) and a dilute (ten 2-mm slabs each separated by 20 mm) Cu target with a beam of 1.7 GeV/u ^{56}Fe ions at the Berkeley Bevalac. The produced projectile fragments were detected, within a cone of $\pm 1^{\circ}$ opening angle 5.5 m downstream, in ΔE plastic scintillators having succesive thicknesses of 1, 6, and 38 mm. The existence of short-lived "anomalons" should, because of the greater number of interactions in the solid target before decay than in the dilute one, move yields from the upper part of the energy loss spectrum to the lower part. This change in the shape of the measured ΔE spectra should, when taking the ratio of the yields in the ΔE spectra for solid and dilute targets, show up as a line with negative slope. The data were recorded using a "min bias" trigger that rejected events where a beam particle was detected. The measured pulse height spectra were calibrated using the energy loss of the beam particles in the detectors, and the yields from the solid and dilute targets were normalized to the same beam intensity.

Figure 2 shows the ratio of the yields in the ΔE spectra produced by the solid and dilute targets (open circles). The error bars shown are due to statistics only and do not contain the systematic error of 1% due to the normalization. The line is obtained from a least square fit to the data points. A fit to the data for a constant value of the ratio equal to one gave a chi square value of 1.04 per degree of freedom, only slightly greater than the 0.81 value for the line drawn, showing that our data are not significantly different from zero effect. To determine the sensitivity to the various proposed decay scenarios, a Monte Carlo simulation of the experiment was done.

The input to the simulation was taken from existing data on projectile fragmentation at this energy.[3,4] The "anomalon" parameters used in the simulation were taken from refs. 2 and 5. The results of the calculations using these two sets of parameters are shown in Fig. 2. The open and filled squares are the results using the parameters from ref. 2 and ref. 5, respectively. As can be seen from the figure, neither calculation agrees with the experimental data. The lines are least square fits to the calculated points.

Our experiment rules out the proposed decay model[2,5] in which the disappearance of the anomalous short mean free path is due to decay. Our data are consistent both with the nonexistence of anomalons and with the disappearance of the short mean free path effect due to reactions. If 100% of the projectile fragments are anomalons, then our data indicate that their mean lifetime must be at least 5×10^{-11} s. It would then be desirable to search for them in, for example, a double scattering experiment.

We are grateful to Dr. Y. Karant for valuable discussions. This work was supported in part by the Director, Office of Energy Research, Division of Nuclear Physics of the Office of High Energy and Nuclear Physics of the U.S. Department of Energy under Contract DE-AC03-76SF00098.

References

1. E.M. Friedlander et al., Phys. Rev. Lett. 45, 1084 (1980)
2. H.B. Barber et al. Phys. Rev. Lett. 48, 856 (1982)
3. G.D. Westfall et al. Phys. Rev. C19, 1309 (1979)
   W.R. Webber et al., Preprint University of New Hampshire, Durham, New Hampsire 03824
   D.E. Greiner, private communication (1983)
4. H.H. Gutbrod et al., Nucl. Phys. A387, 177c (1982)
5. Y. Karant, private communication (1983)

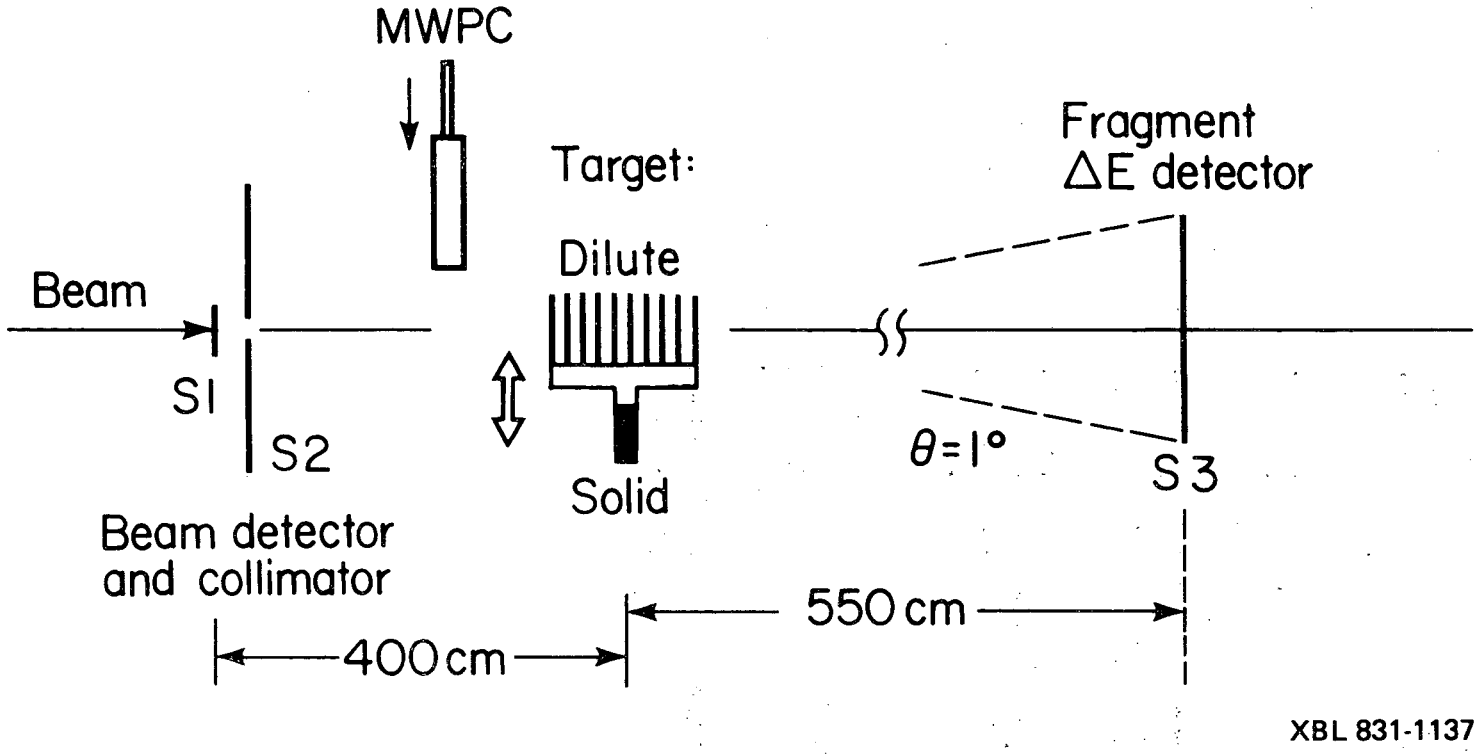

Fig. 1. Schematic view of the experimental layout, S1 and S2 being the beam-defining scintillators. The multiwire chamber MWPC was used for focusing the beam and then retracted. S3 represents the ΔE detectors.

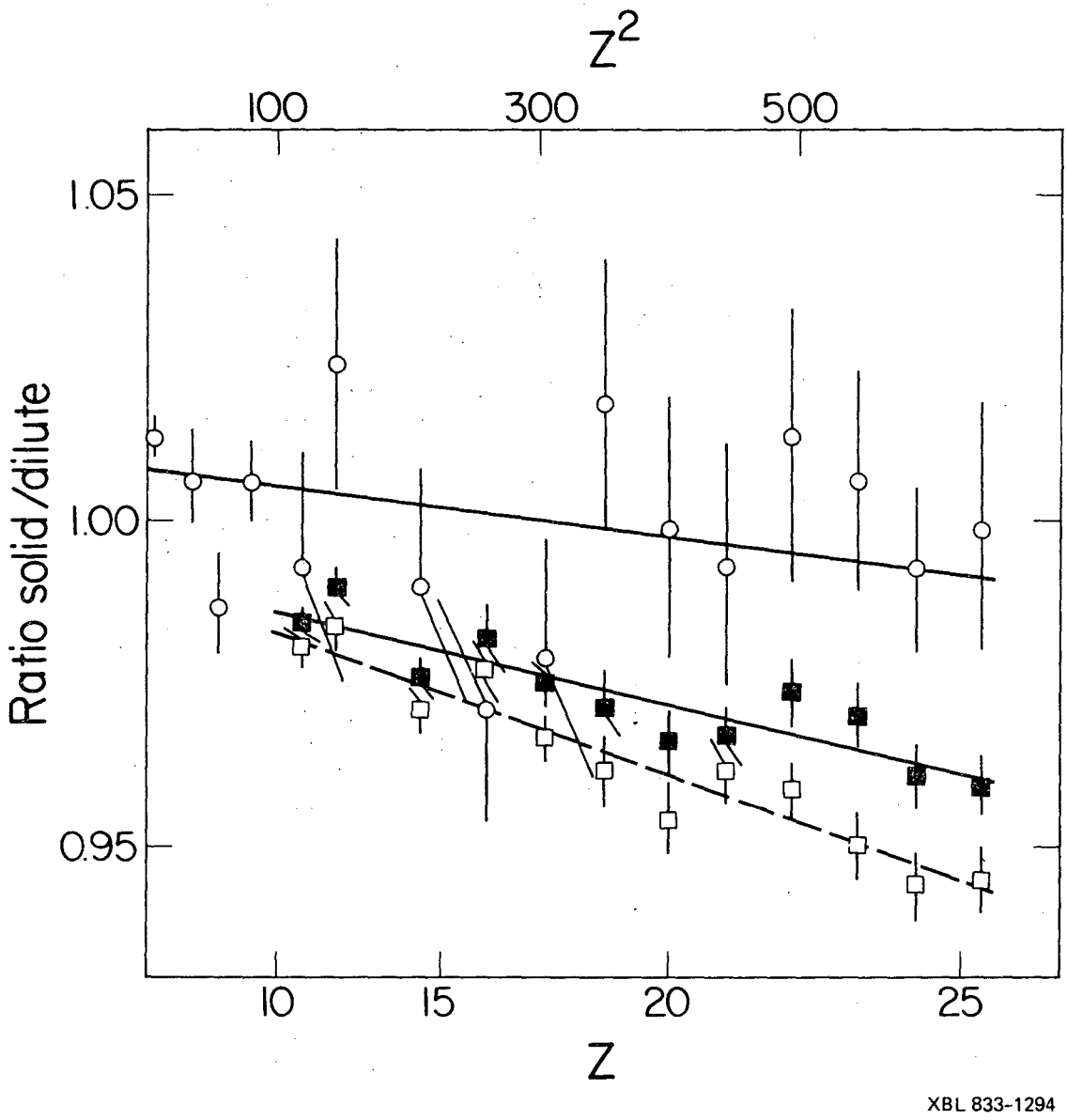

Fig. 2 The ratio of yields in the ΔE spectra produced by solid/dilute targets. Open circles show the data. The 1-mm plastic detector was used to identify charges larger than 10 while for the lower Z values the 6- and 38-mm plastic detectors were used. Open and filled squares show the Monte Carlo simulations.

A SEARCH FOR ANOMALON DECAY BY RADIOCHEMICAL METHODS

by

G. Dersch[a], K. Aleklett[b], R. Beckmann[a], R. Brandt[a], E. M. Friedlander[c], W. Loveland[d], T. Lund[a], P. McGaughey[c], N. Porile[e], G. T. Seaborg[c] and R.Weiner[a]

We present preliminary data on the tests of a radiochemical approach to the investigation of the stability of projectile fragments from relativistic heavy ion collisions. The recent emulsion evidence for anomalously short mean free paths of at least part of such projectile fragments ("anomalons") can be interpreted (most simplistically) by two extreme hypotheses, viz:

a) Anomalons are essentially stable over the distances accessible to the emulsion experiments (∿10 cm) [1] and,

b) Most anomalons return to the nuclear ground state ("normal" cross-section) with a mean life-time comparable to the time necessary for traversal of such distances [2].

Although the experiment to be described is sensitive, in principle, to the presence of stable anomalons, too, its main aim is to test hypothesis b), above.

The method used is identical, in its principle to the one used already in 1941 by Rossi to detect the instability of the muon, viz. the comparison of production/absorption in dense and in diluted targets of the same composition.

In the tests performed to date, identical Cu disks, 1 cm thick and 8 cm in diameter were exposed in pairs to beams of relativistic projectiles in two configurations viz.:

i) in close contact, and

ii) separated by 10 cm of air.

After exposure, spectra of the induced gamma activities were measured, with special attention to the 1369 keV line of ^{24}Na. This isotope is produced with a sizeable cross-section only by hadrons and projectile fragments above ∿1 AGeV, which are well collimated forward.

We define the ratios R1 and R2 as the ratios of initial activities (after correction for ^{24}Na decay) in the two geometrical configurations of the Cu disk pairs. With beam spots ∿2.5 cm in diameter and opening angles of the projectile fragment cones less than 12 degrees the loss of projectile fragments in configuration ii) by "missing" the second disk becomes negligible; hence any difference between R1 and R2 is to be assigned to "decay" of some of the fragments in the longer flight path (i.e. a decrease with time of their reactivity, another formulation for hypothesis b), above).

To date measurements have been completed for exposures to:

1) 24 GeV protons (CERN PS) (where there is no obvious reason to expect anomalon production).

2) 0.9 AGeV ^{40}Ar, and

3) 2.1 AgeV ^{12}C from the BEVALAC.

We remind that previous emulsion experiments with ∿1 AGeV ^{40}Ar have revealed little, if any, anomalon signal, whereas significant signals have been observed with ∿2 AGeV ^{16}O, ^{40}Ar and ^{56}Fe - beams [1-3].

Table 1 shows the ratios R1 and R2, as well as the ratio of ratios Q=R1/R2 from these three exposures. Q=1 would be expected in the absence of "decay effects" (as well as in the absence of anomalons!).

As can be seen the values of Q do not differ significantly from unity although they seem systematically slightly >1. On purely statistical grounds such a fluctuation should occur with a probability of ∿12%.

Measurements on an exposure to a 1.8 AGeV Ar beam are under way. Only a null "decay signal" at the beam energy where an anomalon signal has been detected with the same beam would provide conclusive proof for lack of "decay effects" over a ∿10 cm flight path.

A similar search for "decay effects" using condensed vs. diluted targets with electronic detection of projectile fragments was recently conducted by Gustafsson et al. [4] with a similar negative result. It should however be noted that only projectile fragments of charge > 7 were investigated, whereas ^{24}Na production in our Cu disks is sensitive to the whole charge spectrum.

(a) Philipps University, Marburg/Lahn, Federal Republic of Germany.
(b) Studsvik Science Research Laboratory, S-611 82 Nyköping, Sweden.
(c) Lawrence Berkeley Laboratory, Berkeley, CA. 94720.
(d) Oregon State University, Corvallis, OR. 97331.
(e) Purdue University, W. Lafayette, IN. 47907

TABLE I. R1, R2, and Q ratios for ^{24}Na

BEAM	R1	R2	Q
24 AGeV p	1.08 ± 0.02	1.06 ± 0.03	1.02 ± 0.03
0.9 AGeV ^{40}Ar	1.07 ± 0.02	1.04 ± 0.02	1.04 ± 0.02
2.1 AGeV ^{12}C	1.13 ± 0.01	1.09 ± 0.01	1.03 ± 0.02

REFERENCES

[1]. E. M. Friedlander, et al., Phys. Rev. Lett., 45, 1084 (1980)

[2]. H. B. Barber, et al., ibid, 48, 856 (1982)

[3]. M. M. Aggarwhal, et al., Phys. Lett., 112B, 31 (1982)

[4]. H. A. Gustafsson, et al., LBL Report, 15791 (1983), unpublished

About a Possible Energy Dependence of the Anomalon Effect at Charge Two.

F.Killinger, E.Ganßauge, U.Bieschke, N.Klein, R.Kretschmer, A.Laschek, and W.Weidner
Philipps-University Marburg, West-Germany

Abstract:

The reaction mean-free paths of projectile fragments of charge two seem to be shorter for a few centimeters after their emission than at larger distances from the primary star. This effect is enhanced with decreasing energy of the primary beam. If this can be shown to be true it possibly would explain why the anomalon effect which was established at charges $Z \geq 3$[1-3] has not been found at Z=2 in earlier work[5,6]. Our target was an emulsion stack exposed to a ^{56}Fe beam of around 1.88 A GeV at the Berkeley Bevalac.

Evidence for anomalously short reaction mean-free paths (mfp) of projectile fragments (PF) from high-energy heavy ion collisions in emulsion has been reported by three independent groups[1-3] for PF's of charge $Z \geq 3$ at kinetic energies around 2 A GeV.
This effect was explained by introducing a new kind of particles, called anomalons, with a mean-free path λ too short to be explained by conventional nuclear physics.
One group[4] also reported on search for anomalons at 1 A GeV with no effect being found. This pointed to an energy threshold of the effect between 1 and 2 A GeV. The same group published reasonable statistics on Z=2 PF's at about 2 AGeV although with no effect[5], on the other hand the authors fully agreed with the result at $Z \geq 3$ PF's[2]. Z=2 data are given to a rather large extend originally by B.Judek[6] who repeatedly reported about a strange behaviour of the projectile mfp's.
Although our statistics is very low, we feel that possibly we would understand why neither B.Judek[6] nor the Buffalo group[5] have seen the anomalon effect at Z=2 PF's.
At Marburg we looked for Z=2 PF's from a $^{56}_{26}$Fe beam at 1.88 AGeV which was used at the Berkeley Bevalac for exposing a stack of Ilford G5 nuclear research emulsion. Among around 800 followed α-tracks 246 interacting secondary α's, so called α-stars, have been detected and their location in the emulsion was measured.

Connected with the high charge (Z=26) there is a rather short mean-free path of iron in emulsion ($\lambda \approx 7$ cm). This is the reason why from the 246 stars found there are 147 in between the first three centimeters and 99 in the following ones. The energy of the primary beam is degraded according to the Bethe-Bloch formula $dE/dx = Z^2 \cdot f(\beta)$. Therefore the starting energies of the α-tracks depend rather drastically on the point of origin, X_{OR}, the location of the primary star. Thus, making cuts in the X_{OR} data set of the primary iron beam means grouping the data corresponding to different energy intervals of the secondary projectiles. By doing so and moreover by cutting the data in respect to the distance D from the emission point we find the values listed in Table I.

Table I: Mean-free path's λ^* of secondary α's as function of both, the energy E_o of the α's and the distance D of their origin from the parent star. Integral distribution.

OR cm	E_o GeV/u	$0 < D \leq 3$	$D > 3$ cm	total
0.0	1.88	17.5±1.8 cm(93)	23.3±1.9 cm(153)	21.1±1.3 cm(246)
2.0	1.74	16.8±2.1 cm(60)	21.5±2.3 cm(88)	19.6±1.6 cm(148)
3.0	1.68	15.7±2.4 cm(44)	24.0±3.2 cm(55)	20.3±2.0 cm(99)
4.0	1.61	14.6±2.6 cm(32)	26.4±4.9 cm(29)	20.2±2.6 cm(61)
6.0	1.47	14.4±4.0 cm(13)	44.1±25.5 cm(3)	20.0±5.0 cm(16)

In Table I we see the following: From left to right, i.e. with increasing distance D from the emission point, the mean-free path λ^* increases in each energy group. On the other hand, λ^* decreases rather drastically from top to bottom in the first column, thus with decreasing energy E_o of the originating iron beam. Obvious is this effect only in the first column while in the second E_o seems to be of no influence. With other words, the PF's originated near the emission point are rather sensitive to the energy of the parent beam.

Although our statistics is rather poor we see a distinct trend in this direction, as shown in fig.1. The shaded areas refer to the differential version of Table I as given in Table II.

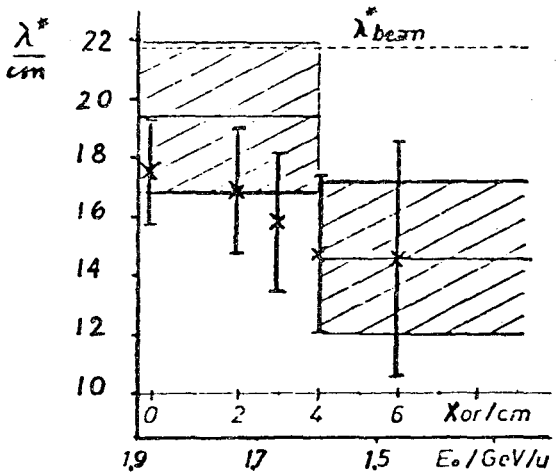

Fig.1: mfp of secondary α's depending on the energy E_o of their parent stars as it corresponds to X_{OR} (Table I, $D \leq 3$ cm).
The broken line gives the value of the primary beam: $\lambda^*_{beam} = 21.8 \pm 0.5$ cm[7]
The shaded areas correspond to the differential distribution as given in Table II.

Let us now compare this representation of our data with the data of B.Judek[6] and P.L.Jain[5]:
B.Judek has done intensive research work on 2.1 AGeV $^{16}_{8}$Oxygen. Her stack was long and she followed many tracks till their very end. But according to Bethe-Bloch the energy decrease of an $^{16}_{8}$O beam in emulsion is only about one tenth of that of an $^{56}_{26}$Fe beam. Therefore she would not have seen the energy effect (see Table III).

And in the energy region around 2 AGeV also we cannot see an effect. B.Judek gives in her above mentioned work[6] one energy grouping, namely "the mfp-transverse momentum dependence of the nuclei from Oxygen fragmentation at different energy intervals" (fig.14 of ref.6).

In the case of P.L.Jain[5] the reason why his group does not find an effect with Z=2 PF's seems to be even more obvious. The authors worked with "short" stacks, one of them being irradiated with ~2 AGeV $^{40}_{18}$Ar. Again the energy decrease compared to iron is about one half, and this means that in a short stack there may be no obvious energy decrease observable.

Table II: Like Table I, but for energy intervals, i.e. differentially distributed.

X_{OR}/cm	E_o/GeV/u	D ≤ 3 cm	D > 3 cm
0-4	1.61 to 1.88	19.4±2.5 cm(61)	22.6±2.0 cm(124)
> 4	1.61	14.6±2.6 cm(32)	26.5±4.9 cm(29)

Table III: Comparison of our data with those of B.Judek[8] and P.L.Jain[5].

	D ≤ 3 cm	D > 3 cm
B.Judek	20.54±1.33 cm(240)	20.13±0.74 cm(736)
P.L.Jain	19.5±1.0 cm(380)	20.3±1.2 cm(286)
this work	19.4±2.5 cm(61)	22.6±2.0 cm(124)
total $1.61 < E_o < 2.1$	19.9±0.8 cm(681)	20.4±0.6 cm(1146)
this work $E_o > 1.61$	14.6±2.6 cm(32)	26.5±4.9 cm(29)

We see from Table II that there is also in our data no effect to be identified if we examine only that energy interval what Jain and Judek have been able to measure. In Table III we compare their data with each other and also with ours. To compare the two energy groups we used the F-test for $F = \lambda_{E>}/\lambda_{E<}$ at D ≤ 3 cm. The probability results in P(>F) = 0.058. To check whether there exists an anomalon effect at all we compare the low energy group near the emission point with the reported beam value λ^*_{beam}=21.8±0.5 cm[7]. The corresponding F-test, using $F = \lambda^*_{beam}/\lambda_{E<}$ at D ≤ 3 cm results in P(>F) = 0.020.
It would be of great interest to enhance the statistics of Z=2 PFs at energies $E_o < 1.6$ AGeV to establish the effect - or to cancel it.

This work was supported by the Bundesminister für Forschung und Technologie, No.06 MR 136 and 158.

References

1) E.M.Friedlander, R.W.Gimpel, H.H.Heckman, Y.J.Karant, B.Judek, and E.Ganßauge, 1980, Phys.Rev.Lett.45, 1084
2) P.L.Jain and G.Das, 1982, Phys.Rev.Lett.48, 305
3) H.B.Barber, P.S.Freier, and C.J.Waddington, 1982, Phys.Rev.Lett.48, 856
4) M.M.Aggarwal, K.B.Bhalla, G.Das, and P.L.Jain, 1982, Phys.Lett.112B, 31
5) P.L.Jain, M.M.Aggarwal, G.Das, and K.B.Bhalla 1982, Phys.Rev.C25, 3216
6) B.Judek, 1977m NRC-report
7) E.M.Friedlander, E.Ganßauge, R.W.Gimpel, H.H.Heckman, B.Judek, Y.J.Karant, and H.Yee, 1981 LBL-report No.12652, p.416, unpublished
8) B.Judek, 1980, private communication

A Search for Topological Correlations in The Interactions of Relativistic Projectile Fragments From Relativistic Heavy Ion Collisions

E.M. Friedlander, H.H. Heckman, and Y.J. Karant

Lawrence Berkeley Laboratory, University of California
Berkeley, California 94720

Following the observation of anomalously short mean free paths among projectile fragments from relativistic heavy ion collisions [1-3] it was a natural next step to investigate what correlations, if any, exist between the characteristics of the events in which "anomalons" are produced, of those which they induce, as well as with their interaction mean free path.

To date there have appeared two indications for such correlations, viz.:

i) The Marburg emulsion group [4] has obtained some evidence for different forward-backward asymmetries (FBA) of target fragments in collisions of He-secondaries from 1.88 AGeV Fe-collisions, according to the distance D of the He-interaction from its origin.

ii) The Cairo group [5] has reported evidence for shorter mean free paths of He-secondaries from 4.5 AGeV C-interactions if the event from which the He-secondary originated had a low multiplicity of target fragments.

We report here the preliminary results of a search from correlations between the properties of production and interaction stars of He-secondaries from the extra-nuclear cascade induced by a beam of 1.88 AGeV Fe. The aim of this investigation, performed to date on a limited subsample of events from stack 3Fe [6], was to identify parameters most sensitive to correlation studies, to be pursued with larger statistics on the whole available material.

Exposure and scanning conditions were described in our preceding abstract [6] concerned with the mean free path measurements. In view of the existing experimental indications, He-secondaries were selected for a first trial run.

The only selection imposed on the events was to exclude stars lying closer than 50 microns to either the emulsion-air or the emulsion-glass interfaces, in order to ensure accurate multiplicity counts. For each He-interaction we recorded the following parameters:

1) Its multiplicities N_h of non-relativistic ($g^*>1.4$) target fragments and n_s, of relativistic secondaries of charge 1.

2) The distance D from the interaction in which the He-secondary originated.

3) The generation of the He-secondary

4) The charge Z^P of the projectile inducing the reaction of origin, and

5) The multiplicity N_h^P of target fragments of this latter interaction grouped in three bins labeled: "0" (N_h^P=0), "1" (N_h^P=1-8), and "2" (N_h^P>8), (the latter almost certainly collisions with AgBr targets).

The data reported here refer to a total of 467 He-interactions of all generations.

The mean values of N_h and n_s were N_h = 7.17±0.31 and n_s =2.66±0.07 respectively. Since $\langle n_s \rangle$ only slightly exceeds 2 (the expected number of surviving fragments of charge 1 from He) the low excess attributable to pion production is hardly adequate for a sensitive search for correlations, except at much higher statistics than available at present. (However the positive N_h-n_s correlation within the He star, well-known from proton-nucleus collisions [7], was clearly observed.)

The search for FBA was conducted in two ways namely:

a) by building composite stars from all He-interactions and

b) by counting the numbers of stars with negative, zero or positive sign of their asymmetry coefficient.

By using method a) no strong effects were observed, although the trend of the FBA coefficient A=(F-B)/(F+B) is the same as the one observed in ref. [4], i.e. A is lower at low D. However, the differences in A hardly exceed the 2 S.D. level (X^2=12.8 with 5 degrees of freedom). Because of the different systematics and methods of analysis (the Marburg group compared the explicit distributions of projected angles of target-fragments, at low and at large D, to obtain ~ 2.5 S.D. significance for different FBA's), the two sets of results cannot yet be added to strengthen the statistical significance and should be considered as preliminary, requiring larger statistical samples for a definite conclusion.

Another hint for a correlation appears if A is binned according to Z^P (Table 1). Again, because of limited statistics, the X^2 is only 5 with 2 DOF. The overall probability of both effects being due to statistical fluctuations is ~1% with the present statistics. Method b) yielded a similarly weak correlation (~2 S.D.).

An interesting correlation was observed between the target fragment multiplicity N_h of the He-interactions and the characteristics (N_h^P and Z^P) of the star of origin (Table 2).

As can be seen the mean N_h-values differ according to the charge Z^P of the projectile (by >2 S.D. in each case) but are of opposite sign if N_h^P is 0 as opposed to N_h^P=1 or 2. The difference $\Delta(\Delta N_h)$ exceeds in significance 3 S.D.

The importance of this observation, if confirmed by larger statistical samples, lies in the fact that it would establish a correlation between the production and interaction mechanisms of relativistic projectile fragments without connection with mesurements of mean free paths.

Further experiments, intended both to increase statistics for He-secondaries and to extend the observations to fragments of higher charges, are under way.

This work was supported by the Director, Office of Energy Research, Division of Nuclear Physics of the Office of High Energy and Nuclear Physics of the U.S. Department of Energy under Contract DE-AC03-76SF00098.

References:

1. E.M. Friedlander, R.W. Gimpel, H.H. Heckman, Y.J. Karant, B. Judek, and E. Ganssauge, Phys. Rev. C27, 1489 (1983).
2. P.L. Jain and G. Das, Phys. Rev. Lett. 48, 305 (1982).
3. H.B. Barber, P.S. Freier, and C.J. Waddington, Phys. Rev. Lett. 48, 856 (1982).
4. N. Klein, et al., private communication
5. M. El-Nadi, O.E. Badawy, M.N. El-Bakry, A. Abdel-Salam, A.A. El-Hamalawy, E.I. Kaalil, A.M. Moussa, and M. El-Nagdy, Abstract, Sixth High Energy Heavy Ion Study and Second Workshop on Anomalons, LBL, June 28 - July 1, 1983.
6. Y.J. Karant, H.H.Heckman and E.M. Friedlander, Abstract, Sixth High Energy Heavy Ion Study and Second Workshop on Anomalons, LBL, June 28 - July 1, 1983.
7. E.M. Friedlander and H.H. Heckman, Relativistic Heavy Ion Collisions: Experiment, LBL report 13854, 1982, to be published in Heavy Ion Science, D. Bromley, Ed., Plenum Press.

TABLE I.

Z^P	:	3-5	6-10	11-25	26
A	:	0.09±0.10	0.17±0.08	0.29±0.08	0.27±0.02

Table II.

N_{hP}	Z^P	N_h	Diff.	Diff. of Diff.
0	2-12	7.5±1.5	(ΔN_h)	$\Delta(\Delta N_h)$
			3.8±1.8	
0	13-25	3.7±0.9		
				6.7±2.2
1-2	2-12	6.0±0.8		
			-2.1±1.2	
1-2	13-25	9.9±0.8		

Particle-Gamma Coincidence Measurements in $^{12}C + ^{12}C$ and $^{12}C + Pb$ Collisions at 2.1 GeV/A Incident Energy, First Results--γ-Ray Spectrum

G. Roche,* J. Carroll,† C.C. Chang,‡ T. Hallman,§ P.N. Kirk,‖ R. Koontz,¶ G. Krebs,‖ L. Madansky,§ T. Mulera,† H. Pugh,¶ L. Schroeder,¶ J. Vicente*

*Université de Clermont-Ferrand, IN2P3, France
†University of California, Los Angeles, CA
‡University of Maryland, College Park, MD
§Johns Hopkins University, Baltimore, MD
‖Louisiana State University
¶Lawrence Berkeley Laboratory, Berkeley, CA

High-energy γ-rays are mainly produced through π° decay in relativistic heavy ion collisions at incident energies in the range 1-2 GeV/A. Other possible weak contributions are: nucleus-nucleus bremsstrahlung, η-meson production, and $\Delta(1232)$ decay. Up to now, only a few experimental studies have been done on this subject (1-3). More recently, γ-ray measurements have been performed to study projectile fragments having an anomalously short interaction length, i.e., the so-called anomalons (4-8). Liss, et al. (9) have searched for single delayed gammas as an eventual decay process. Their negative result does not completely rule out a possible electromagnetic decay of an anomalous state, because their measurement was done at 940 MeV/A, an energy at which it has been suggested (7) that the effect could have disappeared.

We have undertaken a different approach to the study of anomalous fragments. First, the study is done in the target fragmentation region. Second, we look for singly charged anomalous fragments through particle-gamma coincidence measurements. We have focused on the creation and detection of singly charged fragments, which have been extensively studied by Judek (5). For interaction with primary energies up to 5 GeV/A, fragments are found to be anomalous in the range of transverse momenta 120-480 MeV/c, which corresponds in the target region to deuterons of energies in the range 4-60 MeV. On the theoretical side, Frederiksson, et al. (10) suggest the existence of a possible six-quark deuteron state that we estimated could produce a γ-ray around 200-300 MeV. Our experimental method consists then in looking for any sharp line or bump in γ-ray spectra in coincidence with particles and, ultimately, looking for any signal in the particle-gamma invariant mass distribution. Besides this specific aim, our measurements will bring complementary information on the physics first mentioned in the paper. We present here the experimental setup and preliminary results on the measured gamma-ray spectrum.

The experimental configuration is shown in Fig. 1. The multiwire proportional chambers WC2 and WC3 were used for beam alignment and the ionization chamber IC for beam intensity measurement. Photons and charged particles produced in the target T were detected in a thick NaI crystal system (NaI) and two ΔE-E telescopes (TEL2, TEL3), respectively. The detector system NaI consists of a plastic scintillator V used as a charged particle veto, a 1" thick NaI crystal in which the shower is generated, a plastic scintillator C, which detects the γ-ray conversion, and two 5" thick NaI crystals in which the shower deposits the rest of its energy. Besides, the annulary plastic scintillator H signal was used off-line as a veto to

better select the showers emitted around the central axis of the system. The neutron contamination is less than ≈1%, and the overall resolution was determined to be ≈30% at 130 MeV (for minimum ionizing cosmic rays). The telescope TEL2 consists of two 1-mm thick silicon detectors with a 3-in thick NaI crystal, and TEL3 consists of five identical elements made with a plastic scintillator (0.5 inch) and a 5-in NaI crystal. The overall resolutions for TEL2 and TEL3 are, respectively, ≈10 MeV at 50 MeV and 7 MeV at 100 MeV, for protons. The angles between the beam direction and the detector axes are 41° for TEL2, 45° for TEL3, and 124° for NaI, and the azimuthal angles between TEL2/TEL3 and NaI are, respectively, 168/127°.

Gamma-ray spectra have been extracted off-line for both C and Pb targets, both TEL2•NaI and TEL3•NaI coincidence requirements, and the four following conditions:

Condition 1: anything in the particle telescopes satisfying the coincidence requirement,
Condition 2: same as 1 plus a little higher energy threshold in the particle telescopes,
Condition 3: protons in the particle telescopes (20-120 MeV for TEL2, 40-200 MeV for TEL3),
Condition 4: deuterons in the particle telescopes, (30-180 MeV for TEL2, 60-300 MeV for TEL3).

The most inclusive γ-ray measured cross sections are those under condition 1. For conditions 3 and 4, the energy spectra of the charged particles were also extracted, and the invariant mass distributions computed on an event-by-event base. Figure 2 shows an example of γ-ray spectrum

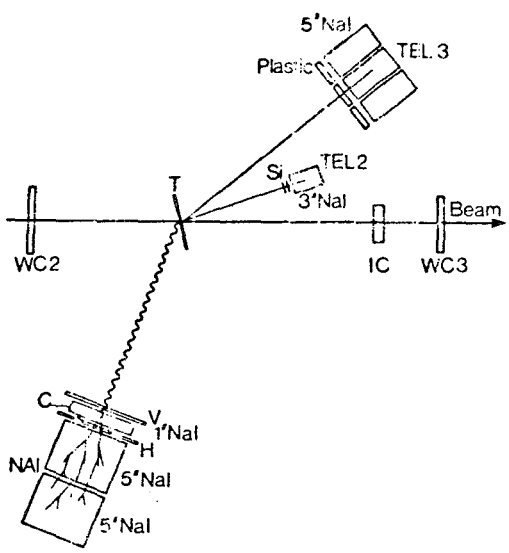

Fig. 1
Experimental setup

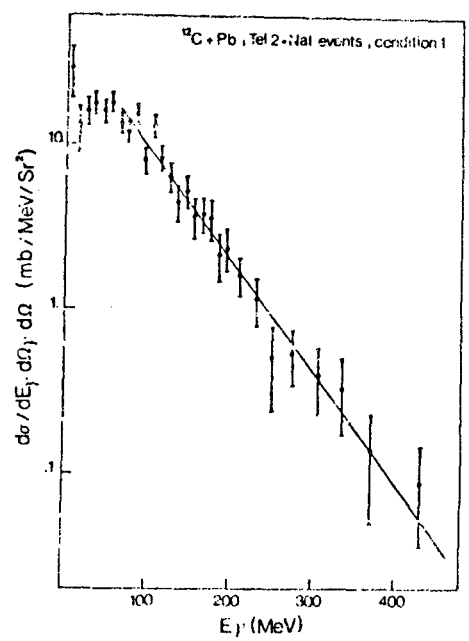

Fig. 2
A γ-ray spectrum

obtained under condition 1, for a Pb target and detectors TEL2•NaI. The solid line is an exponential fit of the spectrum above 90 MeV, writing the fitting function as $A\exp(-E_\gamma/T)$, where A and T are the parameters. Table 1 gives the values of T for our data. These numbers do not seem to depend much on the type of condition, except perhaps for condition 4, where we have a lower value for Pb and a higher one for C (with large errors). They are consistent with Budiansky, et al. (3) measurements at 2 GeV/A incident energy (central trigger), from which one obtains:

$$T = 173 \text{ MeV for Ar + Pb} \rightarrow \gamma\ (30^\circ)$$
$$T = 70 \text{ MeV for Ar + Pb} \rightarrow \gamma\ (90^\circ)$$

We define the "number of γ per trigger" as the quantity n_γ computed from

$$n_\gamma = 4\pi\sigma_\gamma/\sigma_{part}$$

where σ_γ is the cross section integrated over energy for detecting a γ-ray in coincidence with a particle in the telescopes, and σ_{part} is the inclusive cross section integrated over energy for detecting the same particle(s) in the telescopes (this definition assumes isotropy of the γ-ray emission). We also define the "number of π° per trigger" as $N_{\pi^\circ} = n_\gamma/2$. From our measurements, we have found n_{π° in the range ≈1-2 for Pb and ≈0.5 for C, while Budiansky, et al. (3) have published a value of six π°'s per central collision of 2 GeV/A Ar on Pb, which suggests that our data are probably related to more peripheral collisions.

Finally, there are no obvious sharp lines or bumps in our γ-ray spectra or mass distributions so far obtained. More data are being processed, which should allow us to draw stronger conclusions very soon.

Tgt	Condition	T (MeV) TEL2.NaI		TEL3.NaI	
Pb	1	63.9	4.1	62.5	3.0
	2	62.9	4.3	63.1	2.8
	3	59.9	10.0	65.2	4.4
	4	55.7	10.0	50.8	5.8
C	1	88.9	14.9	72.5	5.6
	2	79.0	12.7	70.7	6.5
	3			73.8	7.6
	4			98.5	19.1

Table 1

References

(1) W. Dejarnette, et al., Phys. Lett. 94B, 327 (1980)
(2) T. Hallman, et al., unpublished
(3) M.P. Budiansky, et al., Phys. Rev. Lett. 49, 361 (1982)
(4) B. Judek, Can. J. Phys. 46, 343 (1968)
(5) B. Judek, Can. J. Phys. 50, 2082 (1972)
(6) E.M. Friedlander, et al., Phys. Rev. Lett. 45, 1084 (1980)
(7) P.L. Jain, et al., Phys. Rev. Lett. 48, 305 (1982)
(8) H.B. Barber, et al., Phys. Rev. Lett. 48, 856 (1982)
(9) T.M. Liss, et al., Phys. Rev. Lett. 49, 775 (1982)
(10) S. Frederiksson, et al., 5th High Energy Heavy Ion Study, May 18-22 (1981), LBL-12652, UC-34, CONF-8105104

Studies of Anomalous Projectile Fragments with Lead-Glass, Plastic Track Detectors, and Cerenkov Detectors

P.B. Price
University of California, Berkeley

This is a summary of ongoing as well as recently completed studies of anomalons by members of my group.

1. Search for Delayed Gamma Decays of Anomalous Nuclear States, by T.M. Liss, S.P. Ahlen, P.B. Price and G. Tarlé (Phys. Rev. Lett. 49, 775 (1982)).

We used Pb-glass detectors to search for delayed high-energy γ-rays emitted in flight by projectile fragments of 940A MeV ^{56}Fe interactions with a steel target. Out of 1.6×10^8 interactions we detected only one γ-ray with lab energy E_{lab} between 35 and 1000 MeV. Figure 1 shows regions in the space of fragment-rest-frame photon decay energy $E_0(\approx 2E_{lab})$ versus proper mean lifetime τ_0 which can be ruled out by our data at a 95% confidence level. The dark shading refers to the model of Friedlander et al. in which 6% of projectile fragments are anomalous with λ_a = 2.5 cm in emulsion; the light shading refers to the model of Barber et al. in which 100% of projectile fragments have a mean free path shortened by a factor 1.5 but revert without charged particle emission to normal nuclei in a distance λ = 0.85 cm. Our negative result casts doubt on versions of these and other models in which anomalous states created at ~940A MeV decay electromagnetically to normal nuclei. There is no statistically significant evidence from emulsion studies that anomalons are not created at 940A MeV.

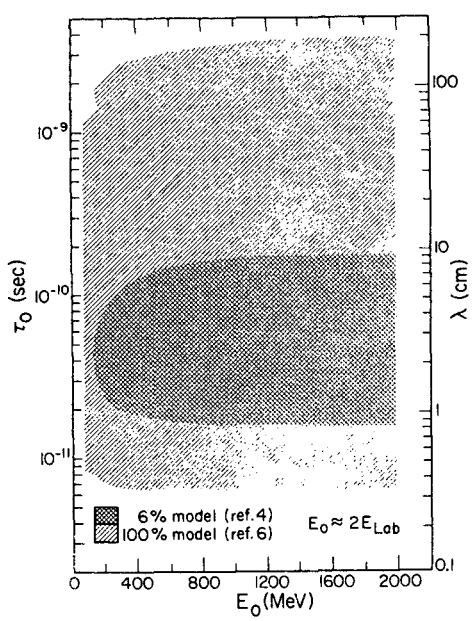

2. Search for Nonintegrally Charged Projectile Fragments in Relativistic Nucleus-Nucleus Collisions, by P.B. Price, M.L. Tincknell, G. Tarlé, S.P. Ahlen, K.A. Frankel and S. Perlmutter (Phys. Rev. Lett. 50, 566 (1983)).

Using dioctyl-phthalate-doped CR-39 detectors with charge resolution σ_Z = 0.06e, we have made the first dynamic search for fractionally charged particles bound to nuclei. (Both one-third and one-half integral charges have been proposed.) We find, from charge measurements in the first 1.7 cm after production, that no more than 3×10^{-3} (95% confidence level) of the projectile fragments of 1.85A ^{40}Ar interactions with $10 \lesssim Z \lesssim 17$ have charges differing from an integer by as much as 0.3e. Figure 2 shows the charge distribution in two sets of measurements. This result, coupled with our positive evidence for anomalons to be summarized in section 3 below, rules out explanations of anomalons based on models in which anomalons have non-integral charge in such charge range.

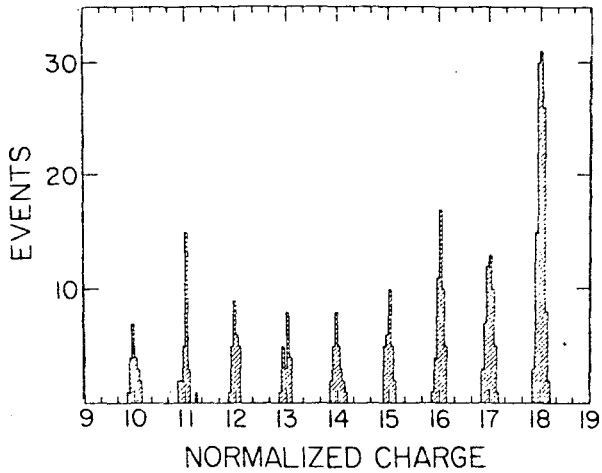

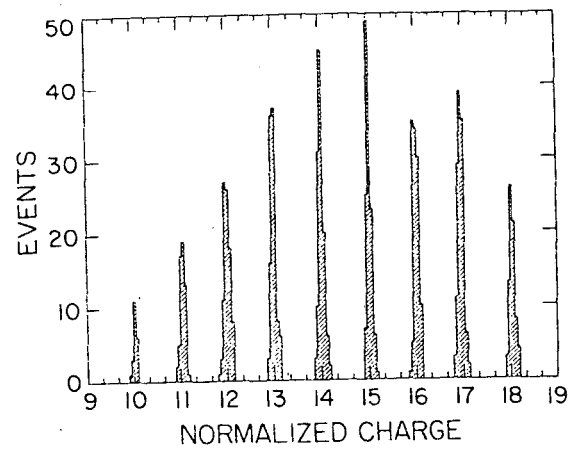

3. Study of Anomalous Fragments of 1.85A GeV ^{40}Ar reactions in CR-39 Detectors, by M.L. Tincknell and P.B. Price.

Tincknell will discuss the results of this study of the dependence of Λ^* on distance from the interaction point for fragments with $10 \lesssim Z \lesssim 17$ in DOP-doped CR-39 detectors. Qualitatively, the main results are as follows:

a) Anomalons are seen using a totally different kind of visual detector from nuclear emulsion. The possible kinds of systematic errors are quite different in these two classes of detectors.

b) Anomalons are produced in collisions with light target nuclei. The composition of CR-39 is $C_{12}H_{18}O_7$.

c) Λ^*/Λ_{beam} is more than 2σ less than unity in the first centimeter and is consistent with unity at greater distances. The recovery distance is shorter in this experiment than in the average of the three published nuclear emulsion studies. A possible explanation is that λ_a is a decreasing function of Z, as suggested by M.H. Mac Gregor. (Our mean charge, $\overline{Z} = 14$, is larger than the mean fragment charge studied in the emulsion experiments.)

d) Both odd-Z and even-Z fragments contain anomalons.

4. Measurements of Charge-Changing Interaction Mean Free Paths of Stable Nuclei with Plastic Track Detectors, by J. Drach, Shi-lun Guo, P.B. Price, M.H. Salamon and M.L. Tincknell.

Before claiming that a detector can measure anomalous mean free paths, it is essential to show that that detector can obtain reliable values of mean free paths of normal nuclei. Using a semi-automated technique to measure diameters of etch-pits in plastic detectors, we have determined $\lambda_{\Delta Z \geq 1}$, the mean free path for charge-changing interactions, for relativistic beams of ^{20}Ne, ^{40}Ar, ^{56}Fe, and ^{238}U at the Bevalac. The results are shown below.

Beam	Medium	$\lambda_{\Delta Z \geq 1}$ (g/cm^2) Our result	Geom. model
2.1 A GeV ^{20}Ne	CR-39($C_{12}H_{18}O_7$)	18.72±1.16	17.99
1.85A GeV ^{40}Ar	"	12.61±0.61	12.55
1.7 A GeV ^{56}Fe	"	10.44±0.44	10.43
0.96A GeV ^{238}U	Tuffak($C_{16}H_{14}O_3$)	4.69±0.15	4.61

We used CR-39 to study the fragmentation of Ne, Ar, and Fe, and we used Tuffak polycarbonate, which has a lower sensitivity and is more suitable for very highly ionizing particles, to study the fragmentation of U. In the uranium case, changes of charge state due to capture and loss of K electrons are common. This adds to the difficulty of detecting nuclear interactions with $\Delta Z = 1$. The uncertainty in our efficiency for detecting such interactions is much smaller than the statistical error.

Our results agree, within counting statistics, with values of $\lambda_{\Delta Z \geq 1}$ predicted by the simple overlap model of Bradt and Peters for the geometric cross section, $\sigma_{geom} = \pi r_0^2 (A_T^{1/3} + A_B^{1/3} - b)^2$, with $r_0 = 1.35$ fm, $b = 0.83$, taken from Westfall et al. (Phys. Rev. C 19, 1309 (1979)), who used silicon detectors to study the fragmentation of an Fe beam. (We took $A_T = 0.089$ for hydrogen target, following Westfall et al.).

The excellent agreement between our measured values and those predicted by the overlap model shows that plastic track detectors can be made to have essentially 100% efficiency for detecting charge-changing interactions of a wide range of projectile nuclei. It also shows that a simple geometric model of nuclei of constant density and skin thickness accounts remarkably well for interaction mean free paths.

5. Comparison of Anomalous Mean Free Paths in Compacted and Dilute CR-39 Stacks, by J. Drach, P.B. Price and M.L. Tincknell.

We are analyzing Λ^*/Λ_{beam} as a function of distance in g/cm^2 from interaction points for fragments with $10 \lesssim Z \lesssim 25$ from 1.7A GeV ^{56}Fe in a compact CR-39 stack (mean density = 1.32 g/cm^3) and a CR-39 stack with periodic air gaps (mean density = 0.16 g/cm^3). If anomalons radioactively decay in a distance less than ~10 cm, the dilute stack should show a weaker depression of Λ^*/Λ_{beam} than the dense stack. An advantage of the dilute stack is that lateral displacements of fragments are amplified by a factor 8 due to the air gaps, making accurate measurements of transverse momenta possible.

The timescale for completion of this work is ~two months.

6. Development of a Segmented Cerenkov Detector for Study of the "Anomalon" Phenomenon, by J.D. Stevenson, J.A. Musser and S.W. Barwick.

We have designed a Cerenkov detector consisting of four 1/8 inch paddles, six 1/4 inch paddles, and two 1/2 inch paddles whose spacing can easily be varied so that enhanced cross sections and radioactive decays can be studied separately.

For a paddle of a given thickness, the charge resolution must be sufficiently good that the probability of charge misidentification is much less

than the probability of a nuclear interaction in the paddle. For a 1/8 inch paddle and $\lambda \sim 10$ cm the charge standard deviation must be less than $\sigma_Z \sim 0.15e$ in order for the technique to work.

Our calibration experiments with Cerenkov paddles have shown that we will achieve the desired charge resolution for paddles of all three thicknesses provided we use wire chambers to permit us to take into account spatial variations in detector response.

We expect to use this new system to study anomalous mean free paths in the fall of 1983.

A Detector for the Measurement of Projectile Fragment Interaction Cross Sections

J.P. Dufour, J.G. Girard, P.J. Lindstrom, D.E. Greiner, D.L. Olson, T.J.M. Symons
Nuclear Science Division, Lawrence Berkeley Laboratory, Berkeley, CA94720

H.J. Crawford
Space Sciences Laboratory, University of California, Berkeley, CA 94720

ABSTRACT

A detector is being developed to measure the charge changing cross sections of secondary and tertiary projectile fragments produced in relativistic heavy ion collisions. This device is designed to provide a high statistics, electronic, analog to the measurements that have been made recently using plastic track detectors. If the detector is successful and the anomalous component present in projectile fragmentation is observed, we intend to use the device in combination with the HISS spectrometer as a filter to study further the anomalous fragments.

DESCRIPTION OF THE DEVICE

Detectors measuring the charge change in a heavy ion collision must by definition rely on an electromagnetic interaction between the fragments and the detection medium itself or with an externally applied electromagnetic field. To date, all measurements of mean free paths of projectile fragments have relied on the ionization of the target medium, which has either been nuclear emulsion or CR39 plastic track detectors. However, other methods are possible such as rigidity measurements in a magnetic spectrometer or macroscopic effects such as Cerenkov and transition radiation.

We believe that Cerenkov detectors have particular promise for the following reasons:
i) At a given velocity, the intensity of the radiation produced is proportional to Z^2, allowing a direct measurement of the fragment charge.
ii) The light emitted is highly directional so that a suitably designed device can isolate the component arising from fragments emitted in a particular angular range.
iii)The energy dependence of the radiation intensity is quite different from that of energy loss by ionization. In particular, low energy, heavily ionizing fragments are below the Cerenkov threshold and make no contribution to the signal.

Against these must be set the obvious disadvantages which include the necessity of using an optically transparent medium as the target and the lack of discrimination of events in which multiple heavy fragments move together at 0 degrees. This, however, is a general criticism of detectors which lack the lateral resolution found in emulsion or track detectors.

We have tested two different detector designs at the Bevalac in order to evaluate the charge and position resolution that can be achieved. Both of

these devices use Lucite as the radiator material and both incorporate strong directional selection on the detected particles. In the first design beam particles pass down the axis of a cylindrical radiator. The light emitted is reflected at the surface of the cylinder and focussed onto a set of photomultiplier tubes which then measure the intensity of the signal (and thus the fragment charge) as a function of depth within the material. In the second, a stack of thin Lucite plates is used. Light is transported out of the plates by multiple total internal reflection at the surfaces of the plate. Since the angle of the Cerenkov light is very close to the critical angle, both of these devices provide excellent directional selection, a typical angular dependence of the detection efficiency being shown in fig. 1. This illustrates that the light from energetic light ions such as protons and alpha particles will be strongly suppressed.

The most important characteristic of any such device is the charge resolution and the distance over which it is necessary to integrate the light in order to achieve this resolution. We have tested our devices with Carbon and Iron beams accelerated by the Bevalac and have been able to obtain satisfactory results, particularly with the segmented radiators. At present, the resolution of the cylindrical device is limited by attenuation of light within the radiator material. This problem can be overcome by changing the method of fabricating the cylinder. In figure 2 we illustrate the resolution that can be achieved by showing a spectrum of ions of charges 24, 25 and 26 measured using a 3mm Lucite radiator. The width of the charge peaks is 0.62 charge units, full width at half maximum. We believe that this resolution, which is close to the theoretical limit for such a radiator, will be sufficient for us to observe the anomalous component that has been reported in the literature.

We are now constructing a device will contain 50 3mm radiators for use in a full scale test of the technique. The only significant change from the devices used so far will be the use of optical glass rather than Lucite for the radiators which should improve both the charge resolution and the uniformity of response of the detector. We hope to measure the mean free path of the secondary fragments ranging from 6mm to 13 cm and also to obtain information on tertiary events and isotopic cross sections.

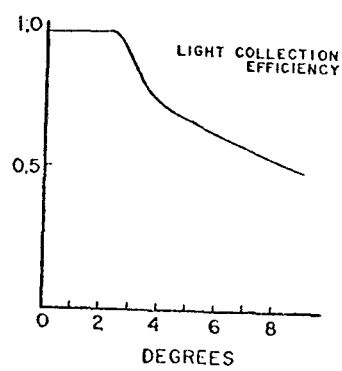

Figure 1. Angular sensitivity of detector.

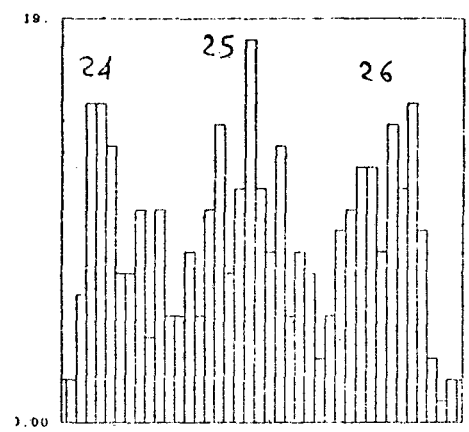

Figure 2. Measured charge spectrum.

Development of a Segmented Cerenkov Detector for Study of the "Anomalon" Phenomenon

J.D. Stevenson, J.A. Musser and S.W. Barwick
University of California, Berkeley

Recent experiments at the Bevalac have suggested that the mean free path of projectile fragments exhibits anomalous behavior for the first two or three cm following an interaction. The experiments performed to date, using nuclear emulsions and plastic track detectors, suffer from a relatively small set of interaction length measurements due to the time-consuming nature of data acquisition associated with these detectors. These experiments do, however, agree that the "anomalon" effect exists. Electronic experiments to date have been restricted to searches for anomalon decays and have all given negative results. There is a real need for a new generation of electronic experiments which directly check the visual detector results.

We plan to look for the anomalon effect using a stack of thin plastic Cerenkov paddles, each of which provides an independent measurement of the projectile fragment charge. Determination of the projectile fragment charge by measurement of the intensity of Cerenkov radiation is superior to ionization measurements because it is insensitive to fragments below the Cerenkov threshold of ~310 MeV/nucleon. Low-energy fragments represent a real danger in analysis of ionization-type experiments since fragments coming to the end of range can mimic nuclear interactions. The chief disadvantage of the use of Cerenkov detectors is their feeble light output. The charge resolution of thin Cerenkov detectors is thus invariably limited by photon counting statistics and efficient light collection schemes are required to achieve satisfactory charge resolution.

The charge resolution requirements of this experiment are quite demanding. The charge resolution must satisfy the requirement that the charge misidentification rate ($P_{Z_{error}}$) be much less than the nuclear interaction rate (P_{int}) in a single detector element. ($R = P_{Z_{err}}/P_{int} << 1$). Table 1 shows values of the ratio R for detectors 3 mm thick and for a fragment interaction length $\lambda = 10$ cm.

Table 1

Charge resolution σ_Z	Error ratio R
0.3e	3.2
0.25e	1.5
0.2e	0.4
0.15e	0.03

From Table 1 it is clear that the charge resolution must be $\sigma_Z \lesssim 0.15e$ in order to have acceptably small misidentification rates.

Figure 1 provides an illustration of the main detector components. Two wire chambers, WC1 and WC2, are located in front of the Cerenkov stack. These wire chambers determine the position of the beam particle as it enters the stack, and allow us to correct for spatial variations in the response of

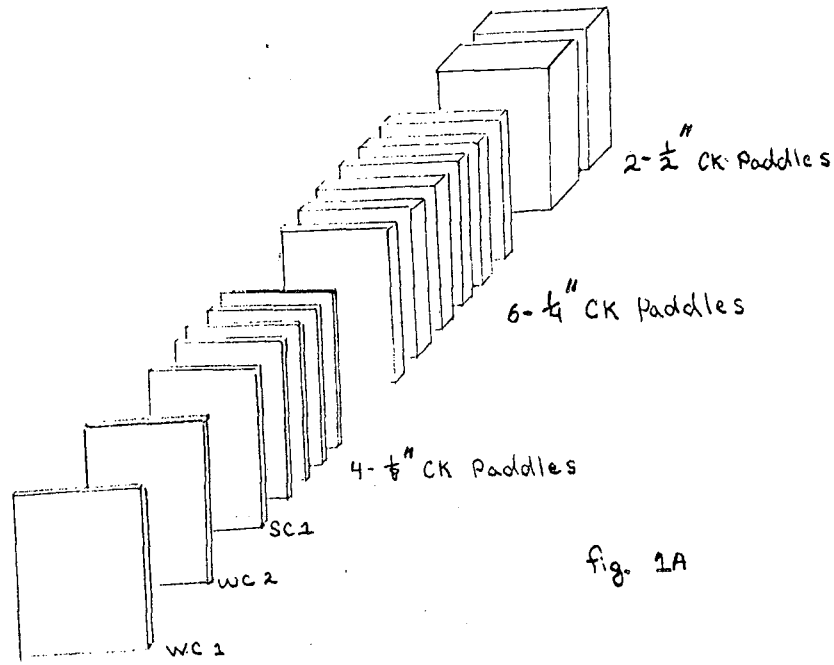

fig. 1A

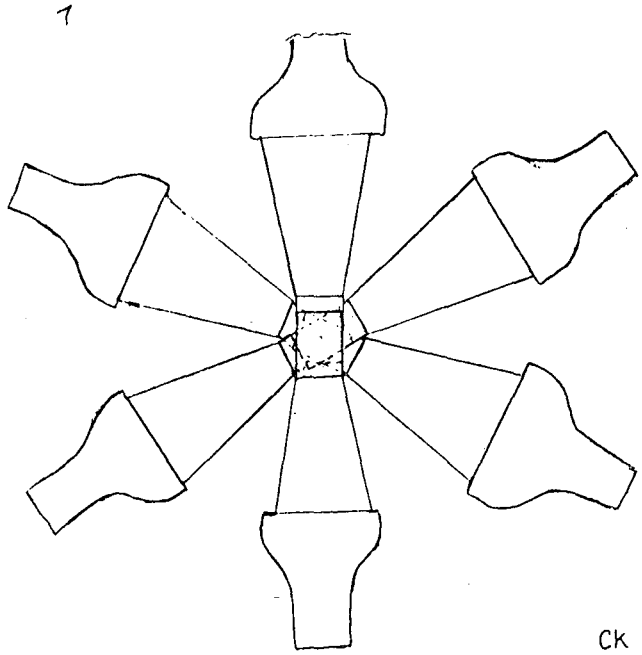

fig 1B
CK Stack front view
(Six paddles hidden)

the Cerenkov paddles. A scintillator paddle, S1, located directly in front of the stack, provides a means of discriminating against particles which have fragmented before entering the first Cerenkov paddle. The Cerenkov stack itself consists of twelve paddles, the first four of which are 1/8" (3 mm) thick, the next six 1/4" (6 mm) thick, and the last two 1/2" (1.2 cm) thick. This configuration represents the minimum necessary to achieve both reasonable position resolution for short mean free paths and sufficient total detector thickness to allow measurement of mean free paths outside the

anomalous region.

The response variation due to photon counting statistics can be determined by measuring the response of the Cerenkov paddles to cosmic ray muons. This has been done for both the 1/8" and 1/4" paddles. The results of these tests indicate that:

$$\sigma_{pe} = (0.30 \pm 0.02)/Z \text{ for the 1/8" paddle}$$
$$(0.20 \pm 0.02)/Z \text{ for the 1/4" paddle}$$

For Z = 18, σ_{pe} = 1.7% for the 1/8" paddle, corresponding to a charge resolution of 0.15e from photoelectron statistics. In order to achieve this resolution in practice, the contribution from spatial variations in detector response must be kept at the 1% level. We have measured the position resolution of our wire chambers and have found it to be ~2 mm, so that the contribution to σ_Z from spatial mapping uncertainties is determined by the characteristic response variations on this scale. We have measured the response map of one of the 1/8" paddles using a 5 MeV Ru β source. We found the maximum response gradient to be <0.5%/mm in the central one square inch of the detector. The charge resolution of the 1/8" and 1/4" paddles should, therefore, be photostatistics limited, while the 1/2" paddles are limited by mapping uncertainties. The charge resolution of the three paddle types based upon the above analysis is:

σ_Z =	0.16e	1/8" paddle
	0.12e	1/4" paddle
	0.11e	1/2" paddle

In conclusion, we have developed and tested a Cerenkov stack detector with the necessary charge and spatial resolution to study the "anomalon" phenomenon. The spacing between paddles can be readily changed to study lifetime of anomalons.

ACTIVE MULTITARGET EXPERIMENT FOR ANOMALONS

M. Enorini, F. L. Fabbri and A. Zallo
INFN, Laboratori Nazionali di Frascati
00044 Frascati, Italy

Anomalons are in fashion despite of their ancient first appearence in photographic emulsions exposed to cosmic rays(1). As matter of fact anomalons do not fit in any conventional picture of nuclear and particle physics. Until now anomalons have been studied in emulsions by exposures at cosmic rays or, more recently, at relativistic ion beams(2, 3, 4). This technique provide an excellent spatial resolution, but does not allow to clarify the behaviour of anomalous fragments in vacuum (or air) and is very poor in statistics and lacking in oriented triggers. Only the counter experiments technique can provide the necessary statistics and investigate if anomalons are spontaneously decaying. We propose to use subsequent active targets in order to trigger on reinteraction of produced fragments. The experimental methods takes advantages from the peculiar feature of anomalons and from their enhanced cross section. The presence of anomalons among the fragments originates an overproduction of secondary interactions. Therefore triggering on successive interactions of the fragments is, straightforward, the best method to evidenciate the existence of anomalons and to improve the selectivity of an experiment. The comparation of the rates of the secondary interactions is directly correlated with the fraction of anomalous fragments, their cross section and the "memory" effect(5).

The use of the silicon solid state detectors as active target, as well as, tracking and charge detectors for the emitted fragments seems appropriate. Solid state detectors have been widely used in the last years. Great technical developments, made possible the building of very thin and large area detectors and their associated fast electronics, have made these detectors a major instrument in high energy physics(6). The assembly of thin silicon devices as multilayer target made them well suited for studying decaying particles such as D-mesons(7). The development of thin strip electrodes and the possibility of operating these detectors as fine grained proportional chambers, the so called microstrip detectors, can provide a spatial resolution until 10 μm(6).

The experimental apparatus is composec by three identical silicon solid state targets, (C_1 C_2 C_3), 2 mm thick, whose relative distances can be con-

tinously varied from ~1 cm to ~15 cm (Fig. 1). An assembly of microstrip chambers M is located after each target to detect the emitted fragments and to measure their charges. Each M telescope is composed by 6 planes (x, y, w coordinates) with 100 μm pitch. The area of the counters is about 4x4 cm^2 and the ion beam is sent on C_1 on a 3x3 mm^2 spot. The electrodes of C_2 and C_3 are shaped in convenient circular areas helping in the reconstruction of the interaction point on the targets. The geometrical acceptance is about $\pm$50 mrad until the third target. The signal of interaction on C_1 is performed comparing the released energy with the expected energy loss of the incident ion. The microstrips are equipped with analogical-digital converter read-out in order to measure the charge of the fragments. In the acquisition logic a constant multiplicity on the six planes of each M telescope, and a multiplicity step between successive telescopes, is required.

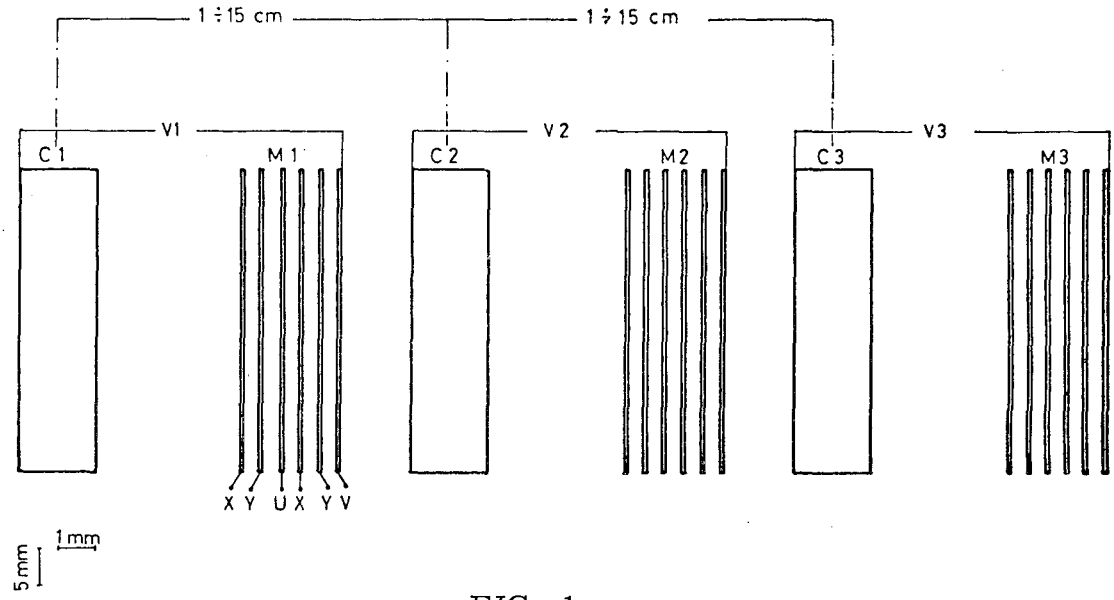

FIG. 1

The sensitivity of this apparatus selecting secondary interactions is much greater than inclusive counting experiment based on fragments reabsorption on the target itself or separate absorber[8, 9]. In fact in these cases the absorption of fragments due to enhanced anomalons cross section, has to be evidenciated in the inclusive flux of the first interaction (no anomalons contribute) and of the secondaries, with relative poor statistics relevance. Moreover no way exists by these methods to select samples of events with increased anomalons presence for deeper analysis. Similar criticism can be applied to the experiments in which an absorber is placed between target and counter[8, 9]. The use of active targets triggerable on interaction, could permit to separate the sample of the secondary interactions where the anomalous effect is operating. If we are able to select the interactions of the fragments of the first and second generation, the excess of interactions due to the anomalon presence is of the order of $f \cdot a$ and $f \cdot a \cdot (fa+2)$ respectively,

where f represents the fraction of anomalons among the fragments, and a is the enhancement of the anomalon cross section respect to the ordinary one. For example, under the condition of 6% of anomalous fragments and a cross section 10 times the geometrical one, we expect an excess of the three successive interactions about 120% of the expected rate for ordinary ions.

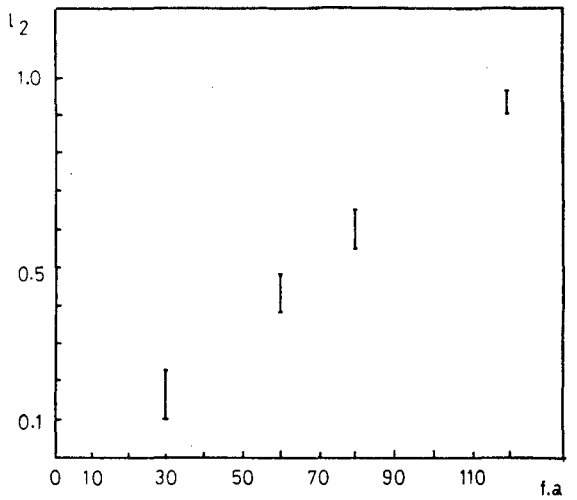

FIG. 2

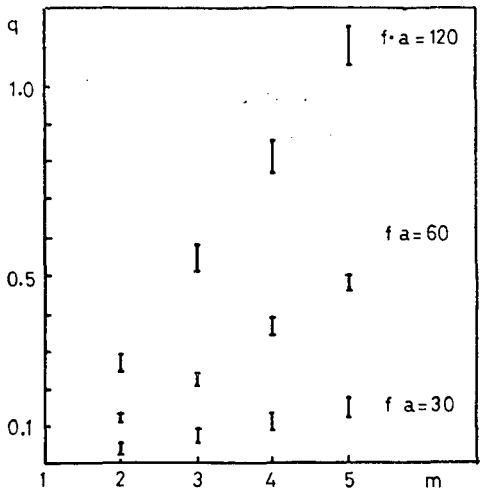

FIG. 3

For N_0 incident ions we evaluated the proper number of interactions on C_1 (N_1), on C_2 originated by a fragment (N_2), and on C_3 originated by a fragment created on C_2 (N_3), taking into account the reabsorption effect on the targets. We report in Figs. 2 and 3 the quantities:

$$L_2 = \left(\frac{N_2}{N_1} - \frac{N_1}{N_0}\right) \Big/ \frac{N_1}{N_0}, \qquad Q = \left(\frac{N_3}{N_1} - \left(\frac{N_2}{N_1}\right)^2\right) \Big/ \left(\frac{N_2}{N_1}\right)^2$$

versus f·a and m, which parametrize the eventual memory effect (m is the ratio between the percentage of anomalons among the fragments emitted by an interacting anomalon and f: m = 1 means no memory effect). Changing the distances between the targets we are able to investigate id the anomalons are stable (Fig. 4). In conclusion the proposed apparatus seems appropriate to investigate both the existence of anomalons and their behaviour. It provides also a way to study the anomalon production and interaction. In fact, if we consider the three generation events and we lock at the interactions on C_1 and C_2, in the case of f = 6% and a = 10 about 50% of the interaction stars are generated by an anomalon instead of the 6% if a non selected sampling of interactions is considered. In this way a study of the Z-distribution of the interacting fragments, on these events, could emphasize favorite Z channels for the anomalon production. The apparatus can also provide the topological configurations of these selected events. Some preliminary data on emulsions seem to indicate a forward-backward asymmetry in the stars originated by anomalons[10], however these result are not conclusive because of poor

statistics.

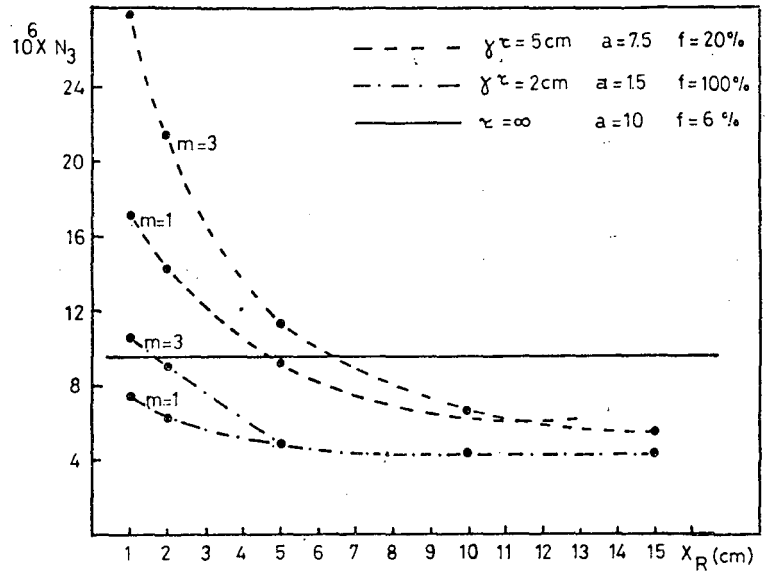

FIG. 4

The momentum distribution of fragments produced by fragmentation of a heavy ion beam, have been investigated in the range of 1-2 GeV/nucleon[11]. The analysis of the selected events, could permit a glimps into the dinamics involved in interactions of an anomalon projectile and the eventual deviations of the fragment momentum distribution from the ordinary one.

(1) A. Milone, Nuovo Cimento Supp. 12, 353 (1954).
(2) E. M. Friedlander et al., Phys. Rev. Letters 45, 1084 (1980).
(3) P. L. Jain and G. Das, Phys. Rev. Letters 48, 305 (1982).
(4) H. B. Barber et al., Phys. Rev. Letters 48, 856 (1982).
(5) E. M. Friedlander et al., LBL preprint 10573.
(6) P. G. Rancoita and A. Seidman, Riv. Nuovo Cimento n. 7 (1982).
(7) E. Albini et al., Phys. Letters 110B, 339 (1982); G. Bellini et al., Phys. Reports 83, n. 1 (1982).
(8) R. D. Amado and A. Dar, Phys. Rev. C27, 1325 (1983).
(9) J. Y. Grossiard, exp. n. 100, Lab. Nat. Saturne (1982).
(10) R. Klein and E. Ganssauge, Fachberiech. Phys. Phillips-Univ. preprint (1982).
(11) D. E. Greiner et al., Phys. Rev. Letters 35, 152 (1975).

χ^2 Analyses of Nuclear Emulsion Anomalous Projectile Fragment Data

Malcolm H. Mac Gregor

Lawrence Livermore National Laboratory
Livermore, California 94550

In a previous paper[1], χ^2 least-squares fits to emulsion data[2-5] were used to demonstrate the existence of a Z-dependence in anomalous projectile fragment (APF) mean free paths (MFP's). In the present paper[6], this work is extended by (a) using some Z-separated data, and (b) applying various isotopic corrections to the "normal" beam projectile MFP's. With a combined Buffalo, LBL, Minnesota, NRC data base, the null hypothesis (no APF effect) is rejected by more than 7 standard deviations.

Nuclear emulsion APF data have been published by the Buffalo[2], LBL-NRC[3] and Minnesota[5] groups. In addition, the LBL and NRC data are available in Z-separated form[7,8]. These data exist in two general representations: Type C data (charge-dependent representation), and Type D data (distance-dependent path length representation).[9] For the present studies, the following combined data bases were set up: CZ = Z-separated LBL and NRC data plus Buffalo and Minnesota data[10]; C = Z-grouped LBL, NRC, Buffalo and Minnesota data[11]; D = LBL + NRC, Buffalo, and Minnesota path-length data[12]. In addition, three different isotopic corrections were applied to the incident projectile beam MFP's: I = straight-line extrapolation from measured ^{6}Li values[13] to standard Z = 8 values; II = asymptotic (D > 2.5 cm) LBL and NRC values for Z = 3-5 and Z = 6-8; III = asymptotic (D > 2.5 cm) LBL, NRC, and Buffalo values for Z = 3-8.

Least-squares fits to the data were made using the parameters $(\bar{\lambda},f,\beta)$ for the APF's, where

$$\lambda(Z) = \lambda_o(2Z)^{-\beta} \tag{1}$$

denotes the APF Z-dependence, f is the APF fraction, and $\bar{\lambda}$ is the average value of $\lambda(Z)$ over the Z-range in question. Figure 1 shows the Z = 3 - 8 χ^2 solution regions for the CZ data[10], using $\beta = 0$ in Eq. 1, and using beam isotope corrections I, II, and III. Since we have no accurate method for choosing among these solutions at present, the different contours represent our uncertainty in determining the APF parameters for the Z = 3 - 8 data (where beam isotope corrections are most important). It should be noted here that all three contours shown in Fig. 1 rule against the null hypothesis for the Z = 3 - 8 charge region (by 3 1/2

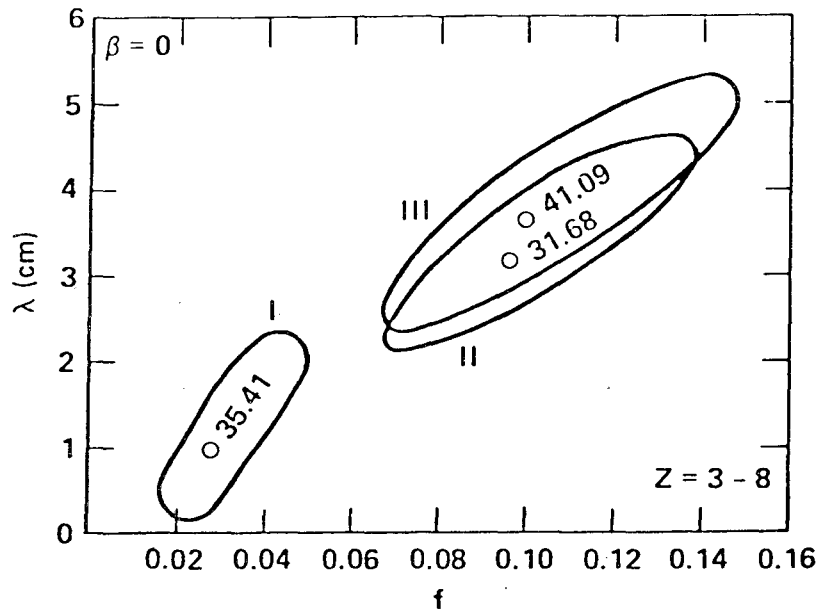

Figure 1. χ^2 contours for the Z = 3 - 8 charge range, using the CZ combined data set with $\beta = 0$ in Eq. 1, and applying beam isotope corrections I, II, and III. Correction II gives the smallest χ^2 sum, but we have no accurate method for choosing among these corrections.

standard deviations or more), which is sufficient to rule out the quasimolecular model of Bayman et al.[14]

Figure 2 shows the χ^2 solution regions for the CZ (left)[10] and C (right)[11] Z = 3 - 26 data, using beam isotope correction I, and using the values $\beta = 0$, 0.5, and 1 for the APF Z-dependence in Eq. 1. As can be seen, the $\beta = 0.5$ and $\beta = 1$ solutions have significantly smaller χ^2 sums than the $\beta = 0$ solutions, thus indicating that the APF's have Z-dependent MFP's. However, the data are not yet accurate enough to enable us to pin down a precise value for β. The null hypothesis (f = 0) is rejected for these solutions by 7 1/2 standard deviations.

Figure 3 gives a χ^2 contour map for the $\beta = 0$, beam isotope correction I, least squares fit to the D data set[12]. As can be seen by this map, the null effect for this solution is also rejected by 7 1/2 standard deviations.

This work was performed under the auspices of the U. S. Department of Energy by the Lawrence Livermore National Laboratory under contract number W-7405-ENG-48.

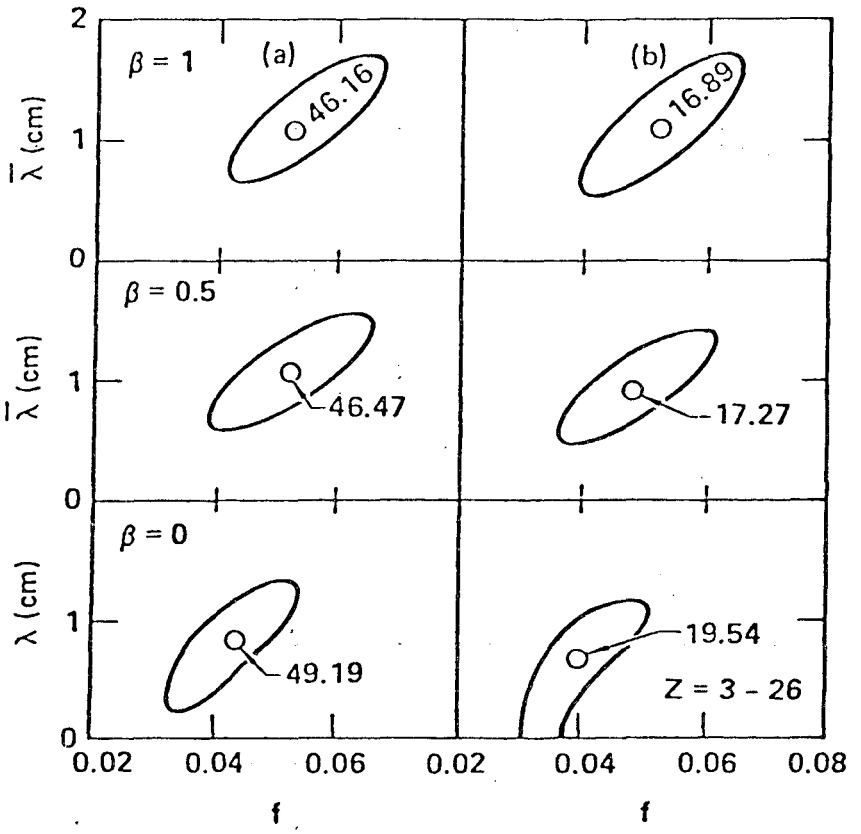

Figure 2. χ^2 contours for the Z = 3 - 26 charge range, using data sets CZ (left) and C (right) with beam isotope correction I. The decrease in χ^2 with increasing β indicates that the APF's have Z-dependent MFP's.

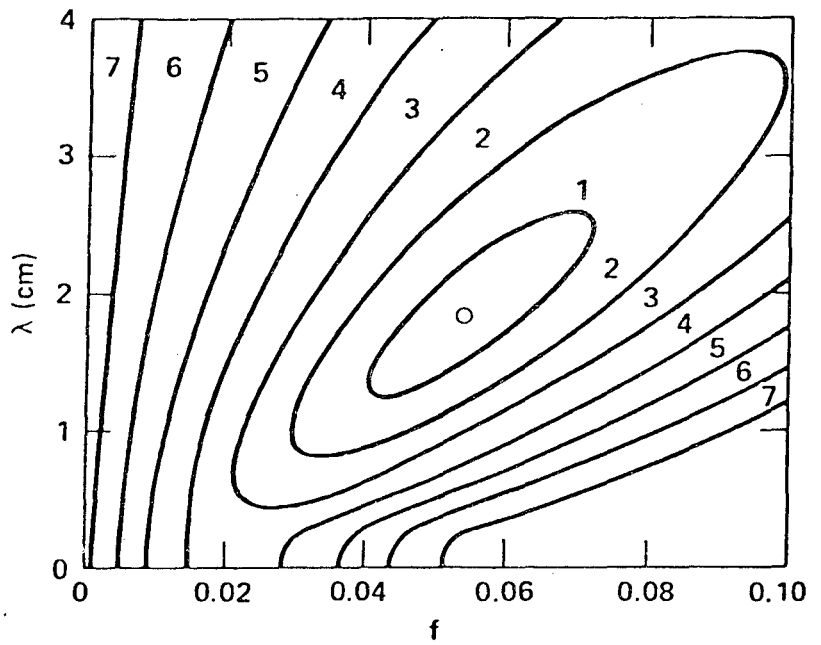

Figure 3. A χ^2 contour map for data set D. The 1,2,3,4,5,6,7 contours correspond to $\Delta\chi^2$ = +1,4,9,16,25,36,49. The null hypothesis (f = 0) is rejected by about 7 1/2 standard deviations.

References.

(1) M. H. Mac Gregor, Phys. Rev. Lett. 49, 1815 (1982).

(2) P. Jain and G. Das, Phys. Rev. Lett. 48, 305 (1982).

(3) E. M. Friedlander, R. W. Gimpel, H. H. Heckman, Y. J. Karant, B. Judek, and E. Ganssauge, Phys. Rev. Lett. 45, 1084 (1980).

(4) E. M. Friedlander, R. W. Gimpel, H. H. Heckman, Y. J. Karant, B. Judek, and E. Ganssauge, Phys. Rev. C27, 1489 (1983).

(5) H. B. Barber, P. S. Freier, and C. J. Waddington, Phys. Rev. Lett. 48, 856 (1982).

(6) M. H. Mac Gregor, Phys. Rev. C (in press).

(7) See Table III in Ref. 4.

(8) B. Judek, private communication. The Z-separated NRC data are available in sixteen pathlength bins, but were regrouped into four pathlength bins to minimize the statistical uncertainties (see Ref. 6).

(9) The data sets denoted here as Type C and Type D data were referred to as Type A and Type B data in Ref. 1.

(10) Data set CZ = NRC Z-separated data (Ref. 8) plus LBL Z-separated Z = 3 - 8 data (Ref. 7) plus LBL Z = 9 - 16 Table I data (Ref. 3) plus Buffalo Table I data (Ref. 2) plus Minnesota Fig. 1 data (Ref. 5).

(11) Data set C = LBL + NRC Table I data (Ref. 3) plus Buffalo Table I data (Ref. 2) plus Minnesota Fig. 1 data (Ref. 5).

(12) Data set D = LBL + NRC Fig. 1 data (Ref. 3) plus Buffalo Fig. 2(a) data (Ref. 2) plus Minnesota Fig. 2 (upper left) data (Ref. 5).

(13) The ^{6}Li incident-beam MFP's used for Isotope Correction I were 14.1 cm for the NRC data and 14.5 cm for the LBL data.

(14) B. F. Bayman, P. J. Ellis, and Y. C. Tang, Phys. Rev. Lett. 49, 532 (1982). See Y. J. Karant and M. H. Mac Gregor, Phys. Rev. Lett. 50, 215 (1983); and B. F. Bayman, P. J. Ellis, and Y. C. Tang, Phys. Rev. 50, 216 (1983).

SESSION II: ANOMALONS—THEORETICAL

IS THE ANOMALON A DINOTOR?

Leonardo Castillejo,
University College London, England

A.S. Goldhaber and A.D. Jackson,
State University of New York at Stony Brook,
NY 11974, U.S.A.

M.B. Johnson,
LAMPF, Los Alamos, NM 87544U.S.A.

Abstract

A model is proposed to explain the anomalous fragments in high energy heavy ion collisions. It consists of a large toroidal bag containing a Fermi sea of quarks confiend by the M.I.T. bag boundary condition. Its shape, stability and lifetime are discussed as are the effects of one gluon exchange in determining the internal quark wave functions.

Introduction

The following salient features have been suggested as characterising the production and interaction of anomalons [1].

a) They are copiously produced, about 5% of fragments could be anomalons,

b) They have long lifetimes $\gtrsim 10^{-10}$ sec.,

c) They have large cross sections for interaction on other nuclei,

d) They are robust, ie they tend to survive collisions.

It is very hard to explain all these features in terms of normal nuclear matter. The phase space requirements of (a) and (b) seem incompatible. To produce anomalons copiously requires them to come from a large region of phase space, while their long lifetimes demands a small phase space region through which they decay. Their large cross-section, (b), can only come about if the nuclear matter of which they are composed is rather diffuse. It is hard to reconcile such a diffuse system with robustness under collisions.

We avoid such contradictions by proposing a model in which normal nuclear matter undergoing high energy collisions creates an abnormal form of quark matter. This quark matter, once it has cooled down, is relatively stable and robust. The production and decay processes have thus been uncoupled and no inherent contradiction remains. The large cross-section for collisions of the anomalous fragments and their robustness would come from the geometrical size and shape of the quark matter. The explicit model we explore is one where the quarks are confined in a large bag of the M.I.T. type [2] and of toroidal shape [3]. This large filled torus we call a dinotor because of its shape and size and perhaps to remind us that the phenomena it is designed to explain may be mythical like the minotor or, like the dinosaur, may disappear.

Calculations of such models will be unreliable, and in particular the very complicated process of formation would be hard to explain in detail. We might envision it as in fig. (1).

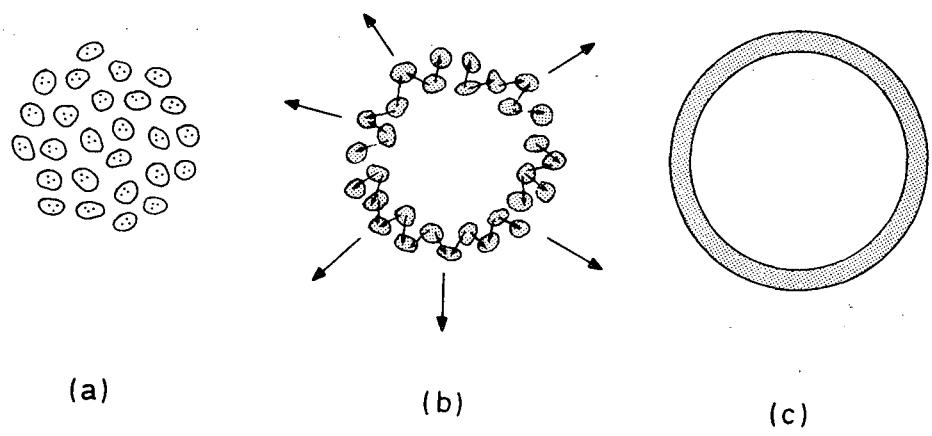

Fig. 1

Initially the nucleus consists of an aglomeration of small bags, each containing 3 quarks in a colour singlet, loosely held together by the pionic degrees of freedom. As the nuclei come together in a head-on collision one nucleus could pass right through the centre of the other, like coring an apple, and would push all the small nucleon bags into a ring-shaped distribution slightly compressed and with individual bags close enough together for them to merge and the quark to move freely from one bag to another. Such a ring would expand rather like a smoke ring and cool down, and there could be a relatively large probability that enough bags had merged to form one continuous toroidal bag containing a large proportion of the quarks. These quarks would no longer be in localised colour singlets of three quarks but each quark spread out uniformly round the torus. During the cooling process the dinotor would emit pions and perhaps a few nucleons would boil off. Such a dinotor could prove stable with a lifetime longer than 10^{-10} sec., the main decay process being one of nucleon "drip" which I shall describe later.

Such a production scenario is clearly too complicated to quantify, but it has the four main features postulated earlier. The production mechanism depends on the geometry and nature of nuclei while the decay of the dinotor depends on the quarks being able to "get their colour together" to escape as nucleons. Furthermore large nuclear densities do not seem necessary since the quark density of the dinotor only slightly exceeds that of nuclear matter. The dimension of the dinotor - a tube about one nucleon thick full of quarks - provides its large cross-section. The choice of a torus for our model rather than a long straight tube is because there are additional mechanisms for increased stability. Circulation of colour currents or coloured magnetic fields can occur within the torus, and also of electric currents which could produce a large magnetic field through the hole of the torus. Such currents could also produce electromagnetic radiation and provide rapid decay to the ground state.

Cross-section of scattering

The dinotor provides a simple geometrical explanation of the large cross-section of anomalons on nuclei. As illustrated in fig. (2) we can compare the

cross-section σ_{ds} for dinotor on nucleus with that of one spherical nucleus on another, σ_{ss}. Suppose a spherical nucleus of atomic number A scatters on another of atomic number A^1. The geometrical cross-section will be

$$\sigma_{ss} = \pi r_0^2 (A^{1/3} + A^{1\,1/3})^2$$

while that of the dinotor of atomic number A and radius a colliding with the nucleus A^1 will be

$$\sigma_{ds} = \left[\frac{1}{2}(1+\frac{1}{\pi})\right] \left(\frac{4}{3}\frac{r_0^3}{a^2} A\right) (4r_0 A^{1\,1/3})$$

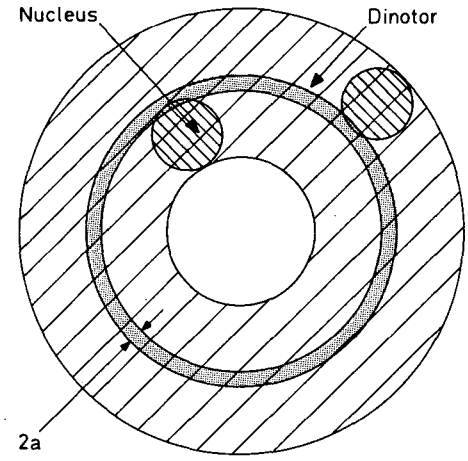

Fig. 2

where the first factor is a crude average over dinotor orientation, the second is the length of the dinotor, assuming it has nuclear density, and the third is twice the diameter of the A^1 nucleus. As an example, A = 64, A^1 = 27 gives $\frac{\sigma_{ds}}{\sigma_{ss}} = 4.4$ if $a = r_0$. So the increased cross-sections are about right.

In such collisions the dinotor would only be struck locally, but since all the quarks are spread uniformly throughout the dinotor the collision is likely to deposit energy among many quarks and this could then be slowly evaporated, rather than destroying the dinotor completely. Furthermore coloured magnetic fields circulating within the dinotor, as suggested by some models, would provide robustness; when a piece is knocked out of the dinotor the broken ends like to join up again to preserve the colour magnetic flux.

Properties of the dinotor

The process of dinotor formation and its collision are too complicated to calculate in detail but there are three properties which must be verified before the model can be taken seriously:

(i) The existence of a local minimum in the energy of quark matter with toroidal geometry.

(ii) The size and density of the dinotor; if the density is too large it is unlikely to be formed.

(iii) The lifetime of the dinotor due to nucleaon "drip" which must exceed 10^{-10} sec.

The first two requirements follow simply by exploring the energy as a function of size and shape parameters, the third requires an estimate of the tunnelling of three quarks out of a dinotor to form a nucleon. These features are insensitive to interactions between the quarks. There is another aspect which is also important but can be less reliably calculated.

(iv) The quark wave functions; these can involve spin-colour correlations within the dinotor.

The quark-quark interaction is now important and a one-gluon exchange model provides a suggestive guide. It is possible that the quarks in the dinotor are not locally in colour singlets. Thus collisions with a fast hadron would effectively provide a non-singlet colour target.

Geometric Size and Stability

The size, thickness and stability of the dinotor is determined by a balance between the bag pressure B and the kinetic energy of the quarks. Quark interactions make only a minor contribution. We shall neglect completely the effects of centre of mass motion which are so necessary to get good fits to the hadron masses in the M.I.T. bag model, and concentrate on the question of stability. Since toroidal coordinates are unpleasant we note that the energy of the dinotor is not much altered if it is replaced by a long straight cylindrical bag of the same radius a and total length L as the torus. The M.I.T. boundary conditions for the quarks will apply on the cylindrical surface and periodic boundary conditions at the ends, because in the dinotor they would be joined up. This "straightening out" of the torus is estimated to have a small effect on the kinetic energy of the quarks.

We now fill the cylinder with a Hartree-Fock wave function of quarks. That is an antisymmetrical product of single particle wave functions ψ_k, which because of the periodic boundary condition must be eigenstates of the momentum.

with eigenvalue k, in the z direction, ie along the cylinder. The possible radial wave functions $\psi_{k=o}(b,\phi)$ correspond to states of definite z component of angular momentum s, and of parity. The mass m of the quarks due to transverse confinement is determined by the M.I.T. bag condition:

$$J_{s-\frac{1}{2}}(ma) = \pm J_{s+\frac{1}{2}}(ma)$$

These Bessel functions are sketched in fig. (3). For angular momentum $s = \frac{1}{2}$ $J_0(mb)$ is the radial wave function of the large components and $J_1(mb)$ of the small components of the Dirac spinor. The total wavefunction curvature needed for confinement is shared between the large and small components to produce an anomalously small mass for the $s = \pm \frac{1}{2}$ states. Fig. (4) represents the low-lying radial energy levels, together with the Fermi sea of longditudinal momenta which correspond to the occupied states within the dinotor.

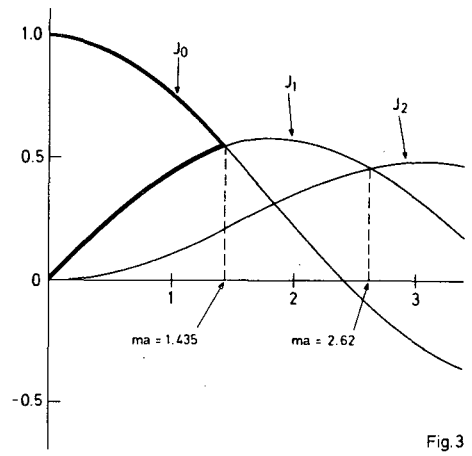

Fig.3

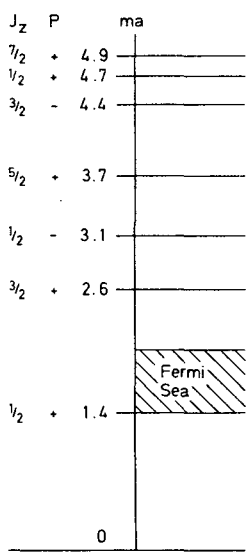

Fig.4

The top of the Fermi sea is well below the next radial excitation, and we can safely neglect all but the lowest $s = \pm \frac{1}{2}$ states. Henceforth we shall refer to these as "spins".

The colour-spin-flavour composition of this Fermi sea will be determined by quark-quark interactions arising from gluon exchange. There are two rather different possibilities. In the first, each momentum state contains 12 quarks - 3 colours, 2 spins, 2 flavours. In the second, the quark gluon interaction

favours having only one Fermi sea with 6 quarks in each momentum state - 3 colours, 2 flavours. Each quark colour has a definite spin. This is not locally a colour singlet, but of course the dinotor as a whole will be a singlet.

To illustrate the stability condition consider a non-relativistic approximation, which is quite good, for 6 quarks in each of N momentum states. Then

$$\frac{E}{N} = 6m + 6\frac{k_F^2}{6} - \frac{e^2}{\pi} k_F V + B\pi a^2 L$$

The terms correspond to mass, kinetic energy, gluon interaction and bag energy with $k_F = \frac{\pi N}{L}$ the Fermi momentum. V is the effective interaction between quarks. Minimizing this with respect to the radius a and $k_F a$ we get a unique local minimum with

$$a^4 = \frac{1}{B}\left(\frac{ma}{\pi}\right) 2\left(\frac{6}{5}\right)^{3/2} \left[(1-\beta^2)\left(\beta + \sqrt{1+\beta^2}\right) - \tfrac{1}{2}\beta\right]$$

$$k_F = \frac{1}{a}(ma)\frac{6}{5}\left[\beta + \sqrt{1+\beta^2}\right]$$

$$\frac{E}{N} = \frac{1}{a}\frac{48}{5}(ma)\left[1 - \tfrac{1}{2}\beta\left(\beta + \sqrt{1+\beta^2}\right)\right]$$

where $ma = 1.435$ and $\beta = \frac{e^2 V}{\pi\sqrt{30}}$. The factors in square brackets are the corrections induced by the quark gluon interaction and for most interactions $\beta < 0.3$. The results scale, in the sense that if the numbers of quarks in each momentum state is doubled from 6 to 12 but the total number $3A$ is kept constant then E/A and k_F decrease by a factor $2^{1/4}$ and the radius a and density ρ increase by the same factor. The bag constant B sets the dimensional scale. The β coefficients from gluon exchange will also change because of the different spin structure of the state, and the choice of which type of Fermi sea belongs to the ground state is determined by competition between these two effects. The β terms are too small to prevent a local energy minimum. Including relativistic kinematics and the momentum dependence of V alters numbers slightly but has no qualitative effect.

In Table (1) some typical data is provided both for 6 quarks and 12 quarks per momentum state. Energies are given per "Nucleon", or 3 quarks. It should be noted that a quark density ρ of about 0.6 fm.$^{-3}$ per quark corresponds to a nucleon density of 0.2 fm.$^{-3}$ which is only slightly higher than nuclear matter density of 0.17 fm.$^{-3}$. Furthermore the equilibrium energy in the dinotor is only 4% higher than the absolute minimum corresponding to the quarks in a large spherical bag.

It is thus clear that there is a local minimum of the energy of the system for a long cylindrical shape which is very stable against changes in the details of the calculation. In all cases the Fermi momenta are well below those which would lead to coupling to other angular momentum or parity states. The model is in some sense robust and depends essentially only on the use of the M.I.T. bag boundary condition for the quarks.

Stability to Nucleon Drip

Is the dinotor a fairly stable object or will it rapidly break up into separate nucleons? There are several forms of decay one can imagine:
(i) Large-scale changes in the parameter, length and radius of the dinotor so that it moves into the deeper minimum corresponding to a spherical bag. Since all the quarks must take part this is very improbable. (ii) A local deformation starts on the surface of the dinotor, say a small bulge containing 3 quarks, which then detaches itself from the dinotor forming a separate bag. This can be thought of as the dinotor "dripping" nucleons. To calculate this properly we would need to know the dynamics of the bag surface, which is poorly understood. We make a simpler model which retains the essential features. I will illustrate this with non-relativistic Schroedinger quarks rather than Dirac ones to simplify the argument but the calculation works just as well relativistically.

In fig. (5a) I have sketched a Fermi sea consisting of momentum states ψ_k with $|k| < k_F$. But instead of single particle states ψ_k, linear combination may equally well be chosen, which are as localised as possible, rather like atomic or molecular orbitals, as in fig. (5b). But even these have a trailing part of their wave function which is spread throughout the whole bag. Before these localised quarks can leave to form their own bag they have to collect up their trailing coloured skirts, since ψ is strictly equal to zero outside the bag. If we calculate this energy adiabatically we have a barrier to nucleon drip and can calculate the probability for the nucleon to tunnel through. To be specific consider the wave function of fig. (5c) which is strictly confined within a distance s

$$\psi_s(z) = \sqrt{\frac{2}{s}} \cos(k_s z)\, \theta(z^2 - s^2)$$

with

$$E(s) = \frac{k_s^2}{2m}, \quad k_s = \frac{\pi}{s}$$

Expand this in terms of the momentum eigenstates of the cylinder of length L

$$\psi_s(z) = \sum_{n=o}^{\infty} \alpha_n \phi_n^{(2)}$$

where $\phi_n(z) = \sqrt{\frac{2}{L}} \cos(k_n z)$ and $k_n = \frac{2\pi}{L} n$.

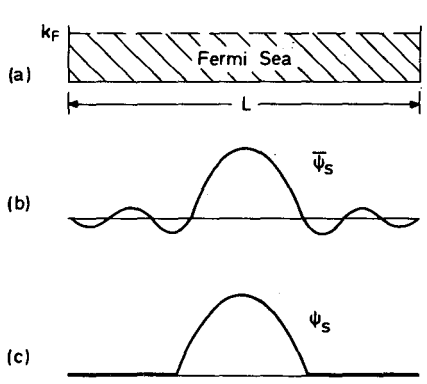

Fig. 5

Now compare this with the localised single particle wave function which most closely resembles ψ_s

$$\bar{\psi}_s(z) = \frac{1}{B} \sum_{n=o}^{N} \alpha_n \phi_n(z) \quad \text{with}$$

$k_F = \frac{\pi}{L} N$ the sum extends only over occupied states and B is a normalizing factor. Its energy will be

$$\bar{E}_s = \frac{1}{B^2} \sum_{n=o}^{N} |\alpha_n|^2 \frac{k_n^2}{2m}$$

Then

$$\Delta E(s) = E_s - \bar{E}_s$$

is the energy a quark needs to collect its colour adiabatically into a region of length S.

A plot of $\Delta E(s)$ is given in fig. (6) for this simple model. On the same plot are some estimates of the energy of a nucleon in a bag when it is "stretched out" to a length s, and its minimum shifted relative to the dinotor by 0, 100, 200 Mev. These absolute energy shifts are too hard to calculate reliably. Now we have a barrier for the nucleon to tunnel through with transmission coefficient

$$T = \exp\left[-6 \int_{s_0}^{\infty} \sqrt{2m\,\Delta E(s)}\, ds\right]$$

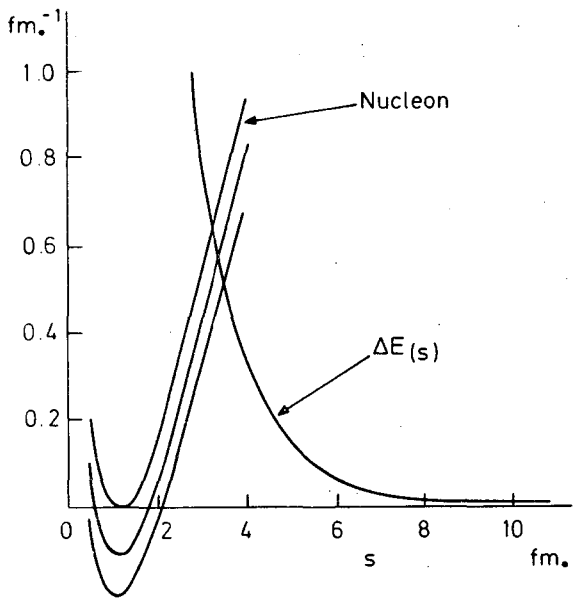

Fig. 6

The mass in this formula has been rather arbitrarily chosen as the transverse quark mass and the factor 6 allows for three quarks to tunnel out. For the three cases considered above the transmission coefficient is

$$T = \begin{cases} 7 \times 10^{-14} \\ 9 \times 10^{-13} \\ 6 \times 10^{-12} \end{cases}$$

This suggests that the lifetime for nucleon drip is greater than 10^{-10}sec. Using relativistic wave functions and including interaction terms makes the whole calculation substantially more complicated and introduces more specific model dependence but does not alter the conclusions.

Quark Wave Functions

The colour-spin content of the quark wave function in the dinotor will be determined by their interactions. If we limit ourselves to one gluon exchange the three graphs of fig.(7) contribute. The self-energy graph has the usual divergences which I would rather not have to calculate. The exchange term exactly cancels that part of the self energy in which the virtual quark of momentum k_s in fig. (7c) is in an occupied level. Two approaches have been followed:

(i) Assuming the self energy is characterless, that is the quarks all get a similar small mass independent of their spin orientations. Then take the direct, fig. (7a), and exchange (7b) diagrams to determine the wave functions. This is the procedure that Jackson and I have followed.

(ii) Relying on the cancellation of the exchange graph with some of the self-energy diagrams, Goldhaber and Johnson include an estimate of the remainder of the self energy by taking a cut-off on the momentum k_s below the excitation of the next radial mode, in the expectation that if wisely chosen the results will not be sensitive to this cut-off.

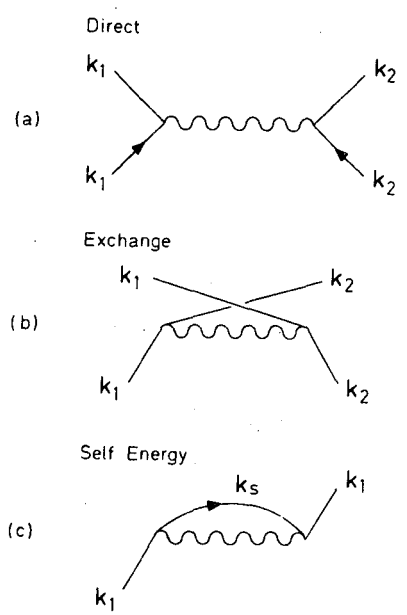

Fig. 7

There is another problem in the calculation. For an infinitely long cylinder the Coulombic exchange interactions have an infrared singularity. This can easily be avoided in the direct term by choosing wave functions which are on the average colour neutral, but it still persists in the exchange and self-energy terms. There are many phenomena which will correct this. For instance, screening of the interaction between two quarks by the intervening Fermi sea. The gluon-gluon interaction also provides a mass for

some of the gluons since they propagate in the presence of an average static gluon field within the bag. All these are strictly higher order effects. Goldhaber and Johnson take some of them into account while Jackson and I have just given the Coulombic gluon a mass comparable to the quark transverse mass and explored the effect of this additional parameter.

The procedure is then straightforward. We parametrise the colour-spin-flavour of the momentum wave functions as generally as possible, consistent with their being Hartree Fock wave functions, evaluate the interaction energy, both direct and exchange, add the kinetic and bag energies and minimize the total with respect to the colour-spin content of the wave functions as well as the bag radius and Fermi momentum. The effects of this procedure on the bag shape are small but the type of wave function can vary dramatically. I shall outline here only the qualitative features.

(a) Direct Interaction terms only:

Several very different configurations have energies which are extremely close to each other so that other effects, not considered here, would dictate the precise form of the ground state. When there are only 6 quarks per momentum state (3 colours - 2 flavours) typical wave functions are:

(i) All quark spins point along the 2 axis but two of the colours have $s = +\frac{1}{2}$ and the third $s = -\frac{1}{2}$. There is a colour current circulating in the $\hat{\underline{\phi}}$ direction within the cylinder and a static magnetic gluon field of λ^8 type along the z direction within the cylinder. In the case of the dinotor this magnetic flux would flow continuously round inside the torus.

(ii) The three colours have "spins" pointing perpendicular to the cylinder axis and 120° apart. The flow of colour current and colour magnetic field is interchanged compared to (i).

(iii) Variants of (i) and (ii) where one colour has spin pointing along the negative z axis, $s = -\frac{1}{2}$, and the other two at an angle $+\phi$ and $-\phi$ respectively to the z axis in a plane including the z axis.

For the direct interaction the "spins" of the three coloured quarks, in a loose sense, like to point as far away from each other as possible. But with the conventional strength of the quark gluon coupling $e^2 \approx 2.0$ the direct interactions by themselves are not strong enough to reduce the energy of the 6 quark per momentum wave function below that of the 12 quark per momentum state. The latter is of course a strict local colour singlet state, with no spin-colour correlations, and the direct interactions contribute to zero energy.

(b) Exchange plus direct interactions

The exchange interaction, again in a rather loose sense, pulls in the opposite direction to the direct terms. It tends to favour the spins of all three colours pointing in the same direction, particularly the z direction. There is a large contribution from the Coulombic gluon whose strength is parametrised by a gluon mass. Even with a large gluon mass nearly twice as large as the quark transverse mass the exchange terms are strong enough to favour a 6 quark per momentum wave function. The state corresponds to all the quarks having the same spin $s = \frac{1}{2}$ in the z direction. This indeed reminds one of the smoke ring which suggested the toroidal configuration in the first place.

Including a quark mass independent of colour, flavour or spin, to make some allowance for the self-energy graph, changes these quantitative conclusions rather little until the quark mass approaches the transverse confining mass. Interactions then start getting rapidly very weak.

Conclusions

The dinotor is a multiquark state whose main features depend essentially only on the M.I.T. bag boundary condition. Whether or not the anomalon as at present experimentally observed, corresponds to this state of matter is a completely open question. The dinoter has several of the features demanded - size, long lifetime, stability, robustness. And if the M.I.T. bag, with its boundary condition, is a good model for the colour confinement of many quarks systems, then we should expect to see the dinoter or one of its descendents some day.

Acknowledgements

It is a pleasure to thank the organisers of this meeting for their invitation and support and the State University of New York at Stony Brook for the many opportunities they have provided for visits there.

Table 1

System of non-interacting Quarks	N° of quarks per momentum	E/A Mev	k_F fm^{-1}	a fm	ρ fm^{-3}
Large Sphere: Relativistic	12	855	1.47	-	.651
Cylinder: Relativistic	12	823	1.23	1.54	.624
Cylinder: Non-relativistic	12	942	1.08	1.46	.612
Cylinder: Non-relativistic	6	1120	1.28	1.23	.514

References

[1] B. Judek, Can. J. Phys. 50, 2082 (1972)

E.M. Friedlander, R.W. Gimpel, H.H. Heckman, Y.J. Jarent, B. Judek and E. Ganssange, Phys. Rev. Lett. 45, 1084 (1980), Phys. Rev. C27, 1489 (1983) and references therein. For the most recent review of the experimental situation see the summary talk at this Workshop by I. Otterlund.

[2] A. Chodos, R.L. Jaffe, K. Johnson, C.B. Thorn and V.F. Weisskopf, Phys. Rev. D9, 3471 (1974)

A. Chodos, R.L. Jaffe, K. Johnson and C.B. Thorn, Phys. Rev. D10, 2599 (1974)

T. De Grand, R.L. Jaffe, K. Johnson and J. Kiskis, Phys. Rev. D12, 2060 (1974)

[3] G.F. Chapline, 5th High Energy Heavy Ion Study - 1981 - LBL - 12652 showed that toroidal quark nuclei are stable and have similar densities to normal nuclear matter and proposed them to explain the anomalons.

Spontaneously Broken Symmetries in Nuclear Physics

J. Boguta

Accelerator and Fusion Research Division
Lawrence Berkeley Laboratory
University of California
Berkeley, CA 94720

1. Introduction

2. Relativistic Nuclear Physics

3. Finite Nuclei

4. Properties of a Nuclear Lagrangian

5. Chiral Symmetry and Catastrophe Theory

6. ω_μ as a Gauge Boson

7. SU(2)XU(1) Gauge Field Theory of Nuclear Interactions

8. Hadroids

This work was supported in part by the Director, Office of Energy Research, Division of Nuclear Physics of the Office of High Energy and Nuclear Physics of the U.S. Department of Energy under Contract DE-AC03-76SF00098.

Introduction

The purpose of this work is to explore the consequences of spontaneously broken symmetries in nuclear physics. This might seem an odd task to undertake in that spontaneously broken symmetries have played no substantial role in understanding nuclear structure. It becomes meaningful, though, in a field theoretic description of nuclear interactions.

There are two types of spontaneously broken symmetries that are relevant in a relativistic field theory approach to nuclear structure and nuclear dynamics. The pion plays an important role in both. It can be viewed as the realization of chiral symmetry in the Goldstone mode. T.D. Lee and G.C. Wick showed a number of years ago that such realization of chiral symmetry implies the existence of a new solution to the field equations, leading to a new nuclear configuration.[1] The other form of spontaneously broken symmetry that is relevant is gauge invariance. The consideration of spontaneously broken gauge field theory in the context of nuclear physics is a logical consequence of the relativistic field theory program, initiated by J.D. Walecka, to describe nuclear interactions.[2]

That a nucleus could be a relativistic system was investigated by Duerr, Johnson and Teller a long time ago.[3] Their idea was motivated by the desire to understand two essential properties of nuclear interactions. These are the spin-orbit splitting and energy dependence of the real part of the optical potential. They classified nuclear interactions according to the Lorentz transformation properties. One part is taken to be a Lorentz scalar, which generates attraction, the other a Lorentz vector, yielding repulsion. To explain the spin-orbit interaction and the observed energy dependence of the optical potential requires the fields to be of colossal strength. They find the scalar potential to be $\sigma \approx -450$ MeV and the vector potential to be $\omega_0 \approx 350$ MeV. Nucleons moving in such potentials are very different from quasi-free nucleons, as nonrelativistic theory assumes. The reason that the binding energy is small is that these two large potentials cancel in the binding. The effective mass of the nucleon still remains quite small, $m^*/m_N = 0.56$.

The assumption that the nucleus is a relativistic many-body system is supported by a number of recent calculations. A detailed investigation reveals that a relativistic approach can account for many known single particle properties of nuclei, such as charge and matter distribution, single particle energy levels, and total binding energies.[4] A simple relativistic model describes these properties better than sophisticated nonrelativistic Hartree-Fock calculations.[5] Another area in which the relativistic approach has done well is in describing nucleon-nucleus scattering.[6] The Dirac phenomenology reproduces known scattering data extremely well, in particular, the analyzing power and spin-rotation function.[7] The last area in which the relativistic approach is proving itself useful is in understanding Coulomb energy anomalies.

Relativistic Nuclear Physics

Nuclear Matter

The physical starting point of a relativistic description of nuclear interactions is the known bulk properties of symmetric, N = Z, nuclear matter. To recall, nuclear matter saturates at a density of about $0.145/fm^3$ with a binding energy of -15.96 MeV.[8] It has a compressibility of about 210 ± 40 MeV. The saturation properties of nuclear matter are considered as given and not deduced from nucleon-nucleon interactions. This is an essential point. We start from known properties of the medium and the single particle wave functions in that medium. Since the mass of the nucleon in matter is assumed to be much smaller than in vacuum, the expansion of the single particle wave function in the medium in terms of free nucleon wave functions is very complex. This means that the nucleon in nuclear matter is very different from that in vacuum.

To reproduce known saturation properties of nuclear matter we need to introduce attraction and repulsion. The attraction is generated by a scalar field σ and repulsion by a vactor field ω_μ, in direct analogy with electromagnetism. The simplest renormalizable Lagrangian that can be written is

$$= \bar{\psi}\left(i\gamma_\mu \frac{\partial}{\partial x_\mu} - m_N\right)\psi - \frac{1}{4} F_{\mu\nu}F_{\mu\nu} - g_\omega \bar{\psi}\gamma_\mu\psi\omega_\mu + g_s\bar{\psi}\psi\sigma$$

$$- \frac{1}{2}\left(\frac{\partial\sigma}{\partial x_\mu}\right)^2 - \frac{1}{2} m_\omega^2 \omega_\mu\omega_\mu - U(\sigma) \tag{1}$$

where

$$F_{\mu\nu} = \frac{\partial}{\partial x_\nu}\omega_\mu - \frac{\partial}{\partial x_\mu}\omega_\nu \tag{2a}$$

$$U(\sigma) = \frac{a}{2}\sigma^2 + \frac{b}{3}\sigma^3 + \frac{c}{4}\sigma^4 \tag{2b}$$

In the mean field approximation the field operators are replaced by their expectation values in the ground state. For infinite, rotationally invariant nuclear matter the field equations are

$$\frac{\partial U}{\partial\sigma} = -g_s\rho_s \tag{3a}$$

$$m_\omega^2\omega_0 = g_w\rho_v \tag{3b}$$

$$\vec{\omega} = 0 \tag{3c}$$

where

$$\rho_s = \frac{4}{(2\pi)^3}\int d^3k \frac{m^*}{\sqrt{k^2+m_N^{*2}}} = \sum_k^{k_F} \bar{\psi}_k \psi_k \tag{4a}$$

$$\rho_v = \frac{2}{3\pi^2} k_F^3 = \sum_k^{k_F} \psi_k^+ \psi_k \tag{4b}$$

with

$$m_N^* = m_N + g_s\sigma \tag{5}$$

The properties of infinite nuclear matter can be studied as a function of g_s/m_s , g_ω/m_ω , b/g_s^3 , c/g_s^4 . Let

$$C_s = g_s/m_s \; m_N \tag{6a}$$

$$C_v = g_\omega/m_\omega \; m_N \tag{6b}$$

For a given set of (C_s,C_v) nuclear matter can be saturated. This still leaves the compressibility and the effective mass as free parameters. To see their effect we plot in Fig. 1 the equation of state. The dots correspond to the equation of state computed by a many-body hypernetted chain approximation using realistac potentials.[9] We can make two comments. First, the low density part of the equation of state is insensitive to the compressibility. The high density part of the equation of state is not a unique function of compressibility.[10] Second, the sophisticated many-body calculation for the equation of state can be well reproduced by the relativistic model both at low and high nuclear densities. Thus the physical content of our model is not trivial.

To explore the physical content of the model we consider the effective potential a nucleon experiences in nuclear matter of various densities. This has also been computed in the hypernetted chain approximation.[11] In our case the potential is given by

$$U_{eff} = E - \sqrt{(E - g_\omega\omega_0)^2 + m_N^2 - m_N^{*2}}^{\;1/2} \tag{7}$$

where the fields are obtained by solving the field equations of Eq. (2) at the appropriate densities. In Fig. 2 the comparison is shown. At normal nuclear densities and at low nuclear densities the physics of both calculations is much the same. The relativistic calculation can be done on a hand calculator.

Finite Nuclei

To describe finite nuclei we need to introduce Coulomb interaction and symmetry energy. The simplest Lagrangian with these interactions is given by

$$\mathcal{L} = -\bar{\psi}(\gamma_\mu \partial_\mu + m_n)\psi - \frac{1}{2}[(\partial_\mu \sigma)^2 + U(\sigma)] - \frac{1}{4} F_{\mu\nu}F_{\mu\nu} - \frac{1}{4} \hat{G}_{\mu\nu} \cdot \hat{G}_{\mu\nu}$$

$$- \frac{1}{4} H_{\mu\nu}H_{\mu\nu} - \frac{1}{2} m_v^2 \omega_\lambda \omega_\lambda - \frac{1}{2} m_v^2 \hat{R}_\mu \cdot \hat{R}_\mu + i g_v \bar{\psi} \gamma_\lambda \psi \omega_\lambda$$

$$+ i g_r \bar{\psi} \gamma_\lambda \hat{\tau} \cdot \hat{R}_\lambda \psi + i e \bar{\psi} \gamma_\mu \frac{(1+\tau_3)}{2} \psi A_\mu - g_s \bar{\psi} \psi \sigma$$

$$U(\sigma) = \frac{a\sigma^2}{2} + \frac{b\sigma^3}{3} + \frac{c\sigma^4}{4} \tag{8}$$

The field equations for the mesonic fields are

$$\frac{d^2\sigma}{dr^2} + \frac{2}{r}\frac{d\sigma}{dr} = \frac{\partial U}{\partial \sigma} + g_s \left\{ \rho_s^{(n)} + \rho_s^{(p)} \right\} \tag{9a}$$

$$\frac{d^2\omega_o}{dr^2} + \frac{2}{r}\frac{d\omega_o}{dr} = m_v^2 \omega_o - g_v \left\{ \rho_v^{(n)} + \rho_v^{(p)} \right\} \tag{9b}$$

$$\frac{d^2 R_o^{(o)}}{dr^2} + \frac{2}{r}\frac{dR_o^{(o)}}{dr} = m_v^2 R_o^{(o)} - g_r \left\{ \rho_v^{(n)} - \rho_v^{(p)} \right\} \tag{9c}$$

$$\frac{d^2 A_o}{dr^2} + \frac{2}{r}\frac{dA_o}{dr} = e\rho_v^{(p)} \tag{9d}$$

$$\rho_s = \sum_\ell \bar{\psi}_\ell \psi \tag{10a}$$

$$\rho_v = \sum_\ell \psi_\ell^\dagger \psi \tag{10b}$$

If we take $C_s = 16.6$ and $C_v = 12.6$, which correspond to nuclear matter compressibility of 210 MeV and $m_N^*/m_N = 0.75$, then the properties of closed shell nuclei can be easily computed by solving the above field equations self-consistently. We note that the two-body interaction is not specified at all. In Fig. 3 some of the results are shown. The agreement with known data is quite good. In particular, the results for ^{90}Zr and ^{208}Pb are significant. In Fig. 4 we show some of the best nonrelativistic calculations for charge distribution in these nuclei. As one can easily see, our results are far superior.

The importance of relativistic effects can be assessed by looking at the size of the small component of the wave function. An interesting nucleus for this is ^{16}O. Here the effect of the small component can be easily seen. In nonrelativistic quantum mechanics the $p_{1/2}$ and $p_{3/2}$ wave functions vanish at the origin. In the Dirac equation the $p_{1/2}$ wave function does not vanish. The size of the small component is directly measured by $^{+}$ $^{-}$. In Fig. 5 this difference is plotted. We see that the small component accounts for about 5% of the density at the origin or 25% of the wave function. Nonrelativistic calculations for the properties of ^{16}O usually predict a hole in the charge distribution at the origin. None is observed. We suggest that the absence of the dip at the origin is a consequence of relativity.

Properties of a Nuclear Lagrangian

A nucleus experiences all known interactions of nature. Thus, our aim should be to encompass as many of these interactions as possible in a renormalizable field theory describing a nucleus. The following interactions should be considered:

A) Pion

To a good degree of approximation the pion is a Goldstone boson. The nucleon acquires its mass through spontaneous breaking of chiral symmetry. Since an enormous amount of nuclear data pertains to pionic interactions, a relativistic chiral field theory is very desirable.

B) The rho meson

In nuclei the separation of neutrons from protons requires the expenditure of energy. This is the so-called symmetry energy. Its importance is quite apparent in nuclei with a large imbalance of neutrons to protons, such as ^{208}Pb. This symmetry energy is due, in a relativistic field point of view, to the rho meson field. Thus, in describing nuclear structure nonabelian vector field plays an important role. The requirement of renormalizability of the field theory can be met by introducing the vector field through a SU(2) local gauge principle.

C) Electromagnetic interactions

The mesonic fields themselves carry charge. Thus, we need to describe these electromagnetic interactions as well. A consistent electromagnetic theory of nuclear interactions requires an expression of the electromagnetic current in terms of mesonic and baryonic degrees of freedom. The only known way of doing this is through a local gauge principle. In view of the fact that the SU(2) field carries charge, the gauge group that can give a consistent current operator for nuclear interactions is SU(2)XU(1). The powerful implications of this gauge group for nuclear interactions will be considered.

The following sections of this work are devoted to the implementation of the above ideas.

Chiral Symmetry and Catastrophe Theory

The easiest way of realizing chiral symmetry of the pion is through the Gell-Mann and Levy model. It has a sigma field for nuclear interactions, as well as the desired chiral properties for the pion. Surprisingly, this model has a fatal flaw. It does not possess a normal nuclear matter ground state[12] for any values of the coupling constants! This problem is directly linked to the spontaneous breaking of chiral symmetry. Spontaneous breaking of a global symmetry corresponds to a cusp Catastrophe.[13] These considerations can be made simple and explicit by considering a model of nuclear interactions in which the scalar meson potential functional has a double minimum as a function of σ. A typical $U(\sigma)$ is shown in Fig. 6. For infinite nuclear matter the equations are

$$\frac{\partial U}{\partial \sigma} = -g_s \rho_s \tag{11a}$$

$$m_\omega^2 \omega_0 = g_\omega \rho_v \tag{11b}$$

In Fig. 7 the solutions are shown as a function of Fermi momentum. For each value of k_F the number of solutions is odd. In Fig. 8 the energy per particle is shown. The minimum of the equation of state is the Lee-Wick state. Normal nuclear ground state does not exist. The modification of $U(\sigma)$ will not cure the problem as long as $U(\sigma)$ has a double minimum. Thus we see that a simple model of chiral symmetry immediately leads to fatal trouble. This difficulty is inherent in the model itself.

As long as the sigma field is not coupled to another field, besides the nucleon, the bifurcation problem will persist, as we saw in the above example. This is because of the cusp nature of the bifurcation induced by the double minimum of the potential function $U(\sigma)$.[13] The only way of avoiding the cusp catastrophe is by coupling the sigma field to another degree of freedom, such as the ω_μ field. As a model of seeing this, let's consider the case when the sigma field generates not only the mass of the nucleon but also that of the vector field.[14] Of course, at this stage the theory is not a gauge theory. To this question we shall return shortly.

Let the Lagrangian be

$$\begin{aligned}\mathcal{L} = {} & \bar{\psi} i\gamma_\mu \frac{\partial}{\partial x_\mu}\psi - \frac{1}{4} F_{\mu\nu}F_{\mu\nu} - \frac{1}{4}\lambda(\sigma^2 + \hat{\pi}^2) \\ & - \frac{1}{2}\mu^2(\sigma^2 + \hat{\pi}^2) - g_s\bar{\psi}(\sigma + i\hat{\tau}\cdot\hat{\pi}\gamma_5)\psi - g_\omega\bar{\psi}\gamma_\mu\psi\omega_\mu \\ & - \frac{1}{2} g_\omega^2 (\sigma^2 + \pi^2)\, \omega_\mu\omega_\nu - \frac{1}{2}\left(\frac{\partial\sigma}{\partial x_\mu}\right)^2 - \frac{1}{2}\left(\frac{\partial\hat{\pi}}{\partial x_\mu}\right)^2\end{aligned} \tag{12}$$

The mass of the vector field is generated by the chiral doublet. The field equations for infinite nuclear matter are

$$\frac{\partial U}{\partial \sigma} - g_\omega^2 m_V^* \omega_0^2 = - g_s \rho_s \tag{13a}$$

$$m_V^{*2} \omega_0 = g_\omega \rho_V \tag{13b}$$

$$m_V^* = m_\omega + g_\omega \sigma \tag{13c}$$

The solution to these field equations, with $g_s = 8.35$ and $m_\sigma = 650$ MeV, is shown in Fig. 9. The point $\sigma = 0$ is a solution to the field equations, but it is isolated for $\rho_V = 0$. Otherwise the system would carry infinite energy. We also have a normal solution. The equation of state is shown in Fig. 10. The bifurcation problem disappeared, as claimed. The equation of state has only one minimum and not two, as desired by Lee-Wick. Nevertheless, there is a new finite nuclear state.

The implication of chiral symmetry for nuclear structure can be quite subtle in nature. Chiral symmetry is spontaneously broken, as shown in Fig. 11. This implies that $\sigma = \pm\sigma_0$ are acceptable solutions for the vacuum state. By choosing $\sigma = +\sigma_0$, we pick out a preferred solution. But, in fact, the other state, $-\sigma_0$, still satisfies the field equations. Thus, if we could hide it inside a nucleus, say, then all the necessary boundary conditions of the problem are met, and we realize a new solution to the field equations. The two configurations of the sigma field are schematically shown in Fig. 12. The one with a kink in the field will lead to kinky nuclei.

The field equations to solve for such nuclei are

$$\frac{d^2\sigma}{dr^2} + \frac{2}{r}\frac{d\sigma}{dr} - \lambda(\sigma^2 - \sigma_0^2)\sigma + g_\omega^2 \sigma \omega_0^2 = g_s \rho_s \tag{14a}$$

$$\frac{d^2\omega_0}{dr^2} + \frac{2}{r}\frac{d\omega_0}{dr} - m_V^{*2}\omega_0 = -g_\omega \rho_V \tag{14b}$$

$$\frac{dU}{dr} = (m_N^* + E - g_\omega \omega_0)V - \frac{K}{r} U \tag{14c}$$

$$\frac{dV}{dr} = (m_N^* - E + g_\omega \omega_0)U - \frac{K}{r} V \tag{14d}$$

where

$$= \frac{1}{r}\begin{pmatrix} iU(r) \\ V(r)\hat{\sigma}\cdot\hat{n} \end{pmatrix} \Omega_{jlm}(n) \tag{15}$$

The numerical solutions to the equations are obtained by starting the iteration process with a reasonable square well for $\sigma(r)$. In Fig. 13 the density profile for the abnormal and normal state of ^{4}He is shown. The abnormal state has a smaller rms radius, and thus we expect such a nuclear state to have a longer mean free path than a normal nucleus.

ω_μ as a Gauge Boson

The above considerations suggest that a simple way of reconciling the pathologies of the linear chiral model is to make the mass of the vector field dynamic. This was achieved by the sigma field. A better version of this mechanism is to treat the vector field as a true gauge field. This is done by introducing a Higgs field ϕ that spontaneously generates the ω_μ mass. For the Lagrangian now take

$$\mathcal{L} = \frac{-1}{4} F_{\mu\nu}F_{\mu\nu} - \bar{\psi}(i\gamma_\mu d_\mu)\psi - g_s\bar{\psi}(\sigma + i\gamma_5\hat{\tau}\cdot\hat{\pi})\psi \frac{-1}{2}(d_\mu\phi)^2$$

$$- \frac{1}{2}\left(\frac{\partial\sigma}{\partial x_\mu}\right)^2 - \frac{1}{2}\left(\frac{\partial\hat{\pi}}{\partial x_\mu}\right)^2 - U(\sigma^2 + \pi^2, \phi^*\phi) \tag{16}$$

$$d_\mu = \frac{\partial}{\partial x_\mu} - ig\omega_\mu \tag{17a}$$

$$U(\sigma^2 + \hat{\pi}^2, \phi^*\phi) = a(\sigma^2 + \hat{\pi}^2)^2 + b(\sigma^2 + \hat{\pi}^2) + c(\sigma^2 + \hat{\pi}^2)\phi^*\phi$$
$$+ d(\phi^*\phi) + e(\phi^*\phi)^2 \tag{17b}$$

The interaction between the Higgs field ϕ and the chiral singlet $\sigma^2 + \hat{\pi}^2$ is necessary. Such a gauge field theory was considered by T.D. Lee in a different context of abnormal matter theory.[15)]

In vacuum, the pattern of spontaneous symmetry breaking can be determined by minimizing U with respect to the Higgs field and the scalar field (take $\hat{\pi} = 0$). We then have

$$\frac{\partial U}{\partial\sigma} = 4a\sigma^3 + 2b\sigma + 2c\,\phi^*\phi = 0 \tag{18a}$$

$$\frac{\partial U}{\partial\phi^*} = c\phi\sigma^2 + 2d\phi^*\phi\phi + e\phi = 0 \tag{18b}$$

and

$$\phi^*\phi = -\frac{1}{d}(e + c\sigma^2) \tag{19a}$$

$$\sigma = \pm\sqrt{\frac{ce-2b}{4a-c^2/d}} \tag{19b}$$

$$m_N = g_s\sigma \tag{19c}$$

$$m_V = g_V\sigma \tag{19d}$$

For given values of a,c,d, the values of e and b can be found so that

$$\sigma_o = \frac{m_N}{g_s} \tag{20a}$$

$$\phi_o = \frac{m_V}{g_V} \tag{20b}$$

The desired values of e and c are

$$e = -\left[\sigma_o^2 c + 2\phi_o^2 d\right] \tag{21a}$$

$$b = -\left[\phi_o^2 c + 2\sigma_o^2 a\right] \tag{21b}$$

Thus a gauge field theory of the omega meson can be easily constructed, which also leads to a chiral symmetric theory.

The gauge nature of the vector field has interesting consequences, as first shown by Nielsen and Olesen.[16] A solution to the gauge field theory is found that possesses a topological quantum number. For this, let's consider a solution to the field equations that is cylindrically symmetric. Let the Higgs field be

$$\phi = e^{i\varphi} U(r) \tag{22}$$

where φ is the azimuthal angle.

The field equations for the vector field are given by

$$\frac{\partial F_{\mu\nu}}{\partial x_\mu} = j_\nu \tag{23}$$

where

$$j_\mu = \frac{1}{2}\, ig \left(\phi^* \frac{\partial}{\partial x_\mu} \phi - \phi \frac{\partial}{\partial x_\mu} \phi^* \right) + g^2 \omega_\mu \phi^* \phi \tag{24}$$

If we let

$$\vec{\omega} = \frac{\vec{r} \times \hat{\varepsilon}_z}{r} W(r) \tag{25}$$

then the field equation is, in cylindrical coordinates

$$\frac{d}{dr}\left(\frac{1}{r}\frac{d}{dr}\left[rW(r)\right]\right) - U(r)^2\left(g^2 W(r) - \frac{g}{r}\right) = 0 \tag{26}$$

We see that asymptotically

$$W(r) \to \frac{1}{gr} \tag{27}$$

and thus the line integral

$$\oint \omega_\mu dx^\mu = n \frac{2\pi}{g} \tag{28}$$

This is the amount of flux that cuts the x-y plane. The number n is integer and its origin is topological in nature.

SU(2)XU(1) Gauge Field Theory of Nuclear Interactions

There exist no nuclear data to reject the hypothesis that nuclear interactions are described by SU(2)XU(1) gauage field theory. In fact, there are a number of supporting considerations for this hypothesis. Nuclear structure shows that global SU(2) is an exceedingly good symmetry of hadronic interactions. Observed breaking of global SU(2) is almost completely accountable by the electromagnetic interaction. Breaking of global SU(2) must be very small in nuclear physics. This is understandable in terms of the fact that γ-ρ° mixing is very small. The mixing angle is

$$\sin\theta_H = \frac{e}{g_\rho} \tag{29}$$

Since global SU(2)XU(1), with a small mixing angle, is in accord to know data so well, it is reasonable to attempt a local extrapolation of this symmetry and study the consequences of such an assumption. Furthermore, the extension of global SU(2)XU(1) to a local gauge symmetry is motivated by the fact that the only way of building renormalizable nonabelian field theories is through a local gauge principle. Thus, for a consistency of the theoretical program to describe nuclear interactions through a field theory, it is necessary to introduce the local extension of SU(2)XU(1).

We shall discuss two different consequences of local SU(2)XU(1) gauge group for nuclear physics. First, we show that the gauge group implies charge asymmetry of nuclear interactions. Of course, this charge asymmetry will be very small. The second implication of the gauge group is that nuclear forces undergo a metamorphosis.[17] This metamorphosis is accompanied by a new quantum number, whose origin is topological in nature and does not correspond to an invariance of the Lagrangian.

SU(2)XU(1) gauge theory of nuclear interactions can be easily constructed. Let the fermion doublet be

$$= \begin{pmatrix} p \\ n \end{pmatrix} \tag{30}$$

The right- and left-hand parts of the wave function are assumed to transform the same way. This implies that parity is conserved, as it must be. The charge of the Higgs field is indicated by

$$H = \begin{pmatrix} h^+ \\ h^o \end{pmatrix} \tag{31}$$

The symmetry is spontaneously broken by the choice of the potential functional

$$V = \lambda/4\ (H^+H - H_o)^2 \tag{32}$$

The covariant derivative acting on doublets is

$$d_\mu \psi = \left(\frac{\partial}{\partial x_\mu} + \frac{i g_\rho}{2} \hat{\tau} \cdot \hat{R}_\mu + \frac{i g}{2}\ B_\mu\right)\psi \tag{33}$$

The Lagrangian is then given by

$$\mathcal{L} = -\frac{1}{4} \hat{F}_{\mu\nu} \cdot \hat{F}_{\mu\nu} - \frac{1}{4} G_{\mu\nu} G_{\mu\nu} - \frac{1}{2} (d_\mu H)^2 - V - \bar{\psi}(i d_\mu \gamma_\mu)\psi \tag{34}$$

$$\hat{F}_{\mu\nu} = \frac{\partial}{\partial x_\mu} \hat{R}_\nu - \frac{\partial}{\partial x_\nu} \hat{R}_\mu + g_\rho \hat{R}_\mu \times \hat{R}_\nu \tag{35}$$

$$G_{\mu\nu} = \frac{\partial}{\partial x_\mu} B_\nu - \frac{\partial}{\partial x_\mu} B_\mu \tag{36}$$

where $\hat{R}_\mu$, B_μ are the SU(2) and U(1) fields, respectively. The mass matrix is diagonalized by the following choice of the fields

$$\rho_\mu^\pm = R_\mu^\pm \tag{37a}$$

$$\rho_\mu^o = \cos\theta_H\ R_\mu^o - \sin\theta_H B_\mu \tag{37b}$$

$$A_\mu = \sin\theta_H\ R_\mu^o + \cos\theta_H\ B_\mu \tag{37c}$$

with

$$\tan\theta_H = \frac{g}{g_\rho} \tag{38}$$

The A_μ field has zero mass and corresponds to the photon.

The Lagrangian can be expanded in terms of ρ_μ, A_μ fields. The electromagmagnetic current operator is then

$$J_\mu^{EM} = \bar{\psi}\gamma_\mu \frac{(1+\tau_3)}{2}\psi + (\hat{\rho}_\nu \times \hat{F}_{\mu\nu})_3 + \left[\hat{\pi} \times \left(\frac{\partial}{\partial x_\mu} \hat{\pi} + g_\rho \hat{\pi} \times \hat{\rho}_\mu\right)\right]_3 \tag{39}$$

and the Lagrangian has the following terms of interest.

$$\mathcal{L} = \frac{-g_\rho}{2}\bar{\Psi}\hat{\tau}\rho_\mu\gamma_\mu\Psi + g_\rho\hat{\rho}_\mu \cdot \left[\frac{\partial}{\partial x_\mu}\hat{\pi} \times \hat{\pi}\right] \tag{40}$$

$$+ \frac{1}{2}\frac{e^2}{g_\rho}\bar{\Psi}\gamma_\mu\Psi\rho^0_\mu + \ldots$$

Of particular interest is the term $\frac{e^2}{2g_\rho}\bar{\Psi}\gamma_\mu\Psi\rho^0_\mu$. It shows that global SU(2) will be violated in our theory. That is, nuclear forces are predicted to be charge asymmetric. This charge asymmetry will be very small, of order e^2/g_ρ. Such a small charge symmetry breaking is not ruled out by nuclear data. The effect of local SU(2)XU(1) gauge field theory for known nuclear structure is very small. The group's full impact appears somewhere else.

Besides the normal Yukawa type solutions, the gauge group possesses a whole class of other solutions. They are characterized by the fact that in these states, the vector field becomes long ranged, and it is accompanied by a new topological quantum number. Such a state is called an hadroid.[17] To see this, we discuss Nambu's results for SU(2)XU(1).[18]

For a solution to exist, we must have

$$d_\mu H = \left(\frac{\partial}{\partial x_\mu} + \frac{ig}{2\rho}\hat{\tau}\hat{R}_\mu + \frac{ig}{2}B_\mu\right)_{r\to\infty} H = 0 \tag{41}$$

This implies that

$$gR^i_{\rho\mu} + g\,B_\mu\,(H^+\tau^i H) = -iH^+\tau^j\frac{\overleftrightarrow{\partial}}{\partial x_\mu}H \tag{42}$$

If R and R are defined with respect to H^+ H then we have

$$gR^i_{\rho\mu\perp} = -\,(H^+\tau^j H)\,\frac{\partial}{\partial x_\mu}\,(H^+\tau^k H)\,e^{ijk} \tag{43a}$$

$$gR^i_{\rho\mu\parallel} = -\,\xi i(H^+\tau^i H)\,H^+\frac{\overleftrightarrow{\partial}}{\partial x_\mu}H \tag{43b}$$

$$gB_\mu = -\,\eta i\,H^+\frac{\overleftrightarrow{\partial}}{\partial x_\mu}H \qquad + \eta = 1 \tag{43c}$$

$$gG_{\mu\nu} = \eta f_{\mu\nu} \tag{44a}$$

$$gF^i_{\rho\mu\nu} = -\frac{\partial}{\partial x_\mu}(H^+\tau^j H)\,\frac{\partial}{\partial x_\nu}(H^+\tau^k H)\,\varepsilon^{ijk} + \xi f_{\mu\nu}(H^+\tau^i H) \tag{44b}$$

$$f_{\mu\nu} = -2i \left(\frac{\partial}{\partial x_\mu} H^\dagger \frac{\partial}{\partial x_\nu} H - \frac{\partial}{\partial x_\nu} H^+ \frac{\partial}{\partial x_\mu} H \right) \tag{44c}$$

For a given Higgs field we can find a solution $\hat{R}_\mu$ and B_μ.

Non-Yukawa type solutions emerge if the Higgs field is given a nontrivial asymptotic dependence on angle. For example, let

$$H = \hat{\tau}\cdot\hat{r} \begin{pmatrix} 0 \\ U(r) \end{pmatrix} \tag{45}$$

Define $$\hat{\phi} = H^+\hat{\tau}H \tag{46a}$$

$$= \frac{1}{r^2} \begin{pmatrix} 2xZ \\ 2yZ \\ x^2+y^2-z^2 \end{pmatrix} \tag{46b}$$

Then another set of solutions is generated by the Higgs field of the type

$$H = \hat{\tau}\cdot\hat{\phi} \begin{pmatrix} 0 \\ t(r) \end{pmatrix} \tag{47}$$

This type of construction can be continued.

Interesting consequences of the hadroid phase can be inferred without much work. First, the number of hadroid states for a nucleus is limitless. This follows from the sequential construction of the Higgs fields for these states. Furthermore, the electromagnetic properties of an hadroid nucleus must be different from that in the normal state. The solution of SU(2)XU(1) gauge field theory has a nonvanishing magnetic field, even for a 0^+ nucleus. This is a unique signature of the hadroid.

Hadroids

The physical picture of nuclear structure given by the SU(2)XU(1) gauge invarian Lagrangian is as follows: For small excitations around the vacuum state, the isotopic nuclear interactions are mediated by a massive rho field. For nuclear matter it gives the correct value of the symmetry energy. It also plays an important role in determining the structure of a nucleus such as ^{208}Pb. The small mixing angle precludes any significant deviations from known nuclear properties obtainable from global SU(2) isotopic spin invariance. A significant prediction is that there is a very small charge

asymmetry in nuclear interactions. The sign and magnitude agree with recent experiment.

In the hadroid phase the classical balance of nuclear forces is altered. The isotopic spin field becomes long ranged and pionic solitons can exist. Change in the character of the isotopic force will manifest itself in the increased interaction of the hadroid with other nuclei. Such phenomenon has been observed in projectile fragments and reported at this Workshop. The excitation of such anomalous nuclear fragments, according to the present model, must be in the isotopic degree of freedom. Those reactions that can excite isotopic spin degrees of freedom must be the most efficacious in creating the hadroid.

Theoretically speaking, the proposition that nuclear interactions are described by a SU(2)XU(1) local gauge invariant Lagrangian is a natural one to make. A consistent relativistic quantum field theory of nuclear interactions must at least have this invariance. The fact that the rho meson is charged requires its gauging, if a consistent electromagnetic theory of nuclear interactions is to be obtained. Besides the requirements of consistence, the theory predicts a number of extraordinary nuclear states, whose existence can be checked by experiment.

The author acknowledges illuminating discussions with B.D. Serot and H. Pugh. This work was supported in part by the Director, Office of Energy Research, Division of Nuclear Physics of the Office of High Energy and Nuclear Physics of the U.S. Department of Energy under Contract DE-AC03-76SF00098.

References

1. T.D. Lee and G.C. Wick, Phys. Rev. D9, 2291 (1974)
2. J.D. Walecka, Ann. Phys. 83, 491 (1974)
3. H.-P. Duerr and E. Teller, Phys. Rev. 101, 494 (1956)
   M.H. Johnson and E. Teller, Phys. Rev. 98, 783 (1955)
4. J. Boguta, Phys. Lett. 106B, 241, 245, 250, 255 (1981)
   J. Boguta, Nucl. Phys. A372, 386 (1981)
5. J.L. Friar and J.W. Negele, in Advances in Nuclear Physics, ed. M. Baranger and E. Vogt, vol. 8 (Plenum, New York) p. 219
6. L.G. Arnold, B.C. Clark, and R.L. Mercer, Phys. Rev. 19C, 917 (1979)
7. B.C. Clark, S. Hama, R.L. Mercer, L. Ray, and B.D. Serot, Phys. Rev. Lett. 50, 1644 (1983)
8. W.D. Myers, in Droplet Model of Atomic Nuclei (IFI/Plenum, New York) p. 5
9. B. Friedman and V.R. Pandharipande, Nucl. Phys. A361, 502 (1981)
10. J. Boguta and H. Stöcker, Phys. Lett. 102B, 289 (1983)
11. B. Friedman and V.R. Pandharipande, Phys. Lett. 100B, 205 (1981)
12. A.K. Kerman and L.D. Miller, Field theory methods for finite nuclear systems and the possibility of density isomers, MIT-CTP PUB 449, unpublished
    J. Boguta, Remarks on density isomers, Argonne National Laboratory report, unpublished
13. R. Thom, Structural stability and morphogenesis (Benjamin, Reading, MA, 1975)
14. J. Boguta, Phys. Lett. 120B, 34 (1983)
15. T.D. Lee, Phys. Reports 23C, 254 (1976)
16. H.B. Nielsen and P. Olesen, Nucl. Phys. B61, 45 (1973)

17. J. Boguta, Phys. Rev. Lett. 50, 148 (1983)
18. Y. Nambu, Nucl. Phys. B130, 505 (1978)

Figure Captions

Fig. 1a Energy per particle as a function of nuclear matter density ρ_V for various compressibilities and effective masses. The dots are the result of hypernetted chain calculation.

Fig. 1b Energy per particle as a function of density ρ_V for fixed compressibility and different effective masses.

Fig. 1c Pressure P as a function of density for various choices of the parameters. The dots are hypernetted chain calculations of ref. 9.

Fig. 2 Optical potential in nuclear matter as a functon of density and particle energy. FP is the hypernetted chain calculation of ref. 11.

Fig. 3a Charge distribution in ^{16}O as predicted by the relativistic model.

Fig. 3b Charge distribution in ^{40}Ca as predicted by the relativistic model.

Fig. 3c Neutron distribution in ^{40}Ca as predicted by the relativistic model.

Fig. 3d Charge distribution in ^{90}Zr as predicted by the relativistic model.

Fig. 3e Charge distribution in ^{208}Pb as predicted by the relativistic model.

Fig. 4a Charge distribution in ^{90}Zr predicted by nonrelativistic models.

Fig. 4b Charge distribution in ^{208}Pb predicted by nonrelativistic models.

Fig. 5 Difference in the vector and scalar particle densities. It measures the size of the small component of the wave function.

Fig. 6a Potential functional with a double minimum that is not symmetric.

Fig. 6b Plot of $\partial u/\partial\sigma$ and the scalar density ρ_S for various ρ_V. The intersections are solution to the field equations.

Fig. 7 Solutions of the field equations for various Fermi momenta k_F. The number of solutions is always odd.

Fig. 8 Energy per particle as a function of the Fermi momentum. The normal ground state does not appear because the line bifurcates.

Fig. 9 Solution to the field equations in the dynamical model. The point $m_N^* = 0$ is isolated, thus preventing bifurcation.

Fig. 10 Energy per particle as a function of density. The dynamical model removes the bifurcations.

Fig. 11 Potential functional $U(\phi)$ as a function of ϕ that corresponds to the equation of state of Fig. 10.

Fig. 12. Schematic representation of the normal and abnormal field configuration allowed by chiral symmetry.

Fig. 13. Proton densities in abnormal ^4He and ^{12}C. The densities are surface peaked. A normal ^4He density profile is shown. The abnormal state has a longer mean free path than a normal nucleus would have.

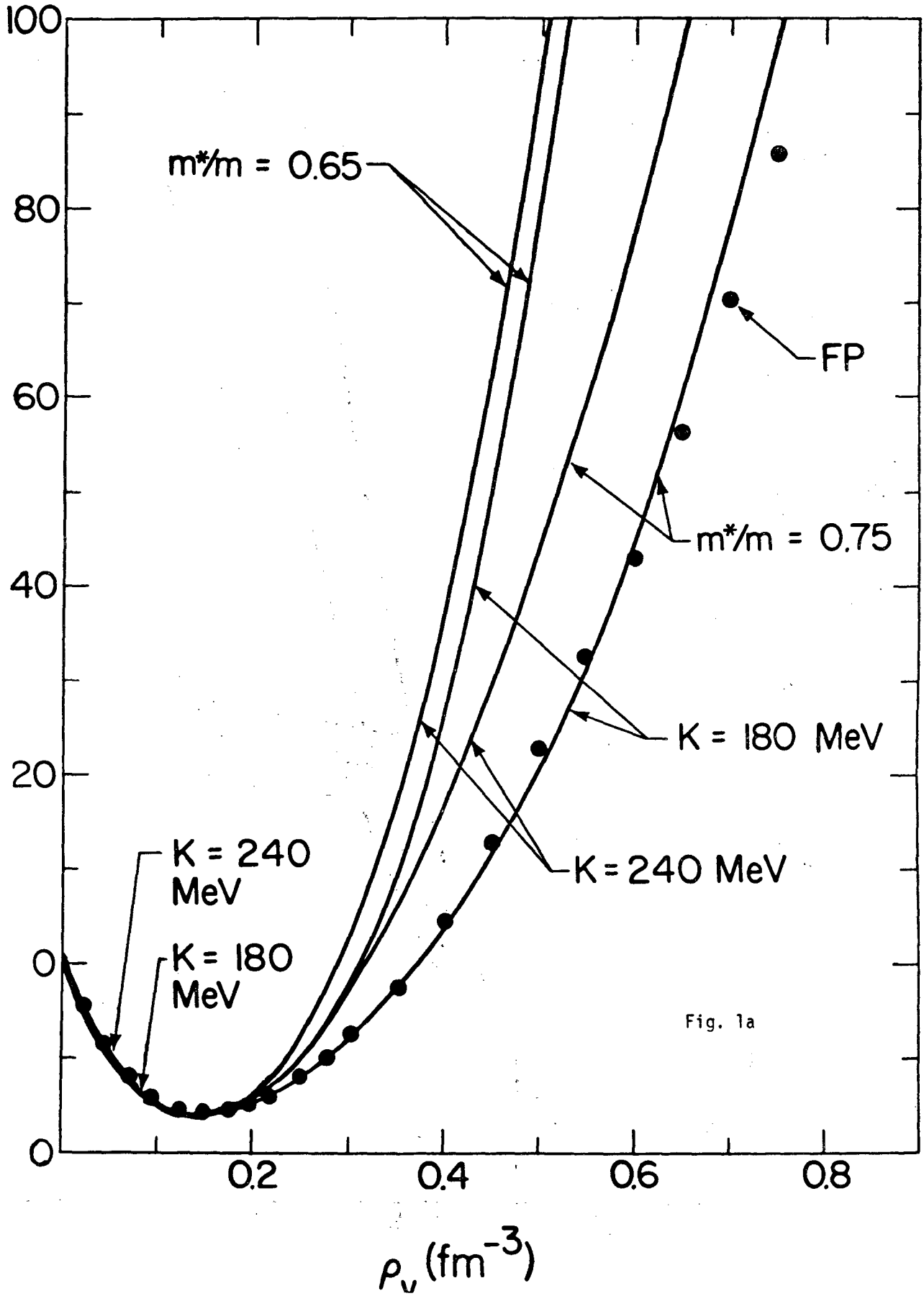
100
80
60
40
20
0
0
0.2
0.4
0.6
0.8
m*/m = 0.65
FP
m*/m = 0.75
K = 180 MeV
K = 240 MeV
K = 240 MeV
K = 180 MeV
ρ_ν (fm^{-3})

Fig. 1a

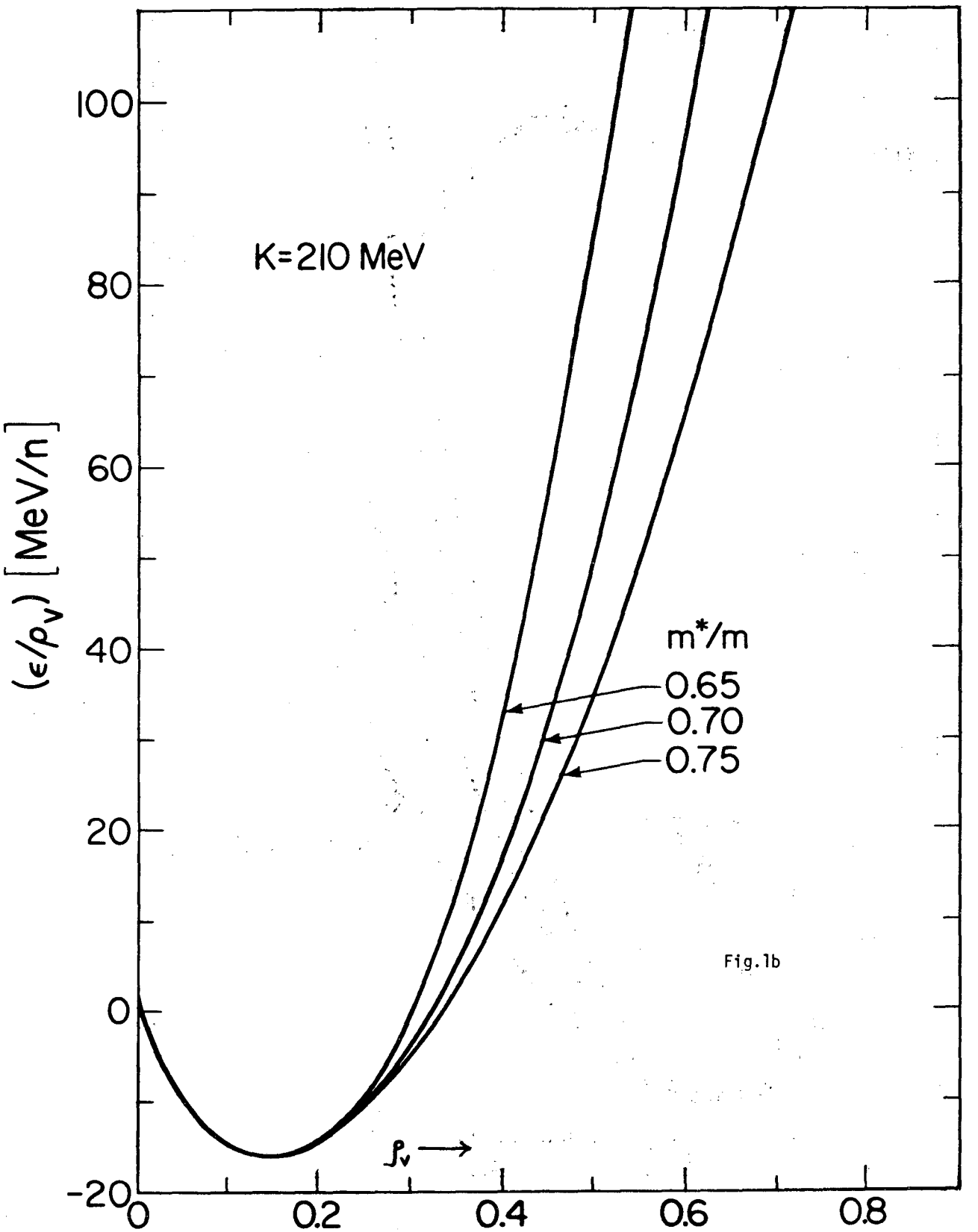
K=210 MeV
m*/m
0.65
0.70
0.75
(ϵ/ρ_v) [MeV/n]
$\rho_v \longrightarrow$
100
80
60
40
20
0
-20
0
0.2
0.4
0.6
0.8

Fig.1b

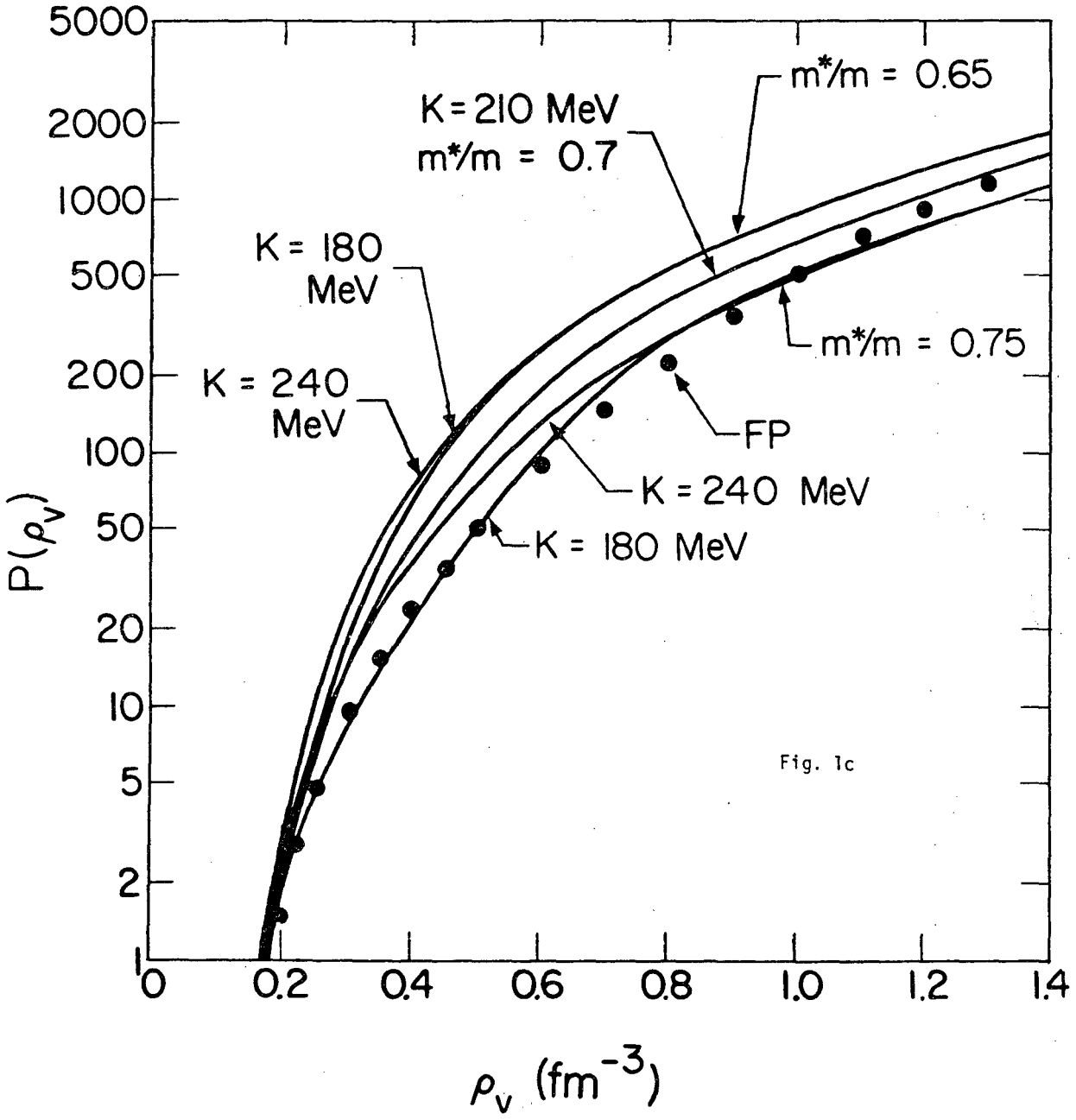
5000
2000
1000
500
200
100
50
20
10
5
2
1
0
0.2
0.4
0.6
0.8
1.0
1.2
1.4
P(ρv)
ρv (fm-3)
m*/m = 0.65
K = 210 MeV
m*/m = 0.7
K = 180
MeV
K = 240
MeV
m*/m = 0.75
FP
K = 240 MeV
K = 180 MeV

Fig. 1c

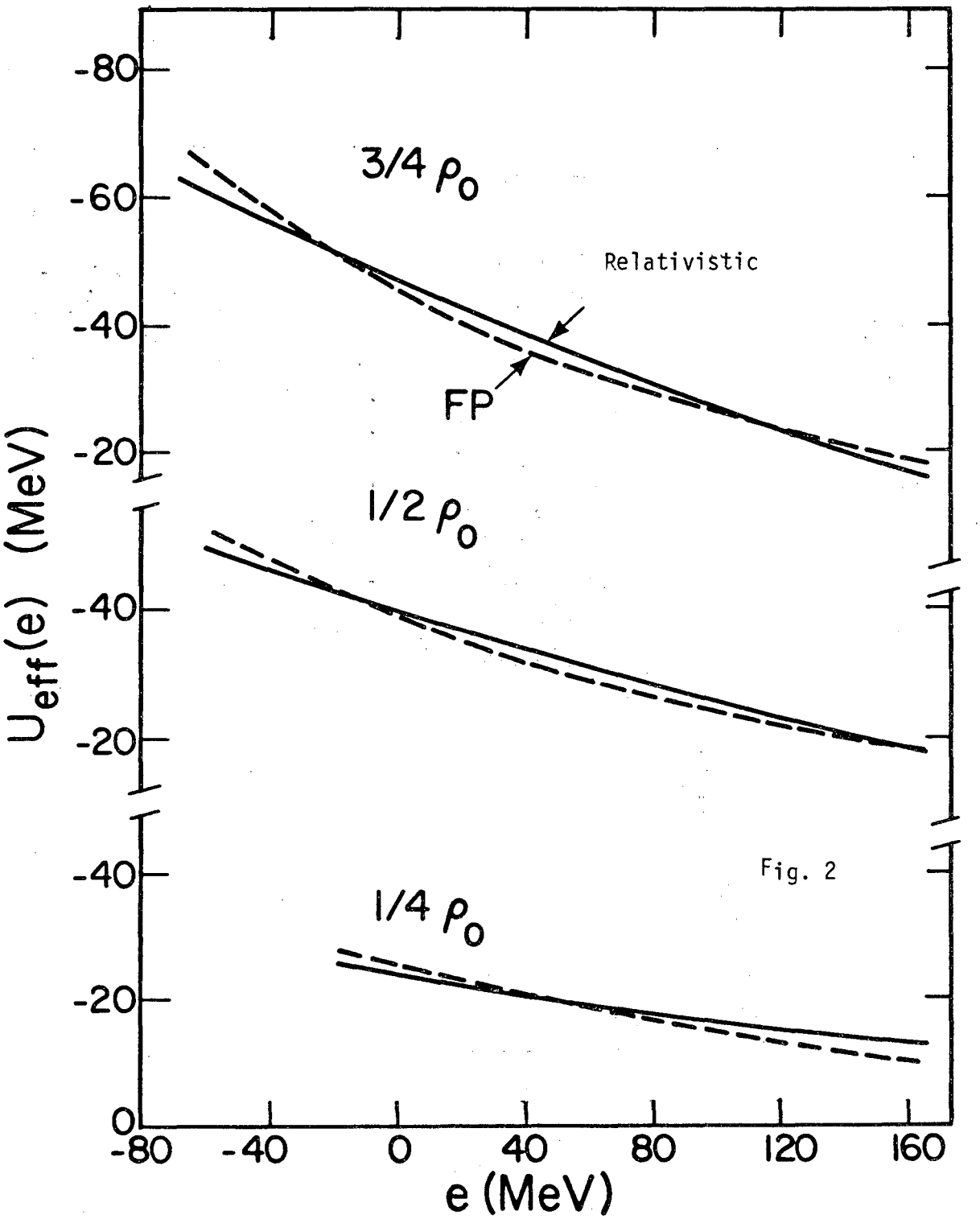

Fig. 2

XBL 824-404

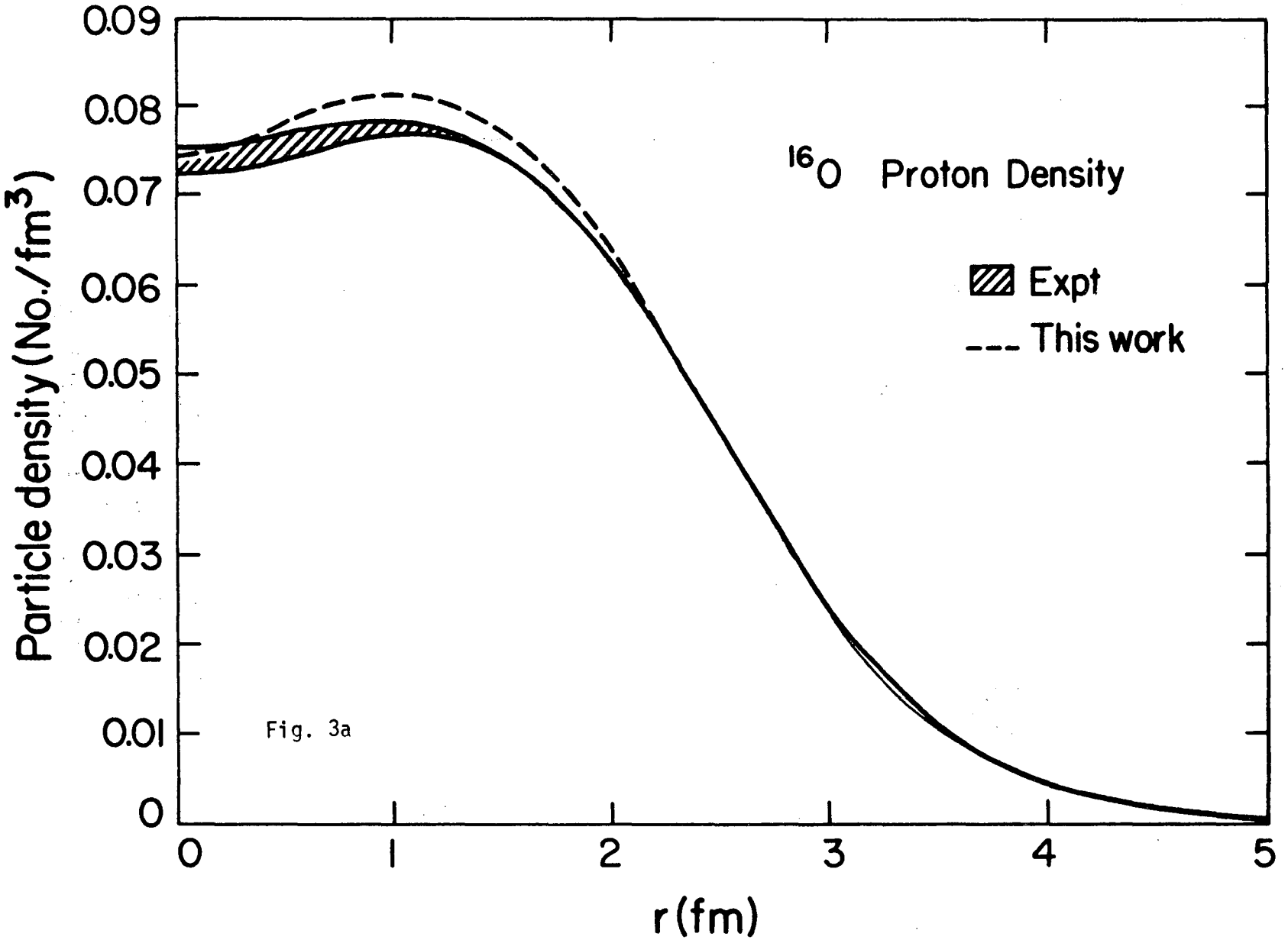

Fig. 3a

XBL 816-1015

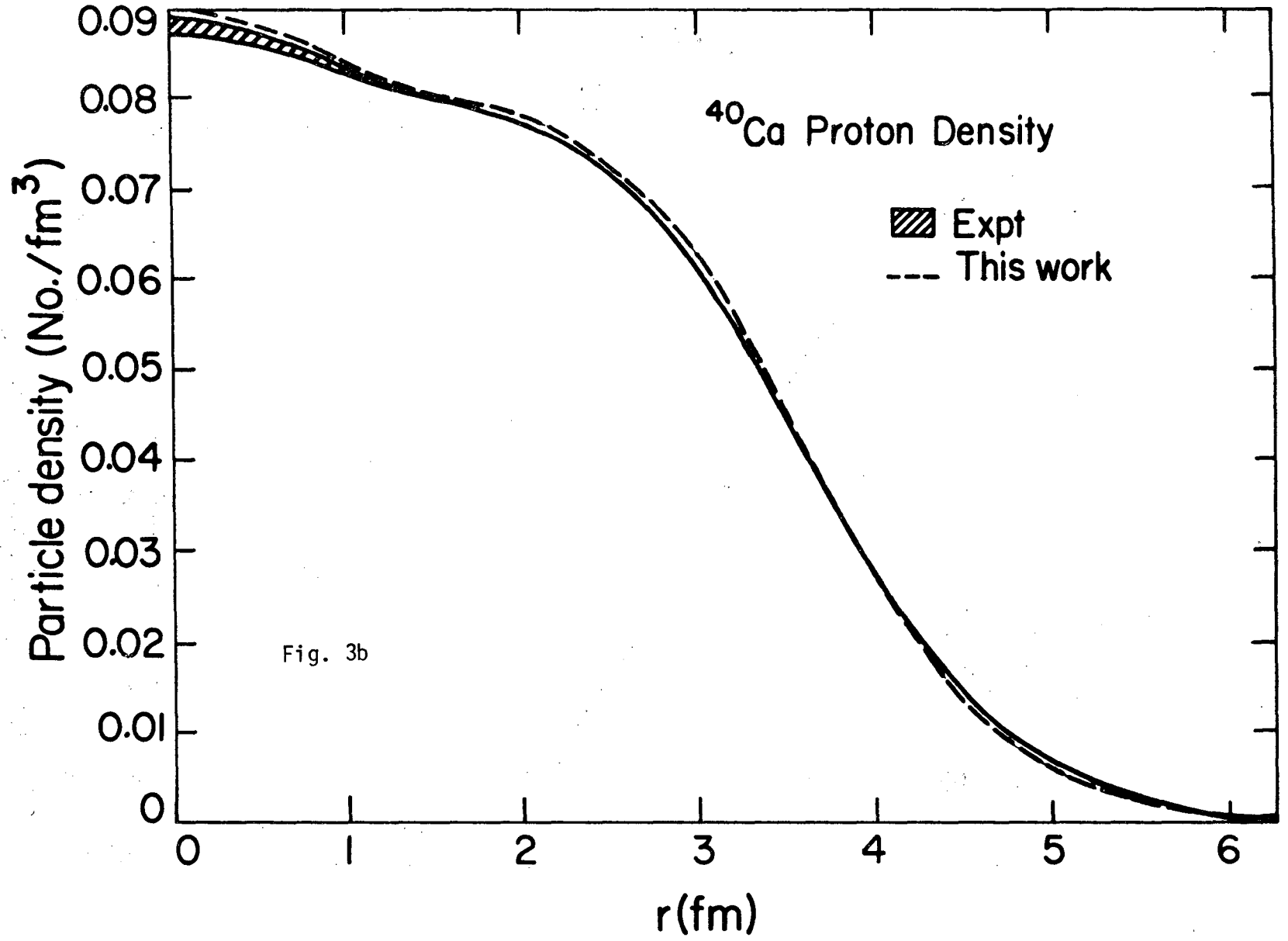

Fig. 3b

XBL 816-1016

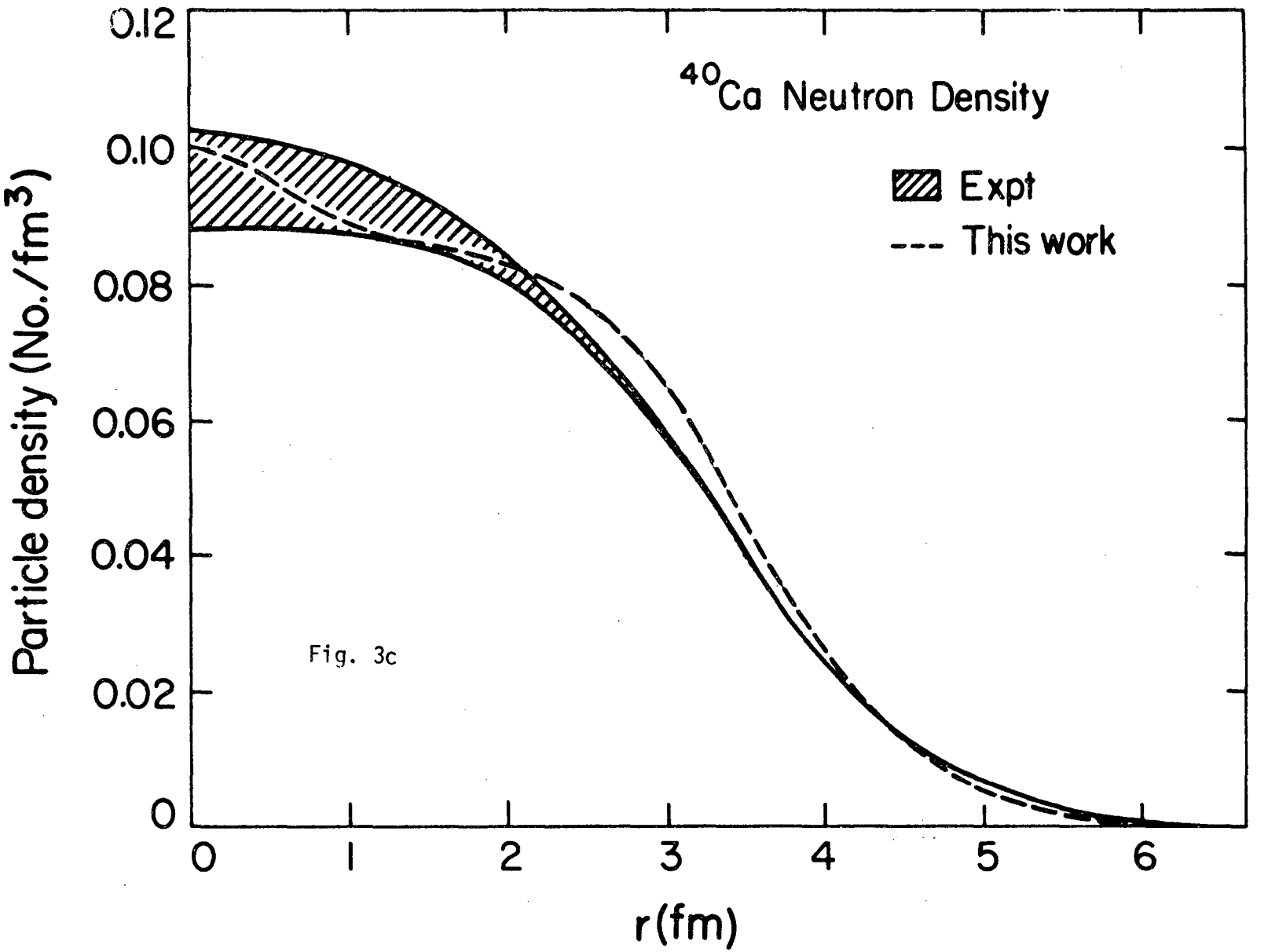

Fig. 3c

XBL 816-1014

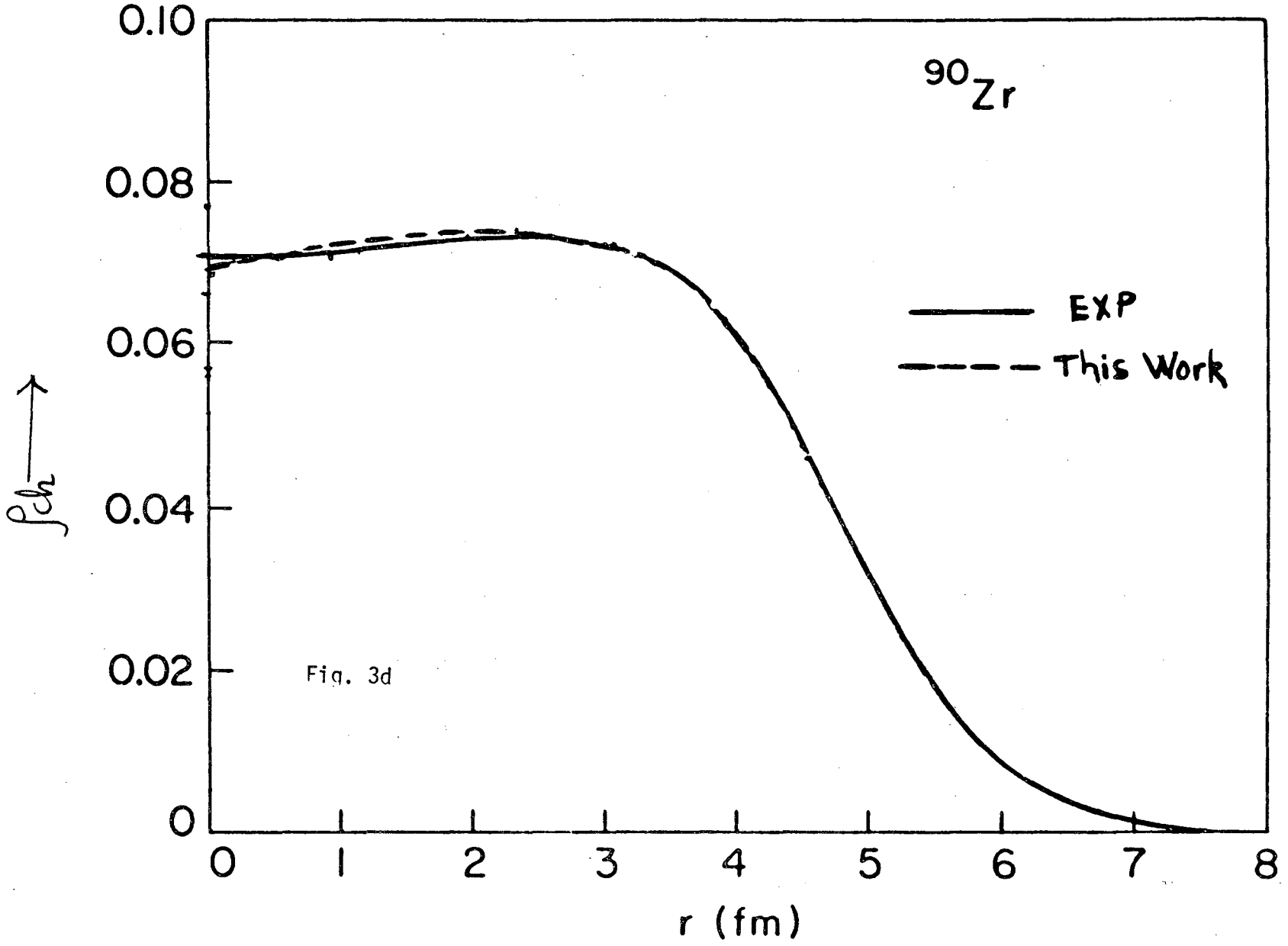

Fig. 3d

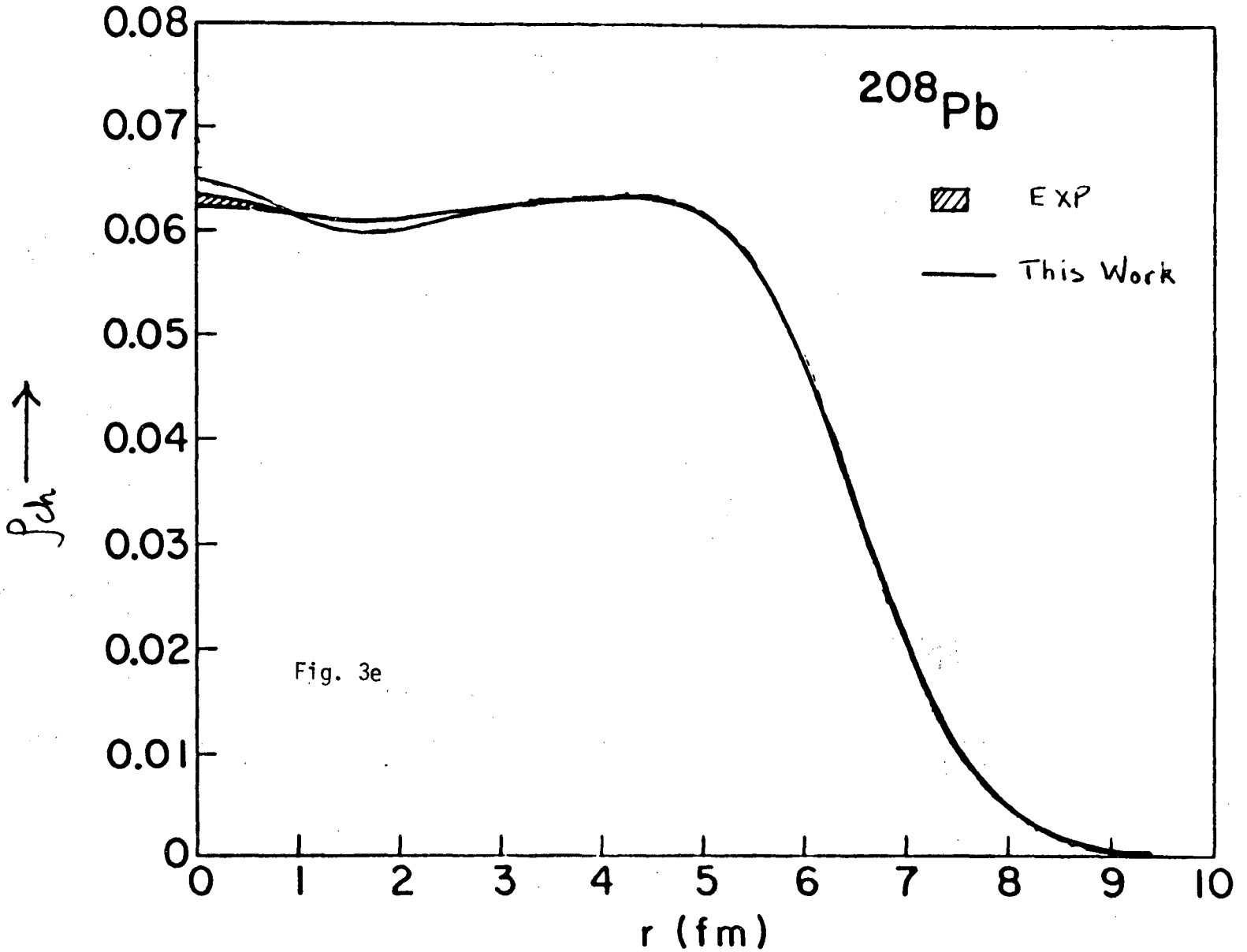
0.08
0.07
0.06
0.05
0.04
0.03
0.02
0.01
0
0
1
2
3
4
5
6
7
8
9
10
r (fm)
ρ_{ch}
^{208}Pb
EXP
This Work

Fig. 3e

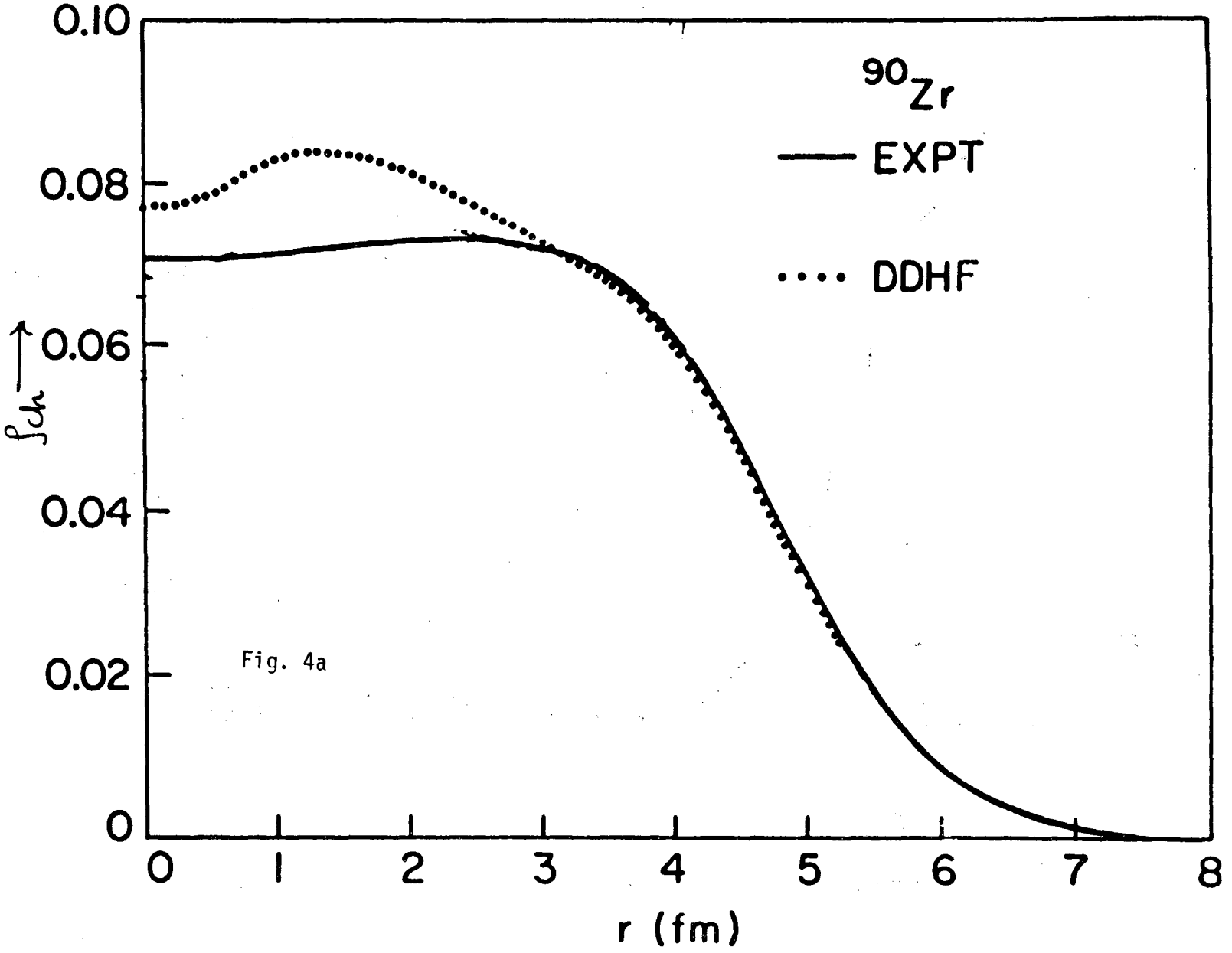

Fig. 4a

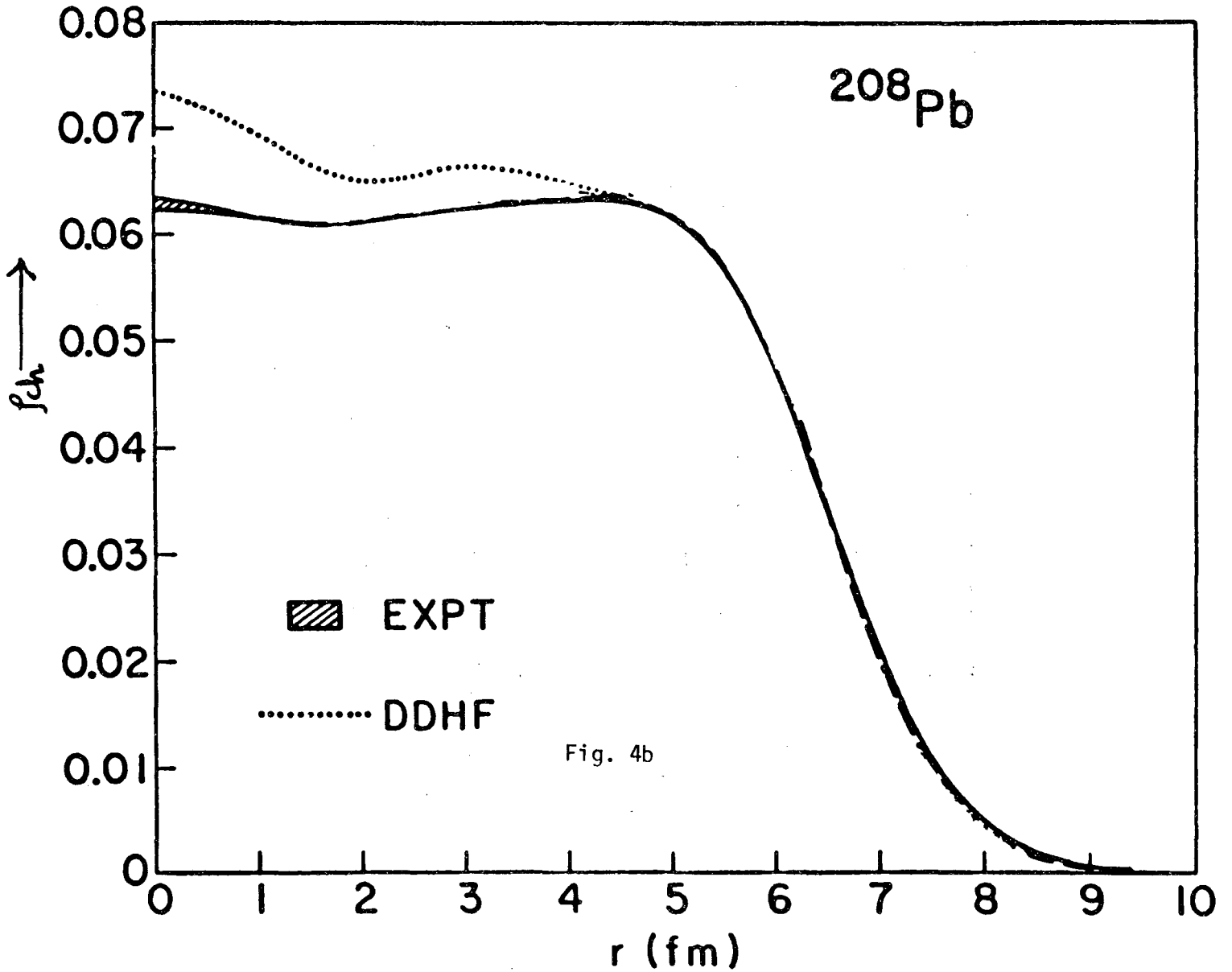
0.08
0.07
0.06
0.05
0.04
0.03
0.02
0.01
0
ρ_{ch}
^{208}Pb
EXPT
DDHF
0
1
2
3
4
5
6
7
8
9
10
r (fm)

Fig. 4b

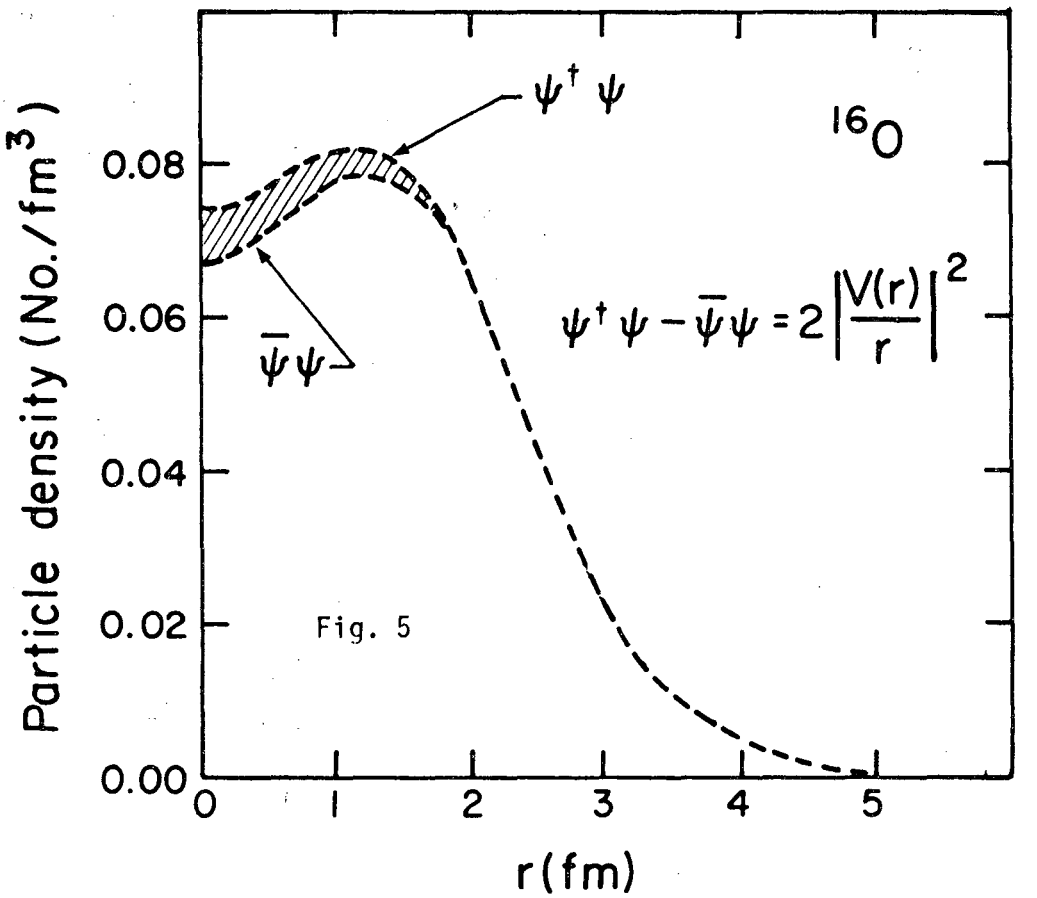

Fig. 5

XBL 811-25

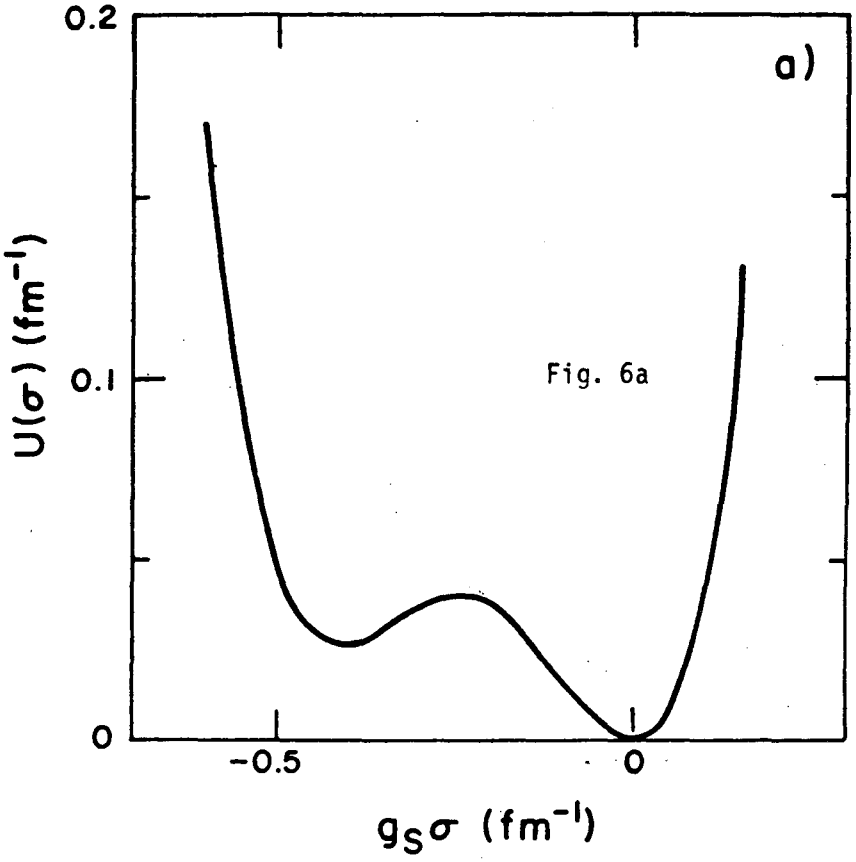

Fig. 6a

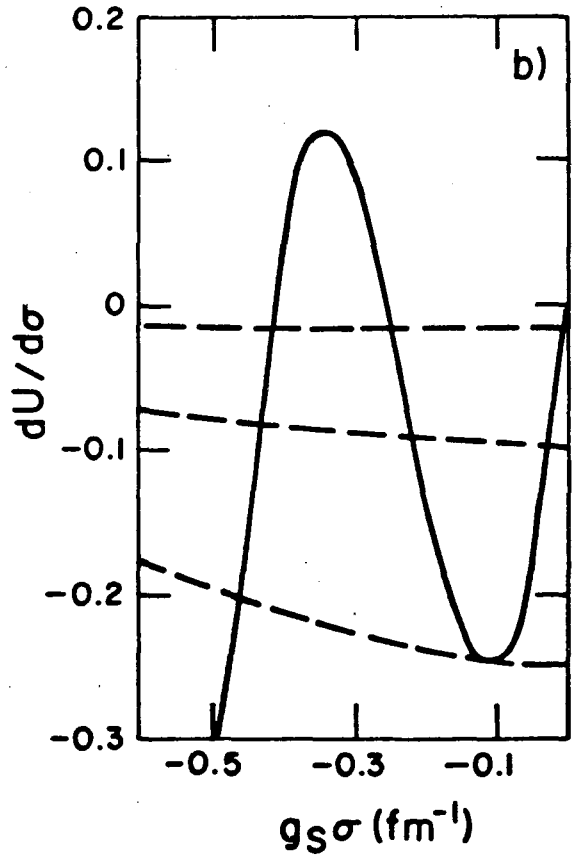

Fig. 6b

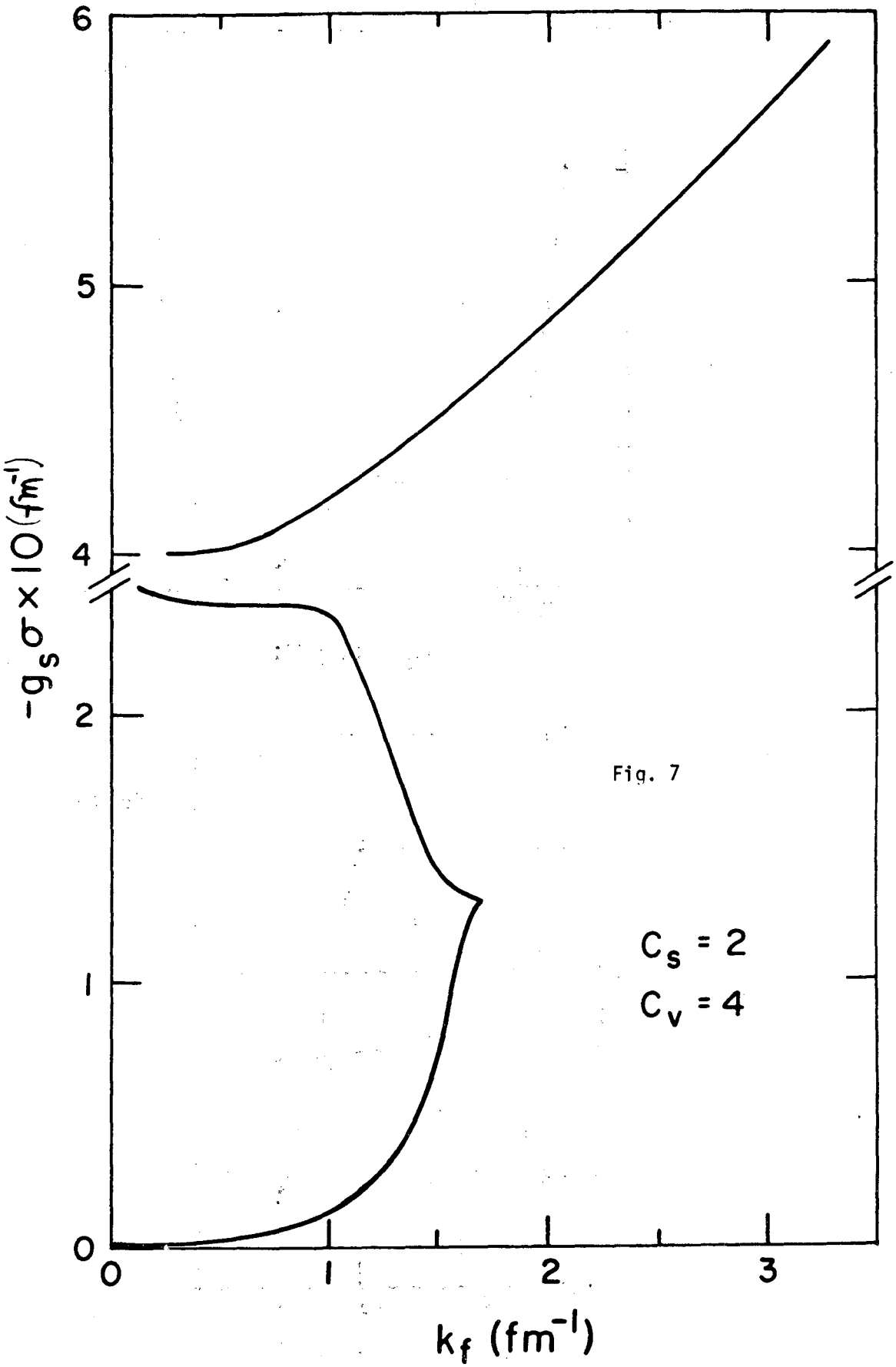

Fig. 7

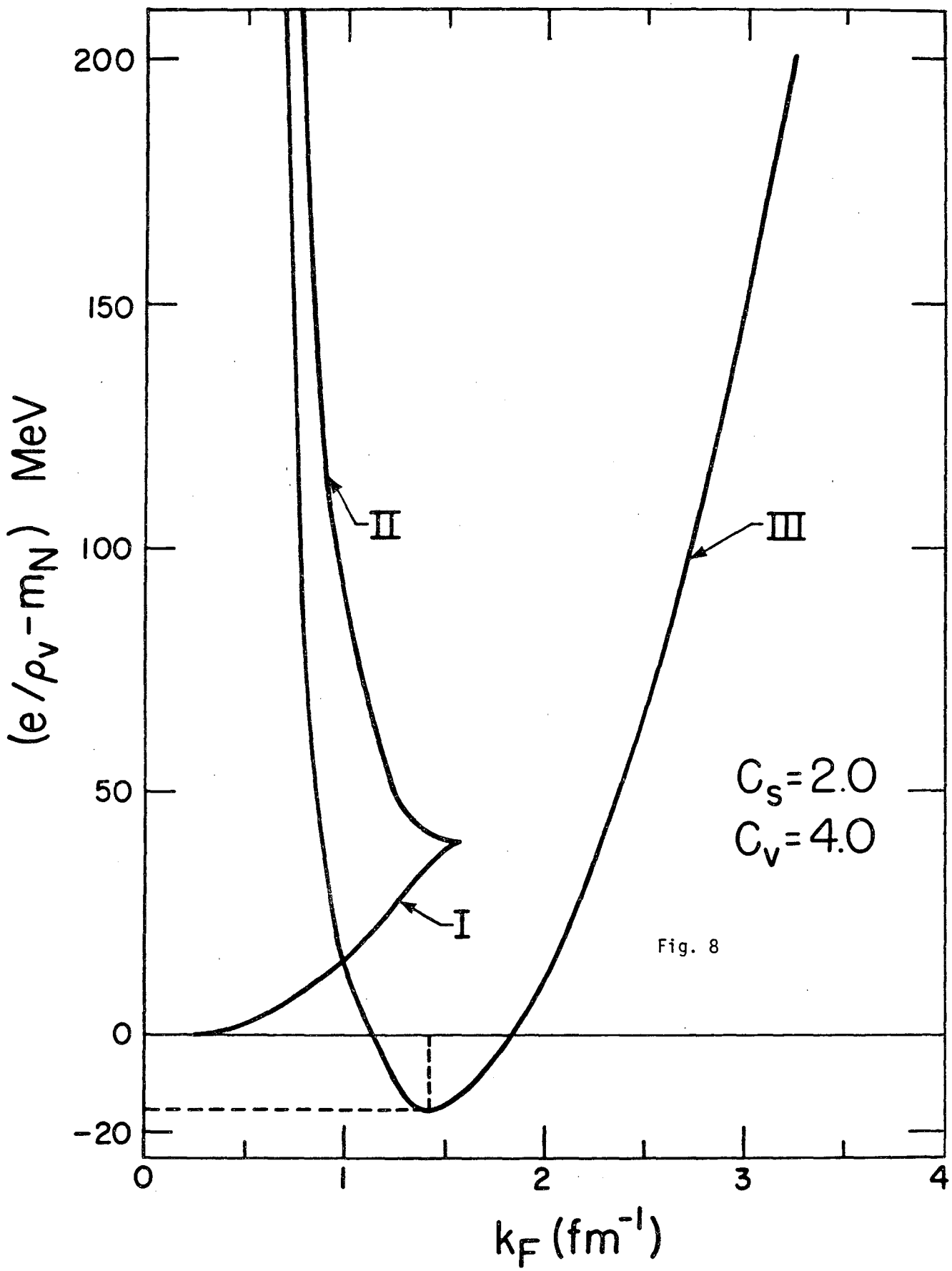

Fig. 8

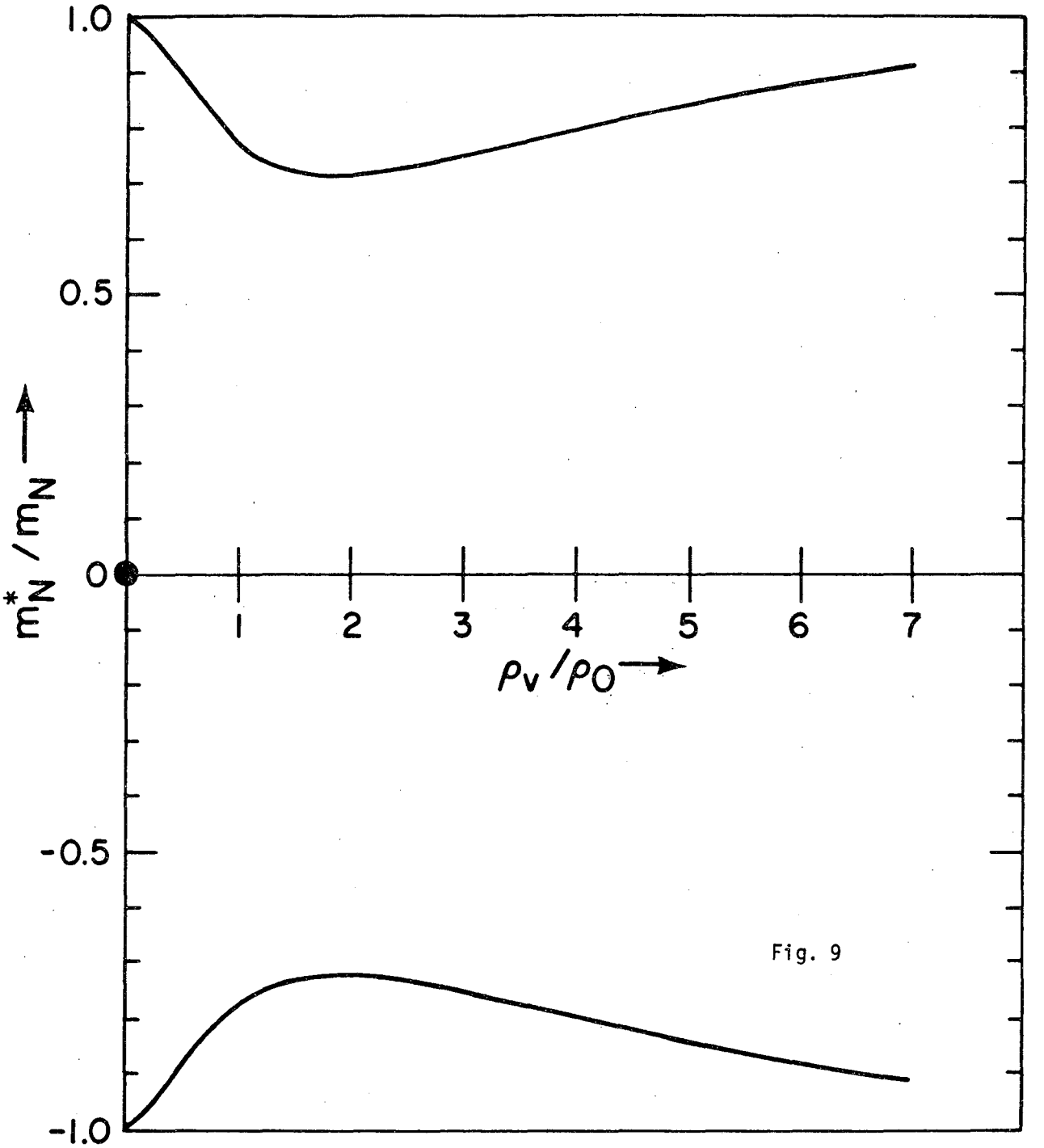

Fig. 9

XBL822-4468

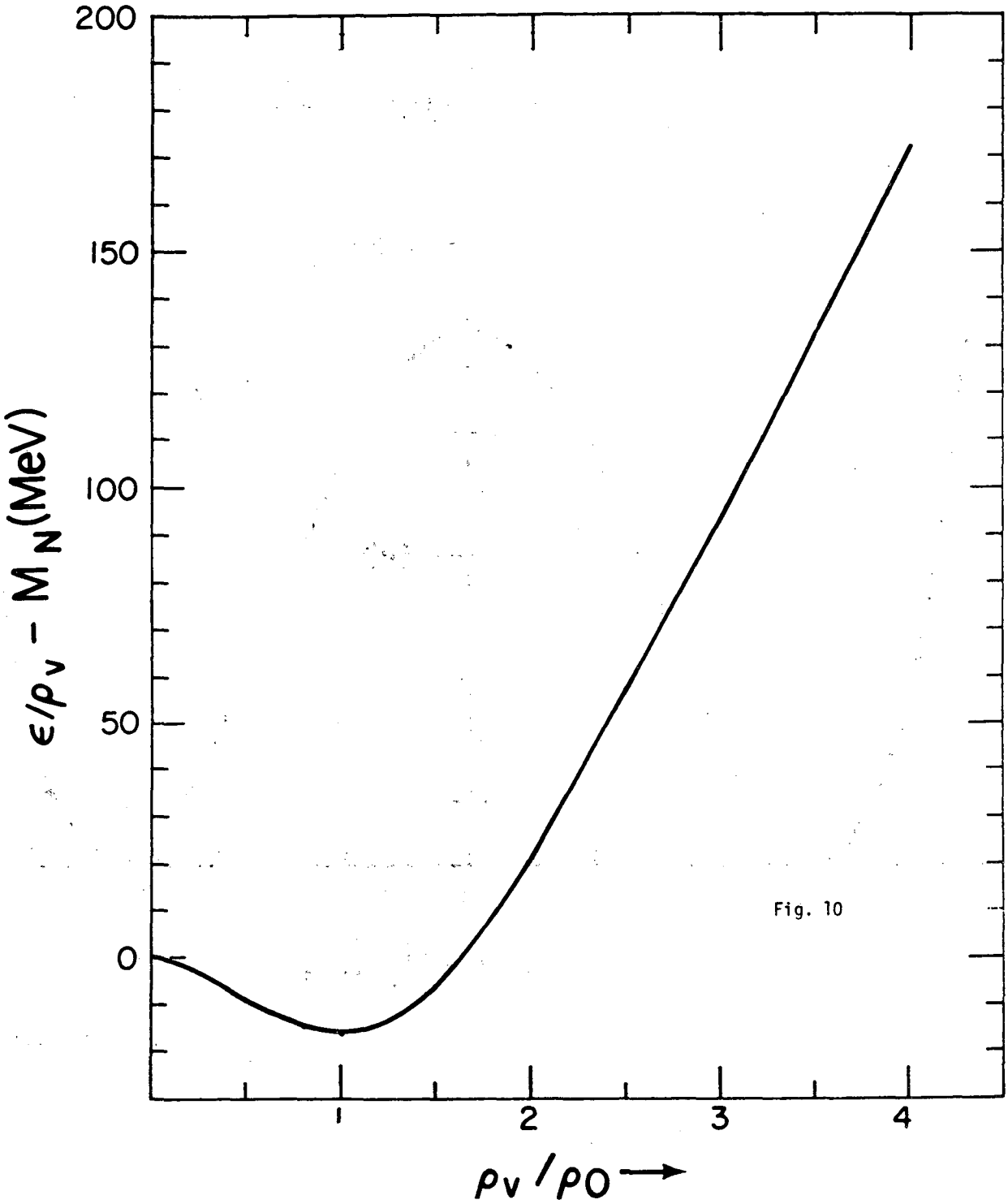

Fig. 10

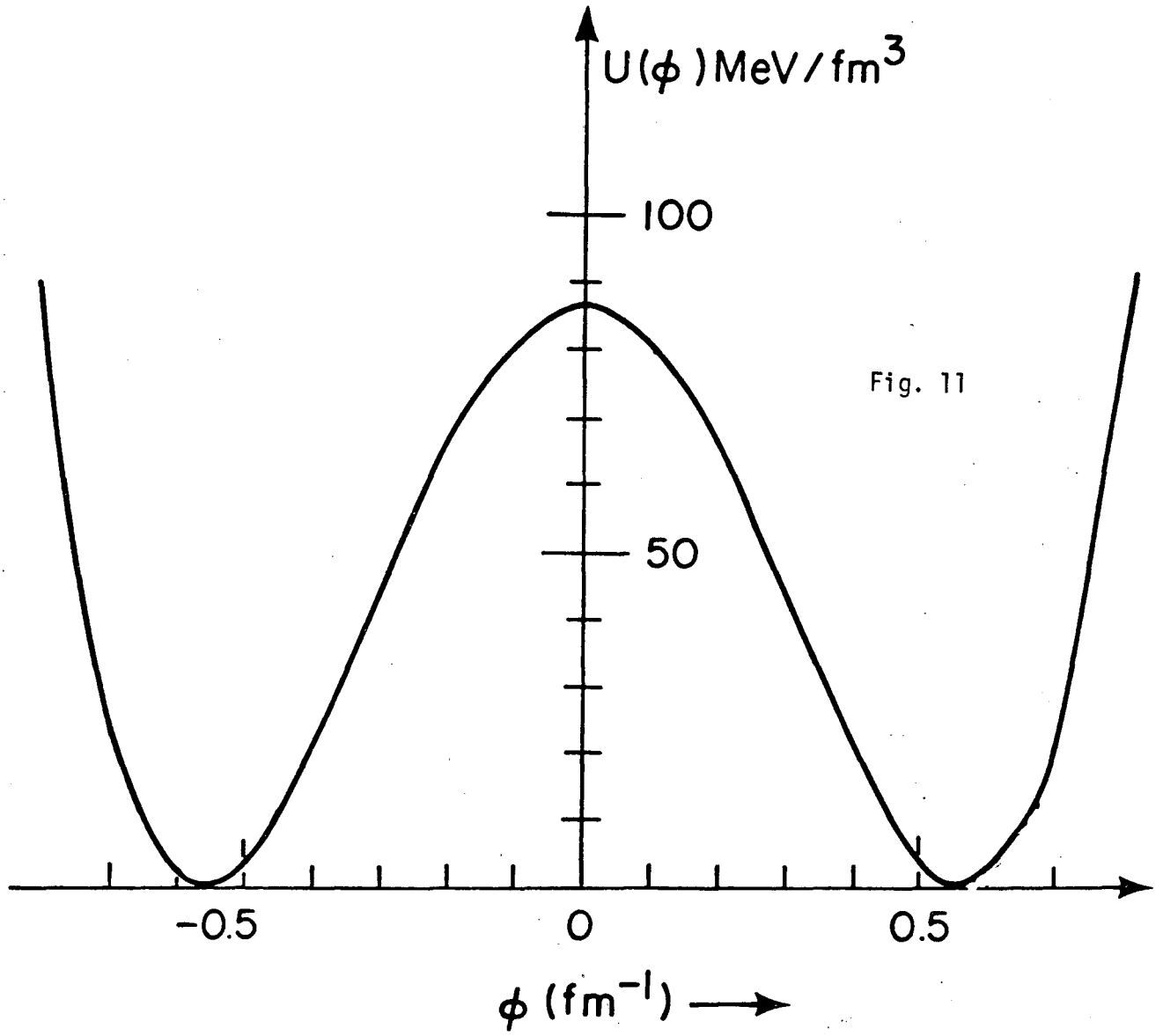

Fig. 11

XBL822-4465

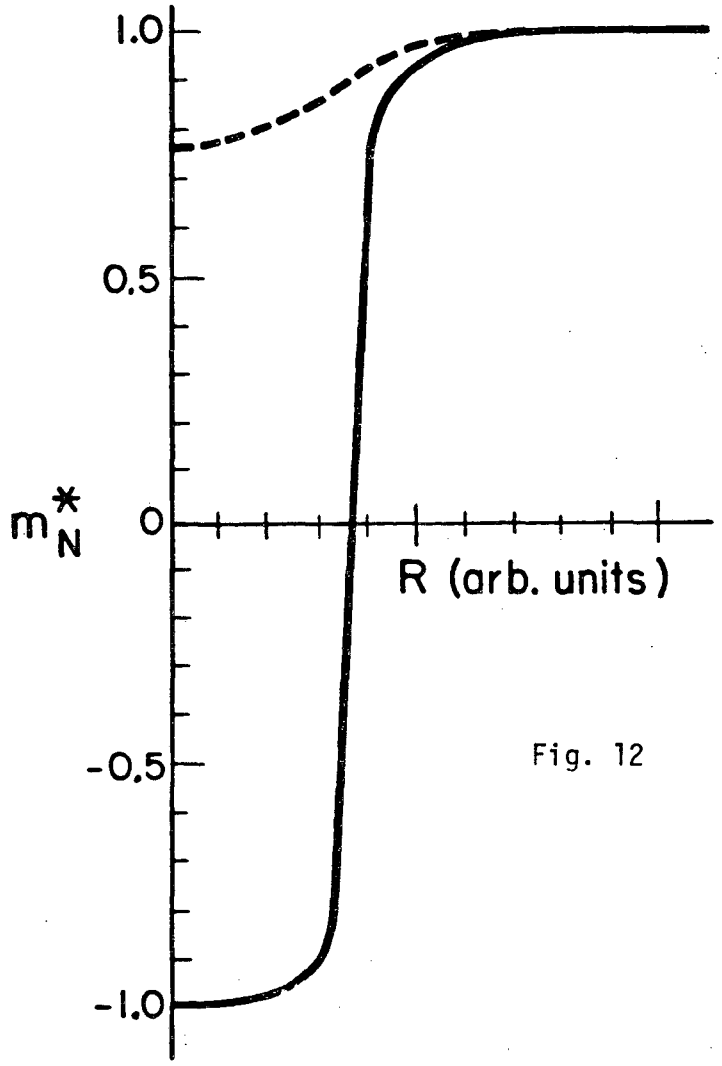

Fig. 12

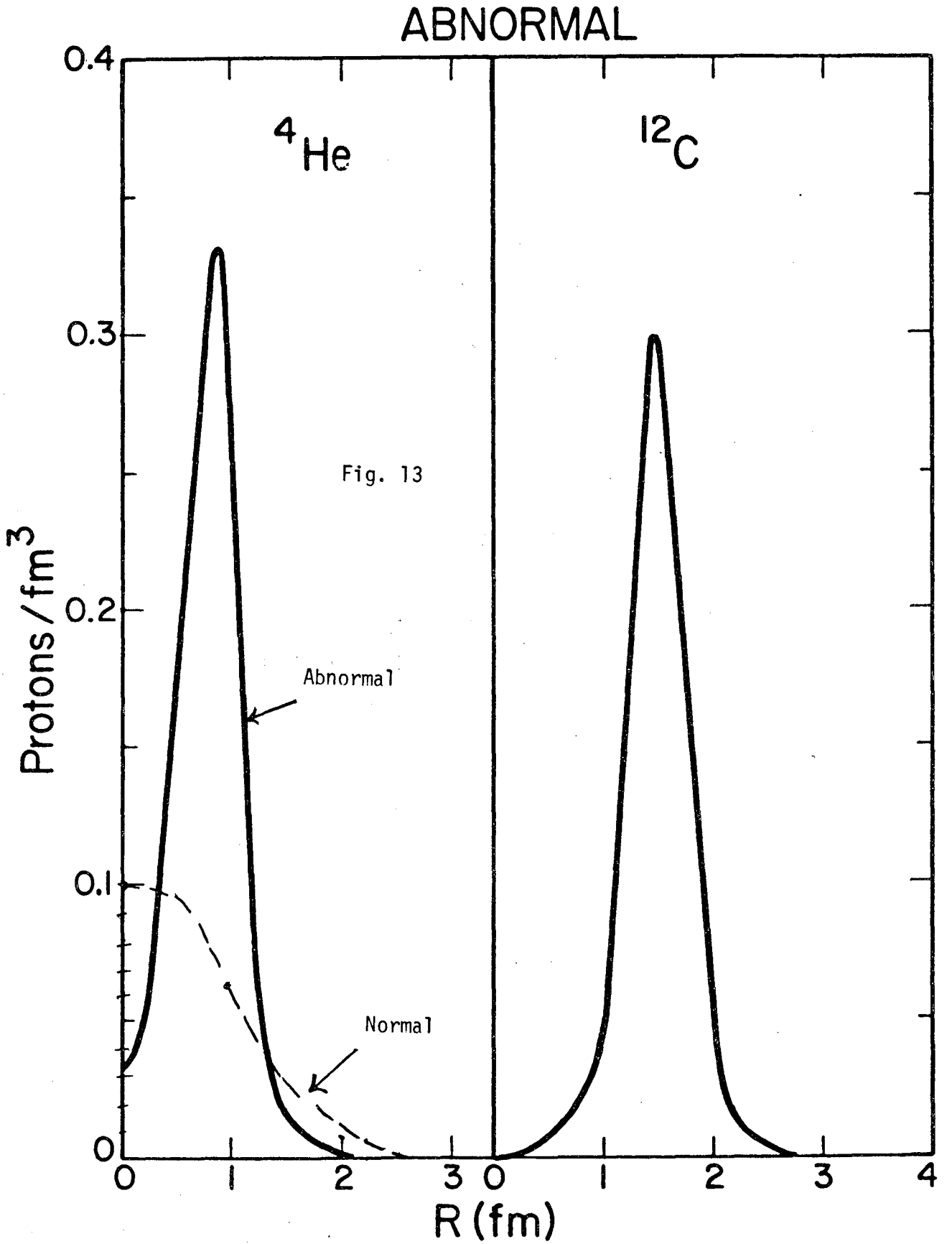
ABNORMAL
^{4}He
^{12}C
Protons/fm^3
0.4
0.3
0.2
0.1
0
Abnormal
Normal
0
1
2
3
0
1
2
3
4
R (fm)

Fig. 13

QUASI-MOLECULAR STRUCTURES IN NUCLEAR SYSTEMS

Y. C. Tang
School of Physics, University of Minnesota, Minneapolis, Minnesota, USA 55455

Abstract: Theoretical and/or experimental evidence is presented to show that there exist quasi-molecular structures in light, medium, and heavy systems. At relativistic energies, an impulse mechanism, which can effectively excite the quasi-molecular states, is described. Plausible arguments are given, which suggest that the observation of anomalons and the asymmetric fission in the Au-region may both be related to the existence of quasi-molecular structures in nuclei.

1. INTRODUCTION.

Recent experiments to study the interactions of relativistic heavy ions in nuclear emulsions have led to the following interesting observations:

(i) The production of projectile fragments which have anomalously short mean free paths [1-4]. These fragments are now often referred to as anomalons.

(ii) A large asymmetric-fission yield in the interaction of relativistic Au projectiles with emulsion nuclei [5]. This is an important discovery, since it was frequently believed that symmetric fission predominates if the fissioning nucleus has fewer than 132 neutrons [6].

The purpose of this talk is to show that both of these phenomena may be associated with the existence of quasi-molecular structures or states (QMS) in medium and heavy nuclei. As will be discussed below, these states can be appreciably excited by an impulse mechanism which is especially effective at relativistic energies.

Because of the indistinguishability of the nucleons, it is of course not possible to give a precise definition for the quasi-molecular structure [7]; therefore, only a rather pictorial description will be presented here. An QMS is considered as a relatively weakly bound or quasi-bound structure consisting of nucleon clusters which do not overlap strongly with one another. For such a structure, the characteristic features are: (i) it has a large spatial extension and is strongly deformed with a large intrinsic quadrupole moment, (ii) it has large reduced width for decaying into constituent clusters, and (iii) there exist rather well-formed rotational bands with large moments of inertia.

The reason for the existence of QMS is quite well understood. It is associated with the observation that the intracluster interaction is strong, but the intercluster interaction is comparatively weak [8,9]. From a microscopic viewpoint, these particular features arise as a consequence of the Pauli principle and the fact that the nucleon-nucleon potential has a strong triplet-even tensor part and a large Majorana component.

The best-known example of a quasi-molecule is the nucleus ^{8}Be in its lowest 0^+, 2^+, and 4^+ states. Each of these states is unbound and the alpha-particle reduced width is very large, close to the single-particle limit. In addition, a theoretical calculation [10] using the generator-coordinate method [11] has shown that the average separation distance between the alpha clusters is even slightly larger than the sum of their rms radii. These findings indicate that ^{8}Be can indeed be reasonably viewed as having a molecule-like structure made of two alpha clusters.

In sect. 2, we discuss the theoretical and experimental evidence of the presence of QMS in light, medium, and heavy systems. An impulse mechanism, which can effectively excite these states at relativistic energies, is then described in sect. 3. In sect. 4, we present plausible suggestions regarding the possible significance of QMS in explaining the observation of anomalons and asymmetric fission in the Au-region. Finally, in sect. 5, concluding remarks are made.

2. EXISTENCE OF QUASI-MOLECULAR STRUCTURES IN NUCLEAR SYSTEMS.

2.1. QMS in light systems

It is well known that nuclei exhibit different kinds of behavior. Some of these are due to single-particle features, while others are connected with collective motions of the nucleons. The relative importance of the various types of behavior can change significantly from nucleus to nucleus and even from one level to the next.

The interesting phenomena of structure change have particularly been noticed in light nuclear systems. For instance, in the nucleus ^{7}Li, the lowest four levels are QMS having predominantly an t + α cluster configuration, while the level at 7.47 MeV experiences a change in structure and has instead an n + ^{6}Li cluster configuration (see fig. 1). In the self-conjugate 4n-nuclei, the study of structure change has especially been carried out (for a comprehensive review, see ref. [12]) and the result can be schematically summarized by the so-called Ikeda diagram [13] depicted in fig. 2 where the unlabelled smaller circles represent α clusters. From this figure, it is seen that there appear between the ground-state series dominated by shell-model character and the series formed by complete dissociation into α clusters many intermediate quasi-molecular-like series of states. Because of the relatively weak nature of the intercluster interaction, the dissociation energy is rather small compared to the internal energies of the clusters and, consequently, structure change can already occur in the region of low excitation. As a specific example, consider the nucleus ^{16}O. The 0^+ ground state can be

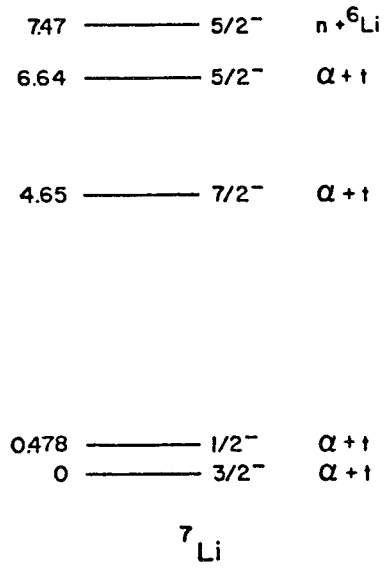

Fig. 1: Cluster structure of ^{7}Li.

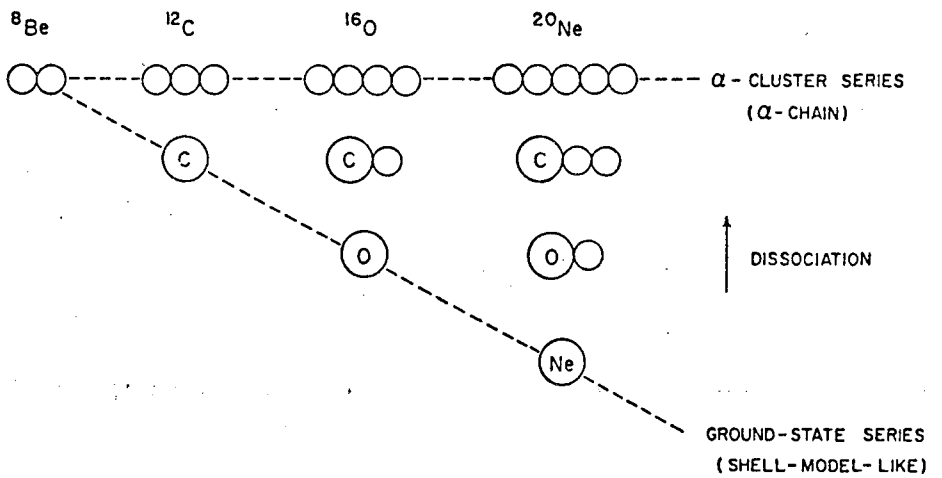

Fig. 2: Ikeda diagram of structure change in self-conjugate 4n-nuclei.

reasonably well described by a shell-model wave function, but the second 0^+ state has been shown by Suzuki [14] to have an $\alpha + {}^{12}C$ weak-coupling structure, with the ^{12}C cluster mainly in its ground state. The 4α linear-chain structure, originally proposed by Morinaga [15], may also have been experimentally found. The 2^+, 4^+, and 6^+ states [16], appearing at 17.13, 18.02, and 19.32 MeV, respectively, follow the energetic sequence of a rotational band with a very large moment of inertia. The 0^+ member of this band has, however, not yet been observed, although a theoretical study [17] did indicate that it may occur with an excitation of about 16.8 MeV.

There is no doubt that a large number of highly-deformed QMS exist in light systems. Some of these have even rather long lifetimes. For instance, the 3α linear-chain state of ^{12}C at 7.65 MeV has a half-life of about 10^{-17} sec, very long on the nuclear time scale. On the other hand, it is not at all clear whether there exists any light QMS with a lifetime as long as, say, 10^{-11} sec. This is an interesting question which certainly merits careful theoretical and experimental investigations.

2.2. QMS in medium-weight systems

For the discussion of QMS in medium-weight nuclei, we shall concentrate on ^{32}S as an example, since this particular nucleus has received detailed attention from many research groups. The possible existence of similar states in other nuclei of this mass region will be only briefly mentioned in this subsection.

As a first step, it will be useful to have a qualitative understanding of the main characteristics of the deformation energy or potential-energy surface. For this it is important to recognize that the ground and low-excited states of ^{32}S cannot be described by a cluster structure of two unexcited ^{16}O clusters [i.e., $(1s)^4(1p)^{12}$ configuration] in relative motion. In these states, at least one of the clusters must be an excited $^{16}O^*$ cluster. To have a configuration with two unexcited ^{16}O clusters in close proximity would require such strong correlations among the nucleons that,

because of the Pauli principle, the gain in potential correlation energy in keeping the ^{16}O clusters unexcited would not be sufficient to compensate for the resultant large increase in relative kinetic energy between these clusters. In the oscillator shell-model description of the low-lying states in ^{32}S, this implies that some of the nucleons have to be lifted up to the 2p-1f and higher oscillator shells.

The above discussion has been schematically and interestingly illustrated by Harvey [18] . In fig. 3a, two unexcited ^{16}O clusters at $\pm\infty$ are shown in a Cartesian representation with filled 1s and 1p orbits characterized by the oscillator quanta n_x, n_y, and n_z in the x, y, and z spatial directions. As these two clusters gradually approach each other along the z-axis, one finds that an excited intrinsic state of ^{32}S (denoted as $^{32}S^*$) is eventually formed which has the structure of an ^{28}Si prolate intrinsic state plus four nucleons in the 2p-1f shell. To reach the intrinsic structure of the ^{32}S ground state where the latter four nucleons should be in the 2s-1d shell, one requires instead (see fig. 3b) that, with one ^{16}O in its ground state, the other has to be in a 4p-4h state, presumably that observed at about 6-MeV excitation.

With a reasonable assumption, the intrinsic matter quadrupole moments Q_0 of the ^{32}S ground-state structure and the $^{32}S^*$ excited-state structure are given by 69 r_0^2 and 194 r_0^2, respectively, where r_0 is a radius parameter related to the radius R of the nucleus by the equation $R = r_0 A^{1/3}$. With this information and the discussion given in the preceding paragraph, Harvey suggested [18] that, along the potential-energy surface, the fission path for $^{32}S \rightarrow {}^{16}O + {}^{16}O$ must follow the hatched curve shown in fig. 3c. Indeed, constrained Hartree-Fock calculations [19,20] did find that this is a correct suggestion. In particular, the calculation of Zint and Mosel [19] showed that, for the states in the first and second potential wells, the intrinsic matter quadrupole moments are equal to 90 and 390 fm^2, respectively . This means that the values of r_0 should be appropriately chosen to be about 1.1 and 1.4 fm for these respective states, indicating that ^{32}S in its ground state is a more compact system than when it is in an excited state belonging to the second potential minimum.

The considerations given above can be generalized to other nuclei in this mass region. Based on symmetry arguments [18,21] , one can show that if the compound nucleus of an A + B system has more than six protons or six neutrons beyond the filled 1s and 1p shells, the potential-energy curve will generally have two minima, suggesting the possibility of the formation of highly-deformed QMS. For example, the nucleus ^{28}Mg, containing sixteen neutrons, may have quasi-molecular states of $^{14}C + {}^{14}C$ cluster structure [22] .

For the purpose of explaining terminology, a schematic diagram for the ^{32}S intrinsic or deformation energy is given in fig. 4 for a Hartree-Fock calculation constrained with respect to the c.m. separation distance. The states in the first well, having shell-model-like character and possessing weak clustering correlations, are referred to as class-I states, while those in the second well, having quasi-molecular structure and containing strong clustering features, are referred to as class-II states. In addition, it should be mentioned that the class-II states have sometimes been further

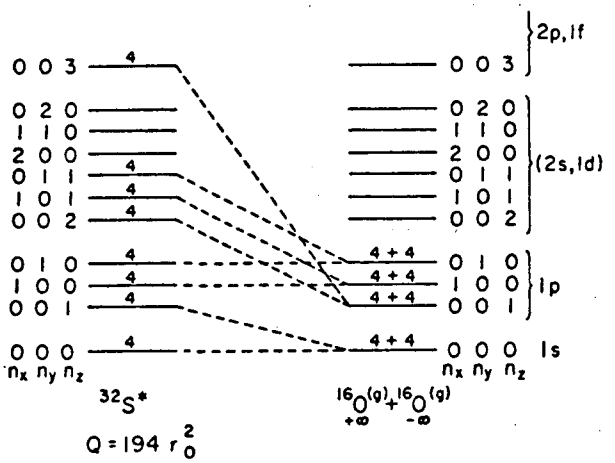

Fig. 3a: Schematic diagram of $^{32}S^*$ reached by the $^{16}O + ^{16}O$ configuration (adapted from ref. [18]).

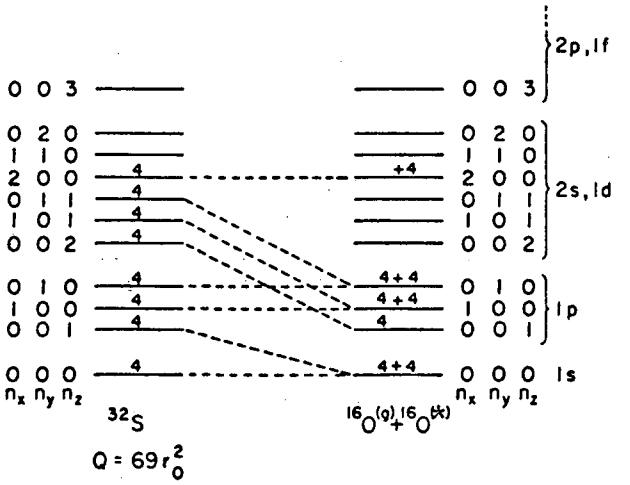

Fig. 3b: Schematic diagram of ^{32}S reached by the $^{16}O + ^{16}O^*$ configuration (adapted from ref. [18]).

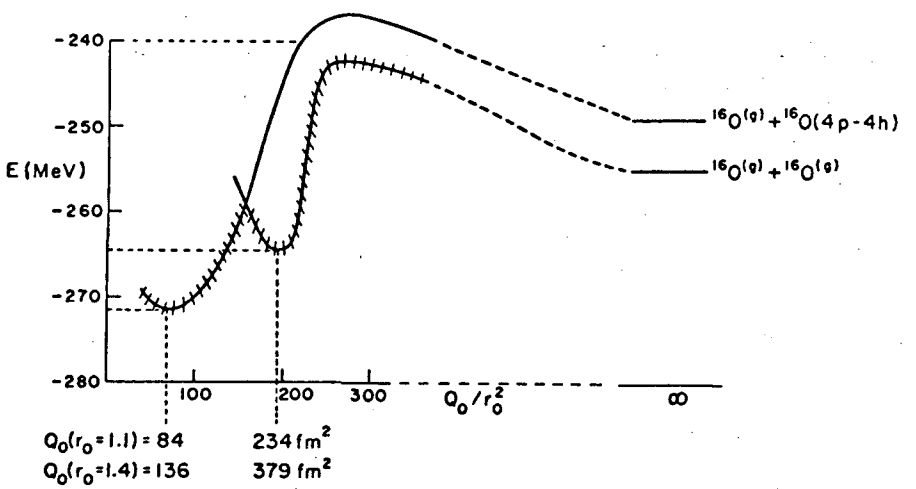

Fig. 3c: Schematic representation of the potential-energy surface in $^{32}S \rightarrow ^{16}O + ^{16}O$ (adapted from ref. [18]).

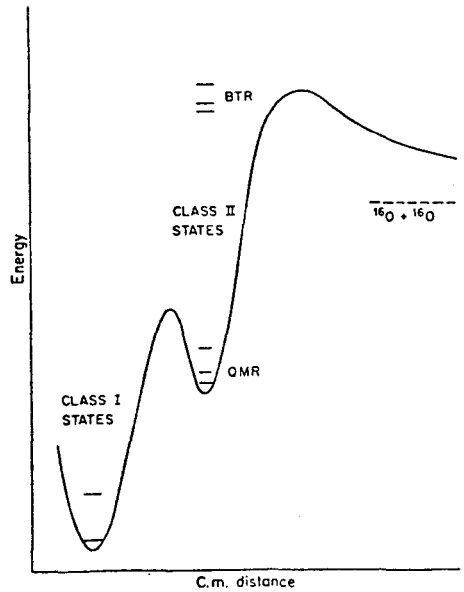

Fig. 4: Schematic diagram for the ^{32}S intrinsic energy as a function of the c.m. distance.

classified into two types of nuclear resonances. The barrier-top resonances (BTR) (also known as orbiting or surface-wave resonances) have short lifetimes and are responsible for the gross structures in the excitation functions and back-angle oscillations in the angular distributions. These resonances have been carefully studied experimentally by Bromley [23] and others. The quasi-molecular resonances (QMR) lie deep in the energy pocket and constitute well-formed rotational bands with large moments of inertia.†

The existence of class-II states in ^{32}S is supported by resonating-group calculations. In fig. 5, we show the $^{16}O + ^{16}O$ phase shifts δ_L calculated by Ando et al. [24] with the nucleon-nucleon potential V2 (m = 0.65) of Volkov [25]. Here one notes that there exist a BTR band with the bandhead at about 11 MeV and two QMR bands at lower energies.††

At present, the best quantitative study in ^{32}S seems to be that of Schultheis and Schultheis [26], utilizing the microscopic α-cluster model. These authors have performed an elaborate calculation with variation after projection. The results they obtained show a QMR band with the bandhead at an excitation energy of 7.5 MeV and a rotational constant of 77.7 keV. By studying the experimental energy spectrum of ^{32}S, they have tentatively identified the QMR 0^+, 2^+, and 4^+ states as the states determined experimentally [27] with excitation energies of 8.507, 9.065, and 10.276 MeV, respectively. In addition, it was found that the intrinsic state has a strong degree of $^{16}O + ^{16}O$ clustering, with the density distribution showing a distinct necked-in configuration (see fig. 6). The overlap between the intrinsic states for the QMR band and the ground-state band turned out to be very small, being only equal to 4×10^{-9}.

It is our belief that the QMR 0^+ state in ^{32}S is likely to be found in the 7 to 10 MeV excitation-energy region. This implies that the QMR states are stable against fission but are unstable against γ-decay and light-ion emission. The lifetimes should, however, be very long, since the light-ion processes have to proceed below the Coulomb and centrifugal barriers and all the transitions (except transitions among class-II states which are not of interest here) are additionally inhibited because of the very small overlap between class-I and class-II intrinsic states.

---

†In the following, the term QMS will be used to denote either the QMR or the BTR, or both of these types of resonances collectively.

††The number of QMR bands depends on the type of nucleon-nucleon potential used in the calculation [24].

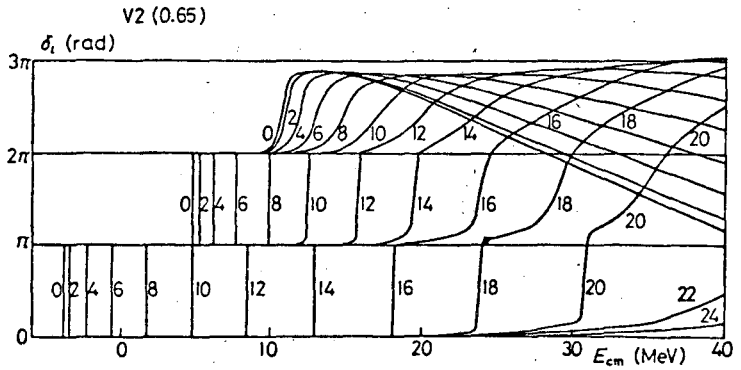

Fig. 5: Resonating-group phase shifts of $^{16}O + ^{16}O$ scattering (from ref. [24]).

It should be mentioned that our present understanding concerning the nature of QMS in medium-weight nuclei is mainly qualitative. In particular, there is no reliable estimate of the lifetimes of these states. For such an estimate, one will have to perform even more sophisticated many-nucleon calculations that those presently available.

2.3. QMS in heavy systems

There is strong experimental evidence that QMS, or fission isomers as they are frequently called, exist in actinide nuclei [6]. At present, about thirty isomers have been located in the region of the periodic table with $92 \leqslant Z \leqslant 97$ and $141 \leqslant N \leqslant 151$. They are long-lived and highly prolate-deformed; for example, the isomer ^{240}Am has a spontaneous half-life of about 10^{-3} sec and a large intrinsic quadrupole moment of 32.7 ± 2.0 b [28].

The existence of fission isomers suggests that the deformation-energy function (fission barrier) $\tilde{V}_{def}(\beta)$ should have two minima with respect to the deformation parameter β. In fig. 7, we show a schematic plot of $\tilde{V}_{def}(\beta)$ for an actinide nucleus having a neutron number $N \approx 146$. Here one sees that, because of structure effects, the fission barrier has two humps at deformations β_2 and β_4, with a deep second minimum occurring in-between at deformation β_3.

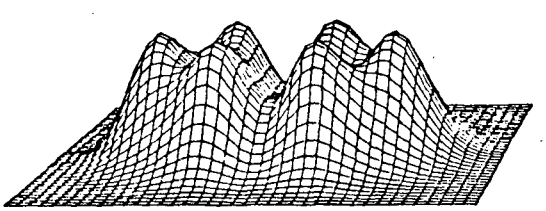

Fig. 6: Density of the intrinsic state of the QMR band in ^{32}S. The plot is for a cut along the axis connecting the centers of the ^{16}O substructures (from ref. [26]).

From the cluster viewpoint, the occurrence of such a double-humped fission barrier can be qualitatively understood [7]. The existence of a first minimum at a nonzero β value ($\beta = \beta_1$) accounts for the observation that the ground state of a nucleus with $N \approx 146$ is permanently deformed. This minimum occurs as a consequence of the formation of energetically favored substructures by the nucleons outside of the closed 82-proton and 126-neutron shells, which leads to a prolate deformation of the nucleus. If the deformation is increased

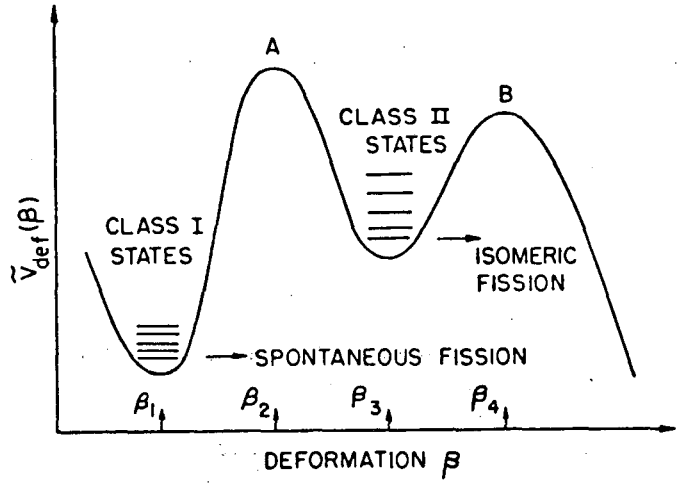

Fig. 7: A schematic plot of the deformation energy for an actinide nucleus having a neutron number around 146.

beyond β_1, then the deformation energy will increase until β reaches the value β_2. This increase is connected with the fact that some nucleons are excited out of the 82-proton and 126-neutron shells, thus breaking somewhat these favored configurations. Upon further increasing the value of β, then one expects that the energetically favored closed-shell substructures with N = 82, N = 50, and Z = 50 will come into play, and the formation of these substructures will bring an energy gain and thereby a decrease in the deformation energy. This decrease tends to be not too abrupt however, because there is a repulsive component in the effective interaction potential between these closed-shell substructures, representing the effect of the Pauli principle. At the second minimum where $\beta = \beta_3$, the formation of the closed-shell substructures with N = 82 and Z = 50 is mainly completed. With a further increase in β, $\tilde{V}_{def}$ is expected to increase again because these substructures themselves now become somewhat deformed which is energetically unfavored. This increase in $\tilde{V}_{def}$ will continue until β is equal to β_4. Beyond which, the decrease in Coulomb energy starts to become the dominant factor and $\tilde{V}_{def}$ then decreases monotonically all the way to the scission point.

To explain the extensive set of fission data available in the mass region A = 210 - 258, Gönnenwein et al. [29] proposed a two-mode hypothesis in which one fission mode (cluster mode) is determined by energetically favored cluster correlations, while the other fission mode (liquid-drop mode) is due to liquid-drop effects only. For all nuclei lighter than fermium (Z = 100), the cluster and liquid-drop modes correspond, respectively, to asymmetric and symmetric fission. Proceeding from this viewpoint, these authors have further given convincing arguments that, for fissioning nuclei with relatively low excitation, the cluster mode should prevail if favored closed-shell structures of N = 82, Z = 50, and N = 50, corresponding to the cluster configuration at the second energy minimum discussed in the preceding paragraph, can be built into the heavy and light clusters, respectively. An immediate consequence of this assertion is that, for nuclei with N < 132, strong asymmetric deformations will not generally occur and symmetric fission should be the dominant decay mode.

For conventional, low-energy fission induced by the absorption of a

photon, a neutron, or a charged light or heavy ion, the above conclusion was indeed found to be valid [6] . Here the experimental finding was that, with N < 132, the mass distribution is generally symmetric and the probability of observing binary products with a large difference in fragment masses is generally quite small. Recently, however, there is evidence to suggest that this conclusion may have to be modified. In an experiment [5] where relativistic gold nuclei (^{197}Au) with an initial kinetic energy of 1 GeV/nucleon were sent into emulsion stacks, it was observed that there occur a number of binary fission events, with each event accompanied by the simultaneous appearance of either no other charged-particle tracks or a very small number of proton and/or alpha-particle tracks. Out of these fission events, an appreciable fraction (about 30%) appears to be asymmetric fission events in which one fragment has a proton number around 26, and another fragment has a proton number around 52 (the uncertainty in charge identification is about 1 or 2 units). This is an astonishing discovery, which obviously demands that our present understanding of the fission process be further examined. In the following, we shall discuss the possibility that, by properly identifying the QMS and by taking into consideration an impulse mechanism (impulse fission), one may explain this observation of a large asymmetric fission yield in the Au-region.

3. IMPULSE MECHANISM AT RELATIVISTIC ENERGIES

In the preceding section, we have discussed the theoretical and/or experimental evidence for the existence of QMS in various nuclear systems. Now, the important question is: how are these states excited in relativistic collisions? To answer this question, we note that, in the case of fission in the Au mass region, there is clear experimental indication for the interaction involved to be peripheral in nature. This suggests that the excitation of the QMS is possibly effected by an impulse mechanism which proceeds in the following manner [4]. With the abrasion of a small number of nucleons or nucleon clusters, a projectile fragment (PF) remains. Let us now view the peripheral interaction between this fragment and an emulsion target in the Lorentz frame of the PF. As the target nucleus moves by with relativistic speed, the nucleons in the PF will experience, on the average, an attractive nuclear impulse and a repulsive Coulomb impulse, both of short duration and in the transverse direction. Because the nuclear force is short-ranged, it is clear that nucleons located in the near side of the PF will receive a much stronger nuclear impulse than those located in the far side. This is illustrated schematically in fig. 8, where b is the impact parameter and the small dots in the PF represent neutrons. As a result of these impulses, the nucleons in the near side will acquire an appreciable transverse linear momentum, but the amount of angular momentum tranferred to the PF perpendicular to the reaction plane will be quite small. The consequence of this is that there should be a substantial probability for the excitation of highly-deformed, low-angular-momentum states, such as the QMS.

It should be pointed out that the impulse mechanism is effective mainly at relativistic energies. If the incident kinetic energy per nucleon does not satisfy the criterion of being much higher than the Fermi energy (≈ 40 MeV), the projectile nucleons will have sufficient time to react to the changing field of the target nucleus as it goes by. The result is that

the PF will more likely be excited to a class-I higher-angular-momentum state than to a class-II low-angular-momentum state.

Based on the model discussed above, Bayman and Fricke [30] have made a simple calculation to estimate the excitation energy E^* acquired by the PF as a function of the impact parameter b. In this calculation, each nucleon in the PF, considered as a sphere of uniform density, is interacting with the target nucleus through an optical potential of Woods-Saxon shape. This latter potential is assumed to have a depth parameter of 50 MeV and geometry parameters determined entirely by the size of the target nucleus. Finite-range effects of the nucleon-nucleon potential are not taken into account in this calculation. The results at a kinetic energy of 1 GeV/nucleon for ^{32}S and ^{197}Au projectiles interacting with various nuclei are shown in fig. 9, where the solid arrow indicates the impact parameter for grazing collision. To correct for the finite range ($\approx$ 2 fm) of the nuclear force, we have made a crude compensation by simply shifting the solid arrow to the left by an amount equal to the difference between the rms radius of the folding potential and the matter rms radius of the target nucleus. This shift results in a compensated grazing distance indicated by the dashed arrow.

For ^{32}S, the values of E^* for grazing collisions are equal to 1.6, 17.0, and 25.2 MeV when the target nuclei are C, Br, and Ag, respectively. These values should be compared with the excitation-energy value of 7-10 MeV estimated for the QMS 0^+ state. In the case of ^{197}Au, the situation is rather similar. Now, the E^* values for grazing collisions are 2.4, 36.7, and 57.0 MeV for target nuclei of Ne, Br, and Ag, respectively. Here the quantity to be compared with is the barrier height for symmetric fission in the Au-region, which is equal to about 20 MeV [6].†

Keeping in mind the crudeness of the calculation, one can make the following qualitative conclusions:††

(i) The impulse mechanism does yield excitation energies of the desirable magnitude required for an appreciable excitation of the QMS.

(ii) The heavier nuclei (Br-Ag) may play a more effective role than the lighter nuclei (C-N-O) in the emulsion.

(iii) Especially in the ^{32}S case, it is noted that the E^* value from the carbon target is a fair fraction of the QMS excitation energy, indicating that the lighter elements in the emulsion must still be considered when the detailed behavior of the PF is the subject of the investigation.

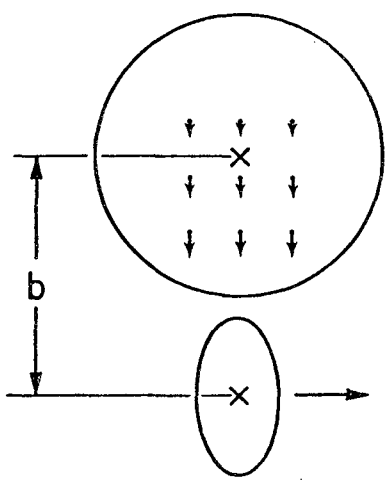

Fig. 8: A schematic plot of an impulse mechanism.

†The barrier height for asymmetric fission may be substantially smaller.

††To reach more definitive conclusions, one must perform a better calculation which takes into account finite-range effects, surface transparency for light nuclei, etc.

4. ANOMALONS AND ASYMMETRIC FISSION

4.1. Anomalon production

We propose now that the PF with anomalously short mean-free-path (mfp) or anomalons are, in fact, QMS of rather low angular momentum. This proposal is made in view of the following observations:

(i) The reaction cross section of the QMS is much larger than that of the corresponding normal nucleus. Again, consider ^{32}S as an example. The calculation of Schultheis and Schultheis [26] showed that the intrinsic proton quadrupole moment has a very large value of 208 fm^2, corresponding to that of a classical uniformly-charged spheroid of axis ratio 2.3 (remember that the actual density distribution has a necked-in configuration). Using these values one can estimate that, as far as reactions at relativistic energies are concerned where geometrical arguments are valid, the cross-sectional area presented by the ^{32}S anomalon is about 2.5 times larger than that presented by a normal ^{32}S nucleus.

(ii) The QMS may have a lifetime longer than 10^{-11} sec. Without an elaborate calculation, it is of course not possible to give a precise estimate of the QMS lifetime. However, the overlapping argument mentioned in subsect. 2.2 does indicate that it is not unreasonable to expect such a large value. In this respect, we should mention again that there are QMS in actinide nuclei which are known to have long lifetimes; for example, the experimentally determined half-life of the fission isomer of ^{242}Am is 14 msec [6] .

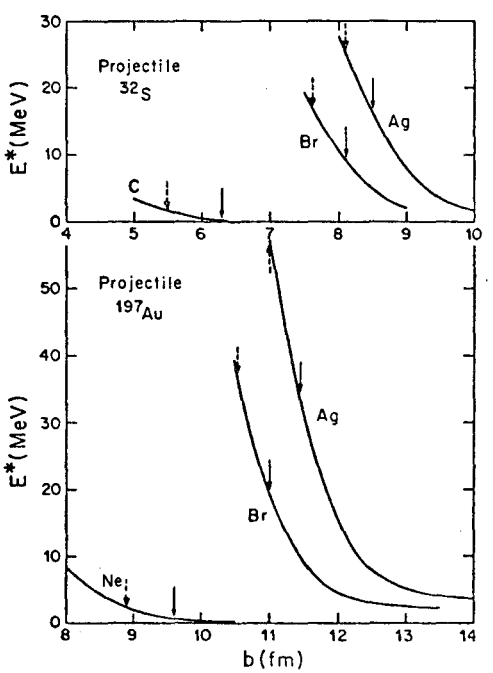

Fig. 9: Excitation energy E^* as a function of the impact parameter b.

(iii) The production probability of the QMS may be large. Here again, a detailed calculation will be necessary to yield reliable information. Because of the many-nucleon nature of the problem, such a calculation is, however, expected to be extremely difficult. Meanwhile, it should be noted that, in the related phenomenon of asymmetric fission in the Au-region, a large yield has been experimentally observed [5] . This can be considered as an indication that the impulse mechanism, which excites the compound nucleus or PF directly into its collective degree of freedom, is capable of yielding a large magnitude for the production probability.

Accepting the proposal of QMS as anomalons, we can proceed to discuss the following effects:

(a) Local-mfp effect, i.e., variation of the mfp λ of the PF with distance D from the point of origin. To discuss this

effect, let us further consider ^{32}S. For this nucleus, the normal mfp is about 10 cm. On the other hand, according to the discussion above, the QMS may have a much shorter mfp equal to about 5 cm. Assuming a production probability of 50%, one then finds that $\lambda(D < 2.5 \text{ cm}) = 6.8$ cm and $\lambda(D > 2.5 \text{ cm}) = 7.8$ cm. The difference of 1 cm is comparable to the observed effect [1] .

(b) Memory effect. The ^{32}S calculation of Schultheis and Schultheis [26] further showed that the QMS in its low-angular-momentum state has a larger radius and a more diffused surface than the corresponding normal nucleus. In addition, it was found that the intrinsic structure of the QMS has a neck of substantial thickness. This means that, when the QMS interacts with a target nucleus in a peripheral collision, only a very small number of nucleons will be abraded owing to the abnormally low density in the surface region and the PF will continue forward with just a small reduction in its size. From the viewpoint of the intrinsic structure, one can reach the same conclusion by noting that, after the abrasion of a small fragment, matter will flow across the neck to yield another necked-in configuration. Thus, it is rather natural to expect a memory effect in the QMS anomalon model.

(c) Isotope effect. Even for a fixed value of Z, the projectile fragments do not have a homogeneous composition. In addition to nuclei within the valley of stability, there may also appear in PF long-lived neutron-rich isotopes such as ^{9}Li, ^{16}C, and so on. Because of anticipated low abundances, the effect on mfp arising from the presence of such isotopes is generally not expected to be of major significance. However, there are special situations where a careful account of the isotope effect should be made. One such situation is the Z = 2 (He) case, where even a rather small fraction of ^{6}He may cause the appearance of a seemingly anomalous behavior. The reason is as follows. The isotope ^{6}He is a lightly bound, particle-stable system and the isobaric-spin partner of ^{6}Li in its excited T = 1 state. Its mfp in emulsion should be substantially shorter than that of ^{6}Li (T = 0 ground state), which is about 14.5 cm. A reasonable guess would be, say, 10 cm, which is much shorter than the mfp of either ^{3}He or ^{4}He in emulsion. As a numerical example, we take $\lambda(^{3}He \text{ or } ^{4}He) = 20$ cm, $\lambda(^{6}He) = 10$ cm, and a 10% population of ^{6}He, and study the local-mfp effect. The result is $\lambda(D < 3 \text{ cm}) = 18.3$ cm and $\lambda(D > 3 \text{ cm}) = 19.1$ cm. Although the difference in these two λ-values is fairly small, He-fragments are abundantly produced and one may be able to detect a difference of this magnitude in the future.

(d) Projectile effect. Only one interesting question will be discussed here. This question is: could the ^{6}He population in the Z = 2 PF depend sensitively on the type of projectile used? The answer is possibly in the affirmative. In anomalon investigations, the projectile used is usually ^{56}Fe which has 26 protons and 30 neutrons. If we view this nucleus as consisting of a Z = 20, N = 20 core plus 6 protons and 10 neutrons in the outside region, then the neutron-richness of the surface may cause an enhancement of ^{6}He production in the projectile fragments. This is in contrast to the case where ^{12}C or ^{16}O nuclei are used as projectiles; here, no such enhancement is expected and the ^{6}He population should be rather low. Thus, the observation of a local-mfp effect in the Z = 2 case may be projectile-dependent, a possibility which is certainly worth looking into.

(e) Detector effect. In addition to nuclear emulsion, CR-39 with composition $C_{12}H_{18}O_7$ has recently also been used as track detector. So we are now faced with the question as to which of these two types of detectors is more

appropriate in studying the anomalous behavior of the PF. Our discussion in sect. 3 indicates that heavier nuclei Br-Ag may be more effective in exciting the QMS than lighter nuclei C-N-O. This would imply that anomalons may be more readily produced in nuclear emulsion than in CR-39, although it is our belief that some anomalous effects may still be observed in the latter detector. In making these statements, we should mention again that we are relying entirely on the E^*-results shown in fig. 9. These results were obtained from a calculation [30] which is based on non-relativistic concepts and is quite crude at this stage. Therefore, it would be prudent to view these statements as merely suggestive and postpone more definitive conclusions until a better calculation has been performed.

(f) Energy-threshold effect. There was suggestion [31] for the existence of an energy threshold below which the anomalous behavior may be quite insignificant. In the QMS anomalon model, energy-dependent effects arise because the impulse mechanism is effective in exciting the QMS only at relativistic energies. As is discussed in sect. 3, such a mechanism will, in particular, be ineffectual when the kinetic energy per nucleon is not much higher than the Fermi energy. Thus, an energy threshold may very well exist, although the lack of a detailed calculation prevents us from making any quantitative statement at this moment.

(g) Odd-even effect. The question here is [32]: do odd-Z and even-Z PF show different anomalous behavior? Our opinion is that they probably do not. If one adds a proton to the ^{32}S anomalon, the resultant structure may have slightly larger binding; however, the nucleus will remain in its QMS and there may be only a slight reduction in the geometrical size. Thus, any odd-even effect is not expected to be appreciable.

Finally, we wish to discuss the often-asked question concerning the lowest value of Z below which anomalous behavior is not expected to be present. In the case of QMS consisting of binary clusters, the discussion in subsect. 2.2 indicates that such structure with a sufficiently long lifetime may not exist below Z = 12. However, there may appear in the lower-Z region other exotic structures such as the linear-chain structure mentioned in subsect. 2.1. For such structures, the main problem is that there is no reliable calculation to give us any information about the lifetime. Clearly, much work has yet to be done in order to establish whether or not these exotic structures may turn out to be low-Z anomalous projectile fragments.

4.2. Asymmetric fission in the Au-region

The observation by Freier and Waddington [5] of a large asymmetric fission yield in the Au-region is a new and exciting discovery in the field of nuclear fission. According to the two-mode theory of Gönnenwein *et al.* (see subsect. 2.3), one must now look for the QMS or binary-cluster state which is responsible for such a fission process. In constructing this state, it is important to keep in mind energetically-favored substructures and symmetry-energy considerations [7] . The general guidelines are: (i) closed-shell cluster configrations with a few outside nucleons play a dominant role in determining the characteristics of asymmetric fission, and (ii) the neutron-to-proton ratio in each cluster must be nearly the same as that in the original compound nucleus; i.e., $N_h/Z_h \approx N_\ell/Z_\ell \approx N/Z$, where (N,Z), (N_h,Z_h), and (N_ℓ,Z_ℓ) represent the neutron and proton numbers of the

compound nucleus, the heavy cluster, and the light cluster, respectively. By assuming in addition that, near the scission configuration, the surplus nucleons form the neck joining the two clusters and that there is nearly equal scission probability anywhere along the neck, one can then obtain a reasonable account of the essential features of the primary fragment mass distribution.

We discuss now the neutron and proton configurations of the heavy and light clusters. First, we note that, for nuclei around Au, the neutron-to-proton ratio is about 1.5. Then, to comply as closely as possible with the guidelines mentioned above, we choose $(N_h,Z_h) = (82,50)$ for the heavy cluster and $(N_\ell,Z_\ell) = (28,20)$ for the light cluster. With this choice, the neutron-to-proton ratios are $N_h/Z_h = 1.64$ and $N_\ell/Z_\ell = 1.40$. This will leave a neck that is proton-rich, except in the unlikely event that, during the peripheral collision between the Au projectile and an emulsion target nucleus, most of the abraded nucleons were protons. To produce these doubly-closed-shell clusters and a proton-rich neck requires some redistribution of the original nuclear charge. The important point to note here is that this charge redistribution could be facilitated as a consequence of the sharp Coulomb impulse received by the compound nucleus. In conventional experiments where low-energy particles initiate the formation of fissioning compound nuclei, such a mechanism is not readily present. As a result, the probability of exciting class-II configurations in these experiments is not appreciable and asymmetric fission yield in the Au region was found to be quite small.

After scission takes place across the neck, the resulting light fragment will have a proton number between 20 and about 28, in agreement with the recent experimental finding of Freier and Waddington [5]. This indicates that the new features discussed here, namely, impulse excitation of class-II configurations and charge redistribution by Coulomb effects, are important and should be incorporated into any complete theory of nuclear fission.

It should be mentioned that there was experimental evidence for asymmetric fission even in lighter elements. The 190-MeV [33] and 600-MeV [34] proton-induced fission of Ce (natural composition; Z = 58) showed that the mass distribution is asymmetric with mass peaks at about 50 and 80 mass units.† This suggests that doubly-closed-shell configurations with $(N_h,Z_h) = (50,28)$ and $(N_\ell,Z_\ell) = (28,20)$ may be involved in the fission process and QMS may be present also in this mass region.

To complete our discussion, we consider again asymmetric fission in the Au-region. When the compound nucleus is on its way to scission, the neck becomes more and more stretched, and this stretching will in turn exert a significant influence on the structures of the heavy and light clusters. Thus, it is distinctly possible that, after scission takes place, the resulting fragments may be left in their respective excited class-II configurations. For the light fragment, the discussion in

---

†Asymmetric mass distributions have also been observed for Pr with Z = 59 [33] and La with Z = 57 [34]. It would be of interest to perform an experiment in which relativistic La projectiles are sent into emulsion or other suitable target.

subsect. 2.1 indicates that the QMS involved may have an C + Ca or other similar cluster configurations. For the heavy fragment, the observation of asymmetric fission in Ce, mentioned in the preceding paragraph, suggests that here the QMS may have a binary-cluster nature with $(N_h, Z_h) = (50,28)$, $(N_\ell, Z_\ell) = (28, 20)$, and a few loosely bound nucleons. If, in addition, one assumes that these QMS happen to have also sufficiently long lifetimes, then some of the fragments from asymmetric fission will behave as anomalons†—a very interesting and intriguing possibility!

Although the above suggestion is quite speculative, there is, in fact, some experimental evidence in its support. In their experiment with Au projectiles, Freier and Waddington ([5] and private communication) found that 11 out of 14 asymmetric-fission fragments interacted in the emulsion stack, resulting in mfp values which are only about 49% of the expected values for the corresponding normal nuclei. This is in sharp contrast to the situation occurring in symmetric fission where they found that only 3 out of 22 fragments created further interactions within the emulsion. Thus, even though the number of events is not large, the evidence is quite convincing that asymmetric-fission fragments may indeed be anomalous. In this respect, it should be noted that heavy fragments from asymmetric fission of uranium have the same character as those from asymmetric fission in the Au-region. Therefore, it will be of great interest to examine the nature of the heavy fragments when relativistic uranium projectiles interact peripherally with emulsion nuclei and undergo asymmetric fission.

5. CONCLUSION

In conclusion, I wish to make the following statements:

(i) Quasi-molecular structures may exist in many regions of the periodic table.

(ii) At relativistic energies, the impulse mechanism is very effective in exciting the quasi-molecular states.

(iii) The observation of anomalons and the asymmetric fission in the Au-region may both be related to the existence of quasi-molecular structures in nuclei.

Many remarks given in this talk are not only qualitative but also speculative. It is my hope that much theoretical and experimental work will be performed in the future to either support or disprove these remarks.

Acknowledgments

I would like to take this opportunity to express my gratitude to B. F. Bayman, P. J. Ellis, P. S. Freier, and C. J. Waddington for valuable discussion and constructive criticisms. Also, I wish to thank S. Fricke and

†The possibility that asymmetric-fission fragments may be anomalon-like was first mentioned to me by Freier and Waddington.

B. F. Bayman for the permission to quote their results prior to publication.

This work was supported in part by the U. S. Department of Energy under Contract No. DOE/DE-AC02-79 ER 10364

REFERENCES

1. E. M. Friedlander, R. W. Gimpel, H. H. Heckman, Y. J. Karant, B. Judek, and E. Ganssauge, Phys. Rev. Lett. 45, 1084 (1980) and Phys. Rev. C27, 1489 (1983).
2. P. L. Jain and D. Das, Phys. Rev. Lett. 48, 305 (1982).
3. H. B. Barber, P. S. Freier, and C. J. Waddington, Phys. Rev. Lett. 48, 856 (1982).
4. B. F. Bayman, P. J. Ellis, and Y. C. Tang, Phys. Rev. Lett. 49, 532 (1982).
5. P. S. Freier and C. J. Waddington, submitted to Phys. Rev. Lett. and contribution to this workshop.
6. R. Vandenbosch and J. R. Huizenga, Nuclear Fission (Academic Press, New York, 1973).
7. K. Wildermuth and Y. C. Tang, A Unified Theory of the Nucleus (Vieweg, Braunschweig, Germany, 1977).
8. K. Ikeda, in Proc. of the INS-IPCR Symposium on Cluster Structure of Nuclei and Transfer Reactions induced by Heavy Ions, edited by H. Kamitsubo, I. Kohno, and T. Marumori (IPCR Cyclotron Progress Report, Supplement 4, 1975), p. 23.
9. V. G. Neudatchin and Yu F. Smirnov, in Progress in Nuclear Physics, edited by D. M. Brink and J. H. Mulvey (Pergamon, London, 1969), Vol. 10, p. 275.
10. A. Arima, H. Horiuchi, K. Kubodera, and N. Takigawa, in Advances in Nuclear Physics, edited by M. Baranger and E. Vogt (Plenum, New York, 1972), vol. 5, p. 345.
11. D. M. Brink, in Proc. of the Intern. School of Physics, "Enrico Fermi", Course 36, Varenna, edited by C. Bloch (Academic, New York, 1966), p. 247.
12. Y. Fujiwara, H. Horiuchi, K. Ikeda, M. Kamimura, K. Katō, Y. Suzuki, and E. Uegaki, Prog. Theor. Phys. (Suppl.) 68, 29 (1980).
13. K. Ikeda, N. Takigawa, and H. Horiuchi, Prog. Theor. Phys. (Suppl.) extra number (1968) 464.
14. Y. Suzuki, Prog. Theor. Phys. 55, 1751 (1976); 56, 111 (1976).
15. H. Morinaga, Phys. Rev. 101, 254 (1956).
16. P. Chevallier, F. Scheibling, G. Goldring, I. Plesser, and M. W. Sachs, Phys. Rev. 160, 827 (1967).
17. D. M. Brink, H. Friedrich, A. Weiguny, and C. W. Wong, Phys. Lett. 33B, 143 (1970).
18. M. Harvey, in Proc. of the 2nd Intern. Conf. on Clustering Phenomena in Nuclei, College Park, Maryland, 1975, edited by D. A. Goldberg, J. B. Marion, and S. J. Wallace (National Technical Information Service, U. S. Department of Commerce, Springfield, Virginia, 1975), p. 549.
19. P. G. Zint and U. Mosel, Phys. Lett. 58B, 269 (1975).
20. S. J. Krieger and C. Y. Wong, Phys. Rev. Lett. 28, 690 (1972).
21. P. Kramer, in Proc. of the Intern. Symposium on Clustering Phenomena in

Nuclei, Tübingen, 1981, edited by P. Kramer and R. Schultheis (Tübingen University Press, 1981), p. 171.
22. D. Baye, in Proc. of the Intern. Conf. on the Resonant Behaviour of Heavy-Ion Systems, Aegean Sea, Greece (1980), p. 103.
23. D. A. Bromley, in Proc. of the 2nd Intern. Conf. on Clustering Phenomena in Nuclei, College Park, Maryland, 1975, edited by D. A. Goldberg, J. B. Marion, and S. J. Wallace (National Technical Information Service, U. S. Department of Commerce, Springfield, Virginia, 1975), p. 465.
24. T. Ando, K. Ikeda, and A. Tohsaki-Suzuki, Prog. Theor. Phys. 64, 1608 (1980).
25. A. B. Volkov, Nucl. Phys. 74, 33 (1965).
26. H. Schultheis and R. Schultheis, Phys. Rev. C25, 2126 (1982).
27. P. M. Endt and C. van der Leun, Nucl. Phys. A310, 1 (1978).
28. C. E. Bemis, Jr., J. R. Beene, J. P. Young, and S. D. Kramer, Phys. Rev. Lett. 43, 1854 (1979).
29. F. Gönnenwein, H. Schultheis, R. Schultheis, and K. Wildermuth, Z. Phys. A278, 15 (1976).
30. B. F. Bayman and S. Fricke, private communication.
31. M. M. Aggarwal, K. B. Bhalla, G. Das, and P. L. Jain, in Proc. of the Fifth Heavy-Ion Conference, University of California, Berkeley, California (1981).
32. M. L. Tincknell and P. B. Price, contribution to this workshop.
33. F. D. Becchetti, J. Jänecke, P. Lister, K. Kwiatowski, H. Karwowski, and S. Zhou, Phys. Rev. C28, 276 (1983); F. D. Becchetti, private communication.
34. H. Å. Gustafsson, G. Hyltén, B. Schrøder, and E. Hagebø, Phys. Rev. C24, 769 (1981).

Anomalous Nuclei and a Nonstatic Metastable σ-τ Phase

F. Palumbo
INFN, Laboratori Nazionali di Frascati
00044 Frascati, Italy

Recent experiments[1, 2] have confirmed previous observations[3] of light anomalous nuclei. These nuclei are characterized by a lifetime of a least 10^{-11} s and by a cross-section which exceeds the geometrical bound by one order of magnitude[1].

A cross-section exceeding the geometrical bound is something so extraordinary that it seems to us to be worthwhile considering any mechanism which could possibly explain it, even if an explicit calculation is not possible at present. We, therefore, make here some qualitative considerations relating such cross-sections to a possible metastable σ-τ phase[4] (spin-up protons and spin-down neutrons displaced with respect to spin-down protons and spin-up neutrons).

Let us suppose that under the compression caused by the collision a nucleus be led to a σ-τ phase. If the separation energy between the nucleons with $\sigma_3\tau_3 = 1$ and the nucleons with $\sigma_3\tau_3 = -1$ has a local minimum at a separation distance d_0, and if such separation distance is reached during the collision, after the collision the nucleus will remain for some time in the σ-τ phase. In such a state the phases $\sigma_3\tau_3 = \pm 1$ will oscillate around d_0 generating a coherent pion field according to the equation

$$(\Box + m_\pi^2)\,\phi_3 = \frac{f}{m_\pi}\,\partial_k S_{k3} = \frac{f}{m_\pi}\,\partial_k \langle \bar{\psi}\sigma_k\tau_3\psi \rangle . \qquad (1)$$

If the oscillation takes place along the 3-axis with frequency ω

$$\langle S_{k3}\rangle = \langle S_{33}\rangle\big|_{t=0}\,\delta_{k3}\exp[i\omega t], \qquad \phi_3 = \phi_3(\vec{r}, t=0)\exp[i\omega t] \qquad (2)$$

and $\phi_3(\vec{r}, 0)$ will satisfy the time-independent equation

$$[\Delta - (m_\pi^2 - \omega^2)]\,\phi_3(\vec{r}, 0) = \frac{f}{m_\pi}\,\partial_3 \langle S_{33}\rangle\Big|_{t=0} \qquad (3)$$

showing that the pion has an effective Compton wave-length $1/\sqrt{m_\pi^2 - \omega^2}$.

Our suggestion is that this increased Compton wave-length (combined with the dislocation d_0)might explain the observed cross-section.

Note that it is essential to have a nonstatic σ-τ phase[5]. A static one[6] can give rise to coherent effects, but cannot explain a cross-section which exceeds the geometrical bound.

To establish theoretically the existence of this metastable phase is a formidable problem due to the essential role played by the short-range $\mathcal{N}\mathcal{N}$ and $\Delta\mathcal{N}$ interactions. It is not known in fact whether these interactions will favour or disfavour a first-order phase transition.

Very much delicate is also the problem of the life-time. If the nucleus were to decay by a single step the observed lifetime could probably be explained. The transition probability should in fact be of the order of $|\langle\varphi(r_\perp, z)|\varphi(r_\perp, z+d_0)\rangle|^{2A}$, φ being a typical single-particle wave function.

But the lifetime could be drastically reduced by a cascade decay. Due to the high degree coherence of the σ-τ phase, however, the steps of the cascade could not be s. p. transitions. Every step should involve the rearrangement of a number of particles, and it does not appear impossible to us that such a number be so high that the lifetime do not be substantially reduced.

(1) E. M. Friedlander et al., Phys. Rev. Letters 45, 1084 (1980).
(2) P. L. Jain and G. Das, Bull. Am. Soc. 26, 549 (1981); M. M. Aggarwal et al., Bull. Am. Soc. 26, 549 (1981).
(3) E. M. Friedlander et al., Phys. Rev. Letters 45, 1084 (1980).
(4) F. Calogero, in 'The Nuclear Many-Body Problem', ed. by F. Calogero and C. Ciofi degli Atti (Roma, 1972), Vol. 2, p. 535; F. Calogero and F. Palumbo, Lett. Nuovo Cimento 6, 663 (1973); A. B. Migdal, Zurn. Eksp. Teor. Fiz. 63, 1993 (1972) (English translation: Sov. Phys. JETP 36, 1052 (1973)). For a review see for instance F. Palumbo, in 'Second Intern. Conf. on Recent Progress in the Many-Body Theories, Mexico City 1981, Lectures Notes in Physics (Springer-Verlag, 1981), p. 462.
(5) F. Palumbo and N. Lo Iudice, Phys. Rev. Letters 46, 1054 (1981); Frascati preprint LNF-81/66 (1981).
(6) G. Do Dang, Phys. Rev. Letters 43, 1708 (1979).

Pion Condensates as anomalons

G.N.Fowler*, S.Raha, R.M.Weiner
Physics Dept.,University of Marburg,Germany,
*also of University of Exeter,England

The observation of abnormally small mean free paths in heavy ion reactions (anomalons) continues to puzzle the nuclear physics community; most of the explanations suggested so far are "exotic" in the sense that they are based on assumptions which are rather ad hoc and for which there is no convincing independent theoretical (not to say experimental) support.

In this paper we propose a solution to the anomalon problem in terms of another phenomenon which has been studied intensively and for which there exists an appreciable consensus that it should occur in nuclear matter under appropriate conditions; we refer to pion condensates. The pion field outside a nucleus in which a condensate exists can have a much longer range than the pion field outside a normal nucleus. It is this longer range which determines the scattering cross section of the nuclear fragment. Physically this enhancement comes about because the change in the vacuum state characteristic of nuclei with pion condensates continues for some distance outside the nucleus.

As a theoretical description of pion condensates, we use, as customary, the chiral σ model with spontaneous symmetry breaking.[1] In this model, outside the nucleus $\langle vac|\sigma|vac\rangle \neq 0$, where σ is the scalar mate of the π field. Inside the nucleus, the existence of the pion condensate is characterized by $\langle vac|\sigma|vac\rangle = 0$ and obviously $\langle vac|\pi|vac\rangle \neq 0$ The quantity $\langle vac|\sigma|vac\rangle \equiv v$ must therefore change as we pass from inside to outside nuclear matter so that we should really think of v as a function of the space coordinates. Similar arguments hold also for the π field so that $\langle vac|\pi|vac\rangle$ and hence $\langle vac|\pi^2|vac\rangle \neq 0$ at $r \leq R$ and also $\lim_{r\to\infty} \langle vac|\pi^2|vac\rangle = 0$. It is therefore necessary to consider the equation of motion of v (and π) outside nuclear matter with the boundary conditions which account for the existence of the pion-condensate inside the nucleus of radius R. These conditions are $v(r \leq R) = 0$ and $\langle vac|\pi|vac\rangle \neq 0$ for $r \leq R$.

The Lagrangian density outside the pion condensate is given by

$$\mathcal{L} = \frac{1}{2}\left\{\left(\frac{\partial\sigma}{\partial x_\mu}\right)^2 + \left(\frac{\partial\pi}{\partial x_\mu}\right)^2\right\} + \frac{\mu^2}{2}\left\{\sigma^2+\pi^2\right\} - \frac{\lambda^2}{4}\left\{\sigma^2+\pi^2\right\}^2 + c\sigma \qquad (1)$$

The free pion mass m_π is related to the parameter μ by

$$m_\pi^2 = -\mu^2 + \lambda^2 f_\pi^2 \qquad (2)$$

where f_π is the pion decay constant; the effective, coordinate dependent pion mass $\tilde{m}_\pi$ is given by

$$\tilde{m}_\pi^2 = -\mu^2 + \lambda^2 v^2 = m_\pi^2 + \lambda^2(v^2 - f_\pi^2) \quad (3)$$

Furthermore, as usual in the σ model, we take

$$C = v m_\pi^2 \quad (4)$$

The equation of motion for σ is

$$\frac{\partial^2 \sigma}{\partial x_\mu^2} - \mu^2 \sigma + \lambda^2 \sigma^3 + \lambda^2 \sigma \pi^2 - C = 0 \quad (5)$$

which must be solved with appropriate boundary conditions. In addition to the condition at r=R one has to demand $\lim_{r\to\infty} v = f_\pi$.

Taking the vacuum matrix element of (5), we have

$$\frac{\partial^2 v}{\partial x_\mu^2} - \mu^2 v + \lambda^2 \langle vac|\sigma^3|vac\rangle + \lambda^2 \langle vac|\sigma\pi^2|vac\rangle - C = 0$$

We now assume, as usual, that the vacuum matrix element of the σ field is the dominant one (essentially treating σ as classical) and find

$$\frac{\partial^2 v}{\partial x_\mu^2} - \mu^2 v + \lambda^2 v^3 + \lambda^2 v \langle vac|\pi^2|vac\rangle - C = 0 \quad (6)$$

where we have used the relation $\sigma^2 = v^2$ in (6).

In the chiral symmetric σ model[2], in the limit M_σ, λ large, one has

$$v^2 + \langle vac|\pi^2|vac\rangle = f_\pi^2 \quad (7)$$

and this equation is approximately satisfied also for softly broken chiral symmetries, which is our case.

Eq.(6) could be solved if one would know $\langle vac|\pi^2|vac\rangle$ at r>R (we are only interested in v outside the condensate). However it is easy to show that if we assume $\langle vac|\pi^2|vac\rangle=0$, we underestimate the enhancement of the range and hence the anomalon effect. In other words, $\langle vac|\pi^2|vac\rangle=0$ is a conservative approximation which we are entitled to make in order to prove our point. Then by combining eqs.(4) and (6), one has, in the static limit,

$$\nabla^2 v + \lambda^2 f_\pi^2 v - \lambda^2 v^3 = 0 \quad (8)$$

This non-linear equation can be solved numerically (cf.below). However, in order to get a feeling for its implications it is worthwhile to study its asymptotic behaviour.

Scaling the variable r by $r' = \lambda f_\pi r$ and by $v' = v/f_\pi$ and linearising by

$$v' = 1 - \delta$$

we find

$$\nabla'^2 \delta = 2\delta$$

so that v approaches the limit f_π as

$$v' \to 1 - B\frac{\exp(-\sqrt{2}r')}{r'} \quad (9)$$

for $r\to\infty$, where B is a constant.

Thus the effective pion mass $\tilde{m}_\pi$ which is responsible for the range of the pionic field reaches its physical value m_π from below at some distances R_a outside the nuclear radius and this constitutes the range enhancement we referred to earlier. It seems reasonable to interpret this R_a as the effective radius of the anomalon, to be distinguished from the density radius R introduced before. For normal nuclei, these two radii coincide since outside normal nuclei pions are on mass shell.

We have considered, as an example, a numerical solution of eq.(8) for an anomalon of radius $R \sim 1.75/m_\pi$ with $\lambda^2=5.63$ and f_π =125 MeV[3]. Assuming, for the sake of concreteness, that the pion-condensate anomalon has a density of $2\rho_o$, where ρ_o is the normal nuclear matter density, the normal nucleus with the same A

has a radius of $R_n \sim 2.2/m_\pi$. R_a as defined above is $\sim 3.2/m_\pi$ for this case. In a geometrical estimate, this gives an enhancement of the anomalon cross section $(\sigma_a/\sigma_n) \sim (R_a/R_n)^2 = 2.1$. It is easy to check that even for $\rho \sim 4\rho_o$, one gets $\sigma_a/\sigma_n > 1$.

Given that we have underestimated the range enhancement by our conservative approximation on $\langle vac|\pi^2|vac\rangle$, we conclude that pion condensates represented by the boundary condition $v(R) = o$ can in principle explain one of the two main characteristics of anomalons, namely their larger cross sections.

The other property is their metastability (lifetime $\gtrsim 10^{-11}$ sec.). This feature follows also automatically if anomalons are condensates since we are faced then with a (meta) stable phase of nuclear matter.

Finally the "memory" effect of anomalons can now be understood in this context, because in order to produce the condensate phase, a higher than normal density is necessary. Once this is achieved in the first collision, the probability to observe an anomalon in successive reactions is enhanced due to two factors: (i) a higher than normal density already exists and (ii) the primary anomalon can survive.

The advantage of the present approach over the other models lies, in our opinion, in the fact that more than any other model, it is based on accepted concepts and that the discovery of pionic condensates in relativistic heavy ion reactions was generally expected, although there was less agreement on what the signals of these objects would be. The fact that so far no experimental evidence for condensates was reported has been in a certain sense almost as puzzling as the discovery of anomalons. We suggest that these two unsolved problems have a common solution and the non-observation of pion condensates is possibly due to the fact that the identification of the proposed specific signals might be more difficult in the first reaction where the normal and condensed phase coexist, than in a second or higher order reaction, where the condensed phase (anomalon) has been separated out. Herefrom it follows that some specific signatures of pion condensates (e.g. abnormal Z/A ratios) should be looked for in anomalon scattering. Another consequence of this anomalon theory is that the anomalon being also a coherent state, Bose-Einstein correlations of identical pions emitted by anomalons in anomalon + nucleus collisions should display coherence effects[4] much in excess of those observed in normal events.

Furthermore, the coherence property might lead to superscattering[5,6], i.e. effects in which the cross-section is proportional to A_o^2, where A_o is the anomalon mass number.

Finally, if the anomalon phenomenon is due to a long range field some specific effects like smaller momentum transfer than in "normal" nuclear reactions should be observed[7].

References

1) B.W.Lee, Chiral Dynamics, Gordon and Breach, New York, 1972

2) C.-K.Au and G.Baym, Nucl. Phys. A 236, 500 (1974)

3) J.L.Basdevant and B.W.Lee, Phys.Rev.D2, 1680 (1970)

4) G.N.Fowler and R.M.Weiner, Phys.Lett. 70B, 77 (1977); Phys.Rev. D 17, 3118 (1978)

5) S.Raha and R.M.Weiner, Europhysics Conference Abstracts 5D, 354 (1981)

6) G.N.Fowler, S.Raha, and R.M. Weiner, Comtex Series (ed.J. Cerny).

7) P.J.S.Watson has reached a similar conclusion (private communication)

Nuclear Chromodynamics and "Anomalons"*

Y.E. Kim and M. Orlowski
Department of Physics, Purdue University
West Lafayette, IN 47907

We propose a new theoretical explanation of "anomalons"[1] based on a unified theory of nuclear chromodynamics formulated recently by us.[2]

In our theory for the np system, the $^3S_1$ deuteron wave function (we neglect the $^3D_1$ component for simplicity) is written as

$$\psi_d(r) = N(E_d)\phi_n\phi_p\chi_{E_d}(r \geq r_o) + A(E_d)\phi_s(r \leq r_o) \tag{1}$$

where ϕ_n and ϕ_p are the three-quark (3q) colorless nucleon bags of radius R with normalization $\langle\phi_n|\phi_n\rangle = 1 = \langle\phi_p|\phi_p\rangle$. $\chi_{E_d}(r \geq r_o)$ is the deuteron wave function generated from the boundary-condition model (BCM) potential of Lomon and Feshbach[3] (LF) and is normalized, $\langle\chi_{E_d}|\chi_{E_d}\rangle = 1$. $\phi_s(r \leq r_o)$ with its amplitude $A(E_d)$ is also normalized, $\langle\phi_s|\phi_s\rangle = 1$, and represents a quark compound bag (QCB), consisting of gluons and six quarks (6q), which we call "soul" and denote by the letter s. r_o is the radius of the "soul" QCB and lies somewhere in the transition region, $R < r_o < 2R$.

The continuity of the probability current at r_o leads to the energy independent boundary condition (BC)

$$\frac{\chi'_{E_d}(r_o)}{\chi_{E_d}(r_o)} = \frac{\phi'_s(r_o)}{\phi_s(r_o)} \quad . \tag{2}$$

In addition to the above BC, the "soul" state, ϕ_s, must satisfy the requirements of the perturbative quantum chromodynamics (QCD) at short distances such as the asymptotic freedom and scaling laws.

The scattering state ψ_d^o at a compound resonance energy, $E = E_r$, (excitation of ϕ_s) can be viewed as a quasi-bound $^3S_1$ state and is written as

$$\psi_{\overset{o}{d}}(r) \propto N(E_r)\phi_n\phi_p\chi_{E_r}(r \geq r_o) + A(E_r)\phi_s(r \leq r_o) \tag{3}$$

where $\chi_{E_r}(r \geq r_o)$ is the $^3S_1$ scattering solution at E_r generated from the LF two-nucleon potential[3] and is orthogonal to $\chi_{E_d}(r \geq r_o)$, $\langle\chi_{E_r}|\chi_{E_d}\rangle = 0$. The subscript $\overset{o}{d}$ stands for "angel" deuteron which is a maximum "soul". At the resonance energy, $E = E_r$, $A(E)$ has a maximum and its shape determines the lifetime, $\tau = \hbar\Gamma^{-1}$, of the "angel" deuteron resonance, Γ being the total width of the *angel* resonance. Using the resonating group method approach the six-quark (soul) probability amplitude $A(E_d)$ in the deuteron bound state is determined by the resonance energy E_r, the partial width Γ_{np} of the deuteron channel, deuteron binding energy and the ratio $x = |\chi_{E_d}(r_o)/\chi_{E_r}(r_o)|$. In other words, ex-

*Supported in part by the National Science Foundation.

perimental knowledge of resonance parameters pertinent to the soul state ϕ_s allows us to determine its probability in the deuteron bound state. In our opinion, a good candidate for such six quark compound state is the dibaryon resonance recently observed by Kamae et al.[4] in the deuteron photodisintegration. Our arguments for the justification of the identification of the *angel* state with Kamae resonance are given in ref. 2. The Kamae resonance occurs at $E_r \approx 2.35$GeV with $\Gamma \approx 0.34$GeV corresponding to $\tau \approx 2.2 \times 10^{-24}$sec. The total width Γ is less certain than resonance pole energy E_r. Assuming that the partial width $\Gamma_{np} \approx 10$-50 MeV, we obtain the probability of *soul* component of deuteron, $|A(E_d)|^2 \approx 1.3$-6%.[2]

It is natural to expect a considerable admixture of the "soul" ϕ_s in heavier nuclei due to the presence of correlated n-p pairs. The excitation threshold energy of ordinary nuclei to *angel* states by incident projectile (say proton) is expected to be ~ 0.5 GeV C.M. but will be smeared out mostly due to Γ ~ 0.34 GeV, many different ways to distribute energy and much less due to the Fermi motion of the pair in the nucleus. The lifetime of *angel* nucleus will be in the same order as the lifetime of a free *angel* , ~ 10^{-24}sec. Since the *angel*-nucleus is a resonance, we expect an enhancement of the cross section in the neighborhood of the resonance pole for the specific channel which proceeds via the *angel* resonance.

The energy range within which the enhancement occurs will depend on the details of the size and structure of projectile and target particles. The magnitude of enhancement will depend especially on the probability of finding a correlated $^3S_1$ np pair in the target nucleus for the entrance channel, i.e. channel initiating a reaction. For this reason we expect that the enhancement will be larger for lighter nuclei. Because of the enhancement of the cross section due to the *angel* resonance, the mean free path (mfp) in emulsion of the pertinent projectile fragments will be shorter. Since the excitation is a compound excitation and its energy of 0.5 GeV is comparable or greater than the total binding energy of a nucleus with $A \leq 60$, the *angel* nucleus, once produced, will explode creating an almost isotropic *angel* star due to its short lifetime and nucleon correlations inside the nucleus imposed by the Pauli exclusion principle. Such signature and the excitation threshold behavior may have been already observed in high-energy proton-nucleus reactions.[5,6]

For nuclei with A > 60 the excitation energy of ~ .5GeV is less than the total energy of the nucleus and hence the *angel* may have a longer lifetime and the decay mode of such heavy nuclei might be different from lighter nuclei. It would be interesting to verify this point experimentally.

The direct evidence for the threshold behavior of *angel* $\mathring{d}$-excitation should be found in high-energy deuteron-nucleus reaction, since we expect that the enhancement of the cross section due to $\mathring{d}$ resonance pole will be most clearly exhibited in this case. The most recent data by V.G. Ableev et al.[7] from $d + C^{12} \rightarrow p + X$ reaction at a deuteron momentum of 8.9 GeV/c has a shoulder in the proton spectrum corresponding to the production of a dibaryon resonance with an estimated mass from 2.0 to 2.2 GeV. This dibaryon resonance may correspond to the $\mathring{d}$ resonance. Obviously further measurements with other nuclear targets are needed to clarify the nature of $\mathring{d}$.

Situation in high-energy heavy-ion collisions is more complicated since there are several mechanisms for producing *angel* excitations. An *angel* state can be excited either in the target nucleus or in the projectile nucleus during

the collision. An enhanced cross section due to the *angel* excitation implies a shorter mfp. Another possibility is that both the projectile and target nuclei undergo an ordinary nuclear reaction first and then at a later stage create an *angel* (two-step process) in a coherent excitation. The latter situation would not affect the mfp. There is some experimental evidence for the threshold behavior of *angel* excitations in high-energy heavy-ion collisions. The anomalous effect for the secondary projectile fragments (PF) is seen in the cases of ^{56}Fe beams with energies of 1.88 and 2.0 GeV A (0.94 and 1 GeV A, respectively, for the primary PF's in the two-nucleon C.M.)[1,6] but not seen with 1 GeV A (0.5 GeV A C.M.).[6] It would be interesting to see if the anomalous effect will go away at much higher energies.

We should point out the differences between our explanation of anomalously short mfp and other interpretations proposed so far. In our picture all tracks recorded in the emulsion are associated with normal nuclear fragments. So far it is commonly believed that the shorter tracks are associated with anomalous nuclear fragments with extremely long lifetime ($\geq 10^{-10}$sec.) which have cross section one order of magnitude larger than the ordinary one and which nevertheless have the same characteristics as ordinary nuclear fragments. We find it difficult to believe that such longlived particles remained undiscovered until now. The anomalously short mfp is explained in our model by the enhancement of the cross section of *normal* nuclear fragments due to the excitation of anomalous shortlived nuclear matter states, for which the six-quark compound angel state is a very likely candidate. Moreover in our model this anomalous effect, d̊ Kamae) resonance, and evidence for the presence of six-quark state in the deuteron are consistently explained. Obviously these different effects are related to each other and would require a unified description.

We like to comment on the point emphasized strongly in the recent studies of anomalons that the primaries do not display anomalously short mfp at short distances, since this seems to be the crucial argument for the creation and existence of anomalons in the secondary beams. First we believe that there is not enough experimental evidence for this claim. The primary beams consisted so far of ^{16}O, ^{56}Fe or ^{40}A.[1,6] But the cosmic ray experiments[8] show that in the case of Li, the anomalous effect is also observed in the primary beam. On the other hand it was found that He (Z=2) particles do not exhibit the anomalous effect in any generation.[9] It is probable that the anomalous effect will be found in the primary deuteron beam. The negative result of the search[10] for anomalous nuclear states cast also doubt on the existence of longlived anomalons.

We note that all experimental works on "anomalons" reported at this conference are either consistent with or in support of our model. In particular, the experimental works of Klein et al.[11] and Killinger et al.[12] give the most direct support of our model. From their analysis of the emulsion data obtained with ^{56}Fe (1.88 GeV A), ^{3}He (1.88 GeV A) and ^{4}He (2.1 GeV A) primary beams, Klein et al.[11] show that many "large" stars ($n_h \geq 9$) induced by the short-track ($\leq$ 3 cm) secondary α's have the characteristic of our isotropic *angel* stars with small forward-backward asymmetry. The experimental work of Killinger et al.[12] exhibits the energy dependence (threshold and resonance behavior) of the anomalously short mfp predicted by our model. They find that the mfp depends sensitively on the kinetic energy of the PF's and decreases drastically with decreasing energy (degraded toward the *angel* resonance energy) of the primary ^{56}Fe beam (initial energy of 1.88 GeV A) *only* at short distances ($\leq$ 3 cm). The two types of the data analysis carried out by Klein et al.[11] and Killinger et al.[12] should be refined and be applied to existing and future emulsion data to provide further clarification of the basic points of our model.

For further experimental verification of our predictions, we suggest emulsion experiments with d, Li, B, N, etc. primary beams in the energy range of 0.1 ~ 1.4 GeV C.M. Ultimately, it would be desirable to do counter (spectrometer) experiments for the inclusive and exclusive proton-nucleus and nucleus-nucleus scattering in the kinematic phase space where the energy transfer to the target (or projectile) covers the *angel* excitation of ~ 0.5 GeV C.M. The results of these (difficult) scattering experiments can provide not only the basic quantitative understanding of the "anomalons" but also of the quark degrees of freedom in nuclei.

We wish to thank Professor Andy Hirsch for bringing many references on "anomalons" to our attention.

References

1) E.M. Friedlander et al., Phys. Rev. C27, 1489 (1983) and references quoted therein.

2) Y.E. Kim and M. Orlowski, "A Unified Theory of Quantum Chromodynamics and Nuclear Dynamics", Purdue Nuclear Theory Group Preprint, 1983, submitted to Physical Review Letters.

3) H. Feshbach and E.L. Lomon, Ann. Phys. (N.Y.) 29, 19 (1964); E.L. Lomon and H. Feshbach, Ann. Phys. (N.Y.) 48, 94 (1968).

4) T. Kamae et al., Phys. Rev. Lett. 38, 468 (1977). H. Ikeda et al., Phys. Rev. Lett. 42, 1321 (1979).

5) R. Kaczarowski and E. Makowska, Nucl. Phys. 74, 348 (1965); J.A. Gaidos et al., Phys. Rev. Lett. 42, 82 (1979) and private communication.

6) P.L. Jain and G. Das, Phys. Rev. Lett. 48, 305 (1982).

7) V.G. Ableev et al., Nucl. Phys. A393, 491 (1983).

8) B. Judek, Can. Journ. Phys. 46, 343 (1968).

9) P.L. Jain et al., Phys. Rev. C25, 3126 (1982).

10) T.M. Liss et al., Phys. Rev. Lett. 49, 775 (1982); Gustaffson et al. and G. Dersch et al., both contributed papers in this volume.

11) N. Klein et al., contributed paper in this volume.

12) F. Killinger et al., contributed paper in this volume.

Some Anomalon Phenomenology

P. J. S. Watson
Theory Group, S.I.N.,CH 5234 Villigen,Switzerland
Physics Dept.,Carleton University,Ottawa,Canada K1S 5B6

The list of what we do not know about anomalons is depressingly long.A shopping list of unknowns is*)

a) Mass difference ($\delta m = m_{A_n} - m_N$) from nearest "normal" state?
b)lifetime ? (or could it be stable?)
c)decay mode ? (weak,electromagnetic or strong?)
d)enhanced cross-section due to large geometrical size or long-range force?
e)produced in light ion collisions?(and if not,why not?)
f)charge states?(fractional? negative?)
g)cross-sections Z-dependent?
h)implications of large cross-sections?(e.g. forward peaking?)
i)associated production or solo?
j)nuclear excitation (c.f. giant dipole) or elementary particle (c.f. hypernucleus)

Obviously some of these questions are interconnected,and in this talk I will attempt to show how some can be answered (1).

The first point to note is that if 6% of projectile fragments are anomalous,then so are 6% of target fragments.These stop in 10^{-11} s, long before they have time to decay.Hence any evidence of anomalon decay should be visible at the end of target fragment tracks.If,e.g.,$\delta m \sim 200$ MeV then some events should decay via pion emission,which would be a most unusual event,with a fast track leaving a slow one.If $\delta m \sim 50$ MeV, then a weak or electromagnetic decay would still give a nuclear recoil of 5 μ for an α-particle,which would be clearly visible but has probably never been searched for.If no decays can be seen,then there seem to be 4 possibilities:

1) $\delta m < 20$ MeV
2) $T_{1/2} > 1$ week (the approximate time before the emulsion is developed)
3) the decay proceeds by a low energy cascade
4)the recoiling nucleus is heavy.

It seems very unlikely that they can be stable.Anomalons are produced in roughly 50% of heavy ion collisions at E > 1 GeV/nucleon. Taking today's cosmic ray flux and integrating over the lifetime of the universe gives a concentration of $10^{-16\pm2}$ anomalons/nucleon in terrestrial matter,which is incompatible with fractional charge models

* This assumes the canonical 6% , m.f.p. = 2.5 cm.,model.

and barely compatible with isotope searches. Note that until the decay can be observed, the crucially important question of associated production cannot be answered.

The problem of long range forces can be partially answered. If we consider a long-range force between anomalon and nucleon of the form

$$V(r) = g\, a^{N-1} / (a^2 + r^2)^{N/2}$$

then the cross-section can be calculated in an eikonal approximation. The conclusion is that for $N > 3$, one must have $a^2 \sim \sigma$, unless g is implausibly large. In other words, the only possibility is a $1/r^2$ or $1/r^3$ interaction: the others are short range.

If the anomalon is taken to be a hard object with a Gaussian scattering amplitude

$$f(q) = \frac{i\,\sigma}{4\pi k} \exp(-q\, R^2/16)$$

then it is possible to make quantitative predictions using a Glauber model. This has a number of testable consequences, in particular:

1) the A dependence of scattering from target nuclei is strongly reduced. This implies that anomalons must produce fewer large stars (i.e. interactions with Ag and Br). Unfortunately the quantitative results (fig I) are such that it is essential to look at light fragments.

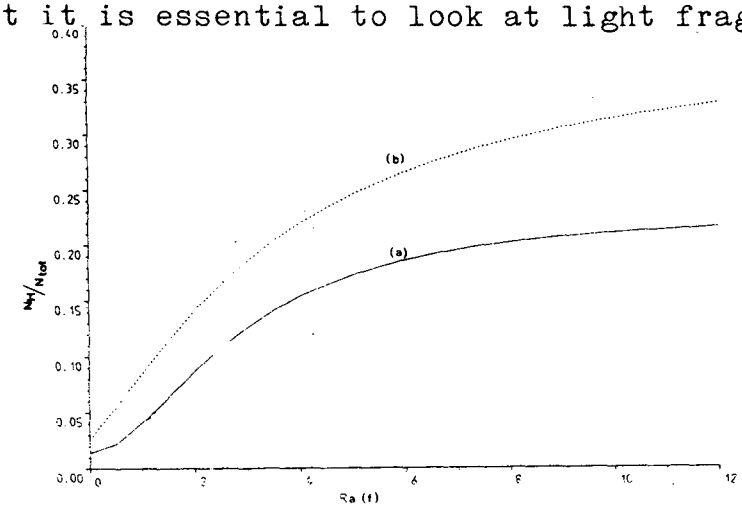

Fig I. Proportion of hits on H. vs. anom. rad. a) Glauber model b) soft sphere

2) the effective anomalon radius is 6 fm

3) the cross-section is strongly forward peaked, (fig II) implying that less momentum is transfered. This should mean both that the anomalous nucleus is less likely to break up, and the target stars will be more symmetrical in the laboratory frame.

4) pion production should be sharply reduced, because the typical momentum transfer is too small to produce (e.g.) an N^*.

Unfortunately these predictions are true only for a "pure" anomalon. Hence it is crucially important to study low Z fragments. In a pure nuclear ('soft') model, the anomalon has a large radius but its components are nucleons. Hence the

individual scattering processes will have a fairly large (~500 MeV/c) momentum transfer, so only the first prediction holds.

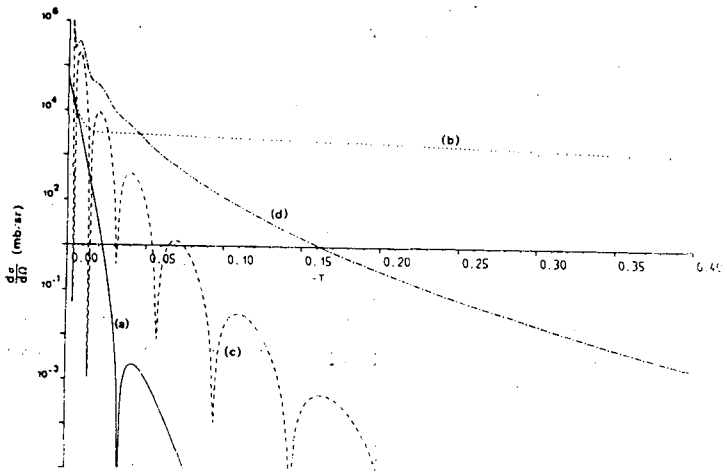

Fig II
do/dt for scattering off 0
a)P elastic
b)P inelastic
c)An elastic
d)An inelast.

Finally there is the light ion problem.There are several related points here.There is no direct evidence that anomalons are not produced in light ion collisions,except for the Carleton-N.R.C scan of D-D film (see R. Saly's talk).The gut feeling that many experimentalists seem to have that 'if they were there,we would have seen them' is false,as one can easily convince oneself by scanning a few frames.However there is evidence that there are no unusual stable multibaryon states.For example, a search by de Boer et al. (2)at S.I.N. for negatively charged heavy objects (pi-neuts) has limits at the atto-barn level!(fig 3).Similarly Kyle et al. (3) have looked at

$$\pi^+ D \dashrightarrow \pi^- (MM)^{+++}$$

and have seen no peak above the level of 50 nb/sr up to the PP threshold

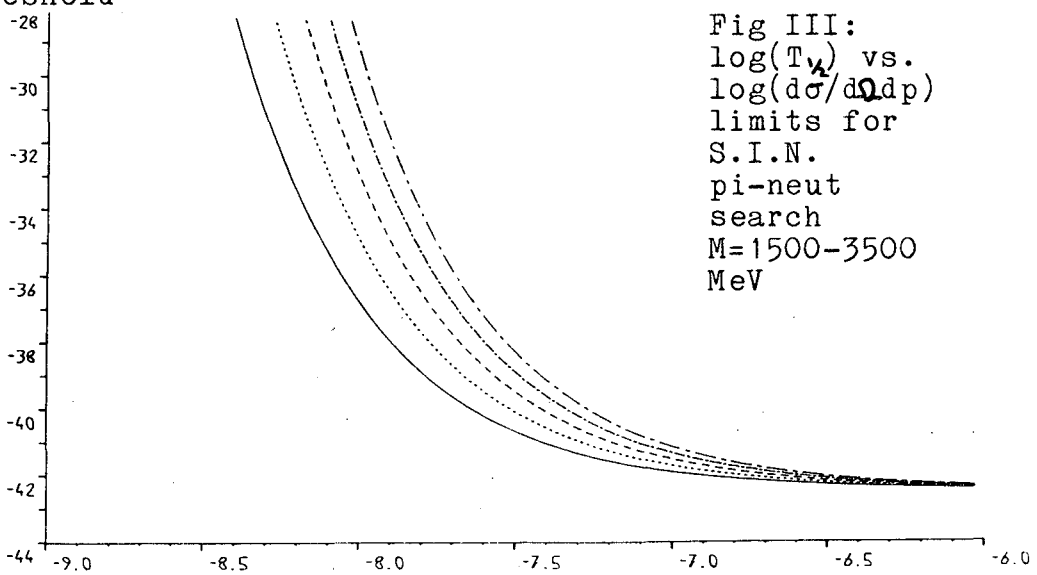

Fig III:
$\log(T_{1/2})$ vs.
$\log(d\sigma/d\Omega dp)$
limits for
S.I.N.
pi-neut
search
M=1500-3500
MeV

There are two obvious possibilities:either the phenomenon is a purely nuclear one,or there are suppression factors operating in light (PP) collisions.If the anomalon is a multi-quark object,(e.g. 6)then its production in

P P --> An + (X)

will be severely suppressed by the requirement that a baryon Regge trajectory must be exchanged. The second is specific to broken colour models: if the interaction between coloured states is quasi-confining, then production in PP will be reduced by a tunneling factor, which can easily be $\sim 10^{-8}$ compared to a nuclear collision. Finally it is interesting to note that if the large cross-section is related to an extended distribution of matter, then even simple wave-function overlap arguments will reduce production by $\sim 10^{3}$. In this connection, one should note that an extended object has a large moment of inertia, implying an unusually closely spaced rotational band. Thus instead of appearing as a sharp spike in a missing mass plot, it would appear as a superposition of narrow states, smeared into a wide peak. It seems reasonable to conclude that there are no light anomalons with exotic quantum numbers, but there is no real evidence about more normal states. This provides problems for quark models, since they rather naturally lead to negatively charged states.

Parts of this work were done in collaboration with W.J.Romo, R. Saly and M.K.Sundaresan. I am grateful to F.Deboer for permission to quote results prior to publication.

(1) P.J.S.Watson et al. Phys. Rev D27, 1468 (1983)
P.J.S.Watson Phys Letts, in press.
(2) F. Deboer et al. S.I.N. preprint (in preparation)
(3) G Kyle et al. unpublished.

Limits on Anomalon Production in Deuterium-Deuterium Collisions at 7.9 GeV/c

R.L. Clarke, D.N. Fernandes, J.E. Hardy, R.J. Hemingway, D. Kessler, A.H. Lefcoe, C. Loken, A.C. McPherson, J.L. Pinfold, W.J. Romo, R. Saly, M.K. Sundaresan, P.J.S. Watson and J.L. Wolfson

Department of Physics, Carleton University, Ottawa, Canada

B. Judek and M. Losty
Division of Physics, National Research Council, Ottawa, Canada

Until now the most reliable observations of anomalons have been in the secondary fragments produced by relativistic heavy ions incident on heavy targets [1]. It is widely believed that the phenomenon does not occur (e.g.) in proton-proton collisions: however it appears that no search has ever been made. If we assume that they are not produced in p-p collisions, there are three (not mutually exclusive) possible reasons. Firstly the simplest anomalon may be a multi-quark state[2] ($n > 3$), and hence production in p-p would require baryon number exchange which would cause a large suppression. Secondly if the anomalon is an extended system, naive wave-function overlap arguments would suggest that it is far more efficient to start from an extended system (such as a heavy nucleus). The third argument is an extension of the second for a class of models based on broken colour[3] where confinement is no longer complete. It is consistent with what is known from high energy collisions that colour confinement is exact up to a distance of (say) 3f, but beyond that free coloured states can escape.

These three arguments suggest that a useful system to look in would be the deuteron. In particular, in the demon deuteron model[2], one would expect anomalons to be fairly readily produced. Furthermore, if low baryon number anomalons exist, independent of any specific model, the relative simplicity of bubble chamber techniques would allow statistically significant results to be accumulated very rapidly.

With these thoughts in mind, we have made a search for anomalous behaviour in the interactions of secondary particles produced in deuteron-deuteron collisions. This note reports our finding from a scan of bubble-chamber film taken at the Alternating Gradient Synchrotron at Brookhaven.

The experiment (No. 341), a Princeton-Rutgers collaboration, exposed the BNL 80-in. deuterium bubble chamber to an almost pure ($\geqslant$97%) beam of 7.9-GeV/c deuterons[4]. Some of this film has been acquired from Rutgers University and scanned at Carleton.

The scan was performed in two parts. In the first part[5], we defined a fiducial volume of length 1m and searched for primary beam interactions leading to at least one fast secondary track (defined by a template to have a projected momentum of at least 1 GeV/c). This momentum cut was imposed to avoid the complication of a large variation in the cross section for secondary-particle-deuteron collisions, particularly in the resonance region. Above 1 GeV/c, these variations will be, at most, a factor of 2.

Each fast secondary track has been followed to see whether or not it interacted before leaving the fiducial volume. In the event of a secondary interaction, all fast tertiary tracks have been followed - and so on. Table I summarizes the scanning statistics from a total of 6763 incident beam tracks

and 2646 recorded interactions. The track lengths reported here have been measured on the scan table and converted into chamber space assuming the momentum component normal to the "scan-table plane" is zero.

From measured cross sections, the primary-beam mean free path would be 155 cm. For the secondary interactions, which have a range of incident momenta 1-8 GeV/c, we expect the mean free path to lie within the interval 140-200 cm for d-d, 280-400 cm for p-d, and 320-470 cm for $\pi^{\pm}$-d collisions[6]. In our 100-cm-long scanning volume, with an average potential path for secondaries of about 50 cm (small compared to the expected mean free paths), we do not need to know either the composition or the momentum distribution of the secondaries. We can define the mean free path for the nonhomogenous secondaries as

$$\lambda(\ell)=\Delta\ell/\ln[N(\ell)/N(\ell + \Delta\ell)]$$

where $N(\ell)$ is the number of secondaries which did not interact up to the distance ℓ from primary interaction and $\Delta\ell$ is a small interval of ℓ. Expressing $N(\ell)$ as $N(\ell)=\Sigma f_i \exp(-\ell/\lambda_i)N(0)$ then, for the above quoted mean free paths λ_i within the interval 140-470 cm and all reasonable values of the composition fractions f_i, we find that $\lambda(\ell)$ is only a slowly varying function of ℓ. In particular, over the interval 0-100 cm, $\lambda(\ell)$ is almost constant; e.g.,

$$|\lambda(0) - \lambda(50)|/\lambda(50) < 0.01$$

The measured value for the entire interval 0-100 cm was obtained at 338 ± 15 cm.

From the emulsion data[1] we can deduce that anomalons would have an m.f.p. of ~10 cm in liquid deuterium. Figure 1 displays the measured secondary mean free path $\lambda(\ell)$ as a function of distance from the primary interaction. Superimposed are curves which represent the expectation values of $\lambda(\ell)$ for a 6% admixture of anomalons with λ_{AF}=10, 30 and 50 cm assuming a single mean free path of 338 cm for the rest. Clearly the data do not support anomalon production with these characteristics. We can use a maximum likelihood method to put

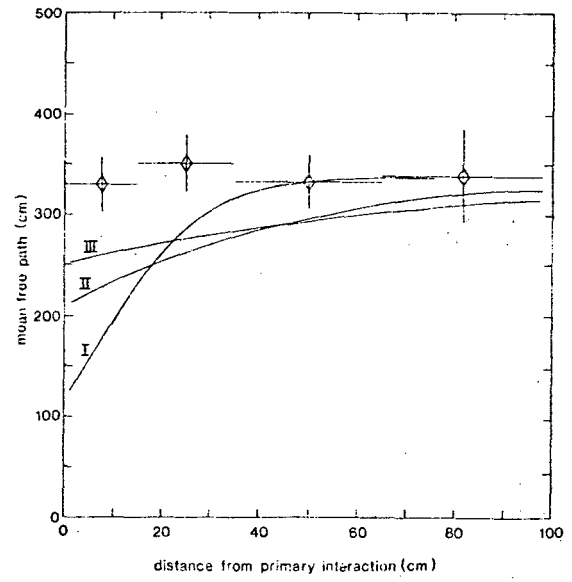

FIG. 1. Measured secondary mean free path as a function of distance from the primary interaction. Curves I, II, and III represent the expected behaviour for a 6% anomalon admixture with mean free paths of 10, 30 and 50 cm, respectively.

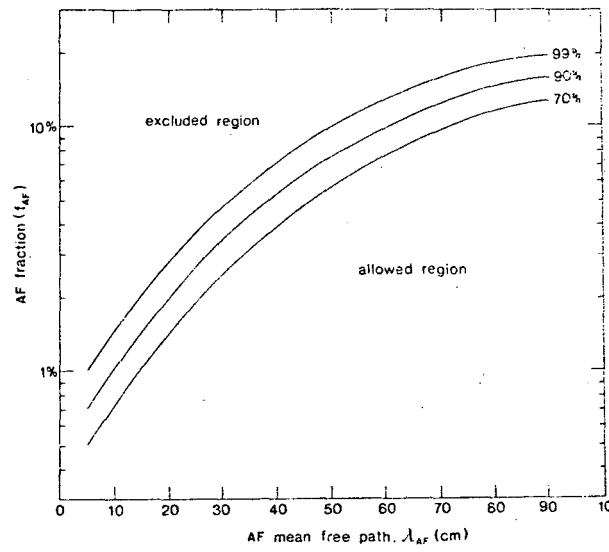

FIG. 2. Confidence-level contours showing the excluded region as a function of AF mean free path (λ_{AF}) and AF fraction (f_{AF}).

limits on the fraction (f_{AF}) of anomalons as a function of m.f.p. (λ_{AF}). The results are shown in Figure 2. Notice that we are insensitive to very short tracks as it is difficult to determine their momentum.

It is somewhat provocative that the m.f.p.'s for negative secondaries, tertiaries and quaternaries are considerably shorter. The effect in negative secondaries can be explained as a somewhat higher production of Σ^-(~300μb) than might be expected. However a Monte Carlo model suggests that only one quaternary should have been observed (instead of four). The same Monte Carlo indicated that it would be extremely difficult to improve the limits significantly using only secondaries. We have therefore commenced a second scan to concentrate on these features. To improve the statistics, we have extended the length of the fiducial volume from 1 meter to 1.5 meters. In our second scanning run, all negatively charged secondaries were followed, as in the first run, but only those positively charged secondaries were followed that gave rise to at least one tertiary track with a projected momentum of at least 1 GeV/c. Table II gives a preliminary summary of the scanning statistics accumulated in our scan of 1 roll of film (1194 frames). Included in Table II are a number of tracks that were so short that the measurements carried out with templates were unable to determine whether or not their momenta exceeded 1 GeV/c. In the bracketed data all of these questionable tracks have been excluded. As is seen from the tables there is no evidence for anomalous behaviour of the negatively charged secondary tracks. On the other hand, there still seems to be some evidence of a decrease in mean free path of the positively charged tracks as the order of interaction increases, although the sample size is still quite small. However, when all tracks with questionable momenta are removed from consideration (cf. Table II) the calculated mean free paths seem to be consistent with normal behaviour, i.e. the absence of any anomalous behaviour.

Despite a lack of evidence for anomalous behaviour in our analysis of the data obtained to this date, the sample size is still quite small and the scanning project continues. It should be noted that this technique is complementary to emulsion results, and cannot be assumed to contradict it. In particular, if Otterlund's suggestion[7] that the anomalous m.f.p. in emulsion is ~1 cm, this would lower the estimate of the m.f.p. in deuterium to 5 cm which lies at the limit of the technique described here.

We thank R.J. Plano for providing us with the film, the optical constants, and the facilities at Rutgers to perform a short feasibility study. We thank P. Patel (McGill) and T.S. Yoon (University of Toronto) for the provision of a Vanguard scanning table and the Physics Department staff at Carleton University for rebuilding it. This research has been supported in part by the Canadian Institute of Particle Physics and the Natural Sciences and Engineering Research Council, Canada.

References

(1) See (e.g.) E.M. Friedlander et al, Phys. Rev. C27 1489 (1983) and references therein.

(2) W.J. Romo and P.J.S. Watson, Phys. Lett. 88B, 354 (1979); Y. Karant, LBL Report No. 9171, 1979 (unpublished); S. Fredriksson and M. Jandel, Phys. Rev. Lett. 48, 14 (1982).

(3) G.F. Chapline, Phys. Rev. D 25, 911 (1982); R. Saly, M.K. Sundaresan, and P.J.S. Watson, Phys. Lett. 115B, 239 (1982).

(4) A.T. Goshaw and M.J. Bazin, Phys. Rev. Lett. 25, 50 (1970); A.T. Goshaw et al., ibid. 25, 249 (1970).

(5) R.L. Clarke et al., Phys. Rev. D 27, 2773 (1983).

(6) V. Flaminio et al., CERN-HERA Reports Nos. 79-01, 79-02, and 79-03 (unpublished).

(7) I. Otterlund et al., these proceedings.

TABLE I. Summary of mean-free-path measurements (first scan).

	All secondaries	Negative secondaries	Tertiaries	Quaternaries
Number of tracks	3527	159	414	20
Number of interactions	510	30	41	4
Total path length (m)	1722.0	63.5	120.6	4.1
Mean free path (cm)	338±15	212±39	294±46	102±51

TABLE II. Summary of mean-free-path measurements (second scan).

	Negative secondaries	Tertiary Tracks	Quaternary Tracks
Number of tracks	382 (376)	1118 (1103)	107 (99)
Number of interactions	63 (57)	165 (150)	15 (8)
Total path length (m)	198.7 (198.6)	451.4(450)	29.1 (28.9)
Mean free path (cm)	315±40 (348±46)	274±21 (300±24)	194±50 (361±128)

Are "Anomalons" a Bag Ful'o Colorful Nucleons?

By F.Kruse and C.C.Noack

Fachbereich Physik, Univ.Bremen, F.R.Germany

One of the more intriguing explanations of the possible existence of "anomalons" (if they do exist)[1] would seem to be in terms of internal color excitations of nuclei. While it follows from confinement in QCD that isolated nuclei (as well as isolated nucleons) must be in color singlet states, the same is not necessarily so for nucleons bound together in a small region of space, viz. a nucleus. Thus one can envisage a nucleus in a color-excited state as composed of localized 3q-systems (i.e. nucleons) which, however, are not all color singlets. We have investigated a particularily simple example of such a model which retains as many of the features of "normal" nuclei as possible, and at the same time stays close to the physical picture of the M.I.T. bag model. We call this a "nuclear bag".

Consider the simplest case, that of 2 bound nucleons. According to the SU(3) reduction formula

$$3 \otimes 3 \otimes 3 = 1 \oplus 8 \oplus 8 \oplus 10$$

a colored baryon could either be an octet or a decuplet. But since the two baryons must couple to a total color singlet, and neither $8 \otimes 10$ nor $10 \otimes 10$ contains a singlet, this leaves us with the octets only. Indeed, totally antisymmetric 3q-states which are color octets but otherwise carry the quantum numbers of the nucleon ($S = 1/2$, $T = 1/2$, $Y = 1$) can be constructed. Thus our basic assumption is that the exotic nuclear states we are considering are M.I.T. - like bags, but with octet nucleons rather than quarks as their constituents. This is not identical with a multi-quark bag [2], since our octet nucleons retain their identity as localized objects; they are, in a sense, elementary.

An immediate (if unexpected) consequence of this model is that, in an $A = 2$ system, there are, aside from the usual nuclear states[3] with ($T + S$) odd (for which the 2 color octets couple symmetrically), also states with ($T + S$) even, because the two octets in the above reduction formula are different and thus can be coupled antisymmetrically.

With these changes from the M.I.T. model, we have computed masses M^* and radii R of the lowest-lying states of such nuclear bags. Regarding the bag model parameters, we have taken the following attitude:

(i) bag constant B: there is no apparent reason why a nuclear bag should have the same volume energy and thus the same bag constant as the M.I.T. bag. We allow B (subject to $B > 0$, of course) to be a free parameter (cf., however, the comments below),

(ii) constituent mass m_8: Obviously we must take m_8, the mass of an octet nucleon, to satisfy $m_8 \geq m_1 \equiv m_N$. It can, however, be shown that m_8 approximately satisfies the inequalities

$$1 - \frac{1}{2}\left(\frac{x}{m_8 R}\right)^2 \lesssim \frac{M^*}{A\, m_8} \lesssim 1 + \frac{4}{3}\left(\frac{x}{m_8 R}\right)^2 \quad ;$$

here A is the number of nucleons in the bag, and x, as usual, is a solution of the bag equation

$$x = \tan x \cdot [1 - m_8 R - \sqrt{\{x^2 + (m_8 R)^2\}}] \quad .$$

For R larger than the usual nuclear radius, we have $\left(\frac{x}{m_8 R}\right)^2 \ll 1$, and thus $M^* \approx A\, m_8$. Since from the anomalon experimental data[1] we expect the excitation energy per nucleon, $E^* := (M^* - M)/M$ to be less than 0.5, we have simply set $m_8 := m_N$,

(iii) zero-point energy Z_0: as with B, we let Z_0 be a free parameter (subject to $Z_0 > 0$),

(iv) one-gluon exchange correction ΔE: with similar assumptions as in the M.I.T. model[4], we find

$$\Delta E_E = 0$$

and

$$\Delta E_M = [9 - 6S(S+1)] \cdot \Delta E_M(\mathrm{MIT})$$

where $\Delta E_M(\mathrm{MIT})$ is the M.I.T. color-magnetic correction for the proton. Note that, for $A = 2$, the color-magnetic correction is independent of isospin T.

Some typical results of our calculation are given in Table I below. In the first line of each of the two sets, we took as input the "observed" anomalon radius R[1], and assumed the excitation energy per nucleon E^* to be zero. The fitted bag constant B then comes out smaller than the M.I.T. value by a factor of 10. In the second line, on the other hand, we have used the M.I.T. values for B and Z_0 as input. The nuclear radius then comes out smaller than the normal nuclear radius[5].

TABLE I

	E^*	R [fm]	$B^{1/4}$ [GeV]	Z_0
A = 2 :				
input E^*, R	0	5.8	0.014	0.48
input $B^{1/4}$, Z_0	0.24	0.97	0.146	1.84
A = 4 :				
input E^*, R	0	6.3	0.014	0.76
input $B^{1/4}$, Z_0	0.19	0.99	0.146	1.84

The results we obtained in other cases (up to A = 32) show the same general tendency: an anomalously large nuclear radius can be obtained in this model, but only at the expense of an unconvincingly small bag constant B.

While our results thus seem to point more against the validity of the model of a "nuclear bag" than they support it, it must be kept in mind that some of our assumptions regarding parameters may be just too crude, and not well-founded. We feel in particular that a more careful treatment of the gluon interaction (we have more or less used similar methods of treating this correction as were used in the original M.I.T. model calculations) might change the results significantly. In addition, more experimental information, above all about the excitation energy E^* of the anomalous nuclei, would give a better foothold for any attempt at explaining anomalons, including ours.

1) E.M.Friedlander, Phys.Rev.Lett. 45, 1084 (1980)
2) cf. K.Johnson, Acta Physica Polonica B 6, 865 (1975)
3) We assume L = 0 for the lowest-lying states.
4) T.de Grand et al., Phys.Rev. D 12, 2060 (1975)
5) The same result - a smaller than normal nuclear radius - is also obtained in the multi-quark bag model; cf. Ref. 2 .

SESSIONS III and IV:
HEAVY ION COLLISIONS AT BEVALAC ENERGIES

Results Obtained Using the Plastic Ball

H.G. Ritter, H.A. Gustafsson, H.H. Gutbrod, B. Kolb, H. Löhner, B. Ludewigt, A.M. Poskanzer, T.R. Renner, H. Riedesel, A. Warwick, F. Weik, and H. Wieman

Gesellschaft für Schwerionenforschung, Planckstrasse 1
D-6300 Darmstadt 11, West Germany
and
Nuclear Science Division, Lawrence Berkeley Laboratory
University of California, Berkeley, CA 94720

Introduction

Single particle inclusive experiments, and experiments that additionally measure a few correlations like the associated multiplicity, have provided the main contribution to our present understanding of high energy heavy ion collisions. The results from those experiments are in overall agreement [1] with calculations of the cascade [2,3] and hydrodynamical [4] models. In the cascade model the collision of two nuclei is simulated as a cascade of nucleon-nucleon collisions using measured N-N cross sections. The hydrodynamical model, on the other hand, describes the nuclear collision as that of two fluids and makes use of a nuclear equation of state relating thermal and compressional energy densities to pressure. The pressure field dominates the expansion phase and leads to collective flow of the reaction products in a preferred direction. The observation of such effects in inclusive experiments is not well established [5,6]. Collective effects that manifest themselves in the shape of the event in phase space are expected to be seen best in complete event detectors that measure the final state as exclusively as presently possible by measuring most of the charged particles emitted in the reaction. In addition, those detectors are well suited to test macroscopic concepts such as equilibrium and temperature. Global methods like the sphericity or thrust analysis [6] take into account all the correlations measured in the event and are specially designed to determine the shape of an event in phase space and thus to define a reaction plane.

Recent data from the Plastic Ball experiment about the study of nuclear stopping and thermalization and on global analysis are presented in this report. Of course, data from 4π detectors like the Plastic Ball can be analyzed under many different aspects. Especially, the characterization of events according to charged particle multiplicity, presently still the best experimental approximation to impact parameter selection, has yielded new and unexpected results, e.g., about the production of composite particles [7] and two particle correlations [8].

Experiment

The Plastic Ball [9] is a segmented multielement detector that covers 96 of the total solid angle. The general layout of the spectrometer is shown in fig. 1. The Plastic Wall, placed 6 m downstream from the target, covers the angular range from 0 to 10 degrees and measures time of flight, energy loss, and position of the reaction products. In addition, the information from the inner counters (0 to 2 degrees) is used to produce a trigger signal.

The Plastic Ball covers the region between 10 and 160 degrees. It consists of 815 detectors, where each module is a ΔE-E telescope capable of identifying the hydrogen and helium isotopes and positive pions. The ΔE measurement is performed with a 4-mm thick CaF_2 crystal and the E counter is a 36-cm long plastic scintillator. Both signals are read out by a single photomultiplier tube. Due to the different decay times of the two scintillators, ΔE and E information can be separated by gating two different ADCs at different times. The positive pions are additionally identified by measuring the delayed $\pi^+ \rightarrow \mu^+ \rightarrow e^+$ decay. The quality of the particle identification is shown in fig. 2 for the hydrogen and helium isotopes.

Figure 3 shows the acceptance of the Plastic Ball experiment for protons in the plane of rapidity versus transverse momentum. In the different areas charged particles can be identified with different quality. Different projectile-target combinations have been measured with a minimum bias trigger and with a trigger configuration that selects central reactions. Results from 400 MeV/u Ca on Ca, 400 MeV/u Nb on Nb, and 800 MeV/u Ne on Pb are presented.

Nuclear Stopping and Thermalization

Thermalization among the participant nucleons in high-energy nuclear collisions is predicted by thermal models and is a necessary condition for the determination of temperature. It is characterized by the fact that the originally longitudinal motion of the projectile is equally distributed over all available degrees of freedom (longitudinal and transversal). A necessary but not sufficient condition for thermalization is that [10]

$$\frac{1}{2} \sum_i p_{i\perp}^2 = \sum_i p_{i\parallel}^2$$

or (1)

$$R = \frac{2 \sum |p_{i\perp}|}{\pi \sum |p_{i\parallel}|} = 1$$

A global stopping of the two nuclei at small impact parameters would show up in a ratio R = 1 or even larger if hydrodynamical flow into transverse direction exists. In the presence of transparency this ratio would always be below 1. Data that fulfill the necessary condition of R = 1 may indicate the existence of a nuclear fireball if, in addition, their energy spectra are of Maxwell Boltzmann shape in the center of mass.

In fig. 4 (top) contour lines of the yield of events in the plane $2/\pi \sum_i |p_{i\perp}|/A$ vs $\sum_i |p_{i\parallel}|/A$ are shown for the system Ca + Ca, the minimum bias trigger applied. Most of the yield is far away from the R = 1 (isotropy) region. The peak at small $p_\perp$ but large $p_\parallel$ corresponds to peripheral reactions and is dominated by projectile fragments. This contribution vanishes as the trigger is changed to a "central" one. Figure 4 (middle) shows central trigger events with a charge particle multiplicity larger than 30. The maximum of the yield is shifted toward the diagonal but only a few events reach R = 1, which, for large multiplicities and absence of any two jet structure, corresponds to a full stopping of the nuclei. In the lower part of fig. 4 for the reaction of 400 MeV/u Nb + Nb the central

trigger events with charge particle multiplicities beyond 55 are fulfilling the stopping condition (R = 1) on the average.

The observed difference between the Ca + Ca and the heavier Nb + Nb system allows two different interpretations: The Ca nuclei are too small to stop one another, so a transparency remains in the longitudinal direction, or only a subvolume is fully stopped and eventually thermalized, but the surface zones show some transparency and therefore the differences are caused by the various surface-to-volume ratios of Ca and Nb. However, one has to keep in mind that the high multiplicity cuts correspond roughly to an impact parameter selection from 0 to 3 fm, where in these symmetric systems still large parts of the nuclei might pass one another rather undisturbed. Although spectator fragments are excluded within $\theta_{lab} \leq 2^\circ$ with our central trigger condition, there are still some "leading particles" left outside of $\theta_{lab} = 2^\circ$. Any one of these particles strongly enhances the parallel momentum component, thus reducing the ratio R.

Global Analysis

It has been pointed out that event shape analysis might be able to distinguish between predictions of cascade and hydrodynamical models. To do this the thrust [11-13] and sphericity [12,14] analyses used in high energy physics [6] have been proposed. Because the thrust vector cannot be calculated analytically, the sphericity method generally has been used.

The sphericity tensor

$$F_{ij} = \sum_{\nu} p_i(\nu)\, p_j(\nu)\, w(\nu)$$

is calculated from the momenta of all measured particles for each event. It is appropriate to choose the weight factor $w(\nu)$ in a way that composite particles have the same weight as the individual nucleons of the composite particle at the same velocity. In this paper the weight $w(\nu) = 1/(2m)$ as proposed in ref. 14 (kinetic energy flow) is used. Other coalescense invariant weights such as $1/p$ [12] have been proposed and have been used in our analysis. The sphericity tensor approximates the event shape by an ellipsoid whose orientation in space and aspect ratios can be calculated by diagonalizing the tensor.

The shapes predicted by hydrodynamical and cascade calculations are quite different. The hydrodynamical model predicts prolate shapes along the beam axis for grazing collisions. With decreasing impact parameter the flow angle increases up to 90 degrees for zero impact parameter events and the shape becomes prolate [11,13,14]. This behavior is independent of projectile and target mass. Cascade calculations, on the other hand, predict finite nontrivial flow angles only for very heavy systems [14].

A rigorous comparison of experimental data with predictions is only possible if the theory calculates all observed quantities by generating a large number of complete events. Those events have to be filtered with the known experimental acceptance and efficiency of the detector. Most models, however, have not yet reached sufficient sophistication: cascade models do not include composite particles, and hydrodynamical codes do not yet produce

event-by-event fluctuations. This makes a useful comparison difficult, and it is not yet clear that the differences between the two models will show up after all distortions are taken into account.

Another big obstacle in extracting information from a flow analysis is fluctuations due to finite particle effects. Recently, Danielewicz and Gyulassy [15] have shown that those distortions strongly depend on multiplicity and that the flow angle, θ, if properly weighted by the Jacobian ($\sin\theta$), is much less severely shifted towards higher values than the aspect ratios. It now can be shown that the results of the flow analysis of the 400 MeV/u Ca + Ca data [16] (fig. 5), even though they differ from cascade predictions, can be explained with finite number distortions by assuming prolate shapes along the beam axis [17]. Deviations from cascade predictions seen in the analysis of asymmetric target projectile combinations measured with the streamer chamber [18,19] seem to be inconclusive as well because the data points in the flow plot do not fall in the region where, despite the distortions, nontrivial flow angles and aspect ratios can be detected.

It is hoped that heavier symmetric systems are less sensitive to distortions and that possible macroscopic effects can more easily be detected. As shown in fig. 6, the Nb + Nb data at 400 MeV/u reach flow angles up to 30 degrees (peak maximum) for the highest multiplicity bins, whereas predictions from the Yariv-Fraenkel cascade [2], filtered with the exact acceptance and efficiency of the Plastic Ball never deviate significantly from 0 degrees even for the highest multiplicity events. The fact that finite flow angles are seen in the data indicates that in those events there exists a plane defined by the flow axis and the beam axis, which will be called the reaction plane. All events can be rotated by the azimuthal angle φ determined by the flow analysis so that their individual reaction planes all fall into the x-z plane, with the z-axis being the beam axis. For those rotated events rapidity plots in the reaction plane [13,20] can be calculated. The use of $p_\perp/m$ as proposed in ref. 13 is only of theoretical interest as the phase space vanishes. However, the invariant cross sections dp_x/mdy (in plane) and dp_y/mdy (out of plane) can be plotted, where p_x is the projection of the perpendicular momentum into the reaction plane and p_y the projection into the plane perpendicular to the reaction plane. Figure 7 shows these plots for 400 MeV/u Nb + Nb data and cascade calculations for events with charged particle multiplicities between 40 and 50, the second highest multiplicity bin considered here. The depletion near target rapidities is due to experimental acceptance. The two cascade plots and the out-of-plane data plots are symmetric around the beam axis, whereas the in-plane data plot is clearly asymmetric. Taking into account the multiplicity dependence of the rapidity plots (not shown here), two distinctly different trends can be observed. The outer low-intensity contour lines seem to follow the trend indicated by the $dN/d\cos\theta$ distribution. At low multiplicity they can be described by ellipsoids elongated along the beam axis. With increasing multiplicity the ellipsoids are more and more turned relative to the beam axis. The peak in the rapidity distributions, resulting largely from the projectile remnants, on the other hand, is rather independent of multiplicity. It clearly shows a perpendicular and longitudinal momentum transfer to the spectator nuclei. The longitudinal degradation of about 0.05 units in rapidity is not dependent on multiplicity, and the perpendicular momentum transfer varies only slightly

from about 30 to 50 MeV/c per nucleon as a function of multiplicity. The deflection angle of the projectile remnants always stays below 10 degrees.

As can be seen from figs. 6 and 7 cascade calculations are not able to reproduce the data. An exact comparison with predictions from hydrodynamical model calculations is not possible as the impact parameter is not known experimentally. However, comparison with cascade events indicates that the highest multiplicity bin of the data contains events whose impact parameter can be as large as 3 to 4 fermis. Considering such large impact parameters the hydrodynamical predictions [13] seem to be in qualitative agreement with the dN/d cos θ distributions. The deflection of the spectator matter is a collective effect that might be due to the effect of a nuclear potential and should be explained, e.g., by classical equation of motion calculations [21].

For asymmetric systems the flow analysis is usually performed in the center of mass of all the measured particles. The velocity β_{obs} of this system in the beam direction should depend on the impact parameter and thus on the multiplicity of charged particles m_c. Figure 8 shows a contour plot of m_c as a function of the observed velocity β_{obs} for the reaction 800 MeV/u Ne + Pb. This velocity varies from that of the nucleon-nucleon system β_{NN} for the most peripheral collisions up to the velocity of the compound system β_{comp}. It significantly overshoots the fireball system velocity β_{FB} even though only about one-third of all particles (and preferentially the faster ones) are detected. This strongly indicates not only that the projectile is stopped as, e.g., predicted by a clean-cut fireball model [22] but that the target nucleus as a whole stops the projectile. The emission pattern of this "compound" system can be studied by a flow analysis. The flow angle distributions dN/dcosθ for the different multiplicities all peak at 0 degrees, but for the highest multiplicities they become flat and angle independent, indicating isotropic emission. The same pattern is suggested by the rapidity plots.

Conclusions

The ratio R of perpendicular to longitudinal momentum per nucleon shows that even for the most violent reactions in the Ca on Ca case at 400 MeV per nucleon there is always some transparency left, whereas in the Nb case the two nuclei are stopped in average and the participant nuclei seem to form an expanding fireball. The fact that for Nb finite flow angles are observed must not necessarily be in contradiction to this statement as the event-by-event variations of R are quite large, and only the rather crude classification of events according to the observed charged particle multiplicity has been studied so far.

The dN/d cos θ distributions show no finite flow angle for the Ca case but reach angles of up to 30 degrees for Nb. However, in both cases a clear collective deflection of the spectator nuclei that is nearly independent of multiplicity is observed. It will be necessary to study the energy and mass dependence of those effects and to compare with cascade and hydrodynamical calculations as well as with events generated with the Fai-Randrup code [23] where parameters like perpendicular and longitudinal momentum transfer can be adjusted before final conclusions about collective effects in relativistic nuclear collisions can be drawn.

References

1) S. Nagamiya and M. Gyulassy, LBL-14035 preprint
2) Y. Yariv and Z. Fraenkel, Phys. Rev. C20 (1979) 2227
3) J. Cugnon, et al., Nucl. Phys. A352 (1981) 505
4) A.A. Amsden, F.H. Harlow, and J.R. Nix, Phys. Rev. C15 (1977) 2059
A.A. Amsden, A.S. Goldhaber, F.H. Harlow, and J.R. Nix, Phys. Rev. C17 (1978) 2080
H. Stöcker, W. Greiner, and W. Scheid, Z. Physik A286 (1978) 121
5) R. Stock, et al., Phys. Rev. Lett. 44 (1980) 1243
H. Stöcker, et al., Phys. Rev. Lett. 47 (1981) 1807
6) S. Brandt and H. Dahmen, Z. Physik C1 (1979) 61
S.L. Wu and G. Zoberning, Z. Physik C2 (1979) 107
7) T.R. Renner, H.A. Gustafsson, H.H. Gutbrod, B. Kolb, H. Löhner, B. Ludewigt, A.M. Poskanzer, H. Riedesel, H.G. Ritter, A. Warwick, F. Weik, and H. Wieman, contribution to this conference
8) H. Wieman, H.H. Gutbrod, H.A. Gustafsson, B. Kolb, H. Löhner, B. Ludewigt, A.M. Poskanzer, T.R. Renner, H. Riedesel, H.G. Ritter, A. Warwick, and F. Weik, contribution to this conference
9) A. Baden, H.H. Gutbrod, H. Löhner, M.R. Maier, A.M. Poskanzer, T. Renner, H. Riedesel, H.G. Ritter, H. Spieler, A. Warwick, F. Weik, and H. Wieman, Nucl. Instr. and Meth. 203 (1982) 189
10) R. Stock, in Proceedings of 5th High Energy Heavy Ion Study, LBL-12652
11) J. Kapusta and D. Strottman, Phys. Lett. 103B (1981) 269
12) J. Cugnon, J. Knoll, C. Riedel, and Y. Yariv, Phys. Lett. 109B (1982) 167
13) H. Stöcker, L.P. Csernai, G. Graebner, G. Buchwald, H. Kruse, R.Y. Cusson, J.A. Maruhn, and W. Greiner, Phys. Rev. C25 (1982) 1873
14) M. Gyulassy, K.A. Fraenkel, and H. Stocker, Phys. Lett. 110B (1982) 185
15) P. Danielewicz and M. Gyulassy, Lawrence Berkeley Laboratory Preprint 15721, submitted to Physics Letters B
16) H.G. Ritter, in Proc. 3rd Intl. Conf. on Nuclear Reaction Mechanism, ed. E. Gadioli (Varenna, Italy, 1982)
H.H. Gutbrod, H. Löhner, A.M. Poskanzer, T. Renner, H. Riedesel, H.G. Ritter, A. Warwick, F. Weik, and H. Wieman, in Proc. Intl. Conf. on Nucleus-Nucleus Collisons (Michigan State University, East Lansing, MI, 1982), Lawrence Berkeley Laboratory Preprint 14980
17) P. Danielewicz, private communication, 1983
18) H. Stroebele, R. Brockmann, J.W. Harris, F. Riess, A. Sandoval, H.G. Pugh, L.S. Schroeder, R.E. Renfordt, T. Tittle, and M. Maier, Phys. Rev. C27 (1983) 1349
19) A. Huie, D. Beavis, S.Y. Fung, W. Gorn, D. Keane, J.J. Lu, R.T. Poe, B.C. Shen, and G. VanDalen, Phys. Rev. C27 (1983) 439
D. Beavis, S.Y. Chu, S.Y. Fung, W. Gorn, A. Huie, D. Keane, J.J. Lu, R.T. Poe, B.C. Shen, and G. VanDalen, Phys. Rev. C27 (1983) 2443
20) H. Stöcker, G. Buchwald, G. Graebner, J. Maruhn, W. Greiner, K. Fraenkel, and M. Gyulassy, Michigan State University Preprint MSUCL 409
21) A.R. Bodmer, C.N. Panos, and A.D. MacKellar, Phys. Rev. C22 (1980) 1025
22) J. Gosset, H.H. Gutbrod, W.G. Meyer, A.M. Poskanzer, A. Sandoval, R. Stock, and G.D. Westfall, Phys. Rev. C16 (1977) 629
23) G. Fai and J. Randrup, Lawrence Berkeley Laboratory Preprint 14248 and Nuclear Physics, in press

Figure Captions

Fig. 1. General layout of the Plastic Ball experiment.

Fig. 2. Particle identification spectrum for 655 modules after gain-matching with (dashed line) and without (solid line) scattering out reconstruction.

Fig. 3. Plastic Ball acceptance in the plane rapidity versus transverse momentum.

Fig. 4. Contour plots of the perpendicular momentum per nucleon as a function of the parallel momentum per nucleon for 400 MeV/u Ca on Ca for two different trigger selections (top) and for 400 MeV/u Nb on Nb.

Fig. 5. Flow plot for 400 MeV/u Ca on Ca.

Fig. 6. Frequency distributions of the flow angle θ for different multiplicity bins (data and cascade calculations).

Fig. 7. Contour plots (linear contours) of the projection of the transverse momentum in and out of plane as a function of cm rapidity.

Fig. 8. Contour plot (linear contours) of the charged particle multiplicity as a function of the velocity of the cm system of the measured charged particles.

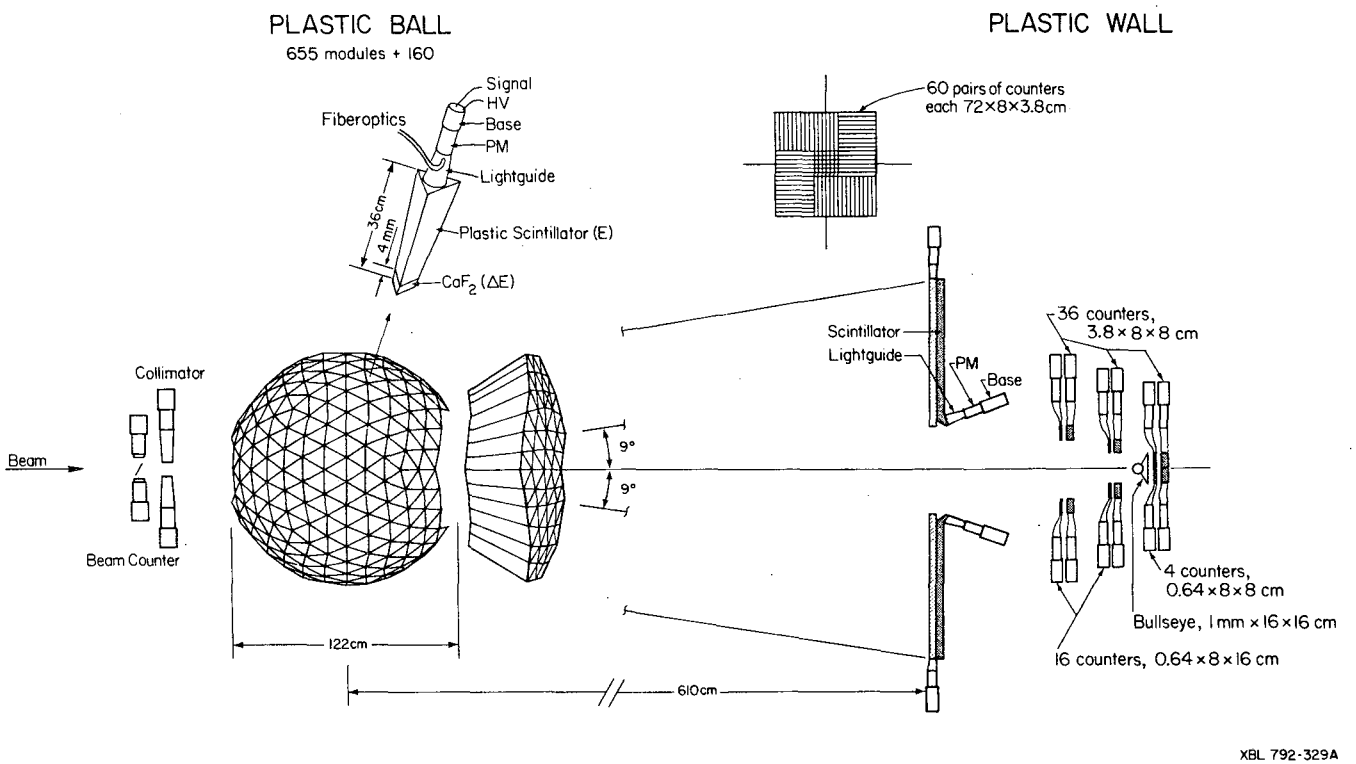
PLASTIC BALL
655 modules + 160
Signal
HV
Base
PM
Fiberoptics
Lightguide
36cm
4mm
Plastic Scintillator (E)
CaF2 (ΔE)
Collimator
Beam
Beam Counter
122cm
9°
9°
610cm
PLASTIC WALL
60 pairs of counters
each 72×8×3.8cm
Scintillator
Lightguide
PM
Base
36 counters,
3.8×8×8 cm
4 counters,
0.64×8×8 cm
Bullseye, 1mm × 16×16 cm
16 counters, 0.64×8×16 cm
XBL 792-329A

Fig. 1

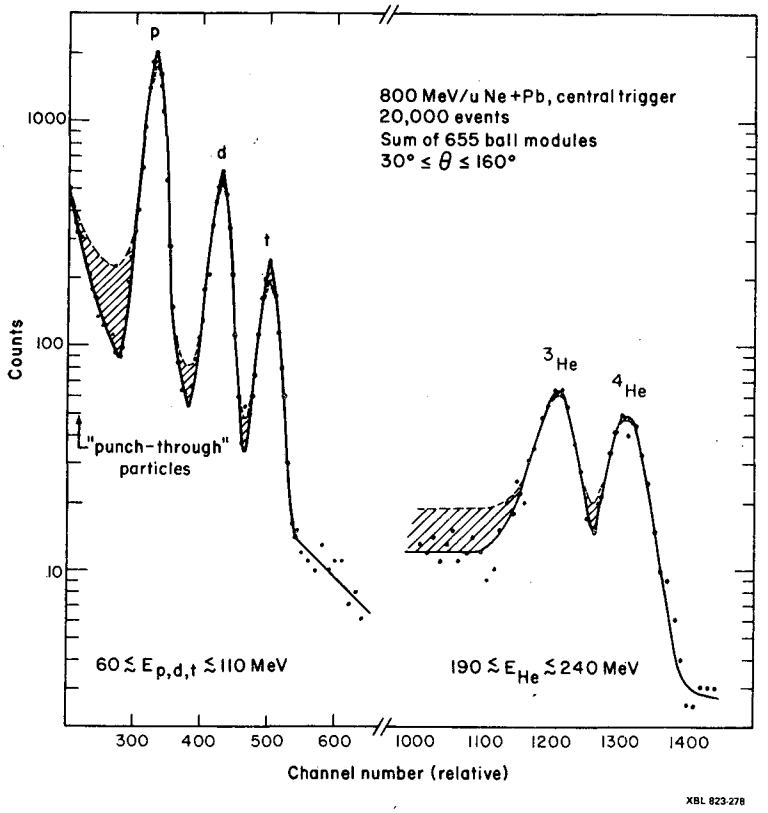
p
d
t
800 MeV/u Ne+Pb, central trigger
20,000 events
Sum of 655 ball modules
30° ≤ θ ≤ 160°
Counts
1000
100
10
"punch-through" particles
3He
4He
60 ≲ Ep,d,t ≲ 110 MeV
190 ≲ EHe ≲ 240 MeV
300
400
500
600
1000
1100
1200
1300
1400
Channel number (relative)
XBL 823-278

Fig. 2

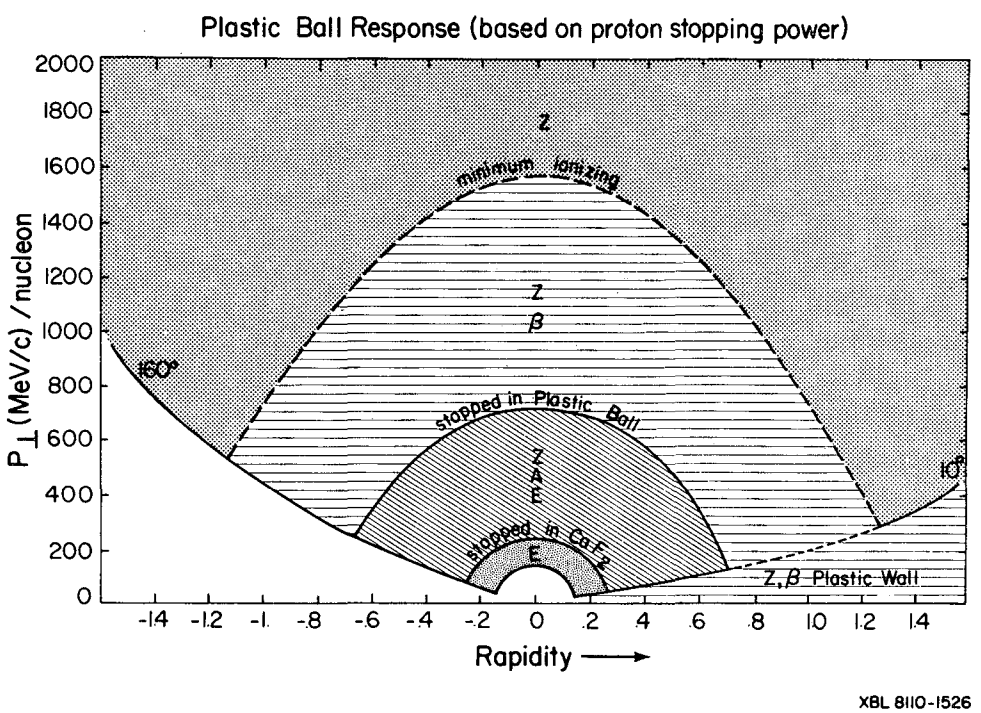
Plastic Ball Response (based on proton stopping power)
P⊥ (MeV/c) /nucleon
2000
1800
1600
1400
1200
1000
800
600
400
200
0
Z
minimum ionizing
Z
β
160°
stopped in Plastic Ball
Z
A
E
stopped in CsI
E
10°
Z, β Plastic Wall
-1.4
-1.2
-1.
-.8
-.6
-.4
-.2
0
.2
.4
.6
.8
1.0
1.2
1.4
Rapidity
XBL 8110-1526

Fig. 3

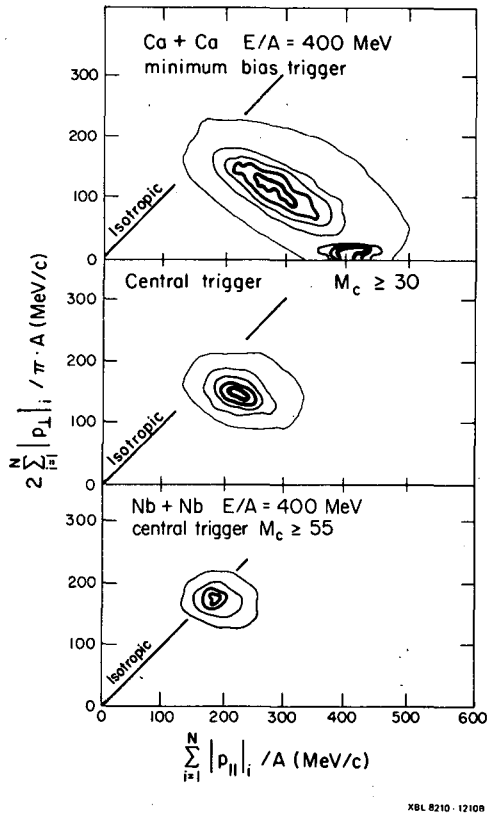
Ca + Ca E/A = 400 MeV
minimum bias trigger
Isotropic
Central trigger $M_c \geq 30$
Isotropic
Nb + Nb E/A = 400 MeV
central trigger $M_c \geq 55$
Isotropic
$2\sum_{i=1}^{N}|p_\perp|_i / \pi \cdot A$ (MeV/c)
$\sum_{i=1}^{N}|p_\parallel|_i / A$ (MeV/c)
XBL 8210-12108

Fig. 4

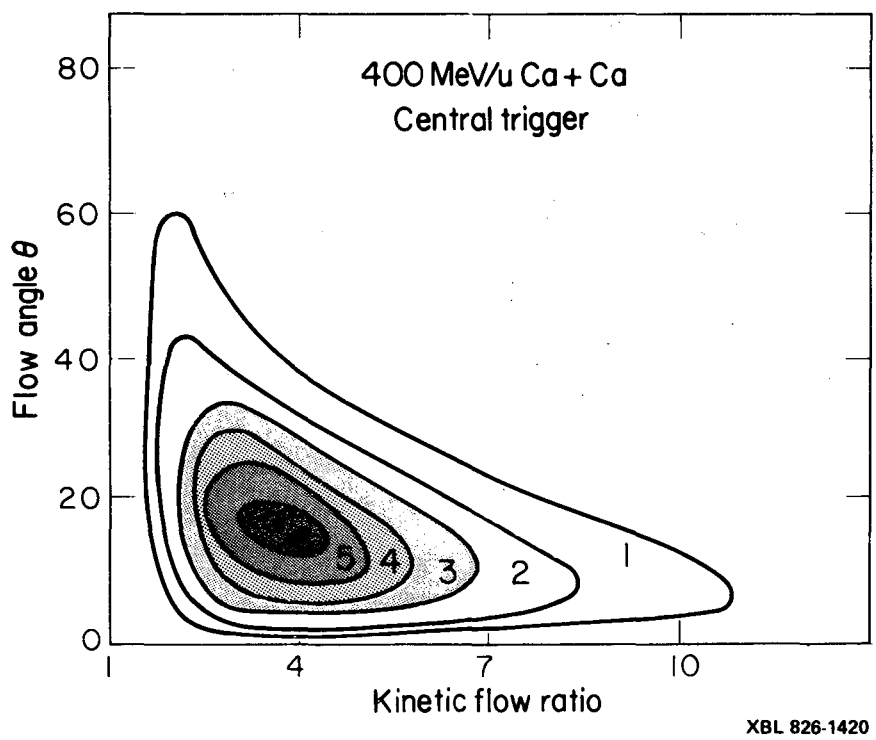
400 MeV/u Ca + Ca
Central trigger
Flow angle θ
Kinetic flow ratio
1
2
3
4
5
XBL 826-1420

Fig. 5

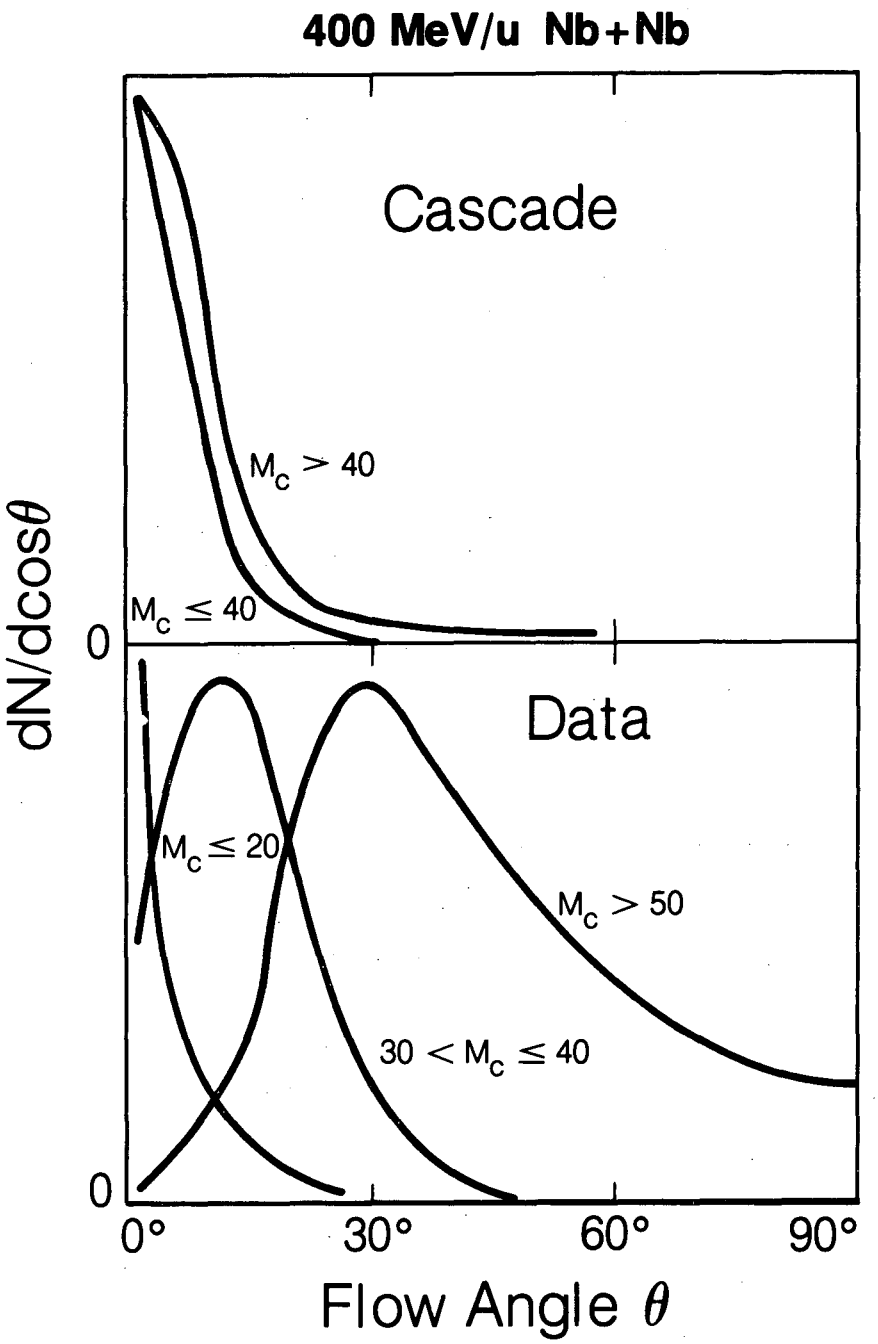

XBL 835-244

Fig. 6

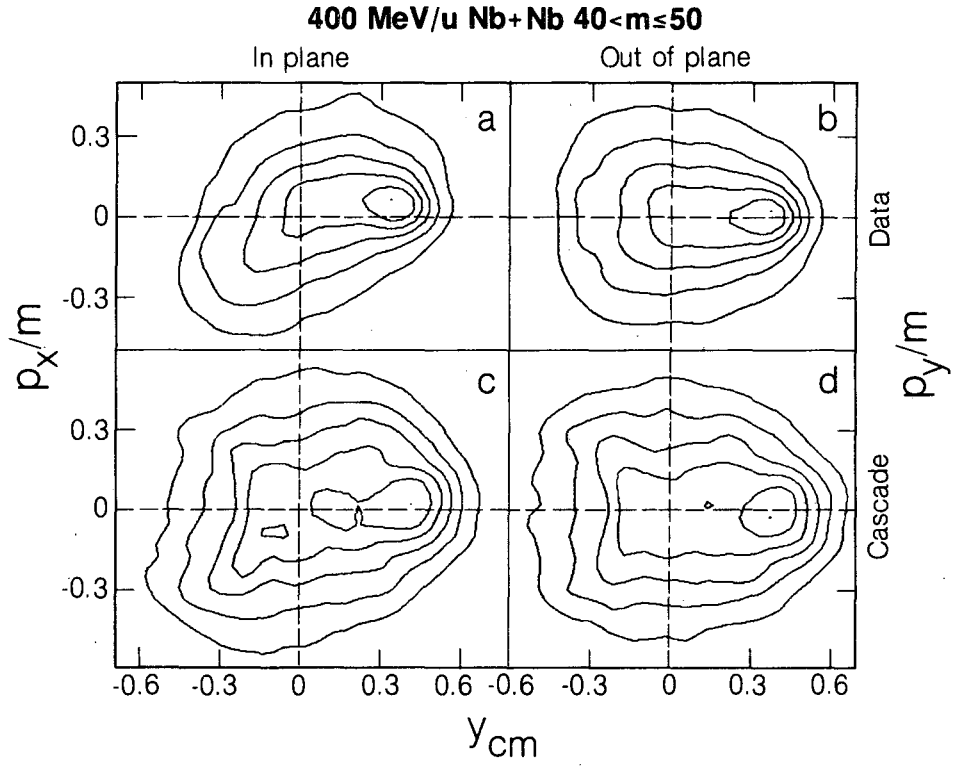

XBL 835-243

Fig. 7

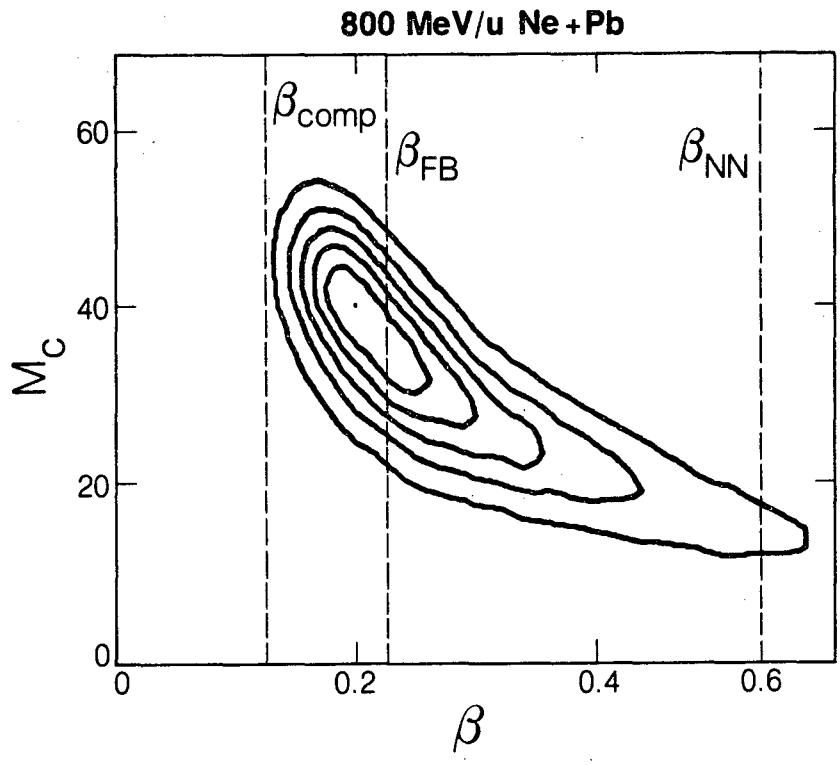

Fig. 8

XBL 835-245

Search for Flow in the Reaction Ar + Pb

R.E. Renfordt,[1] R. Brockmann,[2] J.W. Harris,[2] M. Maier,[2] F. Riess,[2]
A. Sandoval,[2] R. Stock,[2] H. Ströbele,[2] K.L. Wolf,[2] H.G. Pugh,[3]
L.S. Schroeder,[3] D. Schall,[1] and K. Tittel[1]

University of Heidelberg, W. Germany (1)
Gesellschaft für Schwerionenforschung, Darmstadt, W. Germany (2)
Lawrence Berkeley Laboratory, Berkeley, CA 94720 USA (3)

Interactions between Ar projectiles and lead are studied in terms of global observables. The Streamer Chamber at the Berkeley BEVALAC was used to record all charged particles produced in collisions between 0.8 GeV/u Ar projectiles with a Pb_3O_4 target. A hardware trigger selected central collisions with Pb nuclei corresponding to a trigger cross section of 1 barn. In a geometrical picture this is equivalent to an impact parameter range of 0-5 fm.

Three views of the Streamer Chamber pictures were recorded on film. All visible tracks were measured on three views and reconstructed in space. Particle identification and separation was achieved by visual inspection of track granularity and by kinematical cuts. Five hundred events have been analyzed so far. Significant experimental biases were found only for particles around target rapidity, where absorption in the target, proton/deuteron ambiguities, and Streamer Chamber inefficiencies are important. Therefore, further analysis was restricted to the particles emerging in the forward direction in the event participant center-of-mass system, computed event by event from only those particles having transverse momenta above 270 MeV/c (see ref. 1). The experimental data were compared to 400 events generated by the intranuclear cascade code of Cugnon et al.[2] in the same impact parameter range as selected by the hardware trigger. In addition, we compare our data to events generated by a Monte Carlo program using an isotropic angular distribution, the same mean multiplicity ($\langle M \rangle = 48$) and the same slope parameter for the energy spectrum ($E_0 = 110$ MeV) as observed in the data. The experimental inefficiencies were folded into the cascade events as well as into the isotropic Monte Carlo events.

The total baryonic transverse energy in the forward hemisphere of each event ($E_t = \sum_{i=1}^{N} \left\{ \sqrt{P_{t_i}^2 + M_i^2} - M_i \right\}$, N = Number of baryons in the event) was used to define subsamples of events corresponding to different impact parameter (b) ranges. Figure 1 shows the correlation between the total transverse energy and b as determined from the cascade events.

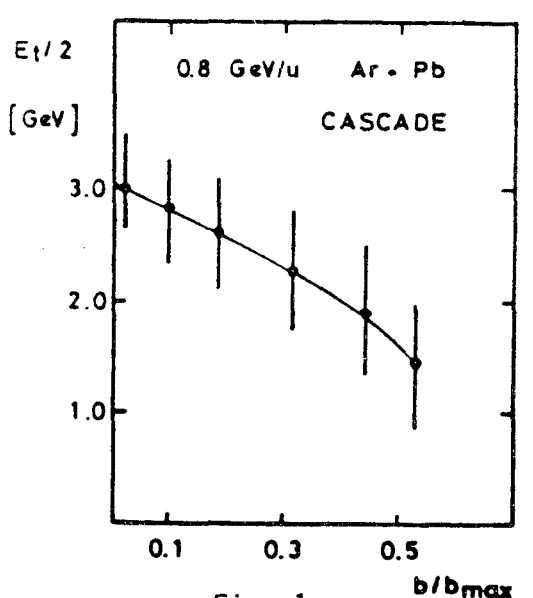

Fig. 1

In Fig. 2 contour plots of the mean longitudinal ($p_{\parallel}$) versus mean transverse (p_t) momentum per event[3] are presented for both the experimental data and the cascade events, together with subsamples selected for high E_t ($E_t > 2.6$ GeV, i.e., small impact parameter). The cascade events have a significantly higher fraction of events with rather high $p_{\parallel}$. For high E_t both data sets are rather isotropic and centered around the symmetry line. The slight excess in P_t for the data is due to the bias introduced by the E_t selection since it is also seen (not shown here) in the isotropic Monte Carlo events.

Differences between data and cascade can be analyzed in more detail by studying the E_t-dependence of the deflection angle and aspect ratio of the momentum flux tensor.[4] Since b is an a priori unmeasurable quantity we use instead the total transverse energy and determine the bias introduced by this selection criterium with cascade generated events.

The histograms in Fig. 3 show the angular distribution of the main axis of the momentum tensor with respect to the beam direction for the data and cascade events. For high E_t the data show an isotropic distribution whereas the cascade events are still dominated by rather small deflection angles.

A more detailed evaluation of this difference is obtained by the following method:[5] the azimuthal orientation of the main axis of the momentum flux tensor is computed for each event; then each event is rotated around the beam such that the momentum tensor has the same azimuthal angle for all events; finally, for each subsample of events, corresponding to different E_t intervals, a single momentum tensor (formed by the superimposed events) is computed, thus eliminating fluctuations caused by the limited number of particles in a single event.

In Fig. 4 the perpendicular component of the momentum within the reaction plane (defined as the plane spanned by the beam and the main axis of the flux tensor) after the rotation and summation as described above is plotted versus the parallel momentum component $p_{\parallel}$ for a subsample of events with $E_t < 2.6$ GeV in a linear plot (4a). The numbers at the contour lines indicate the number of particles. A finite deflection angle can be observed. For comparison the component of p perpendicular to the reaction plane is also plotted (4b). The distribution is symmetric with respect to the beam axis as it should be.

Figure 5 summarizes the result of this analysis. The clear difference in the E_t-dependence of θ between data and cascade events (Fig. 5a) emphasizes the earlier finding of an excess in deflection of the data as compared to the cascade events. The deflection angles for the isotropic Monte Carlo events are consistently higher than the data. The aspect ratio R_{32} (Fig. 5b) as derived from the latter event sample varies with E_t as expected from the θ behavior: elongation of the flux tensor for small deflection angles and shapes close to spherical for large angles, which is consistent with a zero deflection angle of an undistorted momentum tensor.[5] The aspect ratios for the experimental data samples indicate near-spherical shapes for the higher E_ts by comparing it to the isotropic distribution, which shows no dependence on E_t. The data indicate a higher

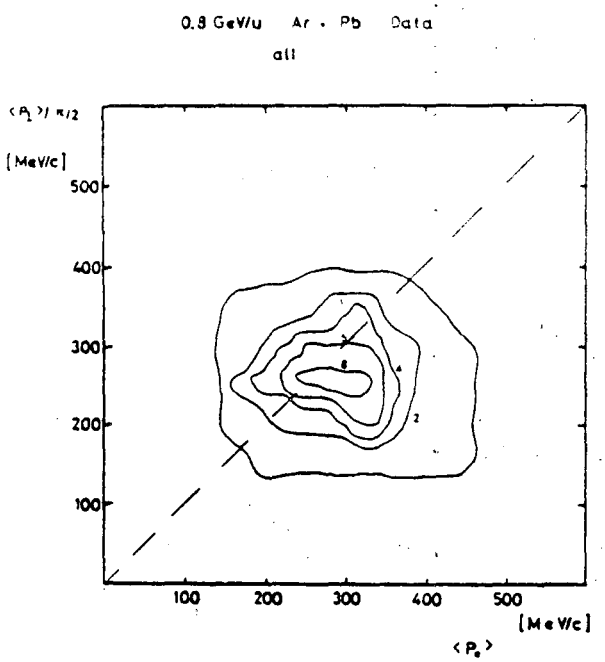

Fig. 2a

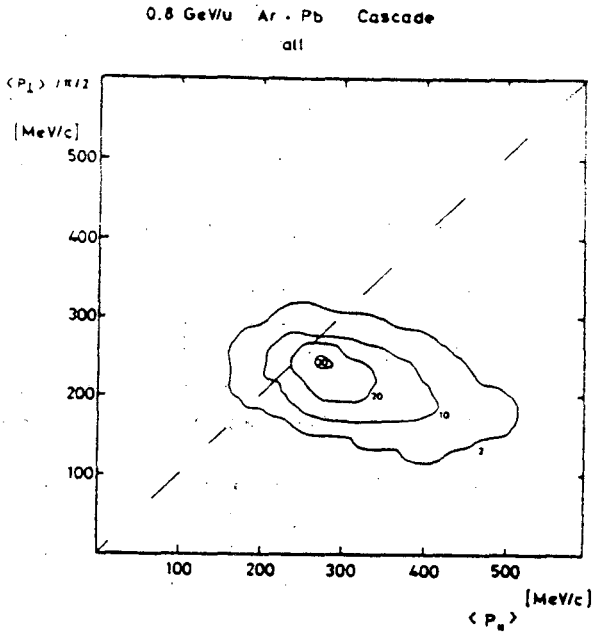

Fig. 2b

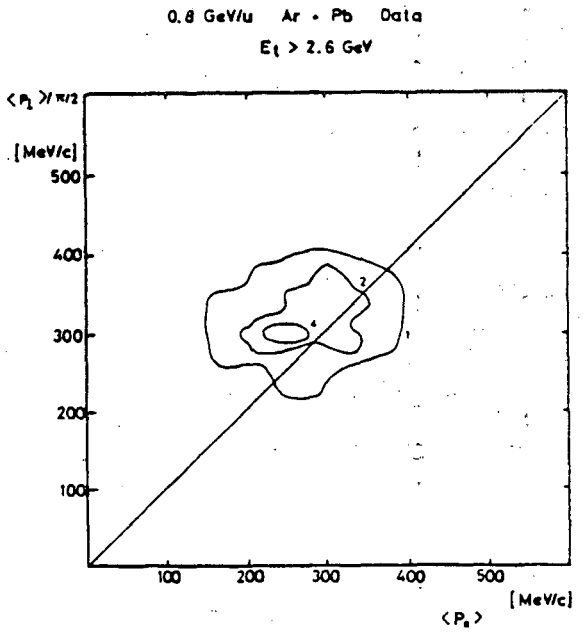

Fig. 2c

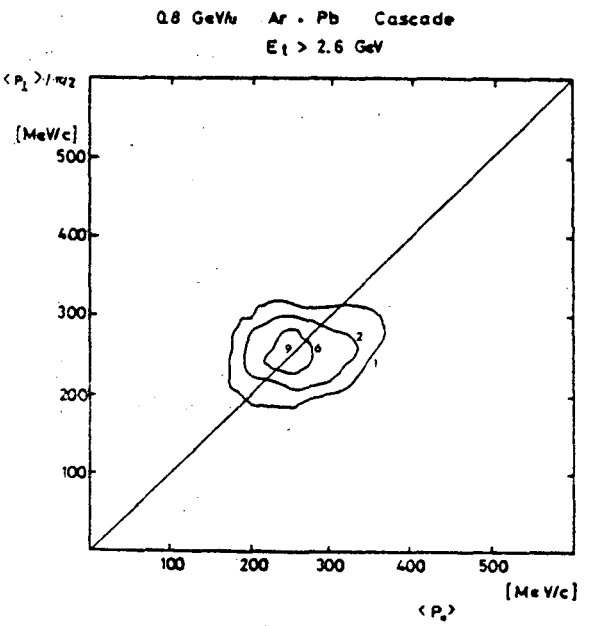

Fig. 2d

Fig. 2. Average transverse momentum versus average longitudinal momentum per event for exp. data (a+c) and cascade events (b+d) with and without a cut in the total transverse energy measured per event.

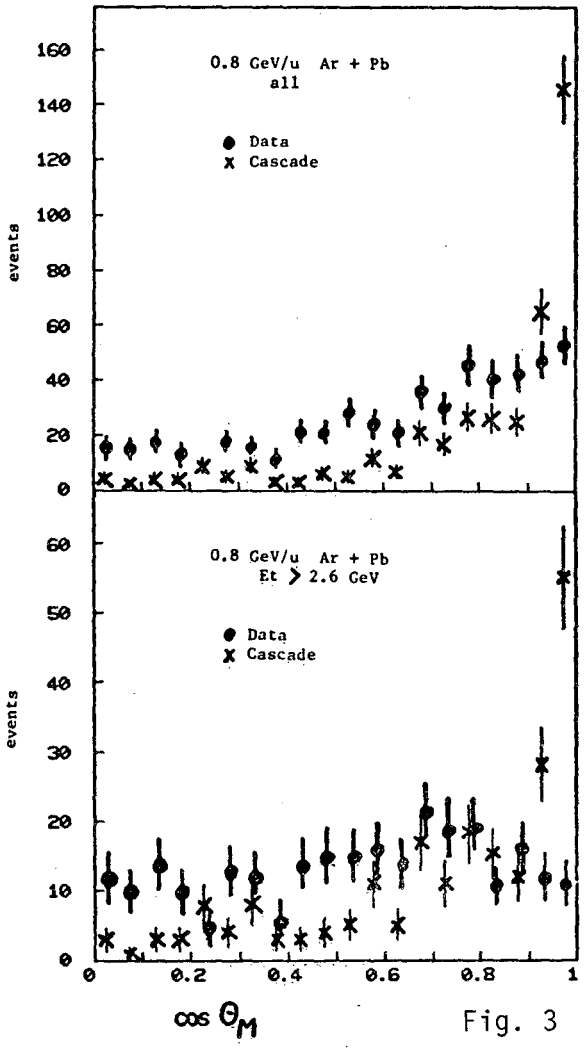

Fig. 3

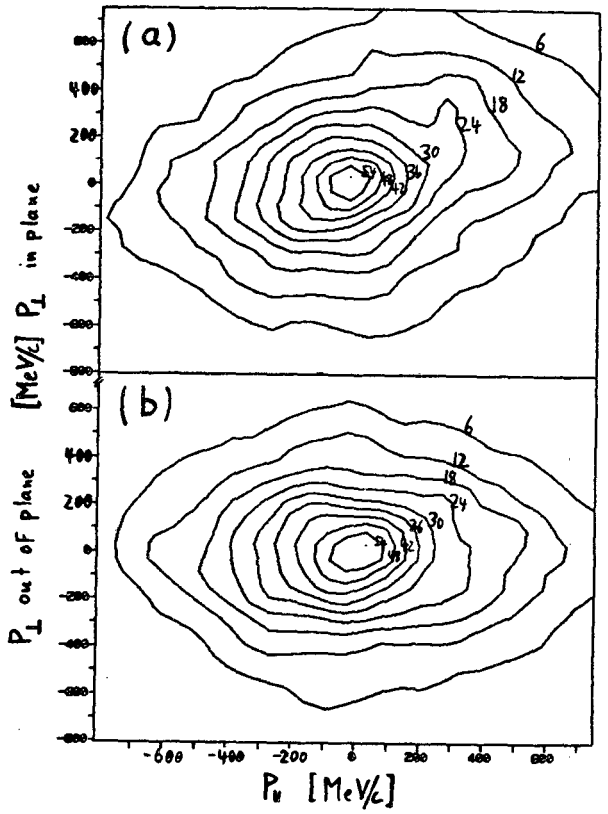

Fig. 4

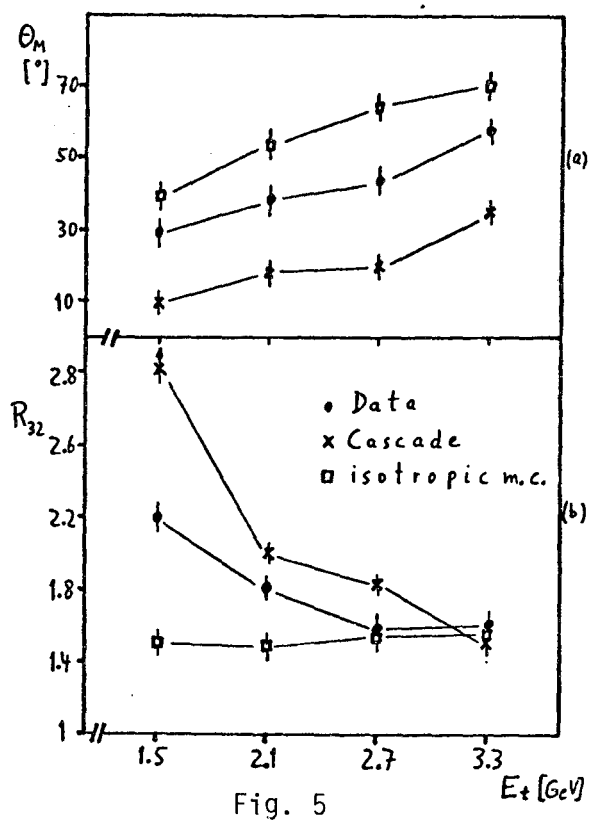

Fig. 5

degree of thermalization than the cascade predicts. The comparison to the isotropic Monte Carlo, on the other hand, indicates a significant deviation from simple thermal behavior. Conclusions about the existence of a bounce-off effect as predicted by hydrodynamical models[6], however, are only possible if detailed predictions are subjected to the same analysis procedures as the experimental data such that systematic biases introduced by these procedures are the same for the model predictions and the data.

We conclude that our experimental data cannot be described satisfactorily by the intranuclear cascade of Cugnon et al. The deviations from the cascade could point towards hydrodynamical flow. However, this can only be verified after the hydrodynamical models are modified such as to be directly comparable to exclusive data.

This work was supported in part by the Director, Office of Energy Research, Division of Nuclear Physics of the Office of High Energy and Nuclear Physics of the U.S. Department of Energy under Contract DE-AC03-76SF00098.

References

1. H. Strobele, et al., Phys. Rev. C27, 1349 (1983).
2. J. Cugnon et al., Nucl. Phys. A379, 553 (1982).
3. R. Stock, Proc. 5th High Energy Heavy Ion Study, LBL-12652 (1981), p. 284.
4. M. Gyulassy et al., Phys. Lett. 110B, 185 (1982).
5. P. Danielewicz and M. Gyulassy, LBL-15721 (1983).
6. J. Kapusta and D. Strottmann, Phys. Rev. C23, 1282 (1981).
   H. Stöcker et al., Phys. Rev. 25, 1873 (1982).

Evidence on the Equation of State of Nuclear Matter at High Densities

J.W. Harris, D. Bangert, R. Bock, R. Brockmann, A. Dacal[1], M. Maier, G. Odyniec, M.E. Ortiz,[1] H.G. Pugh, W. Rauch, R.E. Renfordt, A. Sandoval, L.S. Schroeder, R. Stock, H. Ströbele, and K.L. Wolf[2]

Gesellschaft für Schwerionenforschung, Planckstrasse 1
D-6300 Darmstadt 11, West Germany
and
Nuclear Science Division, Lawrence Berkeley Laboratory
University of California, Berkeley, CA 94720

One of the primary objectives in the study of relativistic nucleus-nucleus collisions is to determine the response of nuclear matter to compression and expansion over a wide range of densities. The nuclear response is fundamental to understanding the formation and collapse of supernovae[1] and the stability of neutron stars.[2] In the early stages of the universe and subsequent stellar evolution, nuclear densities from 0.1 to greater than 10 times normal nuclear matter density (ρ_0) are believed to occur. Likewise, a broad range of densities is expected in nucleus-nucleus collision processes . Furthermore, predictions of phase transitions at both high[3] and low[4] densities are particularly important and appealing.

Predictions of dynamical models[5-8] of widely varying origin yield similar results on the nucleus-nucleus collision process. The one- and two-fluid hydrodynamical models, which assume a short mean free path in nuclear matter, and intranuclear cascade models with diametrically opposite long mean free path assumptions, predict a compression-expansion cycle for the collision process. This is depicted by the results of a hydrodynamical calculation[9] shown in Fig. 1. Densities of 2-4 ρ_0 are predicted in both approaches. However, there has yet been no direct evidence for high density from experiments. Chaotic kinetic effects from heating, represented by an increase in temperature in Fig. 1, during both compression and expansion will dilute any direct signature of the high-density stage of the reaction. In the expansion stage final state interactions and the approach to chemical equilibrium further alter observables that may be linked to high densities. Several experimental approaches have been undertaken to minimize these effects and perhaps gain information on nuclear matter at high densities. To emphasize the collective nuclear effects expected at high densities over the chaotic thermal effects, charged-particle exclusive event analyses using global variables are underway.[10] Another approach is the study of penetrating particles[11] such as K's and Λ's, which are expected to be produced in the early compression stage of the reaction process and rarely absorbed due to strangeness conservation. A third approach, to be used in the following discussion, is the study of pion multiplicities. The interplay between nuclear matter density and pion production was first pointed out by

[1]Instituto de Fisica, UNAM, Mexico City, 21 D.F., Mexico
[2]Cyclotron Institute, Texas A&M University, College Station, Texas 77843.

Chapline et al.[12] in 1973. The sensitivity of pion production to the compressibility of nuclear matter was later calculated explicitly using hydrodynamics by Stöcker et al.[13] and is shown in Fig. 2a. The existence of density isomers would have drastic effects on the pion production as shown in Fig. 2b.

Two effects combine to make pion production over the Bevalac energy range particularly appealing for the study of the high-density stage of the collision process. The elementary pion production cross section increases rapidly as a function of the available energy, and the relative nucleon-nucleon kinetic energy is rapidly degraded in a central nucleus-nucleus collision. As a result, the pion production is heavily weighted towards the compression stage of the reaction. Furthermore, pion multiplicities should be less sensitive to chaotic thermal effects than differential observables. These concepts are supported by the results of cascade calculations[14] shown in Fig. 3. The density increases rapidly as a function of time during the collision process. At the time of maximum density approximately half the baryon-baryon collisions have occurred and the number of pions + deltas reaches a maximum. From this time onward the density decreases, similar to the predictions of hydrodynamical models, and the pion + delta particle number remains constant until there are no longer interactions. A constant pion + delta yield results from a balance of pion- and delta-producing and absorbing reactions. Thus, the eventual pion multiplicity observed after decay of the remaining deltas is established at the time of maximum density and remains relatively constant thereafter, in contrast to differential features which may be altered during expansion.

The present approach[15] is to study the pion multiplicities at various incident energies, which correspond to differing degrees of compression, and compare them to predictions of various models to gain some information on the response of nuclear matter as a function of density. The pion production in hydrodynamical models is very sensitive to the assumptions under which the pions are created. In such models particles are created by incorporating chemical potentials at a predetermined freeze-out density ρ_f. The pion multiplicities are sensitive to the choice of ρ_f. In fact, one would intuitively expect the pions to be produced throughout the nucleus-nucleus collision as in the above cascade model approach and that the freeze-out description is insufficient. The present approach will be to compare data to predictions of the cascade model, which neglects effects of the nuclear medium such as compression and other potential degrees of freedom, and attribute any systematic differences between data and cascade to these effects. Predictions of other models will also be compared to data.

The intranuclear cascade model of Cugnon et al.[8] is a microscopic model of nucleus-nucleus collisions and has been described extensively in the literature. Pion production and absorption are assumed to occur through the delta resonance, i.e., $NN \leftrightarrow \Delta N$ and $\Delta \leftrightarrow \pi N$. This particular model was chosen for use since it contains recent πN and NN cross sections, has no free parameters, and has input data in good agreement with pp, pn, and πp data recently accumulated[16] in the Bevalac energy range.

The experiments[17] were performed by the GSI-LBL Streamer Chamber Collaboration at the Bevalac. A systematic study was made of negative pion

production and the accompanying nuclear disintegration in the interaction of ^{40}Ar + KCl at incident energies 360, 566, 772, 977, 1180, 1385, 1609, and 1808 MeV/u. A total of 4,000 to 10,000 events were accumulated at each energy in both minimum bias and central trigger modes. Each event was categorized by negative-pion multiplicity ($n_{\pi-}$), total charged-particle multiplicity (n_{tot}), and number of charged particles observed in the projectile and target fragmentation regions (n_{spec}). The approximate number of proton participants (n_{part}) in the collision was deduced for each event by subtracting from n_{tot} the number of created charges ($2n_{\pi-}$) and n_{spec}, i.e., $n_{part} = n_{tot} - n_{spec} - 2n_{\pi-}$. The central trigger corresponds to a reaction cross section of 180 ± 20 mb or impact parameters $b < b_{max}$ in a geometrical model with b_{max} = 2.4 fm for ^{40}Ar + KCl. Plotted in Fig. 4 is the observed n_{part} distribution for ^{40}Ar + KCl at 1.8 GeV/u compared to results of a cascade calculation at the same value of impact parameter cutoff as derived from the trigger cross section. This comparison is typical of results at other energies of this study.

The negative pion multiplicities $\langle n_\pi \rangle$ observed in the experiment are displayed in Fig. 5 as a function of incident energy for the ^{40}Ar + KCl system. The $\langle n_\pi \rangle$ increases rather linearly with incident energy, and there are no sharp deviations as predicted in Fig. 2b if density isomers were present. The cascade model prediction for $\langle n_\pi \rangle$ over the impact parameter range $0 < b < 2.4$ fm corresponding to the central trigger of the experiment is also plotted in Fig. 5. It is systematically higher than the experimental $\langle n_\pi \rangle$ by factors ranging from 4.0 at 360 MeV/u to 1.35 at 1808 MeV/u. This overestimate of $\langle n_\pi \rangle$ is also present for other systems studied at similar energies in the streamer chamber: 1.41 for He + KCl (977 MeV/u), 2.09 for Ar + KCl (772 MeV/u), and 2.43 for Ar + BaI_2 (772 MeV/u). For comparison, using the p + ^{48}Ti (730 Mev) data of Cochran et al.,[18] the $\langle n_\pi \rangle$ cascade data ratio is 1.2 ± 0.2. The discrepancy between the cascade values of $\langle n_\pi \rangle$ and those observed in the experiment increases rather dramatically with the mass of the colliding system. A closer look at the cascade results shows that the baryon density increases to values of 1.9, 3.0, and 3.4 for the He + KCl, Ar + KCl, and Ar + BaI_2 systems, respectively, and that the overestimate factor for $\langle n_\pi \rangle$ is directly proportional to the density. This concept of density increase or compression is not present in proton-nucleus and pion-nucleus collisions where cascade models have been found to work quite well[19] in describing pion production and absorption. If the overestimate in $\langle n_\pi \rangle$ is indeed related to the density a systemataic analysis of the response of nuclear matter under compression can be undertaken.

The internal energy per nucleon can be written as

$$E(\rho,T) = E_0 + E_c(\rho) + E_t(\rho,T) \tag{1}$$

where E_0 is the ground state energy, $E_c(\rho)$ is the compressional energy, and $E_t(\rho,T)$ is the thermal energy at a given temperature T and density ρ. However, in the cascade model there is no compressional energy and $E(\rho,T)$ is

$$E(\rho,T) = E_0 + E_t(\rho,T) \qquad \text{(cascade)} \quad . \tag{2}$$

Thus, at a given internal energy per nucleon the cascade model will have an excess amount of thermal energy due to lack of compressional energy. This excess thermal energy results in an overprediction of the number of pions $\langle n_\pi \rangle$ at a given energy per nucleon as pointed out in Fig. 5. In fact, the same value of $\langle n_\pi \rangle$ is observed in the data at an energy E as predicted by the cascade at a lower energy E'. Quantitatively, this difference in cm energy E - E' can be interpreted as the compressional energy assuming the same amount of thermal and ground state energies are included in the cascade and data to produce equal numbers of pions. Clearly, this is only a first approximation. It is presently impossible to disentangle the compressional energy from other effects of the nuclear medium. However, these nuclear medium effects are indeed those which must be understood in ultimately determining the response of nuclear matter at high densities.

Before studying the compressional energy as a function of density, a closer look at the nuclear matter densities predicted by the cascade model is necessary. The density in the cascade approach is derived simply by counting the number of nucleons in a sphere centered in the participant cm system after transforming all nucleons to this cm frame. The size of the sphere cannot be so large that it extends into regions outside the colliding nuclei. On the other hand, it must be large enough so the density is not dominated by fluctuations due to the small number of nucleons inside the sphere. The density as a function of time during the collision, shown in Fig. 3a for 977 MeV/u Ar + KCl, was determined from a sphere of diameter 3.0 fm. A density $\rho = 4\rho_0$ corresponds to 10 nucleons within such a sphere. Smaller sphere sizes become dominated by fluctuations, thus the choice of 3.0 fm diameter for the sampling sphere of Ar + KCl. Displayed in Fig. 6 is the so-determined maximum density as a function of incident energy for Ar + KCl central collisions. Also shown is the mean density weighted by the $\pi + \Delta$ production rate. Although somewhat lower, it reflects the maximum density and will be used in the subsequent pion-related analysis. Both densities increase with incident energy up to approximately 1.2 GeV/u where the densities saturate. The cascade has reached the onset of nuclear transparency where the number of collisions is no longer sufficient to randomize the initial longitudinal motion. Furthermore, excitation to higher resonances above the $\Delta(1232)$ becomes important at these higher energies[20] and their inclusion into the cascade would decrease the transparency. For heavier systems this transparency should occur at even higher energies.

The compressional energy per nucleon $E_c = E - E'$ may now be read from Fig. 5 and plotted against the mean density observed in Fig. 6 at the corresponding energy E. The resulting plot of the nuclear matter equation of state is shown in Fig. 7. Values of E_c - 10 MeV are plotted to account for the ground state binding energy of mass 40 nuclei (E_0 = 10 MeV in eq. 1), which is not present in the Cugnon cascade (E_0 = 0 in eq. 2). The dashed lines are parabolae representing equations of state without phase transitions for compressibility constants K = 200 and 250 MeV. The best fit to the data occurs with K = 240 MeV, a rather "stiff" equation of state. Note that above 1.2 GeV/u incident energy the values of E_c are constant as is the case for the densities in Fig. 6. In addition, analysis of the 772 MeV/u $^{40}Ar + BaI_2$ system yields a point in Fig. 7 in good agreement with those of the Ar + KCl system.

The $^{139}La + ^{139}La$ system was recently studied at 950 MeV/u in the streamer chamber using a central trigger corresponding to a reaction cross section of 358±40mb or $b \leq 3.4$ fm in a geometrical model. As expected, the charged-particle multiplicities ($\langle n_{tot} \rangle = 97 \pm 11$) are much higher than for the lighter systems studied previously. Negative pions are significantly easier to detect than the more abundant positively charged particles due to their opposite curvature. The mean negative pion multiplicity $\langle n_{\pi^-} \rangle = 7.2 \pm 0.6$ is shown in Fig. 8 along with the Ar + KCl points from Fig. 5. Results of the cascade model for La + La with $b \leq 3.4$ fm are also shown in Fig. 8. The cascade overpredicts the $\langle n_{\pi^-} \rangle$ by a factor of 2.8 at 950 MeV/u.

An identical procedure to that used for the Ar + KCl system may be undertaken to derive an additional point for La + La on the equation of state plotted in Fig. 7. Displayed in Fig. 9 are a) the maximum baryon density and b) numbers of pions and delta-particles as a function of time in 1.0 GeV/u $^{139}La + ^{139}La$ collisions with impact parameters $b \leq 3.4$ fm. The mean baryon densities are slightly higher for $^{139}La + ^{139}La$ ($\langle \rho_\omega \rangle = 3.8 \pm 0.2\ \rho_0$) than for Ar + KCl ($\langle \rho_\omega \rangle = 3.4 \pm 0.2\ \rho_0$) at 1.0 GeV/u. Like the Ar + KCl system for $b \leq 2.4$ fm the number of pions + delta-particles ($n_{\pi+\Delta}$) in the $^{139}La + ^{139}La$ system for $b \leq 3.4$ fm reaches a peak at the time of maximum density. However, in $^{139}La + ^{139}La$ the $n_{\pi+\Delta}$ decreases by 15% from this time until the end of the collision. This difference between the $n_{\pi+\Delta}$ plateau in Ar + KCl and the slight decrease in $n_{\pi+\Delta}$ for $^{139}La + ^{139}La$ may be attributed to an interplay of two effects: 1) increased pion-absorption in the factor 3.5 larger volume for $^{139}La + ^{139}La$ and 2) increased stopping power of $^{139}La + ^{139}La$ reducing pion production in the later stages of the collision. Thus, in the later stages of $^{139}La + ^{139}La$ collisions a slight increase in pion-absorbing processes and/or decrease in pion-producing processes primarily due to the larger volume will tilt the balance present in the Ar + KCl system. Nevertheless, the total pion multiplicity n_π in $^{139}La + ^{139}La$ reflects the high-density stage of the collision since both n_π and ρ_{max} increase with incident energy and the decrease in $n_{\pi+\Delta}$ is small and present at each calculated energy. The compressional energy per nucleon at 950 MeV/u taken from Fig. 9 is $E_c = E - E' = 106$ MeV/u. Plotting $E_c - E_0$ (10 MeV/u) = 96 MeV/u versus the mean baryon density $\rho_\omega = 3.82\ \rho_0$ at 950 MeV/u, an additional point is added to an expanded Fig. 7 and displayed in Fig. 10. This point for $^{139}La + ^{139}La$ agrees reasonably well with the previous data for Ar + KCl and Ar + BaI_2.

A comparison of the observed Ar + KCl pion multiplicities to predictions of various models strongly supports the concept that the pion multiplicity reflects the high-density stage of relativistic nucleus-nucleus collisions. Displayed in Fig. 11 are the data[17] along with predictions of the fireball,[21] cascade,[8] hadrochemical,[22] and hydrodynamical[23] models. The fireball model like the cascade, which was discussed previously, contains only a thermal energy component (as in eq. 2) and drastically overpredicts the multiplicity by a factor of ~3. The hadrochemical model, which solves the characteristic equations of hydrodynamics, uses an ideal gas equation of state. Since this is analogous to a Boltzman approach, the hadrochemical model predictions should be similar to those of the cascade. However, the initial assumption of a complete overlap of the two nuclei with density

$\rho = 2\rho_0$ and subsequent radial explosion are probably unrealistic. The reduction of energy available for pion production into collective flow in the hadrochemical model reduces the predicted pion multiplicities from an expected result similar to the cascade prediction down to the values shown in Fig. 11. The hydrodynamical model, on the other hand, inherently incorporates compression by using an equation of state and generally underpredicts the pion multiplicities unless some form of viscosity is added to increase the thermal energy available for pion production.[9] In other words, the basic zero mean free path assumption of hydrodynamics results in too much compressional energy (in eq. 1) and subsequent collective flow and thus necessitates the addition of viscosity to increase the thermal energy available for pion production. The hydrodynamical curve in Fig. 11 is a calculation after adjusting the viscosity. The dependence of the pion production on the freeze-out density in the present hydrodynamical models was discussed earlier in this paper. Comparison of these predictions with the observed pion multiplicities suggests the existence of compression and the importance of the interplay between the compressional and thermal degrees of freedom.

It has been suggested[24] that the compressional effects reflected in the pion multiplicities can be explained in terms of multi-nucleon pion absorption. This idea is based primarily on a suggestion[25] that 100-200 MeV pions impinging on a nucleus are absorbed on 3-5 nucleons. However, subsequent comparison between pion- and photon-absorption[26] on nuclei yields similar spectra suggesting the two absorption mechanisms are the same (i.e., Δ production) rather than multinucleon absorption. Furthermore, the pion multiplicity data tend to rule this out along with the possibility of an onset of such "exotic" pion absorption mechanisms at higher densities. The cascade model removes pions by the $\pi NN \rightarrow \Delta N \rightarrow NN$ two-step process. The rate of this process should be linear in the nuclear density due to the independence of the two steps. For multinucleon pion absorption the pion would interact simultaneously with n correlated nucleons and the density dependence of this process would be steeper $\sim\rho^n$. This "exotic" multinucleon pion absorption would be enhanced at higher densities. As observed in Table I, this explanation cannot serve as an explanation of these observations. For a given system (^{40}Ar + KCl) the overestimate of the pion multiplicity by the cascade decreases with increasing density. If "exotic" multinucleon pion-absorption were present, the largest discrepancies should be seen at the highest energies for a given system. It is just the opposite.

In summary, evidence has been presented that supports the idea that the pion multiplicity $\langle n_{\pi^-}\rangle$ reflects the maximum density attained in central relativistic nucleus-nucleus collisions. A comparison of the $\langle n_{\pi^-}\rangle$ data with predictions of vastly different models (hadrochemical, hydrodynamical, fireball, and cascade) suggests the presence of high-density nuclear matter. A systematic discrepancy between the observed $\langle n_{\pi^-}\rangle$ and those predicted in the cascade model correlates with the predicted density increase (as seen in Table I for various systems at similar energies) and anticorrelates with incident energy (as in Table I for one system at different energies). This latter observation argues against "exotic" multinucleon pion absorption. Removing energy from the pion-producing degrees of freedom at high densities

into potential degrees of freedom, excluded from the cascade model, explains these observations. Disregarding higher order corrections and simply associating this excess energy with the compressional energy, a parabolic nuclear matter equation of state is derived with a compressibility constant K = 240 MeV. Furthermore, the present analysis suggests that for ^{40}Ar + KCl collisions no more than one-third of the available cm energy can be associated with the compressional energy that would manifest itself as collective flow. However, the tremendous overestimate of the cascade model for the $\langle n_{\pi^-} \rangle$ of ^{139}La + ^{139}La results in approximately one-half of the cm energy going into compressional energy, neglecting other potential degrees of freedom. Thus the magnitude of the compressional energy may be approaching that of the chaotic thermal energy, and searches for collective effects may become feasible for heavier systems. Clearly, other explanations may be possible, but they are most likely related to changes in the dynamical behavior of nuclear matter at high densities (such as the possible quenching of Δ production in dense nuclear matter due to the size of the Δ wave function). Of course, such phenomena are not included in the cascade model. In fact, it may be necessary to develope a description in terms of a more fundamental quark model approach due to the high densities involved.

We thank M. Gyulassy and H. Stöcker for stimulating discussions and J. Brannigan for his assistance at the LBL Streamer Chamber. This work was supported in part by the Director, Office of Energy Research, Division of Nuclear Physics of the Office of High Energy and Nuclear Physics of the U.S. Department of Energy under Contract DE-AC03-76SF00098.

References

1. H.A. Bethe, et al., Nucl. Phys. A324 (1979) 487.
2. J.M. Irvine, Progress in Particle and Nuclear Physics, Vol. 2 (1979) p. 201, Pergamon Press.
3. A.B. Migdal, Rev. Mod. Phys. 50 (1978) 107 and references therein.
   V. Ruck, et al., Z. Phys. A277 (1976) 391.
   M. Gyulassy and W. Greiner, Ann. Phys. 109 (1977) 485.
4. M.W. Curtin, H. Toki, and D.K. Scott, MSU Preprint MSUCL-373 (1982).
   P. J. Siemens, Texas A M preprint (1983), submitted to Nature.
5. H. Stöcker, et al., Phys. Rev. Lett. 44 (1980) 725.
6. J.R. Nix and D. Strottman, Phys. Rev. C23 (1981) 2548.
7. Y. Yariv and Z. Fraenkel, Phys. Rev. C20 (1979) 2227 and C24 (1981) 488.
8. J. Cugnon, et al., Nucl. Phys. A352 (1981) 505 and A379 (1982) 553.
9. H. Stöcker, et al., Nucl. Phys. A387 (1982) 205c.
   M. Gyulassy, et al., Phys. Lett. 110B (1982) 185.
10. H. Ströbele, et al., Phys. Rev. C27 (1983) 1349.
    H.G. Ritter, et al., proceedings of this conference.
    A. Huie et al., Phys. Rev. C27 (1983) 439.
11. J.W. Harris, et al., Phys. Rev. Lett. 47 (1981) 229;
    S. Nagamiya, Proc. 5th High Energy Heavy Ion Study, LBL-12652 (1981) 144;
    A. Schor, et al., proceedings of this conference.
12. G.F. Chapline, M.H. Johnson, E. Teller, and M.S. Weiss, Phys. Rev. D8 (1973) 4302.
13. H. Stöcker, W. Greiner, and W. Sheid, Z. Phys. A286 (1978) 121.
14. Slightly modified version of code of J. Cugnon, et al., (see ref. 8).

15. R. Stock, et al., Phys. Rev. Lett. 49 (1982) 1236.
16. F. Shimizu, et al., University of Tokyo preprint (1982).
G. Alexander, et al., Nucl. Phys. B52 (1973) 221.
V. Flaminio, et al., CERN-HERA 70-03 (1979).
17. A. Sandoval, et al., Phys. Rev. Lett. 45 (1980) 874.
18. D.R.F. Cochran, et al., Phys. Rev. D6 (1972) 3085.
19. M. Sternheim and R. Silbar, Phys. Rev. D6 (1972) 3117;
Y. Yariv and Z. Fraenkel, to be published;
For pion absorption, results of the Cugnon code are in quantitative agreement with data of K. Nakai, et al., Phys. Rev. Lett. 44 (1980) 1446.
20. University of California Lawrence Radiation Laboratory report UCRL-20000 NN (1970).
21. S. Bohrmann and J. Knoll, Nucl. Phys. A356 (1981) 498.
22. I. Montvay and J. Zimanyi, Nucl. Phys. A316 (1979) 490.
23. H. Stöcker, et al., Phys. Lett. 81B (1979) 303.
24. R. Malfliet and B. Schurmann, KVI preprint KVI-418 (1982).
25. R.D. McKeown, et al., Phys. Rev. Lett. 44 (1980) 1033.
26. R.D. McKeown, et al., Phys. Rev. Lett. 45 (1980) 2015.

TABLE I. The overestimate of $\langle n_{\pi^-} \rangle$ in the cascade model versus the data is tabulated as a function of incident energy and the colliding system. The mean density calculated in the cascade model is listed in parentheses. (*the incident energy for $^{139}La + ^{139}La$ was 950 MeV/u).

energy (MeV/u)	system			
	$^{4}He + KCl$	$^{40}Ar + KCl$	$^{40}Ar + BaI_2$	$^{139}La + ^{139}La$
360		4.50 (2.6 ρ_0)		
556		2.50 (2.8 ρ_0)		
772		2.09 (3.0 ρ_0)	2.43 (3.4 ρ_0)	
977	1.41 (1.9 ρ_0)	1.85 (3.4 ρ_0)		2.76 (3.8 ρ_0)*
1180		1.53 (3.5 ρ_0)		
1385		1.46 (3.4 ρ_0)		
1609		1.31 (3.4 ρ_0)		
1808		1.31 (3.4 ρ_0)		

Figures

Fig. 1. Results of a hydrodynamical calculation[5] for the compression and expansion of matter for incident energies E_{lab} = 0.2, 0.4, and 0.8 GeV/u. Shaded areas represent the temperature increase due to viscosity. Two different equations of state, solid curve ($\sim\rho$) and dashed curve ($\sim\rho^2$), are displayed.

Fig. 2. Mean pion multiplicity $\langle n_\pi \rangle$ per nucleon plotted versus incident energy as predicted by the hydrodynamical model of ref. 13. a) Results of a soft (K_0 = 100 MeV) and a stiff (K_0 = 300 MeV) nuclear equation of state are shown. b) Results of a calculation with a density isomer in the equation of state. Curve a is the normal nuclear matter curve (K_0 = 300 MeV) and curves b and c have secondary minima in the equation of state at $\rho = 5\rho_0$ with binding energies B_1 = 0 and -140 MeV, respectively, as depicted in the insert.

Fig. 3. Results of a cascade model calculation for central collisions ($b \leq 2.4$ fm) of ^{40}Ar + KCl at 977 MeV/u. Plotted as a function of time during the collision are the a) baryon densities in units of ρ_0, b) cumulative number of baryon-baryon collisions, and c) numbers of pions and delta-particles.

Fig. 4. Distribution of the number of proton participants as derived in the text for central collisions of ^{40}Ar + KCl at 1.8 GeV/u. The curve is the result of the cascade prediction for central collisions with $b \leq 2.4$ fm.

Fig. 5. The mean negative pion multiplicity (triangles) as a function of incident energy for central collisions of ^{40}Ar + KCl. Open circles represent the results of cascade calculations. The vertical lines for $E_{lab} \geq 1.4$ GeV/u represent estimates of the uncertainty of the calculation due to multiple pion production from single NN collisions, which are not included in the calculations. Horizontal arrows are values of $E_c = E - E'$, the compressional energy per nucleon, determined at each experimental point (see text).

Fig. 6. Maximum density as a function of the incident energy predicted by the cascade model for ^{40}Ar + KCl. The circles represent the mean density, which is the maximum density weighted by the rate of pion plus delta production, which is the derivative of the top curve of Fig. 3c.

Fig. 7. Values of E_c plotted as a function of the mean baryon density. Points determined at 1.6 and 1.8 GeV/u are identical to that at 1.4 GeV/u and are not shown. The dashed curves represent parabolic equations of state with compressibility constants K = 200 and 250 MeV.

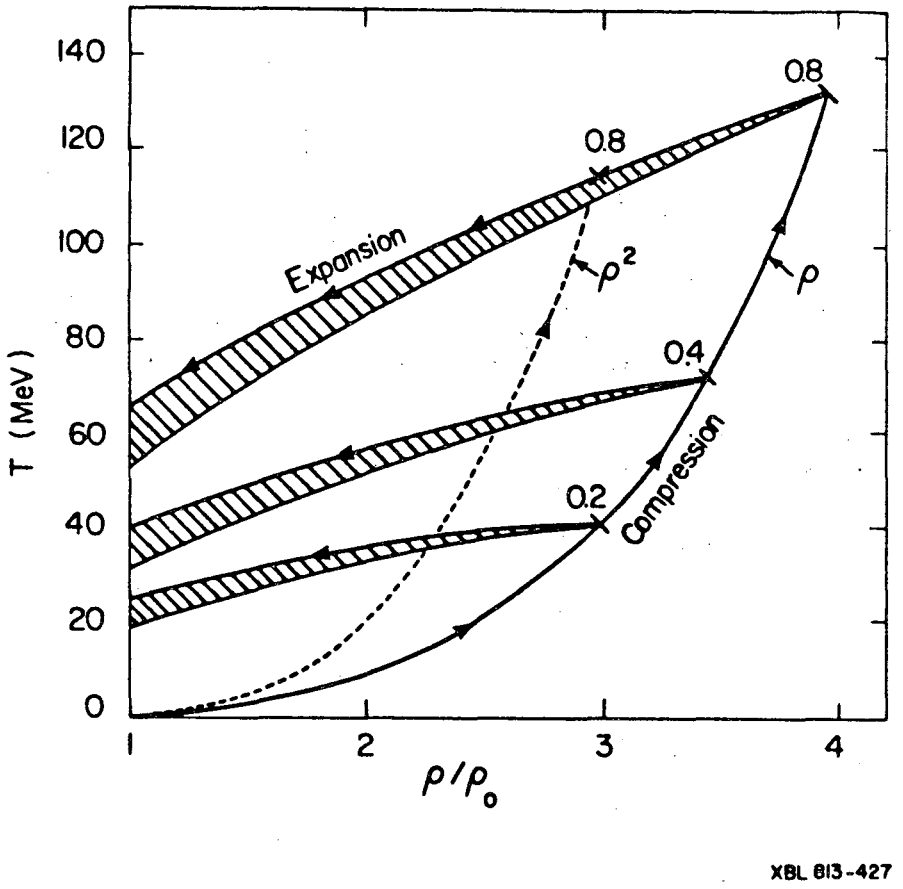
T (MeV)
140
120
100
80
60
40
20
0
1
2
3
4
ρ/ρ₀
0.8
0.8
0.4
0.2
Expansion
Compression
ρ²
ρ
XBL 813-427

Fig. 1.

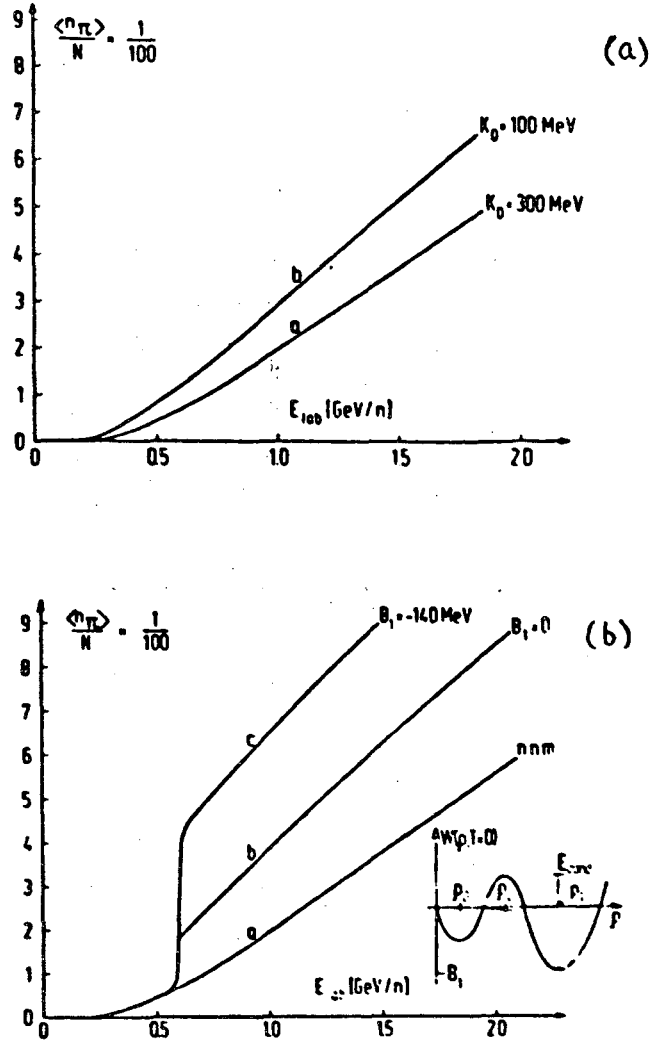
(a)
⟨nπ⟩/N = 1/100
K₀ = 100 MeV
K₀ = 300 MeV
b
a
E_lab [GeV/n]
0
0.5
1.0
1.5
2.0
(b)
⟨nπ⟩/N = 1/100
B₁ = -140 MeV
B₁ = 0
nnm
c
b
a
E_lab [GeV/n]
AW(ρ,T=0)
B₁

Fig. 2.

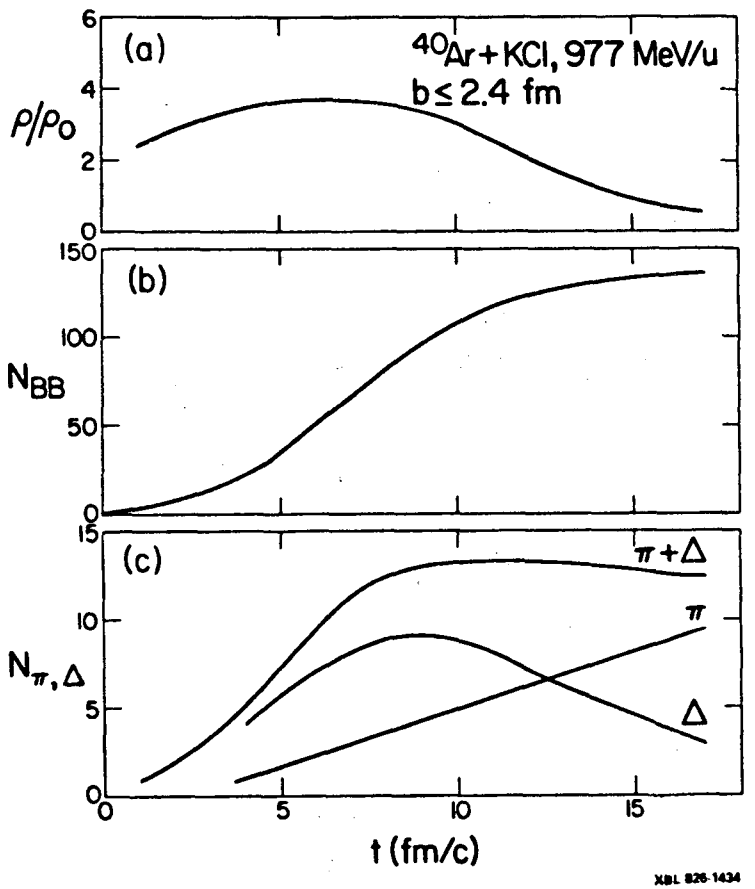
(a)
^{40}Ar+KCl, 977 MeV/u
b≤2.4 fm
ρ/ρ₀
(b)
N_BB
(c)
π+Δ
π
Δ
N_π,Δ
t (fm/c)
XBL 826-1434

Fig. 3.

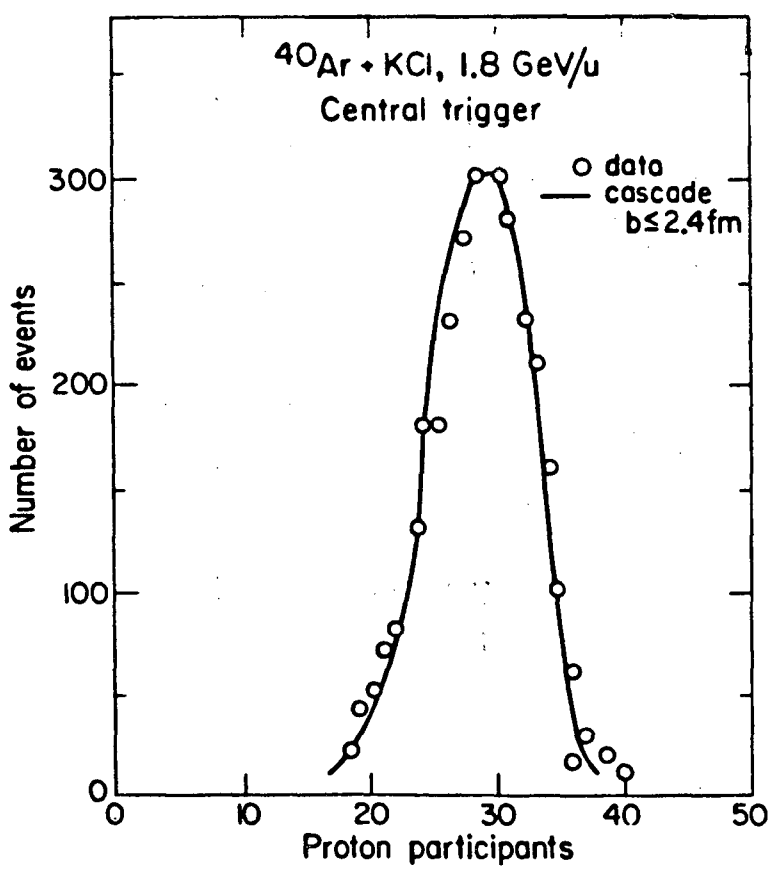
^{40}Ar + KCl, 1.8 GeV/u
Central trigger
data
cascade
b≤2.4fm
Number of events
Proton participants

Fig. 4.

Fig. 5.

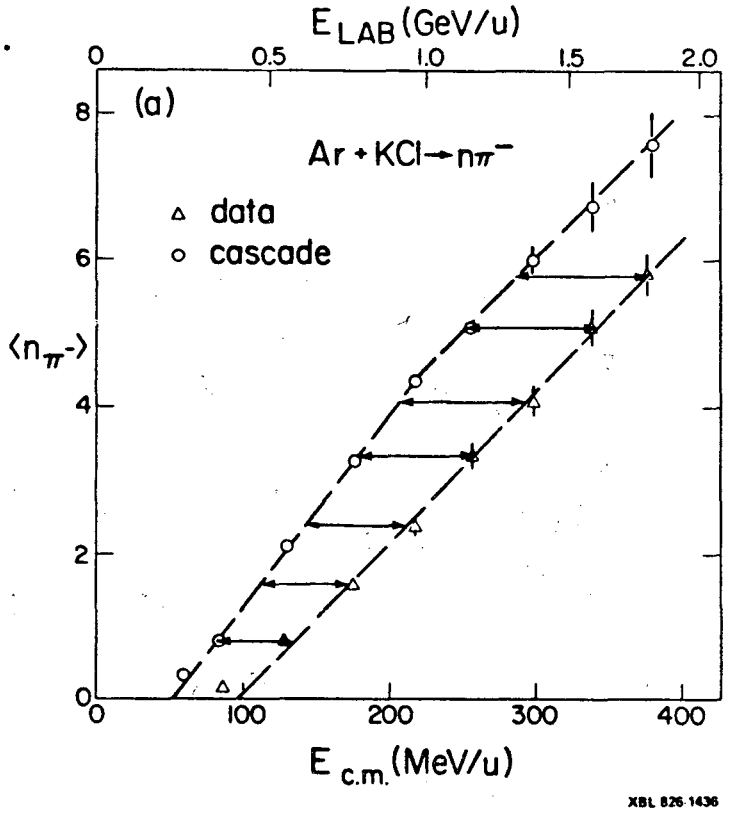

Fig. 6.

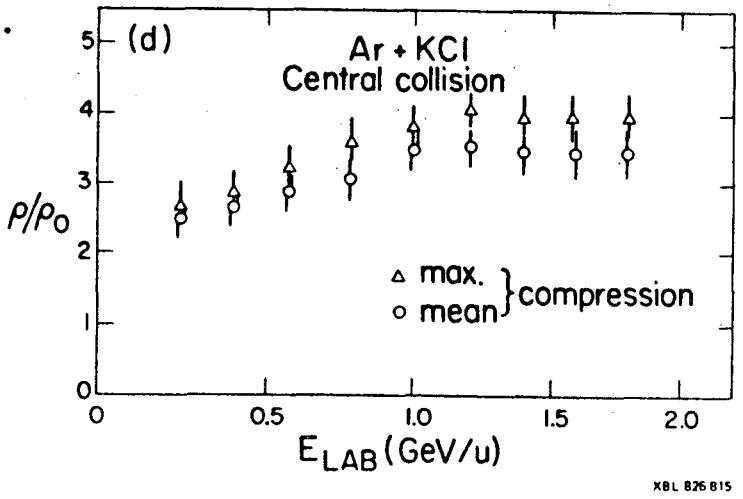

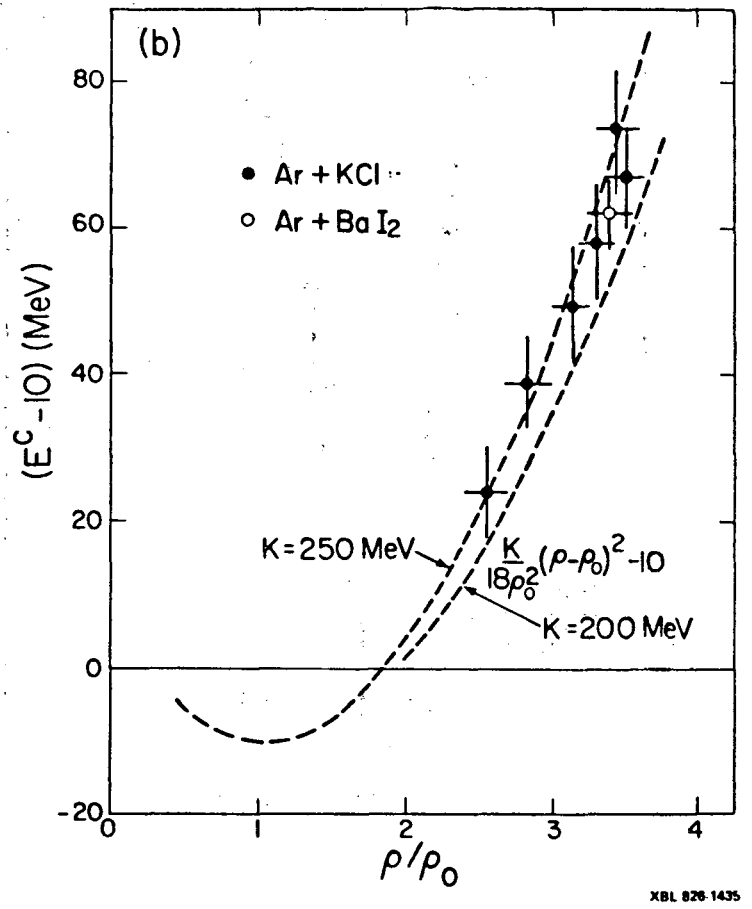

Fig. 7.

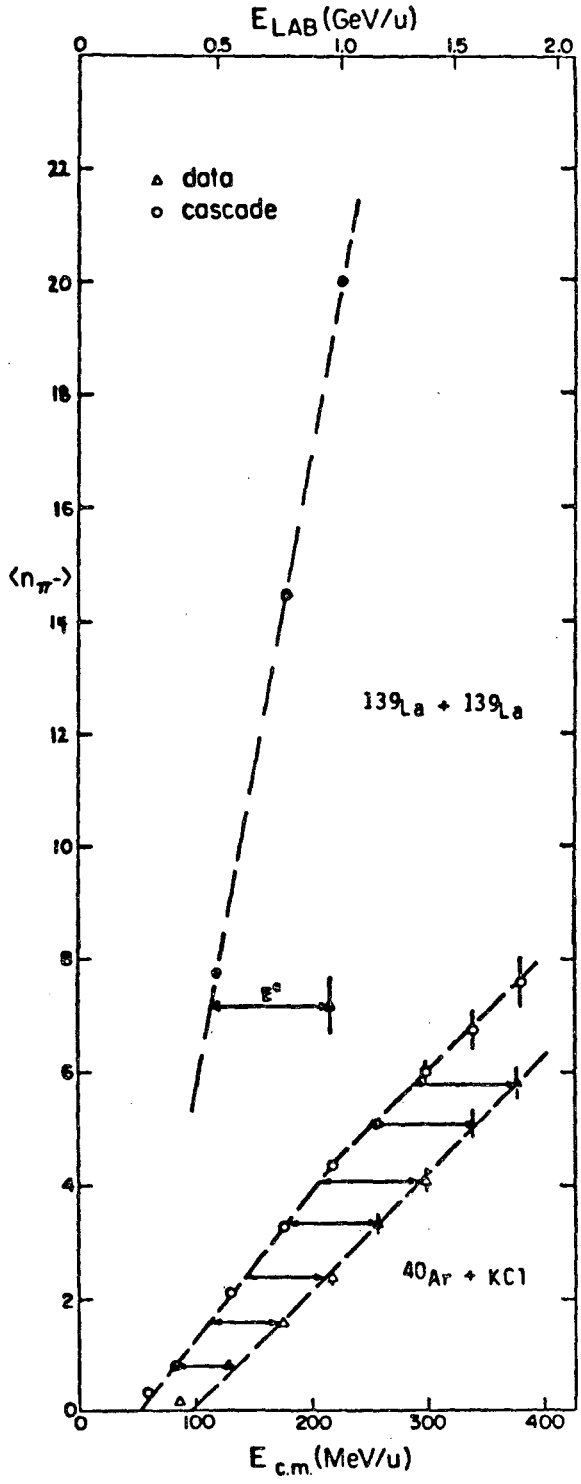
E_LAB (GeV/u)
0
0.5
1.0
1.5
2.0
data
cascade
⟨n_π-⟩
139La + 139La
40Ar + KCl
E_c.m. (MeV/u)
0
100
200
300
400

Fig. 8.

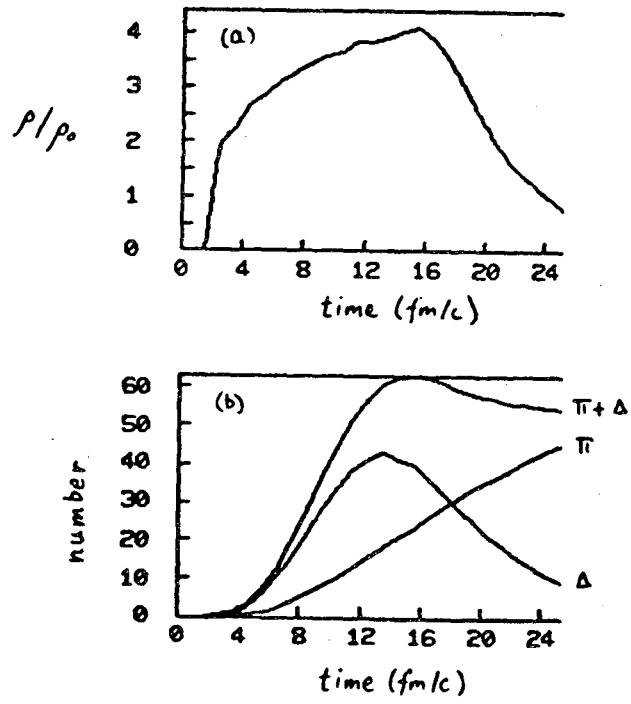
ρ/ρ₀
(a)
time (fm/c)
(b)
number
π + Δ
π
Δ
time (fm/c)

Fig. 9.

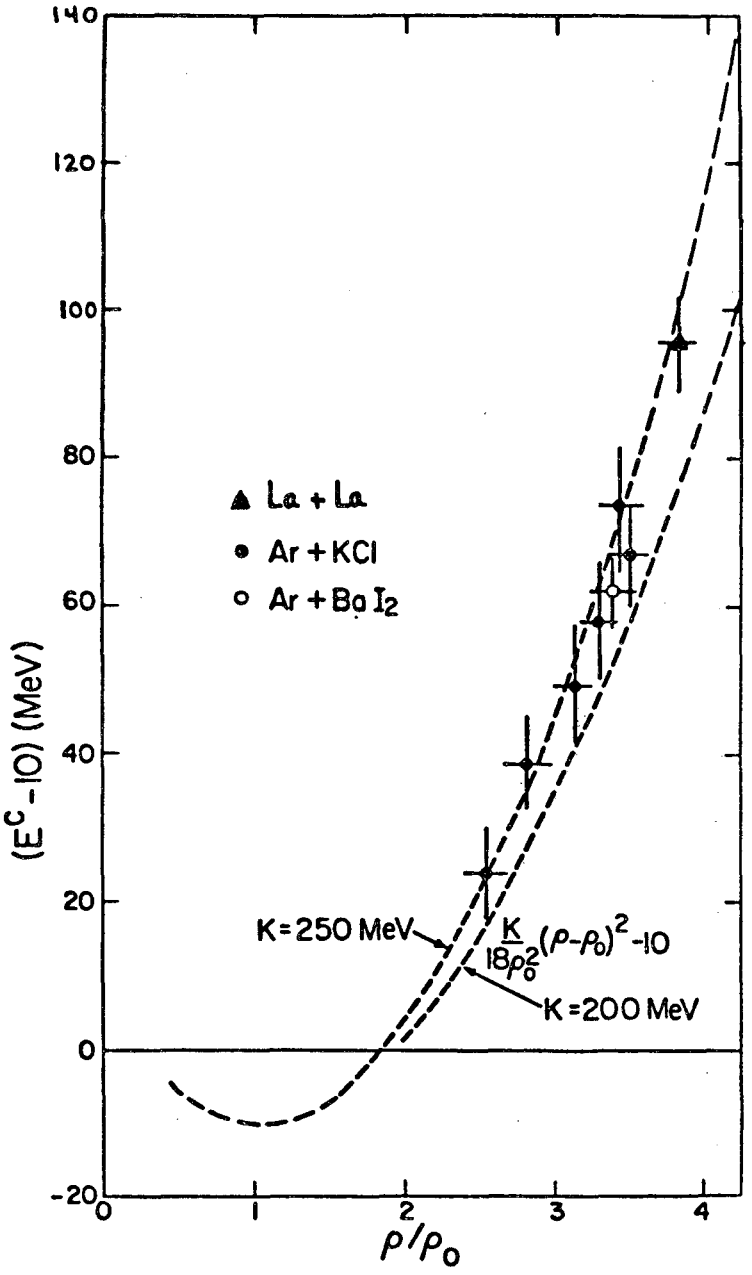
140
120
100
80
60
40
20
0
-20
0
1
2
3
4
(E^C-10) (MeV)
ρ/ρ_0
La + La
Ar + KCl
Ar + Ba I_2
K=250 MeV
$\frac{K}{18\rho_0^2}(\rho-\rho_0)^2-10$
K=200 MeV

Fig. 10.

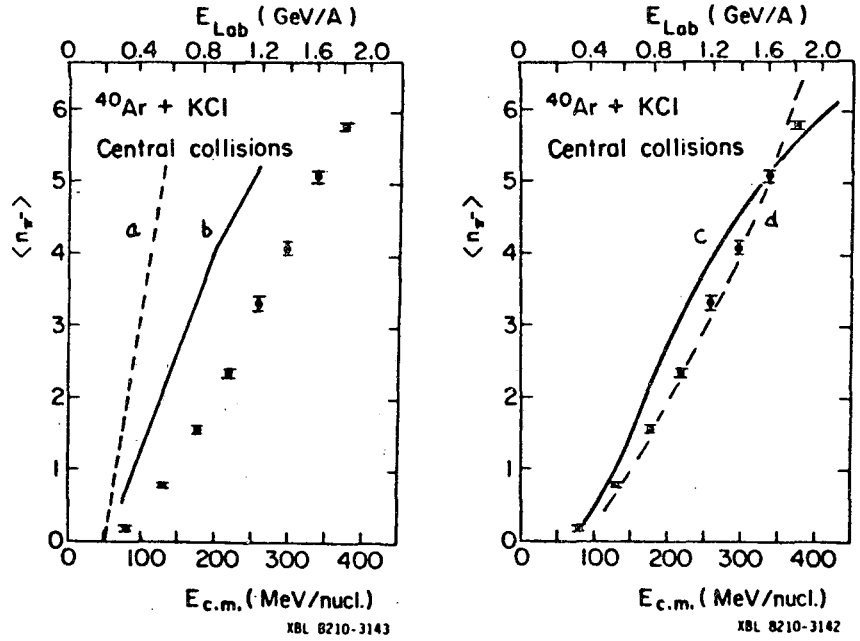
E_{Lab} (GeV/A)
0 0.4 0.8 1.2 1.6 2.0
^{40}Ar + KCl
Central collisions
a
b
c
d
$\langle n_\pi^- \rangle$
0 1 2 3 4 5 6
0 100 200 300 400
$E_{c.m.}$ (MeV/nucl.)
XBL 8210-3143
XBL 8210-3142

Fig. 11.

Collective Effects in Subthreshold Pion Production

Eckart Grosse
GSI Darmstadt

Talk given at the VI. High Energy Heavy Summer Ion Study
and II. Workshop on Anomalons, Berkeley 1983

Introduction

One of the main aims in the field of nucleus-nucleus collisions at higher energies is the production and study of hot dense nuclear matter with properties very different from its ground state. A necessary condition for the production of such exotic nuclear matter is the fast transformation of most of the energy of the relative motion into internal energy of compression or heat; such a fast transformation requires the fast slowing down of the relative motion.

The production of mesons represents an ideal probe for the study of such violent nucleus-nucleus collisions since mesons are produced only by the participant parts of the colliding nuclei and thus originate solely from the internuclear collisions zone. This is in contrast to the observation of nucleons whose spectra also show components caused by the emission from the spectator portions of target and projectile. Pions are the mesons to be produced at the lowest projectile energies; below the production threshold for free N-N-collisions of 280 MeV/u they can still be created either through a single N-N-collision where the intrinsic Fermi motion provides an extra boost or alternatively through a cooperative production mechanism involving a collective interaction of all or at least a large portion of the nucleons from the two collision partners. From the observed production cross section and its dependence on target and projectile mass, on projectile energy and on pion energy and angle one can hope to identify the relevance of the suggested alternatives.

Experiments

Experiments on the production of pions from nucleus-nucleus collisions at intermediate projectile energies have been performed at different accelerators using magnetic spectrometers[1,2] and scintillation detector telescopes[3]; both techniques are similar in their rather low solid angle of around 10 msr; the first method can achieve an energy resolution of 0.5 to 3 MeV. The good energy resolution is needed for the spectroscopy of distinct nuclear states excited by the completely coherent pionic fusion process, which has been observed[4] recently with ^{3}He projectiles; but with heavy ions the expected small cross sections cannot be observed easily with such low solid angle instruments. For reaction mechanism studies through the more abundant statistically emitted pions acting as "probing particles" neutral pions are especially well suited, because they can escape from the collision zone undisturbed by the Coulomb field of the reaction fragments. Their decay into two high energy gamma rays allows their detection even for very low momenta; these long wavelength pions may probe a large volume of nuclear matter coherently without being influenced by strong differential absorption effects.

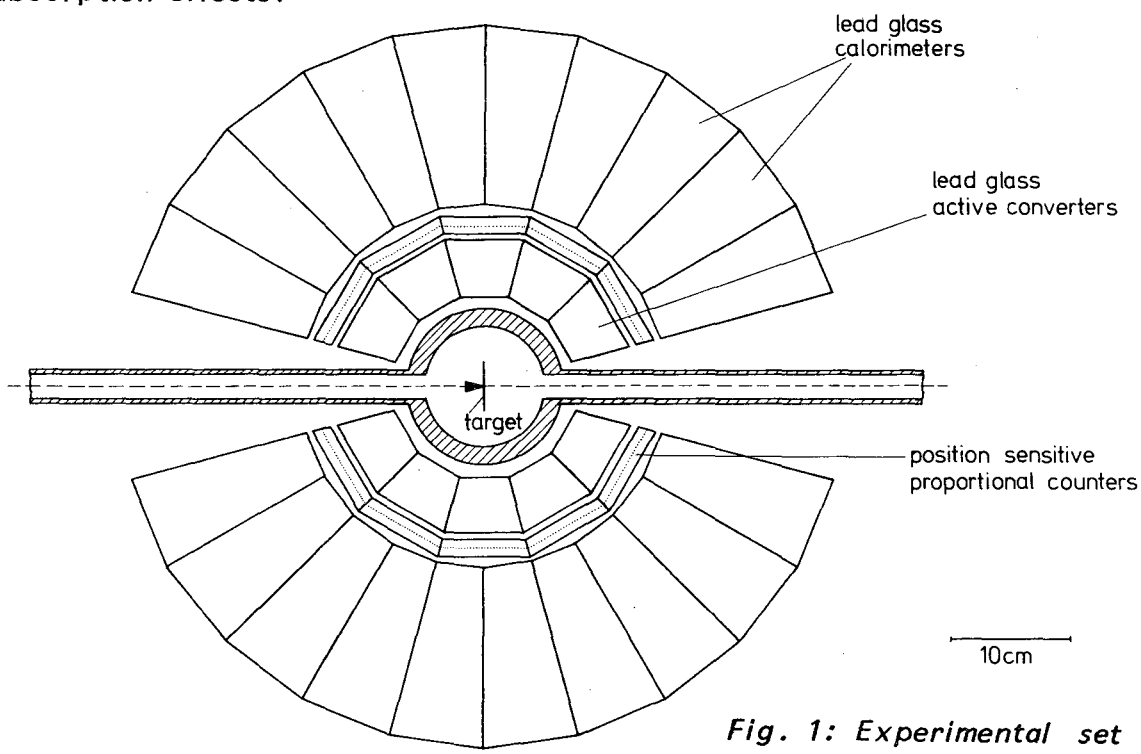

Fig. 1: Experimental set up for the detection of γ's and π^0's.

The production of π^0's in collisions of ^{12}C and ^{18}O projectiles of 60-84 MeV/u from the CERN synchrocyclotron and of ^{40}Ar ions of 44 MeV/u produced by GANIL was studied with targets ranging from C to U using a new lead glass spectrometer. This π^0-hodoscope developed on the basis of an instrument used previously[5] for lower energy pions is shown in Fig. 1. It consists of two concentric rings of lead glass Cherenkov detectors with position sensitive multiwire proportional chambers in between; they determine the position of the electrons and positrons produced in the inner ring, which thus acts as an active converter, whereas the outer, the calorimeter ring, measures their remaining energy.

The detection efficiency for γ's and π^0's was calculated by Monte Carlo techniques using the Electron Gamma Shower (EGS) code system[6]. The calculations[7] were adjusted with π^0's of very low energy from the $\pi^-(p,\pi^0)n$ reaction. For them the efficiency is around 3%, whereas in an intermediate energy range from 10 to 200 MeV it is around 1% nearly independent of π^0 angle. It should be pointed out that the instrument covers all pion emission angles; as an effect of the π^0 decay kinematics the detector elements missing along the beam line cause only a small disturbance. The rather high sensitivity of the set-up allowed experiments to be carried out for angle integrated π^0 production cross sections as low as 50 pb/MeV. The background - e.g. from cosmic rays - can be suppressed very effectively by requiring the two gamma rays to yield the proper invariant mass of the π^0 although the invariant mass resolution of the instrument is rather moderate ($\sim$45%) due to its moderate energy resolution.

Another source of background due to chance coincidences of an abundant low energy component in the singles gamma spectra (cf. Fig. 2) limited the instantaneous count rate which could safely be taken in some of the experiments. As can be seen from the figure, this non coincident radiation falls off much steeper to higher gamma ray energies than that part of the spectrum known from its coincidence properties to originate from the π^0 decay. This excess radiation, which is especially intense at and below 80 MeV, is identified with nucleus-nucleus bremsstrahlung; its intensity and exponential slope indicate - according to classical bremsstrahlung formulae[8] - a rather violent slowing down of the collision partners.

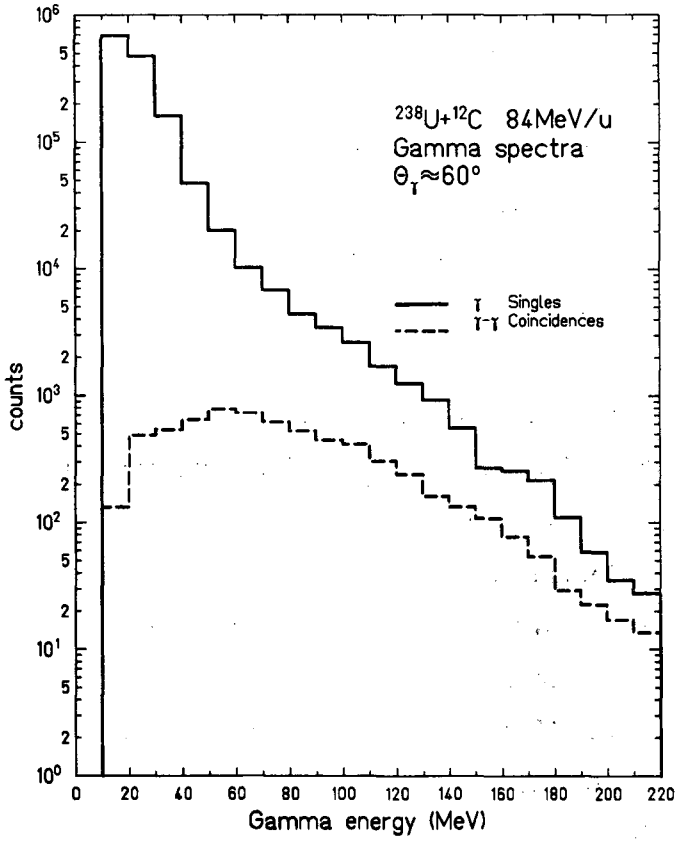

Fig. 2: Gamma ray spectra observed in single and coincidence mode from $^{12}C+^{238}U$ collisions at 84 MeV/u. 1 count corresponds to approximately 1 nb/MeV.

Analysis of the pion spectra

The π^0 spectra from the ^{12}C + ^{12}C collision at 84, 74 and 60 MeV/u - Lorentz transformed into the c.m. system - are shown in Fig. 3. The exponential fall off in the spectra suggests a description on the basis of a thermal emission process. Such a description has been discussed and applied to the charged pion emission studied at the two higher energies; this analysis is contained in a contribution[9] to this workshop. Since the neutral and charged pion data are in accord with each other, it is sufficient to repeat briefly the results of the respective analysis[9] of the neutral pion data, which - due to the highly efficient set-up as discussed above - have significantly better statistics. The analysis[9] allows the extraction of an average number of conjugate particles emitted together with the pion from the collision zone, whose temperature is obtained from the damping of the available kinetic energy assuming microcanonical equilibrium. Since it is not obvious how many nucleons from target and projectile participate in the equilibration process, the number which is actually determined[10] is the reduction factor in the number of degrees of freedom in the

final state relative to the case where all participating nucleons emerge as free particles. In other words, this factor determines the averaged atomic mass number of the fragment, associated with the emission of a pion. From the data taken at 84 MeV/u this number turns out to be 2.4, whereas at 60 MeV/u it is nearly 4. At the lower energy obviously more degrees of freedom are frozen, i.e. less and consequently larger fragments are emitted.

The above mentioned contributed paper[9] also contains an evaluation of the pion production yield expected from N-N-collisions when the Fermi momentum is taken into account. An exact prediction is difficult since: (1) the tails of the Fermi distribution are unknown; (2) the "elementary" cross section for NN→πNN is not well known at low pion momentum and unknown off the energy shell, i.e. inside a nucleus; (3) at low energies Pauli blocking effects are very large. In spite of these ambiguities it is obvious[9,10] that the contribution from N-N-collisions is very small and can be neglected in our spectra.

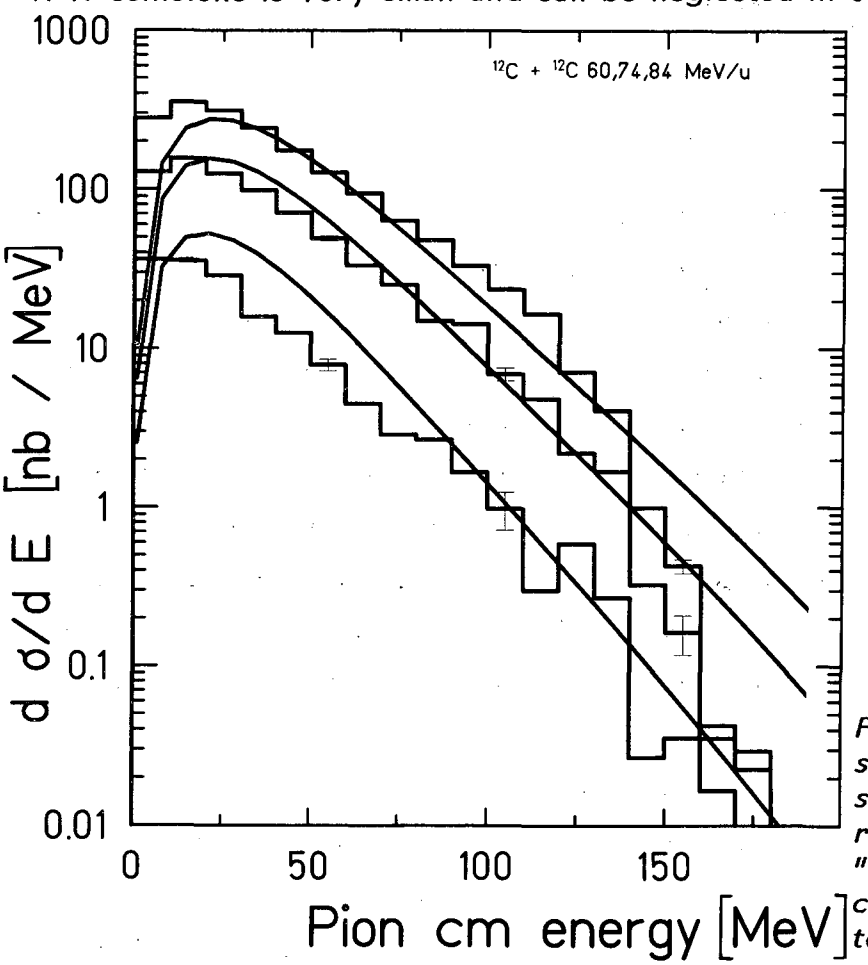

Fig. 3: Angle integrated π^0 spectra from $^{12}C+^{12}C$ collisions. The drawn lines represent the result of a "pionic" bremsstrahlung calculation as mentioned in the text.

The drawn lines in Fig. 3 are from another type of analysis which also yields spectra falling off exponentially. In this analysis[12] the pions, as Goldstone bosons of the strong interaction, are assumed to be produced from the slowing down of the strong field in the two colliding nuclei during the collision - analogous to the emission of γ-quanta in nucleus-nucleus electromagnetic bremsstrahlung. The data taken at different incident beam energies and with different nuclei can be described simultaneously by using as the only fit parameter the slowing down length (corresponding to a slowing down time which is inversely proportional to the initial relative velocity). A Fermi type time dependence of the velocity is assumed along a straight line trajectory and the Coulomb energy between the two partners is subtracted beforehand, since the deceleration caused by the long range Coulomb field is slow and does not contribute to the high Fourier components necessary to create pionic bremsstrahlung.

Pion angular distributions

In the center of mass system the angular distributions of the π^0's produced from ^{12}C + ^{12}C collisions are forward-backward symmetric around a minimum at

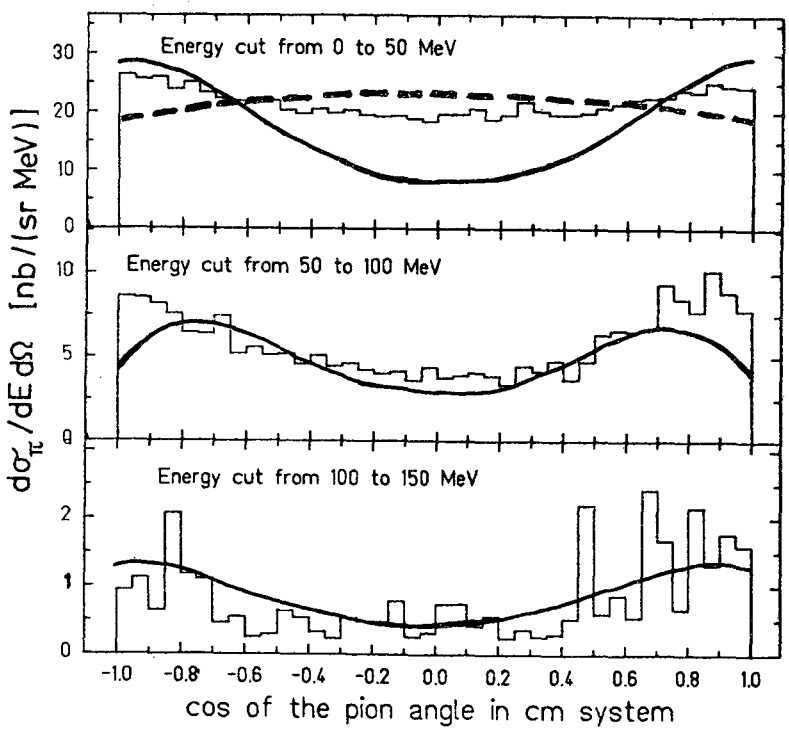

Fig. 4: Angular dependence of the π^0 production cross section from $^{12}C+^{12}C$ at 84 MeV/u, integrated over three spectral regions. For the lowest region there is a large distortion in the data which could explain the difference to the "pionic" bremsstrahlung calculation (drawn lines for coherent, dashed line for incoherent sum, renormalized).

90°; as can be seen from Fig. 4 the anisotropy increases with increasing pion energy. The fact that the cross section assumes a minimum at 90° indicates[12] a destructive interference of the pion intensity emitted from the target with that originating from the projectile. Such an interference pattern obviously requires a coherence between the two sources which, since we are dealing with the emission of bosons of axial vector character, implies a coherence of the nuclear spin directions. This is confirmed by comparing the experimental angular distributions to those calculated[12] coherently resp. incoherently (cf. Fig. 4).

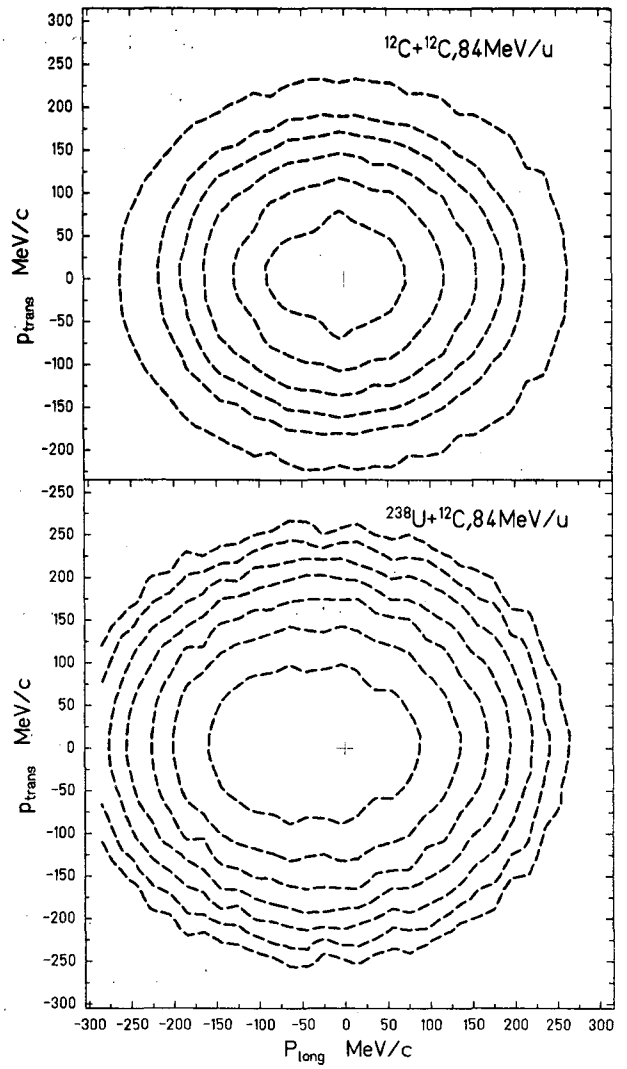

Fig. 5: Contour plot of the production cross section in the π^0 momentum space Lorentz transformed into the c.m. system for the $^{12}C+^{12}C$ system. The $^{12}C+^{238}U$ data are plotted in the same system to demonstrate how the center of the contours is shifted. The cross section rises by 42% between subsequent contours.

Requiring a forward-backward symmetry also for the asymmetric system $^{12}C + ^{238}U$ enables one to determine the mean velocity of the source emitting the pions. This is best seen in a contour plot of the cross section in the π^0 momentum space (i.e. versus its transversal and longitudinal momentum). The low momentum parts of the pion distributions from the two collision systems are shown in such a plot in Fig. 5. The center of the contours observed with

^{12}C on ^{238}U is shifted considerably as compared to ^{12}C on ^{12}C; this is characteristic for the emisson from a much slower source (nearly as slow as the compound nucleus system indicated by the cross of the dotted lines). This is a strong indication for a cooperative production of the π^0's from at least a big portion of the two nuclei acting as a whole. It is unlikely that the observed pattern can be explained by rescattering and absorption of pions emitted symmetrically from a source moving with the velocity of N-N collision systems; this is borne out from the large wavelength of the pions and the consequently large mean free path.

Target mass and projectile energy dependence

The total cross section for the production of π^0's from the bombardment of different targets with ^{12}C and ^{18}O beam of 84 MeV/u is plotted in Fig. 6 versus the target mass; it increases much more slowly than linearly with the mass. A linear dependence is expected for a collision of two clouds of free weakly interacting nucleons with Fermi motion, whereas a thermal pion production is expected to be proportional to the number of participant nucleons; the corresponding thin lines[13] also overpredict the cross section at large A considerably. The production by the two nuclei as a whole should be characterized by a proportionality to the product of the two nuclear surfaces $A_1^{2/3}*A_2^{2/3}$; the data seem to follow such a trend as given by the thick lines in Fig. 6.

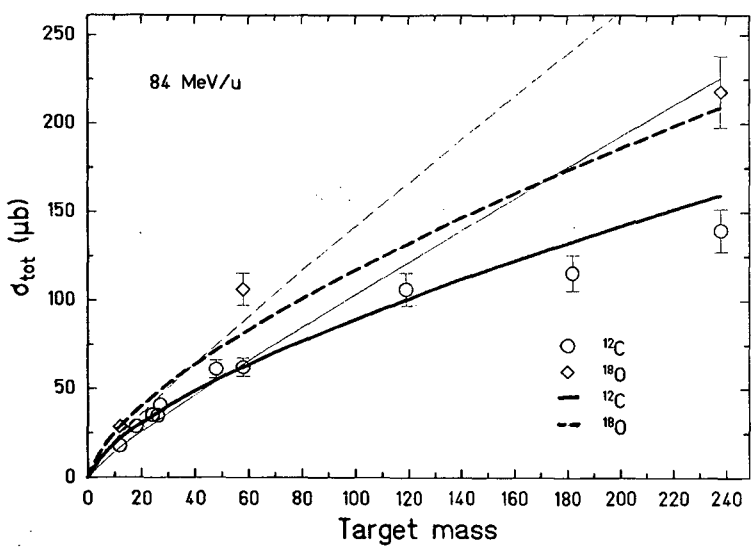

Fig. 6: Integrated cross section for ^{12}C and ^{18}O projectiles versus the target mass. The error bars indicate the relative uncertainties; in absolute scale there is an additional ambiguity of 25% (see text for meaning of lines).

The π^0 production cross section as shown in Fig. 7 rises very quickly with increasing beam energy. Our three data points for the ^{12}C + ^{12}C system at different projectile energies are reproduced quite well by the "pionic" bremsstrahlung calculation. It is very surprising that this calculation - using the same characteristic stopping length of 1 fm - also is in reasonable agreement with the measured production[14] yield from ^{40}Ar on ^{40}Ca at 44 MeV/u (after a renormalization to target and projectile mass using the semiempirical mass dependence shown in Fig. 6). (Even a data point obtained recently[15] by the Stony Brook - Oak Ridge - GSI collaboration with a similar set up at the ^{14}N beam of 35 MeV/u is in rough agreement to this calculation.) This remarkable consistency of the model and its parameters over a wide range of masses and energies gives strong support to the underlying picture. Unfortunately such pionic bremsstrahlung calculations are not yet available for nonidentical collision partners, where a large amount of data exists.

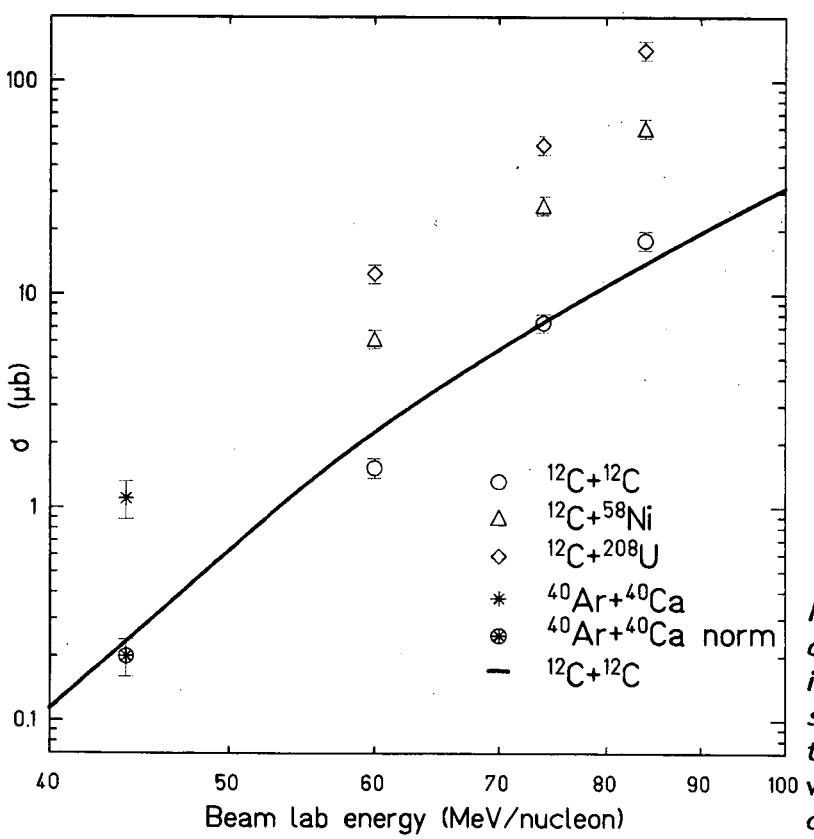

Fig. 7: Beam energy dependence of the total inclusive π^0 production cross section for ^{12}C projectiles; the data point for ^{40}Ar+^{40}Ca was also renormalized for comparison.

Conclusion

Concluding one can say that cooperative effects in the pion production from collisions of 60-84 MeV/u ^{12}C and ^{18}O projectiles as well as ^{40}Ar ions of 44 MeV/u with targets from A = 12 to A = 232 seem to be established. The picture[12] of a coherent bremsstrahlung like pion emission caused by a collective deceleration of the projectile (resp. an acceleration of the target) describes the data reasonably well. It is tested by also observing[10] electromagnetic bremsstrahlung, i.e. high energy gamma rays. Using the slowing down parameters from the analysis of the π^0 spectra one calculates electromagnetic bremsstrahlung[8] with an intensity of about the same order of magnitude as that part of the observed gamma spectra which is not originating from π^0 decay. This consistency indicates the possibility to perform a detailed study of the internuclear collision dynamics and especially the slowing down process by observing bremsstrahlung of the strong and electromagnetic interactions simultaneously. From the analysis of the pion production data available so far it appears that at energies around 60 MeV/u violent nucleus nucleus collisions are occuring in which a big portion of the kinetic energy is taken out of the relative motion through a fast slowing down process taking place within about 1 fm.

Acknowledgements

The work presented here was performed in a close and stimulating collaboration with H. Noll, who will submit his Ph.D. thesis on it to the University of Frankfurt; we gratefully acknowledge the intense support from our collegues C. Brendel and W. Rösch from TH Darmstadt, P. Braun-Munzinger from SUNY Stony Brook; and H. Dabrowski, H. Heckwolf, O. Klepper, C. Michel, W.F.J. Müller and H. Stelzer from GSI. For the experiments at GANIL the help of colleagues from CEN Saclay, the University of Caen and GANIL has been needed heavily and is acknowledged gratefully. Thanks are also due to G. Bertsch, J. Bondorf, W. Greiner, B. Jakobsson, J. Knoll, B. Müller, R. Shyam, R. Stock and D. Vasak for interesting discussions and for making their results available prior to publication.

References

1. W. Benenson et al., Phys.Rev.Lett. 43(1979)683
   J.P. Sullivan et al., Phys.Rev. 25C(1982)1499
2. E. Aslanides et al., Strasbourg report CRN/PN 82/16 , to be publ.
3. T. Johansson et al., Phys.Rev.Lett. 48(1982)732
   B. Jakobsson, Nordic Meeting on Nuclear Physics, Fuglso, August 1983
   J. Julien, 3rd International Conference on Nuclear Reaction Mechanisms, Varenna, June 1982
4. Y. Le Bornec et al., Phys.Rev.Lett. 47(1981)1870
5. M. Lebrun et al., Nucl.Instr.Meth. 166(1979)151
6. R.L. Ford and W.R. Nelson, The EGS Code System, SLAC Report 210
7. Ch. Michel, XXI. Meeting on Nuclear Physics, Bormio, January 1983
8. J.D. Jackson, Classical Electromagnetics, New York
9. R. Shyam and J. Knoll, contribution N° 41 to this workshop
10. E. Grosse, XI. International Workshop on Gross Properties of Nuclei, Hirschegg, January 1983
11. G. Bertsch, Phys.Rev. C15(1977)713
12. D. Vasak et al., Phys.Scripta 22(1980)25, Phys.Lett. 93B(1980)243 and to be published;
    W. Greiner, Conference on Heavy Ion Physics and Nuclear Physics, Catania, May 1983
13. J. Cugnon, J. Knoll and J. Randrup, Nucl.Phys. A360(1981)444
14. H. Heckwolf et al., GANIL experiment No. 19, to be published
15. P. Braun-Munzinger et al., MSU experiment, to be published

COINCIDENCE EXPERIMENTS BETWEEN PIONS ($\pi^{\pm}$) AND FORWARD CHARGED PARTICLES FROM INTERMEDIATE ENERGY HEAVY ION COLLISIONS

J. Julien, M. Boloré, X. Charlot, J-M. Hisleur, R. Legrain, G.S. Pappalardo[+], J. Poitou, Centre d'Etudes Nucléaires Saclay, DPh-N, France.

T. Johansson[++]
The Gustaf. Werner Inst. Uppsala, Sweden

C. Guet, M. Maurel, B. Million, C. Ristori
Centre d'Etudes Nucléaires, Grenoble, France

V. Bellini, G. Lanzano, A. Palmeri
INFN and University Catania, Italy

Pions being one of the most commonly produced particles in heavy ion collisions, one ought to have a very clear understanding of the associated pion production mechanism. Data obtained from subthreshold pion production inclusive measurements (1,2) can be compared with the predictions of some of the conventional models. Nevertheless they are not sufficient to discriminate among these different models. For that, a necessary step is the realization of exclusive measurements.

This paper describes an attempt of coincidence experiment between charged pions and forward emitted charged particles. A few results from a preliminary analysis of the data are presented.

The experiment was carried out with the ^{12}C beam (85 MeV/A) of the CERN Synchrocyclotron (May 1983). The duty cycle was about 40 %. A plastic scintillator range telescope was used to detect pions. The telescope consisted of 11 plastic scintillators allowing to detect and to identify pions between 20 and 90 MeV. The method to separate π^+ and π^- is very efficient and allows to get reliable ratios $N\pi+/N\pi-$ (3,4). To detect forward charged particles, 3 thin scintillators (2 mm thick) C_1, C_2, C_3 were used, followed by two C_4 and C_5 scintillators, 5 mm thick. Four other thicker scintillators were also used at a little longer distance from the target. The figure 1) shows the experimental set up. The covered angular range was between 4 and 15 degrees.

The target was a ^{12}C foil 150 mg thick and the beam current was equal to 1 nA. The telescope was located at $\theta = 90°$ with a subtented solid angle of 15 msr. The pion telescope was also used to detect protons in coincidence with forward emitted particles in order to compare charged particles spectra in coincidence with pions or protons.

The figure 2) represents the time of flight difference between protons or pions stopped in the fourth element of the telescope (T_π = 20 MeV, T_p = 50 MeV) and the charged particles ($Z > 2$) travelling through the C_1, C_2 and M_1 scintillators. The number of random coincidences is pratically zero. One can deduce from the peak positions and the FWHM that the energy range of the frag-

[+] On leave from INFN Catania.
[++]Present address CERN, Geneva, Switzerland.

ments in coincidence is equal to 85 ± 25 MeV/A. The time peak for pions was obtained after a very careful pion identification. In fact electrons detected in the telescope can produce an appreciable broadening of this peak. The figure 3) shows a scatter plot of the energy deposited in the C_5 and M_1 scintillators of the forward wall. It is clear that the charge separation is satisfactory from Z = 2 up to Z = 6.

The figure 4) represents the relative yields for the different charge values ($Z \geqslant 2$) in the cases of inclusive fragment production, and of fragments in coincidence with protons and pions respectively. In spite of the low counting rate, pions have been observed in coincidence with Z = 2 to Z = 6 fragments. The charge distribution of the fragments in coincidence with protons and pions look similar. Future and more elaboratored experiments should give more precise energie and charge distributions of the fragments in coincidence with pions allowing a characterization of the peripheral or central nature of the pion production reaction.

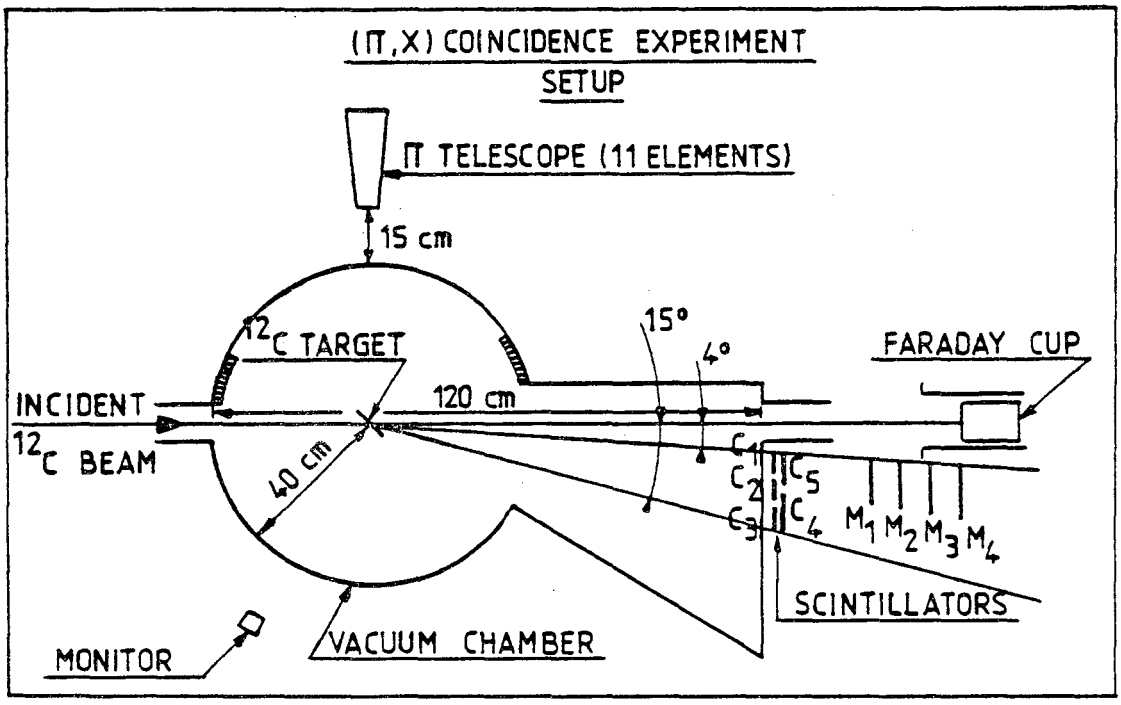

9 Scintillators were used to detect forward charged particles : C_1, C_2, C_3 : 2mm thick - C_4, C_5 : 5mm thick - M_1, M_2, M_3, M_4 were respectively 10, 20, 30, 10 mm thick .

Target thickness : 150 mg/cm^2 . ^{12}C BEAM : 8.10^8 particles/s .

Fig. 1

Fig. 2

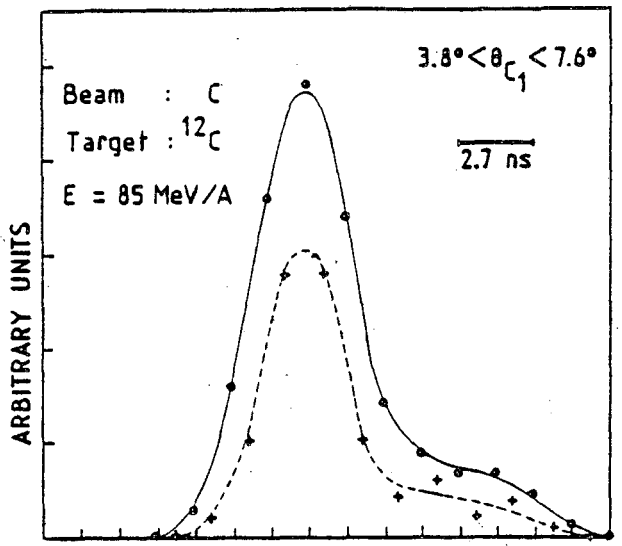

TIME OF FLIGHT DIFFERENCE BETWEEN PIONS (+) OR PROTONS (•) STOPPED IN THE FOURTH ELEMENT S_4 ($T_\pi \simeq 23$ MeV, $T_p \simeq 50$ MeV) AND CHARGED PARTICLES DETECTED IN C_1, C_5, M_1 ELEMENTS OF THE FORWARD WALL. THE FWHM IS ABOUT 4 ns FOR PIONS AND PROTONS. The line is to guide the eye.

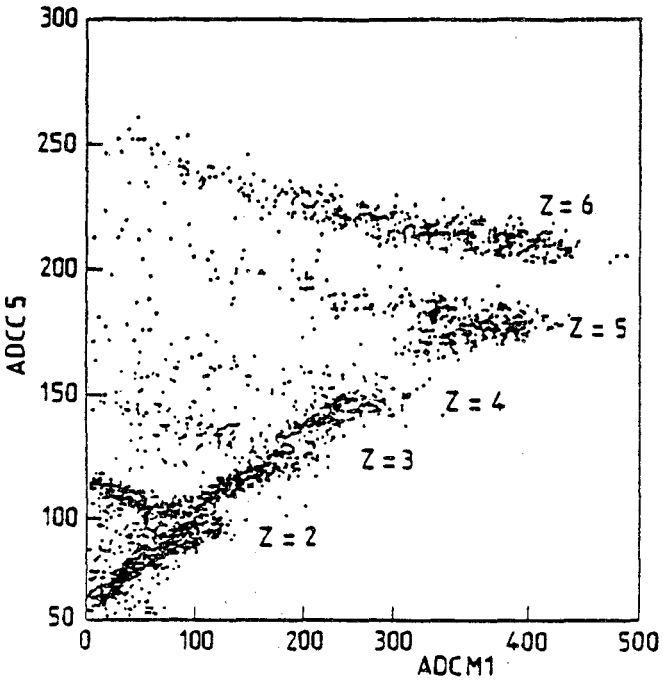

SCATTER PLOT OF ENERGY DEPOSITED IN THE C_5 AND M_1 SCINTILLATORS OF THE FORWARD WALL FOR FRAGMENTS INCLUSIVE PRODUCTION

Fig. 3

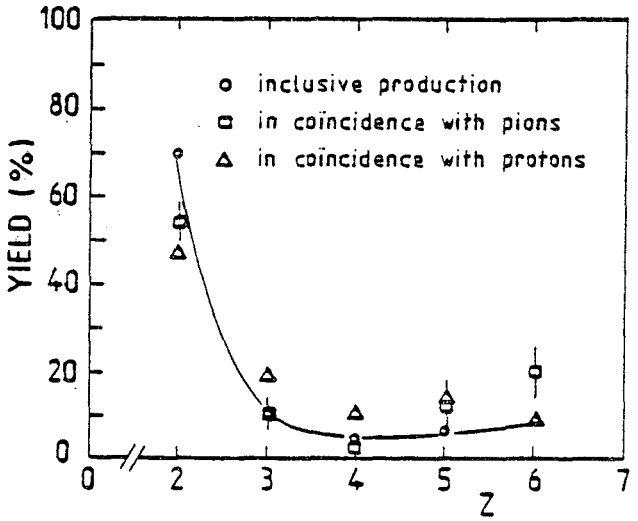

RELATIVE YIELDS FOR THE DIFFERENT CHARGE VALUES ($Z \geqslant 2$) IN THE CASES OF FRAGMENT INCLUSIVE PRODUCTION, OF FRAGMENTS IN COIN-CIDENCE WITH PROTONS AND PIONS RESPEC-TIVELY. The line is to guide the eye

Fig. 4

Références :

1) T. Johansson et al., Phys. Rev. Lett. 48 (1982) 732.
2) V. Bernard et al.. To appear in Nuclear Physics.
3) J. Julien, Proc. of the 3 rd. Inter. Conf. on Nuclear Reaction, Mechanisms, Varenna, 1983.
4) J. Julien et al.. To be published.

CURRENT STATUS OF HIGH ENERGY CASCADE MODELS

E. A. Remler

College of William and Mary, Williamsburg, VA 23185

Normally a status report describes progress towards a commonly perceived goal. In the present case however, few physicists share or even have a perception of where such a goal might stand and therefor how to move towards it. Some doubt the goal stands; some that it is worth attempting. It is therefor necessary to begin by describing where the cascade model stands on a kind of map of theories. That is, to describe its status relative to other approximations to Quantum Mechanics. In addition I will say why the area near it in theory space is worth further exploration. Finally the current status of such explorations will be described.

Figure 1 is a sketch of part of the map. For orientation, some neighboring approximations are also shown. The sketch is necessarily rough not only because I am ignorant of most of it but also because it's multi-dimensionality and multiple connectedness cannot be represented in two dimensions. The following discussion will hopefully help decipher it.

Theories designed to predict exculsive measurements generally start with Schroedinger's time dependent equation for the wave function and approximate it. Conversely, to predict inclusive measurements, it is generally advisable to approximate the quantum Liouville or von Neumann equation ($h = 2\pi$)

$$\partial\rho/\partial t = [-iH,\rho]$$

which is the exact time evolution equation for the density operator. The matrix elements of this operator equation can be written in the Wigner representation defined as follows[1]

$$(\vec{x},\vec{p}|\rho) = \int d\vec{y}\, e^{i\vec{p}\cdot\vec{y}} \langle \vec{x}-\tfrac{1}{2}\vec{y}|\rho|\vec{x}+\tfrac{1}{2}\vec{y}\rangle$$

where $\vec{x} = (\vec{x}^{(1)},\ldots,\vec{x}^{(A)})$, $\vec{p} = (\vec{p}^{(1)},\ldots,\vec{p}^{(A)})$ are each 3A dimensional position and momentum vectors for the A-body system and $(\vec{x}\vec{p}|\rho)$ is called the Wigner representative of the density operator ρ. It is also convenient to abbreviate $\vec{x},\vec{p}$ by ϕ which therefor denotes a point in 6A dimensional classical phase space. The equation of motion in the Wigner representation takes on the form

$$\partial/\partial t(\phi|\rho) = \int d\phi'(\phi|\mathcal{L}|\phi')(\phi'|\rho) \equiv (\phi|\mathcal{L}|\rho)$$

$$d\phi' = h^{-3A}\, d\vec{x}'\, d\vec{p}'$$

For local momentum independent potentials

$$= \mathcal{L}_c + \mathcal{L}_Q$$

$$(\phi|\mathcal{L}_c|\phi') = -(v\cdot\partial/\partial\vec{x} + f\cdot\partial/\partial\vec{p})\delta(\phi,\phi')$$

$$\delta(\phi,\phi') = h^{3A}\delta(\vec{x}-\vec{x}')\delta(\vec{p}-\vec{p}')$$

$$(\phi|\mathcal{L}_Q|\phi') = \frac{1}{24} V(\vec{x}) \; (\overleftarrow{\partial}/\partial\vec{x} \cdot \overrightarrow{\partial}/\partial\vec{p})^3 \; \delta(\phi,\phi') + \ldots$$

Thus the quantum part of the Liouville operator is a series whose successive terms are of order $(\Delta x_V \, \Delta p_\rho)^{-(2n+1)}$ where Δx_V is the smallest length parameter in the potential and Δp_ρ is the system's width in momentum. For large enough $\Delta x_V \, \Delta p_\rho$ we may expect to be able to neglect the quantum term and are left with classical mechanics. When the density operator describes a pure state packet, the momentum width is the inverse spatial width, the classicality condition is that the potential varies negligably over the packet's size and the validity of the classical limit becomes a corollary of Ehrenfest's theorem. It is not clear whether the classical limit is also valid in the more general case of mixed state densities with large momentum width but not correspondingly small spatial width.

The classical Liouville equation

$$\partial/\partial t \; (\phi|\rho_t) = -(\vec{v} \cdot \partial/\partial\vec{x} + \vec{f} \cdot \partial/\partial\vec{p}) \; (\phi|\rho_t)$$

can be numerically solved on the computer by approximating the initial state as a sum of delta functions

$$(\phi|\rho_o) \cong \sum_{\nu=1}^{N} \delta(\phi,\phi_\nu)/N$$

Typically the ϕ_ν would be chosen at random according to the phase space probability distribution function $(\phi|\rho_o)$. N is the number of members of the classical statistical ensemble described by the density. As N increases the approximation converges weakly, that is

$$\lim_{N\to\infty} \frac{1}{N} \sum_{\nu=1}^{N} g(\phi_\nu) = \int d\phi \, g(\phi)(\phi|\rho_o)$$

for a reasonable smooth and fixed $g(\phi)$. Therefor this approximation's accuracy for calculating expectation values of observables, which are always overlap integrals of the above form, linear in the density, increases with N. Conversely, for calculation of a quantity such as the entropy

$$S = -\mathrm{Tr}\,(\rho \; \ell n \; \rho)$$

which is non-linear in the density, the delta function approximation cannot be directly used. Inserting the approximation into the classical Liouville equation shows that the density's time dependence is given by

$$(\phi|\rho_t) = \frac{1}{N} \sum_{\nu=1}^{N} \delta(\phi,\phi_\nu(t)); \quad \phi_\nu(o) = \phi_\nu$$

$$\frac{d}{dt}\vec{x}_\nu = \vec{v}_\nu$$

$$\frac{d}{dt}\vec{p}_\nu = \vec{f}_\nu$$

Here we see Newton's equations and point particle dynamics appearing merely as secondary constructs in a method devised to solve the classical Liouville equation. Furthermore, generally speaking, for more than one particle, this will be the only practical method of calculating $(\phi|\rho_t)$. It has this power because importance sampling is built into it. That is, the larger the value of $(\phi|\rho_t)$ the more the computer time spent in approximating it in the neighborhood of ϕ. This will also be true of the other non-classical approximations to the quantum Liouville equation to be discussed next.

The cascade model evolves from an approximation to the quantum Liouville equation in a limit which is quite distinct from the classical limit just discussed. Although cascade has obvious classical features, the practice of calling it 'classical' should be avoided because it confuses two physically distinct regimes. I have therefor suggested calling it a type of quasi-classical (as distinct also from semi-classical which implies a short wave-length limit) approximation. The meaning of 'quasi-classical' will be explicated later.

It can be shown that[1] for collisions involving large dilute systems the Liouvillian can be approximated by

$$\cong \mathcal{L}_o + \sum_{a<b} J_{ab}$$

where $\mathcal{L}_o$ is the free streaming term

$$(\phi|\mathcal{L}_o|\phi') = -\vec{v} \cdot \partial/\partial\vec{x}\ \delta(\phi,\phi')$$

and the J_{ab} are two-body ('jump') operators which provide the interaction and have kernels given by

$$(\phi^{(a)}\phi^{(b)}|J_{ab}|\phi'^{(a)}\phi'^{(b)}) = \delta(\Phi^{(ab)},\Phi'^{(ab)})\ h^3\delta(\vec{x}^{(ab)}-\vec{x}^{(ab)\prime})$$

$$\times|\vec{v}^{(a)}-v^{(b)}|\delta(x^{(ab)}[-\delta(\vec{p}^{(ab)}-\vec{p}^{(ab)\prime})\sigma_T^{(ab)} + \sigma^{(ab)}(\vec{p}^{(ab)};\vec{p}^{(ab)\prime}]$$

Here $\Phi^{(ab)}$ is the position and momentum of the center of mass of particles a and b while $\vec{x}^{(ab)}$ and $\vec{p}^{(ab)}$ are their relative positions and momenta

$$\vec{x}^{(ab)} = \vec{x}^{(a)}-\vec{x}^{(b)}; \quad \vec{p}^{(ab)} = \frac{1}{2}(\vec{p}^{(a)}-\vec{p}^{(b)})$$

The total cross-section is $\sigma_T^{(ab)}$ and the differential (with respect to momentum) cross-section is $\sigma^{(ab)}(\vec{p}^{(ab)};\vec{p}'^{(ab)})$. This expression assumes only elastic scattering and neglects spin, isospin etc., but can easily be generalized.

One important proviso attached to the above is that J_{ab} must be treated like a pseudo-potential in ordinary scattering theory. Thus the expansion of the propagator[1][2]

$$e^{\mathcal{L}t} = e^{\mathcal{L}_o t} + \int_o^t dt_1 e^{\mathcal{L}_o (t-t_1)} \sum_{a<b} J_{ab} e^{\mathcal{L}_o t_1}$$
$$+ \int_o^t dt_1 \int_o^{t_1} dt_2 e^{\mathcal{L}_o (t-t_1)} \sum_{a<b} \sum_{a'<b'} (1-\delta_{aa'}\delta_{bb'})$$
$$\times J_{ab} e^{\mathcal{L}_o (t_1-t_2)} J_{a'b'} e^{\mathcal{L}_o t_2} + \ldots$$

produces a multiple scattering series; that is, terms in which any one J_{ab} appears twice in succession are absent. This is already implied by the fact that the J_{ab} are in terms of cross-sections and not e.g. potentials and therefor approximate the net effect of the interaction between a and b over a period which is long compared to their interaction time.

The cascade model is related to this approximation in much the same way as classical point dynamics was related to the classical approximation of the Liouville equation. The initial density is again replaced by a sum of delta functions. This additional approximation however now requires that the be slightly altered since point particles interacting via a zero range potential have no chance of meeting. This is done by changing

$$\delta(\vec{x}^{(ab)}) \rightarrow \delta(z^{(ab)})\ \theta(B^{(ab)} - |b^{(ab)}|)/\sigma_T^{(ab)}$$

in the expression for J_{ab}. Here $z^{(ab)}$ is the separation between a and b along their relative velocity direction, $\vec{b}^{(ab)}$ is their relative impact parameter two-vector and

$$B^{(ab)} = (\sigma_T^{(ab)}/\pi)^{1/2}$$

is their interaction radius. This will negligably affect large, dilute systems to the extent that their spatial distribution change slowly on the scale of the interaction radius.

Inserting this interaction into the expansion of $e^{\mathcal{L}t}$ shows that particles a and b will scatter into $\vec{p}^{(ab)}$ from $\vec{p}^{(ab)'}$ with relative probability $\sigma^{(ab)}/\sigma_T^{(ab)}$ if they pass within an interaction radius of one another on the impact parameter plane. This is just the form of the cascade model implemented by Cugnon.[3] As was the case with the classical model, one can express the cascade model in the form of the following equations of motion

$$\frac{d}{dt}\vec{x} = \vec{v}$$

$$\frac{d}{dt}\vec{p}^{(a)} = \sum_{b\neq a} |\vec{v}^{(a)} - \vec{v}^{(v)}| \delta(z^{(ab)} - \varepsilon)\theta(B^{(ab)} - |\vec{b}^{(ab)}|)\vec{I}^{(ab)};\ \varepsilon = 0^+$$

where now, $\vec{I}^{(ab)} = -\vec{I}^{(ba)}$ is a stochastic impulse with probability distribution function determined by the differential cross-section.

The diluteness condition appears to rule out any relevance of the cascade model to nuclei which, on the scale set by the interaction radius, are close packed. How can one then account for the fact that it produces reasonable parameter free fits to much of the particle-nucleus and nucleus-nucleus

non-elastic spectra. In fact one can show that[4][5] because this data is highly inclusive (sums over many final states) and because the elementary two-body cross-sections involved are strongly peaked forward, cascade becomes identical to the Glauber approximation (neglecting relatively small shadowing corrections) for low momentum transfers where the latter is known to provide a good quantum-mechanical description. This is true for their descriptions of the scattering state inside as well as outside the nucleus. Furthermore, contributions to such spectra from large angle quasi-free two body collisions inside the nucleus are by definition well represented by cascade. Cascade's predictive success is therefor due to the fact that it happens, by special circumstance, to handle fairly well both of these mechanisms and these in turn determine most of such non-elastic spectra. Furthermore, this success is real and not just 'due to statistics'.

There are many things which cascade does not describe. Any part of a spectrum dominated by coherent scattering by correlated clusters[4] in the nucleus (such as very possibly the high momentum transfer p+nucleus $\rightarrow$ p'+x cross-section) is out of cascade's present scope (although practical schemes to rectify this have been proposed)[5]. Evaporation and fission spectra must also be treated separately.

In addition to such examples, there are other important cascade predictions which cannot be trusted for perhaps less obvious reasons. One of these is nuclear densities during heavy ion collisions.[6] Cascade's derivation explicitly involves spatial coarse graining with a grain size larger than the interaction radius.[1] This shows up most clearly in the arbitrary and unrealistic prescription it uses to determine $d\vec{p}/dt$. The choice of prescription has no affect on dilute systems and, for reasons discussed, has little affect on the bulk of spectra from (non-dilute) nuclear systems but, should strongly influence many other things including densities during collisions. Evidence of this is the fact that the equation of state of a system actually obeying cascade's equations of motion, would be that of a perfect gas. Clearly no model with a finite grain size can predict details at a finer level. Unfortunately most questions of current interest in heavy ion physics lie at levels finer than that reached by cascade.

Another important area of trouble for cascade is pion production.[7] One reason is that in the dilute limit, where the model is correct, no pion absorbtion takes place. Therefor no theoretical guidance as to its form can be obtained in an internally self-consistent manner. Since pion reabsorbtion is a dominating mechanism in nuclear pion production, this is a serious defect. In any case there are no commonly accepted non-relativistic quantum mechanical models which could be used to derive approximations to the Liouvillian for the nucleon-pion system. Since pion production is an important energy degradation mechanism for nucleons, this difficulty also strongly affects cascade's predictions of nuclear densities discussed in the previous paragraph.

Having discussed some of cascade's ills it is time to mention cures. That cures can be developed in a systematic fashion is perhaps the main point I wish to make in this talk! In principle the procedure is straightforward and the same as for any model. Having obtained cascade[1] by a well defined but not well justified (for non dilute systems) sequence of approximations,

one can go back and improve each approximation as much as possible. This would not be possible if the sequence were not even well defined! In the present case the practical limits to this procedure have hardly been explored and certainly not reached.

A simple, practical and physically transparent first step goes as follows. Divide the two body potential into a long and short range part as illustrated in Figure 2 (for prototype nucleons). The long range part V_L must have a smallest length parameter Δx satisfying

$$\Delta x \, \Delta p >> 1$$

where Δp is the momentum width of measurements the theory is designed to predict. Now re-define the interaction radius $B^{(ab)}$ and the probability distribution function for the impulse $I^{(ab)}$ so that particles a and b, moving according to

$$\frac{d}{dt}\vec{x} = \vec{v}$$

$$\frac{d}{dt}\vec{p}^{(a)} = \sum_{b\neq a} -\partial V_L^{(ab)}/\partial\vec{x}^{(a)} + |\vec{v}^{(a)} - \vec{v}^{(b)}|\,\delta(z^{(ab)} - \varepsilon)\,\theta(B^{(ab)} - |\vec{b}^{(ab)}|)\,\vec{I}^{(ab)}$$

scatter with the observed two-body cross section (averaged over the momentum width). Clearly the interaction radius will now be smaller and the impulse's probability distribution fuction will be flatter. The decrease in interaction radius should reduce the unrealistic behavior of the model with respect to nucleon densities simply because the grain has been refined. The long range classical force term takes into account some of the coherence effects in multiparticle collisions and also clustering during the final expansion phase of heavy ion reactions.

There are a number of other refinements which are already suggested by work that has been done.[5] These include how to phenomenologically take into account scattering by compact multiparticle clusters and, how to alter the form of the stochastic impulse term to a more realistic form as dictated by a Wigner transform of two body transition matrices. It is not possible to discuss these here.

It is worthwhile to point out that the simple refinement suggested above is certainly feasible and may in fact even reduce computation time if properly implemented. Experience with many-body theories seems to indicate that details of force laws and other aspects of dynamical models are unimportant for most questions of interest (equations of state, transport coefficients, ...critical indices!). One should therefor calculate the long range force term in a way which puts a premium on computational speed as opposed to accuracy. Similarly the impulse term can probably be taken to be spherically symmetric. Finally, the stochastic term will occur less frequently due to its reduced interaction radius. These points all tend to reduce computation time.

In summary, improved approximations such as those outlined above, should lead to theories describing particles moving according to some combination of deterministic plus stochastic force laws. I propose to call such theories

quasi-classical. As indicated in Figure 1 they occupy a broad area in theory space which includes both the classical and cascade models as 'limit points'. Only the very preliminary work referred to in this paper has been done to derive quasi-classical theories from the full von Neumann equation. This work suggests that quasi-classical theories should be systematically derivable by coarse graining the phase space representation of the density operator. It will be necessary to make the grain size as small as possible for such theories to be applicable to non-dilute systems and to answer current questions of interest about intermediate states during heavy ion collisions. The minimum value of the grain size is set by the fact that Wigner functions can generally become negative. Too small a grain will therefor give rise to 'negative valued probabilities'. Although it may be possible in the future to implement such a concept in a fashion similar to that discussed above, I have assumed for now that this limitation bounds the concept of quasi-classical theories and indicated it by the dotted line in Figure 1. The area within this line is virtually unexplored and forms the only sure theoretical foundation for further progress in heavy ion physics.

REFERENCES

1. E. A. Remler, Ann. Phys. 95, 455 (1975).

2. E. A. Remler, Phys. Rev. C18, 1786 (1978), Appendix.

3. J. Cugnon, Nuc. Phys. A387, 191c (1982).

4. E. A. Remler and A. P. Sathe, Phys. Rev. C18, 2293 (1978).

5. E. A. Remler, Ann. Phys. 119, 326 (1979).

6. R. Stock, R. Bock, R. Brockmann, A. Dacal, J. W. Harris, M. Maier, M. E. Ortiz, H. G. Pugh, R. E. Renfordt, A. Sandoval, L. S. Schroeder, H. Strobele, K. L. Wolf, Phys. Rev. Lett. 49, 1236 (1982).

7. D. G. Long and M. M. Sternheim, Phys. Rev. C26, 1558 (1982).

FIGURE CAPTIONS

Figure 1 illustrates a number of points which will be stated here without proof. The text describes some of them in more detail. 1: The Schroedinger equation for the wave function is equivalent to the von Neumann equation for the density matrix. The time deisplacement operators are the Hamiltonian and Liouvillian respectively. 2: Approximations to the Schroedinger equation are useful mainly for (nearly) exclusive measurement predictions (corresponding to the entropy of the initial and final states $\to 0$), whereas to the von Neumann equation, mainly for (highly) inclusive ones (entropy of initial and/or final states $\to \infty$). 3: The classical limits of the Schroedinger and von Neumann equations are different. One leads via the short wavelength approximation to the WKB approximation, the other via an expansion in a phase space volume parameter to classical statistical mechanics (SM). 4: The OPTICAL, CASCADE, FLUID, MASTER (EQUATION).....Models are all obtained by projections. 5: Cascade in particular is obtained by coarse graining which is a projection defined in terms of the density operator's representation in classical phase space (Wigner representation). 6: Quasi-classical theories are obtained by using a finer grain than in cascade which is necessary for non-dilute systems.

Figure 2 shows schematically how a nucleon-nucleon type potential is to be divided into a long and short range part.

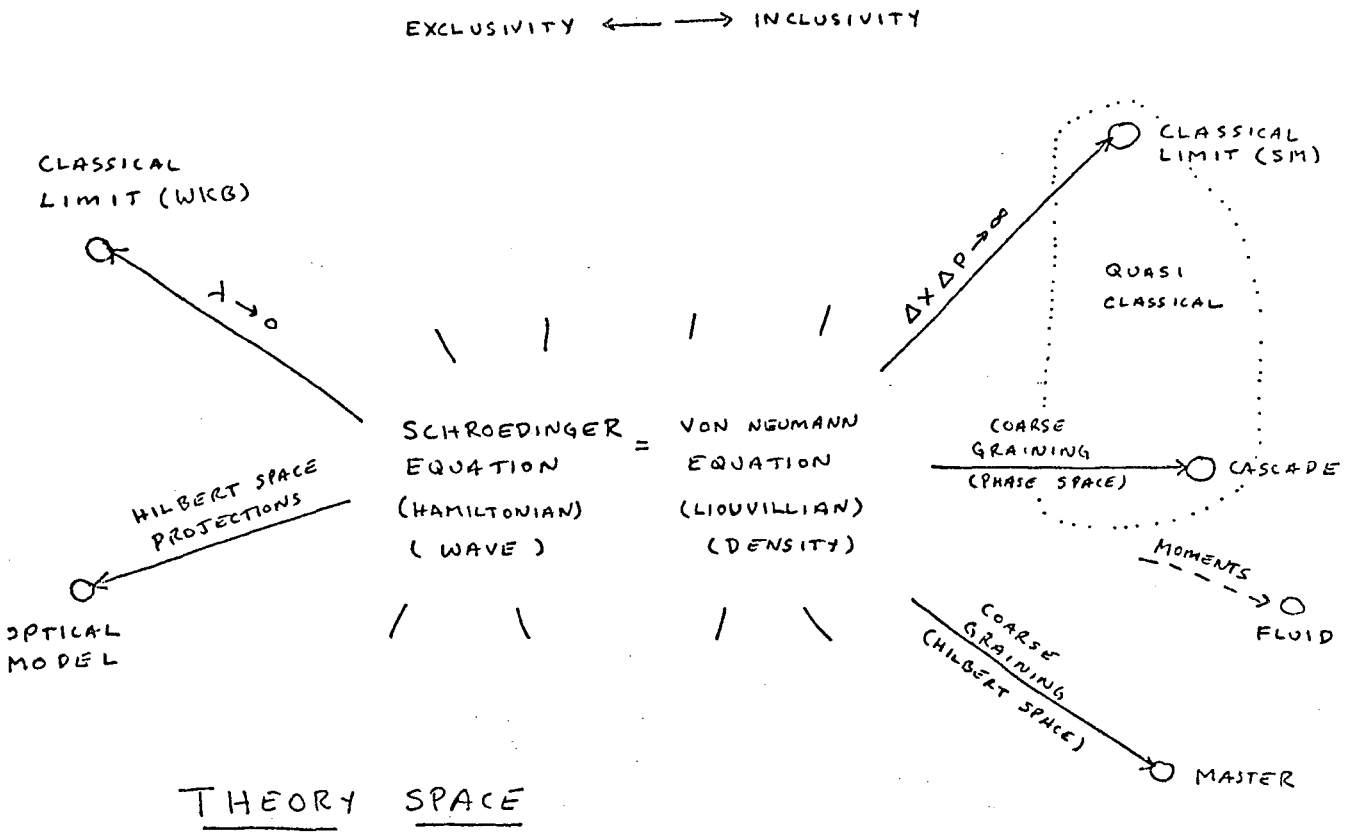
EXCLUSIVITY ⟷ INCLUSIVITY
CLASSICAL LIMIT (WKB)
ħ → 0
CLASSICAL LIMIT (SM)
ΔxΔp → ∞
QUASI CLASSICAL
SCHROEDINGER EQUATION (HAMILTONIAN) (WAVE)
=
VON NEUMANN EQUATION (LIOUVILLIAN) (DENSITY)
COARSE GRAINING (PHASE SPACE)
CASCADE
HILBERT SPACE PROJECTIONS
MOMENTS
OPTICAL MODEL
FLUID
COARSE GRAINING (HILBERT SPACE)
MASTER
THEORY SPACE

FIG. 1

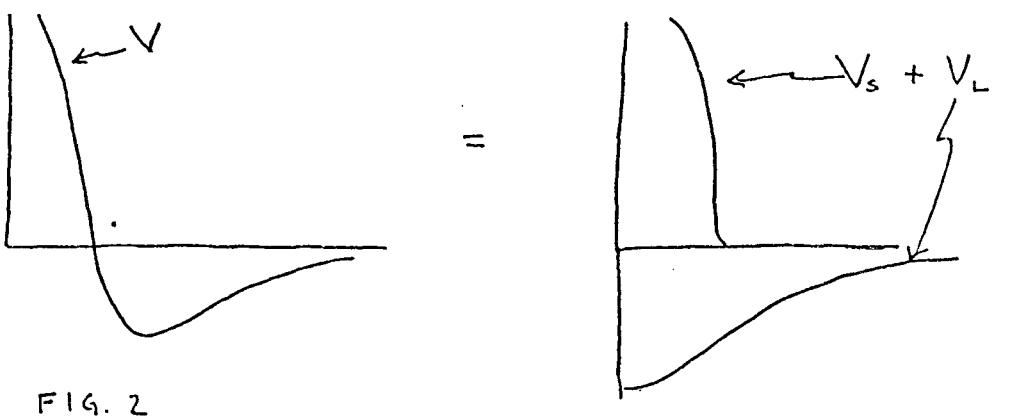
V
=
$V_S + V_L$

FIG. 2

SCALING PROPERTIES IN THE HYDRODYNAMICAL DESCRIPTION OF NUCLEUS NUCLEUS COLLISIONS AT INTERMEDIATE ENERGIES+

N.L. BALAZS

Department of Physics, State University of New York at Stony Brook, New York 11794, U.S.A.

B. SCHÜRMANN and K. DIETRICH

Physik-Department, TU München, D-8046 Garching, W. Germany

and

L.P. CSERNAI

Physik-Department, TU München, D-8046 Garching, W. Germany
and
Central Research Institute for Physics, 1525 Budapest, Hungary++

Abstract: Simple scaling properties of heavy ion reactions at intermediate energies are discussed which follow from the hydrodynamical equations. The measured as well as the calculated hydrodynamical inclusive cross sections exhibit scaling in certain kinematical regions. The fireball model obeys the same scaling laws, but leads to a differential cross section with a qualitatively different shape. The experimental data we analyzed did not show evidence for a hydrodynamical flow.

In the present work the scaling properties of the hydrodynamical evolution of the system and of the calculated differential cross section derived thereof are studied. The collision process may be separated into three stages which are (i) the initial compression stage, (ii) the subsequent quasi-isentropic expansion, and (iii) the final break-up of the nuclear matter. In this contribution we concentrate on the expansion phase (ii). For the treatment of the stages (i) and (iii) we refer to /1/.

For simplicity we consider a nonrelativistic fluid-dynamical model which is reasonable for energies up to ≈ 500 MeV/N

+Supported by the Bundesministerium für Forschung und Technologie

++Permanent address

and central collisions. The basic question is whether we can find some connection between the observable properties of heavy ion reactions for different initial energies per nucleon (E_0 in the cm system) and for different masses A where A=A/2 + A/2 with identical projectile and target masses A/2. To answer this question we shall separate the dimensional physical parameters from the dimensionless general properties of the system. To achieve this we introduce the characteristic mass m_1, the temperature T_1, the length l_1, the time t_1 and the velocity u_1, and specify through them dimensionless quantities denoted by a tilde:

$$\begin{aligned} \vec{r} &= l_1 \tilde{\vec{r}} \quad , \\ t &= t_1 \tilde{t} \quad , \\ \varrho(\vec{r},t) &= (m_1/l_1^3)\,\tilde{\varrho}(\tilde{\vec{r}},\tilde{t}) \, , \\ \vec{u}(\vec{r},t) &= u_1 \tilde{\vec{u}}(\tilde{\vec{r}},\tilde{t}) \, , \\ T(\vec{r},t) &= T_1 \tilde{T}(\tilde{\vec{r}},\tilde{t}) \, . \end{aligned} \tag{1}$$

Here, ϱ is the mass density distribution normalized as $\int \varrho(\vec{r},t)\, d^3r = m\,A$. If we choose the characteristic scaling parameters as

$$\begin{aligned} m_1 &= m\,A \quad , \\ u_1 &= |\vec{u}_0| = (2E_0/m)^{1/2} \quad , \\ l_1^3 &= (4\pi/3)\, r_0^3\, A \quad , \end{aligned} \tag{2}$$

then the characteristic dimensionless hydrodynamical functions are independent of the total mass number A and of the cm energy E_0 before the collision (i.e. at t="$-\infty$"). In general this initial independence of A and E_0 of the scaled variables may not persist as the collision proceeds, but there are examples where it also holds in the later development of the system /1/. We assume in the following this initial independence, and we can then study the later development of the system in a mass- and energy-independent manner.

For simplicity we consider the nonrelativistic dynamics of a nonviscous fluid which may be reasonable on the basis of the numerical results of /2,3/. The corresponding hydrodynamical equations can then be written in a dimensionless form as

$$m_1 \left[\frac{\partial \tilde{\varrho}}{\partial \tilde{t}} + St\, \tilde{\vec{\nabla}} (\tilde{\varrho} \cdot \tilde{\vec{u}}) \right] = 0 \quad , \tag{3}$$

$$\frac{\partial \tilde{\vec{u}}}{\partial \tilde{t}} + St\, (\tilde{\vec{u}} \cdot \tilde{\vec{\nabla}})\, \tilde{\vec{u}} = - St\, \tilde{c}_s^{\,2} \frac{\tilde{\vec{\nabla}} \tilde{\varrho}}{\tilde{\varrho}} \quad , \tag{4}$$

with

$$St = u_1 t_1 / \ell_1 \tag{5}$$

which is sometimes called the Strouhal number, and the dimensionless velocity of sound $\tilde{c}_s$. Since the velocity of sound c_s is known to be of the same order as the thermal velocity we have made the natural assumption that the sound velocity scales with the same velocity u_1, i.e. $c_s = u_1 \tilde{c}_s$. By choosing the time scale as

$$t_1 = \ell_1 / u_1 = r_0 (4\pi A/3)^{1/3} / (2 E_0/m)^{1/2} \tag{6}$$

we put St = 1 for all masses and energies. As a consequence, if two dimensionless solutions a and b are identical initially ($t = 0$, $\tilde{t} = 0$) they remain identical at a later time $t_a = t_b$. However, the corresponding physical times are not equal but in contrast are

$$t_a = \frac{\ell_{1a}}{u_{1a}} \cdot \frac{u_{1b}}{\ell_{1b}} t_b = \left(\frac{A_a}{A_b}\right)^{1/2} \cdot \left(\frac{E_{0b}}{E_{0a}}\right)^{1/2} t_b \quad . \tag{7}$$

Thus the properly scaled similar solutions are similar to each other at different physical times. This is of importance in heavy ion reactions where the hydrodynamical expansion lasts for a given time t_{BU} until the break-up of the nuclear fluid. The observable quantities may exhibit scaling properties only if the break-up times satisfy (7).

As a consequence of the previous considerations, the one-nucleon inclusive double-differential cross section can be written in the following form:

$$\frac{d\sigma}{dE\,d\Omega} = \left(\frac{A}{2}\right)^{5/3} \frac{1}{E_0} \tilde{G}(X, \Theta) \ , \tag{8}$$

where $\tilde{G}(X,\Theta)$ is a universal structure function depending on the dimensionless energy $X = E/E_0$ and the cm scattering angle Θ. It can be shown that the differential cross section derived from the thermal model has the same mass number and energy dependence but that the function $\tilde{G}$ is different. We have checked the prediction of eq.(8) by analyzing some of the experimental data of /4/. To make such an analysis meaningful, the quasi free contribution to the measured cross section has first to be subtracted out. We did this by using the results of /5/ for the calculation of the quasi free contribution. The outcome of our analysis is summarized in fig. 1. The following conclusions can be drawn: (i) After subtraction of the quasi free contribution the structure function $\tilde{G}$ has an approximate universal behaviour, (ii) The position of the maximum of $\tilde{G}$ agrees with that of the thermal $\tilde{G}$ but disagrees with the one of the hydrodynamical $\tilde{G}$, (iii) The fall-off of $\tilde{G}$ with X is much steeeper than for the thermal model. These results suggest that neither the thermal nor the hydrodynamical model is appropriate for the interpretation of the data studied. Probably the analyzed systems are

still too light to show hydrodynamical flow. The need for systematic experimental data for heavier systems and for a variety of incident energies is obvious.

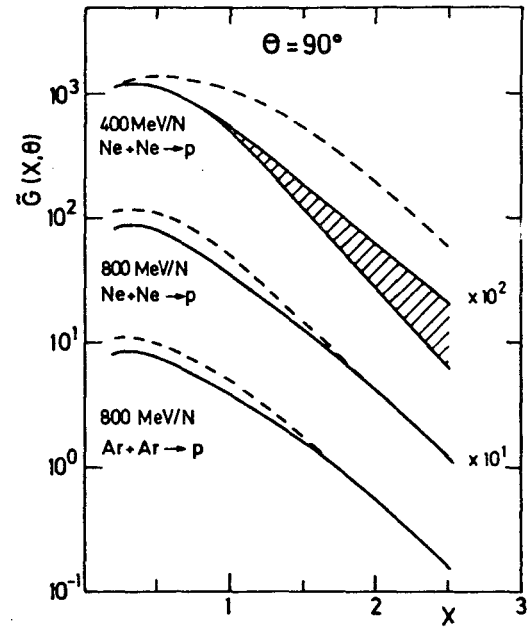

Fig. 1. Structure functions in the cm system, extracted from the experimental proton inclusive data of /4/. Full lines : The quasi free component is subtracted. Dashed lines : The quasi free component is included. The hatched area denotes the uncertainties in the subtraction procedure at 400 MeV/N.

References

1. N.L. Balazs, B. Schürmann, K. Dietrich and L.P. Csernai, to be submitted to Nucl. Phys. A (1983).

2. L.P. Csernai and H.W. Barz, Z.Phys. A296 (198o)173.

3. G. Buchwald, L.P. Csernai, J.A. Maruhn, W. Greiner and H. Stöcker, Phys.Rev. C24 (1981)135.

4. S. Nagamiya, M.-C. Lemaire, E. Moeller, S. Schnetzer, G. Shapiro, H. Steiner and I. Tanihata, Phys.Rev.C24(1981)971.

5. H.-J. Pirner and B. Schürmann, Nucl. Phys. A316(1979)461; B. Schürmann and J. Randrup, Phys.Rev. C23(1981)2766.

Inclusive Measurements of Pions and Light Fragments in 800 MeV/nucleon $^{139}_{57}$La + $^{139}_{57}$La Collisions

X.Bai[a], H.Hamagaki, O.Hashimoto, K.Kimura[b], T.Kobayashi, Y.Miake[c], S. Nagamiya[c], G.Shapiro, Y.Shida and I.Tanihata

Institute for Nuclear Study, University of Tokyo, Tanashi, Tokyo 188, Japan
LBL, University of California, Berkeley, California 94720, USA
a) Institute of Atomic Energy, Beijing, China
b) Department of Physics, Kyushu University, Fukuoka, Japan
c) Department of Physics, University of Tokyo, Hongo, Tokyo, Japan

With the upgraded BEVALAC at LBL, it has now become possible to study high energy heavy ion collisions with projectiles as heavy as uranium. Although in the past the projectiles were limited to relatively light mass nuclei such as C, Ne and Ar due to accelerator capability, measurements of inclusive spectra of pions and light fragments have brought us fundamental information on the reaction mechanism[1]. However, it has been difficult to detect clear signatures of collective phenomena in the reaction by measuring inclusive spectra because the mean free path of a nucleon is comparable to the reaction size in the lighter mass system. With much heavier projectiles such as La or U, we can now expect a better chance of observing nuclear collective phenomena since the reaction size will be significantly larger.

The 800 MeV/nucleon La beam was accelerated at the upgraded BEVALAC. The beam intensity on the target was as high as 10^6 particles/spill. The magnetic spectrometer was used to measure negative pions in the momentum range above 150 MeV/c and light fragments between 400 MeV/c and 2000 MeV/c at laboratory angles of 15,20,40,60,80 and 90 degrees. The experimental set up was the same as that described in Ref 1) except that the spectrometer was modified so that we can handle events with higher multiplicities. In addition, two sets of ΔE-E counter telescopes were installed to detect protons and deuterons in the momentum range from 350 MeV/c to 700 MeV/c at laboratory angles between 80 and 120 degrees.

In Fig. 1 and 2, preliminary data for momentum distributions of protons and pions at various laboratory angles are shown. In these spectra ,we see characteristics similar to those observed in the lighter nucleus collisions. In Fig. 3 and 4 are shown proton and pion energy distributions at CM 90 degrees for the La + La reaction together with the C + C, Ne + NaF and Ar + KCl reactions. We will briefly mention three interesting points :

(1) The slope parameter in the case of La (~82 MeV) is slightly larger than that for Ar (~79 MeV). In the light mass system, it was observed that the heavier the projectile and the target masses are, the less steep is the slope of CM 90 degree spectra. This tendency holds for La, but the difference in the slope parameter between La + La and Ar + KCl seems to be small.

(2) In the CM 90 degree spectrum for proton shown in Fig. 3, the shoulder structure of the spectrum in the low energy region, which is common to a lighter mass system, appears less distinct in La + La. The exponential slope seems to extend down to very small kinetic energy in contrast to the lighter nucleus case. We can say the system looks more equilibrated because of a larger number of collisions before the proton comes out of the reaction region ,since the system

is much larger.
(3) The slope parameter of the pion spectrum for La seems to be somewhat steeper than that for Ar.

Those points may indicate that the characteristics of the La + La collision at 800 MeV/nucleon starts deviating from those generally observed in lighter mass systems. Data analysis is still in progress for inclusive spectra as well as for two particle coincidence spectra.

We would like to thank Prof. H. Steiner and Prof. O.Chamberlain for continuous encoragement and stimulating discussions throughout the experiment. This experiment was supported by the INS-LBL collaboration program, Institute for Nuclear Study, University of Tokyo.

REFERENCE

1) S.Nagamiya, M.C.Lemaire,E.Moeller,S.Schnetzer,G.Shapiro,H.Steiner and I.Tanihata, Phys. Rev. C24,971(1981)

0.8 GeV La + La --> π^- + X preliminary data

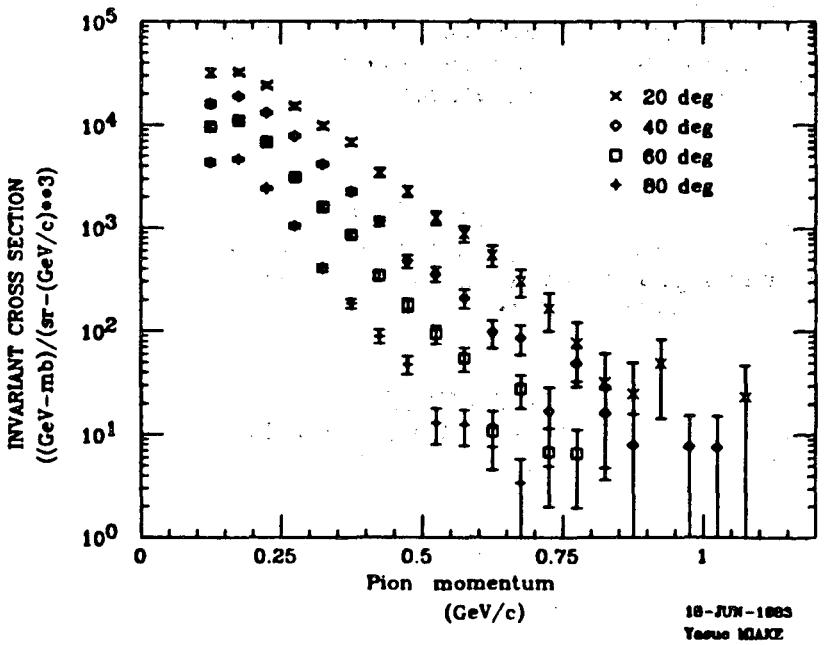

0.8 GeV La + La --> p + X preliminary data

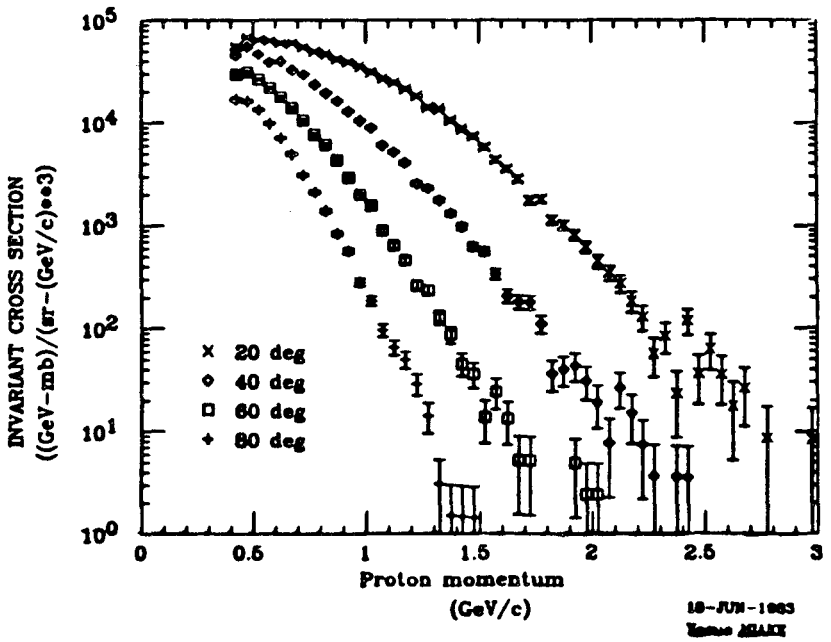

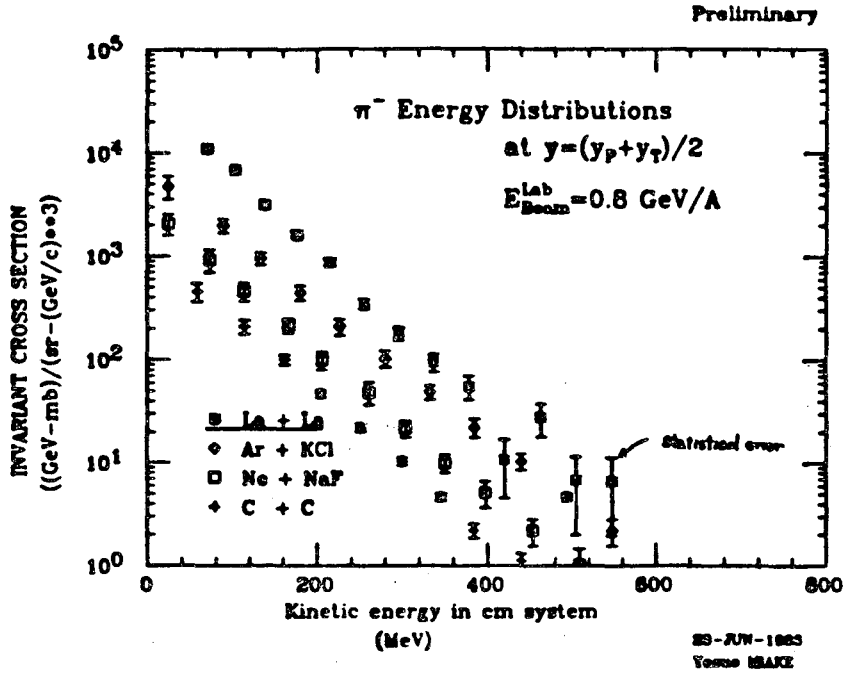

Fig.3 Pion energy distributions at CM 90 degrees in 800 MeV/nucleon La + La collisions together with C + C, Ne + NaF and Ar + KCl collisions.

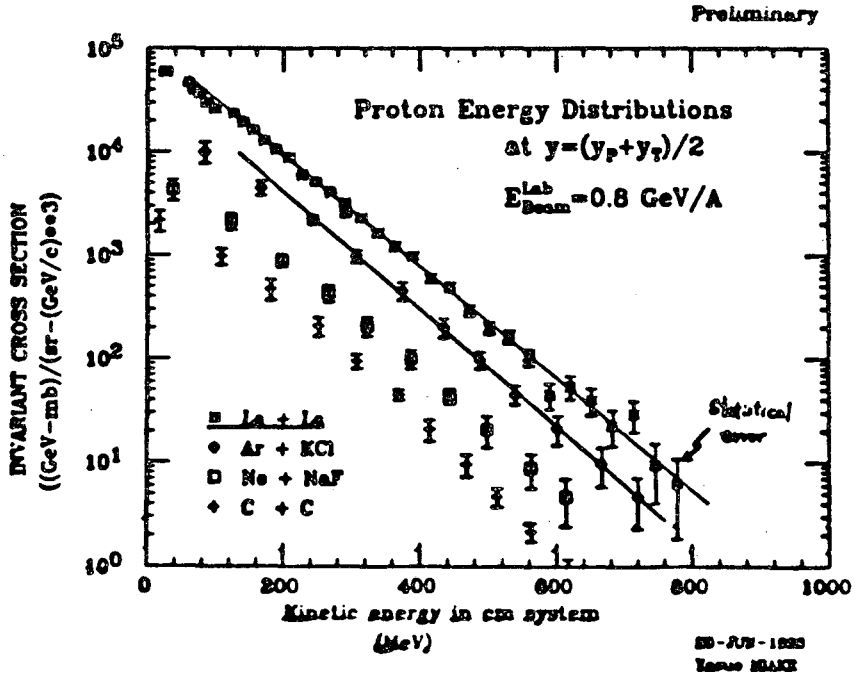

Fig.4 Proton energy distributions at CM 90 degrees in 800 MeV/nucleon L½ + La collisoions together with C + C, Ne + NaF and Ar + KCl collisions.

Production of Light Fragments with High P_T at CM 90 degrees in 800 MeV/nucleon ^{12}C + ^{12}C collisions

X.Bai[a], H. Hamagaki, O. Hashimoto, S. Kadota, K. Kimura[b], Y. Miake[c], S. Nagamiya[c], K. Omata, Y. Shida, I. Tanihata and N. Yoshikawa

Institute for Nuclear Study, University of Tokyo, Tanashi, Tokyo, Japan
LBL, University of California, Berkeley, California, USA
a) Institute of Atomic Energy, Beijing, China
b) Department of Physics, Kyushu University, Fukuoka, Japan
c) Department of Physics, University of Tokyo, Hongo, Japan

In the past years, there have been intensive studies of inclusive spectra in high energy heavy ion collisions, which supplied us a battle field for various theoretical models. The spectra of protons and light fragments generally show a shoulder shape at around the kinetic energy corresponding to free nucleon-nucleon scattering and then the cross sections decrease exponentially with the kinetic energy of the emitted particles. Although numerous theories have been developed to reproduce the general feature of the spectra, it has been very difficult to determine which is a right theory because most theories can explain the data qualitatively. In the hope of getting more discriminative inclusive data, we have carried out an experiment to measure spectra of protons and light fragments with very high momentum at CM 90 degrees where the cross section was expected to be extremely small. Our interest was how the kinetic energy of a projectile can be concentrated to emit a very energetic proton at CM 90 degrees. If some very hot matter is created in the reaction, then we can expect a less steep exponential slope in the higher energy region where the normal component becomes smaller. On the other hand, available phase space is gradually narrowed as the particle kinetic energy becomes closer to the kinematical limit (the absolute limit is 3.8 GeV for 800 MeV/nucleon C + C) and thus the slope of the spectrum tends to be steeper with increasing kinetic energy, since the nucleus-nucleus system does not have an infinite heat bath.

The experiment was designed to measure inclusive spectra of protons and light fragments emitted to CM 90 degrees with extreme high energy (E_K^{CM} > 700 MeV or P_{Lab} = 2 ~ 3 GeV/c) as well as correlations between particles emitted ± 90 degrees in the CM frame.

We studied the 800 MeV/nucleon ^{12}C + ^{12}C reaction using a newly completed HISS(Heavy Ion Spectrometer System) facility at the BEVALAC. The common part of the HISS consists of a superconducting magnet (diameter:2 m, gap:1 m, B_{max}:30 kG), two large drift chambers (1 m x 2 m) and time of flight hodoscopes (2 m x 3 m, 2.5 m x 4 m). The schematic view of the experimental setup is shown in Fig 1. The very large magnetic volume of the magnet (18 KG x 2 m diameter) enabled us to sweep out low momentum charged particles which have large yields. It was also essential to have a long time-of-flight path (~ 10 m) to discriminate between deuterons, tritons and protons because yields of composite particles surpass the proton yield by almost two order of magnitude in the momentum region of P_{Lab} ~ 2 GeV/c . Furthermore, the very good position resolution of the drift chambers made it possible to select good trajectories against large background. The scatter plot of TOF vs 1/p is shown in Fig. 2, which demonstrates how the proton yield is small compared to deuteron and triton yields.

A preliminary spectrum of protons at CM 90 degrees is shown in Fig. 3a. At first glance, we see an exponential decrease of the cross section up to the CM kinetic energy ~1100 MeV. The cross section is already 8 orders of magnitude smaller than the maximum cross section at zero energy. How can we kinematically obtain such high energy particles from the 800 MeV/nucleon C + C reation ?. The free nucleon-nucleon scattering gives to a proton only 182 MeV kinetic energy. If we boost incident nucleon kinetic energy by 270 MeV/c Fermi motion, it can reach only 400 MeV. In order to obtain a kinetic energy of 1100 MeV, about 900 MeV/c Fermi momentum is needed. Even if we take into account a cluster in the target nucleus, it is not possible to produce such high energy nucleons at CM 90 degrees. The maximum energy of kinematically allowed protons for the 800 MeV proton + C reaction is then 420 MeV at CM 90 degrees. To reach a kinetic energy of 1100 MeV in the 800 MeV/nucleon C + C reaction, almost four nucleons ,both from target and projectile, should collide and transfer the kinetic energy to the proton and recoil nucleus. If we take into account the Fermi momentum, then two nucleons from the target and projectile should give their kinetic energy to the proton. The above consideration indicates that the production of the very high energy protons requires at least a few nucleons both from the target and projectile. If we look more closely at the proton spectrum, a deviation from the single exponential decrease will be noticed. The dashed line in Fig. 3a is a fitted line in ref 1). It is clear that the proton energy distribution is not fit by a single exponential slope. This steeper exponential decrease of the cross section in the higher kinetic energy region will be due to the effect of phase space limitation in the momentum range measured in the present experiments.

In Fig. 3 b and c, the deuteron and the triton spectra are shown. A distinct bend of the deutron spectrum is observed at around 400 - 600 MeV, the position of which corresponds to the shoulder of the proton spectrum. The solid lines in Fig 3b and c are the spectrum shape calculated from the proton spectrum based on a coalescence model. Both in the deuteron and the triton spectra, the coalescence model seems to hold remarkably well in the entire kinematic domain from 0 to 1100 MeV. Further analysis is still under way.

We would like to thank Prof. H. Steiner and Prof. O. Chamberlain for continuous encoragement and stimulating discussions through the experiment. We also acknowledge the collaboration of the member of HISS group at every stage of the experiment. This work is supported by the INS-LBL collaboration program, Institute for Nuclear Study, University of Tokyo.

REFERENCE

1) S.Nagamiya, M.C.Lemaire,E.Moeller,S.Schnetzer,G.Shapiro,H.Steiner and I.Tanihata, Phys. Rev. C24,971 (1981)
2) M.C.Lemaire,S.Nagamiya,E.Moeller,S.Schnetzer,G.Shapiro,H.Steiner and I.Tanihata, LBL Report LBL-8463(1979)

LAYOUT OF THE EXPERIMENTAL SETUP FOR E512

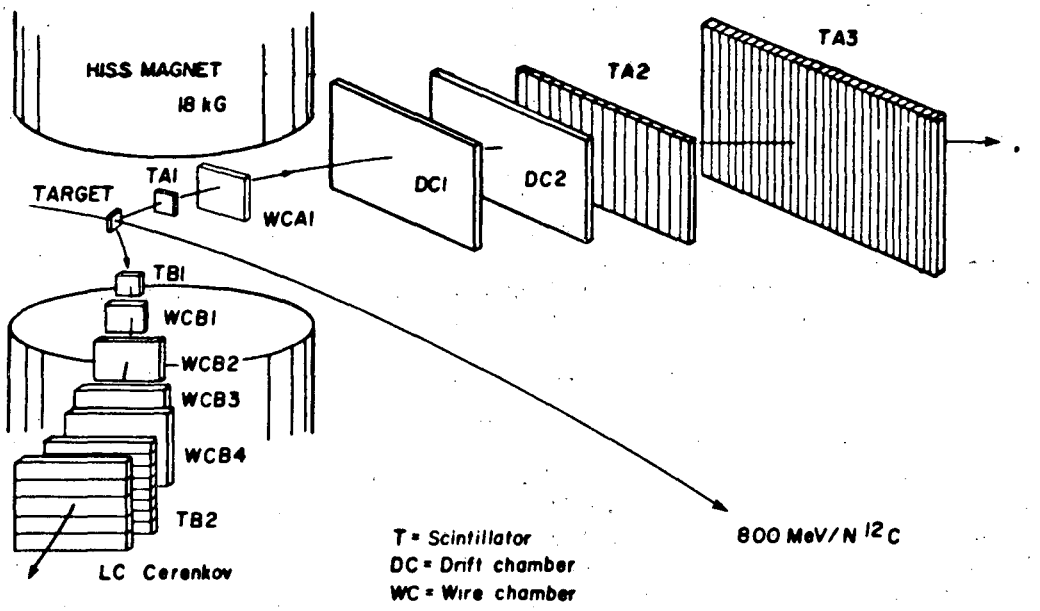

Fig.1 Schematic view of the experimental setup.

XBL 8210 1240

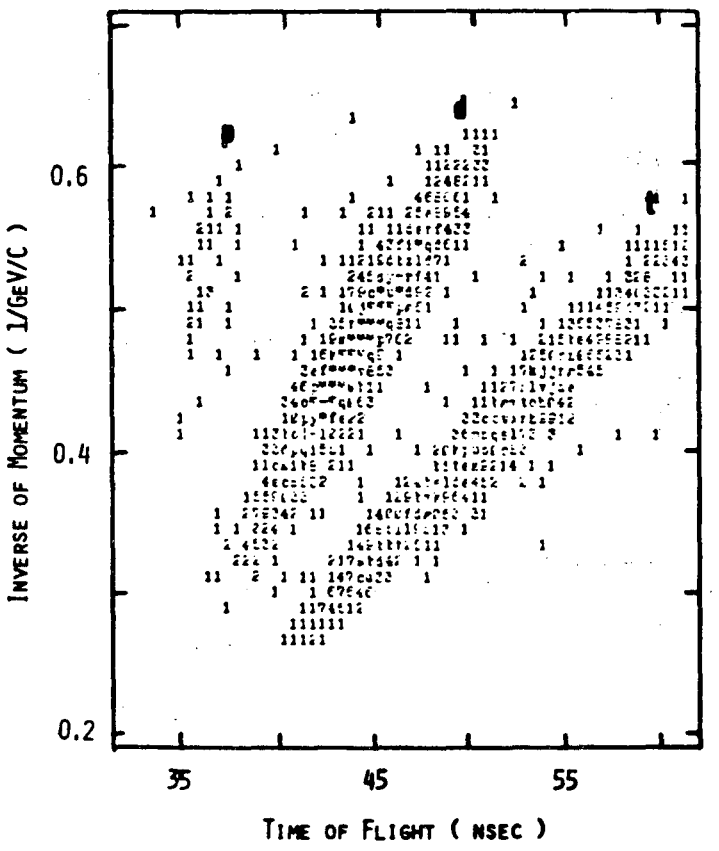

Fig.2 A scatter plot between the inverse of momentum (1/p) and the time-of-flight.

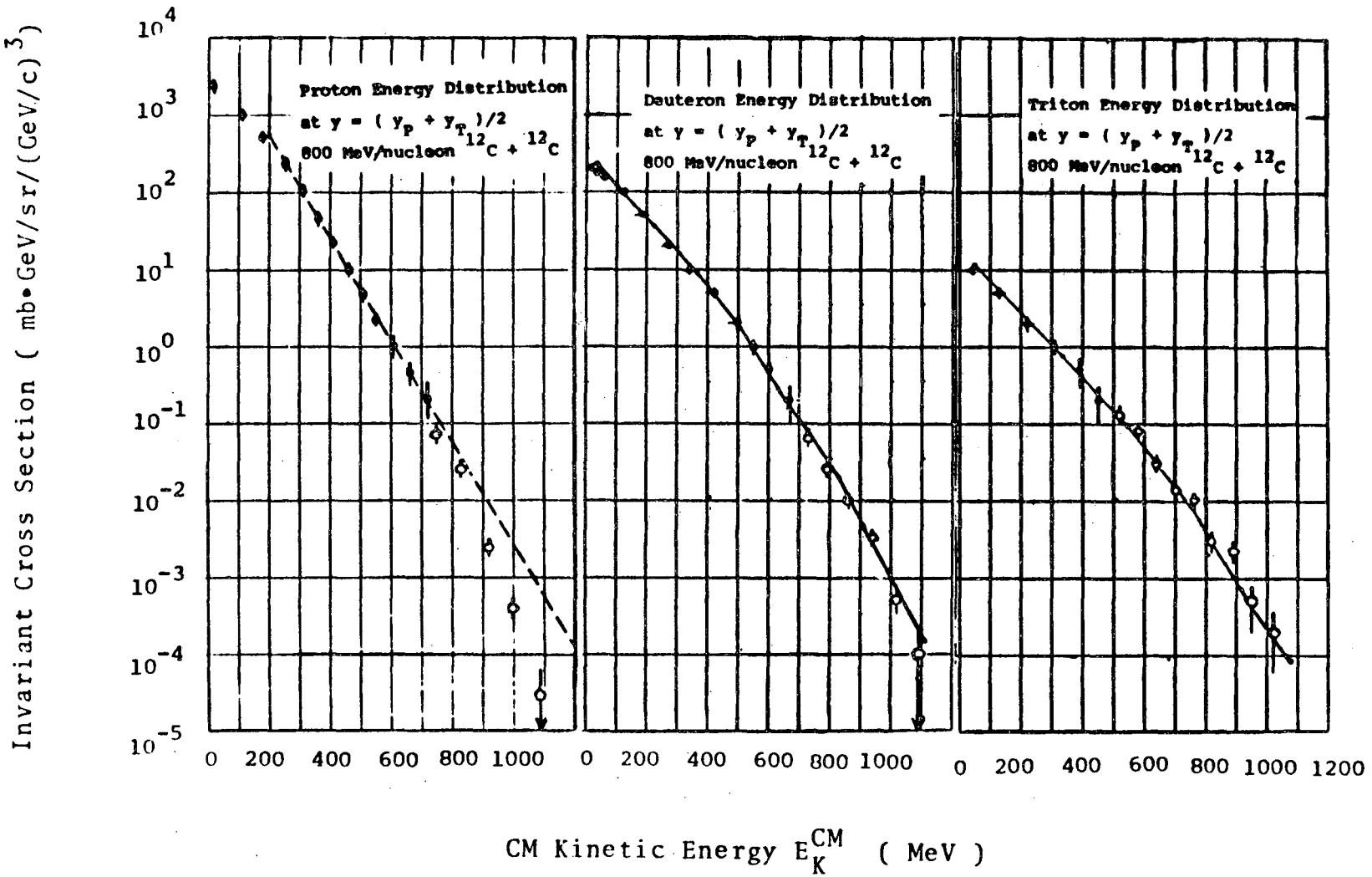

Fig. 3 Invariant cross sections for Z = 1 fragments as a function of kinetic energy at CM 90 degrees. Black points are taken from ref 2. Open points are present results.

CRITICAL PHENOMENA AT LOW TEMPERATURE

David K. Scott

National Superconducting Cyclotron Laboratory

and

Departments of Physics and Astronomy and of Chemistry
Michigan State University
East Lansing, Michigan 48824, USA

Phenomenology cannot represent Nature without transgressing experience . . . Experience, says Goethe, is always only half experience

(L. Boltzmann, On the Evolution of the Methods of Theoretical Physics in Recent Times, 1899)*

Abstract

Critical phenomena in high energy heavy ion collisions have long been of interest in view of the possibility of creating new states of nuclear matter in the form of a pion condensate, density isomer, and a quark-gluon plasma. In this paper we discuss critical phenomena which may be relevant at much lower densities and temperatures. Instabilities associated with a liquid-gas phase transition and a nuclear break-up when the compressibility becomes negative are discussed. Although the phenomena are less exotic than those conjectured to occur at high density or temperature, they also rely for their evolution on a hydrodynamical description of nuclear collisions. Questions of time scales, which are important for all types of critical phenomena, are touched upon. Some of the possible experimental signatures, along with present evidence, for the onset of critical behavior are described. A discussion of more general implications of the behavior of the nuclear equation of state at low density and temperature is included. Low temperature critical phenomena have implications on topics as diverse as the nuclear mean free path, anomalons, and the evolution of supernovae.

1. Introduction

The possibility of creating states of matter resembling those prevailing in the early Universe constitutes a major incentive for the study of high energy heavy ion collisions.[1-3] If energy densities of 2-4 GeV/fm^3 can be achieved, then according to quantum chromodynamics, a phase transition to a quark-gluon plasma may occur. Such a transition represents an extreme example of a critical phenomenon which may exist at high temperatures and densities. Many questions on reaching such a state can be raised--whether, for example, there is sufficient time for the phase transition to manifest itself in the brief time

*This quotation was brought to my attention by J.E. Sedlak in the thesis "Nuclear Hydrodynamics with Viscosity and Heat Conduction," University of Wisconsin--Madison, 1982.

during a nuclear collision when high compressions are thought to be reached, and whether phase equilibrium can be sustained by a finite system consisting of a small number of particles. It is of interest, therefore, to explore the consequences of other critical phenomena, which may set in at lower temperatures and densities and which may be attainable with existing accelerators.

In this paper some of these low temperature critical phenomena are explored, viz a fast mechanical instability leading to the break-up of a nuclear system into fragments, and a slower chemical instability involving a transition between gas and liquid phases. Both phenomena rely for their development on a hydrodynamical description of nuclear collisions, and raise issues which may be germane to phase instabilities of more exotic kinds, such as the quark-gluon plasma and pion condensation.

The next section of the paper describes the underlying physics of the instabilities, and is followed in Section 3 with a discussion of the relevant time scales for the processes to be established. Some of the present experimental evidence is discussed in Section 4; more general consequences of the phenomena in the field of heavy ion science are touched upon in Section 5, and the paper in concluded with a summary in Section 6.

Since at present the theoretical prediction of the experimental consequences has only been developed in a phenomenological way, and since few experiments have been carried out at the level of sophistication necessary to confirm the existence of these phase instabilities, the quotation at the beginning of this section--taken from the work of Boltzmann--is therefore quite apt.

2. Critical Conditions at Low Temperature

An accepted picture of high energy heavy ion collisions is shown on the right of Figure 1 and illustrates the division of a reaction in the participants and spectators.[4] This behavior is established in nuclear collisions at high energies and is to be compared with the slower, more gentle, evolution associated with the TDHF description shown at the left. We shall assume that the participant-spectator description is valid at energies of 50-100 MeV/nucleon. (Some justification for this assumption will be presented in Section 6.) The participant zone is initially compressed and heated; during the subsequent expansion, when the density and temperature drop, it is possible that the system passes through conditions favorable to a division into liquid and gaseous phases, thereby influencing the production of complex fragments. Although frequent discussions of this phenomenon have appeared in the literature (see, for example, Refs. 5-7) pertaining to the evolution of neutron stars and supernovae, its possible manifestation during the dynamical evolution of a heavy ion collision has only recently been raised.[8-13] In the following, a simplified analytical treatment is followed to illustrate the basic ideas; more formal treatments can be found in the above references.

Consider the following parameterization of the energy per particle, E, in a nuclear system as a function of temperature, T, and density, ρ;

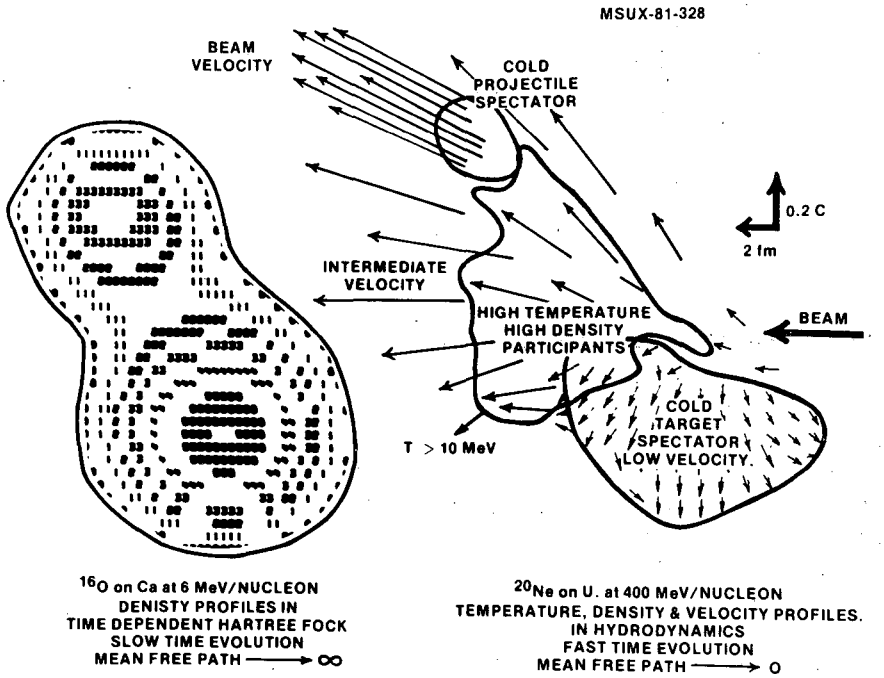

Figure 1. The participant-spectator picture of high energy heavy ion collisions is illustrated at the right by temperature and density profiles calculated with a hydrodynamical model. The participant zone initially contains high density and high temperature nuclear matter. This view of a reaction is contrasted with the picture obtained from a TDHF calculation at low energies shown on the left.

$$E = E_0 + \frac{K}{18}\left(\frac{\rho-\rho_0}{\rho_0}\right)^2 + \frac{\pi^2}{4\varepsilon_F} T^2 \left(\frac{\rho_0}{\rho}\right)^{2/3}$$

which is comprised of the ground state binding energy per particle E_0, the compressional term containing the incompressibility K, and a thermal contribution derived from the low temperature approximation for a Fermi gas; ε_F is the Fermi energy and ρ_0 the normal nuclear matter density of approximately 0.16 nucleons/fm^3. From the free energy F = E - TS, with the specific entropy

$$S = \frac{\pi^2}{2\varepsilon_F} T \left(\frac{\rho_0}{\rho}\right)^{2/3} ,$$

we obtain

$$F = E_0 + \frac{K}{18}\left(\frac{\rho-\rho_0}{\rho_0}\right)^2 - \frac{\pi^2}{4\varepsilon_F} T^2 \left(\frac{\rho_0}{\rho}\right)^{2/3} .$$

The pressure as a function of ρ and T can be calculated from,

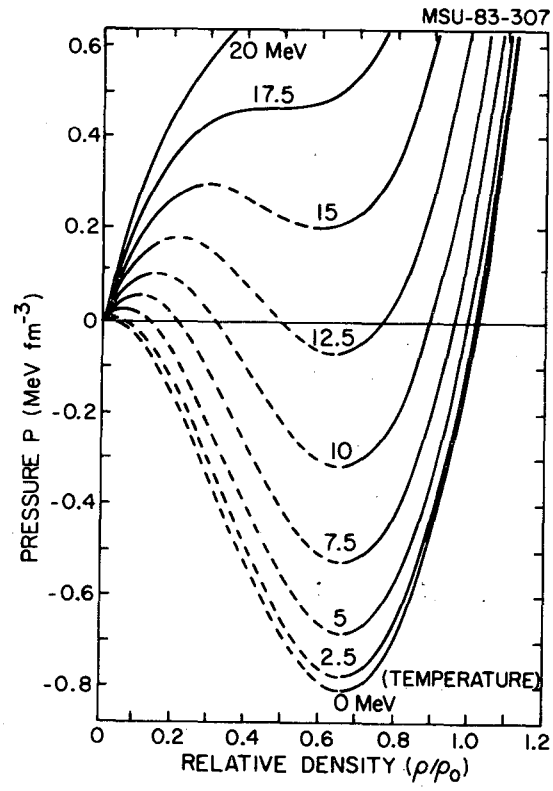

Figure 2. The equation of state for a nuclear system is illustrated by isotherms for pressure versus density. The isotherms separate into two regions which can be identified with liquid and gas phases in a Van der Waals system, connected by a region of negative incompressibility (shown dashed).

$$P = \left(\frac{\partial F}{\partial V}\right)_T = \rho^2 \left(\frac{\partial F}{\partial \rho}\right)_T$$

Results for a more complete calculation[5] are shown in Figure 2, where it can be seen that the equation of state has the form of a Van der Waals system, for the simple reason that the nuclear and molecular systems are analogous; both are subject to short range attractive forces and very short range repulsions.

As in the Van der Waals system, there exist liquid and gaseous phases. For the unphysical region (shown dashed in Figure 2) where the slope of P versus ρ is negative (implying a negative incompressibility) a Maxwellian construction is employed, along which the liquid and gas phases coexist. This region of coexistence is illustrated[11] more clearly in Figure 3, which also shows that as the temperature increases, the apex of the coexistence region coincides with the inflection point of the critical temperature. This point corresponds to the condition,

$$\frac{\partial P}{\partial \rho} = \frac{\partial^2 P}{\partial \rho^2} = 0$$

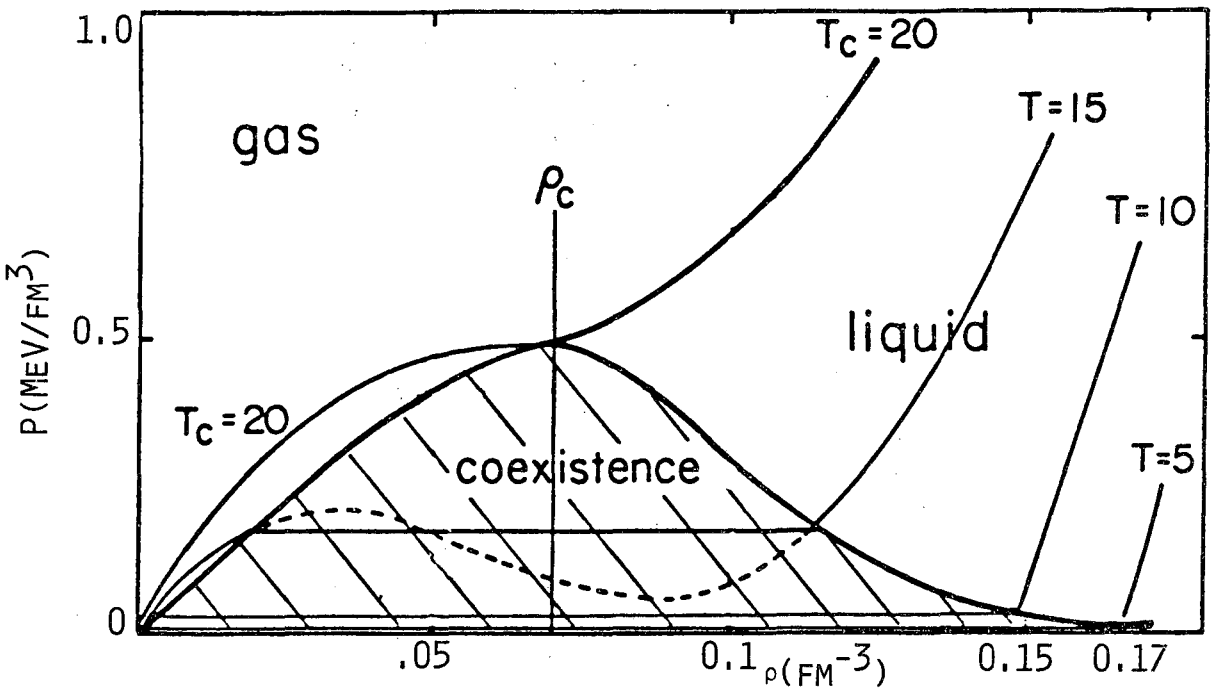

Figure 3. Pressure-density isotherms in which the region of negative compressibility is suppressed (compare Figure 2) by the Maxwell construction describing a phase transition between liquid and gas. The region of phase coexistence is shown by the cross hatching. Above T = 20 MeV only a single gas phase exists irrespective of the density. The critical density is 0.065 fm^{-3}.

A solution of the above analytical expressions with K ≅ 210 MeV, consistent with measurements of the monopole excitation, gives a result close to that obtained from a more detailed analysis, viz $T_c \cong 18$ MeV and $\rho_c \cong 0.07$ nucleons fm^{-3}. For all higher temperatures only a gaseous phase exists.

Most studies of heavy ion collisions at relativistic energies have been conducted in regions where the temperature exceeds 20 MeV. In the later discussion on observable consequences we shall show that temperatures for the participant zone of 20 MeV and lower are generated in collisions below 100 MeV/nucleon, implying that intermediate energy heavy ion studies will be most important for the investigation of these critical phenomena.

Another type of instability, which would occur on a faster time scale than the liquid-gas transition, has also been discussed recently.[14] This concerns a mechanical instability where the compressibility of the nuclear system $K = \rho \frac{\partial P}{\partial \rho}$ becomes negative. Such a region is easily identified in Figure 2 by the dotted lines, but is shown more clearly in Figure 4 where K is plotted as a function of density for different temperatures. The region of zero or negative compressibility falls below the horizontal axis. The corresponding boundary is transposed onto the plot of internal energy as a function of density in Figure 5. Here the region labelled "unstable zone" defines where nuclear matter becomes dynamically unstable. Expressed alternatively the boundary traces out the locus of the tensile stress of nuclear matter as a function of temperature. The authors of Ref. 14 argue that the occurrence of nuclear fragmentation as a dominant reaction process depends on whether the system enters

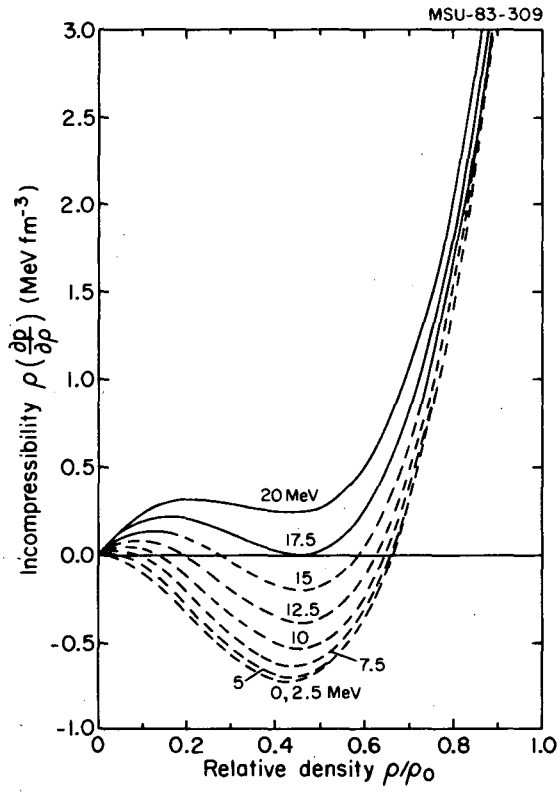

Figure 4. The rigidity $\rho \frac{\partial P}{\partial \rho}$ plotted as a function of density for various temperatures. The region of negative incompressibility, shown dashed in Figure 2, corresponds to the part of the diagram below the horizontal axis. The rigidity of the liquid is much larger than that of the gas.

this unstable region. Since the zone has a boundary of lower than normal nuclear matter density, it is necessary to consider how it can be reached, given that a nuclear system is prepared in a reaction at normal or greater than normal density.

The region labelled "overstressed zone" on Figure 5 defines a boundary which will under certain conditions allow the system to reach the unstable region. Initially a nuclear reaction carries the system from the ground state to some point with higher internal energy. If the energy is transferred by a proton, it is plausible to assume that no significant compression takes place. On Figure 5 the system moves vertically upwards on the diagram from the minimum at normal nuclear density, requiring an injection of approximately 10 MeV per particle. On the other hand, for heavy ion collisions we expect some compression to occur, which prepares the system initially at a point to the right of the minimum of normal density. From this condition it is assumed that the nuclear system will expand along an isentrope until a point of equal internal energy is reached on the left. The justification for an expansion at constant entropy is based on cascade calculations,[15] which indicate that little dissipation takes place; other evidence comes from our knowledge of the monopole vibration, which has a damping width much smaller than its excitation.[16] In Figure 5 the region of appropriate initial conditions which will provide access to the fragmentation zone is defined by the dashed boundary of the shaded region

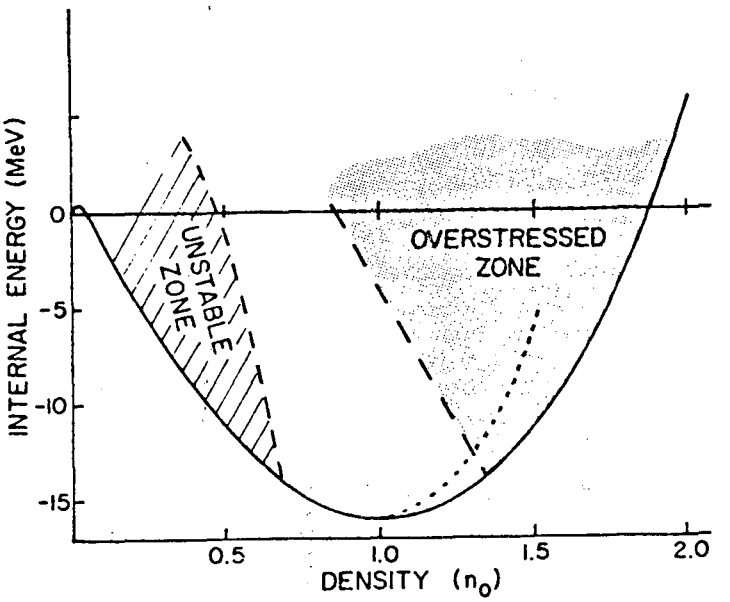

Figure 5. The internal excitation energy per nucleon is shown as a function of relative density. The shaded portion on the left, labelled "unstable zone", defines the region of negative incompressibility. The shaded area on the right defines the overstressed zone from which a nuclear system will be able to reach the unstable zone through an isentropic expansion. The dotted locus extending into the overstressed zone indicates the trajectory expected from theoretical calculations of heavy ion collisions.

labelled "overstressed zone". For example, a compression of 1.4 over normal density is predicted[17] in TDHF calculations at 10 MeV/nucleon (see the dashed line to the left of the S = 0 isentrope in Figure 5), and if it is assumed that all of this excitation energy is thermalised, then the threshold for fragmentation would be lowered to 3 or 4 MeV/nucleon. The corresponding incident energy in the laboratory, assuming again equal participation from target and projectile, would be in the region of 12 MeV/nucleon. Above this threshold the system will always come apart in fragments. An observation of the onset of fragmentation might therefore provide a means of inferring the density at which thermalization takes place; the energy threshold for fragmentation should be an increasing function of the initial density. We shall return to this predicted behavior in Section 5.

3. Time Scales

The mechanical and chemical instabilities we have discussed are quite different in nature. One is a first order transition applicable to processes that occur slowly enough for an equilibrium to be established across the phase boundary. According to the picture of expansion and rarefaction of the initial compressed zone on a time scale commensurate with the frequency of the monopole vibration, this time can be estimated from the typical excitation energy in a

medium weight nucleus,[15] $E \cong \hbar\omega \cong 15$ MeV, resulting in an expansion time of the order 10^{-22} sec. This time scale is the relevant one for a mechanical instability. It is not clear, however, if a liquid-gas chemical instability can be established on this short time scale, since there must exist sufficient time for equilibration to be established across the phase boundary. The time required for this equilibration to occur is of the same order as the evaporation time, an estimate of which can be obtained from the theory of thermionic emission.[18] Thus the current density can be expressed as

$$J = \frac{em}{2\pi^2\hbar^3} T^2 (1 - r) e^{-W/T}$$

where r is the quantum mechanical reflection coefficient (taken as 0), W is the work function (taken as 8 MeV) and T is the temperature. By definition

$$J = \frac{\Delta q}{\Delta t} \frac{1}{A}$$

where A is the surface area of the emitting source. If we set q = e (equivalent to the emission of one nucleon) then $\Delta t = \tau_{evap}$. Assuming a spherical geometry, so that $A = 4\pi R^2$ where $R \cong 3.5$ fm. as determined from the participant-spectator model for intermediate impact parameters[19] and consistent with determinations from pion interferometry measurements,[20] the evaporation time is found to be

$$\tau_{evap} \cong 3.5 \times 10^{-21} \cdot \frac{1}{T^2} \cdot e^{8/T} \text{ sec.}$$

The resulting values given in Table 1 are in good agreement with results deduced from an empirical fit to the measured widths of compound nuclei for A = 20 - 100.[21] Comparing the evaporation time with the time required for disassembly it appears that for $T \gtrsim 8.1$ MeV (henceforth referred to as the breakeven temperature) the liquid-gas phase instability may develop.

Table 1. Nucleon evaporation times as a function of temperature.

T (MeV)	5	10	15	20
t (10^{-22} sec)	6.9	0.77	0.27	0.13

Since a liquid-gas phase instability exists only for temperatures below the critical temperature and above the breakeven temperature, it is obvious that if the breakeven temperature were higher than the critical temperature, the liquid-gas instability would not develop. The critical temperature of approximately 20 MeV predicted in Refs. 10 and 11 was deduced on the assumption that the binding energy per nucleon in nuclear matter is 16 MeV/u compared to the phenomenological binding energy per nucleon of 8 MeV for finite nuclei. A more thorough treatment of this question and of effective mass considerations is given in Ref. 12, where it is shown that in finite nuclei the predicted critical temperature lies between 13.4 MeV and 8.1 MeV depending on the choice

of effective mass. Thus for temperatures above 8 MeV the liquid-gas instability may develop and there is sufficient time for it to do so.

Collision damping has been neglected throughout this discussion. A simple approach[22] to the problem begins with the equation for a damped non-driven oscillator:

$$\ddot{x} + \gamma x + \omega_0^2 x = 0$$

$$x = \rho - \rho_{min}(S)$$

$$\Gamma = \frac{\gamma}{\omega_0^2 - \frac{1}{4}\gamma^2}$$

where γ is the damping coefficient (assumed constant) and ω_0 is the undamped harmonic oscillator frequency. The dimensionless damping coefficient can be deduced from experimental measurements of the monopole oscillation characteristics. The variable ρ_{min} is the value of the density when the excitation energy is a minimum for a given value of the entropy. The damping constant determines the rate at which energy is transferred to thermal energy from the collective motion, thus determining the temperature. For a given value of the density, the entropy can be calculated and ρ_{min} can be determined. Although the oscillation in the density coordinate is not a true harmonic motion we shall use this approximation for small excursions from the equilibrium density. A solution to the above equation is of the form,

$$x \cong Ae^{-\gamma t/2}\cos(\omega t)$$

where

$$\omega^2 = \omega_0^2 - \frac{1}{4}\gamma^2$$

The time required for disassembly is then

$$t \cong \frac{\pi}{\sqrt{\omega_0^2 - \frac{1}{4}\gamma^2}}$$

The empirical full width at half maximum (FWHM) of the monopole excitation is typically $\cong$ 4 MeV for an excitation energy of 15 MeV.[23] Table 2 illustrates how values of the damping constant influence the breakeven temperature for the onset of the liquid-gas instability. In Figure 6 the overstressed region is redefined assuming that the damping constant remains fixed at $\Gamma = 0.27$ (indicative of T = 0 damping) and is not a function of temperature. The minimum

Table 2. Breakeven temperatures for various values of the dimensionless damping constant.

Γ/Γ ($T \cong 0$)	0	5	10	20
$T_{breakeven}$ (MeV)	8.1	7.6	6.9	5.8

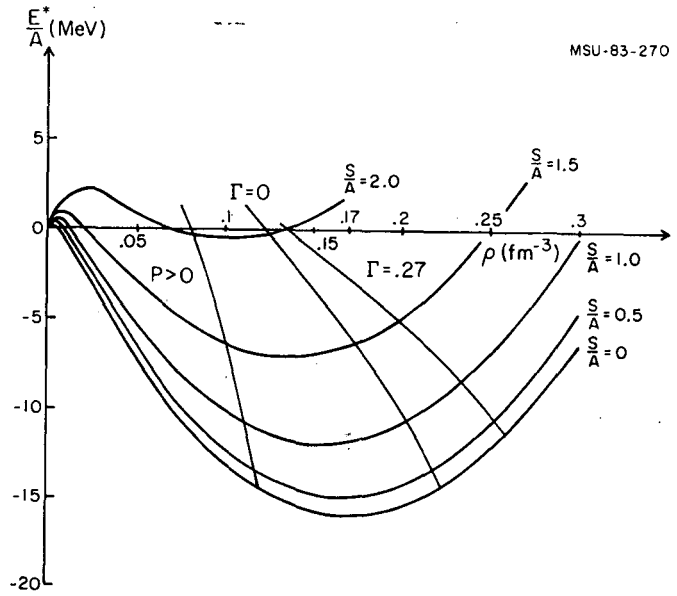

Figure 6. Compared to Figure 5, this figure shows two determinations of the boundary of the overstressed zone. One, labelled $\Gamma = 0$, is identical to that of Figure 5, and the other, $\Gamma = 0.25$, takes into account damping effects during the expansion, increasing the threshold energy for reaching the unstable zone.

excitation energy of the overstressed region becomes 4.75 MeV above the binding energy of normal nuclear matter ($E = -16$ MeV) with $\rho \cong 1.5$ times normal nuclear density. For an equal mass of projectile and target the minimum incident energy required is 4 times the excitation energy, i.e. approximately 19 MeV per nucleon. If this incident energy is insufficient to generate a compression of 1.5 times normal nuclear density, then the minimum required energy will be even larger.

4. Experimental Consequences

The great tragedy of Science--the slaying of a beautiful hypothesis by an ugly fact

T.H. Huxley, Collected Essays

So far there have been few experiments specifically directed at observing the influence of low energy critical phenomena. In this section we review some of the types of data which may be relevant. It is well known that in high energy proton-induced spallation the cross section for fragment production increases dramatically up to energies of a few GeV, followed by a levelling off in the cross section. An example[24] is illustrated in Figure 7 for p + Ag leading to ^{24}Na. The saturation is usually attributed to a limitation of the energy deposition in the nucleus when it becomes transparent to protons of a few GeV. On the other hand, the behavior may be related to the onset of fragmentation when the system reaches the overstressed region.[14] For the system

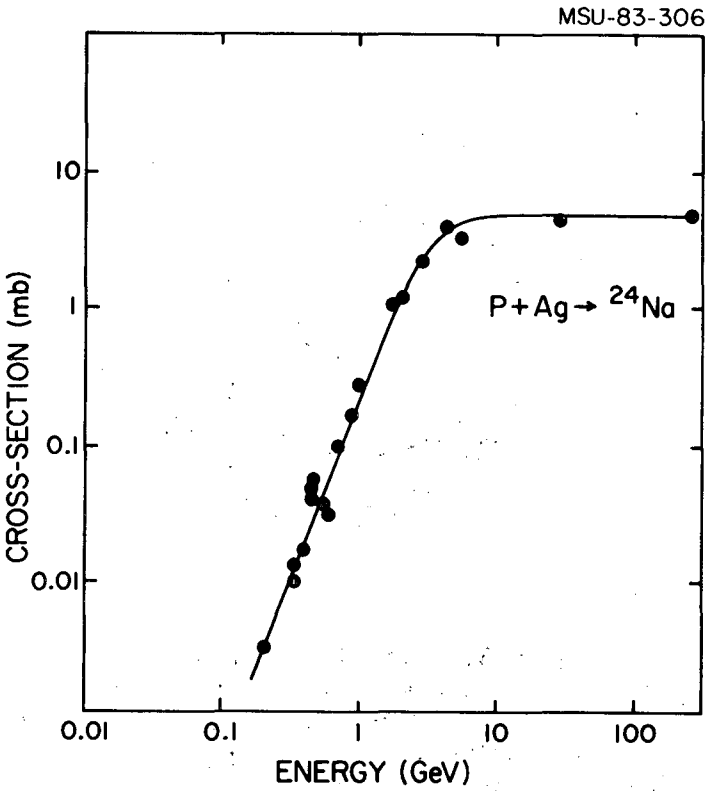

Figure 7. The cross section for the production of ^{24}Na in spallation reactions induced by protons on Ag as a function of incident energy. Following a rapid rise, the cross section saturates at energies above 2 GeV.

p + Ag with about 108 nucleons, our previous discussion would imply that about 1 GeV of energy is necessary. Of clear interest here would be a comparison with heavy ion induced fragmentation in order to discover if the saturation sets in at a lower energy in the presence of some compression. A preliminary comparison of this type is shown[25] in Figure 8, from which there is some indication that a lower threshold may indeed exist in heavy ion proton induced reactions leading to the production of ^{24}Na and Sc isotopes with a Au target.

We should also point out that other approaches to high energy proton induced break-up of a target have recently been discussed; for example,[26] in the process of "cleavage" a high energy proton drills a hole through the nucleus and when the hole expands bonds are broken to release the observed nuclear fragments. A simple argument can be used to show that the energy per particle released in this process may be considerably smaller than the estimate of the energy of 10 MeV/particle required to access the overstressed zone. The cleavage model does appear to give a satisfactory descripton of the absolute production cross sections and energy distribution of the fragments, although so far it has mainly been applied to more massive fragments than have been explained by the models of critical phenomena.

At very high proton energies of 30-350 GeV, the proton induced data have also been interpreted in terms of critical phenomena associated with a liquid-

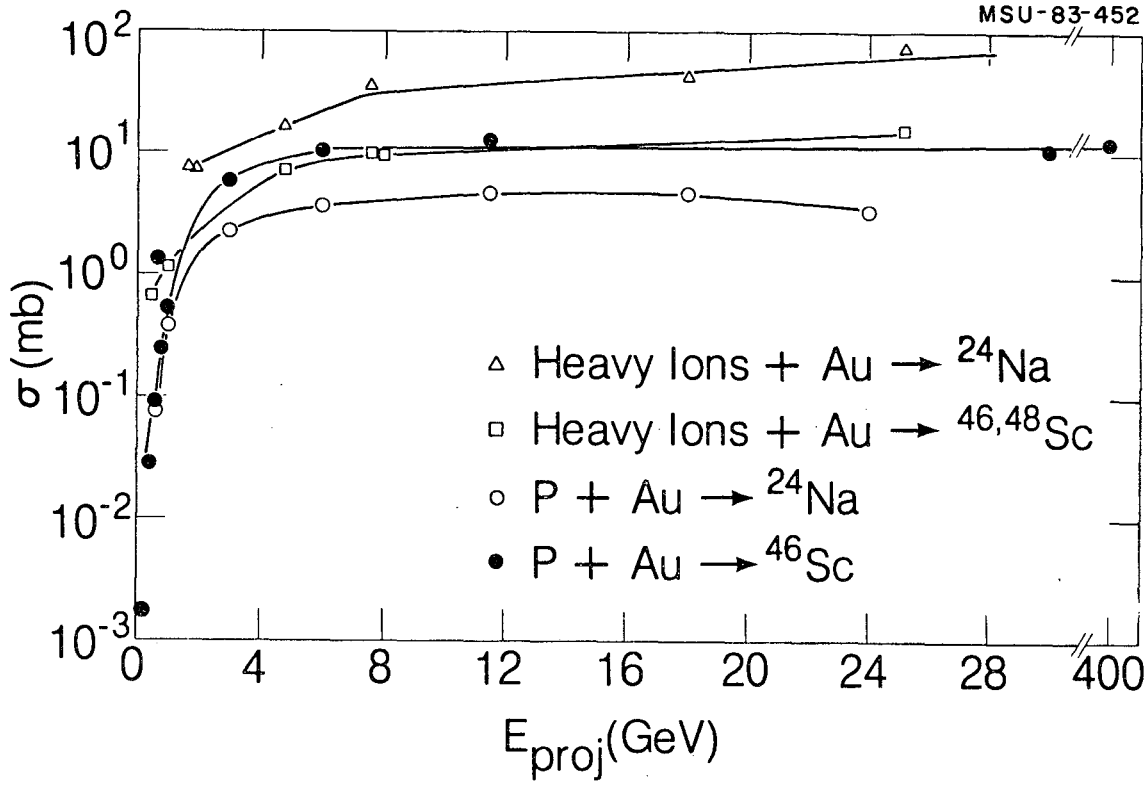

Figure 8. A comparison of yields of ^{24}Na and ^{46,48}Sc in proton and heavy ion induced reactions. There are some indications for differences in the energy at which saturation sets in.

gas phase transition.[27,28] The observation that the mass yield of fragments obeys a power law in fragment mass number, A_F, viz

$$Y(A_F) \propto A_F^{-\tau}$$

with $\tau \cong 2.6$ is taken as a signature for fragment formation near the critical point. According to the theory of condensation in gases and liquids developed by Fisher,[29] this power law describes the size distribution of resulting droplets, and τ is predicted to have a value in the interval $2 < \tau < 3$. An example of the distribution of fragments fitted with this power law is shown in Figure 9, using an exponent of 2.34. Values of the critical density are found to be $\cong \rho_0/2$ in this study; the extracted critical temperature, $T_c \cong 4$ MeV, is, however, well below the value of 17.5 MeV mentioned in Section 2. We recall that this value was appropriate for the case of infinite nuclear matter. When a more complete treatment of effective mass and binding energy corrections are included the value of T_c is lowered[12] to the region 8-13 MeV, but it is still much higher than 4 MeV. We must note, however, that there are difficulties in extracting temperatures from the experimental data, since the values obtained from the distribution of isotopes and energies differ.

The pure power law form applies strictly only at the critical temperature. Following the treatment of Siemens,[30] one can write in general that the

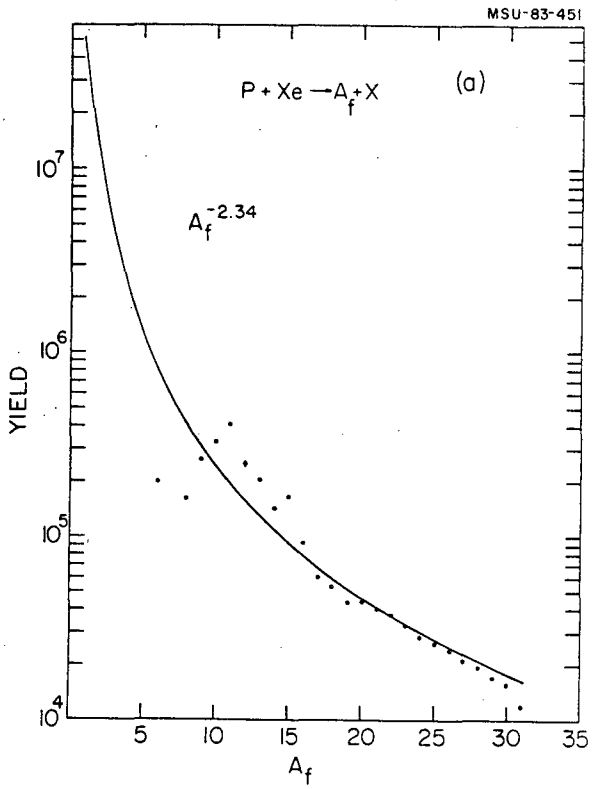

Figure 9. Yield of fragments from the reaction P vs. Xe, typical of the incident energy range from 80 to 350 GeV. The line describes a power law dependence $A_F^{-2.34}$ indicative of critical phenomena of condensation.

probability P_A of finding a cluster A in the fluid is given by

$$P_A \propto A^{-\tau} \exp[-b(T)A^{2/3}]$$

where $b(T) = 4\pi r_0^2(T) \frac{\sigma(T)}{T}$ with $\sigma(T)$ the surface energy coefficient. At zero temperature $\sigma(T)$ takes the value of 1.14 MeV/fm^2, familiar from the liquid drop mass formula. As the temperature is increased the liquid density approaches the critical density of about 0.065 nucleons per fm^3; since the gas density also approaches the critical density, the density difference at the interface vanishes and the surface energy approaches zero.

In Figure 10 a calculation of the surface energy as a function of temperature is shown[31] for three values of compressibility, where the nuclear potential energy is treated within Breuckner's energy-density formalism with appropriate corrections for surface and asymmetry effects. We see that for $K \cong 230$, close to values of the compressibility derived from measurements of the monopole excitation, σ is predicted to vanish at $T \cong 12$ MeV. A rather similar value is obtained by Sauer et al.[32] who parametrize the surface energy coefficient by

$$\sigma = 1.09(1 - 7.16 \times 10^{-3}T^2) \text{ MeV fm}^{-2}$$

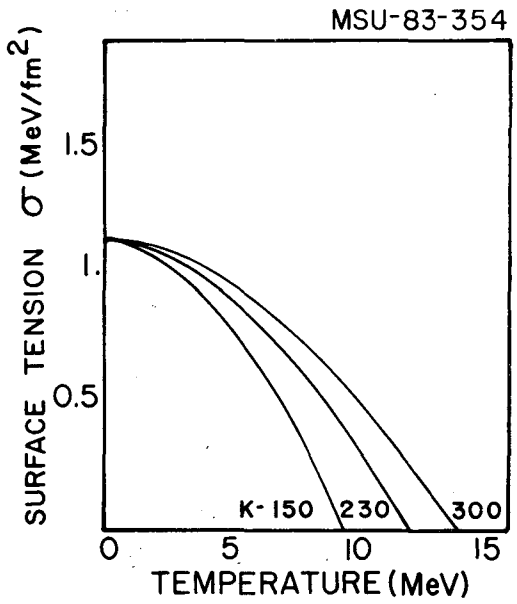

Figure 10. The surface tension σ as a function of temperature for several ground state compressibilities.

which reaches zero at 11.82 MeV. It is encouraging that these deviations result in critical values of the temperature in rather close agreement with the values deduced from studies of the critical temperature of the liquid-gas phase instability in finite nuclei. The consistency implies that studies of fragment production as a function of energy could add to our knowledge of the temperature dependence of nuclear parameters such as the surface energy coefficient. The expected A dependence[30] of the cross section for values of the temperature below near and above the critical temperature are shown in Figure 11. In this calculation a critical exponent of 2.0, a temperature of 8 MeV, and a surface coefficient of 10 MeV were used for $T < T_c$. The dotted line for $T > T_c$ gives a more rapid fall-off as would be predicted, for example, by the coalescence model.[33] In this model the production cross section of a fragment of mass A depends on the Ath power of the single nucleon cross section, giving rise to a steeper A dependence than in the expression for $T = T_c$.

In order to determine the incident energies required in a heavy ion collision to reach temperatures appropriate to the instabilities, we refer to Figure 12 which gives values of temperature derived from a study of particle emission from the participant zone of local high temperature and high density nuclear matter. The temperatures were extracted[34] from the energy spectra of emitted light fragments ranging from protons to ^{12}C in reactions induced by incident projectiles from α particles to Argon. Spectra were fitted with a "moving source model", characterized typically by a velocity half the projectile velocity, i.e. a source of intermediate rapidity such as would be expected if projectile and target contribute roughly equal numbers of nucleons to the formation of the hot zone. At high energies of several hundred MeV/nucleon and above, direct evidence for the existence and size of such a localized zone comes from experiments on two-particle interferometry.[19,35] Although no such convincing proof is yet available at intermediate and low energies, we shall

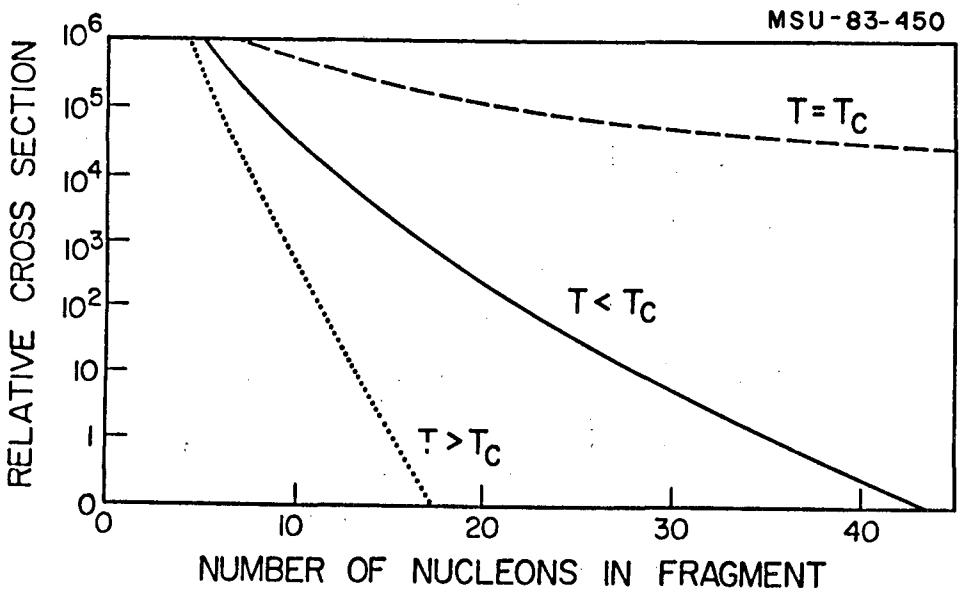

Figure 11. Expected dependence of cross sections on fragment mass A for temperatures above (dotted line), at (dashed line), and about half (full line) the critical temperature T_C. The critical exponent used was 2.0, the surface coefficient was 10 MeV, and the temperature was 8 MeV for the full line (see Ref. 30 for details).

also make use of the results of Figure 3 for the temperature as a function of incident energy.

In part justification we note that the trend of temperatures in Figure 3 is roughly that expected for a Fermi system composed of equal numbers of projectile and target nucleons. Thus, if we write the expression for temperature in a Fermi system as $E^* = T^2/16$, where E^* is the excitation energy per particle and the factor 1/16 comes from the level density parameter, then the result $E = 1/4\ (E_L/A)$ follows, where E_L/A is the incident laboratory energy per particle. Then $T = 2\sqrt{E_L/A}$, and for $T \cong 20$ MeV we obtain $E_L/A = 100$ MeV/nucleon in agreement with the experimental result. Temperatures below the critical value of 18 MeV are therefore appropriate to collisions below 100 MeV/nucleon, placing the observation of the liquid-gas phase instability in the intermediate energy regime.

A power law distribution of fragment cross sections has been found to apply in several other reactions, as for example[36] in the reaction of ^{12}C on Ag at 30 MeV/nucleon, shown in Figure 13. Here the dashed line corresponds to $\sigma_Z \propto Z^{-2.6}$; Z is the charge of the fragment and is roughly proportional to the mass. The authors of this work estimate an upper bound for the temperature reached in the reaction of about 12 MeV, which is the value appropriate for equal participation of target and projectile nucleons as shown in Figure 12. For reactions of this type, in which fragments much heavier than the projectile are produced, it is quite possible that a much larger volume of the target nucleus participates; the associated temperatures would then be commensurately lower. More detailed systematic studies as a function of incident energy will be required to clarify the situation.

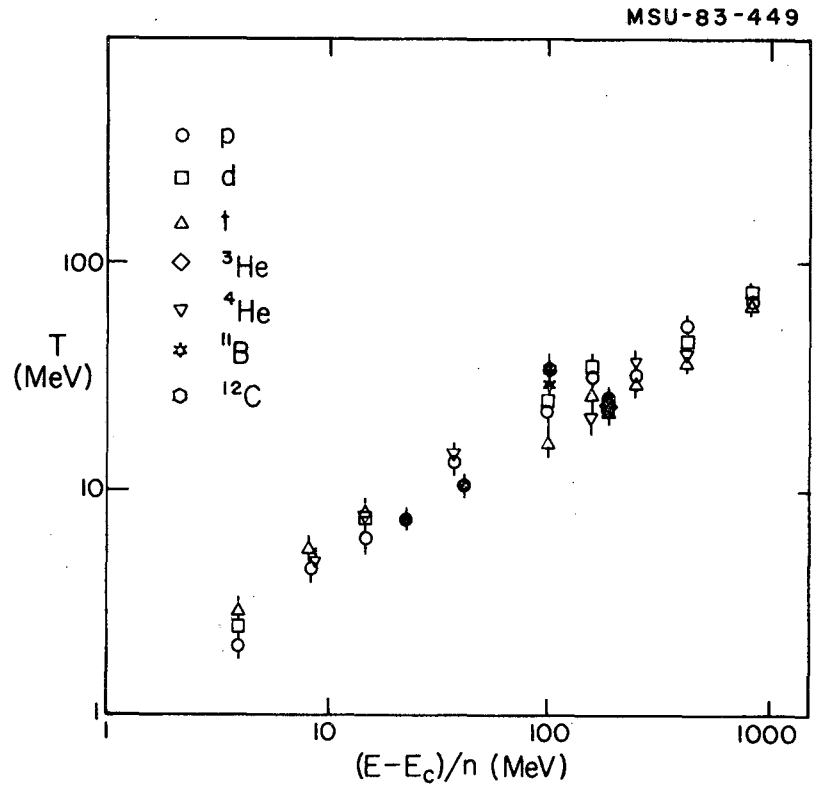

Figure 12. Plot of temperatures as a function of incident energy per nucleon above the barrier, derived from a parameterization of the energy spectra of emitted light fragments with a localized moving source. Results are shown for different emitted fragments p, d, t, ^{3}He, ^{4}He, ^{11}B, and ^{12}C in reactions induced by α, ^{16}O, ^{20}Ne, and ^{40}Ar (see Ref. 34 and references therein for details).

Models which do not explicitly incorporate critical behavior can also be used to explain some aspects of the data we have been discussing. In Figure 13, for example, the data are compared with a statistical model calculation[37] for the idealised case of emission from a completely equilibrated composite system. Isotropic particle emission was assumed, angular momentum effects were neglected, and the level density was assumed to correspond to an ideal Fermi gas at normal density. As indicated by the solid histogram the calculation gives a tolerable account of the data. A similar calculation of the fragment distribution in Figure 9 for high energy proton induced reactions met with comparable success.[38] It bears repeating that only through detailed studies over a range of energies will it be possible to distinguish the different theoretical models, and to confirm the presence of critical phenomena. Other examples of power law behavior are discussed in Refs. 39 and 40.

In the discussion of mechanical instabilities we made use of the cascade result that entropy stays fairly constant during the expansion and cooling of the participant zone. Applying this concept also to the case of a liquid-gas phase instability leads[13] to Figure 14, in which the regions of phase mixture and negative compressibility are defined on a pressure-density diagram with lines of constant entropy. For entropies as high as $S/A \lesssim 3$ the isentropic

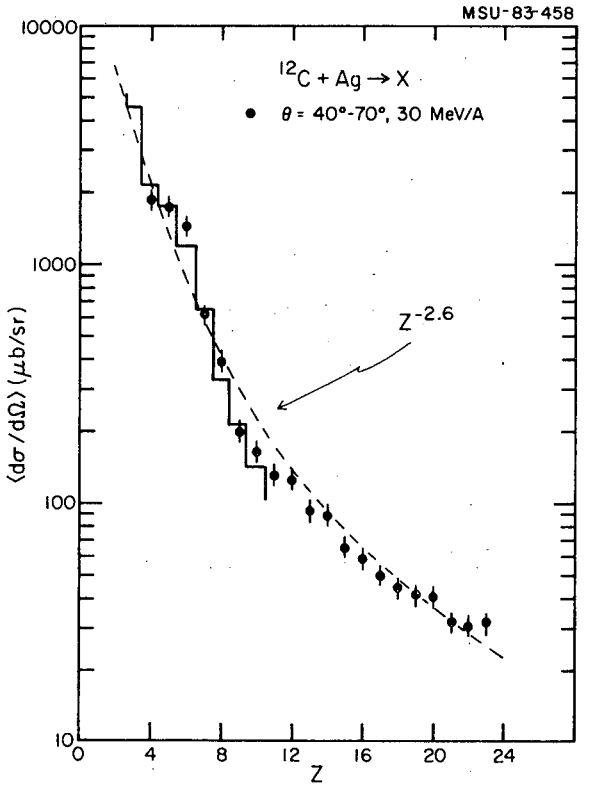

Figure 13. Element production cross sections in the reaction ^{12}C + Ag at incident energy of 30 MeV/nucleon. The dashed line corresponds to a power law dependence $Z^{-2.6}$, and the histogram to a Hauser-Feshbach statistical emission model.

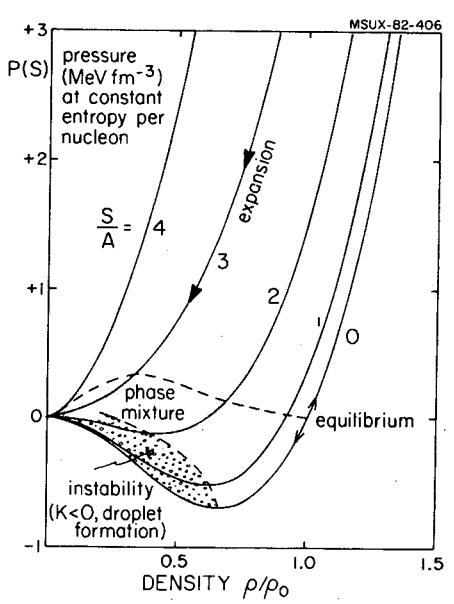

Figure 14. The pressure versus density for a nuclear system as a function of the entropy per particle in the system. The arrows indicate the expansion at constant entropy of the initial compressed and heated zone. The regions of liquid-gas phase admixture and of negative incompressibility discussed for Figures 2-6 are indicated.

lines intersect the region of liquid-gas phase mixture, implying that effects of this instability may be present up to very high bombarding energies of several hundred MeV/nucleon. Now consider a system prepared with initial compression and heating such that the specific entropy S = 2. During the subsequent expansion the temperature and density will drop such that the entropy

$$S = \frac{\pi^2}{2\varepsilon_F} T \left(\frac{\rho_0}{\rho}\right)^{2/3}$$

remains constant. At the intersection with the phase boundary, if a phase transition takes place, the entropy will no longer stay constant but instead the volume will increase at constant temperature along a locus parallel to the horizontal axis in Figure 14. For a system consisting of nucleons only the entropy increase can be derived from the Sackur-Tetrode equation:

$$\frac{S}{A} = \frac{5}{2} + \ln \left(\frac{n_Q}{\rho}\right)$$

where n_Q is the quantum concentration of nucleons. The entropy change is then[13]

$$\Delta S = \ln \rho_{GAS} - \ln \rho_{LIQUID} \cdot$$

Taking values of ρ from Figure 14 we find an entropy increase of $\Delta S \cong 2$ for the case in point. A measurement of entropy as a function of bombarding energy may therefore be a means of detecting the onset of critical phenomena.

Recently it was suggested that a measurement of the yield of complex fragments can be used to measure entropy.[13] In Figure 15 the results of a quantum

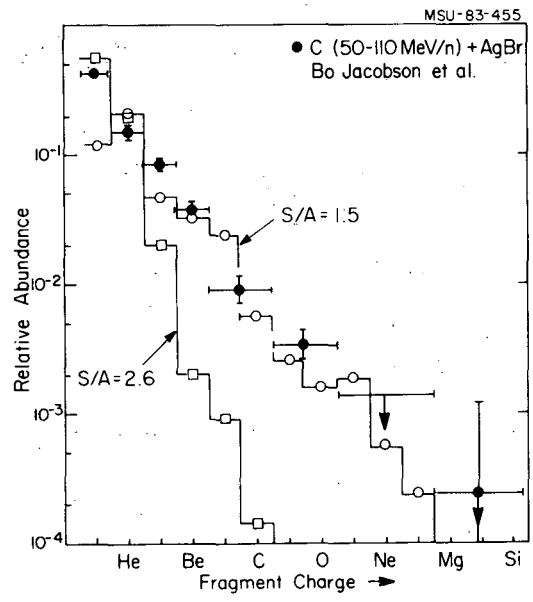

Figure 15. The charge distribution Y(Z) observed in high multiplicity events for the reaction of 50-110 MeV/nucleon carbon in emulsions. The open symbols and histograms are the distributions predicted with a quantum statistical model for two values of the entropy.

statistical model of fragment production are shown for S/A = 1.5 and 2.5. The calculation for S/A = 1.5 is compared with experimental data[41] on complex fragment emission in reactions of ^{12}C in nuclear emulsions at incident energies in the range 50-110 MeV/nucleon. With increasing entropy the yield of heavy fragments decreases rapidly, by two orders of magnitude in the case of nitrogen fragments.

Until recently, emphasis on entropy measurement in heavy ion reactions has focused on the ratio of deuterons to protons emitted from the participant zone, resulting[42] in values which are always in excess of the entropy at the critical point (S ≅ 3.3, see Figure 14). It may be that such light fragments are produced mainly from a gaseous phase. The comparison with heavier fragments emitted from reactions over a wide energy range will be important for establishing the onset of critical phenomena.

5. More General Consequences

The Fairy Tales of Science and the long result of time

Alfred, Lord Tennyson, Locksley Hall

Apart from the intrinsic importance of the critical phenomena, there may also be other less direct consequences which are of interest. Some of these are discussed in this section.

a) Participant-Spectator Model

As we mentioned in the introduction, the participant-spectator model of nuclear collisions is known to be applicable at high incident energies of hundreds of MeV/nuclei; the limit of validity at low energies is unknown but is of interest, since it relates to the question of localization of the energy deposition in a nucleus. A relevant parameter is the temperature dependence of the mean free path, and the results of one calculation[43] are shown in Figure 16. A rather sudden change takes place in the region of 12 MeV, which has its origin in the change of the transport properties of nuclear matter when considered as a liquid or as a gas. There are corresponding sudden changes in heat conductivity and in viscosity. The onset of a localised excitation, or hot spot formation, may therefore set in rather suddenly as a function of energy. Another recent calculation suggests[44] a shortening of the mean free path at approximately 30 MeV/nucleon.

A relevant study is the production of spectator fragments in high energy heavy ion collisions.[45] Such fragments emerge travelling close to beam velocity with a dispersion in momentum determined by the zero point motion of the fragment in the parent projectile, i.e.

$$\sigma^2 = \sigma_0^2 \frac{F(A - F)}{A - 1}$$

where σ is the momentum dispersion, F, A are the mass numbers of fragment and projectile respectively, and $\sigma_0 = P_F/\sqrt{5}$ in the case where the zero point motion is determined by Fermi motion. In Figure 17 the plot of σ_0 obtained[46] from

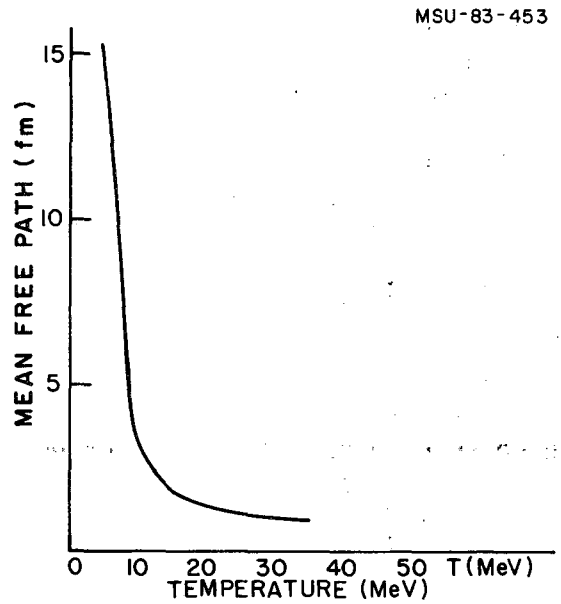

Figure 16. The temperature dependence of the nuclear mean free path. The significant change at T ≅ 10 MeV is associated with the change of mean free path in liquid and gaseous media

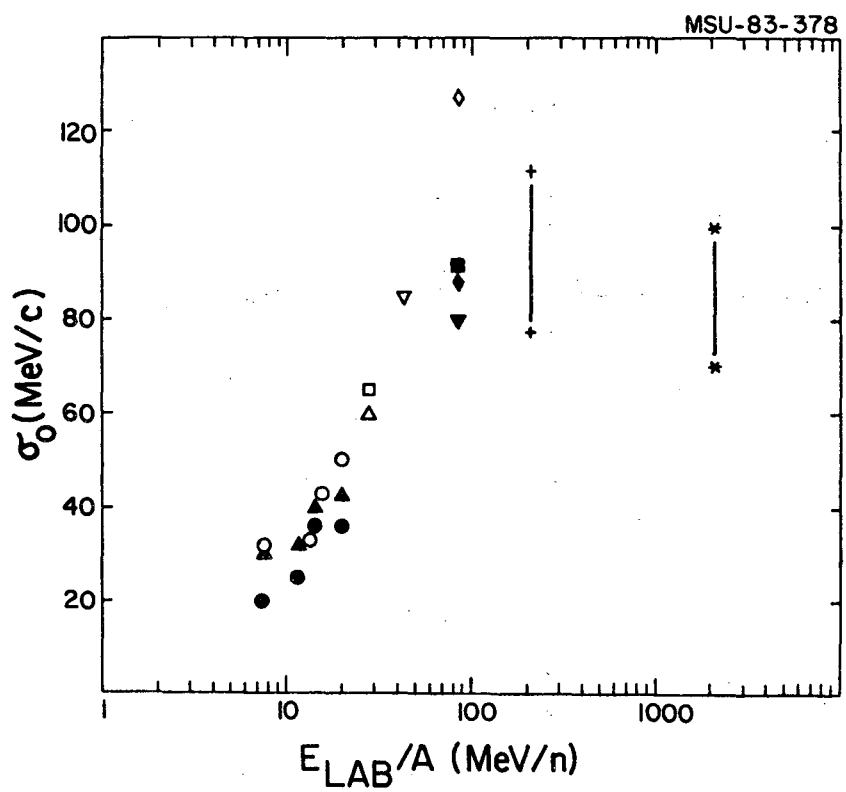

Figure 17. A compilation of several independent measurements of the reduced momentum width parameter σ_0. A large number of such width measurerents have been made at 213 and 2100 MeV/nucleon, and the figure illustrates the full range of the results. There is a tendency for a limiting value of σ_0 to set in at incident energies above 50 MeV/nucleon.

a variety of fragments produced in fragmentation of projectiles ranging from ^{12}C to ^{40}Ar at incident energies up to 2 GeV/nucleon shows that an energy independent limit for $\sigma_0 \cong 90$ MeV/c appears to be established at incident energies beyond $\cong$ 50 MeV/nucleon. According to the participant-spectator model, this could signal the emergence of the spectator picture with an implied onset of the complementary participant localisation. If such an interpretation is substantiated, the energy region of 50 MeV/nucleon may be identifiable with the shortening of the mean free path as a result of the liquid-gas phase transition. Due to critical opalescence it is even possible that in the vicinity of the critical temperature the mean free path may also be influenced by the fluctuations between liquid and gas phases. In macroscopic liquids,[47] a small change of temperature, by as little as a fraction of a degree away from the critical point, can cause the substance to change from being almost opaque to almost colorless. Although no such sharp changes are expected in a finite nuclear system, it is conceivable that some vestige of the phenomenon could persist, and indeed a similar shortening of the mean free path due to critical opalescence has been considered in the case of a phase transition to a pion condensate.[47]

b) Exotic Phenomena

The existence of fragments produced in relativistic heavy ion collisions with interaction lengths much shorter than normal is a topic of great current interest.[49] Among the many possible explanations put forward, some of which have been discussed at this conference, there is one that is closely related to the equation of state in regions of low temperature and density such as we have been discussing. In this domain, cluster formation becomes very important, whereas at high density they are supressed by the Mott blocking mechanism.[50] This blocking--itself in the nature of a critical phenomenon--is mediated by the surrounding hot medium which alters the effective binding energy of the clusters to such an extent that the respective bound states merge into the continuum. The density beyond which clustering is no longer possible is called the "Mott density" and it depends on the velocity of the clusters relative to the surrounding matter. Clusters that move with high velocity are less severely degraded, since the quenching arises essentially from Pauli blocking.

Recent calculations suggest[51] that at very low densities, α-cluster formation may give rise to a new metastable phase. We see from Figure 18 that this region sets in at densities of 1/10 to 1/15 of normal density for temperatures of $T \cong 2$-5 MeV. It develops where the pressure once again crosses zero, corresponding to a stable point on the phase diagram (compare Figure 2). The new region of metastability is shown by the hatching in Figure 19 and disappears at temperatures beyond 12 MeV. This behavior could allow the existence of a low density isomer with a radius much larger than normal nuclei. The authors of Ref. 51 point out that the formation of such α-particle matter may be identifiable with anomalons, although they caution that more detailed estimates of lifetime and the balance of surface and Coulomb energies are necessary to confirm the hypothesis.

The above results, together with the other phenomena discussed in this paper, serve to remind us that the low density and temperature behavior of the equation of state may be a source of interesting new phenomena--like the high density and temperature counterparts. The information provided may also give

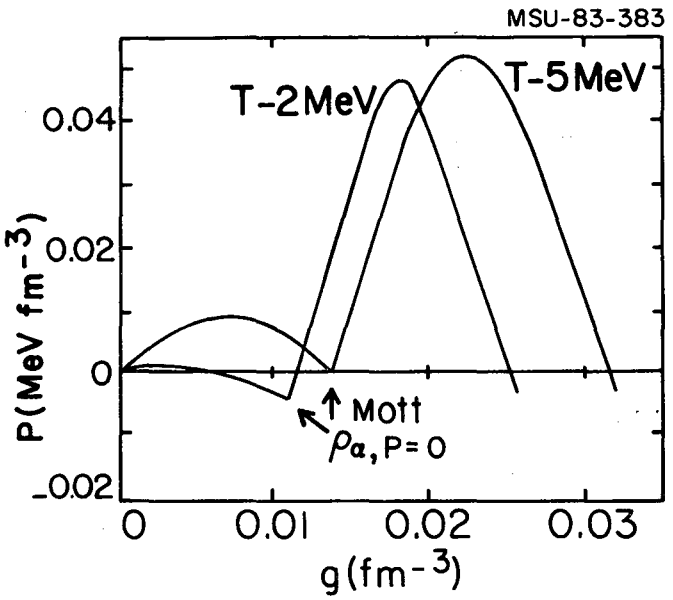

Figure 18. A possible behavior of the equation of state for nuclear matter at very low densities, in which the existence of a new metastable phase determined by clustering effects is predicted. The points labelled $\rho_{\alpha,p}^{MOTT}$ correspond to critical densities beyond which Mott blocking prevents α-cluster formation for zero relative momentum of the clusters relative to the surrounding matter.

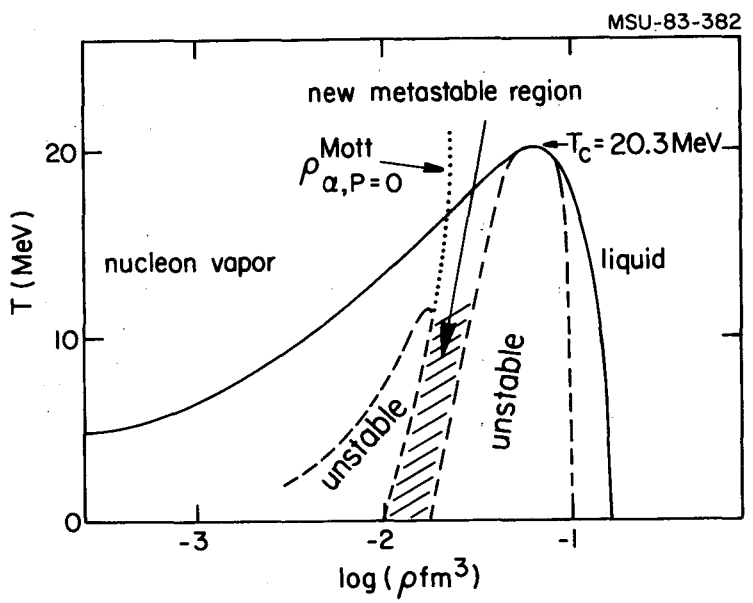

Figure 19. An alternative representation of the phase diagram for nuclear matter showing the coexistence region as well as a predicted new metastable region of α-condensed matter.

insight into other more exotic types of phase transitions, for example to the quark-gluon plasma state expected to be formed when the individual hadron quark bags are forced to overlap by increasing the density or temperature of hadronic matter to high values. Figure 20 gives[52] a P-V diagram for this transition in which three regions are distinguished. There is a hadronic gas region where the pressure rises with reduction in the volume. Eventually the individual hadrons begin to cluster, reducing the Boltzmann pressure since a smaller

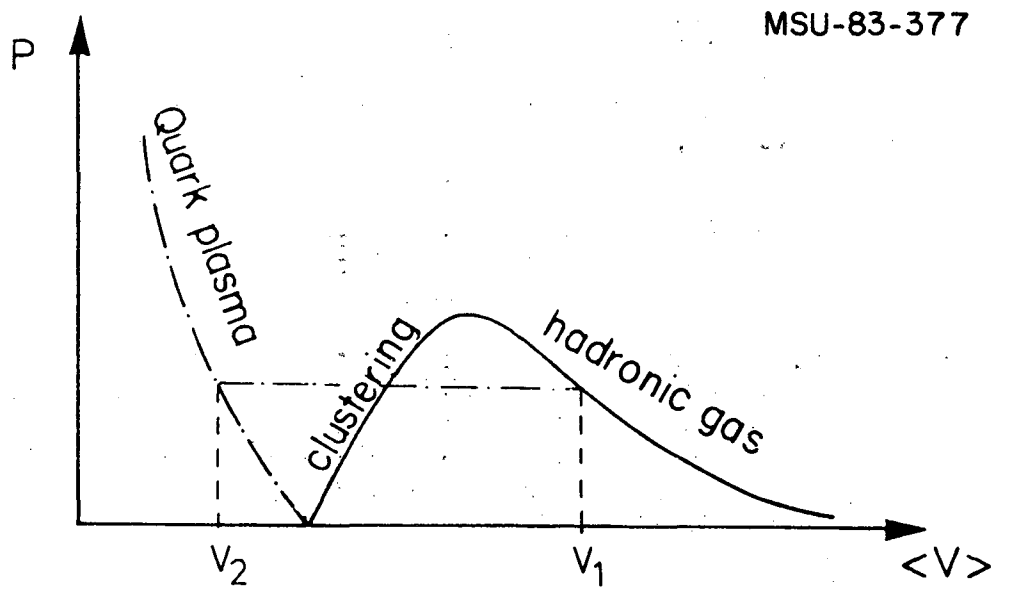

Figure 20. A P-V diagram for hadronic matter. At high densities a phase transition to a quark-gluon plasma is possible. The diagram has a close resemblance to that for the liquid-gas phase transition represented in Figures 2 and 3 for nuclear matter.

number of particles are then present. When the quark-gluon plasma phase is reached the pressure rises again since thereafter only the hadronic constituents are compressed. Clearly this diagram bears a close similarity to Figure 3 which dealt with the analogous problem of liquid condensation from the gas phase. Indeed, many of the problems surrounding the description and the establishment of a phase transition may be rather similar in the two cases--problems, for example, of the time required to establish the transition, the question of the validity of hydrodynamical descriptions of the collision, and so on.

c) Astrophysical Implications

Finally, we mention briefly the interest for astrophysical processes[53,54] of liquid-gas phase phenomena. A well known example of two-phase equilibrium occurs in the crust of neutron stars at temperatures of less than 1 MeV. Also in supernovae, when the inward implosion of collapse is reversed to become an explosion, it is also believed that densities comparable to those in neutron stars are attained with temperatures of 5 to 10 MeV. An understanding of the behavior of matter under those conditions may become possible through studies of nuclear collisions of the type we have discussed in this paper.

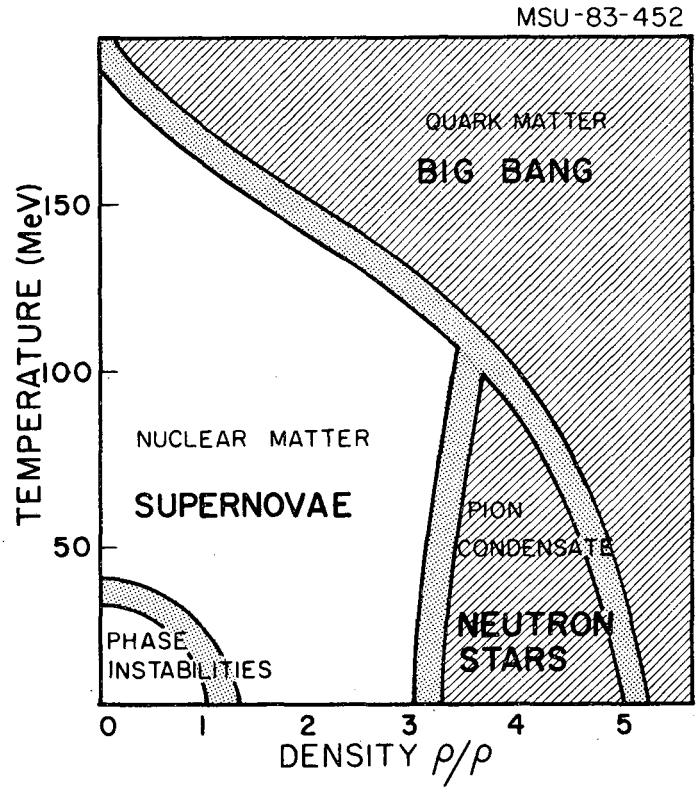

Figure 21. A temperature-density phase diagram for nuclear and hadronic matter. In addition to the exotic phases of quark and pion condensed matter conjectured to occur at high temperature and density, a region of phase instabilities at low temperature and density discussed in this paper is indicated. Each region of phase transition bears a close connection with astrophysical phenomena.

A perspective on the role of the regions of density and temperature we have been discussing is provided by Figure 21. In addition to the three phases of Quark Matter, Pion Condensate, and Nuclear Matter usually displayed, we add an additional region of phase transition, where liquid-gas mechanical instabilities, Mott transitions, and α-condensation may develop. As indicated on the diagram each phase bears a relation to astrophysical phenomena for which the unusual conditions of temperature and density may now become reachable in the laboratory. Thus, while quark-matter may give us our only glimpse of the conditions of matter in the earliest moments of the birth of our Universe, the state of pion condensation--if observed--would simulate conditions prevailing in neutron stars and finally the liquid-gas phase is of direct relevance to supernovae.

6. Conclusion

This paper has dealt with the possibility of investigating critical phenomena in nuclear systems, with particular emphasis on the liquid-gas and mechanical instabilities which can develop at a critical temperatere or at a critical incident energy. Although the phenomena are frequently discussed

and incorporated into calculations of neutron stars and supernovae, the possibility of realising the critical conditions during the evolution of a nuclear collision has only recently been recognised. A study of the approach towards the critical condition can yield information on the temperature dependence of nuclear properties, such as the surface tension. Apart from the intrinsic interest in these phenomena, the phase instabilities may have general implications for the relevance of hydrodynamical concepts in heavy ion collisions and for the localisation of energy deposition through the shortening of the mean free path. The increased interest in the low temperature and low density behavior of the equation of state for nuclear matter has also led to more exotic speculation, for example the creation of metastable phases of α-clustered matter at very low densities, which may be relevant to anomalons. It is also plausible that many of the criteria required for the creation of exotic phases of nuclear matter at high density and temperature, such as the quark-gluon plasma, may be illustrated by phase transitions of the liquid-gas type, the existence of which is based on more accepted knowledge of the equation of state. In particular, questions of time scales and of hydrodynamical behavior are quite pertinent in both cases.

At present there is only sketchy evidence for the existence of critical phenomena of the type we have discussed. The most compelling evidence comes from studies of proton-induced heavy fragment production from a target. Some of the new accelerators will permit new studies of critical phenomena by providing beams of heavy ions over the critical region from 20 to 200 MeV/nucleon. It will take several years for these systematic studies to be completed, because, as we know,

Science moves but slowly, slowly,
creeping on from point to point

Alfred, Lord Tennyson, Locksley Hall

Acknowledgments

I am grateful to many colleagues for discussions, ideas, and data pertaining to this paper. In particular I wish to thank S. Angius, N. Anantaraman, G.F. Bertsch, C.B. Chitwood, M.V. Curtin, G.M. Crawley, D.J. Fields, C.K. Gelbke, B. Hasselquist, B.V. Jacak, J. Kupstas, W.G. Lynch, A.D. Panagiotou, P.J. Siemens, H. Stöcker, H. Toki, B.M. Tsang, H. Utsunomiya, and G.D. Westfall.

My thanks go to Carol Cole for rapid preparation of the manuscript, and to M. Blosser, M. Johnson, and O. McHarris for the illustrations.

This work was supported by the National Science Foundation under Grant No. PHY80-17605.

References

1. M. Gyulassy in Proceedings of the International Conference on Nucleus-Nucleus Collisions (Michigan State University, 1982), eds. G.F. Bertsch, C.K. Gelbke, and D.K. Scott, Nucl. Phys. A400, 31C (1983).
2. H.J. Specht, ibid., p. 43C.
3. H. Satz, ibid., p. 541C.

4. H. Stöcker, J.A. Maruhn, and W. Greiner, Phys. Rev. Lett. 44, 725 (1980).
5. W.A. Kupper, G. Wegmann, and E.R. Hilf, Ann. of Phys. 88, 454 (1974).
6. B. Friedman and V.R. Phandaripande, Nucl. Phys. A361, 502 (1981).
7. D.Q. Lamb, J.M. Lattimer, C.J. Pethick, and D.G. Ravenhall, Phys. Rev. Lett. 41, 1623 (1978); Nucl. Phys. A360, 459 (1981).
8. P. Danielewicz, Nucl. Phys. A314, 465 (1979).
9. M. Barranco and J.R. Buchler, Phys. Rev. C22, 1729 (1980).
10. H. Schulz, L. Munchow, G. Röpke, and H. Schmidt, Phys. Lett. 119B, 12 (1982).
11. M.W. Curtin, H. Toki, and D.K. Scott, Phys. Lett. 123B, 289 (1983).
12. H. Jacaman, A.J. Mekjian, and L. Zamick, Phys. Rev. C27, 2782 (1983).
13. H. Stöcker et al., Proc. of the Int. Conf. on Nucleus-Nucleus Collisions (Michigan State University, 1982), eds. G.F. Bertsch, C.K. Gelbke, and D.K. Scott, Nucl. Phys. A400, 63C (1983).
14. G.F. Bertsch and P.J. Siemens, Phys. Lett. 126B, 9 (1983).
15. G.F. Bertsch and J. Cugnon, Phys. Rev. C24, 2514 (1981).
16. F. Serr, G. Bertsch, and J.P. Blaizot, Phys. Rev. C22, 922 (1980).
17. P. Bonche, S. Koonin, and J. Negele, Phys. Rev. C13, 1226 (1976).
18. J.S. Blakemore in Solid State Physics (W.B. Saunders, Philadelphia, 1974), p. 110.
19. D.K. Scott in Dynamics of Heavy Ion Collisions, eds. N. Cindro, R.A. Ricci, and W. Greiner (North Holland, Amsterdam, 1981), p. 241 and references therein.
20. S. Nagamiya et al., Phys. Rev. C24, 971 (1981).
21. H. Bohning, Proc. of the Int. Conf. on Nuclear Reactions Induced by Heavy Ions, eds. R. Bock and W.R. Hering (North Holland, Amsterdam, 1970), p. 633.
22. M.W. Curtin, H. Toki, and D.K. Scott, Michigan State University Cyclotron Laboratory Preprint MSUCL-426.
23. D.H. Youngblood et al., Phys. Rev. C23, 1997 (1981).
24. R.E.L. Green and R.G. Korteling, Phys. Rev. C22, 1594 (1980) and references therein.
25. K. Aleklett, W. Loveland, P.L. McGaughey, K.J. Moody, R.M. McFarland, R.H. Kraus, Jr., and G.T. Seaborg, Preprints of Contributed Papers to the 6th High Energy Heavy Ion Study and 2nd Workshop on Anomalons (June 1983), Lawrence Berkeley Laboratory Publication LBL-16281, p. 38.
26. S. Bohrmann, J. Hüfner, and M.C. Nemés, Max Planck Institute, Heidelberg Preprint MPIH 1982-V16.
27. J.E. Finn, S. Agarwal, A. Bujak, J. Chuang, L.J. Gutay, A.S. Hirsch, R.W. Minich, N.T. Porile, R.P. Scharenberg, B.C. Stringfellow, and F. Turkot, Phys. Rev. Lett. 49, 1321 (1982).
28. R.W. Minich, S. Agarwal, A. Bujak, J. Chuang, J.E. Finn, L.J. Gutay, A.S. Hirsch, N.T. Porile, R.P. Scharenberg, B.C. Stringfellow, and F. Turkot, Phys. Lett. 118B, 458 (1982).
29. M. Fisher, Physics V3, 255 (1967).
30. P.J. Siemens, Preprint 1983, submitted to Nature.
31. H. Stöcker and J. Burzlaff, Nucl. Phys. A202, 265 (1973).
32. G. Sauer, H. Chandra, and U. Mosel, Nucl. Phys. A264, 221 (1976).
33. S. Das Gupta and A.Z. Mekjian, Phys. Reports 72, 131 (1981) and references therein.
34. S. Angius, M.Sc. Thesis, Michigan State University 1982; S. Angius and D.K. Scott, Annual Report (Michigan State University Cyclotron Laboratory 1981-1982), p. 24.

35. S. Nagamiya, Proc. of Int. Conf. on Nucleus-Nucleus Collisions (Michigan State University, 1982), eds. G.F. Bertsch, C.K. Gelbke, and D.K. Scott, Nucl. Phys. A400, 399C (1983).
36. C.B. Chitwood, D.J. Fields, C.K. Gelbke, W.G. Lynch, A.D. Panagiotou, M.B. Tsang, H. Utsunomiya, and W.A. Friedman, Phys. Lett. B, to be published.
37. W. Friedman and W.G. Lynch, Phys. Rev. C28, 16 (1983).
38. W. Friedman and W.G. Lynch, Phys. Rev. C28, 950 (1983).
39. H.H. Gutbrod, A.I. Warwick, and H. Weiman in Selected Aspects of Heavy Ion Collisions (Saclay, 1982), eds. M. Martinot, C. Ngô, and P. Gugenberger (North Holland-Amsterdam, 1982), p. 177C.
U. Lynen et al., ibid., p. 129C.
41. B. Jakobsson, G. Jönson, B. Linquist, and A. Oskarsson, Z. Phys. A307, 293 (1982).
42. J. Kapusta, Preprint, 1983.
43. S.I.A. Garpman, D. Sperber, and M. Zielinska-Pfabe, Nuov. Cim. 57B (1980).
44. B. Sinha, Phys. Rev. Lett. 50, 91 (1983).
45. D.K. Scott in Proc. of the Int. Conf. on Nuclear Physics (Berkeley, 1980), eds. R.M. Diamond and J.O. Rasmussen, Nucl. Phys. A354, 375C (1981).
46. M.J. Murphy and R.G. Stokstad, to be published, and Lawrence Berkeley Laboratory Publication PUB-5078, 1982.
47. H.E. Stanley, Introduction to Phase Transitions and Critical Phenomena (Clarendon Press, Oxford, 1971).
48. H. Stöcker, J. Hofmann, J.A. Maruhn, and W. Greiner, Progress in Particle and Nuclear Physics, Vol. 4 (1980); M. Gyulassy and W. Greiner, Ann. Phys. 109, 485 (1977).
49. W. Heinrich et al. in Proc. of Int. Conf. on Nucleus-Nucleus Collisions (Michigan State University, 1982), eds. G.F. Bertsch, C.K. Gelbke, and D.K. Scott, Nucl. Phys. A400, 315C (1983).
50. G. Röpke, L. Münchow, and H. Schulz, Nucl. Phys. A359, 536 (1982); Phys. Lett. B112, 13 (1982).
51. R. Schulz, G. Röpke, and M. Schmidt, Z. Phys. A310, 139 (1983).
52. J. Rafelski and M. Danos, Perspectives in High Energy Nuclear Collisions, National Bureau of Standards Publication NBSIR 83-2725, 1983, p. 5.
53. G. Baym and C. Pethick, Ann. Rev. Nucl. Sci. 25, 27 (1975).
54. G.E. Brown, H.A. Bethe, and G. Baym, Nucl. Phys. A375, 481 (1982).

HIGH ENERGY (30-350 GeV) PROTON-NUCLEUS COLLISIONS AND THE DESCRIPTION OF FRAGMENTATION AS A CRITICAL PHENOMENON

A. S. Hirsch, A. Bujak, J. E. Finn, L. J. Gutay, R. W. Minich,
N. T. Porile, R. P. Scharenberg, B. C. Stringfellow, and F. Turkot
Department of Physics and Department of Chemistry
Purdue University and Fermi National Accelerator Laboratory

An inclusive experiment in which nuclear fragments from helium to aluminum were produced in collisions between high energy protons (30-350 GeV) and heavy nuclear targets (xenon, krypton) has motivated the description of fragment production as a critical phenomenon.[1,2] The observation that the mass yield of fragments obeys a power law in fragment mass number, A_f,

$$Y(A_f) \propto A_f^{-\tau} \tag{1}$$

with τ about 2.6 for both targets, was recognized as a possible signature for fragment formation near the critical point of nuclear matter.[1] (Fig. 1) The power law describes the frequency distribution for clusters (fragments) having A_f constituents. Clustering according to a power law with an exponent between 2 and 3 is displayed by many systems near their critical point.[3,4,5] Away from the critical point, the yield is expected to be damped exponentially, thereby suppressing the creation of large clusters.

In pursuing this description of fragment production, we have generalized the classical droplet model by M. E. Fisher for a one component system undergoing a liquid-gas phase transition near its critical point.[6] For a single species substance, the probability to form an ℓ-particle cluster depends on the Helmholtz free energy and the chemical potential per particle

$$Y(\ell) \propto e^{-(f(\ell)-\mu\ell)/kT} \tag{2}$$

The Helmholtz free energy

$$f(\ell) = U(\ell)-TS(\ell) \tag{3}$$

contains bulk and surface contributions to both the cluster binding energy, $U(\ell)$, and entropy, $S(\ell)$. Fisher stated that there existed a term in the free energy which contained the parameter τ. At the critical point, nearly exact cancellation between $f(\ell)$ and μ leaves only the term containing τ and so the power law (1) emerges from (2). This simple description works surprisingly well for real gases from the triple point up to the critical point.[3]

From this point of view, nuclear fragments are formed when the remnant of the proton-nucleus collision approaches its critical point. Precisely how this state is attained cannot be answered at present, but for the sake of argument let us accept the power law (1) as evidence that the remnant is at or in the neighborhood of its critical point. Thus, large density fluctuations occur giving rise to clusters of nucleons, or fragments. The surface free energy is substantially reduced near the critical point, and so the system of fragments is free to disassemble under the influence of Coulomb repulsion. Fragmentation is therefore viewed as a multi-body breakup of the remnant near the critical temperature. We expect that inclusive fragment measurements and those obtained with a heavy fragment trigger will display the same characteristics, since the observation of a fragment is, within this picture, a

signature for the multi-body breakup of the remnant near its critical point. This has recently been confirmed by the data of Warwick et al.[7]

The first step in applying Fisher's model to our data is to parameterize the binding energy term in (3). The natural choice is the Weizsäcker semi-empirical mass formula. The coefficients are in general temperature and density dependent. Following Fisher, the entropy term, S, in (3) contains a bulk term proportional to the number of constituents in the cluster, and a surface term, proportional to the surface area of the cluster or $A_f^{2/3}$. Therefore, we can absorb the heat contribution to the cluster free energy into the appropriate terms in the binding energy parameterization. The Helmholtz free energy becomes

$$f(Z_f,A_f) = a_v A_f - a_s A_f^{2/3} - a_c Z_f^2/A_f^{1/3} - a_a(A_f - 2Z_f)^2/A_f - \delta \qquad (4)$$

where $\delta = a_p/A_f^{.75}$ for odd-odd nuclei, zero for odd-even nuclei, and $-a_p/A_f^{.75}$ for even-even nuclei. The coefficients in (4) represent the volume, surface, Coulomb, symmetry and pairing contributions to the free energy.

Fisher's condensation theory dealt with unimolecular liquids, and thus is not directly applicable to two-component systems. To account for both neutrons and protons we have modified Fisher's model by introducing a chemical potential for each. In addition, we account for the entropy of mixing between neutrons and protons. Finally then, the fragment yield as a function of charge and mass is given by

$$Y(Z_f,A_f) = \frac{C}{A_f^{\tau}} \exp\left[(f(Z_f,A_f) + \mu_N N_f + \mu_Z Z_f)\beta + N_f \ln \frac{N_f}{A_f} + Z_f \ln \frac{Z_f}{A_f}\right] \qquad (5)$$

where $\mu_N(\mu_Z)$ is the neutron (proton) chemical potential and $\beta = 1/kT$.

We have fit our fragment data with the above expression. (See Ref. 2 for parameters.) As the figures in Ref. 2 show, the fit is quite impressive over three orders of magnitude with only 8 free parameters and about 50 degrees of freedom. It should be pointed out that we have not rigorously justified the modifications made to Fisher's theory. However, this model is simple and effective in parameterizing a large quantity of data.

Since the data determine only the products $f\beta$ and $\mu\beta$, we cannot uniquely set the temperature scale. In the simplest approach, we can choose to normalize the parameters by requiring a_v to be equal to its value in normal nuclear matter, 14.1 MeV in the parameterization we have used. With this provision, the critical temperature for nuclear matter is about 3.2 MeV. In the spirit of the classical droplet model, we may estimate that we have included 8 MeV per nucleon of heat in a_v. This would increase the critical temperature to about 5 MeV. Other parameters would be scaled up accordingly. In either case, the temperature obtained is well below the average binding energy per nucleon in a medium to heavy nucleus of 8 MeV.

Let us now discuss the kinetic energy spectra. Several features of the spectra of fragments from targets in our mass range have been previously observed:[8,9,10] 1) the fragments appear to have been emitted from a remnant system, A_r, with a very small velocity along the beam direction, $v/c \sim .002$ for xenon; 2) the fragment (Li and heavier) angular distributions are nearly

isotropic in this moving frame; 3) the kinetic energy spectra indicate that Coulomb repulsion energies are significantly less than tangent sphere values assuming a partner of mass A_r-A_f and charge Z_r-Z_f; 4) the spectra have high energy tails which have an inverse logarithmic slope of about 14 MeV.[11] Point number 4 deserves some elaboration.

We expect that this slope parameter, T', characterizes in some way the system from which the fragment was emitted. In fact, due to momentum conservation, the nucleons comprising the fragment are correlated to the remaining nucleons of the system A_r-A_f, and thus T' depends on both the remnant mass and the fragment mass[12], i.e.,

$$T' = T_o \left(\frac{A_r - A_f}{A_r}\right)$$

It is T_o and not T' which uniquely characterizes the excited remnant. At this point, there is no reason to expect that each fragment is related to a remnant of the same A_r and T_o, yet, when we plot T', obtained from the high energy tails, versus A_f, we obtain a linear relation (Fig. 2). This implies that fragments, on the average, come from a system of approximately 75 nucleons for krypton, and that the remnant system has a T_o of about 14 MeV. Note that a linear relation would not obtain if fragment emission occurred sequentially, since then each A_r would be progressively smaller. The implication is that all the fragments are formed at the same time. Now we must address the question of the nature of the parameter T. If T is interpreted as a thermal temperature, it exceeds by about a factor of two the average binding energy per nucleon in a heavy nucleus. If fragments are formed at an average of 14 MeV temperature, this leads to an excitation energy of about 20 MeV/nucleon using a Fermi gas level density. However, experimental evidence is rather convincing that fragments are formed with substantially less excitation energy, since high excitation energies would lead to alpha particle emission correlated to the hot fragment's motion.[13]

If we accept for a moment the critical temperature, T_c, obtained from the fit to the isotopic data, we see that the temperature equivalent of the ground state mean-squared momentum, i.e.,

$$kT = 2/3 \frac{\langle \vec{p}^2 \rangle}{2M_N} = \frac{1}{5} \frac{p_f^2}{M_N} \qquad (\sim 14 \text{ MeV for a mass 100 nucleus.}^{14})$$

is substantially the greater of the two. Here $\langle \vec{p}^2 \rangle$ is the mean-squared momentum of a nucleon of mass M_N in the nucleus and p_f is the Fermi momentum. Thus, the high energy tails of the kinetic energy spectra may be dominated by the nucleon mean-squared momentum which was present in the cold nuclear target. The additional kinetic energy due to T_c is much smaller. This point of view provides a simple and unified explanation of many facets of the data mentioned above and is consistent with the droplet model of fragmentation which we have developed.

In summary, the power law behavior of the fragment yield from high energy proton-nucleus collisions with heavy nuclear targets suggests that fragmentation may be a critical phenomenon. Parameterizing the fragment Helmholtz free energy in a form resembling the Weizsäcker mass formula has enabled us to fit simultaneously all of the observed fragment yields from a given target. We estimate that the critical temperature for a heavy nucleus is about 3-5

MeV. The high energy tails of the fragment kinetic energy spectra provide evidence that all of the observed fragments are created at the same time from a common system. The tails appear to be dominated by the mean-squared momentum of the nucleon in this system, i.e. Fermi motion. Small Coulomb energies arise naturally in this description since the entire remnant system undergoes disassembly simultaneously.

1. J. E. Finn et al., Phys. Rev. Lett. 49, 1321 (1982).
2. R. W. Minich et al., Phys. Lett. 118B, 458 (1982).
3. C. S. Kiang, Phys. Rev. Lett. 24, 47 (1970).
4. H. E. Stanley, Phase Transitions and Critical Phenomena, Oxford University Press (1971).
5. D. Stauffer, Phys. Rep. 54, 1 (1979).
6. M. E. Fisher, Physics 3, 255 (1967) and Rept. on Prog. Phys. 30, 615 (1967).
7. A. I. Warwick et al., Phys. Rev. C27, 1083 (1983).
8. A. M. Poskanzer et al., Phys. Rev. 3, 882 (1971).
9. G. D. Westfall et al., Phys. Rev. C17, 1368 (1978).
10. Fermilab E442, unpublished.
11. J. A. Gaidos et al., Phys. Rev. Lett. 42, 82 (1979).
12. A. S. Goldhaber, Phys. Lett. 53B, 306 (1974) and Phys. Rev. C17, 2243 (1978).
13. B. D. Wilkins et al., Phys. Rev. C19, 856 (1979).
14. E. J. Moniz et al., Phys. Rev. Lett. 26, 445 (1971).

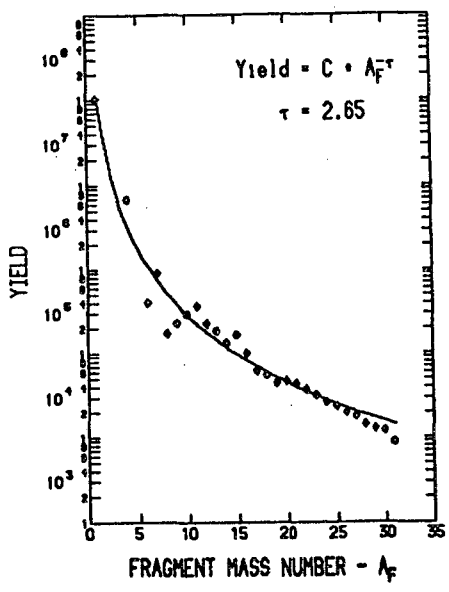

FIG. 1

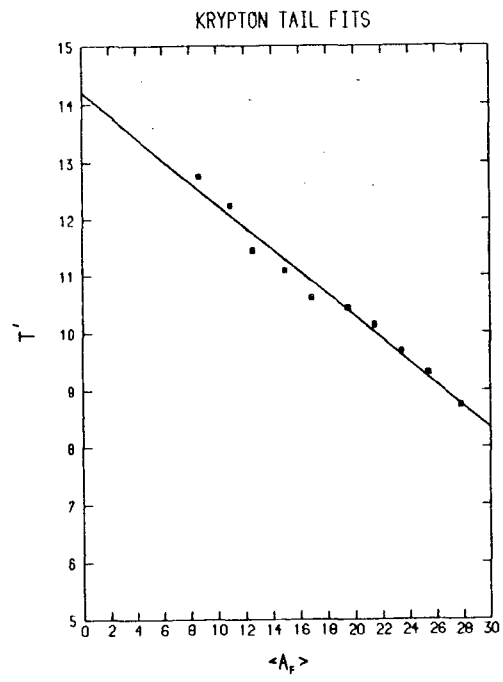

FIG. 2

Aspects of data on the breakup of highly excited nuclei

A.I. Warwick, H.H. Wieman, H.H. Gutbrod, H.G. Ritter, H. Stelzer, F. Weik
Gesellschaft für Schwerionenforschung, Planckstrasse 1
D-6300 Darmstadt 11, West Germany and
Nuclear Science Division, Lawrence Berkeley Laboratory
University of California, Berkeley, CA 94720
and
S.B. Kaufman, E.P. Steinberg, and B.D. Wilkins
Argonne National Laboratory, Argonne, IL 60439

1. Introduction

There is an awakening of theoretical interest in the mechanisms by which nuclear fragments ($4 \leq A < 150$) are produced in violent collisions of heavy ions. With this in mind we review some aspects of the available experimental data and point out some challenging features against which to test the models.

The concept of evaporation is tremendously powerful when applied to pieces of nuclei of low excitation (1 or 2 MeV/u). Current interest focuses on higher excitations, at the point where the binding energy of the system vanishes. This is the transition from liquid nuclei to a gas of nucleons, and it may be that the critical phenomena that certainly exist in infinite nuclear matter will be manifest in finite nuclei under these conditions.

2. Favorable experimental conditions

One might study pieces of nuclear matter at excitation energies corresponding to the zero binding regime by making central nuclear collisions at bombarding energies around 50 MeV/u. However, in these lower energy collisions the multiplicity of fast charged particles is always small making it difficult to pick out central collisions. Furthermore, leading particles and the products of fast knock-out processes are not well separated in rapidity space from the fragments formed in the excited mid-rapidity zone. A clearer approach is to study asymmetric collisions at higher bombarding energies, measuring the products from the highly excited spectator residues. In such collisions the multiplicity of fast charged particles is an excellent parametrization of the violence of each collision and there is a clean rapidity separation between participants and spectators. Figure 1 shows angular distributions of a) heavy fragments from the target residue of a 42 GeV Ne + Au interaction and b) fast light particles from the fireball. The residue is almost stationary in the laboratory frame; the fireball has a large forward velocity. In the most violent collisions of Ne + Au at 2.1 GeV/u we have observed complete disintegration of the Au nucleus into fragments of $A \leq 10$, demonstrating sufficient transfer of energy to the spectator residues in such collisions to make them valuable probes of nuclear matter at zero binding energy.

3. Multifragmentation

For central collisions of asymmetric systems at high bombarding energy (Ne + Au above 250 MeV/u), we have observed[1] the disintegration of spectator residues into several large fragments. It seems likely that such a breakup process corresponds to an excitation energy too large to be appropriate to a conventional evaporation theory and calls for new models.

Figure 2 shows an example of such a measurement. Here a fragment of mass number $20 \leq A < 40$ from Ne + Au is the trigger for the event; these fragments emerge from the highest multiplicity collisions. We plot the multiplicity of coincident fragments as a function of their charge. Note that with 42 GeV Ne + Au one typically observes several neutrons and protons, three heliums, one lithium, one fragment with $4 \leq Z \leq 11$, and one fragment triggering the detectors for this measurement with Z of about 15.

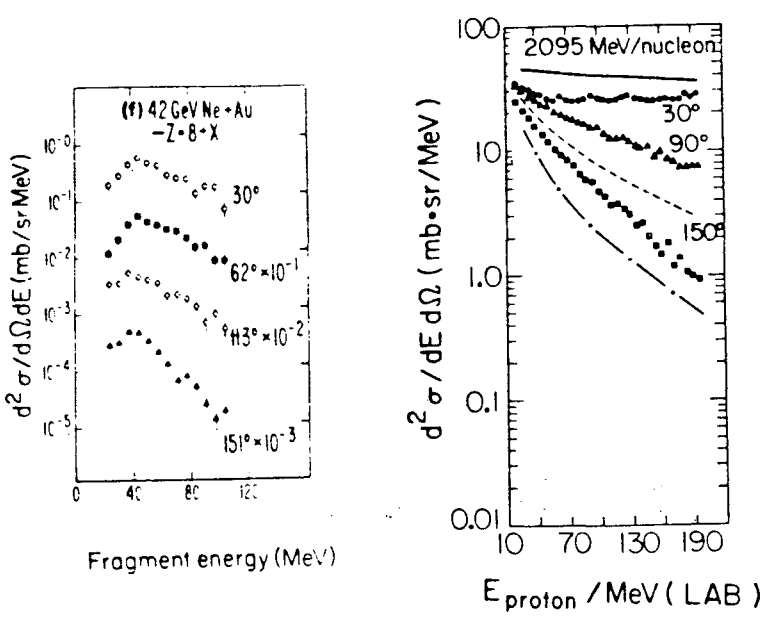

Figure 1. Angular distributions of light and heavy fragments from Ne induced reactions at 42 GeV.

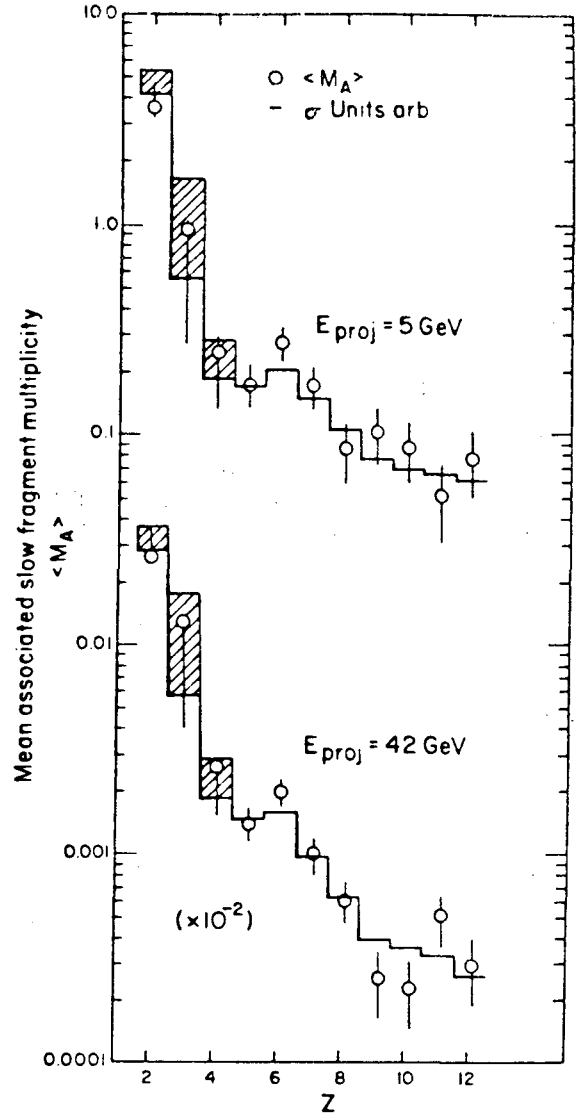

FIG. 2 Open circles show the mean multiplicities of fragments with charge Z associated with a trigger fragment of mass $A = 20-40$ detected at $\theta \simeq 90°$ from the reaction Ne + Au. The histogram represents the singles measurement of fragment yield as a function of fragment charge Z, scaled appropriately for comparison to the measured fragment multiplicities.

4. The mass-yield curve

a) It is important to realize that light and heavy fragments are produced from different classes of collision. In the case of Ne + Au at relativistic energies this can be demonstrated by observing the multiplicity of fast charged particles emitted from each collision.[1] High multiplicities are from large fireballs produced in central collisions and any spectator residues are born out of a violently disturbed system. Low multicities indicate peripheral collisions in which residues have low excitation. Figure 3 shows contours of yield against multiplicity of fast particles and the mass of fragments, from 42 GeV Ne + Au. There is a smooth trend; the highest multiplicity collisions produce the lightest fragments. Note the contribution of peripherally induced fission to the production of fragments around A = 90, accompanied by very few fast charged particles. This can be seen again[2] in fig. 4, which shows the fission yield peaked around 60 MeV, while the deep spallation contribution has a steeply falling spectrum at lower energies. So, for example, one should not attempt to invoke a single mechanism to explain the shape of the entire mass-yield curve.

b) At the low end of the mass yield curve an interesting fact shows up in the yield of the ^{3}He and ^{4}He.[3] The ^{3}He spectrum is very flat while the ^{4}He spectrum contains a very large cross section at low α-energies up to a total yield of 13 barns (fig. 5) with a slope parameter of 14-20 MeV. The conventional view is that alpha particles come from low energy deposition reactions while ^{3}He comes from high deposition energy collisions. We have found, however, that ^{3}He and ^{4}He have the same associated multiplicity of

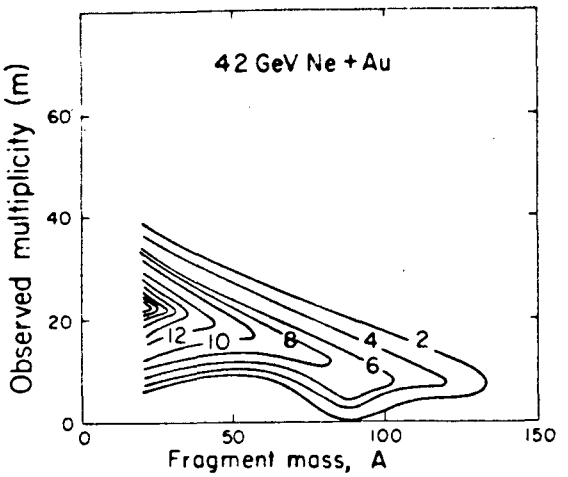

FIG. 3. Contours of fragment yield versus associated observed multiplicity and fragment mass for the reaction 42 GeV Ne + Au.

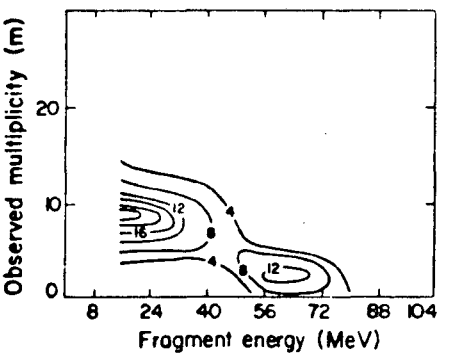

FIG. 4. Contours of fragment yield (arbitrary units) in the mass range $80 \leq A \leq 89$ at $\theta = 90°$ from the bombardment of ^{197}Au by ^{20}Ne projectiles at 250 MeV/u.

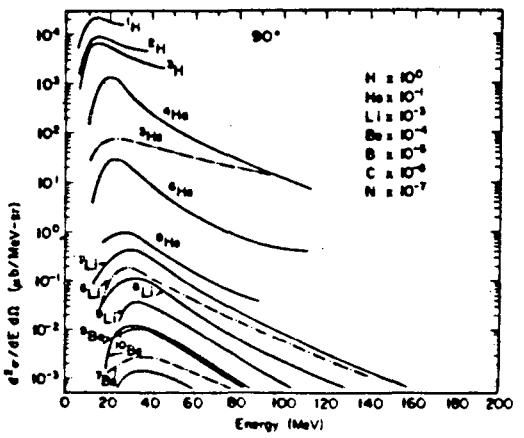

Fig. 5. Hydrogen and helium spectra from 5 GeV proton-U collisions.

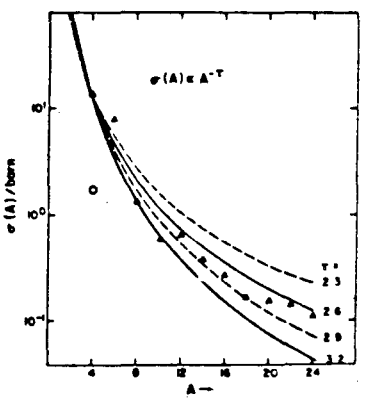

Fig. 6 Fragment yields compared to the power law $\sigma_A \propto A^{-T}$ (with varying from 2.33 to 3.2) of the general condensation model

fast charged particles,[4] suggesting that they are emitted from the same class of collisions. In this case the difference in their spectra can be explained by alpha particles emitted late in the lifetime of the cooling fireball, with a lower characteristic temperature.

c) The observed shape of the mass yield curve for A < 20 can be fit by a simple power law, $\sigma(A) \propto A^{-2.6}$ (fig. 6), following suggestions of ref. 5 using the theory of condensation.[6] We considered this as a possible indication of a liquid-vapor phase transition. However, this same power law appears in the total energy spectrum of particles emitted by cosmic-ray sources.[7]

There one finds for the probability $\phi_p(E)$ to observe a particle of energy E

$$\phi_p(E) \sim (E + E_0)^{-2.6}\ \mathrm{cm}^{-2}\ \mathrm{sec}^{-1}\ \mathrm{MeV}^{-1} \qquad (E_0 = m\,c^2)$$

Rewritten as a function of mass A: $\phi_A(E) \sim (E + A\ 931)^{-2.6}\ \mathrm{cm}^{-2}\ \mathrm{sec}^{-1}\ \mathrm{MeV}^{-1}$.

In the frame moving with the mean particle velocity E is very small compared with E_0 ($E \ll A\ 931$). Thus: $\phi \sim (931 \times A)^{-2.6} \propto A^{-2.6}$.

In applying the condensation theory, temperatures of ~20 MeV have been discussed. In the cosmic-ray sources, however, these high temperatures are

never considered. The coincidence in the power law observed in high energy nuclear reactions and in the particle spectrum of cosmic-ray sources might be fortuitous. On the other hand, it might indicate a common feature of nuclear fragmentation. Within the context of condensation it would point towards much hotter sources in the universe than previously considered.

d) The fireball concept has been extended to include composite particle production up to A = 20.[8,11] These calculations produce a mass yield curve of the correct shape in the range $1 \leq A \leq 11$ with an excitation of ≈20 MeV/u. Beyond mass 12 the model predicts yields less than experimentally observed.

The inability of fireball-chemical equilibrium models to describe the mass yield curve above A ≈ 12 indicates departures from statistical mechanical equilibrium. It is of great interest to see a detailed comparison of this part of the mass yield curve to the predictions of condensation theory. Our data show that the production of fragments up to A ≈ 30 at a given projectile energy are from the same class of violent collisions. Above A ≈ 30 fragments are from more peripheral collisions.

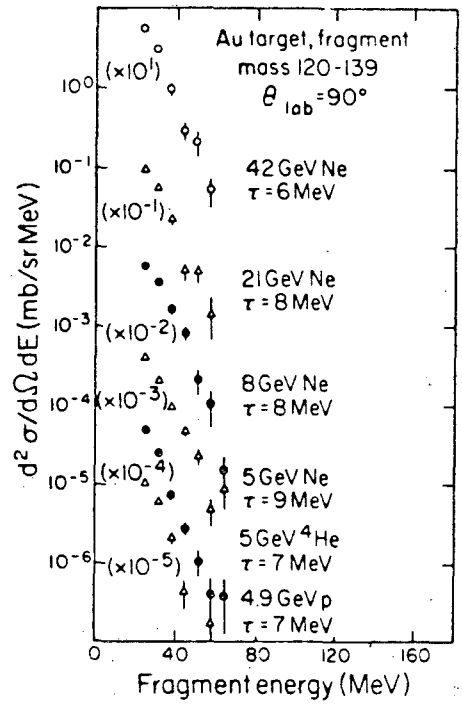

FIG. 7. Double differential cross sections for fragments falling into the heaviest mass bin, for each of the reactions studied. The exponential slope parameters (τ) are from a fit to the tails of the measured spectra.

e) In the upper part of the mass yield curve at 2/3 of the target mass fragments are observed to have spectra with a slope parameter of T_0 ~ 7-9 MeV independent of the projectile size or incident energy (fig. 7). We consider these fragments to be spectator residues from fairly clean-cut abrasion reactions with the spectra reflecting the momentum distribution the fragments had in the target nucleus.[9] However, a small perpendicular momentum transfer has been observed in projectile spectators in 4π data[10] and might also be part of the transverse momentum distribution of these heavy target fragments.

5. Fireball-residue coupling

Examination of the energy spectra of fragments from the residues of violent collisions shows little dependence of projectile mass and energy (fig. 8), and the angular distributions show more or less forward peaking, depending on projectile mass and energy (fig. 9). The size, velocity, and temperature of the fireball, however, varies enormously with projectile mass and energy.

One way to deal with this effect is to decouple the fireball from the residue breakup mechanism, simply allowing enough energy to cross into the residue to produce approximately the same excitation at all projectile energies. Linear momentum is also transferred to the residue to push it forward in accordance with the observed fragment angular distributions. Such a scenario might give rise to equilibrium behavior of the residue and statistical mechanics could then predict the breakup.[11] We find[1] that a residue excited to about 20 MeV/u, breaking up statistically, would approximately reproduce the measured energy spectra. The initial excitation energy is partly used up to break binding as the nuclear remnant breaks up into fragments, according to the statistical mechanical probability distribution. The remaining excitation is shared among the fragments as

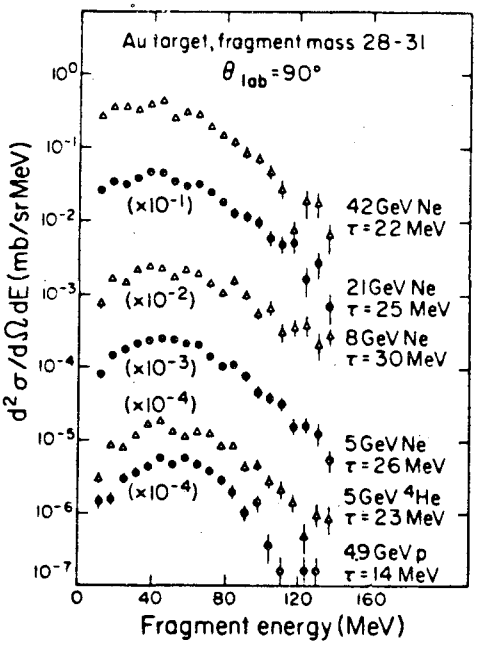

FIG. 8. Double differential cross sections for fragments falling into the lightest mass bin, for each of the reactions studied. The exponential slope parameters (τ) are from a fit to the tails of the spectra.

kinetic energy, and the resulting spectrum (when modified by the final stage Coulomb interaction) almost agrees with the data (fig. 10).

A totally different approach would be to couple the participants to the residue breakup mechanism directly.[12] For example, fast protons from the cascade or fireball could knock out preformed cold clusters of nucleons forming the observed fragments. Early results of such "cracking" phenomena look promising both in describing double differential cross sections and the observed mass yield curve. With regard to the earlier discussed observed power law in the particle spectra of cosmic-ray sources this model does not require high source temperatures.

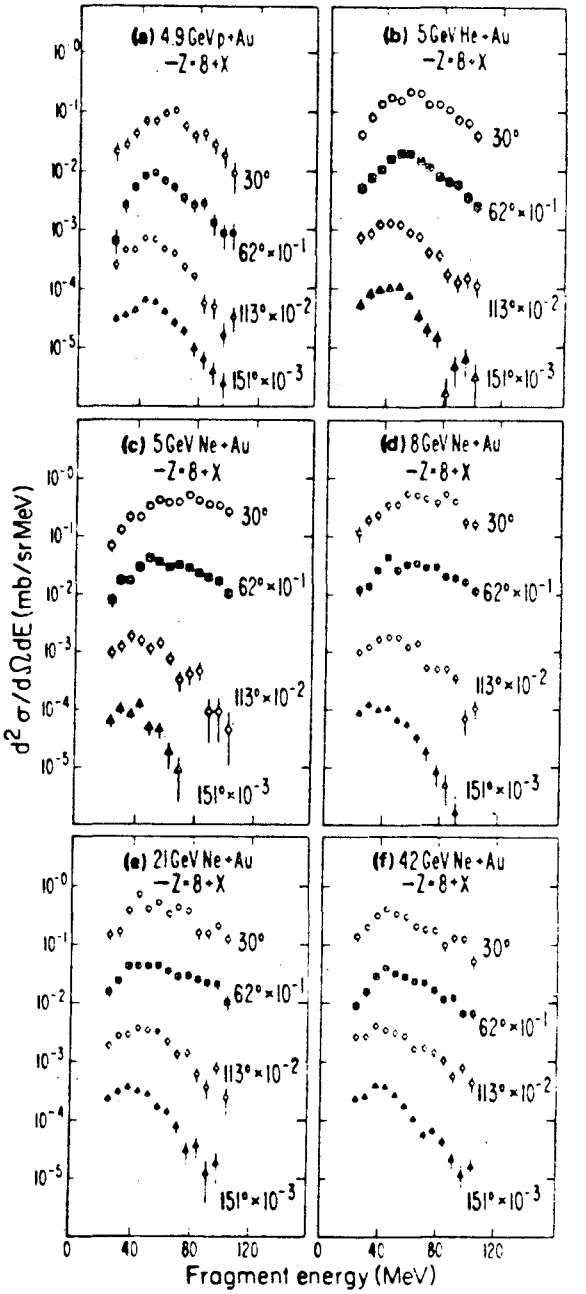

FIG. 9. Angular variation of the spectra of fragments of $Z = 8$ from the reactions (a) 4.9 GeV p + Au, (b) 5 GeV He + Au, (c) 5 GeV Ne + Au, (d) 8 GeV Ne + Au, (e) 21 GeV Ne + Au, and (f) 42 GeV Ne + Au.

6. Change of Mechanism

There are experimental results to show that fragments of a given mass (A = 30, say) originate in the most central collisions at low projectile energies while at higher projectile energies these same fragments are most likely to emerge from violent collisions. Figure 11 shows the multiplicity of fast charged particles for events in which "trigger" fragments or "trigger" protons were detected. The proton trigger comes from the fireball itself, and its detection necessarily weights the data towards the largest fireballs from the most violent collisions. Thus the trend of proton trigger multiplicities is that of the most violent (b ≈ 0) collisions. The fragment trigger multiplicities follow this trend up to 10 GeV projectile energy, showing that these fragments emerge from the most violent collisions. At higher energies,

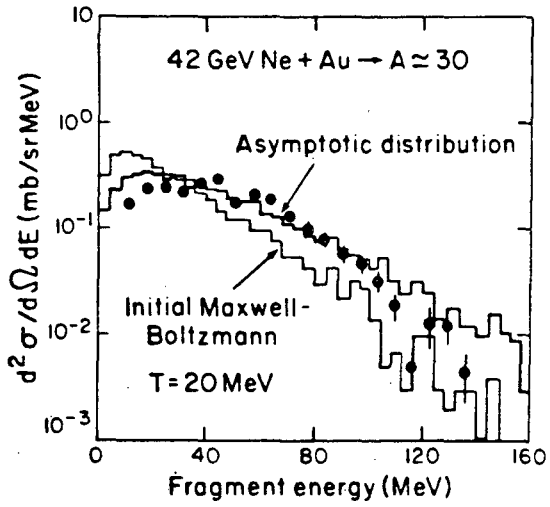

FIG. 10 Results of the Coulomb expansion calculation of the kinetic energy spectra of $A = 30$ fragments emerging from the Au target residue after a central collision induced by a 42 GeV Ne projectile.

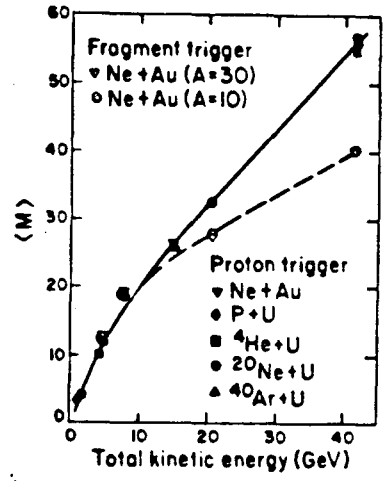

Fig. 11 Average charged particle multiplicity associated with proton emission and with slow light fragment emission into 90° as a function of total projectile energy.

however, the fragments emerge from collisions of less than maximum violence. The corollary is that at projectile energies above 10 GeV one can sometimes cause a Au nucleus to disintegrate completely into fragments of A < 10.

This work was supported in part by the Director, Office of Energy Research, Division of Nuclear Physics of the Office of High Energy and Nuclear Physics of the U.S. Department of Energy under Contract DE-AC03-76SF00098.

References

1) A.I. Warwick, et al. Phys. Rev. C27 (1983) 1083
2) A.I. Warwick, et al. Phys. Rev. Lett. 25 (1982) 1719
3) A.M. Poskanzer, et al. Phys. Rev. C3 (1971) 882
4) H.H. Gutbrod, et al. Nucl. Phys. A387 (1982) 177c
5) J.E. Finn, et al. Phys. Rev. Lett. 49 (1982) 1321
6) M.E. Fisher, Physics 3 (1967) 255
7) S.A. Austin, Michigan State University Cyclotron Laboratory Report MSUCL-333
8) J. Gosset, et al. Phys. Rev. C18 (1978) 844
9) A.S. Goldhaber, Phys. Lett. 53B (1974) 306
10) H.G. Ritter, et al., contribution to this conference
11) G. Fai and J. Randrup, Nucl. Phys. A381 (1982) 557
12) J. Aichelin, private communication

The Asymmetric Fission of Relativistic Gold Nuclei

P.S. Freier and C.J. Waddington
School of Physics and Astronomy, University of Minnesota,
Minneapolis, Minnesota 55455

Abstract. Relativistic gold nuclei have been observed in nuclear emulsions. Among the nuclear interactions detected some 6.0% represent a fission of the projectile nucleus. One-third of these fission events have strongly asymmetric fission products while the other two-thirds are symmetric. This appears to be the first observation of a significant yield of asymmetric fission from nuclei in this mass range.

Two small stacks of Ilford G5 nuclear emulsion pellicles have been exposed to a beam of gold nuclei, $^{197}_{79}$Au, accelerated at the LBL Bevalac to an initial energy of 1.06 GeV per amu. In this report we describe the characteristics of a small subsample of the observed interactions which represent fissioning of the incident nuclei.

We have observed a total of 307 nuclear interactions of Au-nuclei in nuclear emulsions. They were detected by along-the-track tracing of the tracks of Au nuclei which were located by a systematic scan 1 mm below the top edge of the emulsion. Allowing for the intervening matter, and using a modified range-energy relation appropriate for nuclei of such high charge,[1] the initial energy of the nuclei detected in the emulsions was 980 ± 10 MeV per amu. Each nucleus found in this way was traced through the emulsion until it left the individual pellicle, came to rest, or produced an interaction. A total of 18.84 m of track was examined, leading to a total observed mean free path for gold of 6.1 ± 0.4 cm of emulsion (23.4 ± 1.3 g/cm^2). This mean free path is energy independent, as are the characteristics of the interactions. In particular the fissionlike events occurred at all energies.

The interactions observed can be separated into classes based on the degree of breakup of the projectile by considering how much of the initial charge is still carried on fragments with $Z \geq 6$, i.e., not "released". In this sample 42% of the interactions show more than 20 charge units, cu, released, 15% had between 10 and 20 cu released, while 43% show that less than 10 cu were released. Of these latter, 81%, or 107 interactions, have only one residual fragment, while the remaining 24 have the charge carried by two or more fragments. On six of these the lighter fragment has $Z < 10$, while on one the charge is carried on five separate heavy fragments. On the remaining 17 interactions the charge is carried on two fragments, each with $Z \geq 20$. These events represent a splitting of the projectile nucleus into two nuclei and appear to be the result of a fissioning of the nucleus. They are clearly analogous to the similar fissionlike events observed with a $\sim$ 50% probability when uranium beams traverse nuclear emulsions.[2,3] The charges of the two fragments in these interactions are shown in Figure 1.

We will show below that the kinematics of these events are entirely consistent with their representing the fissioning of the excited projectile nucleus, being characterized by modest impulses and energy releases compatible with the changes in binding energies. The validity of this interpretation as a mode of fission is important because 5 of the 18 events we are able to analyze in detail clearly represent an asymmetric mode of fission, with one fragment having approximately half the charge of the other, whereas nine are conventional symmetric fissions and three show appreciable charge loss and are ambiguous.

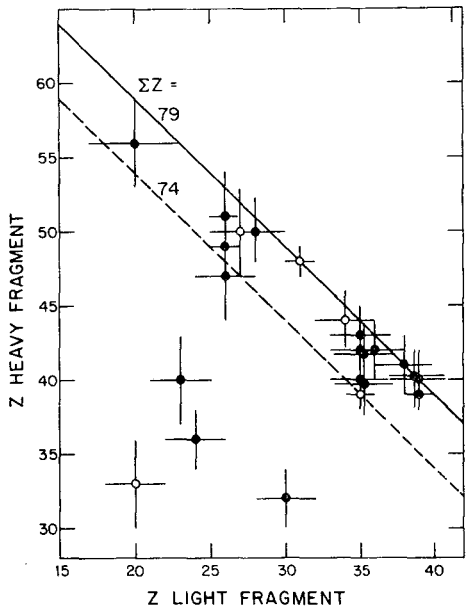

Fig. 1. Plot of the charge on the heavy fragment against the charge on the light fragment. Events that could be kinematically analyzed are shown as solid points. Lines of no charge loss, $\Delta Z = 0$, $\Sigma Z = 79$, and of $\Delta Z = 5$ are given.

Experiments where gold targets have been bombarded by projectiles of various mass and energies have failed to detect any appreciable yield of asymmetric fission.[4-7] Present models of fission appear unable to account for asymmetric fission of elements such as gold. A clear demonstration of the asymmetric fission of gold would thus indicate that an alternate mode of inducing fission exists that had not been previously considered. We have therefore analyzed in detail the kinematics of our events in order to establish that these events are consistent with a fission mode of decay.

Due to the limitations of our technique we can neither measure the mass of the fragments, nor can we observe any neutrons emitted during the interactions. However, we do know rather precisely the energy of the incoming gold nucleus at the point of interaction from the amount of matter traversed and the energy loss rate appropriate for gold nuclei.[1] Furthermore, we can at least estimate the energies of the fragments from their residual ranges if they come to rest, or from the rate of energy loss of secondary low-charged particles produced in further nuclear interactions of the fragments. These energy estimates are dependent on our charge estimates, which in turn depend on measurements of taper characteristics or comparative delta ray counts. Since meson production is generally small at these energies, and none have been observed in these particular interactions, these charge estimates are also constrained by requirements of charge conservation. We have confined our detailed analysis to those cases where the quality of the emulsions at the point of interaction allowed a reliable determination of the angles of emission of each fragment relative to the beam direction. Our kinematic analysis is then principally based on a consideration of the behavior of the transverse momenta of the fragments since these are invariant between the different frames of references. Longitudinal momentum considerations, based on residual ranges of stopping fragments, have been used to confirm and sharpen up charge estimates and are generally consistent with these momenta being larger in those interactions characterized by lower transverse momenta but with total momentum transfers still corresponding to energy transfers of < 1 MeV/nucleon.

We assume, as a hypothesis to be tested, that these fissionlike events can be represented by the following model. The incoming gold nucleus makes a peripheral interaction with a target nucleus of the emulsions. This target nucleus is probably, but not necessarily, a heavy nucleus of Br or Ag. The modest degree of excitation of the target nucleus that is characteristic of all these interactions, as revealed by the small amount of visible energy released (small N_h) is consistent with this model. The momentum of the Au nucleus at the point of interaction is p_o MeV/c per nucleon. In the interaction only a few of the nucleons of the incident nucleus are directly involved and these are either wounded and lose energy to the target nucleons, or

released as neutral, single and doubly-charged fragments that proceed with p_o. The remaining spectator projectile nucleus receives a transverse impulse with a momentum of p_i per nucleon, which should be small enough to imply excitation but not disruption. This excited nucleus then fissions, releasing two fragments and possibly some neutrons. In the fission process the two fragments receive equal and opposite momenta, so that each has a perpendicular, $p_\perp$, and longitudinal, $p_{||}$, momentum component. If we make the further assumption that in the fission process the neutron to proton ratio in the two fragments is constant, $N_1/Z_1 = N_2/Z_2$, so that the total momenta of the fragments scale as the charges, then, even if neutrons are lost during the fissioning, values of p_i and of $p_\perp$ of each fragment can be deduced from p_o, Z_1, Z_2 and the emission angles. From p_i we can determine the impulse energy, E_i, received by the residual nucleus in the collision, which presumably is an upper limit to the excitation energy. Similarly, from the $p_\perp$ values we can determine a lower limit to the energy released per nucleon in the fission process, E_f. In this case these are lower limits due to the neglect of longitudinal momenta. Values of E_i and E_f, expressed as values per nucleon, are given in Figure 2 for every event that could be reliably analyzed and had $\Delta Z \leq 6$.

In order for the nucleus to fission we would expect an excitation of at least 20 MeV, or $E_i \gtrsim 0.11$ MeV/n. Only 5 of the 15 events have E_i more than twice this value, while the remainder are consistent with modest excitation. The mean for all 15 interactions is 0.15 MeV/n, or less than 30 MeV of possible excitation energy. In the fission process we should observe the release of 0.7 to 0.8 MeV/n in binding energy. The actual energy release observed should on average be $\sqrt{2}\, E_f$ and the values of E_f listed are generally entirely compatible with a fission process. The mean E_f is 0.54 MeV/n, corresponding to an average visible energy release of 0.77 MeV/n. The kinematics are thus consistent with our model and we do indeed appear to be observing a form of fission similar to the more conventional mode observed in the reference frame of the fissionable nucleus.

A possible indication that the physics of this unexpected asymmetric fission might be significantly different from the symmetric case is provided by the behavior of the fission fragments. Each of the fragments has been followed until it interacts, is brought to rest, or leaves the stack. For fragments produced by asymmetric fission 11 of 14 interact, while for fragments from symmetric fission only 3 of 22 interact. If the mean free paths, λ, are expressed in Z independent units[8] then the asymmetric fragments have $\lambda = 0.49\bar{\lambda}$ while the symmetric fragments have $\lambda = 2.71\bar{\lambda}$.

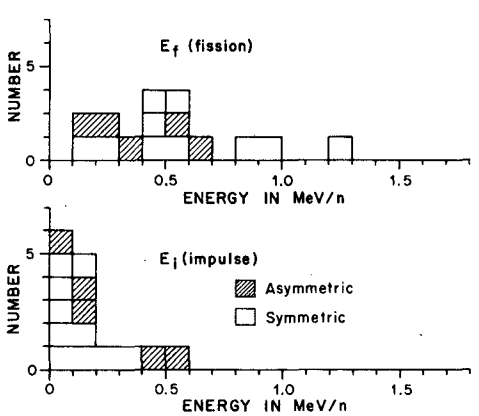

Fig. 2. Histograms of E_f and E_i.

In conclusion, we find that approximately one-third of the pure fissions induced in the Au-nuclei occur via an asymmetric rather than a symmetric mode. This appears to be the first detection of appreciable asymmetric fission in nuclei in this mass range independent of how the fission is induced. A recent report has suggested that asymmetric fission can be induced in still lighter nuclei with $Z \simeq 140$ by energetic proton bombardment.[7] A model for the asymmetric fission of these Au-nuclei which depends on an impulsive induce-

ment during a very peripheral collision with a heavy target nucleus has been proposed,[9] and seems to be consistent with all our data. The bombardment of a gold foil with energetic silver nuclei, in an experiment similar to that of Kaufman et al.,[6] would test these results and the proposed model. Similarly, bombardment with energetic gold nuclei and a search for coincident fissions of both the projectile and the target would be a feasible and definitive test.

Acknowledgements. We are grateful to the staff of the LBL Bevalac for their dedicated efforts in achieving the first beam of relativistic gold nuclei, and in particular to Hank Crawford for all his interest and guidance. We are grateful to Professors Bayman, Ellis and Tang for their stimulating interest in our results. This work was supported by NASA under Contract No. NAS8-27977 and by NSF under Grant No. Phy 8119421.

---

[1]C.J. Waddington, P.S. Freier and D.J. Fixsen, Phys. Rev. A, in press (1983).

[2]P.L. Jain, M.M. Aggarwal, M.S. El-Nagely and A.Z.M. Ismail, Bull. APS 28, 703 (1983).

[3]S.P. Ahlen, G. Tarle and P.B. Price, Science 217, 1139 (1982). Also E.M. Friedlander, H.H. Heckman, and Y.J. Karant, Phys. Rev. C27, 2436 (1983).

[4]R. Vanderbosch and J.R. Huizenga, Phys. Rev. 127, 212 (1962).

[5]F. Plasil, R.L. Ferguson, F. Pleasonton and H.W. Schmitt, Phys. Rev. C7, 1186 (1983).

[6]S.B. Kaufman et al., Phys. Rev. C26, 2694 (1982).

[7]F.D. Becchetti et al., Phys. Rev. C, in press (1983).

[8]H.B. Barber, P.S. Freier and C.J. Waddington, Phys. Rev. Lett. 48, 856 (1982).

[9]B.F. Bayman, P.J. Ellis and Y.C. Tang, private communication.

Angular Correlations Between Target and Projectile Fragments Emitted from ^{238}U + Ag(Br) Collisions at 0.85 A GeV

H. H. Heckman, E.M. Friedlander and Y.J. Karant

Lawrence Berkeley Laboratory, University of California
Berkeley, California 94720

Our examination of inelastic nuclear interactions of ~1A GeV ^{238}U in research emulsions revealed a large range of target/projectile multiplicities, from simple binary fission to complete disintegration of both the uranium projectile and target nucleus into nucleons and light nuclear fragments.[1] A particular class of U-reactions that we have begun to study are those that exhibit the classical target/projectile fragment topologies, selected by the criteria that at least 10 target- and 10 projectile- related fragments are produced in the reaction. Such reactions, when observed in emulsion, are identified with collisions of the incident uranium ions with the heavy component, Ag(Br), of the emulsion. Because of the high multiplicities of both target and projectile fragments, statistically meaningful measurements on the angular correlations between the target and projectile fragments becomes possible on an event-by-event basis.

A 4 x 11 x 1 cm^3 G-5 ILFORD emulsion stack irradiated by 0.96A GeV ^{238}U nuclei has been scanned over the beam profile for a distance of 1 cm from the entrance surface of the stack. Of a total of 399 interactions detected in the interval 0.85 ± 0.10 A GeV, 52 fulfilled the selection criteria. Of these 19 events were deemed unsatisfactory for measurement owing to obscuration by nearby beam tracks and/or the proximity, i.e. $\lesssim$ 40μm, of the event to either the top or bottom surface of the emulsion pellicle, thereby restricting angle measurements of fragments over the entire 4π steradian.

This report describes the status of our measurements on the angular distributions of i) target fragments whose rates of ionization correspond to Z = 1 particles having energies 100 A MeV and ii) projectile fragments, Z 2, emitted within a forward 15-20° cone. All emission angles were determined by measuring the xyz coordinates of two points along each track separated by distances up to ~1mm, depending on the energy, i.e. multiple scattering, and direction of the emitted particle. From these measurements we have obtained the distributions of space - and azimuthal - angles of the target and projectile fragments relative to i) the incident beam vector or ii) relative to their respective angular "center-of-gravity". As will be seen, target and projectile fragments separately show significant asymmetries in the azimuthal distribution suggesting jet-like emission. Thus the c.g. of angles conceptually identifies the vector of the "jet" axis for each class of fragment.

Figure 1 defines the coordinate systems (lab frame) we have used. a) is the "beam" system, where $\underline{i}$ is along the beam axis, with $\underline{k} = \underline{i} \times \underline{j}$ being normal to the beam-emulsion plane. b) is the "jet" system, where the $\underline{i}$ axis

is directed along the angular c.g. (the jet axis) of either the target or projectile fragments, with $\underline{k}' = \underline{i}' \times \underline{i}$. The space angles θ (θ') and azimuthal angles ϕ (ϕ') are indicated in their respective systems.

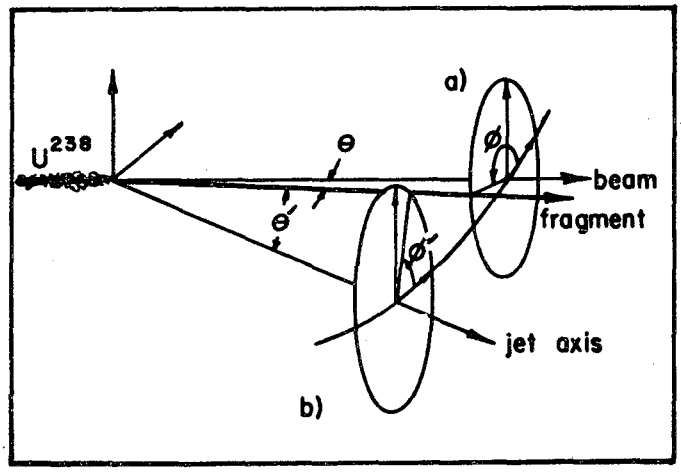

FIG. 1. Coordinate systems: a) Beam system, b) "Jet" system

We have defined the "center-of-gravity" of n fragments to be

i) in azimuth: $\langle\phi\rangle = \tan^{-1} (\sum \sin \phi_i / \sum \cos \phi_i)$

and ii) in space: $\langle\cos \theta\rangle = \frac{1}{n} \sum \underline{r}_i \cdot \underline{i}$,

where $\underline{r}_i$ is the unit vector of the ith fragment.

Fig. 2 presents the differences in the c.g. azimuthal angles, in the beam coordinate system, of the target and projectile ($Z \leq 2$) fragments, i.e., $\Delta\phi = \langle\phi\rangle_{TF} - \langle\phi\rangle_{PF}$, based on 28 events. The data show a strong back to back correlation; all values of $\Delta\phi$ are in excess of 90°, with a mean difference $\Delta\phi = (149 \pm 4)°$ and dispersion D = 23°. These data are compared with those derived from a Monte Carlo simulation of each event assuming the target fragments are uniformly distribution in azimuth. This simulation is necessary in order to remove the bias (spurious asymmetry) inherent to choosing the empirical center of gravity as the angular origin. The calculated distribution $\Delta\phi = \langle\phi\rangle_{TF} - \langle\phi\rangle_{MC}$ has a mean $\Delta\phi = (101 \pm 11)°$ and $D = (56 \pm 8)°$, compatible with that expected for a uniform distribution, namely 90° and 52°, respectively.

The verification that the asymmetries used to identify the c.g. of the azimuthal angle go beyond the above mentioned bias is that the angular distribution of all (643) target fragments measured relative to the c.g. angle $\langle\phi\rangle$ on an event-by-event basis exhibits a stronger correlation with $\langle\phi\rangle$, i.e., a peaking towards 0°, than does the M.C. (isotropic) simulation of

the data. In this case, the dispersion of the distributions are $D_{exp} = (73 \pm 2)^\circ$ and $D_{MC} = (91 \pm 3^\circ)$, the ratio of the variances giving a $P(<F) \sim 10^{-6}$.

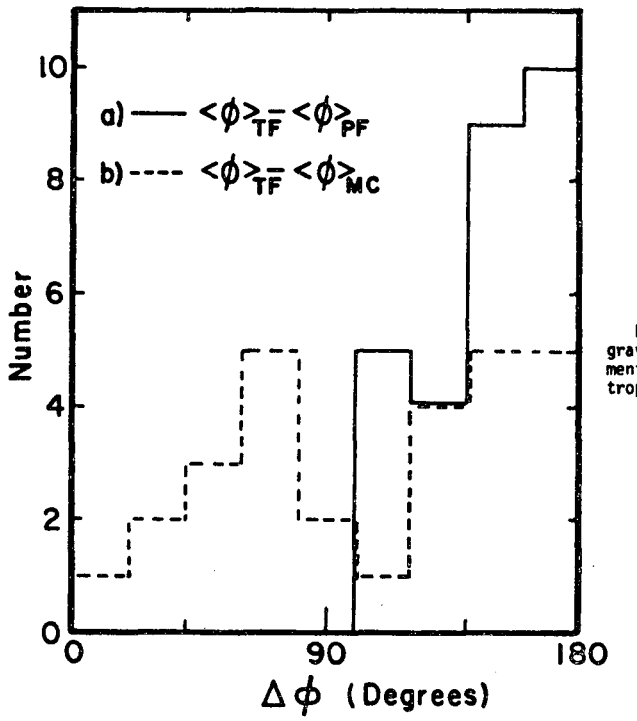

FIG. 2. Distribution of the differences between the center of gravity of the azimuthal angles for a) target and projectile fragments and b) target fragments and Monte Carlo simulation for isotropic emission.

The azimuthal correlations described above imply significant correlations in the angles of emission of the fragments. In Fig. 3 we show the angular distribution of the target fragments in their "jet" frame, where $\cos\theta = 0$ is the jet axis, Fig. 1b. A plot of $\ln(N^{-1}dN/d\cos\theta)$ vs. $\cos\theta$ reveals a forward-peaked distribution, the linear relationship indicated being characteristic of a Boltzmann energy distribution. For a Boltzmann distribution, the ratio of $\beta_{\parallel}$, the longitudinal velocity, to β_0, the characteristic velocity ($\propto \sqrt{T_0[\mathrm{Temp}]}$) of the emitting system, is $\mathrm{erf}(\beta_{\parallel}/\beta_0) = (1 - F/B)(1 + F/B)^{-1}$ (see ref. 2). For the observed value of $F/B \pm 4.3 = 0.6$, $\beta_{\parallel}/\beta_0 \approx 0.6$, i.e., the translational energy $T_{\parallel} \approx 0.4T_0$.

Based on our present data, the "jet" direction of the target fragments are also peaked forward, with on average value of $\langle\cos\theta\rangle \approx 0.6$. The average emission angle of projectile fragments in the same events is $\langle\cos\theta\rangle = 0.9986$ (3°). These angles are incompatible with "bounce-off" (elastic) collisions of the U + Ag(Br) system before break-up, although they are compatible with two-body kinematics provided the excitation energies are about 50 MeV/nucleon.

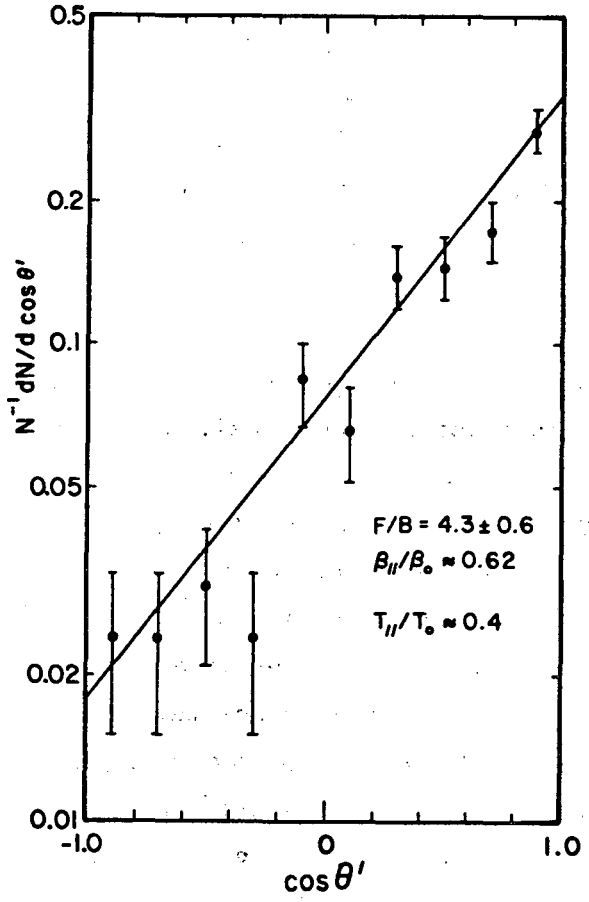

FIG. 3. Angular distribution of targets in the "jet" system.

Beyond the obvious angular asymmetries dictated by momentum conservation, the measurements we have made to date on these high-multiplicity U events suggest that non-trivial angular correlations may be present and extractable from data of the type presented here. One such (hydrodynamical) model that may be applicable for interpretation of the data is that proposed by Beckmann, Raha, Stelte and Weiner[3], whose article stimulated this investigation.

This work was supported by the Director, Office of Energy Research, Division of Nuclear Physics of the Office of High Energy and Nuclear Physics of the U.S. Department of Energy under Contract DE-AC03-76SF00098.

References:

1. E.M. Friedlander, H.H. Heckman and Y. J. Karant, Phys. Rev. C27, 2436 (1983).
2. H.H. Heckman, et al., Phys. Rev. C17, 1651 (1978).
3. R. Beckmann, S. Raha, N. Stelte and R.M. Weiner, Phys. Lett. 105B, 411 (1981).

Azimuthal Angular Correlations between Heavy Projectile Fragments and Light Particles in the Reaction ^{18}O + Ni at 84 MeV/u

W.F.J.Müller, A.Gobbi, K.D.Hildenbrand, A.Olmi, H.Sann, H.Stelzer,
GSI Darmstadt
I.Bock, U.Lynen, MPI Heidelberg
D.Pelte, U.Winkler, Universität Heidelberg
R.Glasow, K.H.Kampert, R.Santo, Universität Münster

At intermediate energies between 30-100 MeV/u the formation of a hot spot has been predicted [1], a reaction mechanism halfway between deep-inelastic scattering and participant-spectator behavior. As a localized excitation the hot spot may decay by particle evaporation as well as by heat conduction to the interior of the nuclear residues. In inclusive measurements in addition to evaporation from target and projectile a source at mid-rapidity has been observed which may result either from hot spot evaporation or from quasi-free nucleon-nucleon scattering [2].

To investigate whether the mid-rapidity source in peripheral reactions is localized at the nuclear surface a coincidence experiment has been done at the 84 MeV/u ^{18}O beam of the CERN-SC. The set-up used to study the correlation between projectile fragments and light charged particles is sketched in fig. 1. Projectile fragments have been detected in 6 scintillators covering the angular range between 1.5° and 4.5°, light particles in a 20 scintillator hodoscope covering a solid angle of 2π between 20° - 80° (forward) and 100° - 160° (backward). The set-up is almost symmetrical around the beam-axis in order to avoid systematical errors.

The azimuthal angular correlation between a projectile fragment and a light particle in the forward hemisphere of the hodoscope is shown for various projectile fragments in fig. 2. In order to select peripheral interactions only events with a total light particle multiplicity of one were used. For projectile fragments heavier than Beryllium a pronounced enhancement of light particles on the opposite side of the projectile fragment shows up which in case of $Z_p=8$ increases to a peak-to-valley ratio of 2:1. In order to derive an asymmetry-coefficient α the distributions were fitted with the expression:

$$R = 1 - \alpha \cos(\Delta\phi)$$

The dependence of α on the projectile charge is plotted in fig. 3 for both the forward and backward hemispheres. In fig. 4 the average asymmetry for

Z_p = 4..8 is shown as a function of the pulse height of the hodoscope-scintillators. Due to quenching effects and the missing particle identification this gives only a rough estimate of the particle energy. In the forward hemisphere the asymmetry increases with growing particle energy whereas at backward angles an asymmetry is observed for small energies only. For more central events where two or more light particles are observed in the hodoscope, the asymmetry is strongly reduced.

An explanation of this angular correlation due to projectile fragmentation can be ruled out since the asymmetry is also observed at backward angles and furthermore the maximum shows up for events where the full charge of the projectile is detected. With similar reasons also hydrogen impurities in the target can be excluded. In a simple hot-spot picture due to the shadowing by the target residue no pronounced peak would be expected at the opposite side of the projectile fragment. The observed asymmetry could be explained by nucleus-nucleon scattering where the projectile interacts with one or a few nucleons of the target. In this case, however, a high transparency of the target nucleus for the scattered nucleon must be assumed.

[1] R. Weiner and M. Weström, Phys.Rev.Lett. 34 (1975) 1523
[2] R. Glasow et al., Phys.Lett. 120B (1983) 71

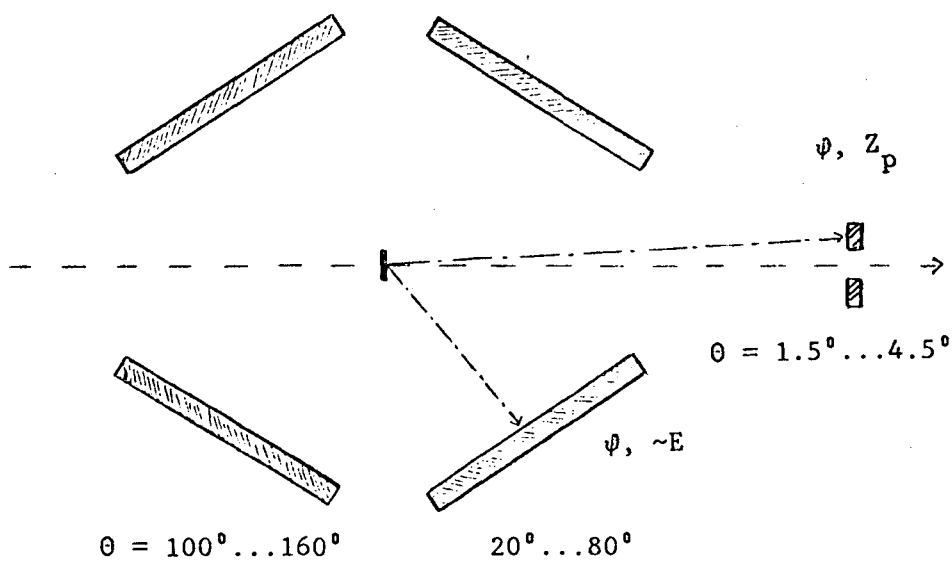

Fig. 1: Experimental set-up.

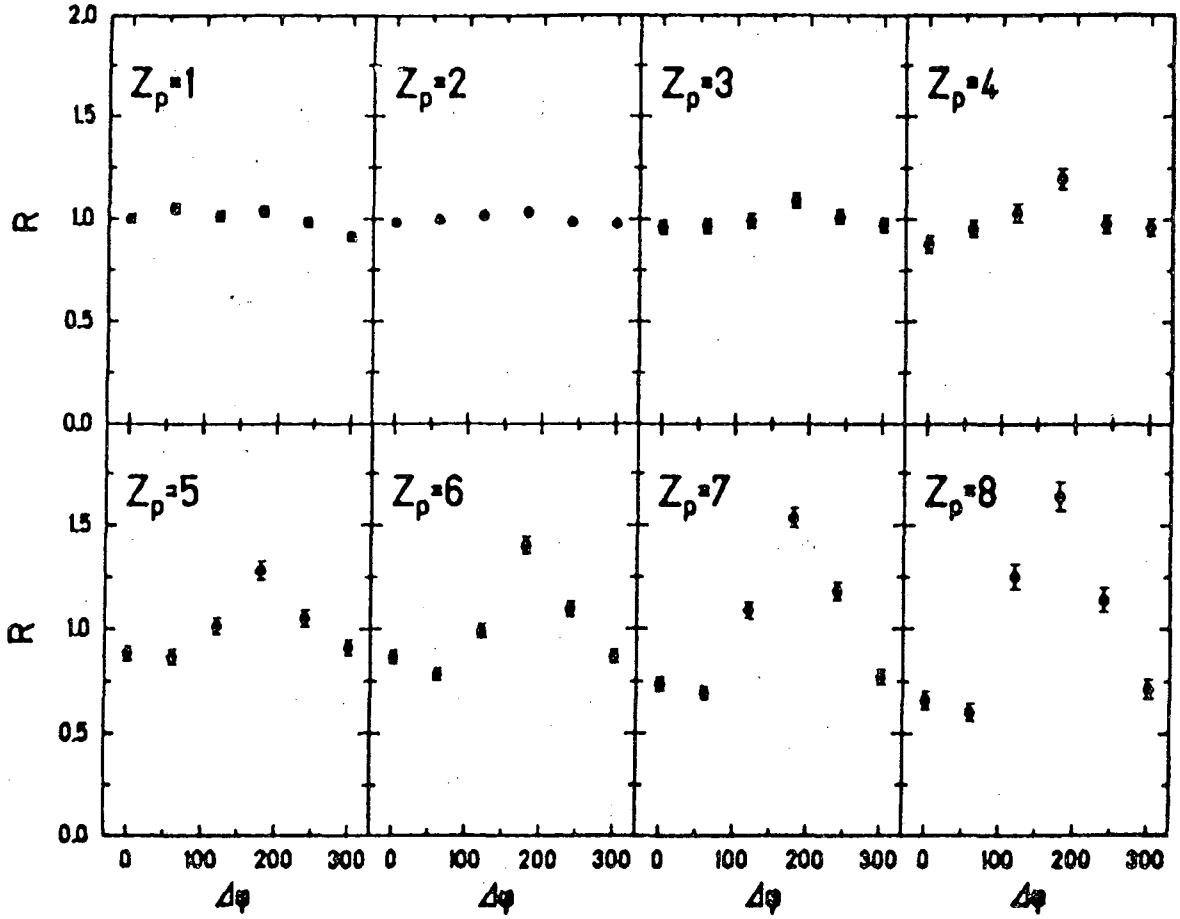

Fig. 2: Angular correlation for different projectile fragments

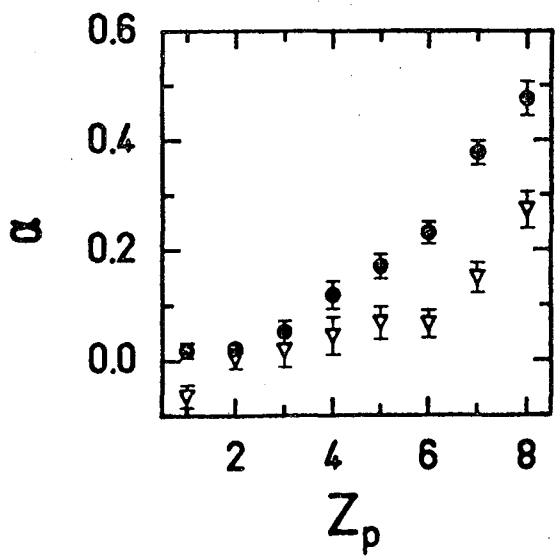

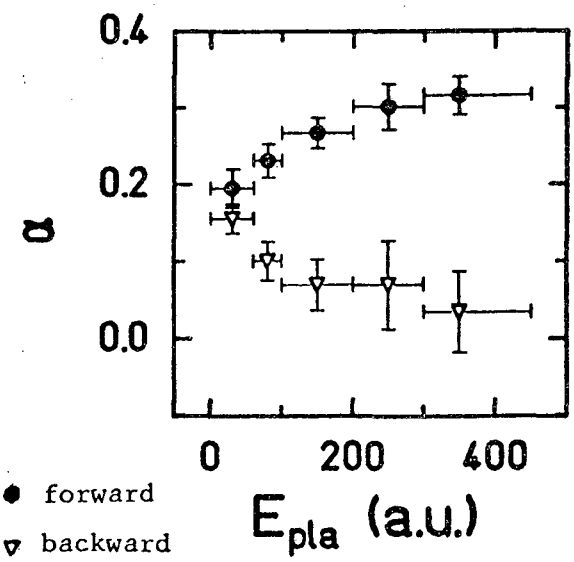

Fig. 3: Asymmetry vs. fragment charge

Fig. 4: Asymmetry vs. pulse height

Subthreshold K^- Production in Nucleus-Nucleus Collisions

A. Shor, J. Carroll, E. Barasch, S. Abachi, V. Perez-Mendez, T. Mulera, P. Fisher, G. Igo, S. Trentalange, K. Ganezer, and F. Kazeminzhad

Nuclear Science Division, Lawrence Berkeley Laboratory
University of California, Berkeley, CA 94720
and
University of California, Los Angeles, CA 90024
and
University of California, Davis, CA 95616

Abstract

We have measured the production cross section and momentum distribution of K^- produced at 0° in $^{28}Si + ^{28}Si$ collisions at an energy of 2.1 GeV/nucleon. The K^- spectrum is approximately exponential. The large yield in the "subthreshold" production of K^- that we observe corresponds to a production rate of $1K^-$ per 50 collisions at impact parameters less than 1f. Productions mechanisms involving collective effects and thermal equilibration are discussed.

Relativistic nuclear collisions (RNC) may demonstrate interesting and possibly exotic nuclear phenomena involving abnormally dense nuclear matter,[1] meson condensation,[2] or a phase transition to quark-gluon plasma.[3] For these nuclear effects to occur, some degree of equilibration or collective interactions among the colliding nucleons must take place. A straightforward indication of thermal or collective behavior is the creation of particles whose production threshold is significantly above the available nucleon-nucleon collision energy. At the maximum Bevalac energy of 2.1 GeV/nucleon, the lightest particle for which production is "subthreshold" is the K^-, which requires an N-N bombarding energy >2.5 GeV.

We have recently measured the momentum distribution of K^- produced at 0° in the reaction $^{28}Si + ^{28}Si$ at 2.1 GeV/nucleon. Negative secondaries produced in the heavy ion collision were momentum selected and transported along a magnetic beam line. Three bends, each followed by a detector station, allowed for multiply redundant measurements and particle identification. The detector stations were instrumented with an array of scintillation counters, focusing liquid Cerenkov counters, and high-pressure gas Cerenkov counters at the first two locations. Time of flight, along with multiple dE/dX measurements, determined particle mass and charge. Identification of the dominant background was made with the liquid Cerenkov counters for $P < 1$ GeV/c and with the gas counters for $P > 1$ GeV/c.

As an example of the good particle separation in our data, we show in figure 1 the results for laboratory momentum of 2.4 GeV/c. The TOF distribution for events that registered at the first two detector stations but that did not trigger the Cerenkov counters is plotted. This data set represents about 600,000 events prior to the Cerenkov cuts. The events in the peak at 0.85 ns are identified as kaons by their mean TOF. Four of these events actually survived to the third detector station to register correlated TOF information, thus confirming that these events were kaons. Cross

sections were determined by taking into account kaon and pion decay, channel acceptance, target thickness, and integrated projectile intensity.

We measured yields of K^- at laboratory momenta of 0.63, 0.73, 0.90, 1.4, 1.9, and 2.4 GeV/c. The invariant K^- cross sections, plotted as a function of the kaon kinetic energy in the nucleus-nucleus center-of-mass frame, are shown in figure 2, which includes the cross section for K^- at P_{lab} = 0.98 GeV/c that we measured in a previous experiment.[4] In these preliminary results from our recent experiment, we have assigned tentative error bars only.

The data, plotted in the c.m. frame, appear to fall off approximately in an exponential manner, with a slope parameter E_0 of about 80 MeV. This may indicate a thermal source at the mid-rapidity region. However, it is difficult to imagine equilibration for a system as small as ^{28}Si. Nevertheless, barring a thermal source, it may be difficult to account for the K^- at the higher momenta. Since the K^- requires a relatively large energy for its creation, it should be produced primarily at or near the mid-rapidity. For the K^- to acquire a momentum significantly larger than $p = m_K \beta_{c.m.} \gamma_{c.m.}$ (which in our case corresponds to 0.5 GeV/c), it would have to be produced coherently or to undergo several hard collisions subsequent to its production. (Note that a kaon at the <u>projectile</u> velocity has a momentum of only 1.5 GeV/c.)

An exponential fit to the seven data points gives a χ^2 value of 1.43. A fit excluding the measured point at 525 MeV gives χ^2 = 0.43 and a temperature of ~80 MeV. This last point is then 2.5 S.D. above the 80 MeV line and could indicate a change in slope.

Several models have been studied in an effort to account for the observed high K^- yields. At 2.1 GeV, the de-Broglie wavelengths of the incoming projectile nucleons are about 0.3 Fermi, certainly much smaller than the internucleon separation. It is therefore reasonable to assume that the nuclear collisions consist of independent N-N interactions. Although N-N collisions at 2.1 GeV are below the K^- production threshold, the nuclear Fermi momentum of the projectile and target nucleons allows for more of the N-N bombarding energy to be used for excitation rather than translational energy. A calculation has been performed[4] that assumed a double gaussian parameterization for the Fermi momentum. Although very good agreement was obtained for subthreshold anti-proton production in proton nucleus collision, calculations for K^- production in nucleus-nucleus collisions were more than twenty times below what we observed. Recent high energy muon and electron scattering experiments[5] report systematic differences between the structure functions in iron and deuterium. These results indicate a distortion in the structure function of nucleons embedded in a nucleus that cannot be attributed to Fermi momenta. Theoretical speculations suggest that these distortions may be due to 6-quark states in nuclei. This effect would change our picture of independent N-N collisions and would have a marked effect on subthreshold production.

We have made an estimate of the effects of intermediate π-N and Δ-Δ interactions on K^- production. A perturbation approach using hadron-hadron center-of-mass energies obtained from a cascade calculation show these effects to be small. Recently C.M. Ko has shown that hyperon-pion interactions

contribute significantly to the K^- production rates.[7] However, his calculations assumed thermal pions and did not take into account finite Δ lifetimes and noncentral collisions, and when these effects are included we estimate that this production mechanism accounts for only about 20% of the yield at 1 GeV/c.

With the present K^- data, we are able to rule out the ϕ-Bremsstrahlung model proposed by K.H. Muller.[8] In his model, ϕ-mesons are radiated by decelerated nuclear matter and decay to K^- that are sharply peaked at the mid-rapidity. It also seems unlikely that the suggestion of $K\bar{K}$-condensation is reasonable since it implies a structure in the K^- spectrum that we do not observe.

Subthreshold K^- production will no doubt shed light on the collision dynamics in nucleus-nucleus collisions, if not on new production mechanisms, and therefore warrants further investigation.

This work was supported by the Director, Office of Energy Research, Division of Nuclear Physics of the Office of High Energy and Nuclear Physics of the U.S. Department of Energy under Contract DE-AC03-76SF00098.

REFERENCES

1. T.D. Lee, Rev. Mod. Phys. 47, 267 (1975)
2. V.P. Berzovoi, et al., Sov. J. Nucl. Phys. 30, 581 (1979)
3. S.A. Chin, Phys. Lett. 78B, 552 (1978)
4. A. Shor, K. Ganezer, S. Abachi, J. Carroll, J. Geaga, G. Igo, P. Lindstrom, T. Mulera, V. Perez-Mendez, A. Sagle, D. Woodard, and F. Zarbakhsh, Phys. Rev. Lett. 48, 159 (1982)
5. A. Bodek, Phys. Rev. Lett. 50, 1431 (1983)
6. R. Jaffe, Phys. Rev. Lett. 50, 220 (1983)
7. C.M. Ko, Phys. Lett. 120B (1983)
8. K.H. Muller, Nucl. Phys. A395 (1983)

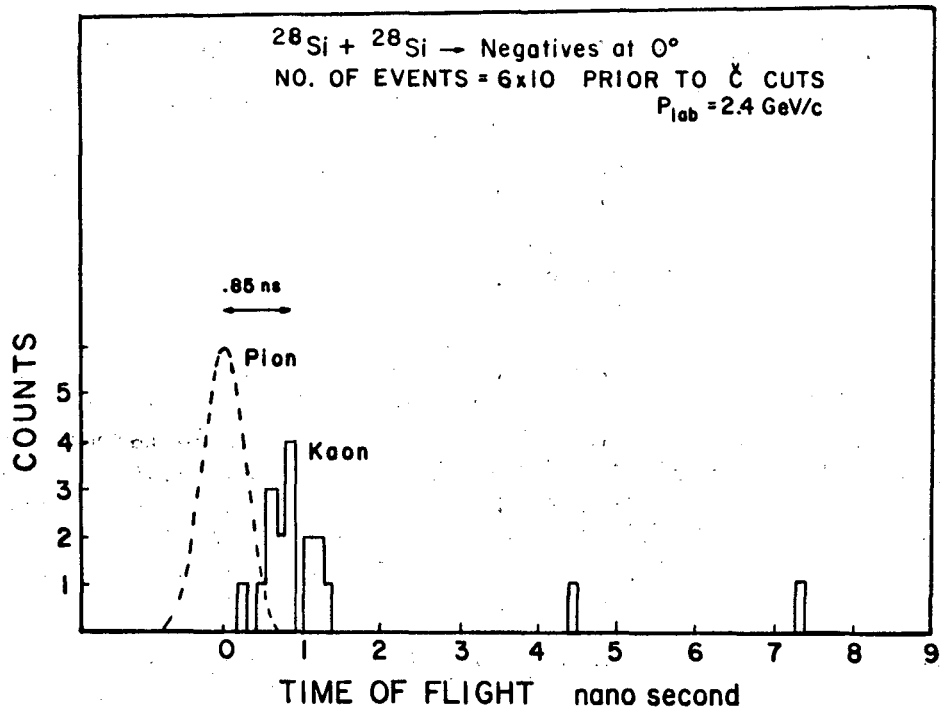

Fig. 1. Time of flight cuts showing the separation between π^- and K^-.

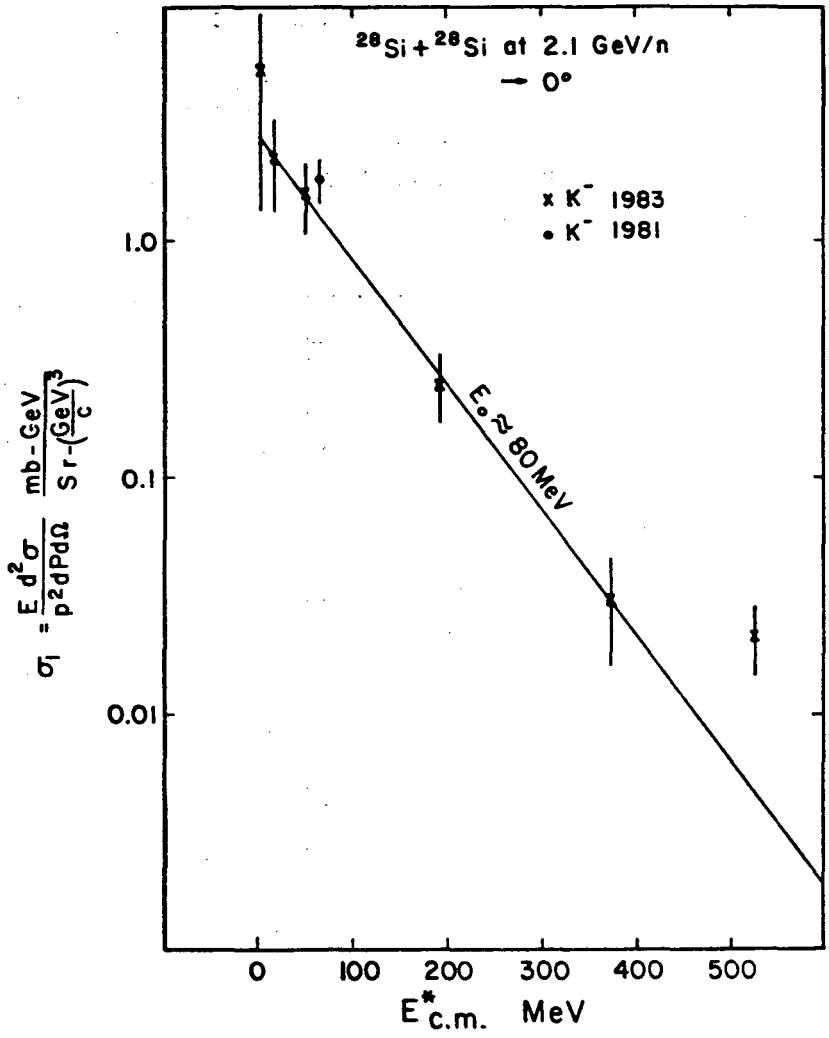

Fig. 2. Energy distribution in the c.m. system of the K^- produced in Si-Si collisions. The line drawn is fitted to the first six points (χ^2 = 0.43/degree of freedom).

NEUTRON EMISSION FROM COLLISIONS OF 390 MeV/u NEON IONS ON LEAD

R. Madey, J.C. Varga, B.D. Anderson, A.R. Baldwin, R. Cecil, and J.W. Watson
Kent State University
Kent, Ohio 44242

G.D. Westfall
Michigan State University
East Lansing, Michigan 48824

We measured neutron time-of-flight spectra at eight angles (viz., 0°, 15°, 30°, 50°, 70°, 90°, 120°, and 160°) from collisions of neon ions with an energy of 390 MeV/u at the center of a (3.43 g/cm^2) Pb target. Flight paths ranged from 8 m at 0° to 3.5 m at 160°. The apparatus measured the time difference between the detection of a neon ion in a beam telescope (consisting of two 0.8 mm scintillators) and the detection of a neutron in one of the eight, mean-timed,[1] neutron detectors.[2] The neutron energy resolution varied from 4% at 100 MeV, to 8% at 400 MeV, to 15% at 800 MeV.

In order to distinguish between peripheral and central collisions, each neutron event was tagged with an associated r-fold ($0 \leq r \leq 14$) coincidence of charged particles with a threshold of 27 MeV for protons. The events were separated into high ($r \geq 4$) and low ($r \geq 0$) associated multiplicity events. Figures 1 and 2 are semilog plots of the neutron spectra for collisions with $r \geq 0$ and $r \geq 4$, respectively. The striking peak in the $r \geq 0$ spectrum at 0° occurs at a neutron energy slightly below the beam energy per nucleon. Comparison of the spectra in Fig. 1 with those in Fig. 2 reveals that the associated multiplicity tag has the greatest effects

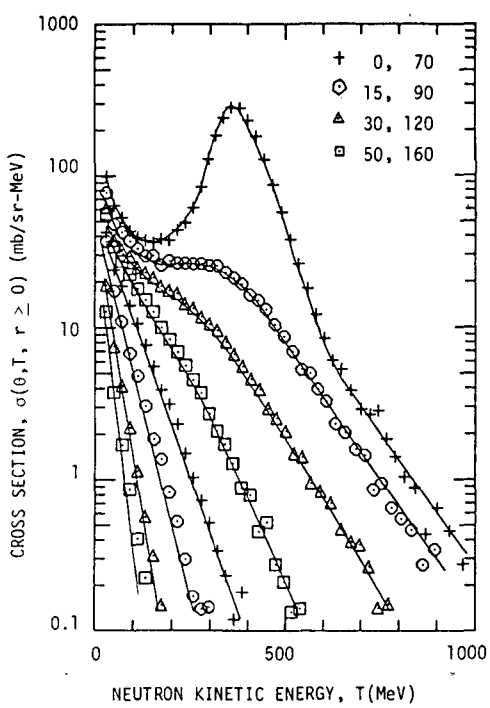

Fig. 1

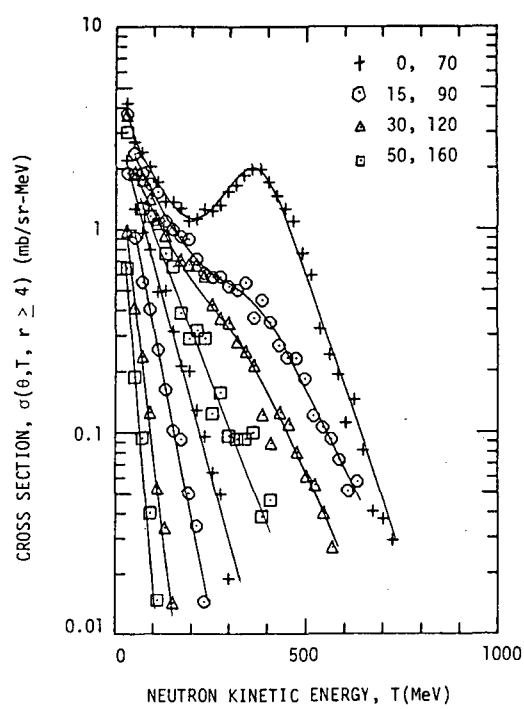

Fig. 2

for neutrons above $\sim$ 100 MeV at forward angles; for example, the cross section $\sigma(r \geq 4, \theta=0°, T = 380$ MeV) is $\sim$ 140 times smaller than the measured inclusive cross section $\sigma(r \geq 0°, \theta=0, T = 380$ MeV), whereas the cross sections at backward angles $\sigma(r \geq 4, \theta \gtrsim 120°, T)$ are only $\sim$ 18.5 times smaller than the inclusive cross sections $\sigma(r \geq 0, \theta \gtrsim 120°, T)$.

The angular distributions of low-energy (e.g., 30, 50, 90, and 150 MeV) neutrons with $r \geq 4$ have nearly the same forward-peaked shape as the inclusive $(r \geq 0)$ angular distributions. For $\theta=120°$, the ratio of the $r \geq 0$ events to the $r \geq 4$ events equals 18.5 ± 0.4 for the measured energy region from 30 to 160 MeV. The inclusive differential cross section $\sigma(r \geq 0, \theta, T)$ and 18.5 times the differential cross section $\sigma(r \geq 4, \theta, T)$ for $r \geq 4$ events are plotted in Figs. 3 and 4, respectively, versus the laboratory angle θ for $0 \leq \theta(\text{deg}) \leq 160$ for neutron energies T = 30, 50, 90, and 150 MeV. These observations of forward-peaked neutron angular distributions for $r \geq 4$ events are in sharp contrast to the proton observations. For low-energy ($\sim$ 10 to 40 MeV) protons, Stock et al[3] observed "relatively flat" angular distributions (from about 30° to 150°) for high-multiplicity events and forward-peaked distributions for low-multiplicity events from the reactions of 393 MeV/u Ne on U and 1.04 GeV/u Ar on U. They concluded that forward emission of low-energy protons was suppressed in central Ne and Ar collisions on heavy targets.

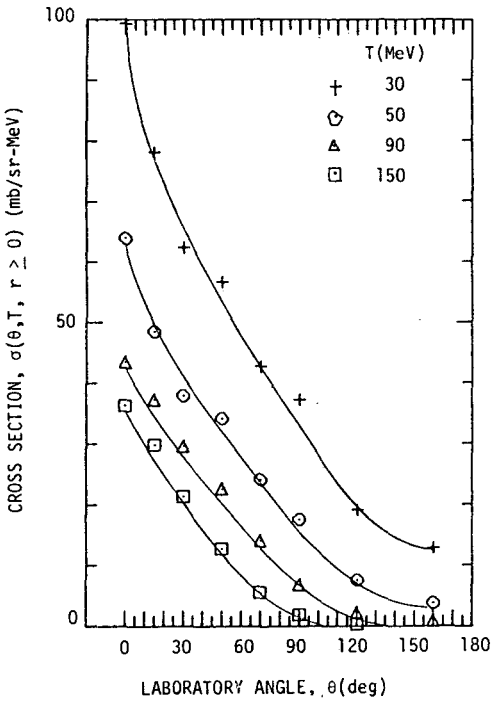

Fig. 3

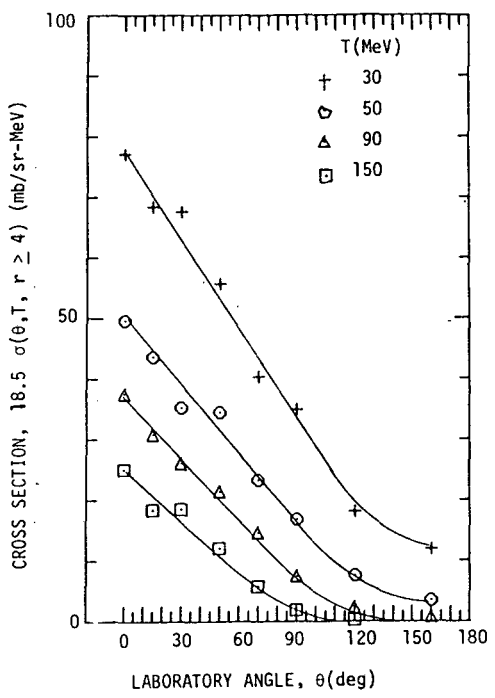

Fig. 4

Actually, the "relatively flat" angular distributions of low- and medium-energy protons reveal broad maxima at large angles. Stöcker et al[4]

reproduced this qualitative feature with a nuclear fluid-dynamics (NFD) model which includes thermal breakup of the system into free particles when the expanding fluid reaches the breakup or freeze-out density. The existence of a collective sideward matter flow cannot be concluded definitively from the proton angular distributions because these distributions can be sensitive to the formation of composite fragments; for example, suppression of protons in the forward direction could occur if the process for formation of composite fragments were enhanced in the forward direction. In contrast to the NFD calculations, the cascade models calculate primordial spectra and reveal the same forward-peaked shape of the angular distributions for both peripheral and central collisions. The angular distributions of low-energy neutrons are similar to the predictions of cascade calculations.[4] The formation of composite fragments is expected to distort primordial proton spectra more than primordial neutron spectra.[5,6] This effect is a consequence of the facts that the neutron-to-proton (n/p) ratio of the initial system is greater than unity, that the formation of deuterons occurs with a higher probability than does the formation of heavier fragments, and that the formation of tritons and helium-3 particles occurs with approximately equal probability. Thus, since the light composite fragments carry away equal numbers of neutrons and protons, the n/p ratio observed in the final system is higher than that expected from the n/p ratio of the initial system.

The neutron angular distributions in Figs. 3 and 4 indicate also that the emission of low-energy neutrons at 0° is suppressed in $r \geq 4$ collisions. In order to examine the degree of the suppression, we plot in Fig. 5 the following ratio as a function of neutron kinetic energy:

$$R = \frac{\sigma(r \geq 0,\ \theta=0°,\ T) - 18.5\ \sigma(r \geq 4,\ \theta=0°,\ T)}{18.5\ \sigma(r \geq 4,\ \theta=0°,\ T)}$$

R is about 0.3 for 30 and 50 MeV neutrons and decreases slightly with increasing neutron energy to about 100 MeV. The increase in R with increasing energy above 100 MeV reflects the fact that central collisions suppress the strong peak which is observed at a neutron energy slightly below the beam energy per nucleon in the inclusive spectrum at 0°.[7] For T = 380 MeV, R ≈ 7.

Figure 6 is a linear plot of the Lorentz invariant cross section $\sigma_I(r \geq 0,\ \theta=0°)$ in the region of the peak at 0° versus the neutron momentum up to ± 200 MeV/c. The solid line is a Gaussian with a half-width of 58 MeV/c and an

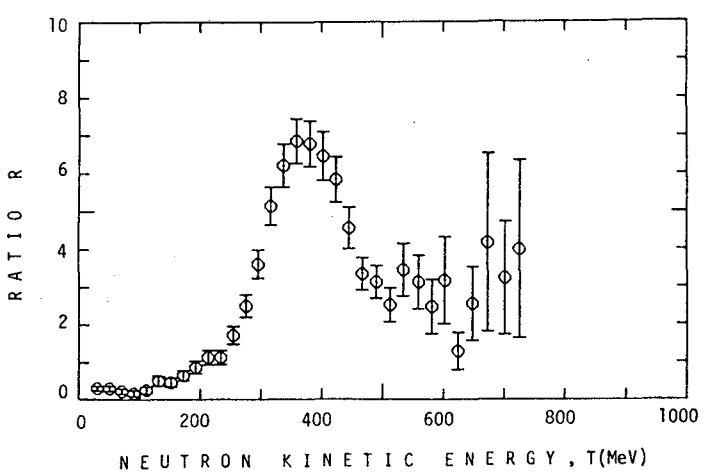

Fig. 5

offset of 27 MeV/c. The Gaussian is fitted to the data over a momentum interval of ± 60 MeV/c. After unfolding the experimental resolution, the half-width of the peak is 55 MeV/c. Figure 7 is a semilog plot of the Lorentz invariant cross section $\sigma_I(r \geq 0, \theta=0°)$ and $18.5\ \sigma_I(r \geq 4, \theta=0°)$ versus the neutron momentum in the rest frame of the projectile for momenta up to ∿ 500 MeV/c. Note that $\sigma_I(r \geq 0)$ falls off exponentially with a change in the slope at $P_0 \sim 200$ MeV/c. The characteristic (1/e) slope is 46 MeV/c below ∿ 200 MeV/c and 78 MeV/c above ∿ 200 MeV/c. Greiner et al[8] found that the longitudinal momentum distribution of protons emitted within a 12.5 m-rad acceptance cone in the fragmentation of (1.05 and 2.1 GeV/u) ^{12}C and (2.1 GeV/u) ^{16}O projectiles was represented by $(d\sigma/dP) \propto \exp(-P_{||}/65)$.

This work was supported in part by the National Science Foundation.

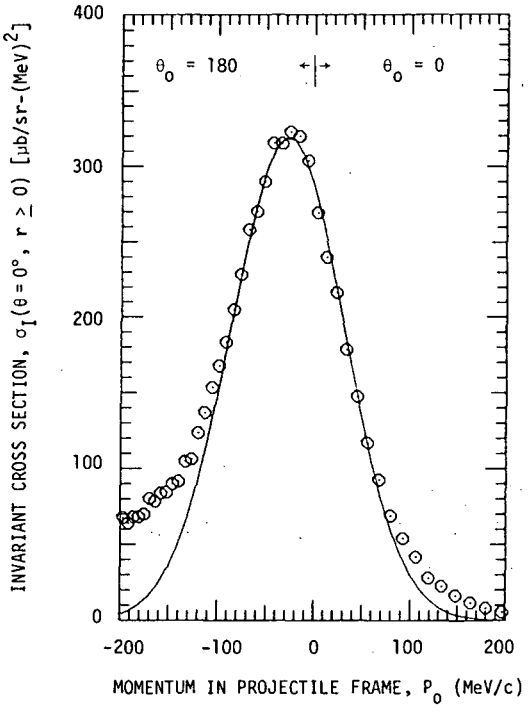

Fig. 6

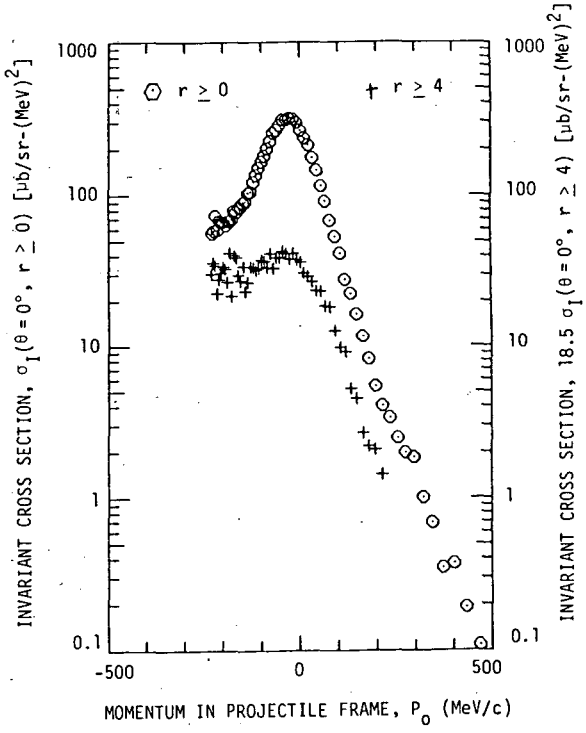

Fig. 7

1. A.R. Baldwin and R. Madey, Nucl. Instr. & Meth. 171 (1980) 149.
2. R. Madey et al, Nucl. Instr. & Meth. ___ (1983), to be published.
3. R. Stock et al, Phys. Rev. Lett. 44 (1980) 1243.
4. H. Stöcker et al, Phys. Rev. Lett. 47 (1981) 1807.
5. J.D. Stevenson, Phys. Rev. Lett. 45 (1980) 1773.
6. J. Randrup and S.E. Koonin, Nucl. Phys. A356 (1981) 223.
7. R. Madey, B.D. Anderson, J.W. Watson, A.R. Baldwin, R. Cecil, J. Varga, and G.D. Westfall, Bull. Am. Phys. Soc. 27 (1982) 25.
8. D. Greiner et al, Phys. Rev. Lett. 35 (1975) 152.

Two-pion Correlations for 1.2 GeV/nucleon Ar on KCl

D. Beavis, S. Y. Chu, S. Y. Fung, W. Gorn, A. Huie, D. Keane,
J. J. Lu, R. T. Poe, G. VanDalen, and M. Vient

University of California, Riverside, California 92521

ABSTRACT

The technique of pion interferometry is used to study the pion source for central collisions of 1.2 GeV/nucleon Ar on KCl. The data are described by a Gaussian source of radius 3.8 ± .5 fm, a lifetime of (18 ± 6) x 10^{-24} sec and a degree of coherence of .74 ± .17.

The properties of the pion source produced in relativistic heavy ion collisions are a major focus of interest.[1-4] Measurement of the space-time structure and the degree of coherence of the pion source would provide important information on the pion emission process and the total reaction mechanism. Studying pion pair correlations through interferometry[5] has proven[6] to be a suitable tool for obtaining such information. In this paper, we report the preliminary results of a pion interferometry analysis for 1.2 GeV/nucleon Ar on KCl central collisions.

The experimental data was obtained using the Lawrence Berkeley Laboratory streamer chamber. The 1.2 GeV/nucleon Ar beam was focused on a .44 gm/cm^2 KCl target located inside the streamer chamber. The chamber was triggered to preferentially select small impact parameter collisions, corresponding to 30% of the reaction cross section. Geometrically, this can be interpreted as selecting collisions with impact parameters of 5 fm or less. The observed average negative pion multiplicity is 2.3 per event. The detection efficiency, incorporating target absorption, scanning losses, and other inefficiencies is estimated to be $\gtrsim$ 90%, giving a corrected value of average negative pion multiplicity per event of 2.5. The observed negative pion multiplicity distribution is given in Fig. 1. The predictions of an effective one-pion fireball model including the trigger selection and detection efficiency are shown in Fig. 1 for values of the critical freeze-out density, ρ_c, of 1/3 (solid) and 1/2 (dashed) the normal nuclear density, ρ_o. For $N_{\pi^-} > 4$ the slope of the negative pion multiplicity distribution is sensitive to the value of ρ_c and the data suggest a value between 1/3 and 1/2 ρ_o. Later we will show that the interferometry analysis suggests a similar value.

The interferometry analysis is performed by fitting the correlated two-π^- cross section with the product of a function C and the uncorrelated two-π^- cross section. The function C contains the effects of Bose-Einstein statistics, dynamical correlations, final state interactions, etc. For a Gaussian space-time pion emitting source[7] with correlations induced only by the quantum statistics one obtains

$$C(\vec{q},q_o) = K[1 + \lambda \exp(-\vec{q}^2R^2/2 - q_o^2 \tau^2/2)] \qquad (1)$$

where $\vec{q}$ and q_o are the center of mass relative momentum and energy of the pion pairs, R is the source radius, τ is the lifetime, λ is a measure of the degree of coherence, and K is a normalization factor.

The uncorrelated two-π^- cross section is generated by combining negative pions from different events with the same negative pion multiplicity. The effect of the final state $\pi^-\pi^-$ Coulomb interaction is corrected for by incorporating a Gamov factor[5] in the uncorrelated two-π^- cross section. The determination of the normalization factor, K, is equivalent to requiring the ratio of correlated to uncorrelated two-π^- cross sections at large relative momentum be unity.

A subsample of 7200 events with $N_{\pi^-} \geq 2$ is used for the interferometry analysis. In addition, a momentum requirement of $P_{LAB} \geq 100$ MeV/c is imposed to minimize multiple scattering effects in the target and electron contamination from photon conversion and Dalitz pairs. The final data sample contains 24,000 pion pairs. All pairs with $q \leq 60$ MeV/c have been reexamined to remove any measurement errors. Our results are:

$$R = 3.8 \pm .5 \text{ fm},$$
$$\tau = (18 \pm 6) \times 10^{-24} \text{ sec},$$
and
$$\lambda = .74 \pm .17.$$

The data and the fit have been summed over the relative energy and displayed in Fig. 2. The large statistics in the region for $q \geq 150$ MeV/c gives an accurate determination of the normalization factor K and decouples the normalization from the source parameters. A Gaussian source radius of 3.8 fm corresponds to a uniform distribution of radius 5.9 fm. Estimating the average number of participant nucleons to be 50, we obtain a critical freeze- out density, $\rho_c \simeq .45\ \rho_o$. This result agrees well with the expectation of the effective one pion fireball model from the multiplicity distribution in Fig. 1.

The lifetime of 18×10^{-24} sec $\simeq$ 4.5 fm/c is quite reasonable for a source radius of 3.8 fm. In addition, models such as the intranuclear cascade[3] suggest most of the pion production occurs for a period of 10 fm/c and therefore agrees well with our Gaussian width of 4.5 fm/c. In the region of phase space where $q \simeq q_o$, Eq. 1 is no longer sensitive to R and τ separately but to $R^2 + \tau^2$. This induces a coupling in the determination of these parameters. In Fig. 3, the likelihood contours for the parameter space of R and τ are shown. A weak correlation in the manner expected is evident.

The determination of the degree of coherence has always been one of the goals of the interferometry analysis. We obtained a value of .74 ± .17 for the degree of coherence suggesting that a component of the pion source may be non-chaotic. The degree of coherence is the only parameter significantly affected by the Gamov correction for $\pi^-\pi^-$ Coulomb interaction. A value of $\lambda \simeq .55$ is obtained without the Gamov factor. The determination of R and λ are strongly coupled as clearly seen by the likelihood contours displayed in Fig. 4. A value of $\lambda = 1$ corresponding to a totally chaotic source lies

within two standard deviations of the minimum and therefore cannot be excluded.

In conclusion, the pion source parameters for central collisions of 1.2 GeV/nucleon Ar on KCl have been measured using pion interferometry. The radius and lifetime of the source are in agreement with the expectations of simple geometrical considerations. The data suggest the pion source may have a coherent component, which can be confirmed with a moderate increase in statistics.

We are grateful to M. Gyulassy and W. Zajc for several useful discussions. We thank the entire Bevalac staff and in particular James P. Brannigan and Dr. Fred Lothrop. This work was supported by the U.S. Department of Energy.

References

1. J. P. Vary, Phys. Rev. Lett. 40, 295 (1978).
2. M. Gyulassy and S. K. Kauffmann, Phys. Rev. Lett. 40, 298 (1978).
3. J. Cugnon, D. Kinet, and J. Vandermeulen, Phys. Rev. C22, 1985 (1980).
4. R. Stock et al., Phys. Rev. Lett. 49, 1236 (1982).
5. M. Gyulassy, S. K. Kauffmann and L. W. Wilson, Phys. Rev. C20, 2267 (1979).
6. S. Y. Fung et al., Phys. Rev. Lett. 41, 1592 (1978); D. Beavis et al., Phys. Rev. C27, 910 (1983).
7. F. B. Yano and S. E. Koonin, Phys. Lett. 78B, 556 (1978).

Figure Captions

Fig. 1. The negative pion multiplicity distribution for central collisions of 1.2 GeV/nucleon Ar on KCl. Predictions of an effective one-pion fireball model (ref. 2) for values of the critical freeze-out density of 1/3 (solid) and 1/2 (dashed) the normal nuclear density.

Fig. 2. The data and fit summed over the relative energy as a function of the relative energy as a function of the relative momentum, q.

Fig. 3. Likelihood contours for 1, 2, ... standard deviations for the radius, R, and the lifetime, τ.

Fig. 4. Likelihood controus for 1, 2, ... standard deviations for the radius, R, and the degree of coherence, λ.

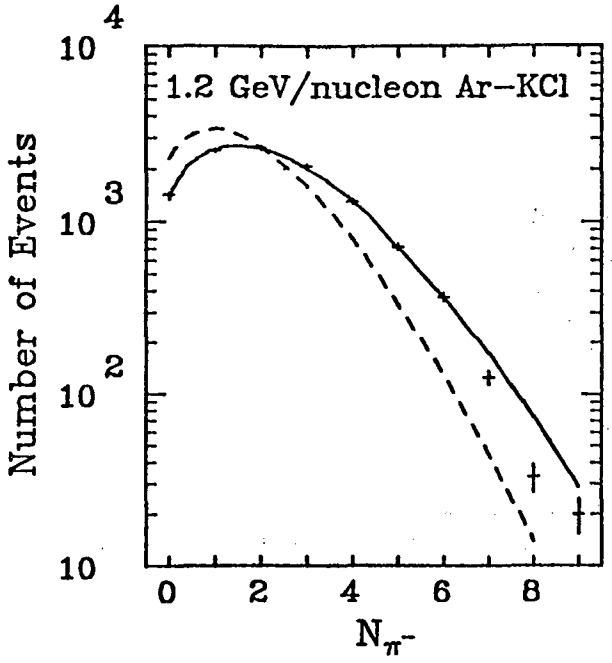

Figure 1

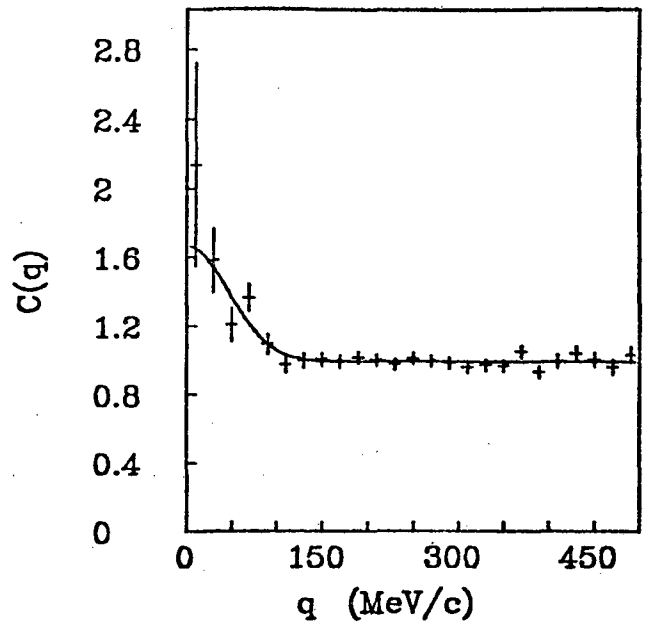

Figure 2

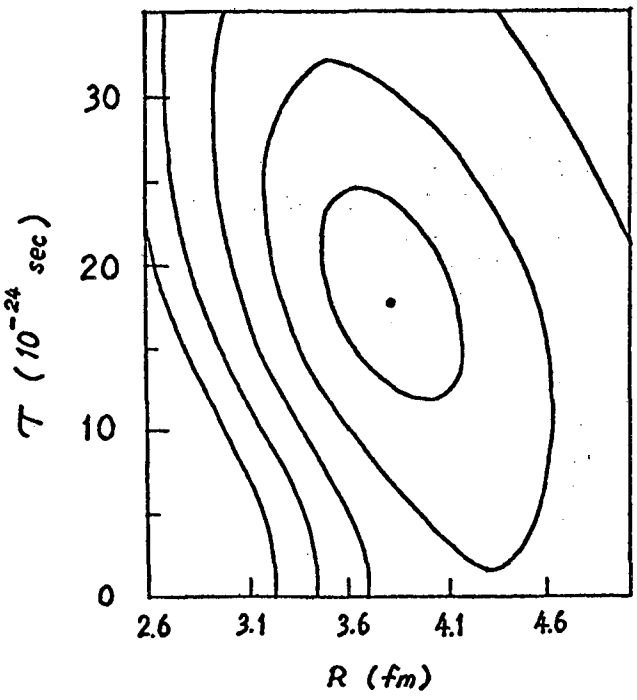

Figure 3

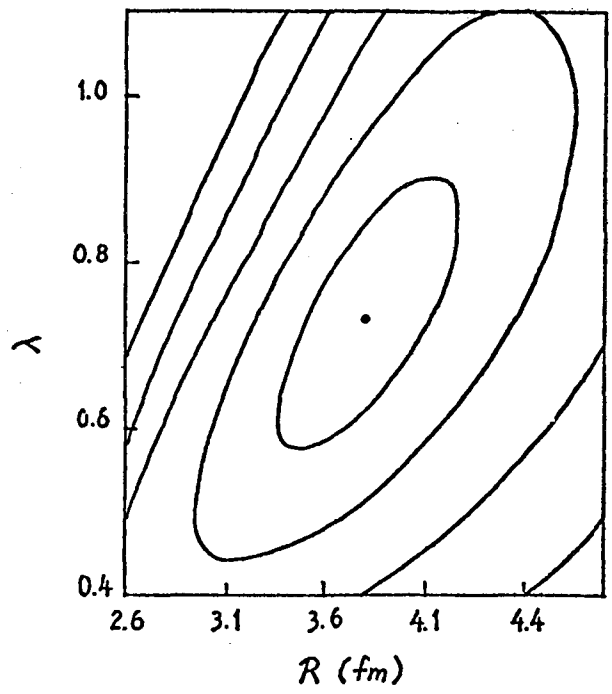

Figure 4

Two Particle Correlations Observed with the Plastic Ball Detector

H. Wieman, H.H. Gutbrod, H.A. Gustafsson, B. Kolb,
H. Löhner, B. Ludewigt, A.M. Poskanzer, T. Renner,
H. Riedesel, H.G. Ritter, A. Warwick, and F. Weik

Gesellschaft für Schwerionenforschung, Planckstrasse 1
D-6300 Darmstadt 11, West Germany and
Nuclear Science Division, Lawrence Berkeley Laboratory
University of California, Berkeley, CA 94720, USA

Three different categories of two-particle correlations are being investigated in the analysis of the Plastic Ball data. The first category, which has already received the most attention by others in the field of relativistic heavy ions, is source size determination using Hanbury-Brown, Twiss type interferometry. Two-pion correlations have been measured for this purpose with a streamer chamber[1] and with a magnetic spectrometer.[2] Source size measurements have also been made with proton-proton correlations[3] following the calculations of Koonin,[4] which include Coulomb and nuclear forces in addition to strictly interference effects. In this category of two-particle correlations the relative velocities are quite low. For protons the kinetic energy in the center of mass of the pair is on the order of 0.5 MeV.

The second category of two-particle correlations deals with low-energy nuclear cluster formation, the kinetic energy in the pair center of mass being in the region 1 MeV to 10 MeV. Here one observes nuclear composites--the formation and decay of particle unstable isotopes and levels such as ^{5}Li.

The third category addresses higher energies, 100 MeV or more in the center of mass of the pair. In this energy region the possibility exists for seeing baryon resonances. For example, delta decay might be observed via π^+-p correlations or dibaryon resonances by π^+-d correlations.[5]

Here we shall be reporting only on preliminary results obtained in the first two categories. So far, source sizes and cross sections have not been extracted as we have mainly been exploring, looking for those areas where the unique features of the Plastic Ball can best be exploited. The most obvious advantage of the Plastic Ball for two-particle correlation measurements is the large solid angle ($\sim 4\pi$) and rapid data collection, which allow better statistics than are easily obtained with other devices. On the other hand, the relatively coarse angular resolution (3.5° to 10°) and the limited energy resolution impose restrictions on the correlations that can be measured. The studies described here have been limited to the possible two-particle combinations of p, d, t, ^{3}He, and ^{4}He with low relative velocities. Particles included in the analysis were stopped in the Ball detector (laboratory angle 10° to 160°) where particle type and energy could be determined. As work progresses the correlations will be compared for various projectile target combinations, but to date our efforts have been concentrated on Ca + Ca at E/A = 400 MeV, the system for which we have the largest data set. These data were recorded using a central collision trigger.

The correlation function $F(\Delta p)$ has been generated in a manner similar to that used in two-particle interferometry studies.[3]

$$F(\Delta p) = nN_s(\Delta p)/N_d(\Delta p)$$

where $N_s(\Delta p)$ is the number of pairs per unit Δp taken from the same event and $N_d(\Delta p)$ are the number of pairs per unit Δp constructed from different events. The momentum Δp is the particle momentum in the center of mass of the pair. The factor n is chosen arbitrarily such that $F(\Delta p)$ equals approximately one at large Δp. This correlation function is closely related to the R correlation function used by Koonin: $F(\Delta p) - 1 \cong R(\Delta p)$. $F(\Delta p)$ is greater than 1 for positive correlations. The particle momentum in the center of mass (Δp) was chosen for this analysis for two reasons. First, this choice is consistent with the variable used in other source size determinations ($\Delta p \cong |\vec{p}_1 - \vec{p}_2|/2$ for pairs of like massed particles). Second, Δp is easily related (nonrelativistically) to Q values and excitation energies (E_x) of clusters formed from the pair, i.e.,

$$\Delta p = \sqrt{2 \frac{m_1 m_2}{m_1 + m_2} (E_x + Q)} \quad .$$

The resulting correlation function for proton-proton pairs is shown in fig. 1. The two solid curves shown with the measured correlation function are predictions[4] for Gaussian sources with rms radii of r_0 = 3 fm and 5 fm and a lifetime of $\tau = 0$. The expected enhancement in the measured correlation function is clearly observed, but it peaks at 30 MeV/c instead of 20 MeV/c, Koonin's predicted value. Also the peak is broader than predicted. Both of these distortions can be blamed on the finite angle subtended by a Plastic Ball detector module. This distortion, however, is probably not a serious problem for a source size analysis, since the integrated peak area should be as sensitive as the peak height to the source radius.

We have found that p-p is not the only two-particle system to show correlations at low Δp. A number of other two-particle systems exhibit stronger correlations, some positive, some negative. The most striking examples appear in figs. 2 and 3. As shown, there is a strong enhancement in the p-^{4}He system at a Δp value corresponding to the decay of the ^{5}Li ground state. Likewise, d-^{4}He has a peak that apparently comes from the decay of the lowest excited levels of ^{6}Li. For the d-d system, on the other hand, there is a negative correlation. At low relative velocity deuterons appear to coalesce into excited states of ^{4}He that decay by another channel. The observed depression in the d-d correlation function extends up to Δp = 150 MeV/c. This is well beyond the Δp = 55 MeV/c instrumental cutoff imposed by the finite angular size of the detectors in the Plastic Ball. The d-d system may be contrasted with the p-t system, which couples to slightly lower values of ^{4}He excitation. In this case there is evidence again of a positive correlation at low Δp.

The results obtained so far show that the Plastic Ball with its large solid angle can be a useful tool for measuring two-particle correlations. The present effort on two-particle correlations will continue along two lines. First, work will continue towards extracting source size information from proton-proton correlations. The initial question is how much does the limited detector angular resolution distort the true correlation function, and is this important? Perhaps the integrated peak in the correlation function is sufficient for source size measurements. There is the additional, more fundamental question, what is the meaning of the source size? Maybe this is the freeze-out radius since correlations from an earlier stage would probably be largely destroyed through later interactions.

The second line of effort will be devoted to extracting relative cross sections for the formation of the particle-unstable isotopes and levels that we have observed. These can then be compared with phase space models such as Fai and Randrup's,[6] which predict yields of stable as well as unstable clusters.

This work was supported in part by the Director, Office of Energy Research, Division of Nuclear Physics of the Office of High Energy and Nuclear Physics of the U.S. Department of Energy under Contract DE-AC03-76SF00098.

References

1. J.J. Lu, et al., Phys. Rev. Lett. 46, 898 (1981)
2. J.A. Bistirlich, et al., LBL-13366, 146 (1982)
3. F. Zarbakhsh, et al., Phys. Rev. Lett. 46, 1268 (1981)
4. S.E. Koonin, Phys. Lett. 70B, 43 (1977)
5. T. Siemiarczuk, J. Stepaniak, private communication, 1983
6. J. Randrup, G. Fai, Phys. Lett. 115B, 281 (1982)

Figure Captions

Fig. 1. p-p two-particle correlation function as a function of the particle momentum in the center of mass of the pair. Solid curves are predictions of Koonin for sources with rms radii of r_0 = 3 fm and 5 fm. The source lifetime is $\tau = 0$. Values of $F(\Delta p)$ greater than 1 indicate a positive correlation.

Fig. 2. Two-particle correlation functions for d-^{4}He coupling to ^{6}Li and p-^{4}He coupling to ^{5}Li. Position of levels known to decay to the pair particles are indicated.

Fig. 3. Two-particle correlation functions for d-d p-t both coupling to ^{4}He. Correlations are shown as a function of the particle momentum in the center of mass of the pair. Position of some ^{4}He excited states are indicated in the p-t system.

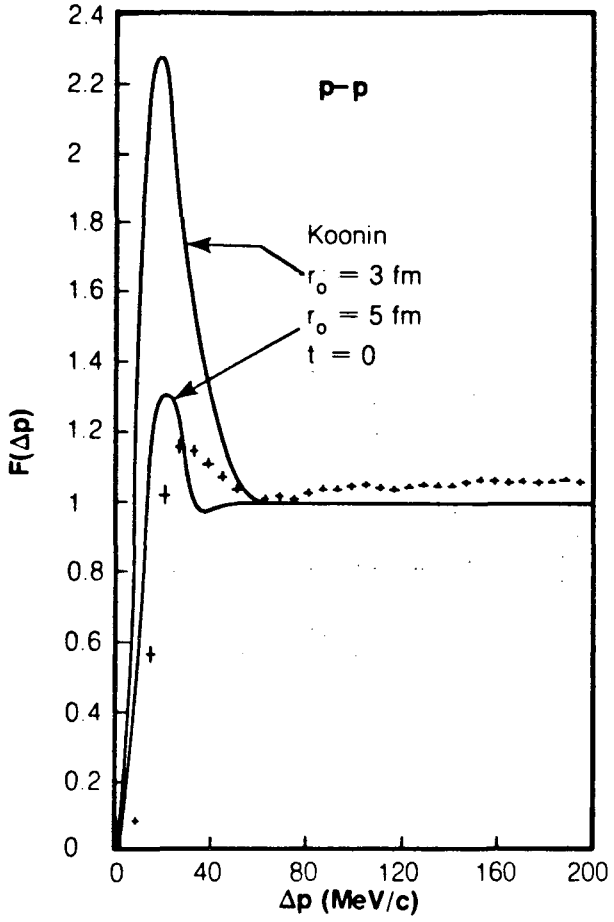

Fig. 1

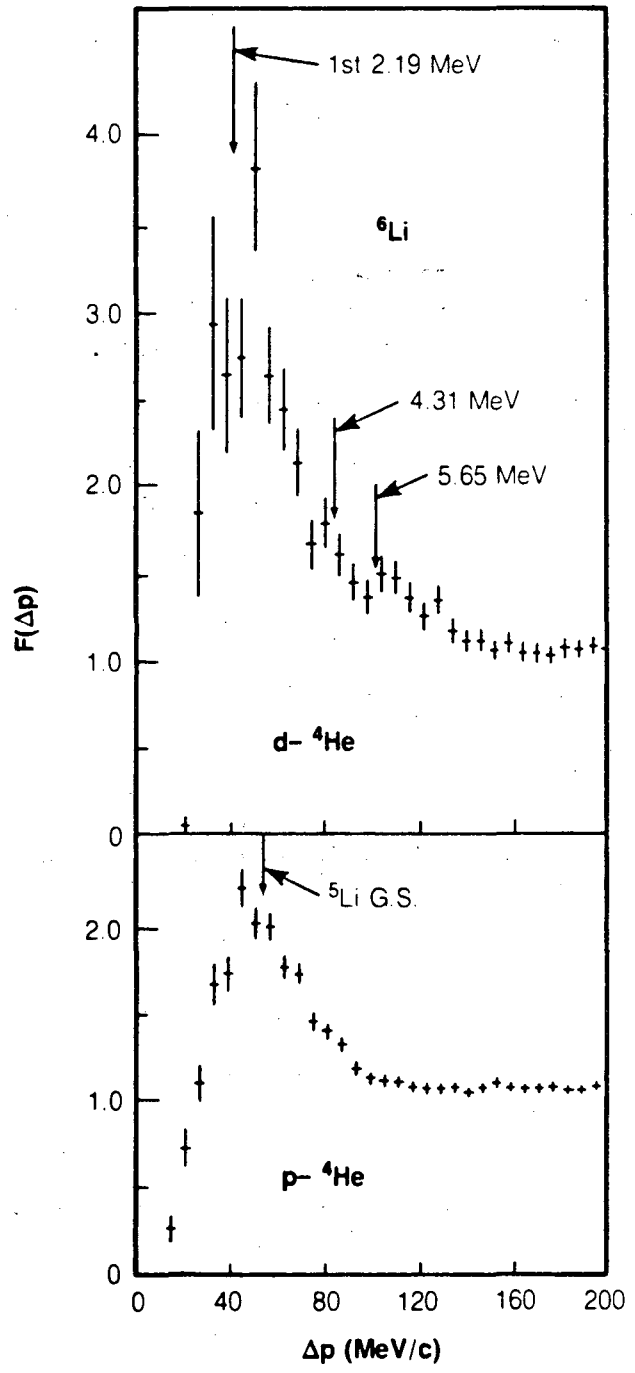

Fig. 2

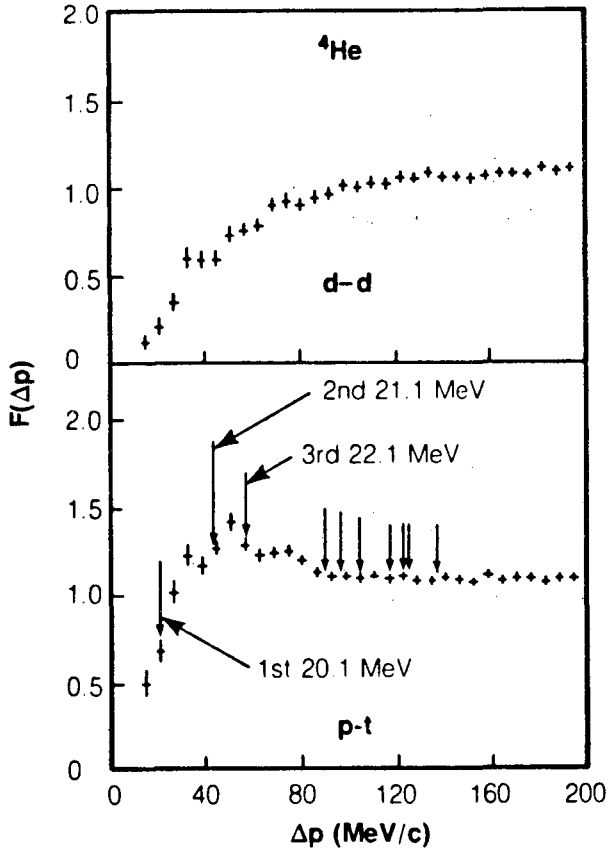

Fig. 3

Composite Particle Production Measured with the Plastic Ball

T.R. Renner, H.A. Gustafsson, H.H. Gutbrod, B. Kolb, H. Löhner, B. Ludewigt, A.M. Poskanzer, H. Riedesel, H.G. Ritter, A. Warwick, F. Weik, H. Wieman

Gesellschaft für Schwerionenforschung, Planckstrasse 1
D-6300 Darmstadt 11, West Germany, and
Nuclear Science Division, Lawrence Berkeley Laboratory
University of California, Berkeley, CA 94720

One of the questions to be answered by studying collisions of nuclei at relativistic energies is whether phase transitions can occur in nuclear matter. Several models have suggested changes in entropy as a signature of such a phase transition (1). More recently a suggestion has been made that one measure of entropy might be the comparison of the deuteron yield to the proton yield (2). A further refinement has been made that proposes measuring the number of real and virtual deuterons to determine entropy. This d-like quantity as defined by Bertsch and Cugnon (3):

$$\text{d-like} = D + 3/2(He3 + T) + 3He4$$

is used in this work.

The measurements of these quantities up until this time has been done with single particle inclusive measurements. As has been shown recently with results from the Plastic Ball such measurements average over impact parameters. Consequently, information about quantities that have a charge particle multiplicity or impact parameter dependence is lost. The results to be reported on in this work indicate just such a dependence of d-like/p-like on charge particle multiplicity, which is defined as follows

$$\text{p-like} = P + D + T + 2(He3 + He4)$$

The detection and identification of composite particles by the Plastic Ball have several limitations affecting the d-like to p-like ratio. First, there is a 40 MeV per nucleon lower threshold, which suffices to exclude target spectator fragments that come from a late stage of the collision from being included in the measurements. Second, the particle identification scheme of the Plastic Ball does not allow a distinction between protons and deuterons above a deuteron energy of about 400 MeV. Further limitations in particle identification make it judicious to use only the yields as measured in the backward hemisphere in the center-of-mass system (which for symmetric systems is just the nucleon-nucleon center of mass) and multiplying them by two. This effectively excludes projectile spectator matter. The $\tilde{d}$-like and $\tilde{p}$-like quantities to be presented are measured in this way.

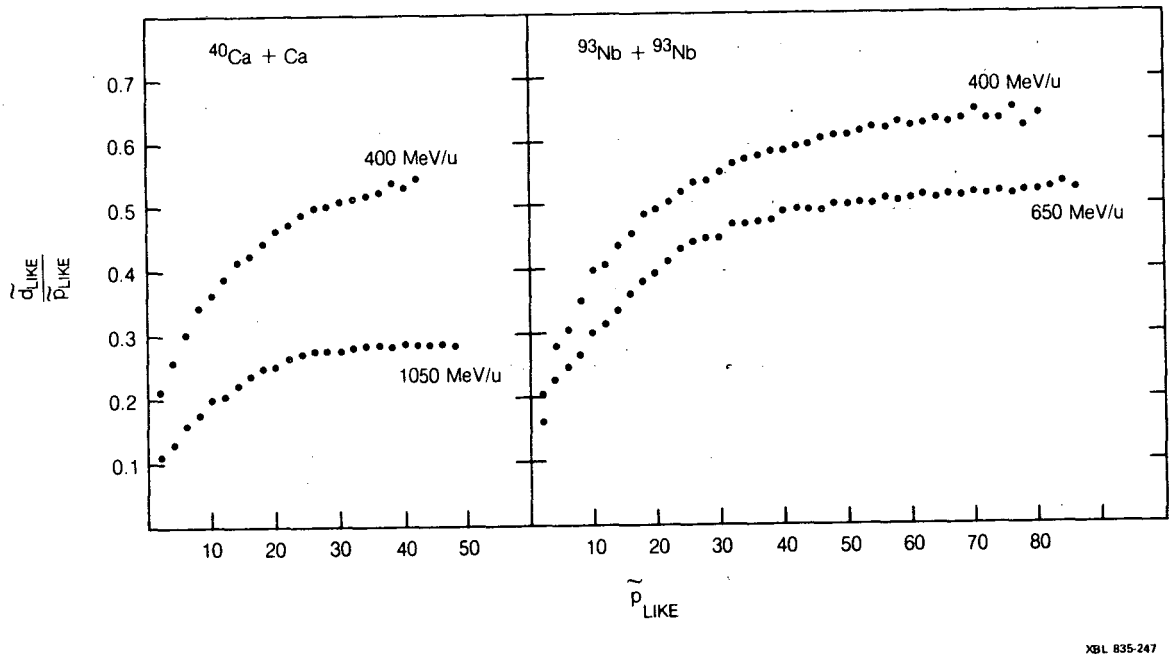

Figure 1

The data as seen in Figure 1 are for the systems Ca + Ca at E/A = 400 and 1050 MeV and Nb + Nb at E/A = 400 and 650 MeV. Clearly, the $\tilde{d}$-like/$\tilde{p}$-like ratios change as a function of multiplicity but also seem to saturate for high $\tilde{p}$-like values. Furthermore, the data show that for a given $\tilde{p}$-like value the ratio depends on the target + projectile system and the bombarding energy. The implications of this await a consensus among theorists on just how to extract entropy from $\tilde{d}$-like to $\tilde{p}$-like ratios. Values extrapolated to high multiplicity, in any case, might be the most appropriate to use.

Fits to these data can be made in terms of the coalescence model, which has been recently improved (4) to include the finite size of the deuteron, as well as the volume of the participant region. The coalescence radius p_0 in momentum space is related to the deuteron radius r_d and the participant radius R by

$$\frac{\tilde{d}\text{-like}}{\tilde{p}\text{-like}^2} = \frac{4}{3}\pi p_0^3 = \frac{N}{\left[1+2(R/r_d)^2\right]^{3/2}}$$

where N is a normalization factor and R can be related to the observed charges by $R = r_0\ (2\ \tilde{p}\text{-like})^{1/3}$ with r_0 a free parameter. Fits varying the normalization and the ratio of r_0/r_d yield an r_0/r_d value of ~0.34 for the systems Ca + Ca at E/A = 400 MeV and Nb + Nb at E/A = 400 and 650 MeV. To extract an r_0 value the value of r_d must be known. The free deuteron radius of 2.2 fm gives values for r_0 that suggest a freeze out density greater than normal nuclear matter. However, a recent paper by Schulz et al. (5) finds the deuteron radius to be a function of temperature and pressure. Their calculations suggest a deuteron size of ~3.9 fm at a temperature of 60 MeV and a density close to normal nuclear matter density. The r_0 extracted

would then be 1.35 fm corresponding to a freeze out density of ~0.8 times the density of normal nuclear matter, which is clearly higher than expected. The question of the deuteron size and the value of the freeze out density remains a puzzle. A more complete phase space calculation of cluster production using the formula of Gyulassy and Remler (6) yields essentially the same values for the freeze out density.

Finally, the formula given above (4) can also be used to extract the $\tilde{d}$-like/$\tilde{p}$-like values for high multiplicities by rewriting it as

$$\frac{\tilde{d}\text{-like}}{\tilde{p}\text{-like}} = \frac{N\ \tilde{p}\text{-like}}{\left[1+2(r_o/r_d)^2(2\ \text{p-like})^{2/3}\right]^{3/2}}$$

For large $\tilde{p}$-like values then the factor of one is negligible and the ratio simply becomes:

$$\frac{\tilde{d}\text{-like}}{\tilde{p}\text{-like}} = \frac{N}{2^{5/2}(r_o/r_d)^3}$$

The values extracted for $\tilde{d}$-like/$\tilde{p}$-like from the fit values of N and r_o/r_d are shown in Table 1. These values as a function of the incident projectile energy will no doubt be of interest in looking for phase transitions in nuclear matter and will be forthcoming from the Plastic Ball. How to determine the entropy of a system from these ratios clearly needs theoretical attention.

Table 1

System	E/A	d-like/p-like
Ca + Ca	400	0.74
Ca + Ca	1050	0.37
Nb + Nb	400	0.83
Nb + Nb	650	0.66

This work was supported in part by the Director, Office of Energy Research, Division of Nuclear Physics of the Office of High Energy and Nuclear Physics of the U.S. Department of Energy under Contract DE-AC03-76SF00098.

References

1. H. Stöcker, W. Greiner, and W. Scheid, Z. Physik A286, 121 (1978)
   H. Stöcker, J. Maruhn, and W. Greiner, Phys. Lett. 81B, 303 (1979)
2. P. Siemens and J. Kapusta, Phys. Rev. Lett. 43, 1486 (1979)
3. G. Bertsch and J. Cugnon, Phys. Rev. C24, 2514 (1981)
   J. Cugnon, Proc. of ICOSAHIR, Nucl. Phys. A387, 191c (1982)
4. H. Sato and K. Yazaki, Phys. Lett. 98B, 153 (1981)
5. H. Schulz, G. Ropke, K.K. Gudima, and V.D. Toneev, Phys. Lett. 124B, 458 (1983)
6. M. Gyulassy and E. Remler, private communication (1983)

Pion Spectra in the Reaction Ar + KCl at 1.8 GeV/Nucleon

R. Brockmann, J.W. Harris, M. Maier, A. Sandoval, R. Stock,
H. Stroebele, and K.L. Wolf*
Gesellschaft fuer Schwerionenforschung
D-6100 Darmstadt, West Germany
and
H.G. Pugh and L.S. Schroeder
Nuclear Science Division, Lawrence Berkeley Laboratory
University of California, Berkeley, CA 94720
and
R.E. Renfordt
Universitaet Heidelberg
D-69 Heidelberg, West Germany

Pion production in the symmetric system Ar + KCl was studied in the energy range 0.4-1.8 GeV/nucleon using the Streamer Chamber Facility at the Bevelac. The main purpose of this experiment was to measure a complete set of pion spectra, in order to test existing and future theoretical models describing the pion production and absorption in nucleus-nucleus collisions at higher nuclear densities. Up to now there exists no theoretical or phenomenological approach that reproduces all the features of the pion production mechanism, though specific aspects are well reproduced by several models.

In the following we report some observations that were made in central collisions at an incoming energy of 1.8 GeV/nucleon, which to our knowledge are not predicted by any of the existing theoretical or phenomenological approaches.

Already in the study of inclusive pion spectra by Nagamiya et al. (1) an interesting variation in the angular anisotropy as a function of pion energy was observed in the reaction Ar + KCl at 0.8 GeV/nucleon.

We observe the same behavior of the angular distribution in central collisions at 1.8 GeV/nucleon, which has been parameterized according to

$$\frac{1}{p_{c.m.}} \frac{d^2\sigma}{dE\,d\Omega} \sim (1 + a \cos^2\theta)$$

In Fig. 1 the parameter "a" is plotted as a function of the kinetic energy E of the pion in the nucleon-nucleon c.m. system. The angular distribution is anisotropic for pions in the kinetic energy region corresponding to delta decay, but for pions with E > 350 MeV the emission again becomes more isotropic.

To our knowledge none of the existing models predicts this behavior. The result for parameter "a" from a nucleus-nucleus cascade calculation (2), which does not include multi-pion production, is also plotted in Fig. 1 and a comparison shows that pions with energies E > 300 MeV observed in the experiment are much more isotropic than those calculated in the cascade.

This pion emission pattern might suggest that the very energetic pions are emitted from a fireball-like interaction region, which is created in the very center of the reaction volume, whereas most of the pions are produced in the reaction NN = delta N = PI NN and subsequent final state interactions.

Further support of this reaction mechanism stems from the transverse-momentum spectrum (pper spectrum) of the pions. In Fig. 2a the pper spectrum is plotted and fitted with a single temperature according to Hagedorn's thermodynamical model (3). The fit gives a temperature of T = 68.2 ± 0.5 MeV; however, this fit is completely rejected by the large value of χ^2, whereas the cascade results are fitted quite well with T = 68.8 ± 5 MeV (Fig. 2b). In Fig. 3 a fit with two temperature components is applied to the data. The two temperatures T1 = 58.7 ± 2 MeV and T2 = 102.4 ± 6 MeV were extracted.

These two temperatures might be interpreted as direct fireball pions (4) with the temperature T2 and pions with temperature T1 originating from decaying deltas.

From the statistical model one would expect a temperature of about T2 = 110 MeV for the fireball pions and for pions originating from completely thermalized deltas of about T1 = 79.6 MeV (5) if one neglects cooling. The temperature of the parent delta distribution in this case is assumed to be equal to the temperature of the lambdas (T = 116 MeV), which was measured previously (6) in the same experiment.

We conclude from the analysis of the pion spectra that there is some experimental evidence that the pions are mainly emitted from deltas, which might to a certain extent be thermalized, whereas a fraction of the pions is emitted from a hot fireball-like very central interaction region. These pions carry the temperature T = 102 MeV, which agrees reasonably with the prediction of the statistical bootstrap model (4), though the forward-backward enhancement of pion emission is not reproduced by this model.

This work was supported in part by the Director, Office of Energy Research, Division of Nuclear Physics of the Office of High Energy and Nuclear Physics of the U.S. Department of Energy under Contract DE-AC03-76SF00098.

References

*Present address: Texas A & M University, College Station, Texas

(1) S. Nagamiya, et al., Phys. Rev. C24, 971 (1981)
(2) J. Cugnon, Nucl. Phys. A379, 553 (1982)
(3) R. Hagedorn, Suppl. Nuovo Cimento 3, 147 (1965)
(4) R. Hagedorn, and J. Rafelski, Phys. Lett. 97B, 136 (1980)
(5) R. Hagedorn, private communication (1983)
(6) J.W. Harris, et al., Phys. Rev. Lett. 47, 229 (1981)

Figure Captions

Fig. 1. Fit parameter "a" as a function of the kinetic energy of the pions in the nucleon-nucleon c.m. system.

Fig. 2a. Transverse-momentum spectrum of the pions fitted with a one-temperature component distribution (see text).

Fig. 2b. Transverse-momentum spectrum of the pions from a cascade calculation with a one-temperature component distribution.

Fig. 3. Same distribution as Fig. 2a but fitted with a two-temperature component distribution.

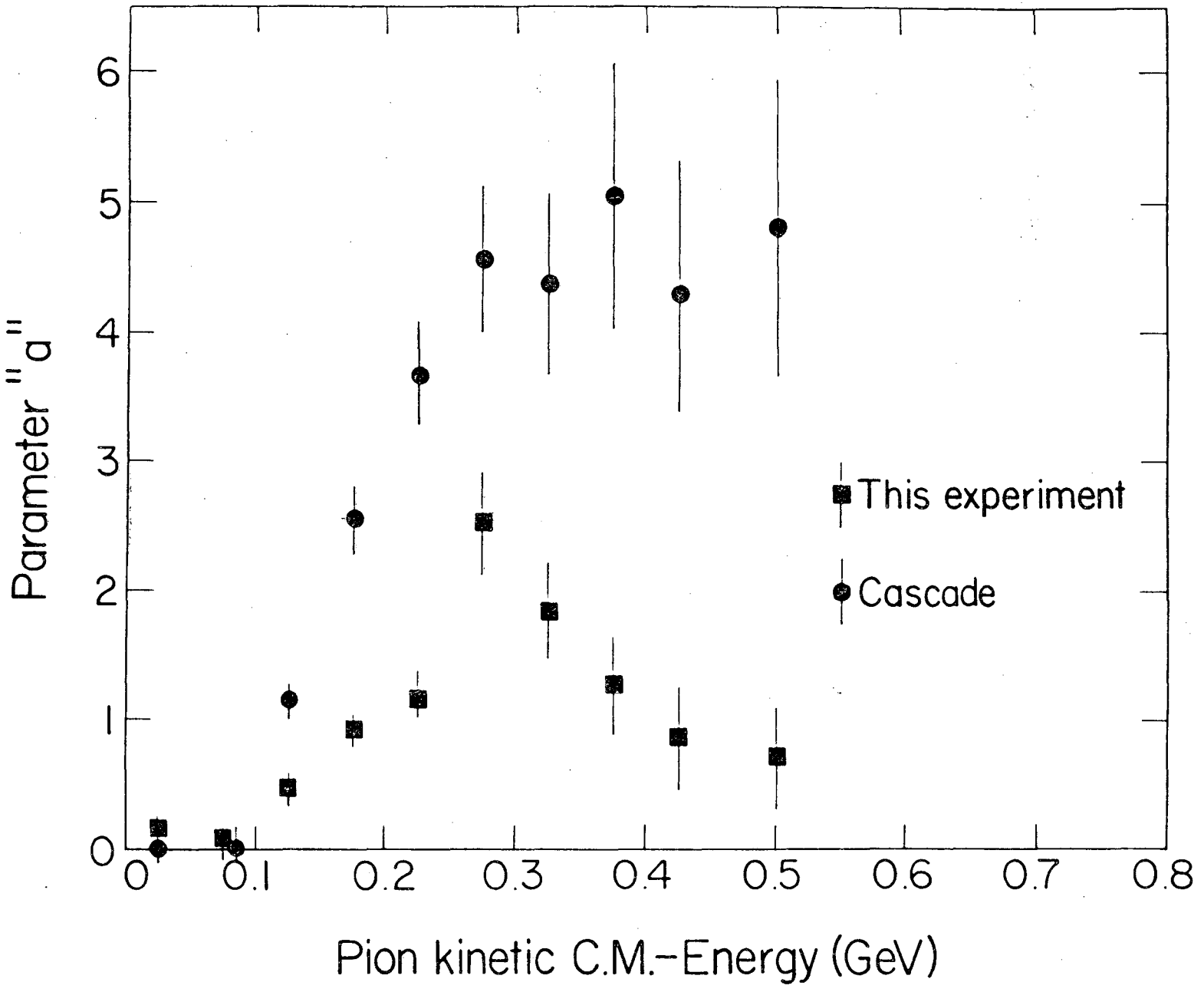
Parameter "a"
0
1
2
3
4
5
6
0
0.1
0.2
0.3
0.4
0.5
0.6
0.7
0.8
Pion kinetic C.M.-Energy (GeV)
This experiment
Cascade

Fig. 1

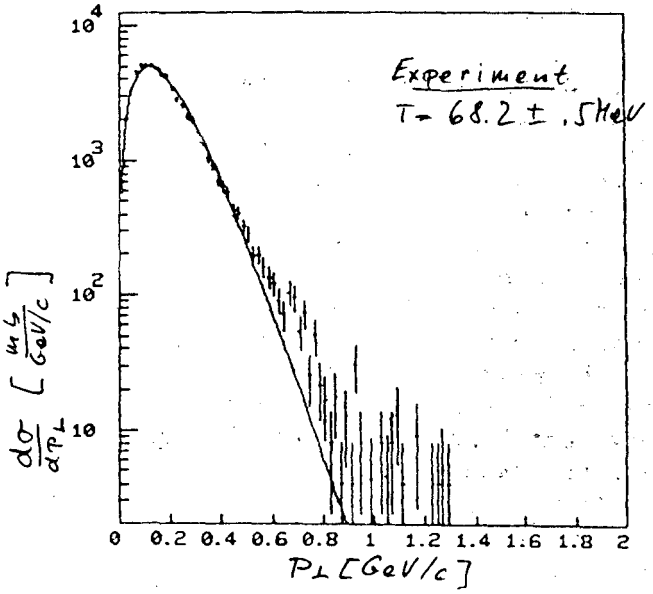

Fig. 2a

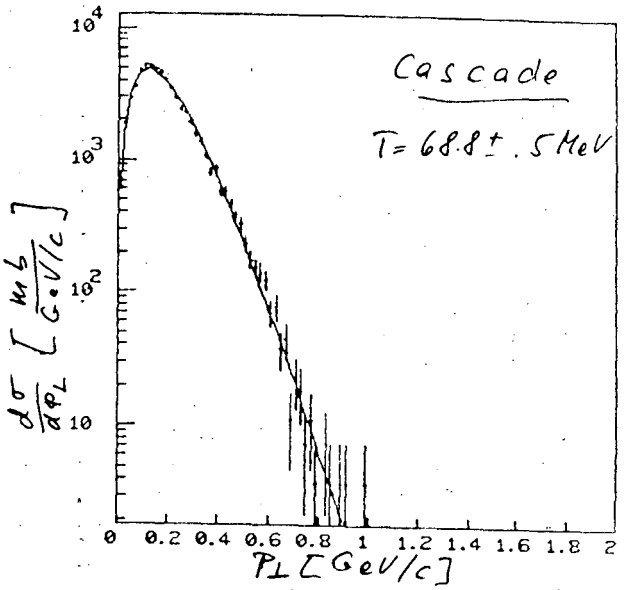

Fig. 2b

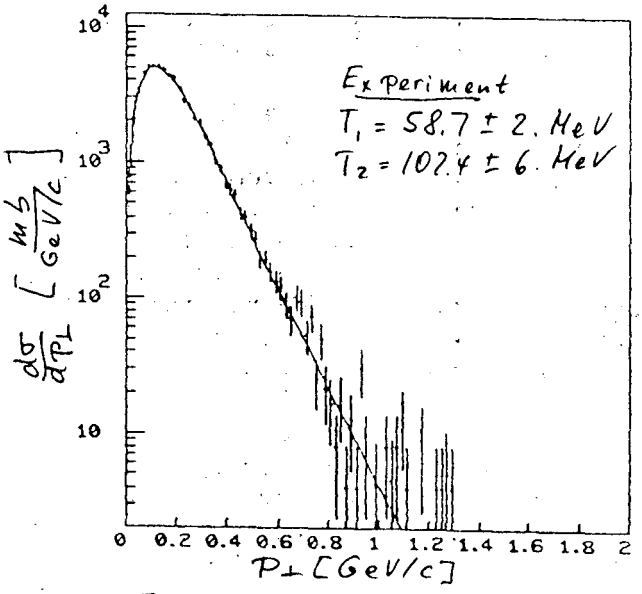

Fig. 3

Au TARGET FRAGMENTATION AT INTERMEDIATE ENERGIES

K. Aleklett, W. Loveland, P. L. McGaughey, K. J. Moody, R. M. McFarland, R. H. Kraus, Jr. and G. T. Seaborg, Lawrence Berkeley Laboratory, Berkeley, CA 94720

Target fragment yields were measured for the interaction of 12.0 and 18.4 MeV/u ^{16}O and 45.8 and 83.8 MeV/u ^{12}C with ^{197}Au.

In Figure 1 we show the isobaric yield distributions for the systems studied in this work along with similar data for lower and higher energy experiments. Because we have previously shown that the product yield distributions are generally invariant (with the exception of the light fragments) in the projectile energy region from 250-2100 MeV/u, we choose to represent all "high energy" distributions with a single distribution from the interaction of MeV/u ^{20}Ne with ^{197}Au. Upon examining the data of Figure 1 one observes three distinct qualitative changes in the product mass distributions with increasing projectile energy. The yields of the light fragments (A<60) increase dramatically with increasing projectile energy. The magnitude of the large central "hump" in the mass distribution (which generally represents fission events) decreases with increasing projectile energy until at the highest energies it is barely, if at all, separable from other processes. In addition the centroid of the fission product mass distribution moves to lower A values representing a decrease in the average mass of the fissioning system. Such a change would, of course, be expected as a consequence of decreasing complete fusion and increasing incomplete fusion with increasing projectile energy. The yields of those fragments whose mass numbers are between that of the target and the fission fragments increase sharply with increasing projectile energy while the yields of trans-target species sharply decrease and appear to be very small at projectile energies of 45 MeV/u and higher.

The comparison of the predictions of the nuclear firestreak model and this data is quite interesting. Perhaps because the firestreak model emphasizes the collective aspects of the reactions, which are more important at intermediate energies, it appears to do a good job in describing the data. It even appears to do a reasonable job of describing the 18.4 MeV/u data.

To describe the fragment yields from a "low-energy viewpoint", we used the generalized sum rule model of Wilczynski et al.[1] to calculate the cross sections for various incomplete and complete fusion reactions. The excitation energy of each of the many resulting products was assumed to be the "optimal" excitation energy as calculated using a semi-classical DWBA by Toepffer[2] and as used by Hubert et al.[3] to calculate the yields of transfer products in low energy reactions. The de-excitation of each primary fragment was calculated using the same DFF code used in the firestreak calculations. The agreement between the calculated and measured fragment yields for the reaction of 12.0 MeV/u ^{16}O with ^{197}Au seems excellent. Satisfactory agreement between the calculations and the data is also seen at 18.4 MeV/u projectile energy but when the projectile energy is raised to 45.4 MeV/u there appears to be a significant difference betwen measured and calculated distributions. This discrepancy may be due to the fact that the only way in which the projectile energy enters into the model is the calculation of the projectile wavelength giving rise to the situation that the angular momentum windows leading to each particular type of transfer are energy independent.

The dramatic increase in the yields of the light fragments with increasing projectile energy is of considerable interest. In Figure 2 we compare the excitation functions for two typical light fragments (^{24}Na and ^{46}Sc) produced in the fragmentation of ^{197}Au by protons and heavy ions. The data used in compiling Figure 2 come from various published and unpublished data and this work. Above some energy, the fragment yields from the proton induced fragmentation become invariant with further increases in projectile energy while the yields from the heavy ion reactions appear to increase slightly with increasing projectile energy. The ratio of yields of a given fragment in proton and heavy ion reactions is greater than the ratio of the total reaction cross sections.

The determination of the relative thresholds for the heavy ion and proton induced reactions may be instructive. No simple linear dependence of the light fragment production cross sections upon $1/E_{cm}$ can be found which indicates more than one mechanism is operating in producing these fragments. This is consistent with previous observations of the binary or non-binary character of these reactions at intermediate and high energies, respectively. Simple comparisons of the data in Figure 2 indicate that the heavy ion reactions have lower thresholds for the production of light fragments than do the proton induced reactions. This situation is predicted by a model due to Bertsch[4] in which the light fragments are produced from unstable nuclear matter reached by an isentropic expansion of overstressed nuclear matter.

References:

1. J. Wilczynski, K. Siwek-Wilczynska, J. van Driel, S. Gonggrijp, D.C.J.M. Hageman, R.V.F. Janssens, J. Lukasiak, and R.H. Siemssen, Phys. Rev. Lett. 45, 606 (1980).

2. C. Toepffer, Z. Physik 253, 78 (1972).

3. F. Hubert, H. Delagrange, and A. Fleury, Nucl. Phys. A228, 415 (1974).

4. G. F. Bertsch (to be published).

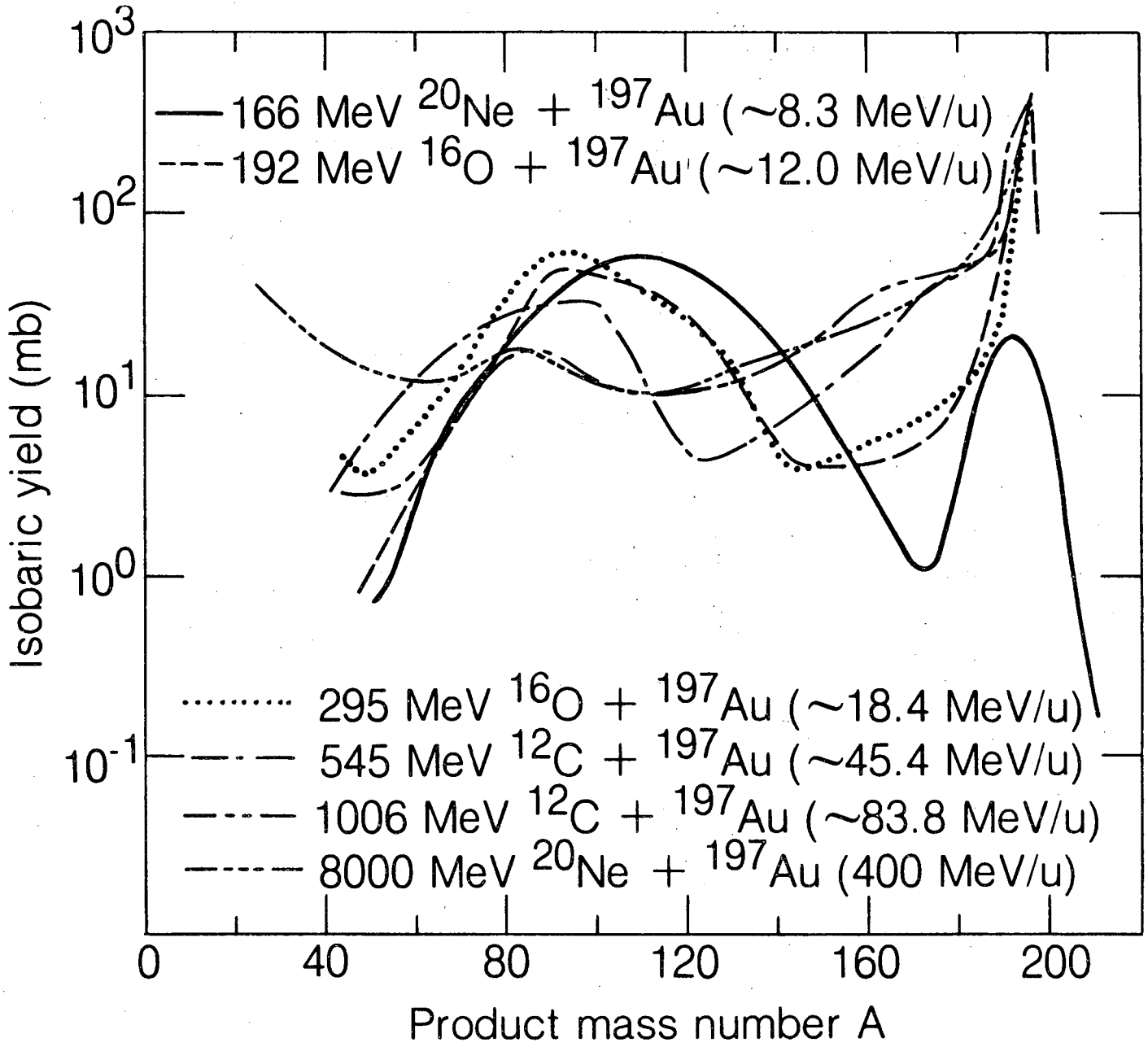
166 MeV ^{20}Ne + ^{197}Au (~8.3 MeV/u)
192 MeV ^{16}O + ^{197}Au (~12.0 MeV/u)
295 MeV ^{16}O + ^{197}Au (~18.4 MeV/u)
545 MeV ^{12}C + ^{197}Au (~45.4 MeV/u)
1006 MeV ^{12}C + ^{197}Au (~83.8 MeV/u)
8000 MeV ^{20}Ne + ^{197}Au (400 MeV/u)
Isobaric yield (mb)
10^3
10^2
10^1
10^0
10^{-1}
0
40
80
120
160
200
Product mass number A

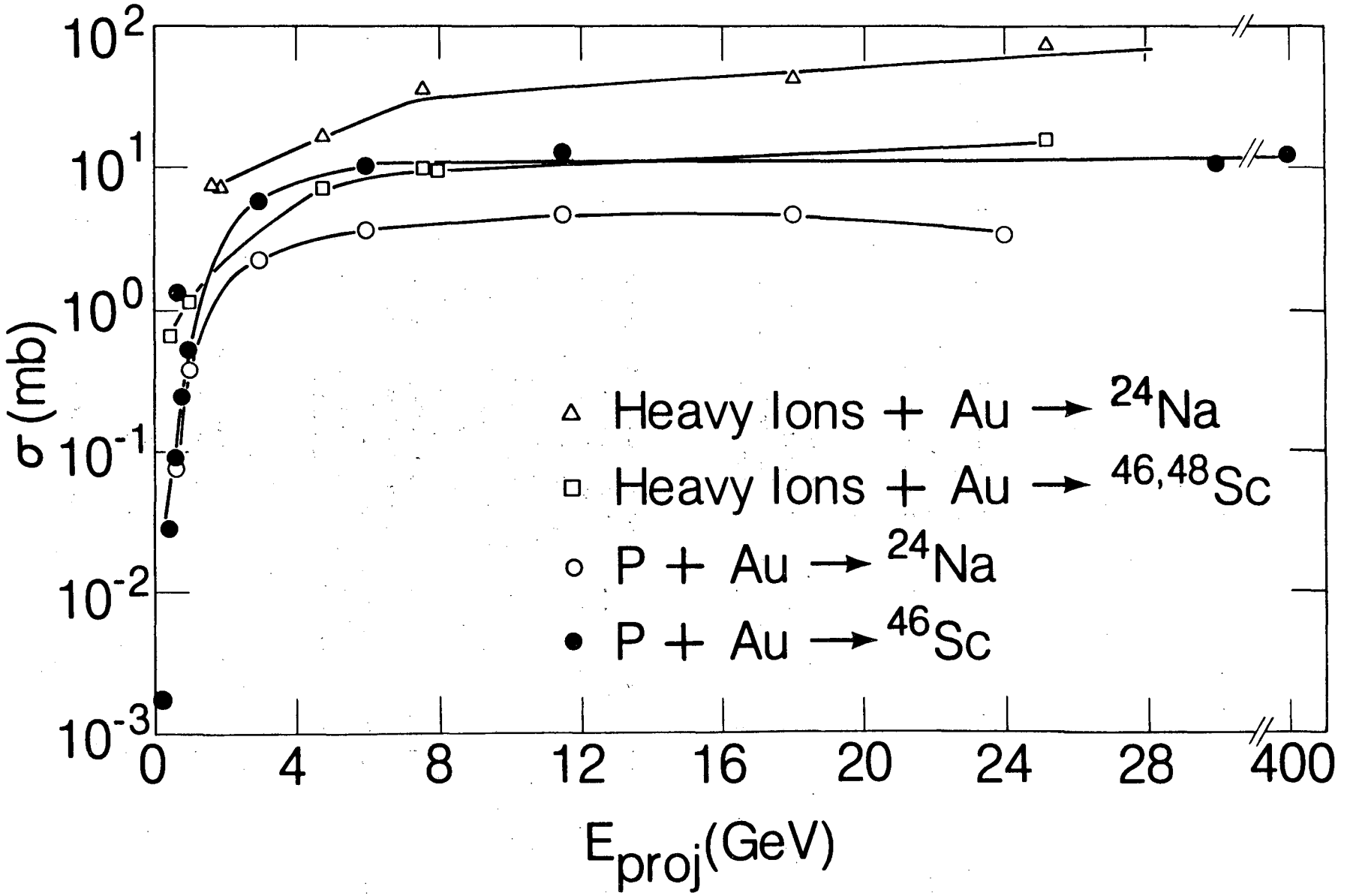
10^2
10^1
10^0
10^{-1}
10^{-2}
10^{-3}
σ (mb)
0
4
8
12
16
20
24
28
400
E_{proj}(GeV)
Heavy Ions + Au → ^{24}Na
Heavy Ions + Au → ^{46,48}Sc
P + Au → ^{24}Na
P + Au → ^{46}Sc

XBL 835-931

PHASE-SPACE CONSTRAINTS ON THE MOMENTA OF PROJECTILE FRAGMENTS

Martin J. Murphy
Nuclear Physics Laboratory
University of Washington
Seattle, WA 98115

ABSTRACT

The model of projectile fragmentation as a fast reaction which samples the nucleon Fermi momenta in the projectile prior to the collision is revised to reflect the fact that the fragment is also a Fermi gas. The results predict fragment momentum distributions which are narrower than those observed.

A fundamental feature of relativistic projectile fragmentation reactions is that, for a projectile of mass A and fragment of mass K, the longitudinal momentum distributions for the fragments in the projectile rest frame have Gaussian shapes whose widths σ can be approximately described by

$$\sigma^2 \cong \frac{K(A-K)}{A-1}\,\sigma_0^2, \qquad [1]$$

where σ_0 is ≈90 MeV/c for most fragment masses[1]. In an early interpretation of these observations, Feshbach and Huang[2] postulated a fast reaction mechanism which samples all possible combinations of ground-state nucleon momenta in the projectile prior to the collision. Goldhaber[3] subsequently showed that if the projectile nucleons have a mean-square momentum equal to $(3/5)p_F^2$, where p_F is the Fermi momentum, then such a sampling has a momentum dispersion of the form of eq. (1), with $\sigma_0^2 = (1/5)p_F^2$. This predicts $\sigma_0 \cong 112$ MeV/c.[3] In a later paper, Bertsch[4] treated the correlations between the momenta of individual nucleons localized in space and calculated a corrected width for ^{40}Ar fragmentation which was 17% smaller than Goldhaber's prediction. The agreement with experiment is compelling. However, there are still more constraints on the nucleon momenta; I shall describe one here which further narrows the momentum distributions, so that the prediction of the fast reaction mechanism is less than the observed widths.

The problem solved by Goldhaber[3] involved only the constraint $\langle p^2 \rangle = (3/5)p_F^2$ on the magnitudes of the individual nucleon momenta in the projectile rest frame. Goldhaber's problem placed no upper limit on the magnitude of any one nucleon's momentum in the projectile frame, and no constraints at all on the final-state nucleon momenta in the fragment rest frame. In reality, the bound-nucleon momenta in both the projectile and fragment are arranged in Fermi distributions with an upper limit on their magnitudes, which we may assume to be the Fermi momentum P_F. I shall show that the more realistic situation of Fermi gases for both the projectile and fragment significantly reduces the phase space available to nucleons in

the fragment, relative to the situation considered by Goldhaber. This has the consequence of narrowing the predicted distribution of a fragment's total momentum in the projectile frame.

To investigate the effects of constraints on the individual nucleon momenta in the projectile and fragment frames, I proceed in the following way: Let $\{\vec{p}_i\}$ designate the A nucleon momenta in the projectile frame, and $\{\vec{p}_j\}$ the momenta of K of these nucleons in the fragment K's rest frame. If the fragment K has a total momentum $\vec{P}_K$ in the projectile frame, then the addition of velocities requires $(1/K)\vec{P}_K + \vec{p}_j = \vec{p}_i$ for the (i=j)th nucleon. First consider the case in which there is no constraint on the magnitudes $\{p_j\}$ for nucleons in the fragment. For any value of P_K, each magnitude p_j can be chosen small enough so that $\vec{p}_j$ can point anywhere in the phase-space sphere of radius p_j. This corresponds to the problem of Goldhaber. If, however, one requires that the projectile and fragment be bound nuclear systems such as Fermi gases, which have well-defined momentum distributions limited by their Fermi surfaces, then for sufficiently large P_K the momenta $\{\vec{p}_j\}$ can no longer have arbitrary directions – each is constrained to the segment of phase space defined by the polar angle β_j ($0 \leq \theta_j \leq \beta_j$). This is illustrated in Figure 1. (The nucleon momentum $\vec{p}_j$ is excluded from the shaded volume.)

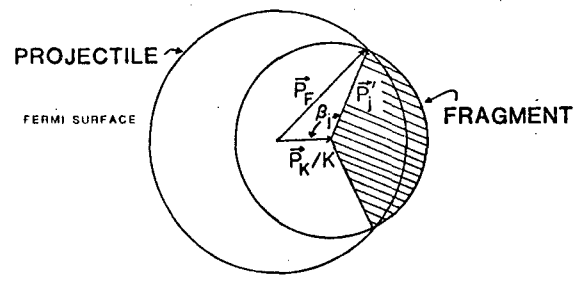

As the total momentum P_K of the fragment increases, the constraint allows less and less phase space for the fragment nucleons.

How does such a phase space restriction affect the width of the fragment's momentum distribution $N(P_K)$? Goldhaber obtained the dispersion σ of $N(P_K)$ by counting the number of ways in which A vectors, taken K at a time, can add up to P_K. I now ask, how many ways can a fragment be assembled of K momenta $\{\vec{p}_j\}$ with, and without, constraints on the directions of the $\vec{p}_j$? The condition on the momenta in the fragment nucleus K is that they satisfy

$$\sum_{j=1}^{K} \vec{p}_j = 0 \qquad [2]$$

Thus the question reduces to determining the number of ways W that the unconstrained $\{\vec{p}_j\}$ can add to zero, and the number of ways W' that the constrained vectors can add to zero. The phase space restriction then reduces each point on the original momentum distribution $N(P_K)$ by a fraction $f(P_K) = W'/W$, and the corrected distribution is

$$N'[P_K] = f[P_K]N[P_K] \qquad [3]$$

This distribution has a new, smaller width σ'.

The quantities W and W' can be obtained by solving the random walk problem in three dimensions. In other words, I ask for the number of ways in which K vectors $\{\vec{p}_j\}$ can add up to a total $\vec{P}=0$, when each vector's magnitude

and direction is specified by a distribution function $\tau_j(\vec{p}_j)$. The formal solution (due to Markoff[5]) is obtained from the Fourier transforms of the functions τ_j:

$$W(0)d^3P = \frac{d^3P}{8\pi^3} \int_{-\infty}^{\infty} d^3k \prod_{j=1}^{K} \int_{-\infty}^{\infty} d^3p_j \, e^{i\vec{k}\cdot\vec{p}_j} \, \tau_j[\vec{p}_j] \qquad [4]$$

If we assume that the nucleon momenta $\vec{p}_j$ have discrete magnitudes ℓ_j and the polar angles θ_j are limited to β_j, then

$$\tau_j = \frac{1}{2\pi\ell_j^3[1-\cos\beta_j]} \, \delta\left[p_j^2 - \ell_j^2\right] H[\theta_j - \beta_j] \qquad [5]$$

where $H(\theta_j)$ is the Heaviside (unit step) function. For unconstrained momenta, $\beta_j = \pi$.

Before discussing the solution of eq. (4), a refinement of the phase space constraint is necessary. So far, I have considered a limit of p_F on the magnitudes of the momenta $\{\vec{p}_i\}$ in the projectile. In fact, the projectile nucleons are arranged in a Fermi sea, in a succession of states of momentum less than or equal to p_F. The K nucleons in the fragment are a sample of this distribution and thus some are limited to momenta much less than p_F in the projectile frame. To accomodate this set of constraints on the fragment nucleons, one can estimate the probability that the jth nucleon in the fragment corresponds to one of the nucleons in the projectile with momentum less than or equal to p_i. Then a weighted mean phase space constraint $\langle\beta_j\rangle$ on $\vec{p}_j$ can be computed to reflect the range of momenta in the projectile.

At this point we have a set of phase space constraints $\{\langle\beta_j\rangle\}$ on the momenta $\{\vec{p}_j\}$ which reflect the fact that the fragment is a Fermi gas, and was made of nucleons from another Fermi gas. The set of K different quantities $\{\ell_j, \langle\beta_j\rangle\}$ were averaged to obtain mean values ℓ and β. This permits use of the solution of Chandrasekhar[6] to eq. 4 for the case $\tau_j(\vec{p}_j) \to \tau(\vec{p})$ and large K:

$$f = \frac{W'}{W} \cong \frac{2\exp\left\{\left[\frac{-3K}{8}\right]\left[\frac{1+\cos\beta}{1+\cos\beta+\cos^2\beta}\right]\right\}}{\left[2-\cos\beta-\cos^2\beta\right]\left[1+\cos\beta+\cos^2\beta\right]^{1/2}} \qquad [6]$$

Equation (6) represents the fractional reduction f in the ensemble of ways a fragment of mass K and total momentum P_K may be formed, when one goes from having no constraints on the nucleon momenta $\{\vec{p}_i\}$ and $\{\vec{p}_j\}$, to a requirement that they form Fermi gases. How large is this effect for observable reactions? Inclusive momentum spectra have been measured for the fragmentation of 213 MeV/N ^{40}Ar projectiles,[7] 1050 MeV/N ^{12}C projectiles,[1] and 2100 MeV/N ^{12}C and ^{16}O projectiles.[1] The experimentally determined reduced widths σ_0 for the momentum distributions, defined according to eq. (1), are shown in Figure 2. Goldhaber's[3] prediction of $\sigma_0 \cong 112$ MeV/c for the fast reaction mechanism is indicated by a dashed line. The reduced widths σ_0' predicted by this calculation are shown by solid lines.

The phase space correction reduces the dispersions σ and introduces a mass dependence in σ_0', so that σ_0' decreases as K becomes small. The dependence on K becomes more pronounced as the projectile becomes smaller. A qualitatively similar mass dependence is present in the data. These features are directly linked to the distributions of nucleon momenta in the projectile and fragment. However, if ground-state Fermi momentum distributions are assumed for the nuclei, the corrected dispersions are systematically narrower than in the observed spectra, sometimes by a large degree. This will be further aggravated by other corrections to the momentum dispersion. For example, the correction by Bertsch[4] for ground state correlations, which has only been calculated for the ^{40}Ar projectile, reduces the width σ_0 in this reaction by an additional 17% for all fragment masses. (The combined correction for ^{40}Ar is shown as a dotted line in Figure 2.) In order to obtain predictions of σ_0 for ^{40}Ar that agree in magnitude with the observations, it would be necessary to increase the nucleon momenta in the projectile by 3% (for K=36) to 11% (for K=16) above the ground state, while keeping the fragment's distribution near the ground state. This corresponds to excitation of the projectile by 2 MeV/N (for K=36) to 7.6 MeV/N (for K=16) prior to fragmentation.

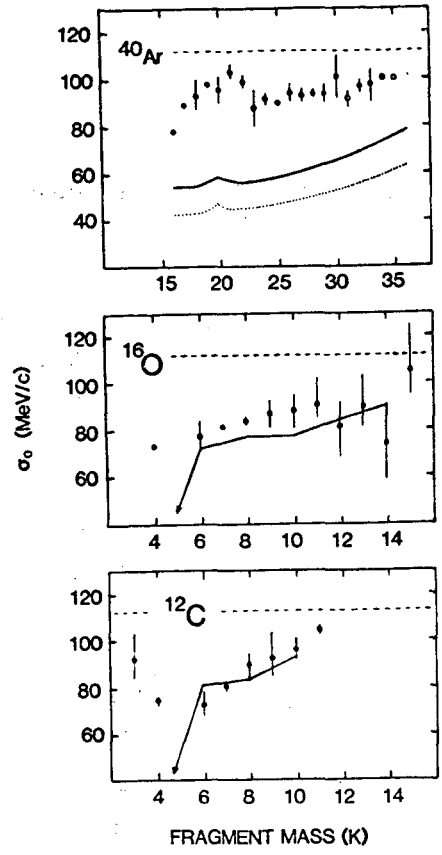

I conclude that the inclusive momentum spectra of projectile fragments reflect the internal momentum distributions of both projectile and fragment, but the relevant distributions are not those of ground state Fermi gases prior to the collision, as had been originally proposed.[2,3] Rather, it is necessary that the projectile momentum distribution be excited above the ground state prior to formation of the fragment in order to predict the observed widths via this formalism.

1. D.E.Greiner, et. al., Phys. Rev. Lett. 35, 152 (1975).
2. H. Feshbach and K. Huang, Phys. Lett. 47B, 300 (1973).
3. A.S.Goldhaber, Phys. Lett. 53B, 306 (1974).
4. G.Bertsch, Phys. Rev. Lett. 46, 472 (1981).
5. A.A.Markoff, Wahrscheinlichkeitsrechung (Leipzig, 1912).
6. S.Chandrasekhar, Rev. Mod. Phys. 15, 1 (1943).
7. Y.P.Viyogi, et. al., Phys. Rev. Lett 42, 33 (1979).

INCLUSIVE K^+-PRODUCTION IN THE MODEL OF TRANSPORT THEORY FOR HIGH-ENERGY NUCLEUS-NUCLEUS COLLISIONS +

W. Zwermann, B. Schürmann, K. Dietrich and E. Martschew
Physik-Department, TU München, D-8046 Garching, W. Germany

Abstract: The inclusive differential cross section for K^+-meson production in the reaction Ne+NaF at 2.1 GeV/N is calculated within an independent multiple collision approach, neglecting the possible influence of the rescattering of the produced kaons by surrounding particles. We use the near-analytical, parameter-free model of transport theory with slight modifications, to determine the momentum distributions of the colliding particles after each number of collisions, taking account of pion production via the delta resonance.

Recently, the inclusive differential K^+-production cross section has been measured in the reaction Ne+NaF at 2.1 GeV/N /1/. The observation of kaons in nuclear collisions is, despite their small production cross section, of great interest, for they might provide us, because of their small interaction cross section with nucleons, with information on the early, violent stage of the collision. The main features of the experimental results are the following: (i) The K^+-spectrum extends to energies far beyond the kinematical limit for kaon production in elementary nucleon -nucleon collisions. (ii) It can be parametrized by a nearly exponential shape with an apparent temperature appreciably higher than that for proton and pion production in the same reaction. (iii) No anisotropy of the K^+-spectrum in the c.m. system of the colliding nuclei is observed. Fermi motion of the colliding nucleons might be a possible explanation for the high energy components in the kaon spectrum. This was already examined by Randrup and Ko /2/. Indeed, the spectrum exceeds the kinematical limit appreciably, but with a reasonable value for the Fermi momentum the resultant slope is much too steep to explain the data. The possibility of kaon production in collisions between multiply scattered nucleons and delta resonances was inspected in /2/ on the basis of the linear cascade model "rows on rows" /3/. Surprisingly, the slope of the kaon cross section remained essentially unchanged. However, in the model of /3/ there is a lack of transverse communication and thermalization cannot take place. This could be a possible reason for the too small cross section at high kaon energies.

In contrast, in the model of transport theory /4/ the nucleons reach thermalization after only a few collisions. This seems to be in accord with recent results obtained by use of the numerical intranuclear cascade model /5/. So the model of transport theory may serve as a good background model for kaon

+Supported by the Bundesministerium für Forschung und Technologie

production in nuclear collisions before other possibilities, like rescattering of the produced kaons or cooperative effects, are considered.

In a multiple collision approach, the inclusive differential cross section for K^+-production in a nuclear collision is given by

$$E\frac{d\sigma}{d^3p} = \sum_{i=1}^{\infty}\sum_{j=1}^{\infty}\frac{\sigma_A(i)}{\sigma_{NN}}\,\frac{\sigma_A(j)}{\sigma_{NN}}\sum_{m=1}^{i}\sum_{n=1}^{j}\mathcal{J}_{mn} \qquad (1)$$

where $\mathcal{J}_{mn}$ is the elementary inclusive differential cross section for K^+-production folded with the momentum distributions of the two colliding particles after m-1 and n-1 collisions, respectively :

$$\mathcal{J}_{mn} = \int d^3p_1\, d^3p_2\, Q^P_{m-1}(\vec{p}_1)\, Q^T_{n-1}(\vec{p}_2)\, E\frac{d\sigma_{el}}{d^3p} \qquad (2)$$

The geometrical weights $\sigma_A(i)/\sigma_{NN}$ denote the number of projectile or target baryons which undergo precisely i collisions before leaving the interaction zone. They are given, in eikonal approximation, by the Glauber-Matthiae factors /6/ with the free total NN cross section σ_{NN}. For the elementary K^+-production cross section we use the parametrization of /2/. Including delta resonances and neglecting the difference between deltas and all higher baryon resonances, we can write the momentum distributions of projectile and target particles as a sum of those for the nucleons and deltas,

$$Q_n(\vec{p}) = \rho_n^N Q_n^N(\vec{p}) + \rho_n^\Delta Q_n^\Delta(\vec{p}) \qquad (3)$$

with the probability $\rho_n^{N(\Delta)}$ of a colliding particle to be a nucleon (delta) after the n-th collision /4/ :

$$\rho_n^N = \rho_N - e^{-\alpha(n-1)}\left[\alpha\rho_N - (1-\alpha)\rho_\Delta\right] \;;\; \rho_n^\Delta = 1-\rho_n^N \qquad (4)$$

Here, α is the branching ratio between elastic and inelastic NN-collisions and $\rho_{N(\Delta)}$ are the equilibrium distributions of nucleons and deltas in a heat bath of temperature τ. This temperature follows from energy conservation. Furthermore, we need an analytic expression for the momentum distributions $Q_n^{N(\Delta)}(\vec{p})$. The Fermi distributions of the cold nucleons can be parametrized by a relativistic Maxwell distribution of width $2\sigma_F^2$, centered around the momentum $\vec{p}_0$ ($-\vec{p}_0$). The distributions of the particles in the thermal limit are relativistic

Maxwell distributions of width $2M_{N(\Delta)}\tau$. So it is a reasonable assumption that the momentum distributions after n collisions are of the interpolating form

$$Q_n(\vec{p}) = \gamma_n(E-\vec{v}_n\cdot\vec{p})\, N_n\, e^{-\frac{M}{\sigma_n^2}\gamma_n(E-\vec{v}_n\cdot\vec{p})} \qquad (5)$$

The parameters $\vec{v}_n$ and σ_n are determined from the average values of momentum and energy obtained in analytic form from the distributions (5). On the other hand, these average values are known from a relativistic formulation of the transport model /4/. The relations between the average values and the parameters $\vec{v}_n$ and σ_n can then be used to calculate the latter /7/. The distributions (5) are thus completely fixed. We note in addition that with the form (5) the functions $\zeta_{mn}(2)$ can be calculated in a good approximation analytically, except for a remaining one-dimensional numerical quadrature.

Our results are shown in figure 1. Although we obtain at high kaon energies a substantial improvement as compared to previous calculations with the linear cascade model /2/, the experimental data are still underestimated by more than an order of magnitude (cf. fig.1).

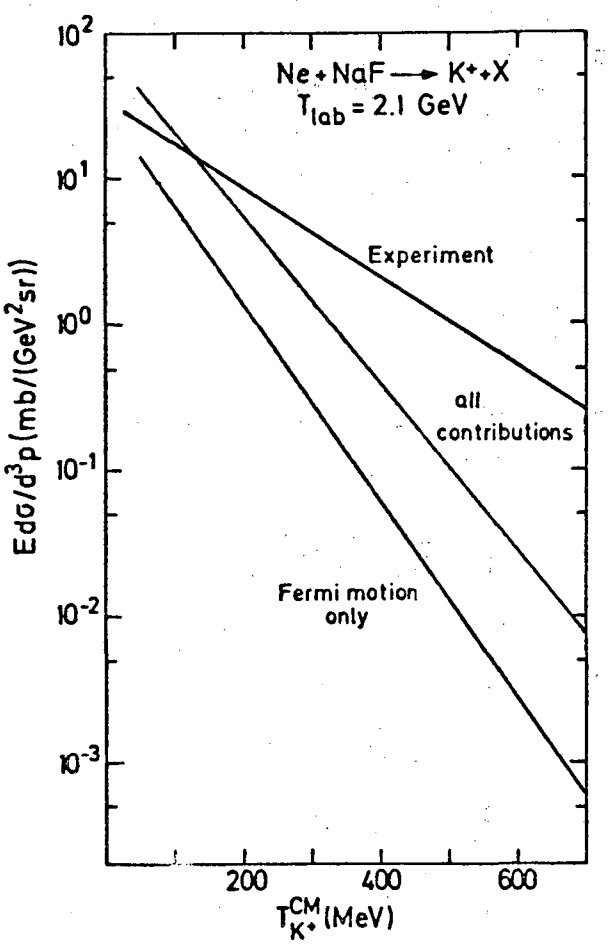

Fig.1. Comparison of our calculations with the experimental data of /1/.

We think that the calculations presented together with those of ref./2/ give a good impression of what to expect from more complex numerical cascade models. The potential power of the present model, namely its near-analytical formulation as well as its ability to yield quantitative results, can be utilized to study the influence of K^+-rescattering on the final kaon spectra /8/ without introducing large numerical errors.

References

1. S. Schnetzer, M.-C. Lemaire, R. Lombard, E. Moeller, S. Nagamiya, H. Steiner, and I. Tanihata, Phys. Rev. Lett. 49 (1982) 989.

2. J. Randrup and C.M. Ko, Nucl. Phys. A343 (1980) 519; LBL-Report 16316, 1983.

3. J. Hüfner and J. Knoll, Nucl. Phys. A270 (1977) 460; J. Knoll and J. Randrup, Nucl. Phys. A324 (1979) 445.

4. H.-J. Pirner and B. Schürmann, Nucl. Phys. A316 (1979) 461; B. Schürmann, K.M. Hartmann, and H.-J. Pirner, Nucl. Phys. A360 (1981) 435.

5. J. Cugnon and D. L'Hote, Nucl. Phys. A397 (1983) 519.

6. R.J. Glauber and G. Matthiae, Nucl. Phys. B21 (1970) 135.

7. W. Zwermann, Diploma Thesis, TU München (1983).

8. J. Randrup, Phys. Lett. 99B (1981) 9; C.M. Ko, Phys. Rev. C23 (1981) 2760.

SUBTHRESHOLD PION PRODUCTION IN NUCLEUS-NUCLEUS COLLISIONS - A CO-OPERATIVE PROCESS!

R. Shyam and J. Knoll
Gesellschaft für Schwerionenforschung, Darmstadt, West Germany

Significant pion production cross-sections have been observed[1] in the collision of two nuclei at the beam energies (<290 MeV/A) where the basic nucleon-nucleon collision can not produce a pion. The earliest suggestion to understand this process dates back to Fermi. It exploits the fact that the initial intrinsic nucleonic motion offers the necessary extra boost for the elementary nucleon-nucleon (N-N) pion production process. This original idea has recently been reconsidered in a "first N-N collision" model for a quantitative explanation of the pion production at beam energies both below and above threshold[3]. However, with decreasing beam energy this model may become insufficient to explain the production rates as well as the shapes of the pion spectra. Other mechanisms like participation of more than two nucleons into the pion production process and the freezing of the degrees of freedom in the final channel, i.e. formation of the composite nuclei may become increasingly important. Near the absolute threshold (minimum beam energy/nucleon required to produce a pion in the nucleus-nucleus collision), the mechanism of "pionic fusion"[4] in which two nuclei as a whole coherently interact with each other and fuse to form a compound nucleus, converting all the available free energy into a pion, becomes the only possible production mechanism.

Before attempting to achieve a detailed microscopic description of the subthreshold pion production process, it is essential to understand clearly the bare kinematical implications of the alternative pion production mechanisms. In particular we carefully rediscuss the single nucleon-nucleon collision mechanism.

The single N-N collision model relies on the one-nucleon spectral function $f_A(P,E)$ and $f_B(P,E)$ of the two colliding nuclei (A and B) in their respective ground states. These distributions which describe the initial intrinsic nucleonic motion (Fermi motion) can in principle be determined by quasi-free electron scatterin experiments (e,e'p) and (e,e'n). However, the form used for these in the literature so far is that of the Fermi-gas model,

$$f_{FG}(P,E) = f(P)\delta(E-\varepsilon(P)) \qquad (1)$$

where $\varepsilon^2(P) = P^2 + (m_o-v_o)^2$.

Here V_o is the depth of the potential well and m_o the nucleon mass. In the more realistic shell model, on the other hand, the particles are distributed in the orbits of discrete energies, and the one nucleon distribution function acquires the following form

$$f_{s.m.}(P,E) = \sum_i f_i(P)\delta(-\varepsilon_i). \qquad (2)$$

Here ε_i represents the binding energy of the ith orbit with a momentum distribution $f_i(P)$. In the limit of the large nuclei, both prescriptions merge in the sense that the classically allowed most probable momentum components follow the Fermi gas distribution. The use of the smooth momentum distribution in eq.(1) (instead of a function with sharp cutt-off at the edge of the Fermi sea), however, brings in an inconsistency into the Fermi gas prescription. Particularly for the large momentum components (which are classically forbidden), this allows the energies of the nucleons to exceed the nucleon separation energies and thus the description of the initial states of the nuclei A and B involves serious errors. Note that the shell model prescription is void of this defect, all

the nucleons remain bound in the initial state irrespective of the intrinsic momenta used. All the calculations based on the single N-N collision model published so far, however, have used the erroneous Fermi gas prescription (in some cases even the binding potential V_0 has been taken to be zero), despite the fact that at subthreshold energies one is particularly sensitive to the classically forbidden momenta. Consequently in the single N-N collision, while the total available c.m. energy varies approximately linearly with the intrinsic momentum in the shell model picture, an additional quadratic dependence follows for the Fermi gas prescription. This means that in the Fermi gas picture a pion can be produced already at far lower intrinsic momenta than in the shell model picture. Thus the calculations performed by the single nucleon-nucleon collision model with the Fermi gas prescription will result in larger yields and flatter slopes of the pion spectra in comparison to those performed with the more accurate shell model prescription as illustrated in fig. 1.

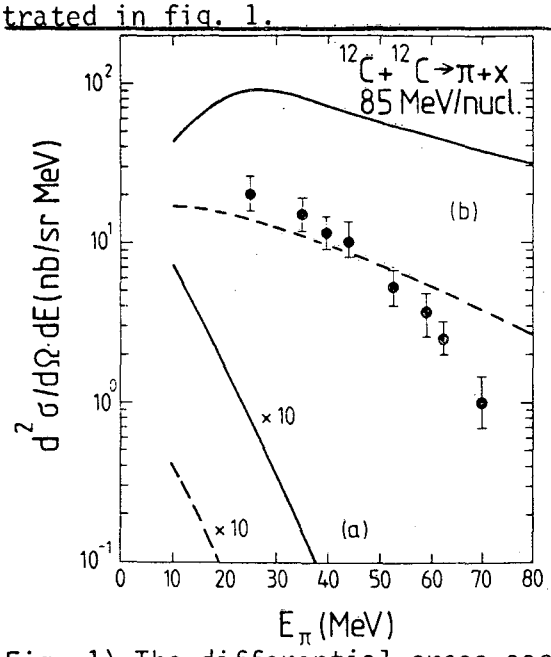

Fig. 1) The differential cross-section for the pions calculated with the single N-N collision model. The group of curves a have been obtained with the shell model prescription (eq. (2)) whereas group b with the Fermi-gas prescription (eq.(1)). The solid curves correspond to the NN → d π channel whereas dashed curves to the NN → NN π channel.

In fact the single N.N. collision model is able to cope neither with the absolute yields nor with the shapes of the experimental spectra. Therefore, in contrast to the other calculations published, there is a need for a further production mechanism besides the single N-N collision picture.

In the shell model picture the kinematical situation changes with the participation of more than two nucleons in the pion production process. As expected, the production threshold opens already at much lower intrinsic momenta in comparison to the single N-N collision picture, and the sensitivity of the process is shifted from the extreme tail region towards the classically allowed components of the momentum distribution. It seems, therefore, that the multi-nucleon collision is a more realtistic picture for the subthreshold pion production.

In order to illucidate the kinematical consequences of the multinucleon production mechanism we have performed the calculations for the pion spectra in the multiple collision picture using the nuclear phase-space model[6,7] with the extension[8] of including the possibility of forming the composited nuclei in the final channel. The results of our calculations are shown in fig. 2. The experimental data are taken from Ref. 2. The calculations have been performed with the shell model prescription for the intrinsic motion. All the curves have been normalized at the value of the cross-section at E_π = 10 MeV. Comparing the curves a and c one can see that although the intrinsic motion of the nucleons in the initial states of the respective colliding nuclei is important, yet it is not sufficient to account for the observed slopes of the experimental

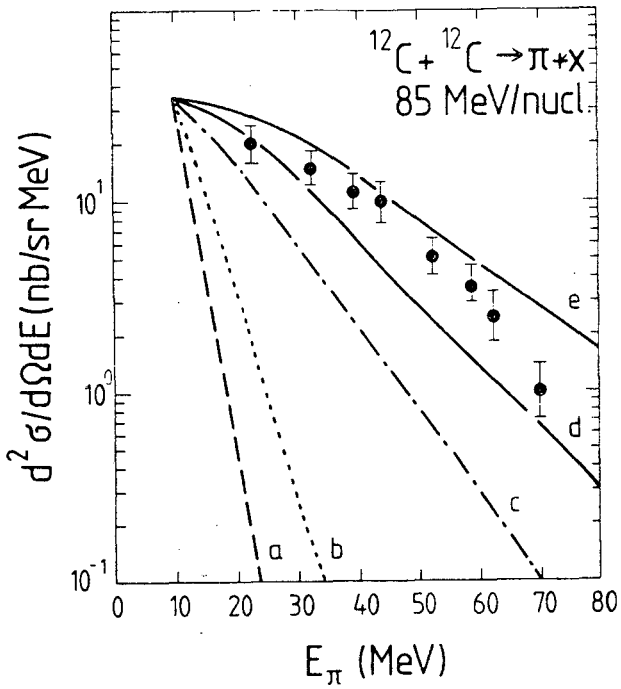

Fig. 2) The differential cross-section for the pion production calculated with the nuclear phase-space model. Various curves have the meaning as follows a) intrinsic motion of the nucleons in the initial states are not included and the final state is supposed to be consisting of only nucleons and pions; b) same as a) but the degrees of freedom in the final state are frozen by a factor of two; c) same as a) but the intrinsic nucleonic motion is included with the shell model prescription; d) same as c) but the degrees freedom in the final channel are frozen by a factor of two; e) same as d) but the degrees freedom in the final channel are frozen by a factor of three.

spectra. The experimental spectra are still too flat, in other words the "temperature"associated with the experimental pion spectra is larger in comparison to the calculated one. If, however, certain kinetic degrees of freedom in the final channel are frozen, the total available energy will be shared less, i.e. the spectra of the outgoing pion could achieve a higher "temperature". This is clearly seen from the curves d and e in fig. 2 where we have frozen the degrees of freedom in the final channel by the factors of 2 and 3 (assuming an averaged atomic mass number of the produced nuclei of two or three) respectively. Curves d and e are much closer to the experimental data.

In conclusion, the single N-N collision process with a correct energy prescription (shell model) for the initial intrinsic nucleonic motion is unable to reproduce the absolute yields as well as the observed shapes of the experimental pion spectra. Rather, co-operative effects are seen to be vital. Effects which are more of collective nature, like the Bremsstrahlung picture[9] or the production due to pionic instability of the compressed nuclear matter[10], have been suggested in the literature. Here we considered those type of effects that emerge from a multiple collision picture, where the sharing of the energy of several nucleons and also the freezing of degrees of freedom in the final channel seem to be vital. The latter effect should reflect itself in a correlation between the produced pion and the associated mass distribution of the nuclear fragments. We feel that our work has provided a necessary and useful background for the future attempts to perform the microscopic calculations for the pion production process in the nucleus-nucleus collisions at the subthreshold energies. One of the challenges for this microscopic calculation would be to also explain the absolute yields of the pion spectra which we left unconsidered in our present kinematical investigation.

References:

[1]W. Benenson et al., Phys. Rev. Lett. 43, 683 (1979)
S. Nagamiya et al., Phys. Rev. Lett. 48, 1780 (1982)
T. Johansson et al., Phys. Rev. Lett. 48, 732 (1982)

[2]B. Jakobsson, Proc. of the Nordic meeting on Nucl. Phys. Fuglso, Denmark, August 1982 (unpublished)

[3]G.F. Bertsch, Phys. Rev. C15, 713 (1977)

[4]K. Klingenbeck, M. Dillig and M.G. Huber, Phys. Rev. Lett. 47, 1654 (1981)

[5]E. Fermi, Prog. Theor. Phys. 5, 570 (1950)

[6]J. Knoll, Phys. Rev. C20, 773 (1979), Nucl. Phys. A343, 511 (1980)

[7]S. Bohrmann and J. Knoll, Nucl. Phys. A356, 498(1982)

[8]R. Shyam and J. Knoll, to be published

[9]D. Vasac et al., Phys. Lett. 93B, 243(1980)

[10]M. Gyulassy, Nucl. Phys. A354, 395 (1981)

PION PRODUCTION FROM PERIPHERAL HEAVY-ION COLLISIONS THROUGH COHERENT ISOBAR AND ISOBARIC ANALOG GIANT RESONANCE FORMATION

P. A. Deutchman, R. L. Madigan, J. W. Norbury, and L. W. Townsend*
Department of Physics
University of Idaho, Moscow, Idaho 83843

ABSTRACT

A spin, isobaric-spin formalism for the coherent production of isobars in the peripheral region of a high-energy heavy-ion projectile along with giant isobaric analog excitations has been improved and extended. These changes include the decay of the nucleonic isobars to pions and the removal of the classical straight line assumption along with generalization of the density of states to four bodies. Formal expressions for the total and a differential cross section for pion angular distributions have been obtained.

INTRODUCTION

In previous work[1-3] we developed a spin, isobaric-spin formalism for the coherent production of projectile isobars with concomitant target excitations to giant isobaric analog states due to peripheral collisions of relativistic heavy ions. However, we did not include the decay of the $\Delta(1236)$ projectile isobars to their various pion and nucleon charge states. These important decays are now included. Furthermore, we have been able to remove the extreme high energy classical straight line assumption where it was assumed that the target center-of-mass motion is undeviated throughout the collision as seen in the projectile center-of-mass frame. The formalism now rests on a complete quantum mechanical footing and makes it possible to develop a formalism that would be applicable over a range of energies. We are also in a position to calculate total cross-sections for the coherent production of nucleonic isobars from a given projectile nucleon which subsequently decays to a given pion and nucleon along with concomitant excitation of the target to a specific spin, isobaric spin giant resonance. We have also just obtained a formal expression for the Lorentz invariant differential cross section for pion production with the hope that a characteristic pion signal might be obtained theoretically from heavy-ion collisions through coherent Δ-formation. Finally, the time dependent matrix elements of our previous formalism forced us to introduce frequencies in order to replace the target with an equivalent phonon spectrum.[1] The fact that we have now developed a formalism with time independent matrix elements allows us to deal strictly with the momentum transferred from the target to the projectile rather than with a phonon spectrum.

FORMALISM

From second order, time-dependent perturbation theory, the transition rate from the initial state to the final state through an intermediate

*Present address: NASA Langley Research Center, Mail Stop 160, Hampton, VA 23665.

resonating state of total width Γ is given by

$$w = \frac{2\pi}{\hbar V^2} \sum_{M_\tau M_\sigma} \frac{|A^{m_{\tau f}\pi_{\tau f}}_{M_\tau M_\sigma}|^2 \; |V^{M_\tau M_\sigma}_{\mu_\tau \mu_\sigma}|^2}{[(E_\pi + E_N) - M_\Delta c^2]^2 + (\Gamma/2)^2} \rho_4(E_f), \tag{1}$$

where $V^{M_\tau M_\sigma}_{\mu_\tau \mu_\sigma}$ is the formation amplitude describing target excitations to a spin-isobaric-spin giant resonance state μ_σ, μ_τ while the nucleonic isobar is coherently formed into a spin-isobaric-spin state M_τ, M_σ. The virtual nucleonic isobar then resonates with virtual energy Mc^2 (which is eventually integrated over) about the isobaric resonant energy $M_\Delta c^2$ and decays with amplitude $A^{m_{\tau f}\pi_{\tau f}}_{M_\tau M_\sigma}$ to a final nucleon of spin-isobaric-spin state $m_{\sigma f}$, $m_{\tau f}$ and final pion of spin-isobaric-spin state $\pi_{\sigma f}$, $\pi_{\tau f}$. The four-body density of states factor $\rho_4(E_f)$ can be transformed into a folded product of three, two-body density of states factors integrated over virtual-mass energies as[4]

$$\rho_4(E_f) = \iint \rho_2(E_{\pi NR,T^*})\rho_2(E_{\pi N,R})\rho_2(Mc^2)\,d(Mc^2)\,dE_{\pi N,R} \;, \tag{2}$$

where the energy in the final state is distributed over the energies of the pion, nucleon, residual projectile and excited target as $E_f = E_\pi + E_N + E_R + E_{T^*}$. The virtual energy Mc^2 is distributed over the energies of the pion and nucleon as $Mc^2 = E_\pi + E_N$. Assuming spin-zero initial projectile and target states, we obtain the total cross section for coherent isobar formation leading to a final pion charge state $\pi_{\tau f}$ which is

$$\sigma(\pi_{\tau f}) = \sum_{M_\tau m_{\tau f}} g^2_{M_\tau m_{\tau f}} \sum_{\mu_\tau \mu_\sigma M_\sigma} (1 - \delta_{\mu_\tau,0}\delta_{\mu_\tau,0})$$

$$\times \left[\tfrac{1}{2}\sum_{m_\tau} C^{m_\tau - \mu_\tau M_\tau}_{\frac{1}{2}\;\;1\;\;3/2}\right]^2 \left[\tfrac{1}{2}\sum_{m_\sigma} C^{m_\sigma - \mu_\sigma M_\sigma}_{\frac{1}{2}\;\;1\;\;3/2}\right]^2 (fA_p)^2 \sigma_{\Delta T}(\omega_\Delta) \;. \tag{3}$$

Similar to Ref. 3, $\sigma_{\Delta T}$ (ω_Δ) is a spin-isobaric-spin-independent total cross section, $(fA_p)^2$ is the projectile coherence factor modified by the fractional peripheral approximation factor f, the bracketed Clebsh-Gordan factors come from the spin and isobaric-spin transitions of a projectile nucleon into a nucleonic isobar, and the round brackets contain the term due to the uncoupled representation.[3] The sums over the Clebsch-Gordan coefficients are formal only since each m_τ and m_σ are determined by spin and isobaric spin conservation. The partial cross section $\sigma(M_\tau, m_{\tau f}, \pi_{\tau f})$ for a given nucleonic isobar state M_τ decaying to a particular final nucleon state m_τ and pion charge state $\pi_{\tau f}$ is defined as $\sigma(\pi_{\tau f}) = \Sigma_{M_\tau m_{\tau f}} \sigma(M_\tau, m_{\tau f}, \pi_{\tau f})$. The isobar branching ratio $g^2_{M_\tau m_{\tau f}} = \Gamma_{M_\tau m_{\tau f}}/\Gamma$ describes the isobar decay into its final channels where the partial width,

$$\Gamma_{M_\tau m_{\tau f}} = 2\pi \sum_{m_{\sigma f}\pi_{\sigma f}} \rho_2(Mc^2)\,|A^{m_{\tau f}\pi_{\tau f}}_{M_\tau M_\sigma}|^2 \;. \tag{4}$$

Hope for the future arises by obtaining the formal expression for the Lorentz Invariant differential cross section for direct comparison to experiments[5] which is

$$\frac{d^3\sigma(\pi_{\tau_f})}{(d^3p_\pi/E_\pi)} = \frac{V}{(2\pi\hbar)} E_\pi \sum_{\substack{M_\tau M_\sigma \pi_{\sigma_f} \\ m_{\tau_f} m_{\sigma_f}}} \frac{|A^{m_{\tau_f}\pi_{\tau_f}}_{M_\tau M_\sigma}|^2}{[(E_\pi + E_N) - M_\Delta c^2]^2 + (\Gamma/2)^2}$$

$$\times \sum_{\mu_\tau \mu_\sigma} [1 - \delta_{\mu_\tau,0}\delta_{\mu_\sigma,0}][\tfrac{1}{2}\sum_{m_\tau} C^{m_\tau - \mu_\tau M_\tau}_{\frac{1}{2}\ 1\ 3/2}]^2 [\tfrac{1}{2}\sum_{m_\sigma} C^{m_\sigma - \mu_\sigma M_\sigma}_{\frac{1}{2}\ 1\ 3/2}]^2$$

$$\times (fA_p)^2\ \sigma_{\Delta T}(\omega_\Delta) \qquad (5)$$

This expression gives identical results to previous results obtained with the straight line assumption; however, it is now possible to consider lower energy heavy-ion reactions even down to threshold.[6]

REFERENCES

1. P. A. Deutchman and L. W. Townsend, Phys. Rev. Lett. 45, 1622 (1980).
2. L. W. Townsend and P. A. Deutchman, Nucl. Phys. A 355, 505 (1981).
3. P. A. Deutchman and L. W. Townsend, Phys. Rev. C 25, 1105 (1982).
4. D. M. Brink and G. R. Satchler, Angular Momentum 2nd ed. (Clarendon Press, Oxford, 1968), p. 104.
5. W. Benenson, *et al.*, Phys. Rev. Lett. 43, 683 (1979); and various references in Proceedings of the Fifth High Energy, Heavy Ion Study, Berkeley, 1981, Lawrence Berkeley Laboratory Report, LBL-12652.
6. V. Bernard, *et al.*, Cosmic and Subatomic Physics Report LUIP8301, 1983.

COMPLEX WKB SOLUTIONS FOR $^{12}C+^{12}C$ SCATTERING

L. W. Townsend, NASA Langley Research Center, Hampton, VA 23665
H. B. Bidasaria, Old Dominion University, Norfolk, VA 23508
J. W. Wilson, NASA Langley Research Center, Hampton, VA 23665

Abstract: WKB solutions for carbon-carbon scattering from 200 to 360 MeV are obtained using a double-folding optical potential with no arbitrarily adjustable parameters. Significant improvements over previous results are obtained when values for the energy-dependent nucleon-nucleon scattering slope parameter are limited to those appropriate to diffractive scattering.

In order to properly assess optimum shield and dosimetry requirements for future manned space flights, an accurate theory of galactic heavy ion interaction and transport for energies above 20 MeV/nucleon is currently under development. As part of this effort, WKB solutions for carbon-carbon scattering at 17, 20 and 24 MeV/nucleon were obtained (ref. 1) utilizing a double-folding potential based upon a composite particle generalization of Watson's multiple scattering series (ref. 2). In that work, surprising agreement with recent experimental results (ref. 3) was obtained although there were no arbitrarily adjusted parameters in the calculation. In this work, improvements to the results given in reference 1 are obtained by restricting the allowed values for the experimental nucleon-nucleon scattering slope parameter to those appropriate to purely diffractive scattering (ref. 4), rather than including values obtained over the entire range of momentum transfers (refs. 5,6).

From reference 1, the double-folding nuclear optical potential is

$$V_N(\vec{x}) = A_P A_T \int d^3\vec{z}\, \rho_T(\vec{z}) \int d^3\vec{y}\, \rho_P(\vec{x} + \vec{y} + \vec{z}) t(e,\vec{y}) \tag{1}$$

where the constituent-averaged two-body amplitude is

$$t(e,\vec{y}) = -(e/m)^{1/2}\sigma(e)[\alpha(e)+i][2\pi B(e)]^{-3/2}\exp[-y^2/2B(e)] \tag{2}$$

The nuclear densities, ρ , in (1) are obtained by analytically unfolding the usual gaussian nucleon charge distribution from the experimentally determined ^{12}C harmonic well charge distribution (see reference 1 for details). The constituent-averaged nucleon-nucleon scattering parameters (α and σ) are taken from the usual compilations (refs. 5-8). Rather than using constituent-averaged values from compilations (refs. 5,6) for the slope parameter, B , values for B were determined from (ref. 4)

$$B = 10 + \frac{1}{2}\ln(s/s_0) \tag{3}$$

where s is the square of the nucleon-nucleon center of mass energy and $s_0 = 1(\mathrm{GeV})^2$. The values obtained from (3) were B 10.6 $(\mathrm{GeV/c})^{-2}$ rather than the values B 4.9$(\mathrm{GeV/c})^{-2}$ used previously (ref. 1). After performing the integrations in (1), the resultant nuclear potential is of the form

$$V_N(\vec{r}) = A_o(1 + A_1 r^2 + A_2 r^4) \exp(-A_3 r^2) \quad (4)$$

with A_0 complex and $A_1 \rightarrow A_3$ real. Values for these parameters are displayed in Table I.

As in reference 1, elastic differential, reaction and total cross sections were determined from standard partial wave analysis using complex WKB phase shifts. Since space limitations preclude displaying the elastic differential cross sections for all the energies considered herein, representative results (for 288.6 MeV) are shown in Figure 1. Also displayed, for comparison, are the previous predictions from reference 1 and representative experimental data from reference 3. The improved agreement between theory and experiment is confirmed by a reduction in the χ^2 per point from 27 (ref. 1) to 17 (this work). Half of the remaining χ^2 contribution is due to the large disagreement in the minima near 15° and 20°. It appears, however, that the angular offset between theory and experiment, noted in reference 1, is largely removed in the present work. The remaining angular disagreements ($\sim$0.1°) may be due to uncertainties in the experimental angles (ref. 3) and/or the calculated value for B. Figure 2 displays values for the total and reaction cross sections, from this work and reference 1, as a function of energy. Also shown are various experimental results (refs. 3,9,10). The most marked improvement is in the agreement between theory and experiment for σ_{tot}. In order to test the hypothesis (ref. 1) that some of the remaining discrepancies, in this energy range, may be due to the poorly determined values for the ratio of real-to-imaginary part of the neutron-proton forward scattering amplitude, α_{np}, we allowed α_{np} to vary as a free parameter while retaining the experimental values for all other nucleon-nucleon scattering parameters. At 288.6 MeV, α_{np} increased from a value of 0.28 (ref. 1) to a fitted value of 0.45. The resultant value for σ_{tot} increased to 2523 mb, which is in better agreement with the experimental value of 2660±80 mb (ref. 3). In addition, the χ^2 per point for the elastic differential cross sections was reduced from 17 to 12. Finally, since it is of current theoretical interest (ref. 9,11), we used the real WKB phases at 288.6 MeV to investigate nuclear rainbow effects. As reported in reference 12, we determine values for the nuclear rainbow angle of $\theta_r \approx 1\text{-}2°$, which although not in agreement with reference 11, are not unexpected since the imaginary nuclear potential, from (4), is quite large (ref. 12).

In summary, substantial improvement in the predicted values for carbon-carbon elastic differential, reaction and total cross sections, when compared with experimental measurements, have been obtained by using the larger values of the slope parameter appropriate to diffractive scattering. The results obtained also suggest that α_{np} in this energy range, may be larger than presently listed in compilations. We gratefully acknowledge fruitful discussions with R. Stokstad of LBL. One of the authors (H.B.B.) was supported in part by NASA Grant No. NCCI-42.

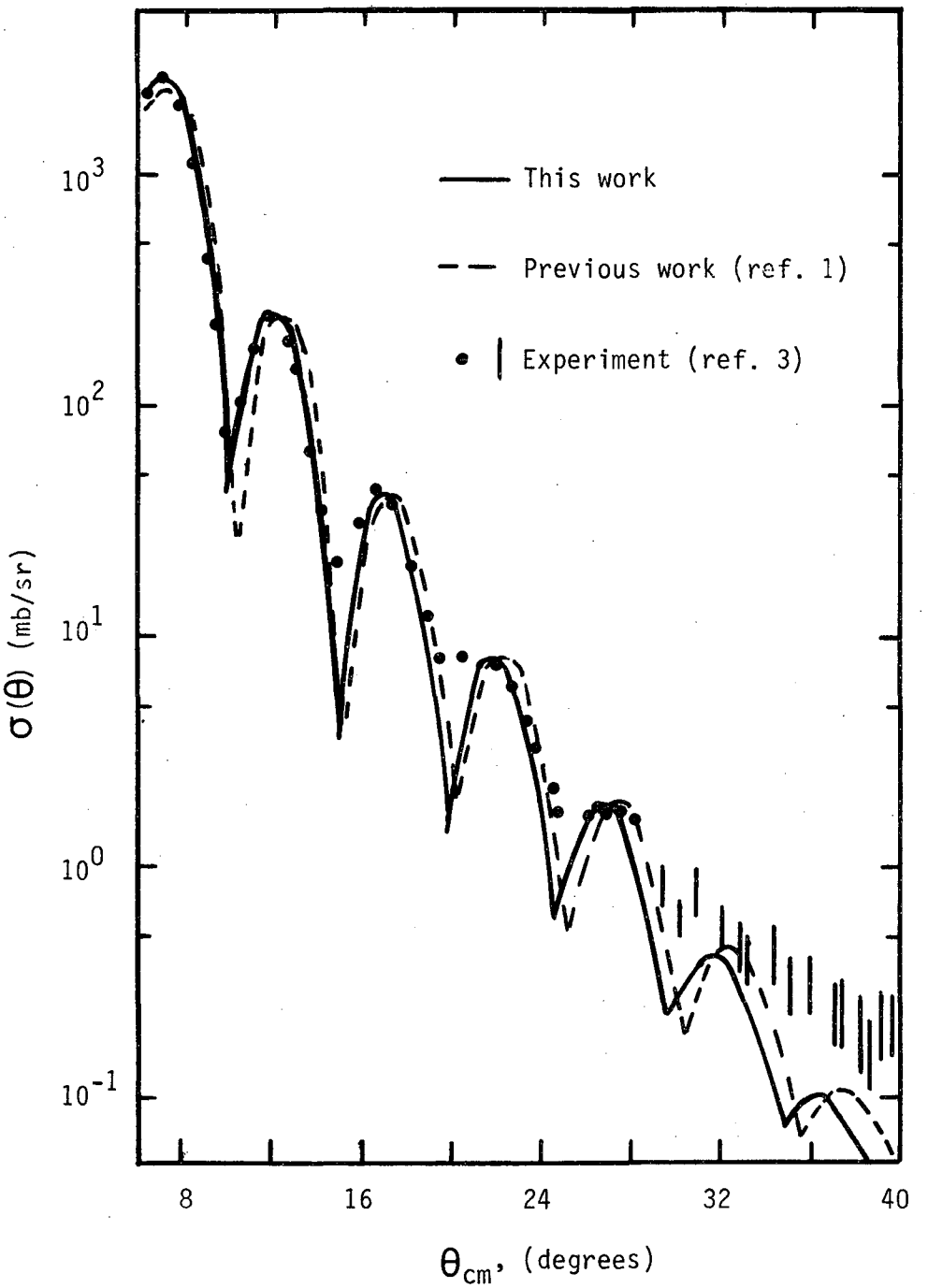

Figure 1. Elastic differential cross sections for 288.6 MeV carbon - carbon scattering.

1. H. B. Bidasaria, L. W. Townsend, and J. W. Wilson, J. Phys. G: Nucl. Phys. 9, L17 (1983).
2. J. W. Wilson and L. W. Townsend, Can. J. Phys. 59, 1569 (1981)
3. A. J. Cole et al, Phys. Rev. Lett. 47, 1705 (1981)
4. F. E. Ringia et al, Phys. Rev. Lett. 28, 185 (1972)
5. K. H. Hellwege (Ed.), Landolt-Bornstein Series Group I, Vol. 9 (Springer-Verlag: New York) 1980.
6. O. Benary, L. R. Price, and G. Alexander, UCRL-20000NN (1970).
7. J. Binstock, Phys. Rev. C 10, 19 (1974)
8. I. V. Amirkhanov et al, Proc. 5th Int. Conf. on High-Energy Physics and Nuclear Structure, Uppsala, Sweden. G. Tibell, Ed. (North Holland: Amsterdam) 1974
9. H. G. Bohlen et al, Z. Phys. A 308, 121 (1982).
10. C. Perrin et al, Phys. Rev. Lett. 49, 1905 (1982).
11. M. E. Brandan, Phys. Rev. Lett. 49, 1132 (1982).
12. J. Knoll and R. Schaeffer, Ann. Phys. 97, 307 (1976).

Table I. Potential Parameters

Energy (MeV)	A_0 (MeV)	A_1 (fm^{-2})	A_2 (fm^{-4})	A_3 (fm^{-2})
204.2	(-286,-774i)	.0650	.0025	.1756
242.7	(-339,-693i)	.0650	.0025	.1756
288.6	(-369,-612i)	.0650	.0025	.1756
300.0	(-372,-594i)	.0650	.0025	.1755
360.0	(-372,-511i)	.0650	.0025	.1755

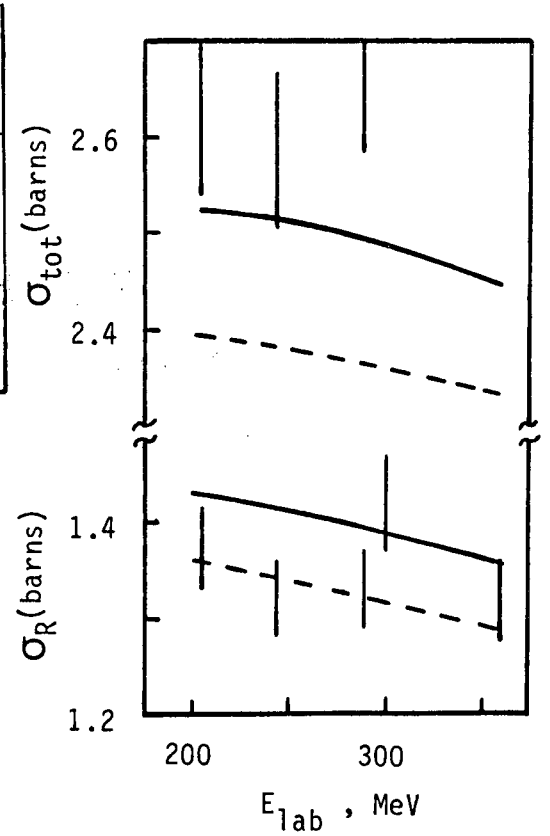

Figure 2. Carbon - carbon total and reaction cross sections for this work (solid lines), previous work (dashed), and experiment (vertical lines) versus energy.

SESSIONS V and VI: HIGH ENERGY REACTIONS

Search for a possible deconfinement phase transition in nuclear matter by proton and anti-proton interactions with nuclei at 200 GeV

I. DERADO

Max-Planck-Institut für Physik und Astrophysik

München, Germany

I would like to report some results obtained at the SPS in CERN by the collaboration Bari-Krakow-Liverpool-MPI München-Nijmegen. The existence of a quark gluon plasma has been speculated upon since the early days of the quark model [1]. Serious information about the parameters and possible nature of the transition of nuclear matter to quark matter has been obtained however only recently with the advent of lattice calculations in QCD [2]. The most remarkable result of these calculations is that the transition temperature could be very low, T_c = 200 MeV, thus it is interesting to look for experimental evidence of a quark-gluon plasma even in existing experimental data [3]. Our recent experiment [4] shows that for a Xenon target we have in the central region about 5 charged particles per unit rapidity, and that objects produced initially evolve into hadrons at considerably later times. This means that we can have for a central collision much higher average energy density [3] than inside the nucleon, which is about 440 MeV/fm^3. At these higher energy densities it has been speculated by many authors that one can produce exotic objects which, in their rest frame, may extend over several fermis.

Data Analysis

The details of our experiment on charged particle production in the collisions of 200 GeV/c protons and anti-protons with Hydrogen, Argon and Xenon targets are published elsewhere [4]. Our present analysis was made possible by use of a streamer-chamber vertex spectrometer with a 4π solid-angle coverage and excellent multitrack efficiency. The magnetic field of 1.5 Tesla gave us good momentum and charge information. A downstream spectrometer, consisting of seven magnetostrictive spark chambers, was used to improve the momentum measurement. The measuring accuracy was $\Delta p/p$ = 0.0025 p (p in GeV) in the streamer chamber and $\Delta p/p$ = 0.0005 p for tracks also reconstructed in the spark chambers. About 10% of the charged tracks with momenta p > 30 GeV/c had to be reconstructed from streamer-chamber data only. This accuracy was important in order to obtain sufficient resolution to perform pion correlation interferometry [5] for measuring the dimensions of the pion production region up to several fermis in size. Our interaction trigger vetoed about 3% of the inelastic events.

Tables I and II show the number of events, tracks and pion pairs for each reaction used in the present analysis.

Investigation of transverse momentum distributions

An increase of $\langle p_\perp \rangle$ with multiplicity has been suggested by cosmic ray measurements of Lattes et al. [6]. Figure 1 shows the $\langle p_\perp \rangle$ as the function of charged multiplicity for the central rapidity region $|y| < 1.5$ for several targets. The rapidity $y = \frac{1}{2}\ln\frac{E+p_\parallel}{E-p_\parallel}$ is calculated in the overall pp center of

mass system. The dashed lines represent $\langle p_\perp \rangle$ for all multiplicities, the values of which are given in Table 2 along with the average multiplicity $\langle n \rangle$ given in Table 2. We see no correlation of $\langle p_\perp \rangle$ with the multiplicity, in agreement with the ISR experiments at CERN [7]. However, clear correlation was observed at much higher energy in a $\bar{p}p$ collider experiment at CERN [8], the results of which are represented by the pair of solid lines (±1 standard deviation) in the $\bar{p}Xe$ diagram of Fig. 1. It was this observation, which was interpreted, within the framework of Landau's thermodynamical model [9], by Van Hove [10] as a possible evidence for a hadronic phase transition.

Determination of the interaction volume from pion correlations

The like-pion interference, observed by G. Goldhaber for the first time, allows to determine the time-space characteristics of the pion emission volume [5]. It is well-known that the two-particle correlation function of identical bosons emitted by two independent one-particle sources with nearly equal momentum p, and opening angle Θ, is described by the formula

$$W = 2[1 + \cos(pR\Theta)] ,$$

where R is the distance between the two sources.

However, this formula holds only for two point sources. To analyse our data we used the specific parametrization for a model of a uniformly radiating disk of radius R and lifetime τ, which was developed by Kopylov and Podgoretskij [11]. In addition to the energy and momentum differences of two pions, calculated in the overall pp CMS by

$$q_o = |E_i - E_j| \text{ and } \vec{q} = \vec{p}_i - \vec{p}_j ,$$

they introduced a new variable

$$q_t = \frac{|(\vec{p}_i - \vec{p}_j) \times (\vec{p}_i + \vec{p}_j)|}{|\vec{p}_i + \vec{p}_j|}$$

where q_t is the projection of $\vec{q}$ onto the plane perpendicular to $\vec{p}_i + \vec{p}_j$. It is closely related to the effective mass $M_{\pi\pi}$ (for $q_o \to 0$, $q_t^2 = m_{\pi\pi}^2 - 4m_{\pi\pi}^2$).

In this model, the number of like sign pairs (N_L) is given by the following expression:

$$\frac{N_L}{N_B} = 1 + \frac{I^2(q_t R)}{1+(q_o \tau)^2} ,$$

where $$I(q_t R) = \frac{2J_1(q_t R)}{q_t R} ,$$

with J_1 being the first order Bessel function and N_B is the number of "background" pairs, i.e. the number of pairs where there are no correlations.

The experimental problem is that one needs to extract only the correlation arising from Bose-Einstein statistics, but not other possible dynamical and kinematical correlations. Therefore, one takes a restricted q_o, q_t kinematical region. For the N_B one usually takes a number of opposite-sign pairs.

Unfortunately the dependence on q_o, q_t of this N_B is not free of dynamical correlations. In fact the $(\pi^+\pi^-)$ mass spectrum and hence the q_t distribution is strongly affected by resonances such as η and ω. A discussion of possible ways to determine N_L and N_B is given in reference [12].

We now summarise the procedure chosen for this analysis: in order to suppress the contribution of resonances we used only pairs with $0.0 < q_o < 0.2$ GeV and $0.002 < q_t^2 < 0.2$ (GeV/c), the lower limit removes possible electron pair contamination. N_B was found by first randomly mixing the transverse components of pions in each event. Then the variables q_t^2 and q_o were computed in the CMS of the interaction in the same manner, as for the non-reshuffled events. Finally N_B was normalised to the total number of like pairs in the q_o, q_t^2 region given above.

The binned experimental correlation function $\frac{N_L}{N_B}$ was fitted, with the least square method to the modified Kopylov-Podgoretskij expression

$$C\left(1 + \lambda \frac{I^2(q_t R)}{1+(q_o \tau)^2}\right) \quad , \tag{1}$$

where C is a normalisation constant and λ the degree of incoherence ($\lambda = 1$ represents a fully incoherent source). The maximum value of the function (1) is given by $C(1 + \lambda)$. Introducing the parameters C and λ, we take into account normalisation problems and contamination by non-Bose-Einstein correlations.

In Fig. 2 we show the experimental correlation function versus q_t^2 for two intervals of q_o, for both incident particles and for hydrogen and xenon targets. The solid line represents the fit of the theoretical expression (eq. 1) to the data. This fit was made simultaneously for both q_o intervals. In Table 3 fitted parameters with the corresponding χ^2 are given. The result for $\bar{p}p$ is in good agreement with a previous experiment [12].

As a check, the fit was tried for different q_t^2 and q_t binnings, four by fifteen instead of two by ten. The fit results were almost the same. We also tried the fit with λ as a fixed parameter: $\lambda = 1$ and $\lambda = 0.5$. For the case $\lambda = 1$, we found results similar to the case where λ was a free parameter. In the case $\lambda = 0.5$, the value of R did not change, but τ was very small ($c\tau \approx 0.01$ for pXe). The fitted values of C, being near one, indicate that our N_B normalisation was reasonable.

Since our interaction volume is probably not of a simple sphere, but more likely an ellipsoid, we tried to make specific cuts, in order to measure its length and width. We define ϑ to be the angle between the beam axis and the momentum vector of the pion pair and ϕ to be the angle between the plane defined by the two pions and that plane defined by the beam axis and the momentum vector of the pion pair. In the part of the data where $|\cos\vartheta|$ is small and $|\cos\phi|$ approximately one, the fitted values of R will be dominated by the length of the interaction volume. To obtain adequate statistics, we used cuts of $|\cos\vartheta| < 0.5$ and $|\cos\phi| > 0.7$. In the complementary data sample the value of R will be dominated by the width of the interaction volume. The results of these fits are also shown in Table 3 (except for $\bar{p}p$ where statistics were inadequate).

The values of the fitted parameters are similar for hydrogen and xenon, which we would not expect if a quark-gluon plasma was produced in the nuclear target. This result rather agrees with the expectation from the additive quark-model, which was found to be consistent with many other aspects of hadron nucleus collisions [4].

Central collisions are expected to be more favourable for the production of a quark-gluon plasma, because they produce a higher energy density. We have accordingly attempted to enrich fractions of central collision events by selecting xenon events with overall pion multiplicity greater than twenty. However, even with these samples we still obtained similar R and $c\tau$ values (see Table 3).

It is interesting to compare the radius of interaction found in this analysis, using elementary projectiles with that found in the BEVELAC experiments using the projectile ^{40}Ar [13]. Their radius is about three times ours, consistent with the larger radius of ^{40}Ar. However, in contrast with our results, their R increases with multiplicity. On the other hand, our radius is twice that found in $e^+ + e^-$ annihilation [14].

Conclusions

We have presented results for correlation between $\langle p_\perp \rangle$ and multiplicity in central rapidity region. No correlation is observed. In the central collisions, i.e. by higher multiplicity, one could expect higher energy density and/or temperature resulting in an increase of $\langle p_\perp \rangle$. Such an increase has been observed in the $\bar{p}p$ collider experiment. However, our energy is much lower than that of a collider.

We have obtained values for the size and lifetime of the pion producing region for both elementary and xenon targets. For both targets the values are similar, with radius about 1.5 fermis. This result is consistent with our previous observation that the proton interacts inside the nucleus in the manner, predicted by the additive quark model [4].

This analysis shows no indication of a deconfinement phase transition in nuclear matter.

References

[1] E.V. Shuryak, Physics Report 61 (1980) 71

[2] See e.g. L. McLerran et al., Phys. Lett. 98B (1981) 195,
T. Engels et al., Phys. Lett. 101 (1981) 89, [1]

[3] J.D. Bjorken, Phys. Rev. D27 (1983) 140 and Fermi Lab-Pub.82/59 Th. August 1982

[4] C. De Marzo et al., Phys. Rev. D26 (1982) 1019

[5] R.H. Brown and R.Q. Twiss, Nature 178 (1956) 1046,
G. Goldhaber et al., Phys. Rev. 120 (1960) 300,
G. Cocconi, Phys. Lett. 49B (1974) 459,
M. Gyullassy et al., Phys. Rev. C20 (1979) 2267

[6] C.M.G. Lattes et al., Phys. Rep. 65 (1980) 151

[7] T. Åkesson et al., Phys. Lett. 119B (1982) 464
M. Faessler, CERN-EP/82-145, 15 Sept. 1982

[8] G. Arnison et al., CERN-EP/82-125, 3 Sept. 1982

[9] L.D. Landau, collected papers, ed. D. Ter Haar, Pergamon, London, 1965, p. 569

[10] L. Van Hove, Phys. Lett. 118B (1982) 138

[11] G.I. Kopylov, Phys. Lett. 50B (1974) 472,
G.I. Kopylov and M.I. Podgoretskij, Sov. J. Nucl. Phys. 19 (1974) 215

[12] M. Deutschmann et al., Nucl. Phys. 204B (1982) 333

[13] S.Y. Fung et al., Phys. Rev. Lett. 41 (1978) 1592,
J.J. Lu et al., Phys. Rev. Lett. 46 (1981) 898

[14] G. Goldhaber, LBL-13291, Sept. 1981

Figure Captions

Figure 1: The average transverse momentum of charged hadrons ($\sqrt{s}$ = 19.4 GeV) as a function of charged track multiplicity in the rapidity interval $|y| < 1.5$. The dashed line is $\langle p_\perp \rangle$ value. The solid lines represent (± 1 standard deviation) the result of a $\bar{p}p$ collider in CERN.

Figure 2: q_t^2 dependence of the correlation function for the two intervals of q_o. The curves are fits of equation (1) to the data.

TABLE 1: NUMBERS OF EVENTS AND PAIRS FOR PROTON AND XENON TARGETS

REACTION	NO. OF EVENTS	NO. OF LIKE PAIRS	NO. UN-LIKE PAIRS	NO. OF LIKE PAIRS AFTER THE CUTS*	NO. OF RESHUF-LED UNLIKE PAIRS AFTER THE CUTS*
p + p	3531	55481	63494	7203	6891
$\bar{p}$ + p	1850	26440	33052	3465	3559
p + Xe	1391	146220	138773	13971	11219
$\bar{p}$ + Xe	1381	155627	157722	15540	12756

* $q_o \leq 0.2\,(\mathrm{GeV})$, $0.002 < q_t^2 \leq 0.2\,(\mathrm{GeV}/c)^2$

TABLE 2: NUMBER OF EVENTS AND AVERAGE TRANSVERSE MOMENTUM AND MULTIPLICITY IN THE RAPIDITY REGION $|y_{CMS}| < 1.5$

REACTION	NO. OF EVENTS	NO. OF TRACKS	$\langle p_\perp \rangle$ GeV/c	$\langle n \rangle$
p + p	3252	17778	0.366±0.002	5.47±0.06
$\bar{p}$ + p	1643	8724	0.366±0.003	5.31±0.08
p + Ne	104	658	0.376±0.010	6.33±0.39
$\bar{p}$ + Ne	82	505	0.372±0.012	6.16±0.40
p + Ar	929	7857	0.376±0.003	8.46±0.18
$\bar{p}$ + Ar	835	7257	0.376±0.003	8.69±0.20
p + Xe	1344	14070	0.363±0.003	10.50±0.18
$\bar{p}$ + Xe	1341	14628	0.359±0.003	10.95±0.18

TABLE 3: FITTED VALUES OF MODEL PARAMETERS (see eqn. 1 in text)

REACTION	Rfm	$c\tau$fm	λ	C	χ^2 (NDF=16)
pp	1.66±.04	1.02±.18	0.96±.08	0.90±.02	9.0
LENGTH	1.02±.08	0.62±.25	1.14±.10	0.65±.02	8.4
WDTH	1.74±.11	1.04±.28	1.04±.15	0.90±.03	13.5
$\bar{p}$p	1.52±.01	1.31±.21	1.23±.12	0.72±.02	29.8
pXe	1.53±.13	0.93±.16	1.27±.11	1.14±.05	25.4
LENGTH	0.82±.05	0.94±.16	1.52±.11	0.78±.03	15.1
WIDTH	1.58±.12	0.89±.17	1.38±.13	1.14±.05	23.2
pXe (N>20)	1.45±.11	0.95±.10	1.55±.16	1.12±.05	21.1
$\bar{p}$Xe	1.47±.11	0.95±.11	1.34±.08	1.07±.05	14.7
LENGTH	1.36±.10	0.78±.28	0.94±.11	1.18±.04	10.9
WIDTH	1.48±.11	0.98±.12	1.43±.11	1.04±.06	11.8
$\bar{p}$Xe (N>20)	1.53±.10	0.95±.16	1.27±.12	1.16±.05	19.1

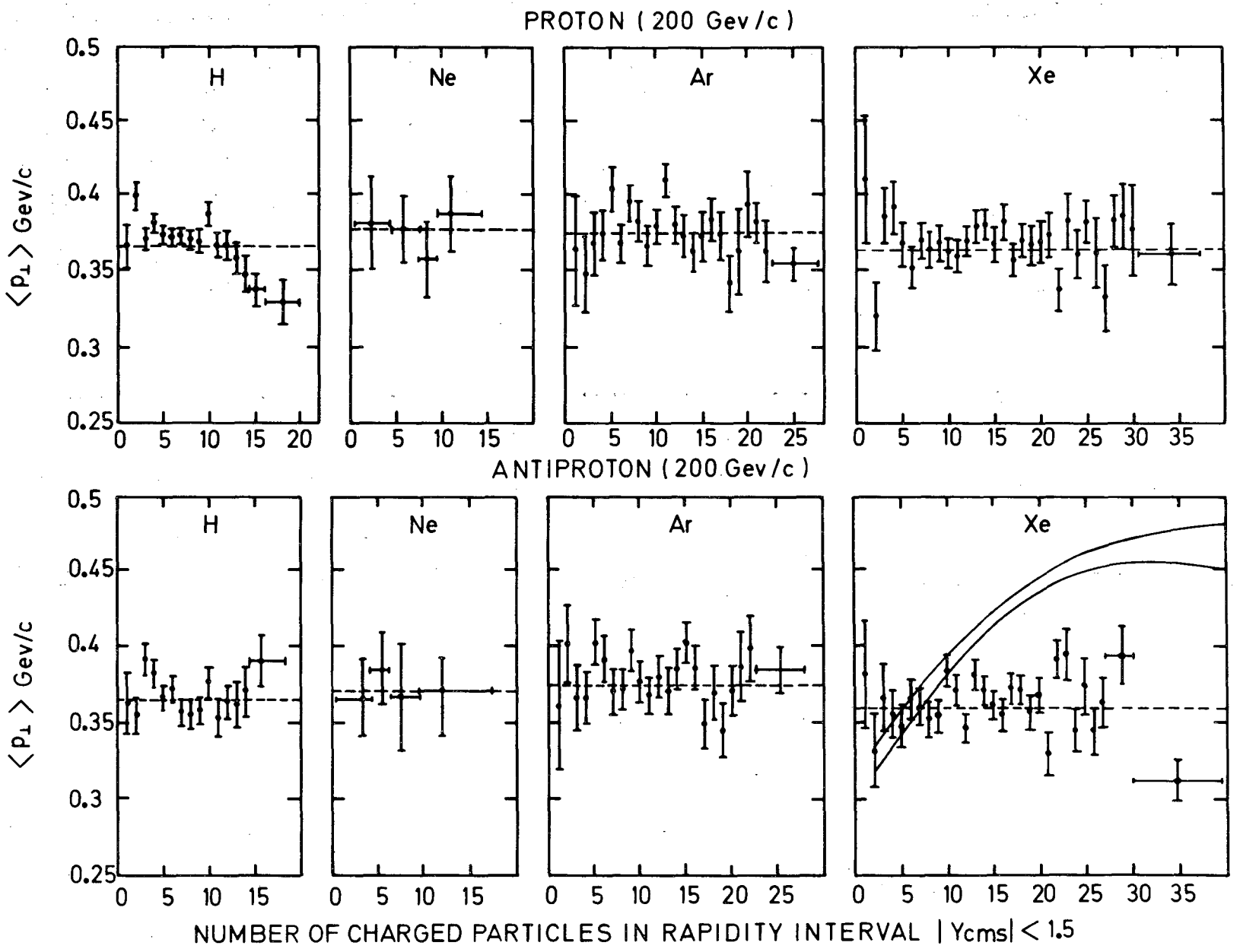
PROTON (200 Gev/c)
ANTIPROTON (200 Gev/c)
H
Ne
Ar
Xe
⟨p⊥⟩ Gev/c
0.5
0.45
0.4
0.35
0.3
0.25
0 5 10 15 20
0 5 10 15
0 5 10 15 20 25
0 5 10 15 20 25 30 35
NUMBER OF CHARGED PARTICLES IN RAPIDITY INTERVAL |Ycms| < 1.5

Fig. 1

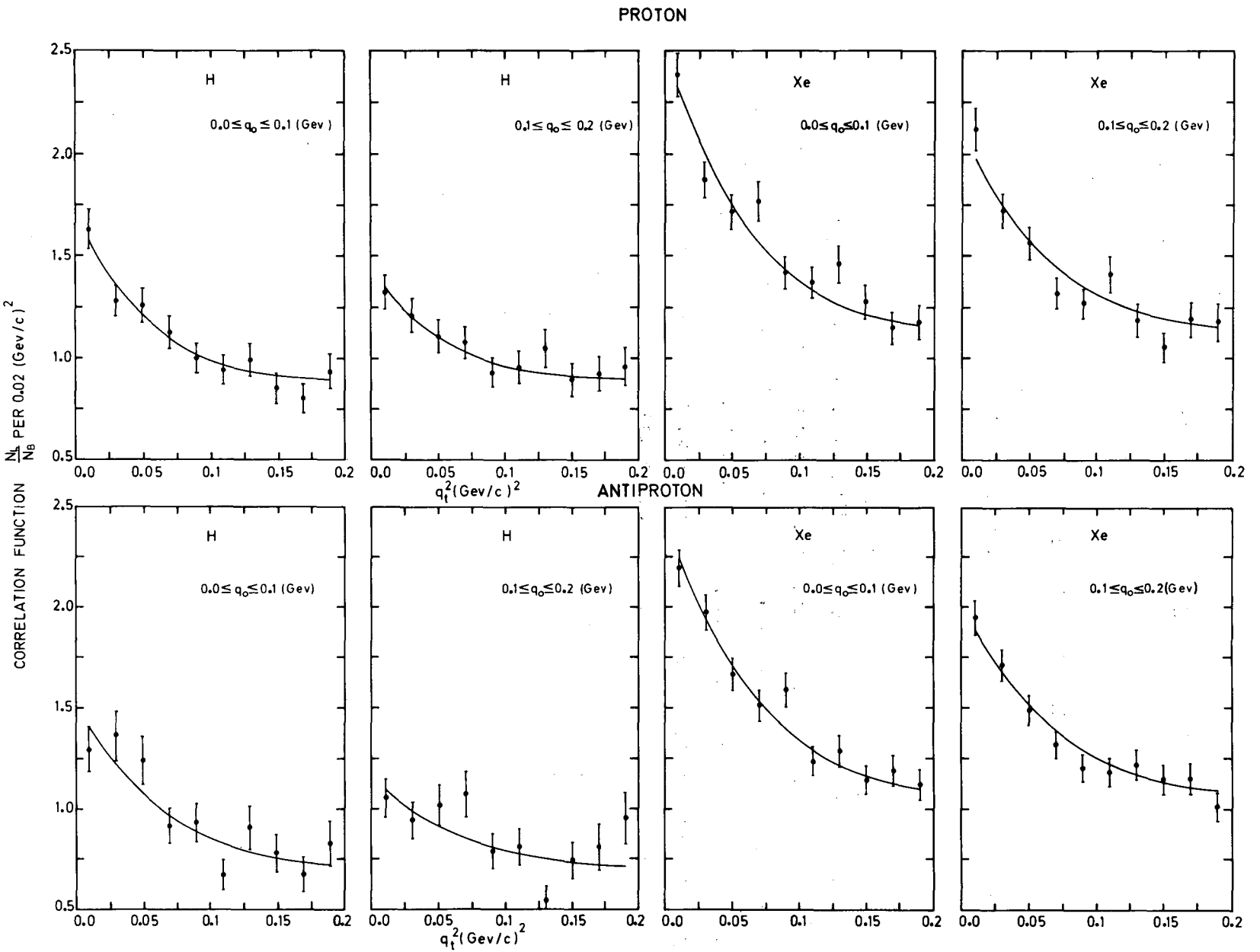
PROTON
ANTIPROTON
CORRELATION FUNCTION $\frac{N_L}{N_B}$ PER 0.02 (Gev/c)^2
H
0.0≤ q_0 ≤ 0.1 (Gev)
H
0.1≤ q_0 ≤ 0.2 (Gev)
Xe
0.0≤ q_0 ≤0.1 (Gev)
Xe
0.1≤q_0≤0.2 (Gev)
H
0.0≤ q_0≤0.1 (Gev)
H
0.1≤q_0≤0.2 (Gev)
Xe
0.0≤q_0≤0.1 (Gev)
Xe
0.1≤q_0≤0.2(Gev)
q_t^2(Gev/c)^2
q_t^2(Gev/c)^2
0.0
0.05
0.1
0.15
0.2
0.5
1.0
1.5
2.0
2.5

Fig. 2

αα and αp Interactions at the CERN ISR.

E. Stenlund

(CERN-Heidelberg-Lund collaboration)

CERN, Geneva, Switzerland.

Abstract

Recent results on two-particle rapidity correlations measured in αα, αp and pp interactions are presented. The experiment was done at the CERN ISR using the Split Field Magnet detector. The true two-particle correlations were isolated by fixing the charged multiplicity. In the framework of a simple cluster model, the cluster widths as well as the cluster multiplicities were found to be the same for αα, αp and pp interactions.

Introduction.

During a short run in 1980 with α-particles in the CERN Intersecting Storage Rings, a large amount of data was collected. Five experiments took data using different experimental set-ups and various triggers.

R 110: π^0 production at very large transverse momenta with a superconducting solenoid magnet and leadglass and lead/scintillator sandwich counters.

R 210: Small-angle elastic scattering, with plastic scintillators and drift tube hodoscopes.

R 418: Elastic scattering at larger angles, inelastic interactions, and large-p_t hadron production, with the SFM detector.

R 806: π^0 production at large p_t, with two liquid-argon/leadplate calorimeters.

R 807: Production of hadrons with large p_t and inelastic interactions, with the AFM detector and two forward calorimeters.

The different physics subjects studied can thus be summarized in the following categories:

Elastic scattering

Quasi-elastic scattering and nuclear break-up

Hard scattering of constituents - Large p_t physics

Inelastic scattering

The subject of this talk has been choosen from the last category, namely, a recent study of two-particle rapidity correlations performed by the CERN-Heidelberg-Lund collaboration (R 418) [1].

Particle correlations have been measured in various hadronic interactions during the last ten years [2,3], and lately also in e^+e^--interactions [4]. The observed correlations were interpreted in the framework of various theoretical models; the most popular ones were the cluster models [5] and, more recently, the string models [6].

When α-particles were accelerated and stored in the ISR, a unique possibility of studying two-particle correlations for interactions of multinucleon systems was provided. Speculations of a phase transition when high enough energy densities are reached, suggest that the size or mass of clusters might be larger in nucleus-nucleus interactions com-

pared to interactions between elementary particles [7]. Also other collective phenomena could lead to an increase of the cluster size.

It may not be realistic to believe that a phase transition will be reached with nuclei as light as α-particles. On the other hand light nuclei provide a simple system where the "normal" nuclear effects on the correlations can be studied. The understanding of these effects might be crucial when one searches for phase transitions using heavier nuclei.

The investigation was organized as follows: First the inclusive correlations were studied and thereafter we turned to the semi-inclusive correlations, by fixing the observed multiplicity. By doing the analysis at fixed multiplicity in terms of a cluster model, we extracted cluster-widths in rapidity and cluster-strengths or decay multiplicities as a function of the total multiplicity and compared these quantities for our different data sets. We believe this to be a sensitive procedure to recognize differences of real dynamic correlations. The main aim of the investigation was to measure and compare correlations in αα, αp and pp-interactions.

Inclusive two-particle rapidity correlations.

The normalized correlation function

$$R(y_1,y_2)=\frac{\rho^{(2)}(y_1,y_2)}{\rho^{(1)}(y_1)\rho^{(1)}(y_2)} - 1, \qquad (1)$$

has the advantage that the detector efficiencies cancel out in the first approximation and has thus been used throughout this investigation.

One problem in comparing αα, αp and pp interactions is to find corresponding energies at which comparisons can be made. When pp-interactions at different energies are compared an energy dependence is clearly seen, i. e. at large absolute rapidities, the value of R decreases with decreasing energy.

If instead the "normalized" rapidity, defined as $\psi=y/y_{inc}$ [8] is used the behaviour changes drastically, i. e. the energy dependence disappears. This suggests that by using the "normalized" rapidity, we can compare correlations from different origin without taking the incident energies

into consideration. In fig. 1 we display the results of such a comparison. Except for the peaks around $y_1 \cong y_2$, the most striking effect is the difference between correlations in αα-interactions and those in pp-interactions. At high absolute rapidities the αα-data flattens out giving $R \cong 0$, thus showing that correlations are absent, in contrast to what is observed for pp-data where large negative correlations are seen in this region.

The data from αp interactions have the following features: When the "triggering" rapidity, ψ_1, is close to 0, the correlations on the α-side (positive rapidities) are close to the ones observed in αα-interactions, while on the p-side (negative rapidities). The function behaves like the one obtained for pp-interactions. When the "triggering" rapidity is shifted to the α-side the R-function becomes similar to the one observed for αα-interactions, and the corresponding behaviour is observed for ψ_1 on the p-side, i. e. here the function follows closely the one obtained from pp-interactions.

It is known since a long time [3] that the main structure of fully inclusive two-particle correlations results from mixing events with different structure in momentum space (here y) and has nothing to do with true two-particle correlations. We have derived a quantitative form for R assuming that all true two-particle correlations are absent, and shown that the change in shape of the particle density with increasing multiplicity leads to a non-uniform R-function. Assumptions:

i) No correlations within events $\Longrightarrow$

$$\rho_n^{(2)}(y_1,y_2)=\frac{n-1}{n}\,\rho_n^{(1)}(y_1)\rho_n^{(1)}(y_2), \tag{2}$$

where

$$\sum_n \Pi(n)\rho_n^{(1)}=\rho^{(1)}. \tag{3}$$

$\Pi(n)$ is the probability of having n charged particles.

ii) Particle densities at any given rapidity y depends linearly on n [9] $\Longrightarrow$

$$\rho_n^{(1)}(y)=n\cdot\alpha(y)+\beta(y). \tag{4}$$

Furthermore we define the average multiplicity associated with a particle at rapidity y (including the particle) as

$$\langle n\rangle_y = \sum_n \Pi(n)\cdot n\cdot \rho_n^{(1)}(y) / \sum_n \Pi(n)\cdot \rho_n^{(1)}(y), \tag{5}$$

and finds

$$R(y_1,y_2) \cong \frac{\langle n^2\rangle}{D^2}(\langle n\rangle_{y_1}/\langle n\rangle - 1)(\langle n\rangle_{y_2}/\langle n\rangle - 1) - 1/\langle n\rangle. \tag{6}$$

Fig. 2 shows a comparison between eq. (6) and the experimental R-functions and indeed the overall behaviour of the experimental R-functions are very well described by eq. (6), apart from the maximum at $y_1 \cong y_2$ which is by essence absent from this equation.

Even if the assumption of linearity in the density, eq. (4), is not fulfilled, this example shows that the R-function has a structure similar to the one observed, also if all two-particle correlations were absent. The conclusion which has to be drawn is the wellknown fact that to get rid of the so called long-range correlations, one has to study R at fixed total multiplicity.

Semi-inclusive correlations.

Fig. 3 shows the R-function for all charged particles at a fixed negative multiplicity, $n_- = 5$, for αα, αp and pp-interactions. The different interactions give similar features with a peak around y_1 of about the same height. It should be noted that the distributions shown in fig. 3 are very similar to what is obtained from fig. 2, if eq. (6) is subtracted from the experimental data.

In order to study systematically whether differences of the width and height of the correlation peak occur for αα, αp and pp-interactions, a parametrization of the peak and the background level is needed. Therefore the data was analysed in the context of a simple independent cluster model. The following assumptions were used:

i) A cluster at rapidity Y decays into K charged particles at rapidities y_i, i=1,2,..,K, so that y_i are uncorrelated and Gaussian distributed with mean Y and width δ.

ii) δ is much smaller than the width of the rapidity distribution of clusters.

iii) Clusters are independent.

The correlation function for fixed multiplicity n is expressed as follows:

$$R_n(y_1, y_2) = \frac{F_n \rho_n^{(1)}(y_a)}{\rho_n^{(1)}(y_1)\rho_n^{(1)}(y_2)} \cdot \frac{1}{2\sqrt{\pi}\,\delta_n} \exp\{-(\Delta y)^2/4\delta_n^2\} - \frac{1-F_n}{n}, \qquad (7)$$

where δ_n is the width in rapidity of clusters produced in events with multiplicity n and F_n is the corresponding cluster-strength defined as $F_n = [\langle K(K-1)\rangle / \langle K\rangle]_n$, where K is the charged multiplicity of the cluster. Furthermore $y_a = (y_1+y_2)/2$ and $\Delta y = y_1 - y_2$.

In fig. 4 the obtained values of δ_n are displayed as a function of the negative multiplicity, n_-. In fig. 4a we have compared δ_n from pp-data at three different energies and the energy independence is clearly seen. In fig. 4b we compare δ_n from $\alpha\alpha$- and αp-data with the δ_n from pp-data and no significant deviations can be detected.

Also F_n is independent of the incident particles but, in contrast to the case for δ_n, an energy dependence seems to be present.

Summary and conclusions.

When two-particle correlations from $\alpha\alpha$, αp and pp-interactions are compared, they show a similar behaviour. The only differences are seen at large absolute rapidities, where the distributions from $\alpha\alpha$-interactions and from the α-side of the αp-interactions give correlations close to zero. This is on the other hand a trivial effect, since most of the particles observed in this region are spectator protons (or heavier fragments) left over from the interacting α-particles.

When the correlations are analysed in the framework of a simple cluster model, the widths as well as the multiplicities of the clusters come out the same for $\alpha\alpha$, αp and pp-interactions. The conclution must be that the mechanisms responsible for the short range correlations are the same for the different kinds of interactions.

We find no trace of collective phenomena from our analysis, and if such

phenomena should be possible to observe, either the energy or the masses of interacting nuclei have to be increased.

Acknowledgements.

I wish to thank S.-Y. Fung for reading and correcting the manuscript and M.Faessler for discussions connected to this talk. I also would like to thank all members of the CERN-Heidelberg-Lund collaboration.

References.

[1] Two-particle Rapidity Correlations in αα, αp and pp Interactions at the CERN ISR, W.Bell et al.. To be published.

[2] See for instance: A.Breakstone et al. ABCHW collaboration, Phys. Lett. 114B(1982)383; K.Alpgard et al. UA5 collaboration, CERN Preprint: CERN-EP/83-20(1983).

[3] See for instance: L.Foa, Phys. Reports 22(1975)1; J.Ranft, Fortschritte der Physik 23(1975)467.

[4] W.Koch, Talk given at the "XIII Int. Symp. on Multiparticle Dynamics", Volendam, the Netherlands, June 1982. DESY Preprint: DESY 82-072(1982) and references therein.

[5] See for instance: O.Czyzewski and A.Krzwicki, Nuovo Cim. 30(1963)603; L.van Hove, Rev. Mod. Phys. 36(1964)655; A.Bassetto, M.Toller and L.Sertorio, Nucl. Phys. b34(1971)1; F.Henyey, Phys. Lett. 45B(1973)469; J.L.Meunier and G.Plaut, Nucl. Phys. B87(1975)74; J.Kubar-Andre, M.Le Bellac and J.Meunier, Nucl. Phys. B93(1975)138; C.Michael, Nucl. Phys. B103(1976)296.

[6] See for instance: A.Veneziano, Nucl. Phys. B117(1976)519; A.Capella, U.Sukhatme and J.Tran Thanh Van, Z. Physik C3(1980)329.

[7] R.Hagedorn, Invited lecture at the "Workshop on Future Relativistic Heavy Ion Experiments", Darmstadt, Germany, October 1980. CERN-preprint: Ref.TH.3014-CERN(1981).

[8] L.van Hove, Phys. Rep. 1C(1971)347; E.Stenlund and I.Otterlund, CERN-preprint: CERN-EP/82-42(1982).

[9] J.Whitmore, Phys. Rev. C27(1976)187.

Figure captions.

Fig. 1: Comparison of the normalized correlation function for all charged particles from αα, αp and pp-interactions. The pp-data are shown as curves. a) $\psi_1=0$. b) $\psi_2=-0.5$.

Fig. 2: Comparison between the normalized correlation function and calculations from eq. (6). a) pp 31+31 GeV, $y_1=0$. b) pp 31+31 GeV, $y_1=-2$. c) αα 62+62 GeV, $y_1=0$. d) αα 62+62 GeV, $y_1=-2$.

Fig. 3: The normalized correlation function at fixed multiplicity ($n_-=5$) for αα, αp and pp-interactions. a) $y_1=0$. b) $y_1=-1.5$.

Fig. 4: The cluster width, δ_n, as a function of the corrected negative multiplicity. a) pp-interactions. b) αα-interactions. The shaded area corresponds to the pp-data from a).

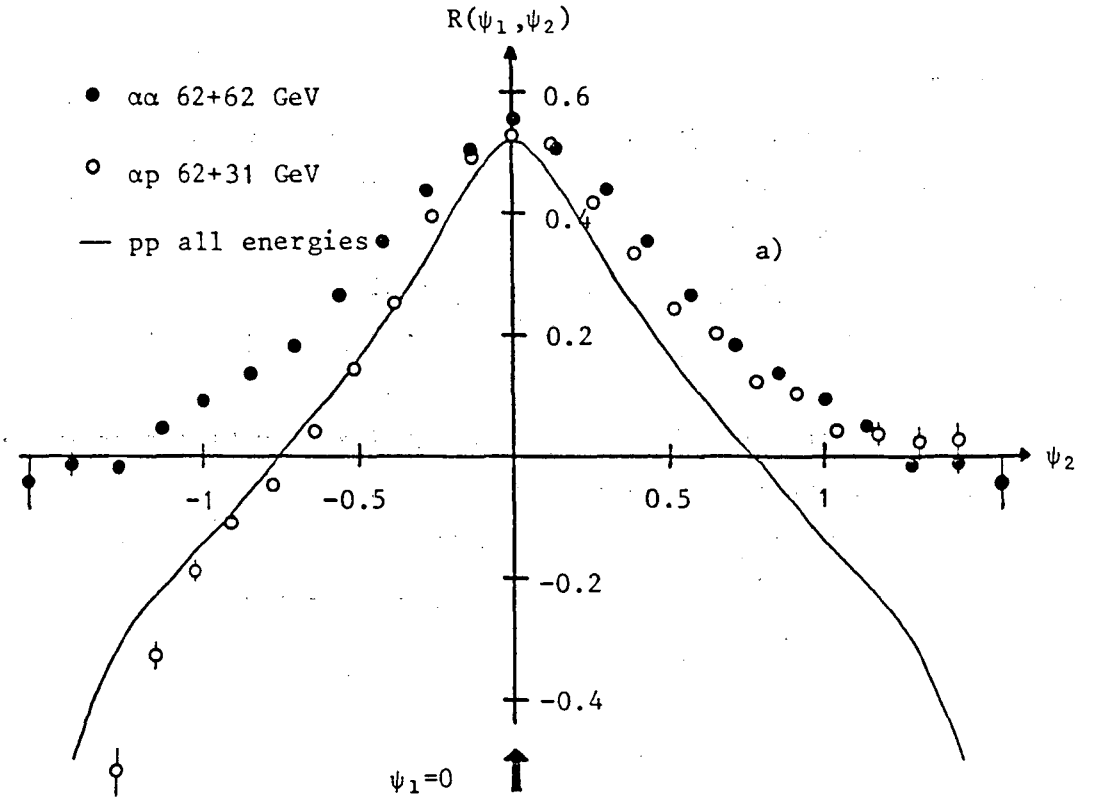
R(ψ1,ψ2)
αα 62+62 GeV
αp 62+31 GeV
pp all energies
a)
0.6
0.4
0.2
-0.2
-0.4
-1
-0.5
0.5
1
ψ2
ψ1=0

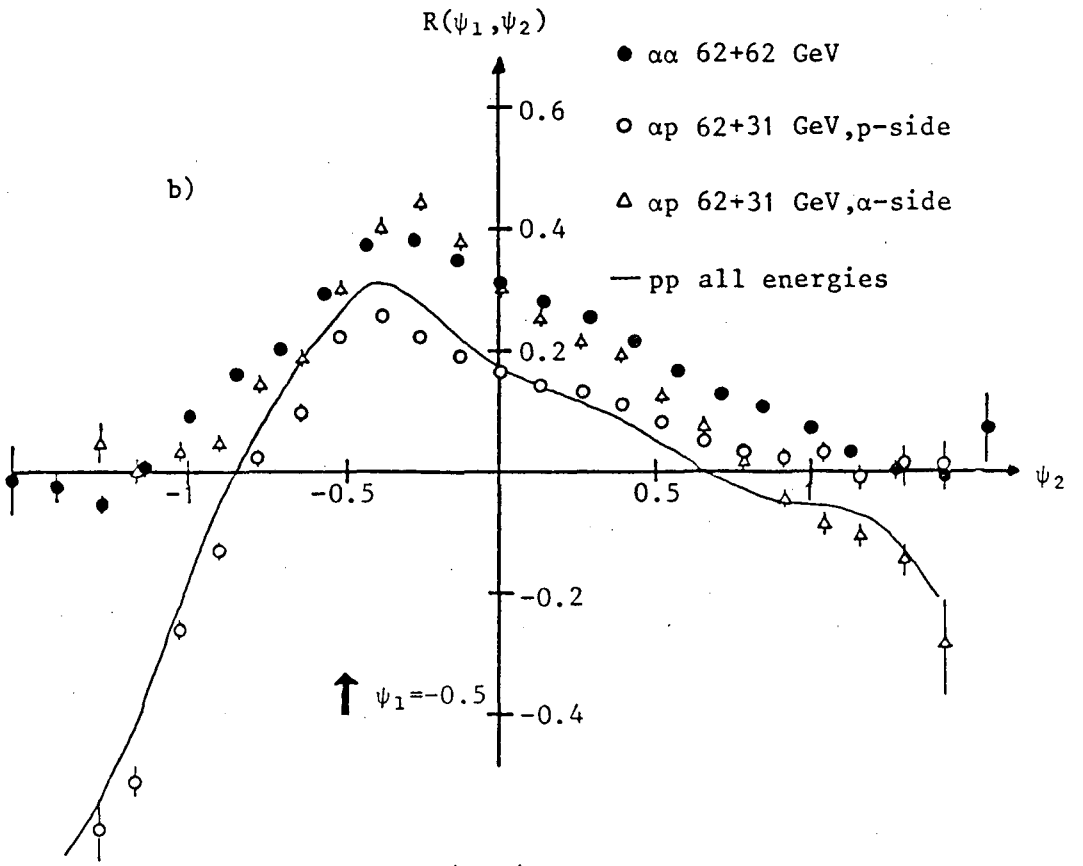
R(ψ1,ψ2)
αα 62+62 GeV
αp 62+31 GeV,p-side
αp 62+31 GeV,α-side
pp all energies
b)
0.6
0.4
0.2
-0.2
-0.4
-1
-0.5
0.5
1
ψ2
ψ1=-0.5

Fig. 1

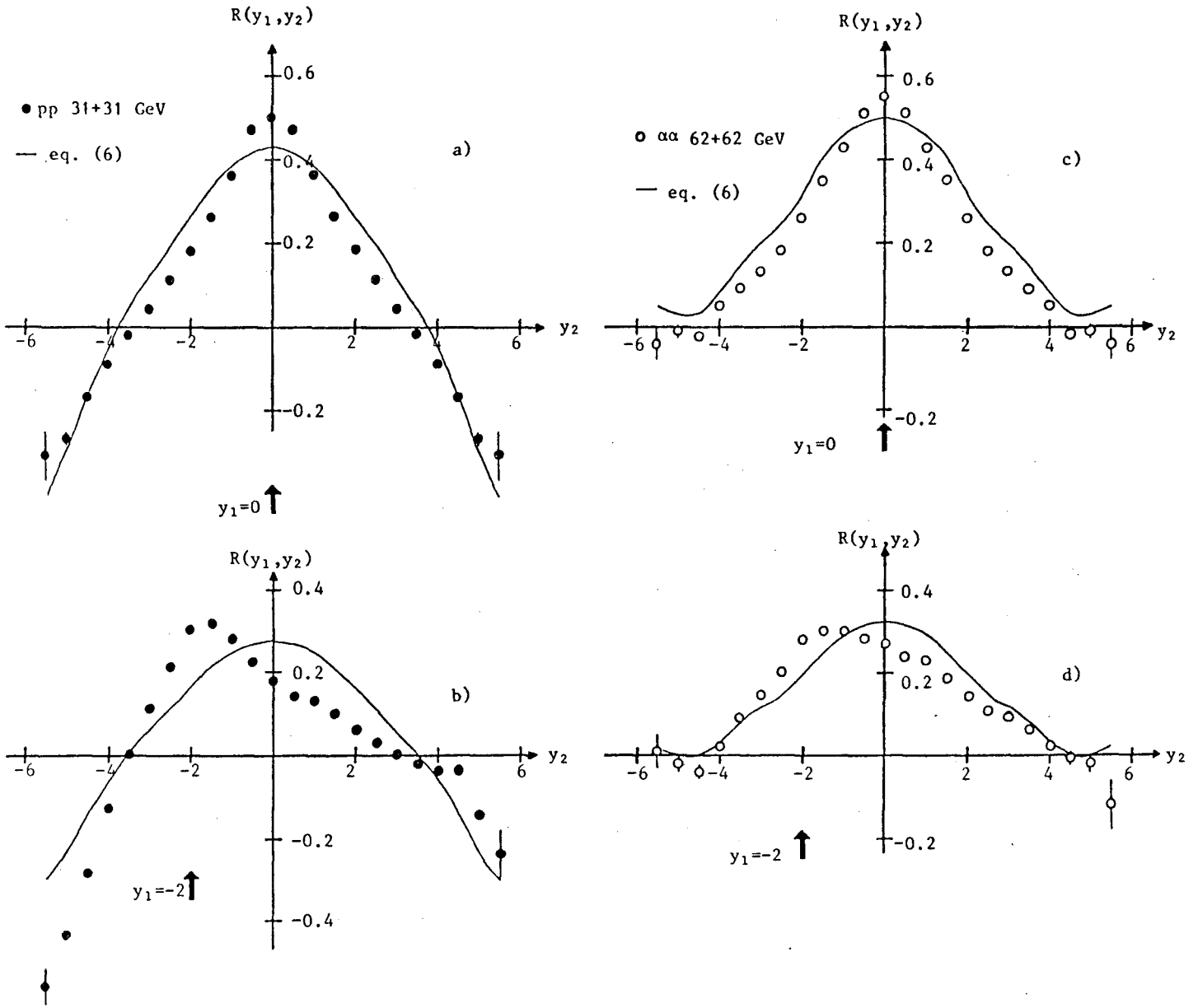

Fig. 2

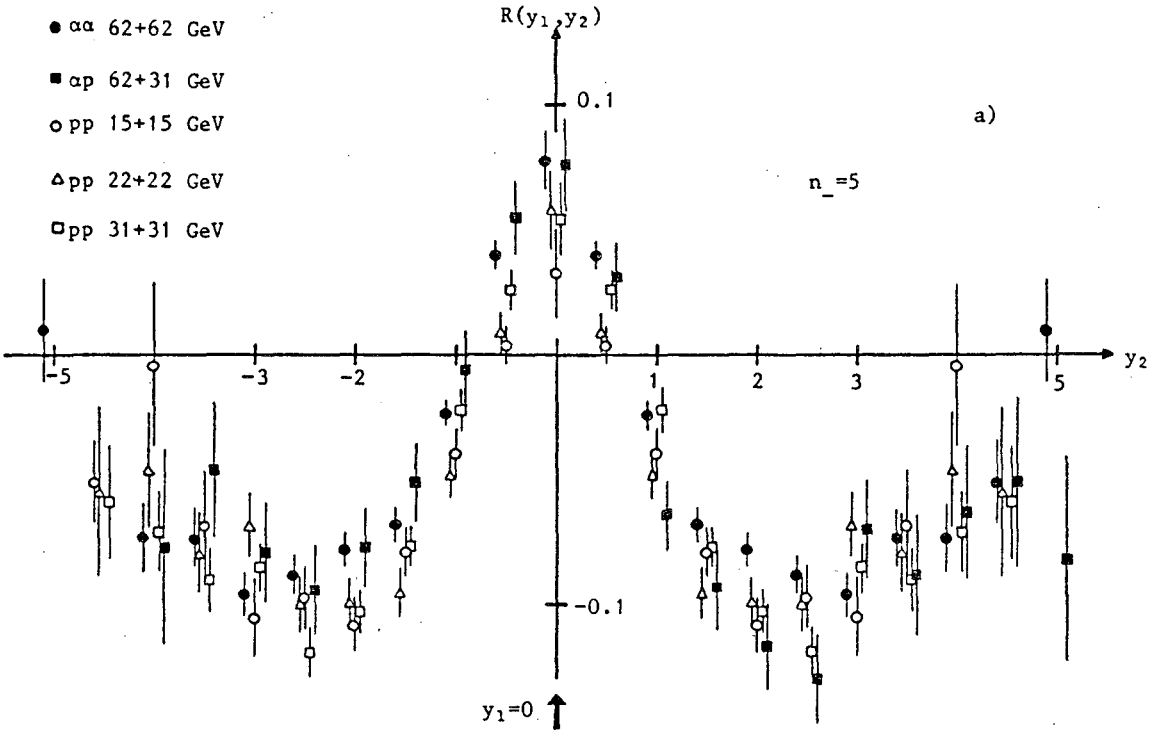
αα 62+62 GeV
αp 62+31 GeV
pp 15+15 GeV
pp 22+22 GeV
pp 31+31 GeV
R(y1,y2)
0.1
-0.1
a)
n_=5
y2
-5
-3
-2
1
2
3
5
y1=0

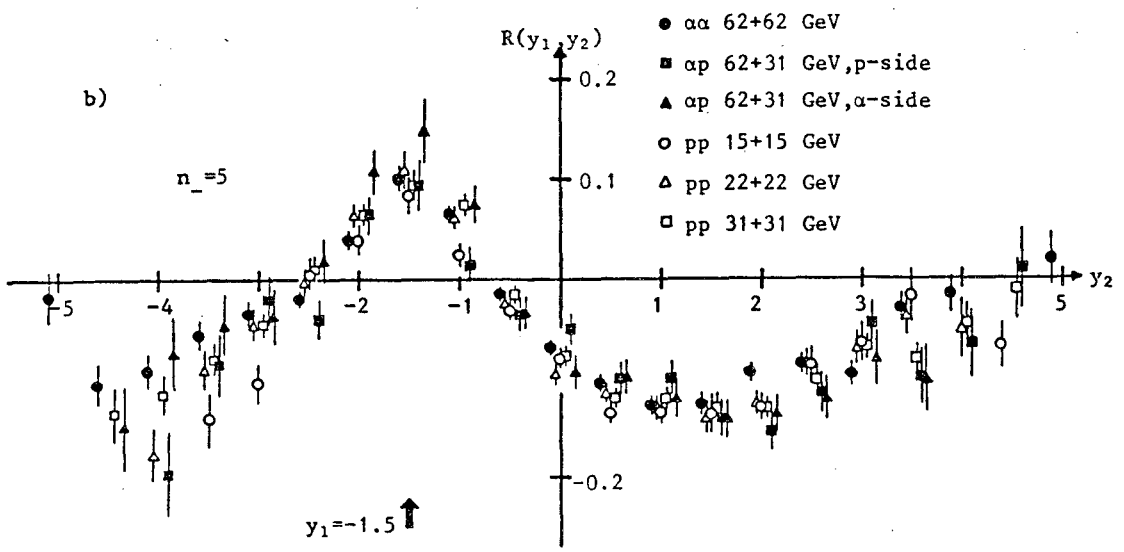
b)
n_=5
R(y1,y2)
αα 62+62 GeV
αp 62+31 GeV,p-side
αp 62+31 GeV,α-side
pp 15+15 GeV
pp 22+22 GeV
pp 31+31 GeV
0.2
0.1
-0.2
y2
-5
-4
-2
-1
1
2
3
5
y1=-1.5

Fig. 3

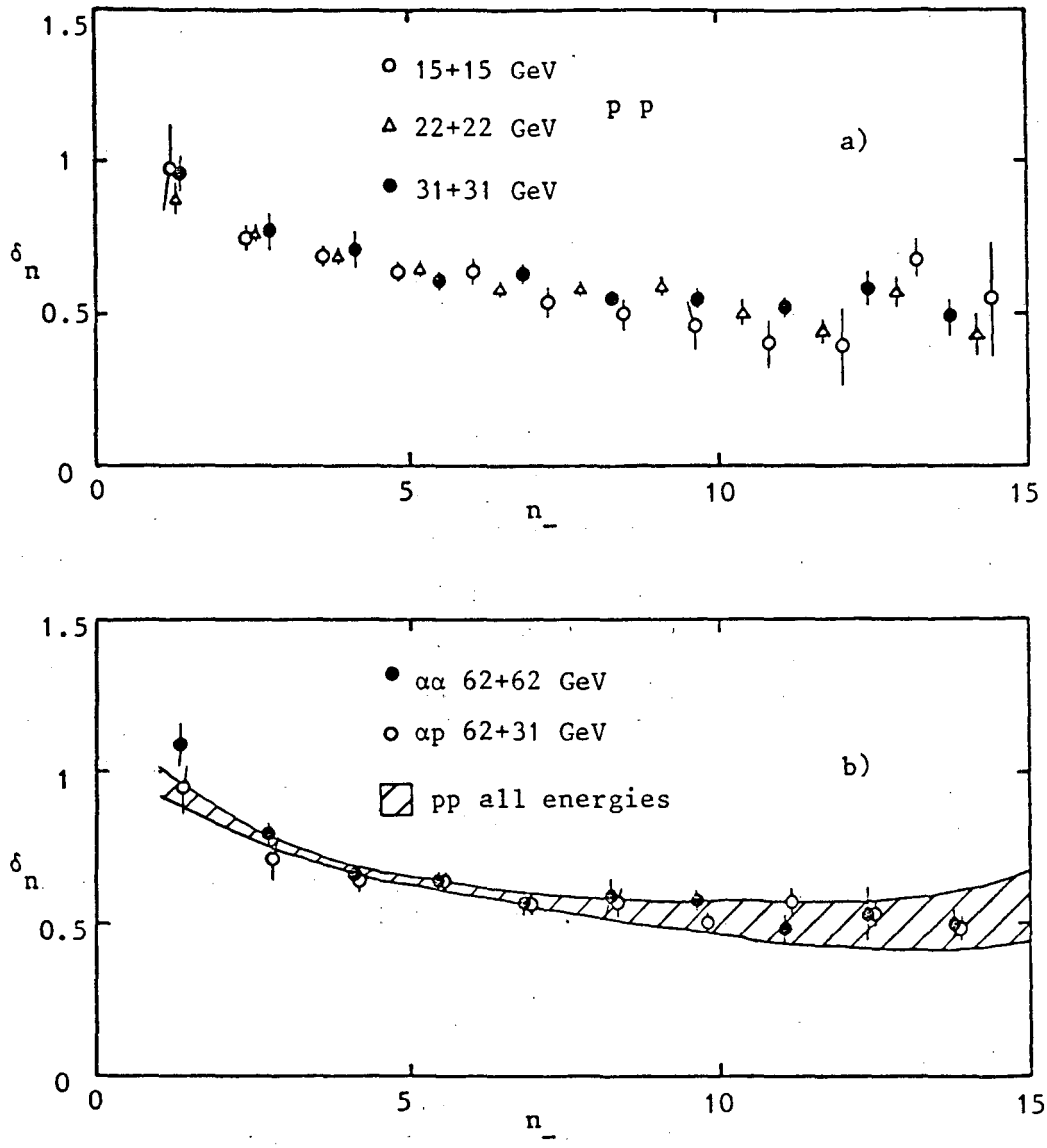
1.5
1
0.5
0
δ_n
0
5
10
15
n_-
15+15 GeV
22+22 GeV
31+31 GeV
p p
a)
1.5
1
0.5
0
δ_n
0
5
10
15
n_-
αα 62+62 GeV
αp 62+31 GeV
pp all energies
b)

Fig. 4

Particle densities in ultrarelativistic heavy ion reactions extrapolated from proton-nucleus collisions.

I. Otterlund, S. Garpman, I. Lund,
Division of Cosmic and Subatomic Physics, University of Lund, Lund, Sweden.

E. Stenlund,
CERN, Geneva, Switzerland.

Rapidity density distributions in central ultrarelativistic heavy ion reactions are estimated from high energy proton-nucleus collisions and compared with some cosmic ray events. Deviations from a simple scaling of pA reactions are observed.

Introduction.

Recent developments of quantum cromodynamics provide great confidence in the existence of a new phase of matter - the quark gluon plasma - which could be reached either by heating up or by compressing nuclear matter [1]. Theoretical studies [2] suggest that the quark-gluon plasma is accessible in ultrarelativistic central heavy ion collisions. Guided by observations in proton-nucleus reactions [3-5] we have estimated rapidity and energy density distributions to be expected in ultrarelativistic heavy ion reactions.

Ultrarelativistic proton-nucleus collisions.

Data from hadron-nucleus reactions agree on the concept of a long formation length for the final hadronic states. Most hadrons are materialized outside the nuclei and they have thereby lost their possibility to interact with nuclear matter. Only slow hadrons can cascade in the hit nucleus.

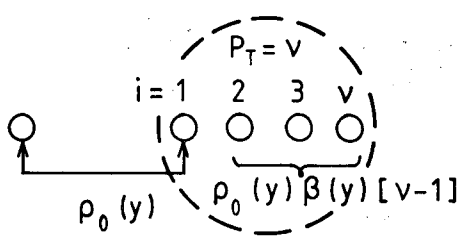

Fig. 1. An artist drawing of a proton-nucleus collision.

We have utilized a picture of pA reactions as illustrated in Fig. 1. The rapidity density is

$$\rho(y)=\frac{1}{\sigma}\frac{d\sigma}{dy} = \rho_o(y) + \sum_{i>1} \beta_i(y)\rho_o(y) \qquad (1)$$

To evaluate $\beta_i(y)$ we examine reactions where the incident proton has passed through layers of nuclear matter of different thickness i.e. different number of participant target nucleons, P_T. This can be done by either increasing the size of the target nucleus, $P_T = \langle\nu(A)\rangle$, or by decreasing the impact parameter in reactions with comparatively heavy nuclei, $P_T = \langle\nu(N_h)\rangle$, ($N_h$ = the multiplicity of charged nuclear fragments). Within the experimental uncertainties a fairly linear dependence between ρ and $\langle\nu\rangle$ is observed showing that the energy flux is not attenuated very much during its passage through the nucleus. If we neglect any intranuclear cascade the contribution from a hit nucleon i, $\beta_i(y)\rho_o(y)$, then ought to be comparatively independent on i, i.e.

$$\sum_{i>1}^{P_T} \beta_i(y)\rho_o(y) = (P_T-1)\beta(y)\rho_o(y) \qquad (2)$$

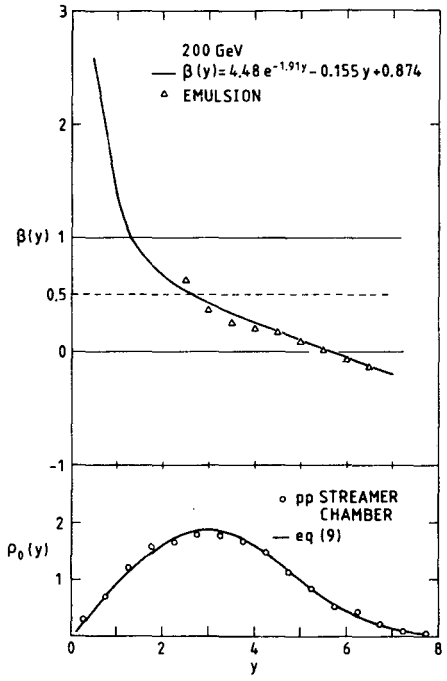

Fig. 2. ρ_o and β estimated from streamer chamber data [4].

a) comparison with the actually measured rapidity densities in pp reactions [4].

b) Comparison between β determined from streamer chamber data (solid curve) and from emulsion experiments (triangles).

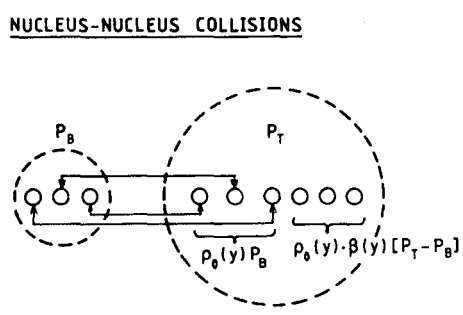

Fig. 3. An artist drawing of a nucleus-nucleus collision.

Fig. 2a compares $\rho(y)$ of produced particles in pp-reactions [4] with $\rho_o(y)$ from the best fit of eq. (1) to the streamer chamber pp-, pAr- and pXe-reaction data [4]. Fig. 2b shows $\beta(y)$ obtained by the fit.

Ultrarelativistic nucleus-nucleus collisions.

We consider central heavy ion reactions and only events where the beam nucleus is so small and the target nucleus so large that the probability is high that all incident nucleons participate in the reaction.

Rapidity densities.

To estimate rapidity densities we assume that each of the (P_T-P_B) participant nucleons contribute to the density with $\beta(y)\rho_o(y)$ particles, while the contribution from the first hit nucleons is $\rho_o(y)\ P_B$ (cf. Fig. 3). P_B is the number of participating projectile nucleons. We then receive the following expression for the densities.

$$\rho(y) = \rho_o(y)\ P_B + \rho_o(y)\beta(y)(P_T-P_B) \qquad (3)$$

$$= P_B\rho_o(y)\ [1 + \beta(y)\ (k-1)]$$

$$\text{where } k = \frac{P_T}{P_B} \text{ and } P_T > P_B. \qquad (4)$$

In the phenomenological model described here the shape of the density distribution in central heavy ion reactions is determined by scaling of the ratio k i.e. pA and BA reactions with the same $k = \langle\nu\rangle$ values exhibit density distribution with similar shapes. The merit of eq. (3) is that it supplies a norm for comparison with experiments. Deviations may tell us that the nuclear environment is of much more importance than considered by only counting the number of participants in the geometrically overlapping volumes.

In central BA reactions the average value of k $(=k_g)$ is determined by the geometrical overlap

$$k_g = \frac{A}{B}\left[1 - \left(1 - \left(\frac{B}{A}\right)^{2/3}\right)^{3/2}\right] \qquad (5)$$

As long as the actually measured distributions, event by event, agree with the distributions

extrapolated with k-values equal or smaller than k_g, the signal for interesting physics is not obvious from rapidity density distributions. However, values of $k \gg k_g$ and large fluctuations from extrapolated distributions may signal that new physics is going on in central heavy ion reactions.

Heavy ion reactions in the hundred of A GeV range.

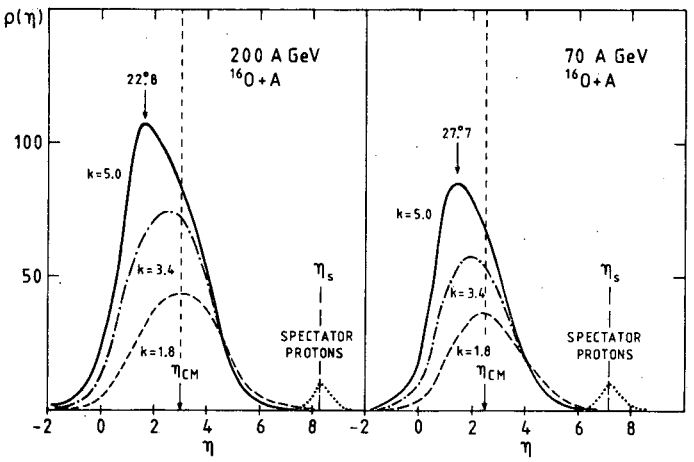

Fig. 4. Rapidity densities for central ^{16}O+A reactions for three different k-values estimated from pEm collisions at 200 and 70 GeV. The expected distribution for spectator protons are shown by the dotted distributions.

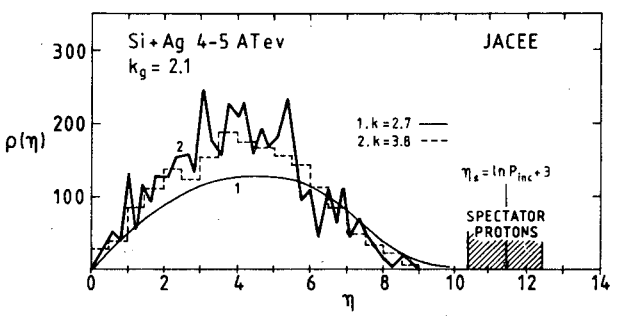

Fig. 5. The particle density distribution in pseudo-rapidity in an event of Si+Ag from the JACEE collaboration [6]. The solid curve and the dotted histogram are extrapolated from proton-emulsion reactions at ~ 3000 GeV. The pEm data are from ref. 8.

Figs 4a and b show $\rho(\eta)$ distributions in central ^{16}O+A reactions at 200 A GeV and 70 A GeV respectively. The distributions are extrapolated from pseudo-rapidity ($\eta = -\ln \mathrm{tg}\,\frac{\theta}{2}$) distributions measured in pEm reactions.

In the upper region of rapidity range extrapolated and measured density distributions should agree because all incident nucleons participate. In the central and lower rapidity range fluctuations are expected. Fig. 4 which shows how the density distributions depends on k, gives some hints on such fluctuations.

Heavy ion reactions in the A TeV range.

One impressive cosmic ray event is from the JACEE collaboration where a Si-nucleus interacts with an Ag-nucleus at an energy of 4-5 A TeV [6]. The rapidity density distribution in this event is shown in Fig. 5. The distributions 1 and 2 in Fig. 5 are extrapolated pEm reactions in two N_h-bins; $6 \leq N_h \leq 10$ (solid curve) and $11 \leq N_h \leq 15$ (dotted histogram).

The JACEE Si+Ag event exhibits a much larger enhancement in the backward direction in the nucleon-nucleon centre of mass system than expected from a simple scaling of pA-data with

$$k_g = \frac{P_T}{P_B} = 2.1$$

Energy densities.

It has been pointed out by Gyulassy [7] that energy densities extracted from central ultrarelativistic cosmic ray events are high. We give here an es-

timate of energy densities in BA events extrapolated from pA-reactions.

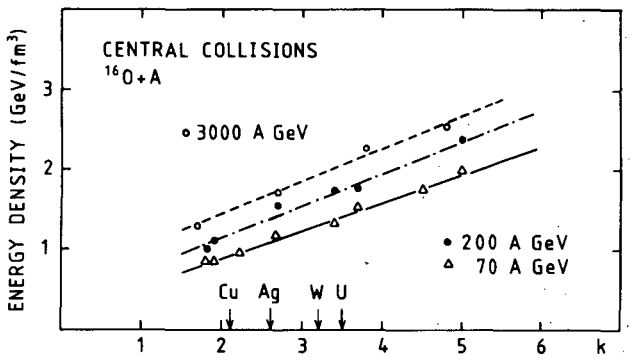

Fig. 6. Energy densities in central ^{16}O+A reactions estimated from proton-emulsion nucleus collisions. The k_g-values for average central reactions with Cu, Ag, W and U are marked in the figure.

Fig. 6 shows the energy density, ϵ, in the region of rapidity where the rapidity density distribution extrapolated from pA reaction exhibits its maximum. This region is defined as $\eta_{max} \pm 0.5$ where η_{max} is the pseudo-rapidity at maximum particle density. The k_g-values for average central reactions with Cu, Ag, W and U are marked in the figure. In single events higher k-values can be reached. Our estimates show that $\epsilon \approx 1\text{-}3$ GeV fm^{-3} could be achived at $\sqrt{s_{NN}} \gtrsim 10$ GeV.

Conclusions.

Rapidity density distributions extrapolated from proton-nucleus collisions supply a norm for comparison with measured particle densities in high energy nucleus-nucleus collisions.

We compare with the average behaviour determined by the clean cut participant - spectator model. Much larger particle densities than given by the geometrical clean cut picture ($k \gg k_g$) may signal new interacting physics.

The JACEE Si+Ag event exhibits a large enhancement in the backward direction in the nucleon-nucleon centre of mass system. This large enhancement signals a violent participation from the target nucleus.

References.

1. L. van Hove, Proceedings of the Bielefeld Workshop on Quark-Gluon Matter and Very High Energy Heavy Ion Collisions; ed. by M. Jacob and H. Satz, World Scientific Publishing Co,. Singapore 1982, p.349 and references therein.

2. H. Satz, Proceedings of the International Conference on Nucleus-Nucleus Collisions, 1982, Michigan State University, East Lansing, Michigan, USA, and University of Bielefeld preprint BI-TP 82/29 (1982).

3. E. Stenlund, I. Otterlund; CERN-EP 182-42 (1982) and references therein.

4. C. de Marzo et al., Max-Planck-Institut für Physik und Astrophysik preprint MPI-PAE/Exp. E1 102 (1982).

5. J.E. Elias et al., Phys. Rev. D22 (1980) 12.

6. JACEE Collaboration, in Proceedings of Workshop on Very High Energy Cosmic Ray Interactions, Univ. Penn. April 1982.

7. M. Gyulassy, Proceedings of the International Conference on Nucleus-Nucleus Collisions, 1982, Michigan State University, East Lansing, Michigan, USA and Lawrence Berkeley Laboratory Report LBL-15175 (1982).

8. J. Babecki et al., Phys. Lett. 52B (1974) 247.
J. Babecki private communicatio

ANALYSIS OF THE HIGH MULTIPLICITY EVENTS IN ULTRA-RELATIVISTIC HEAVY ION COLLISIONS

H. Sumiyoshi
Institute for Nuclear Study
University of Tokyo, Tokyo 188

ABSTRACT

From the view point that a high energy nucleus-nucleus interaction is composed of the multiple nucleon-nucleon collisions, we analyze the multiplicities of the ultra-relativistic heavy ion collisions. Most of the experimental data are well settled within our framework. It is concluded that the multiplicity is insensitive to the quark-gluon plasma (QGP) formation or QGP has not yet been created within the observed events.

1. Introduction

High energy heavy ion collisions are now widely explored of their possibilities to produce the QGP state[1]. As for the problem what could be a clear signal of the formation of the QGP state, it is often considered that abnormally high multiplicity event itself is one of the evidence to assure the formation of the QGP. Our purpose of this paper is to give the standard average multiplicity of the central nucleus-nucleus (A_b-A_t) collisions.

Here, we employ, as one of a reliable model, the multi-chain model(MCM)[2)3)] which can describe well the high energy hadron-nucleus collisions and has already been successfully applied to heavy ion collisions[4]. Especially, the rapidity density dN/dy in the A_b-A_t collision is firstly given over all rapidity range[4].

Based on our calculational results, we can judge whether the multiplicity of an event is abnormally high or not.

2. Total Collision Number in A_b-A_t Interaction

If we take a cylinder approximation of a nucleus, A_b-A_t collisions are considered as follows; $\bar{W}_b$ ($\bar{W}_t$) nucleons in the beam (target) nucleus are wounded and each of them makes multiple interactions with $\bar{\nu}_t$ ($\bar{\nu}_b$) nucleons in the target (beam) nucleus. Those numbers are obtained, by using the probabilistic version of the Glauber formula[5)~7)], as follows;

$$\bar{\nu}_t = \frac{A_t \sigma_{inel}^{NN} \int d^2b_I \int d^2b t_b(b-b_I)\, t_t(b_I)}{\int d^2b_I \{1-\int d^2b t_b(b-b_I)\,[1-\sigma_{inel}^{NN} t_t(b_I)]^{A_t}\}} \tag{1}$$

and

$$\bar{W}_b = \frac{A_b \int d^2b_I \{1-\int d^2b t_b(b-b_I)\,[1-\sigma_{inel}^{NN} t_t(b_I)]^{A_t}\}}{\int d^2b_I \{1-[1-\sigma_{inel}^{NN} \int d^2b t_b(b-b_I)\, t_t(b_I)]^{A_b A_t}\}} \tag{2}$$

where the integration of the impact parameter b_I is restricted within $0 \leq b_I \leq 1.5$ fm to select the central collisions. The average total collision number $\bar{C}$ equals to $\bar{W}_b \cdot \bar{\nu}_t$ $(= \bar{W}_t \cdot \bar{\nu}_b)$. The numerical results of those quantities are enumerated in Table I for various A_b-A_t collisions.

3. Subenergy of a Collision

In each inelastic interaction, the energy momenta $x_+(E+P)$ and $x_- m_N$ are spent for the production of particles. Here the four momenta of the nucleon in the beam (target) nucleus are $(E,\vec{0},P)$ $((m_N,\vec{0},0))$ and $x_\pm$ is the light-like momentum fraction. For simplicity, we take the following equipartition[2] distribution of $x_\pm$;

$$F_\nu(x_\pm) = \begin{cases} \dfrac{\Gamma(\nu Q)}{\Gamma(Q)\Gamma((\nu-1)Q)} x_\pm^{Q-1}(1-x_\pm)^{(\nu-1)Q-1} & \text{for } \nu \geq 2 \\ \delta(1-x_\pm) & \text{for } \nu=1 \end{cases} \tag{3}$$

The free parameter Q is taken to be 1.0.[2] The mean multiplicity of charged particles from each collision, $\langle n_c(s_c)\rangle$, is dominated by the subenergy s_c which is equal to x_+x_-s. Here s is defiend by the initial four momenta of the colliding nucleons. The above approximation of equipartition makes all the collisions being equivalent on the average and then it makes the following discussions drastically simple.

4. Mean Multiplicity in A_b-A_t Interaction

To obtain the average charged multiplicity of A_b-A_t collision, $\langle N\rangle_{A_bA_t}$, we have to get the expression for $\langle n_c(s)\rangle$. As a first step, it may be natural to take $\langle n(s)\rangle_{pp}$ for $\langle n_c(s)\rangle$. The p-p data are well fitted by the formula[8];

$$\langle n(s)\rangle_{pp} = 0.88 + 0.44\ln s + 0.118\ln^2 s \ . \tag{4}$$

In our case, however, about half of the wounded nucleons are neutron in stead of proton, which leads to

$$\langle n_c(s)\rangle = \langle n(s)\rangle_{pp} - 1 \ . \tag{5}$$

There is another important point that we have to notice. Due to baryon number conservation, it is only from $(\bar{W}_b+\bar{W}_t)$ collisions out of $\bar{C}$ that the baryons, which carry the initial baryon numbers of the wounded nucleons, can be produced. As for the $\langle n_c(s)\rangle$, therefore, we take Eq.(5) only for $(\bar{W}_b+\bar{W}_t)$ collisions and $\langle n(s)\rangle_{pp}$ for others. Thus we get

$$\langle N\rangle_{A_bA_t} = \bar{C}\int dx_+\int dx_- \, F_{\bar{\nu}_t}(x_+)F_{\bar{\nu}_b}(x_-)\langle n_c(x_+x_-s)\rangle + \{\bar{C}-(\bar{W}_b+\bar{W}_t)\} \tag{6}$$

5. Numerical Results

The numerical results of Eq.(6) are shown in Fig.1. The dispersions obtained by O. Miyamura[9] using MCM are also shown for some events. The events whose multiplicities are far below the theoretical values may be simply interpreted as the A_b-A_t collisions at larger impact parameters. We can safely say that most of the existing data[10)~17)] of the ultra-relativistic heavy ion collisions, except for the event No.5, can be settled within the MCM.

6. Conclusions

The observed high multiplicity events of the A_b-A_t collisions are not abnormal in the sense that they are well understood by MCM. Therefore, we can conclude as follows: (i) If the QGP state is formed in the process of the observed ultra-relativistic heavy ion collisions, the multiplicity is insensitive whether QGP is formed or not. Or (ii) if the multiplicity could certainly be the clear signal of the QGP formation, the QGP state has not yet been realized in the observed events.

7. Acknowledgement

The author thanks to Dr. O. Miyamura for useful discussions on various points through out this paper. He also thanks to Prof. T. Saito and Prof. T. Ogata for their useful comments on the data.

References

1) For a recent review, see Phys.Rep.88 No.5 (1982) edited by M.Jacob and J.Tran Thanh Van.
2) K.Kinoshita,A.Minaka and H.Sumiyoshi, Prog.Theor.Phys.61(1979),165.
3) K.Kinoshita,A.Minaka and H.Sumiyoshi, Prog.Theor.Phys.63(1980),928.
4) K.Kinoshita,A.Minaka and H.Sumiyoshi, Z.Phys.C8 (1981),205.
5) R.J.Glauber, Lectures in Theoretical Phys. ed. by W.E.Brittin (1959), Vol.1, p.315.
6) A.Capella and A.Krzwicki, Phys.Lett.67B (1977),84; Phys.Rev.D18 (1978),3357.
7) A.Bialas, M.Bleszinski and W.Czyz, Nucl.Phys.B111 (1976),461.
8) W.Thome et al., Nucl.Phys.B129 (1977),365.
9) Private communication with O.Miyamura.
10) K.Rybicki, Nuovo Cim.28 (1963),1437.
11) A.Somogyi et al., Intercosmos collab., Bucharest preprint 1977.
12) S.Tokunaga, J.Phys.Soc.Japan 12 (1957),454.
13) A.A.Loctionov and J.S.Takibaev, Int. Conf. on Cosmic Ray and Earth Storms, p.412, Kyoto (1961).
14) D.Abraham et al., Phys.Rev.159 (1967).1110.
15) ICEF data, Chicago (1962).
16) S.Tasaka et al., Phys.Rev.D25 (1982),1765.
17) JACEE Collab., AIP Conf. Proc.,No.85 Particles and Fields Subseries, No.26, p.552 ed. by V.Berger,D.Cline and F.Halzen AIP, New York 1982.

Table I

No.	A_b+A_t	E(TeV/N)	σ^{NN}_{inel}(mb)	$\bar{\nu}_b$	$\bar{\nu}_t$	$\bar{W}_b$	$\bar{W}_t$	$\bar{C}$	Ref.
1	N+Ag	0.07	31.5	1.76	4.91	13.7	38.3	67.4	10
2	Mg+Ag	0.07	31.5	2.13	4.77	23.4	52.6	111.7	10
3	B+Ag	0.3	32.5	1.65	5.10	10.8	33.5	55.3	10
4	Ca+Pb	0.3	32.5	2.53	6.36	39.6	99.6	251.4	10
5	Si+Ag	0.3	32.5	2.30	4.86	27.3	57.8	132.8	11
6	Li+Ag	0.4	33.0	1.39	5.20	5.9	22.2	30.8	12
7	Si+Ag	0.5	33.0	2.32	4.93	27.3	58.1	134.8	13
8	B+Ag	0.5	33.0	1.66	5.18	10.8	33.8	56.1	10
9	Al+Ag	0.5	33.0	2.29	4.95	26.4	57.0	130.4	10
10	C+Ag	1.2	35.0	1.76	5.46	11.8	36.9	64.7	15
11a	B+Ag	1.5	35.0	1.71	5.48	10.9	34.9	59.5	15
11b	Be+Ag			1.60	5.52	8.9	30.7	49.1	
11c	Li+Ag			1.42	5.58	5.9	23.4	33.2	
12	B+Ag	1.7	35.0	1.71	5.48	10.9	34.9	59.5	15
13	C+Ag	3.0	36.0	1.78	5.61	11.9	37.4	66.6	14
14	Si+Ag	3.6	36.5	2.47	5.43	27.4	60.3	149.0	17
15	He+Ag	4.3	37.0	1.62	6.22	4.0	15.3	24.8	14
16	He+C	7	38.0	1.73	2.24	3.3	4.3	7.4	16
17	Ne+C	7.1	38.0	2.01	2.58	9.4	12.0	24.1	17
18	B+Ag	14	40.0	1.52	6.24	10.9	44.7	68.0	14
19	He+C	27	43.0	1.84	2.44	3.4	4.5	8.3	17
20	Ca+C	100	48.0	2.22	4.47	11.3	22.7	50.3	17

The numerical results of $\bar{\nu}_b$, $\bar{\nu}_t$, $\bar{W}_b$, $\bar{W}_t$ and $\bar{C}$ for various observed A_b-A_t collisions, each of which is assigned an event number.

* $C_5H_8O_2$ target is treated as C in our calculation

Fig.1

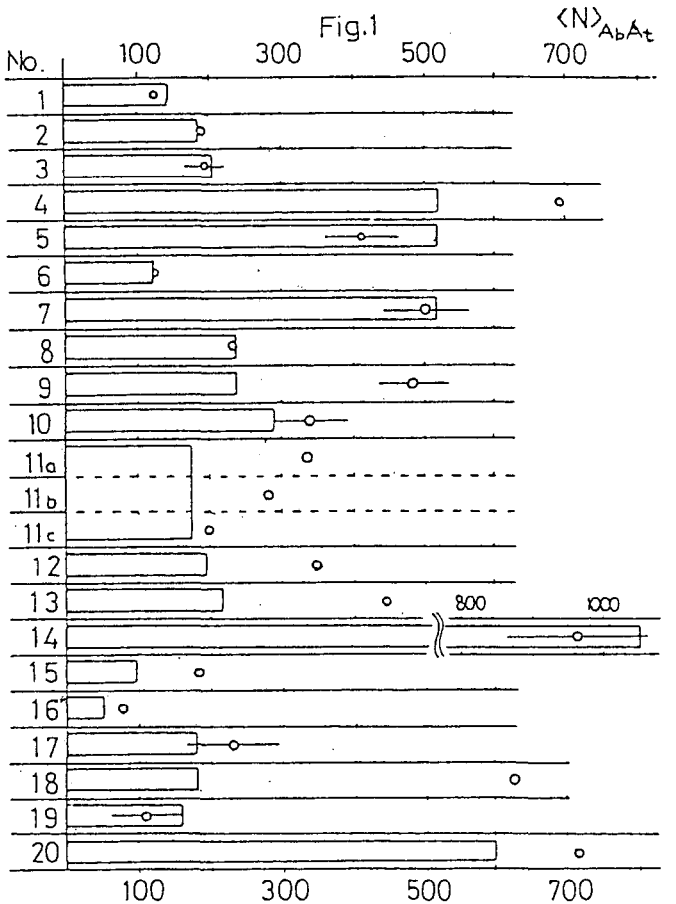

The numerical results of $\langle N\rangle_{A_bA_t}$

For some events the dispersions are shown[9] by the solid lines. If the data shown by the histgram do not exceed the theoretical values, those are not abnormally high multiplicity events.

* Averaged over 10 events.[16]

LEPTON SCATTERING FROM NUCLEAR TARGETS

A. Bodek

Department of Physics and Astronomy
University of Rochester
Rochester, N.Y. 14627 USA

ABSTRACT

Experimental results on deep inelastic lepton scattering from nuclear targets are discussed with emphasis on electron scattering experiments. Also discussed are experiments that have recently been completed and experiments that are about to begin data taking in the near future. A short summary of current theoretical ideas on quark distributions in nuclei is also presented. An analysis of electron scattering and neutrino scattering data from hydrogen and deuterium indicates that nuclear effects in the deuteron are small.

1. Introduction

Deep inelastic lepton scattering experiments using nuclear targets have initially concentrated on the low x and low Q^2 region[1),2)] where the application of the quark-parton model is not valid, and where effects such as nuclear shadowing[3)] were expected to be important. These early experiments, performed initially with electrons, and later also with muons, have indicated that the atomic weight dependence of the structure functions of nuclei was about $A^{1.0}$ at low x ($x \approx 0.1$) and at Q^2 values of about 1.0 $(GeV/c)^2$. Initially, these results were somewhat surprising, because nuclear showing has been observed in photoproduction ($Q^2=0$) experiments[4)] and a continuous transition between photoproduction and electroproduction was expected. These results lead to the early demise of the naive vectro-meson dominance model (VMD) in which the assumption of dominant coupling of the virtual photon to low mass vector mesons implied large shadowing in electroproduction experiments.

Since nuclear shadowing was not observed at low x and $Q^2 \cong 1$ $(GeV/c)^2$, further investigations of the A dependence at larger values of x and Q^2 were not undertaken. The theoretical expectations were that if there were no shadowing effects at low x and low Q^2, then the A dependence at large x and large Q^2 would certainly be linear with A. Later, high Q^2 muon and neutrino scattering experiments were designed to use nuclear targets because such targets were easier to construct than liquid hydrogen and liquid deuterium targets. It was implicitly assumed that aside from Fermi motion corrections, such experiments

determine the structure functions of free nucleons.

The first results from the European Muon Collaboration[5),6),7)] (EMC), which indicated that the ratio of steel and deuterium structure functions was different from 1.0 at large values of Q^2 came as a complete surprise. The trend of the ratio as a function of x was in a direction which is opposite to that expected from Fermi motion effects[8)].

The confirmation of the EMC results did not take long. It was realized that the target walls used in SLAC experiments[9)] E49B and E87 were constructed from aluminum and steel respectively. These experiments, which were carried out in 1970-1972 were designed to measure the structure functions of the proton and the neutron using liquid hydrogen and liquid deuterium targets. The target wall contributions were measured using empty target replicas. The story of the recovery of the old SLAC data is more appropriately suited for publication in an Archeological journal[10)]. It suffices to say that the data was recovered, analyzed and recently published[11),12)].

2. The Experimental Data

The electron scattering data (Rochester-SLAC-MIT[11),12)]) is shown in figures 1a and 1b. The ratio of aluminum to deuterium cross sections shown in figure 1a, spans a range of Q^2. The mean Q^2 of the data is 1.9, 2.2, 2.4, 2.7, 2.4, 3.1, 3.8, 4.2, 5.2, 5.2 7.0, 6.8, 7.5, 8.7, 8.3, 11.8, 11.4, 13.8, and 20.1 $(GeV/c)^2$ for the x bins starting at 0.075 and ending at 0.863, respectively. The data for the ratio of steel to deuterium cross sections, shown in figure 1b, also span a range of Q^2. The mean Q^2 for the steel data is 6.0, 6.4, 7.1, 7.2, 7.6, 6.0, 7.8, 9.7, 11.4, 12.8, 17.0, and 19.3 $(GeV/c)^2$ for the x bins starting at 0.25 and ending at 0.90, respectively.

Also shown in figure 1b is the F_2^{Fe}/F_2^{D} ratio as measured by the EMC collaboration at larger values of Q^2. The EMC data span a Q^2 range from 9 to 27 $(GeV/c)^2$ for x = 0.05, from 11.5 to 90 $(GeV/c)^2$ for x = 0.25 and from 36 to 170 $(GeV/c)^2$ for x = 0.65. In the region of overlap the Rochester-SLAC-MIT data and the EMC data indicate the same effect. The Rochester-SLAC-MIT data extend to higher values of x where the effects of Fermi motion appear to become important. The data have <u>not</u> been corrected for Fermi motion. The curves, calculated by Bodek and Ritchie[8)] indicate what the data should look like if Fermi motion was the only effect present. The trend of the data for $x<0.6$ is opposite to that expected from Fermi motion effects. Also shown in figure 1b is the ratio of the structure functions for copper and deuterium from a low Q^2 ($Q^2 \simeq 1.0 (GeV/c)^2$) experiment[2)] at SLAC, and σ_{Fe}/σ_D as measured in photoproduction[4)] experiments. The experiments, taken together, suggest that at small x and small Q^2 the ratio is considerably reduced. It is possible that the combined effect of the nuclear enhancement at low x and shadowing effects at low Q^2 is the

reason for the rapid disappearance of nuclear shadowing for $Q^2>0$. An important question that must be settled in future high energy and high Q^2 muon scattering experiments is to confirm and determine, within one experiment, the nature of the low x Q^2 dependence.

The Rochester-SLAC-MIT data for the ratio of aluminum and deuterium structure function is shown in figure 1a. Also shown are results from a lower Q^2 experiment[2] at SLAC ($Q^2 \simeq 1.0 (GeV/c)^2$) and photoproduction[4] data. For $x>0.2$, the aluminum data also show a trend which is opposite to that expected from Fermi motion effects. The trend is similar to that observed in the data for steel.

It appears that in the region $0.2<x<0.6$, the Rochester-SLAC-MIT data and the EMC data are consistent. This suggests that the distortion of the valence quarks in the nucleus is Q^2 independent. Fits performed to the electron data over this x region of the form A + Bx yields $A = 1.15 \pm 0.04 \pm 0.011$ and $A = 1.11 \pm 0.02 \pm 0.023$ for σ_{Fe}/σ_D and σ_{Al}/σ_D, respectively. The corresponding values of B are $B = -0.45 \pm 0.08$ an $B = -0.30 \pm 0.06$ for σ_{Fe}/σ_D and σ_{Al}/σ_D, respectively. The slope for aluminum is 1½ standard deviation lower than the slope for steel. The EMC results, yield $A = 1.18 \pm 0.01$ and $B = 0.52 \pm 0.04 \pm 0.21$ for F_2^{Fe}/F_2^D at large Q^2.

3. Normalization and Systematic Errors

In the electron scattering experiments, the data taking from the nuclear targets is interspersed with data for deuterium. Typically, targets are changed every 10 minutes. Computer control of the movable target assembly allows target changes to occur in less than one minute. Therefore, most systematic errors in the cross sections, such as flux monitors calibration, incident and scattered energy calibration, spectrometer solid angle, and most uncertainties in the radiative corrections cancel in the ratio. The target cells are constructed to have the same length in units of radiation length[13]. This makes the radiative corrections for all target essentially identical (i.e. the differences are less than a few tenths percent). Errors which do not cancel are primarily due to the knowledge of the relative target densities and lengths. The normalization errors in the electron data is ±1.1% and ±2.3% for σ_{Fe}/σ_D and σ_{Al}/σ_D, respectively. Other point to point systematic errors have been added to the errors of the points shown in figure 1.

The muon steel and deuterium data are obtained in different data taking periods using targets of different radiation lengths. However, since the same spectrometer is used, some cancellation of systematic errors is expected.

4. Radiative Corrections and Two Photon Effects

The radiative corrections include the effect of photon emission for elastic, quasielastic and inelastic scattering from the nuclear targets. Such photons can be emitted either in the actual scattering process (internal bremsstrahlung) or due to straggling in material before or after the scattering (external bremstrahlung). The radiative corrections for muon and electron experiments are somewhat different and the fact that for $x>0.2$, both muon and electron experiments observe the same effect suggests that the effect is not due to radiative processes. As mentioned earlier, the systematic error in the external bremsstrahlung radiative corrections mostly cancels for the electron data, because targets of the same radiation lengths are used. The radiative corrections for the electron experiments[11),12)] have been calculated as described in Stein et al.[2)] using the procedure of Mo and Tsai[14)]. The corrections, which are typically less than 30% for each target are essentially the same (within a few tenths percent) for targets having the same length in radiation lengths. The internal bremsstrahlung radiative corrections are dominated by photon emission in inelastic scattering processes which are assumed to be the same for all targets. The contributions of the elastic nuclear radiative tail is negligible and the quasielastic tail is small except at the lowest values of x. They are included in the corrections.

The errors in the σ_{Fe}/σ_D ratio from radiative corrections are larger in muon experiments since targets of different lengths are used and energy loss corrections must be applied. The validity of the Mo-Tsai procedure for internal bremsstrahlung in scattering experiments from hydrogen has been checked by the EMC collaboration by detecting photons emitted at wide angles. The rate of photons agreed[15)] with the Mo-Tsai calculation.

One may speculate as to whether the internal bremsstrahlung calculated using the Mo-Tsai procedure is good approximation for heavy nuclear targets. In addition, one may speculate as to whether two photon and $Z\alpha$ corrections affect the conclusions that are obtained using the one photon exchange approximation. At present, there is no experimental evidence to suggest that such affects are important.

The above effects can lead to a difference between electron and positron scattering from nuclear targets. As is known from work comparing elastic e^+p and e^-p scattering the effects of hadronic radiation and two photon exchange make the radiative corrections for the two processes slightly different. A comparison of deep inelastic e^+p and e^-p scattering has been used to place upper limits on such terms. The ratio of the cross sections, as measured by the UCSB group[17)], for e^+p/e^-p is 1.0027 ± 0.0035. An earlier measurement by a SLAC group[18)] yields $e^+p/e^-p = 1.001 \pm 0.008$.

Similar measurements from nuclear targets are also consistent with unity. A comparison of the deep inelastic scattering of μ^+ and μ^-

mesons on carbon at BNL energies[19] yields $\mu^+c/\mu^-c = 1.002 \pm 0.017$. The BCDMS collaboration at CERN have used the comparison of μ^+ and μ^- cross sections on carbon[20] to measure the electroweak asymmetry predicted by the Weinberg Salam model, and obtained $\sin^2\theta_W = 0.19 \pm 0.07 \pm 0.04$. The measured asymmetry of about 1% at high Q^2 was consistent with that expected from electroweak interference and higher order electromagnetic effects calculated[21] assuming a quark parton model and no nuclear affects.

Nevertheless, the effects for high Z elements such as steel as well as for very high Z targets such as lead and gold (which are to be used in more recent experiments[23],[24], must be investigated. Theoretical work on two photon processes in the scattering from nuclear targets has been primarily done for low energy (≃50 MeV) scattering[22]. Further theoretical investigation at higher energies and high Q^2 is progress[39] in order to understand whether $Z\alpha$ terms are important. A comparison of neutrino scattering from heavy targets with that from deuterium would be very interesting as a check on such terms. Such comparisons are presently being pursued.[25]

Another way to check the $Z\alpha$ and two photon terms is by doing Rosenbluth plots. The extraction of $R = \sigma_L/\sigma_T$ relies on a comparison of data taken at different scattering angles. If two photon and $Z\alpha$ terms were important, non linearities would be present in such plots, because then the one photon exchange approximation, and the description of inelastic scattering in terms of two structure functions would not be valid. Such a check is being done by SLAC experiment[23] E139.

5. Experiments in Progress

SLAC experiment E139 has recently completed data taking. Data were taken with deuterium ($^2H_1$), helium ($^4He_2$), berillium ($^9Be_4$), aluminum ($^{27}Al_{13}$), iron ($^{56}Fe_{26}$), silver ($^{107}Ag_{47}$) and gold ($^{197}Au_{79}$) targets. The range of x that has been covered is $0.1 \lesssim x \lesssim 0.8$. Data were taken at $Q^2 = 2$, 5 and 10 $(GeV/c)^2$ and at $Q^2 = 15$ $(GeV/c)^2$ and $x = 0.6$. The experiment has recently been completed (June 30, '83) and preliminary results are expected shortly.

The EMC collaboration[7],[24] has undertaken a program to study the low x and low Q^2 region for $Q^2>0.15$ and $x>3\times10^{-4}$ in order to study the shadowing region. They plan to run with hydrogen ($^1H_1$), deuterium ($^2H_1$), carbon ($^{12}C_6$), iron ($^{56}Fe_{26}$) and lead ($^{207}Pb_{82}$). They expect to get between 250k events and 300k events for each target for $0.15<Q^2<2$ $(GeV/c)^2$ and about 40k events for each target for $Q^2>2$ $(GeV/c)^2$. The data taking period starts in July 1983.

The BCDMS collaboration[20] is planning to study muon scattering[26] from deuterium ($^2H_1$), nitrogen ($^{14}N_7$) and iron ($^{56}Fe_{26}$). This experiment, which will run at the end of 1983 is planning to study the range $0.07 \lesssim x \lesssim 0.65$ for very high Q^2. This experiment is complementary to

SLAC E139 since it will extend the A dependence study to very high Q^2.

6. Neutrino Experiments

Neutrinos offer a unique tool in establishing the origin of the distortion of the structure functions of bound nuclei. For example, the radiative corrections in neutrino experiments are different from those in electron and muon experiments. Neutrino experiments yield information on the valence quark and sea antiquarks separately. This information is important if the low x enhancement, which is observed at high Q^2, is due to an increase in the quark antiquark sea in a heavy nucleus.

Unfortunately, the systematic errors are very large, because data on different target nuclei are obtained in different experiments. Presently, old data from the BEBC bubble chamber at CERN, and data from the 15' bubble chamber at Fermilab are being studied in England and at Columbia University, respectively. The aim is to compare deuterium ($^2H_1$) to neon ($^{20}Ne_{10}$) x distributions. Because the data are from different experiments the systematic effects due to differences in the beams and analysis procedures make their comparisons difficult. A more promising effort is being undertaken at Saclay[25], where CDHS wide band beam data on iron is being compared to BEBC deuterium data. Both experiments have run simultaneously in the same beam, so beam related systematic effects should be small. Systematics due to differences in analysis between the two experiments remain, because it is difficult to measure x in a deuterium filled bubble chamber. Results are expected around the end of 1983. The CDHS group[25] is also investigating the antiquark distributions in hydrogen[35] in order to compare to the antiquark distributions in iron. Results are expected soon[33].

7. Theoretical Explanations

The understanding of the mechanisms responsible for the distortion of the structure functions of nucleons bound in a large nucleus has been the subject of several recent theoretical papers. This include ideas such as multiquark bags[27], pions and quasipions in nuclei[28], delta resonances in nuclei[29], diquark states[30], the percolation of quarks from nucleon to nucleon in a large nucleus[31] and changes in the effective mass and radius of a nucleon bound in the nucleus[32]. However, the understanding of the effect is still in a very qualitative state. The reader is referred to the original references for detail. More references and summary of the theoretical work can be found in references 6 and 7.

8. What about the deuteron, is all the effect due to iron?

It has been suggested[27] that nuclear distortions in the deuteron are small because of the large separation between the neutron and the

proton. A check on nuclear effects in the deuteron can be done in two ways. One suggestion[28] is to compare neutrino cross sections for deuterium to the sum of neutrino and antineutrino cross sections for bydrogen. Antoher way is to study the quantity

$$R = \frac{F_2^{ed}}{F_2^{ep}\left[1 + \frac{1 + d_v/u_v + sea/u_v}{4 + d_v/u_v + sea/u_v}\right]} \equiv \frac{F_2^{ed}}{\left[F_2^{ep} + F_2^{en}\right]_{Free}}$$

as a function of x, where $u_v(x)$ and $d_v(x)$ are the valence quark distributions in the nucleon extracted from neutrino and antineutrino experiments[34),35)] on hydrogen. For $x \gtrsim 0.4$, the sea quark contribution can be neglected. I have used the data of Bodek et al.[9)] for F_2^{ed}/F_2^{ep} and the results from three neutrino experiments on hydrogen for the ratio $d_v(x)/u_v(x)$, as summarized by Eisle[35)]. The errors of the d/u data from the neutrino experiments dominate the error in R. The results, shown in figure 2a indicate that the nuclear distortions in the deuteron are small. For $x<0.4$ I have included a small sea correction using $\bar{u}$, $\bar{d}$ and $\bar{s}$ distributions extracted from CDHS data on hydrogen (Pszola[35)]). I have assigned a 100% error to this correction. This error has been added linearly (outer error bars) to the points for $x<0.4$.

The quantity $\frac{\sigma_{\nu n}-\sigma_{\nu p}}{\sigma_{\nu n}+\sigma_{\nu p}}$ can be extracted from neutrino experiments in a deuterium bubble chamber[36)] by the comparing scattering from bound protons and neutrons. The identification of an event as scattering from a proton versus scattering from a neutron is done by investigating the event topology[36)]. For $x>0.4$

$\frac{\sigma_{\nu n}-\sigma_{\nu p}}{\sigma_{\nu n}+\sigma_{\nu p}} \equiv \frac{\sigma_{ep}-\sigma_{en}}{\sigma_{ep}+\sigma_{en}}$. For $x<0.4$ there are small sea corrections which have been handled as described above. If we assume that nuclear effects in the deuteron cancel in the above ratio, we can use these data (Kitigaki[36)]) in conjunction with F_2^{ed}/F_2^{ep} from Bodek et al. to form the ratio $F_2^{ed}/(F_2^{ep}+F_2^{en})_{Free}$. These results are shown in figure 2(b). Also shown are the expected ratio from Fermi motion effects using the procedures of Atwood and West[37)] (solid line) and Frankfurt and Strickman[38)] (dashed line).

Within the errors, there are no indications of nuclear distortions in addition to those expected from Fermi motion effects. Systematic errors come from the fact that not all the experiments are done at the same Q^2 (scaling violations) as well as experiment related systematic errors. In addition, the neutrino data are preliminary i.e. obtained from conference proceedings. However, it appears that better neutrino data could be used as a check on the Fermi motion calculation.

The Atwood and West technique[37] (also used by Bodek and Ritchie[8]) yields a curve which is typically 1.5 to 2.5% lower than the calculation of Frankfurt and Strickman[38].

References

1) W. R. Ditzler et al., Phys. Lett. 57B, 201 (1975); M. S. Goodman et al., Phys. Rev. Lett. 47, 293 (1981) (see Ref. 11 for a complete list of references).

2) S. Stein et al., Phys. Rev. D12, 1884 (1975).

3) G. Grammer and J. D. Sullivan in Electromagnetic Interactions of Hadrons, edited by A. Donnachie and G. Shaw (Plenum, New York) Vol. 2, p. 195 (1978).

4) D. O. Caldwell et al., Phys. Rev. Lett. 42, 553 (1979); Phys. Rev. D7, 1362 (1973); A. M. Eisner in "Proceedings of the 1979 International Symposium on Lepton and Photon Interactions, Fermilab, Aug. 1979, p. 448; T. B. W. Kirk and H. D. I. Abarbanel ed.

5) J. J. Aubert et al., Phys. Lett. 123B, 275 (1983).

6) Klaus Rith, Freiburg preprint THEP 83/4 to be published in Proceedings of the XVIII Rencontre de Moriond, Electroweak Interactions, LaPlagne, France, March 1983.

7) A. Edwards, in proceedings of the Multiparticle Production Conference, Lake Tahoe, June 1983.

8) A. Bodek and J. L. Ritchie, Phys. Rev. D23, 1970 (1981) and 24, 1400 (1981).

9) A. Bodek et al., Phys. Rev. Lett. 30, 1087 (1973); A. Bodek et al., Phys. Lett. 51B, 417 (1983); A. Bodek et al., Phys. Rev. D20, 1471 (1979).

10) CERN Courier, Vol. 23, p. 90, April 1983.

11) A. Bodek et al., Phys. Rev. Lett. 50, 1431 (1983).

12) A. Bodek et al., UR846 to be published in Phys. Rev. Lett.

13) A. Bodek, Nucl. Intrum. Methods 109, 603 (1973).

14) L. W. Mo and Y. S. Tsai, Rev. Mod. Phys. 41, 205 (1969); Y. S. Tsai, SLAC-Pub-0848 (1971), Lectures given at Nato Advanced Inst. on Electron Scattering and Nuclear Structure, Cagliari, Italy 1970.

15) J. J. Aubert et al., Zeit. Phys. C10, 101 (1981).

16) S. Hartwig et al., Nuovo Cimento 12, 30 (1975) and references therein, see also N. Meister and D. R. Yennie, Phys. Rev. 130, 1210 (1973).

17) D. L. Fancher et al., Phys. Rev. Lett 37, 1323 (1975).

18) L. S. Rochester et al., Phys. Rev. Lett. 36, 1284 (1976).

19) H. Jostlein et al., Phys. Lett. 52B, 485 (1974).

20) A. Argento et al., Phys. Lett. 120B, 245 (1983).

21) D. Yu Bardin et al., Yad Phys. 29, 499 (1979), and Nucl. Phys. B197, 1 (1982).

22) J. Bernabeu and J. A. Penarrocha, Phys. Rev. D22, 1082 (1980); J. A. Penarrocha, Ann. Phys. 135, 321 (1981).

23) R. G. Arnold et al., SLAC experiment E139 (ABMRSS) American University, Bonn, Maryland, Rochester, Saclay, SLAC collaboration. Experiment completed June 30, 1983.

24) EMC collaboration, CERN-NA-28 experiment to run in summer of '83 at CERN (Proposal on shadowing O. C. Allkofer et al., CERN SPCS/82-4, SPSC/P176 (1982). Approved 17 Feb. 1983.

25) A. Para, CDHS (private communication).

26) BCDMS collaboration (CERN-NA-4) experiment to run at the end of 1983.

27) R. L. Jaffe, Phys. Rev. Lett. 50, 228 (1983), H. J. Pirner and J. P. Vary UNI-HD-83-2 in proceedings of the Sixth High Energy Heavy Ion Study LBL June 1983 available as LBL-16281); W. Furmanski and A. Krzywicki-LPTHE 83/11 (1983) (also in LBL-16281); C. E. Carlson and T. J. Havens, Phys. Rev. Lett. 51, 261 (1983); O. Nachtman and H. J. Pirner, Heidelberg preprint THEP-83-08; S. Date WU-HEP-83-4 (Waseda U.).

28) C. H. Llewellyn Smith, Oxford preprint 18/83 and 37/83, M. Erickson and A. W. Thomas, CERN TH-3553 (1983); E. L. Berger, F. Coester, R. B. Wiring, ANL-HEP-PR-83-24.

29) J. Szwed, Carcow preprint TPJU-1/83 (Jagellonian University).

30) J. D. Bjorken, private communication.

31) G. Baym, Physica 96A, 131 (1979).

32) F. E. Close, R. G. Roberts and G. G. Ross, RL-83-051 (1983);

M. Staszel, J. Rozynek, C. Wilk, IFT/9/83-Warsaw (1983).

33) F. Dydak, Talk, Lepton-Photon Conference, Cornell, Aug. 1983.

34) G. R. Farrar et al., Phys. Lett. 69B, 112 (1977), P. Allen et al., Phys. Lett. 103B, 71 (1981).

35) F. Eisele in Proceedings of the 21st International Conference on High Energy Physics, J. Phys. (Paris) Colloq. 43, C3-337 (1982); B. Pszola in Proceedings of "V 82", Balalonfured, Hungary, A. Frenkel, L. Jenik editors (1982), Vol. 2 p. 133.

36) J. Hanlon et al., Phys. Rev. Lett. 45, 1817 (1980); T. Kitagaki, Proceedings of "V 81" Hawaii; C. J. Cence, E. Ma, A. Roberts, ed., Vol. 2 p. 97; A. G. Tenner ibid p. 109; D. Allasia et al., Phys. Lett. 107B, 148 (1981).

37) W. B. Atwood and G. B. West, Phys. Rev. D7, 773 (1973).

38) L. L. Frankfurt and M. I. Strickman, Phys. Lett. 76B, 333 (1978).

39) S. Brodsky and M. Soldate, SLAC (private communication).

Figure Captions

Fig. 1. $\sigma_{A\ell}/\sigma_D$ (b) σ_{Fe}/σ_D the data have been corrected for the small neutron excess and have not been corrected for Fermi motion effects. In addition to the Rochester-SLAC-MIT data (Ref. 11,12), also shown are high Q^2 σ_{Fe}/σ_D data from EMC (Ref. 5), low Q^2 σ_{Al}/σ_D and σ_{cu}/σ_D data from SLAC (Ref. 2) and photoproduction σ_{Al}/σ_D and σ_{Fe}/σ_D data. Normalization errors are not shown.

Fig. 2. $F_2^{ed}/(F_2^{ep}+F_2^{en})_{Free}$ obtained by using F_2^{ed}/F_2^{ep} data and extracting a quantity which is equal σ_{en}/σ_{ep} from quark distributions measured in neutrino experiment. The results indicate that nuclear distortions in the deuteron are small.

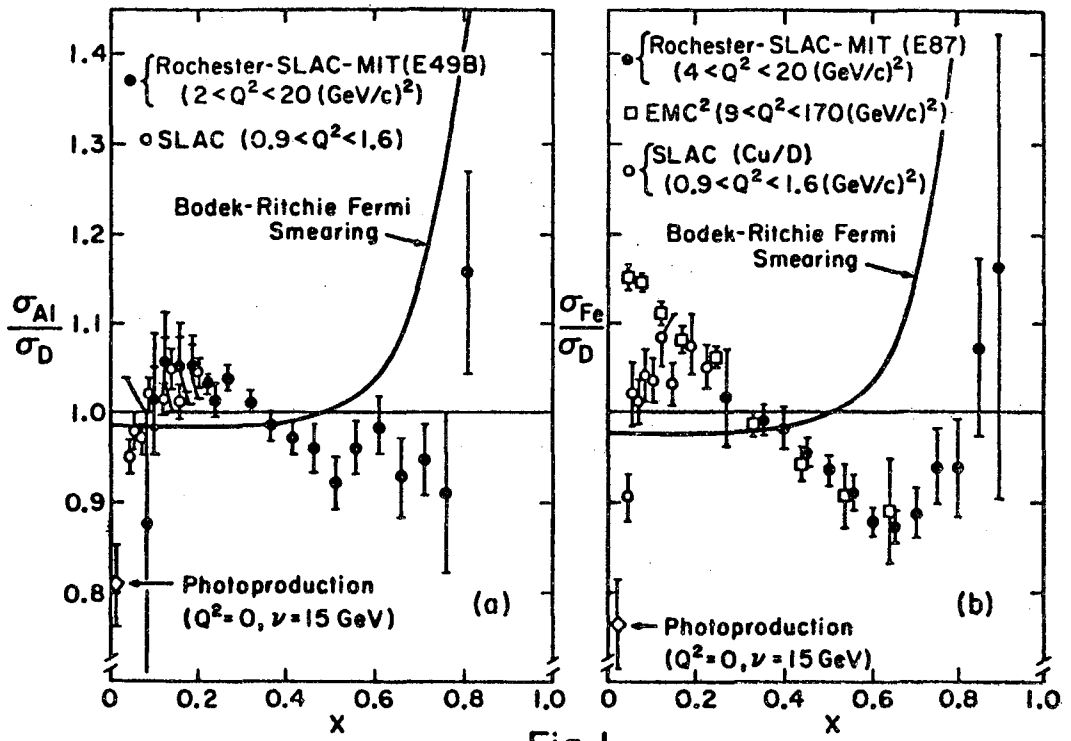
Rochester-SLAC-MIT(E498)
(2<Q²<20 (GeV/c)²)
SLAC (0.9<Q²<1.6)
Bodek-Ritchie Fermi Smearing
Photoproduction
(Q²=0, ν=15 GeV)
(a)
σAl/σD
Rochester-SLAC-MIT (E87)
(4<Q²<20 (GeV/c)²)
EMC² (9<Q²<170 (GeV/c)²)
SLAC (Cu/D)
(0.9<Q²<1.6 (GeV/c)²)
Bodek-Ritchie Fermi Smearing
Photoproduction
(Q²=0, ν=15 GeV)
(b)
σFe/σD
x

Fig.1

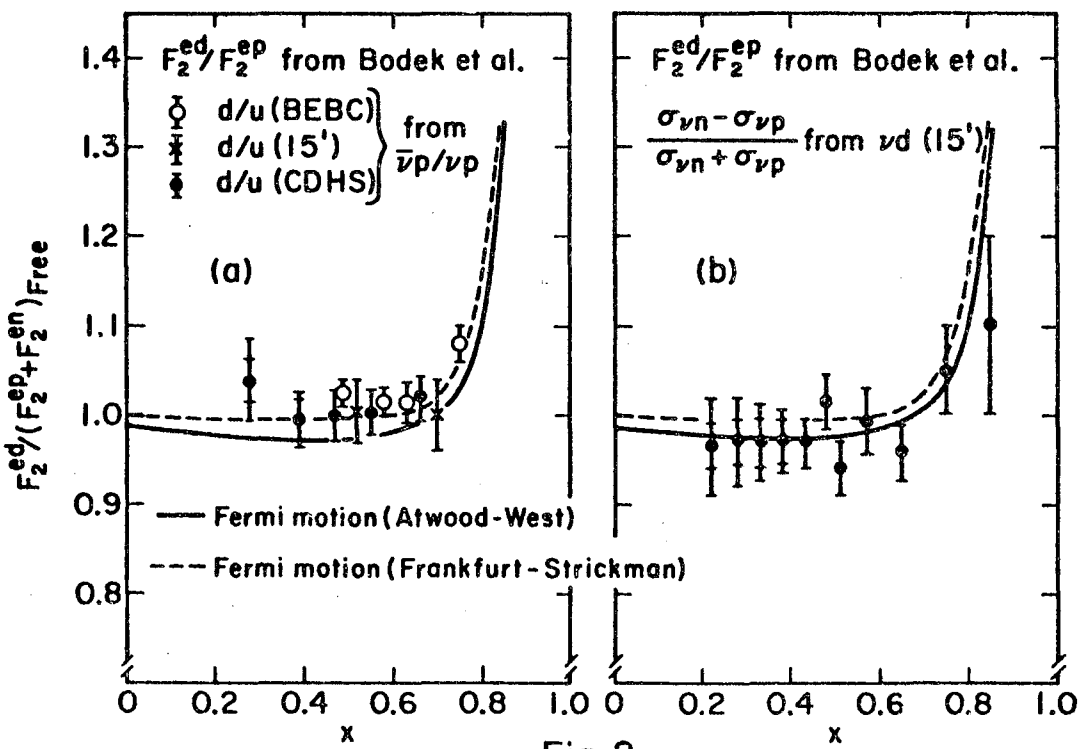
F₂ed/F₂ep from Bodek et al.
d/u (BEBC)
d/u (15')
d/u (CDHS)
from ν̄p/νp
(a)
Fermi motion (Atwood-West)
Fermi motion (Frankfurt-Strickman)
F₂ed/F₂ep from Bodek et al.
(σνn−σνp)/(σνn+σνp) from νd (15')
(b)
F₂ed/(F₂ep+F₂en)Free
x

Fig.2

Deep Inelastic Lepton Scattering and the Quark Structure of Nuclei

James P. Vary†
Arizona Research Laboratories, University of Arizona, Tucson, Arizona
and Physics Department, Iowa State University, Ames, Iowa

and

Hans J. Pirner
Institut für Theoretische Physik, Universität Heidelberg, and
Max Planck Institut für Kernphysik, Heidelberg, FRG

Deep inelastic lepton scattering has proven to be a powerful tool for discovering the substructure of the hadrons. In the same way, we expect that deep inelastic scattering (DIS) from nuclei reveals how that substructure is modified by the nuclear medium. We have presented a model[1] which successfully explained DIS on ^{3}He[2] in terms of 3, 6, and 9-quark clusters. We have recently improved the model by incorporating more realistic nuclear wave functions to determine the effects of Fermi motion and to evaluate the geometrical overlap probabilities of cluster formation.[3] Furthermore, we have included the contributions of sea quarks[4] which are important for understanding the new data with iron targets.[5,6] We have also extended the model to obtain a description of the elastic charge form factor of ^{3}He[7].

Here, we summarize the principal ingredients of the model and present illustrative results for DIS. For a lepton of incident lab energy E, final energy E′ at lab scattering angle θ, we define the lab energy loss $\nu=E-E'$ and the negative of the invariant four-momentum transfer squared, $Q^2=4EE'\sin^2\theta/2$. The scattering occurs from a target nucleus of A nucleons, N neutrons, and Z protons whose mass M is approximated as Am, where m is the nucleon mass. We employ the Bjorken variable $x\equiv Q^2/2m\nu$ which has values $0\leq x\leq A$ and the Nachtmann variable $\xi\equiv 2x[1+(1+Q^2/\nu^2)^{1/2}]^{-1}$ which goes over to x as $Q^2\to\infty$, $\nu\to\infty$ but x fixed. The variable ξ accounts[8] for finite mass corrections to scaling which are important over the range of the ^{3}He data[2] and the low Q^2 Fe data[6], but which are not important for the high Q^2 Fe data.[5]

We write the total invariant structure function for the nucleus as

$$\frac{\nu\, d^2\sigma}{\sigma_M\, d\Omega dE'} = \nu W_2^{tot} = \nu W_2^{in} + \nu W_2^{q-el} , \tag{1}$$

where the Mott cross section $\sigma_M=4\alpha^2(E')^2Q^{-4}\cos^2\theta/2$; α is the fine structure constant; and the inelastic structure function

$$\nu W_2^{in} = \sum_{\substack{\text{quarks}\\ j}} e_j^2 \frac{\xi}{A} \mathcal{P}(\xi) . \tag{2}$$

The function $\mathcal{P}(\xi)$ is the distribution of quarks in the nucleus with momentum fraction ξ/A of the total nuclear light-cone momentum $P^+=E+P_z$. In our quark

cluster model[1] we assume the quarks are found in an i-quark (i-q) cluster (i=3,6,9,...,3A) within the nucleus with probability $\tilde{p}_i$ so that

$$\mathcal{P}(\xi) = \sum_{\substack{\text{clusters}\\ i}} \tilde{p}_i \, \overline{P}_i(\xi) \, , \tag{3}$$

where $\overline{P}_i(\xi)$ is the ξ-distribution of quarks within the cluster. We then write

$$\overline{P}_i(\xi) = \int_0^{\xi^{th}_{i/A}} dy \int_0^{\xi^{th}_{q/i}} du \, \overline{n}_{q/i}(u) \, N_{i/A}(y) \, \delta\left(\frac{u}{i/3} \cdot \frac{y}{A} - \frac{\xi}{A}\right) , \tag{4}$$

where $\overline{n}_{q/i}(u)$ is the distribution of quarks in the i-q cluster with momentum fraction $u(i/3)^{-1}$, $N_{i/A}(y)$ is the distribution of i-q clusters in the nucleus with momentum fraction y/A, and the δ function guarantees momentum conservation. We take cluster masses $m_i = mi/3$ and define the thresholds by

$$\xi^{th}_{i/A} = A \left[\frac{\left[1 + \frac{m_i^2}{M^2} \frac{Q^2}{\nu^2}\right]^{1/2} + 1}{\left[1 + \frac{Q^2}{\nu^2}\right]^{1/2} + 1} \right] \tag{5}$$

$$\xi^{th}_{q/i} = \frac{i}{3} \left[\frac{2}{\left[1 + \frac{4m_i^2}{Q^2}\right]^{1/2} + 1} \right] . \tag{6}$$

Equation (4) may be simplified to read

$$\overline{P}_i(\xi) = A \int_0^{\xi^{th}_{i/A}} dy \, \frac{1}{y} \, n_{q/i}(\xi/y) \, N_{i/A}(y) \, \theta\left(\frac{i\xi}{3y} - \xi^{th}_{q/i}\right), \tag{7}$$

where $n_{q/i}(3u/i) = (i/3)\overline{n}_{q/i}(u)$ and θ represents the usual step function. For 3-q clusters we take $n_{q/3}$ distributions determined by QCD and best fits to data.[9] We terminate the cluster sum in Eq. (3) at 9-q clusters, and we take $n_{q/i}$ for i=6,9 from counting rules and Regge behavior to be:

$$n_{q/6}(z) = 1.762(z)^{-1/2}(1-z)^9 \tag{8}$$

$$n_{q/9}(z) = 2.239(z)^{-1/2}(1-z)^{15} \, . \tag{9}$$

For the Fermi motion of the clusters we take, at present, a simple Gaussian distribution

$$N_{i/A}(y) = \frac{1}{\sqrt{2\pi\sigma^2}} \exp\left[- \frac{(y-i/3)^2}{2\sigma^2}\right] , \tag{10}$$

with σ=0.1152 based upon a simplified analysis of ^{3}He wave functions.[1] Results with more realistic treatment of the Fermi motion in Eq. (7) will be presented elsewhere.[3]

For the ^{3}He data, we may readily use realistic nuclear wave functions to determine the quasi-elastic contribution νW_2^{q-el} in Eq. (1) and to determine the cluster probabilities $\tilde{p}_i$. For these purposes we employ semi-realistic[10] and realistic[11] three-body wave functions for ^{3}He obtained by solutions of the Faddeev equations. For the present analysis of ^{3}He data we will take νW_2^{q-el} to be $\tilde{p}_3$ times the results obtained by the Hannover group.[11] For the probability that a quark is found in an i-q cluster, we compute geometrical overlaps as a function of a critical bag radius R_c[1] using the semi-realistic results of the Los Alamos group.[10] A visual fit to the highest energy ^{3}He data sets is used to determine an optimum R_c value and, hence, the cluster probabilities $\tilde{p}_i$. We show in Figs. 1 and 2 an envelope of results for DIS on ^{3}He corresponding to the choices $R_c \simeq 0.45$ fm ($\tilde{p}_3$=0.93, $\tilde{p}_6$=0.07, $\tilde{p}_9$=0.00) and R_c=0.55 fm ($\tilde{p}_3$=0.83, $\tilde{p}_6$=0.15, $\tilde{p}_9$=0.02) along with the pure quasi-elastic results of the Hannover group[11] for comparison. In order to fit the low ν (high x or ξ) data, we require a substantial contribution from the 6-q cluster. Based upon the results shown here, we estimate a "best fit" to the data is obtained with this improved version of our model using R_c=0.50 fm and the resulting $\tilde{p}_3 \simeq 0.88$, $\tilde{p}_6 \simeq 0.11$, and $\tilde{p}_9 \simeq 0.01$. Analyses with different choices of semi-realistic nuclear wave functions suggest an uncertainty of ±0.05 fm in R_c and ±0.02 on each of the $\tilde{p}_i$ values. In particular, the 9-q cluster probability is determined almost entirely by conservation of probability since the 9-q cluster has only small contributions in this range of data. These results differ only slightly in R_c from the earlier fit[1] with the more substantial changes occuring in the $\tilde{p}_i$ and in νW_2^{q-el}. The nearly unchanged R_c reflects an offsetting influence of short-range correlations between $\tilde{p}_i$ and νW_2^{q-el}.

Let us fix the ingredients determined to fit the ^{3}He data and now address the DIS of leptons from Fe.[4] Here the data[5,6] are presented as a ratio R of cross sections per nucleon of iron to deuterium (D). We assume that R_c is the same in all nuclei and hold it fixed at 0.50 fm but realize that D is less dense than ^{3}He while Fe is more dense. We estimate the effects of these density differences[3] to yield ($\tilde{p}_3$, $\tilde{p}_6$, $\tilde{p}_9$) = (0.95, 0.05, 0) and (0.79, 0.17, 0.04), respectively for D and Fe. Then if we evaluate R for lepton scattering at E=100 GeV, θ=8° and include the strange and charm sea contributions[4]

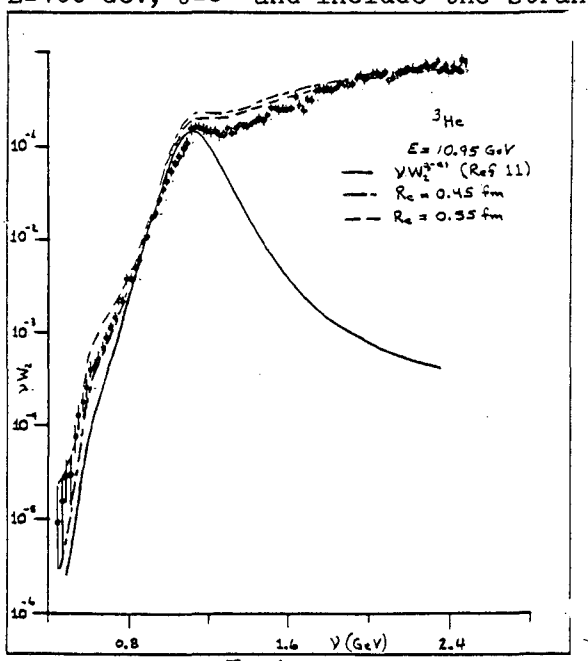

Fig 1

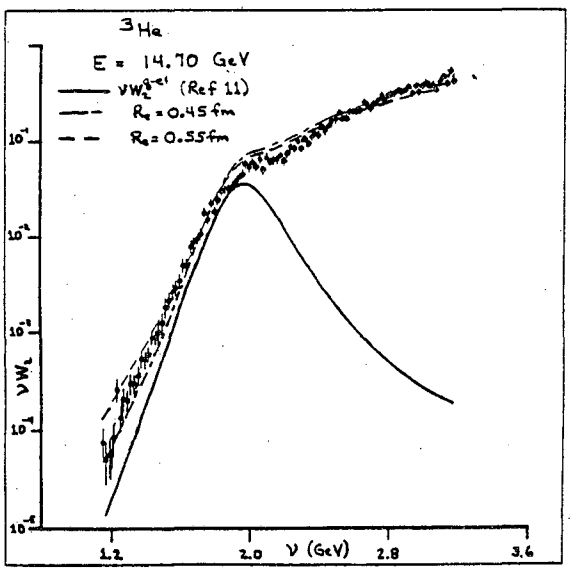

Fig 2

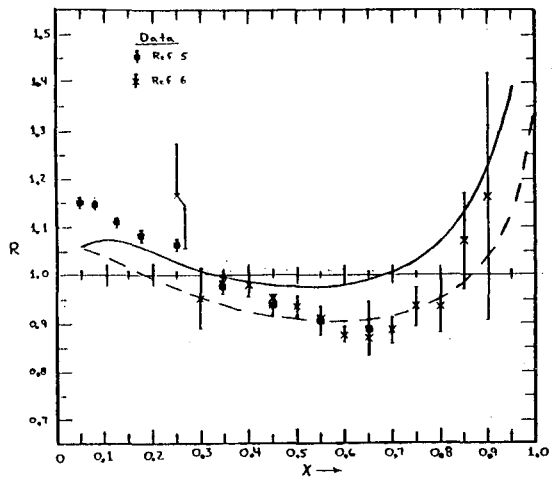

Fig 3

appropriate to $Q^2=20(\mathrm{GeV}/c)^2$ we obtain the solid curve in Fig. 3. The low x region is primarily sensitive to the sea quark contributions. The dip in R below unity is sensitive to the ratio of 6-q cluster contributions in Fe and D. To fit this dip we need to decrease the 6-q cluster probability in D and/or enhance the 6-q cluster probability in Fe. The rise near x=1 is sensitive to the treatment of Fermi motion which is approximated here as the same in Fe and D. Compare the dashed curve for E=20 GeV, the sea at $Q^2=1.8(\mathrm{GeV}/c)^2$ and an arbitrarily increased density effect in ^{56}Fe wherein $(\tilde{p}_3, \tilde{p}_6, \tilde{p}_9)=(0.70, 0.22, 0.08)$.

While the quark cluster model is successful in describing the ^{3}He data, there is a need to improve the description of Fe/D data. Further work on this is in progress.[12]

REFERENCES

†Supported by USDOE contract no. DE-AC02-82ER40068, HENP Division.

[1]H. J. Pirner and J. P. Vary, Phys. Rev. Lett. 46, 1376 (1981); H. J. Pirner and J. P. Vary, Nucl. Phys. A 358, 413C (1981).

[2]D. Day et al., Phys. Rev. Lett. 43, 1143 (1979).

[3]H. J. Pirner and J. P. Vary, to be published.

[4]H. J. Pirner and J. P. Vary, University of Heidelberg preprint UNI-HD-83-02; and to be published.

[5]J. J. Aubert et al., CERN-EP/83-14 (unpublished); Phys. Lett. 105B, 322 (1981).

[6]A. Bodek et al., SLAC-PUB-3041 (unpublished).

[7]J. P. Vary, S. A. Coon, and H. J. Pirner, Proceedings of the Tenth International Conference on Few Body Problems in Physics, Karlsruhe, 21-27 August 1983; Proceedings of the International Conference on Nuclear Physics, Florence, 29 August-3 September 1983; and to be published.

[8]O. Nachtmann, Nucl. Phys. B 63, 237 (1973).

[9]A. J. Buras and K. J. F. Gaemers, Nucl. Phys. B 132, 249 (1978).

[10]J. L. Friar, B. F. Gibson, E. L. Tomusiak, and G. L. Payne, Phys. Rev. C 24, 665 (1981); and private communication.

[11]H. Meier-Hajduk, Ch. Hajduk, P. U. Sauer, and W. Theis, University of Hannover preprint; and private communication.

[12]O. Nachtmann and H. J. Pirner, University of Heidelberg preprint THEP-83-08.

ANOMALOUS BEHAVIOUR OF NUCLEAR STRUCTURE FUNCTIONS REVISITED

W. FURMANSKI and A. KRZYWICKI

Laboratoires de Physique Théorique, Univ. Paris-Sud, Orsay

If a nucleus is regarded as a collection of quasi-free nucleons, the nuclear structure functions are simply proportional to the corresponding structure functions of the nucleon:

$$F(x,A) = A\,F(x,1), \quad 0 < x < 1 \tag{1}$$

Here A is the nuclear mass number and x is the parton momentum scaled by the momentum of one nucleon. Back in 1976 it has been argued by one of us[1] that the conventional picture of the nucleus might not hold when the nucleus is probed during a very short time. A simple parton model has been formulated, illustrating the idea of an "anomalous" behaviour of nuclear structure functions, where eq. (1) is violated. At that time this idea has met with scepticism. Recent experiments[2] have demonstrated, however, that eq. (1) is indeed badly violated. Hence we decided to develop further the ideas of ref. 1.

The picture of a nucleus as a collection of (almost) free nucleons is an extreme view. In a snapshot of a nucleus one would see some hadronic mess: nucleons, excited or not, all kinds of mesons, etc. For short time intervals it is more appropriate to consider quarks and gluons as elementary quanta. This is what we shall do. However, we shall also adopt an extreme viewpoint: we shall neglect correlations between partons. This is an oversimplified picture, but it has the merit of simplicity. We write the probability of a parton configuration in the form[3]

$$dP_{KLM}(X,Y,Z) = C\delta(1-\sum^{K} X_j - \sum^{L} Y_j - \sum^{M} Z_j)\, d\mu_{KLM}(X,Y,Z) \tag{2a}$$

$$d\mu_{KLM}(X,Y,Z) = \frac{\Lambda_S^K \Lambda_G^L}{K!L!} \prod^{K} S(X_j)dX_j/X_j \prod^{L} G(Y_j)dY_j/Y_j \prod^{M} V(Z_j)dZ_j \tag{2b}$$

and $S(0) = G(0) = 1$, $V(Z) \sim Z^{\beta-1}$ for $Z \to 0$ $(\beta > 0)$. Here K is the number of sea quarks and anti-quarks, L is the number of gluons and $M = 3A$ is the number of valence quarks. The variables X_j, Y_j, Z_j are parton momenta scaled by P, the total momentum of the hadronic system. We assume that the average num-

-ber of sea constituents is $\sim$ A like the number of valence quarks. Hence, we set $\Lambda_{S,G} = A\lambda_{S,G}$. Apart from that, the nucleon and the nucleus are treated on the same footing: the functions S,G,V are assumed independent of A. They are determined from nucleon data. Once this is done the extrapolation to A > 1 is unambiguous.

Our physical picture of the nucleus is that of a bag of instantaneously free partons. The partons do not know the size of the bag, their one-particle wave functions do not depend on A. The average number of partons is proportional to A and therefore a single parton seldom gets momentum > P/A. Such anomalous configurations are not strictly excluded, however, and one can argue[1] that their existence represents short-time collective effects in nuclear matter.

Define

$$\Omega_M(T) = \sum_{K\,L} \int \delta(T - \sum^{K} X_j - \sum^{L} Y_j - \sum^{M} Z_j)\, d\mu_{KLM}(X,Y,Z) \tag{3}$$

The structure functions are

$$xF_S(x,A) = \Lambda_S S(x/A)\ \Omega_M(1-x/A)/\Omega_M(1) \tag{4a}$$

$$xF_G(x,A) = \Lambda_G G(x/A)\ \Omega_M(1-x/A)/\Omega_M(1) \tag{4b}$$

$$xF_V(x,A) = Mv(x/A)\ \Omega_{M-1}(1-x/A)/\Omega_M(1),\ v(x) = xV(x). \tag{4c}$$

Here x is the momentum in units of P/A. The determination of functions S,G,V from nucleon data is mathematically non-trivial. The solution of this problem is presented in ref. 4. For A >> 1 the saddle-point approximation to $\Omega_M(T)$ yields

$$xF_{S,G}(x,A) = A\ \lambda_{S,G} \exp -\Lambda x \tag{5a}$$

$$xF_V(x,A) = \frac{3A}{\Gamma(\beta)}\ (\Lambda x)^{\beta} \exp -\Lambda x \qquad (x \lesssim 1) \tag{5b}$$

with $\Lambda = \lambda_S + \lambda_G + 3\beta$. A numerical study shows that the limit (5) is reached rapidly: for A > 20 the error is less than 1%. Since the A dependence of structure functions factorizes at large A, viz. $F(x,A) = Af(x)$ $(x < 1)$, we

predict a striking saturation law:

$$\frac{A'F(x,A)}{AF(x,A')} = 1 \quad , \quad A,A' >> 1 \tag{6}$$

as if anomalous effects in structure functions were absent.

The CDHS data[5] have been used as input in our numerical work. We stick as much as possible to their fits, except that we assume $F_G \sim (1-x)^4$ for $x \to 1$, in agreement with prejudices from large p_t phenomenology. In calculating the ratio σ_{Fe}/σ_D we have two options: 1) Describe the deuteron by our nuclear model, and 2) Assume that deuteron is an exception to the rule and replace it by two free nucleons. The second option is the one which is generally considered as "obviously" more realistic, but we prefer to be careful and we did our calculations for the two extreme cases. The results are shown in fig. 1. The dashed and the solid curve correspond to the options 1) and 2) respectively.

Neither of our curves really fits the data, as one could expect with so crude a model. Nevertheless, we claim a success since we reproduce the most salient features of the data essentially without free parameters: a) we predict $\sim$ 15% enhancement at small x, b)we predict $\sim$ 20% depletion for medium values of x, to be compared with the observed 14%. The dramatic rise of the solid curve for $x > 0.6$ has nothing dramatic in it. With option 2) one is dividing σ_{Fe} by a quantity that tends to 0 for $x \to 1$. As one moves towards x=1 unconventional contributions to D structure functions are certainly important, e.g. it is plausible that option 1) is realistic there. It is amusing that, on the whole, the dashed curve looks better. It is not clear whether this is an accident or whether a parton bag description of D is more realistic than expected.

Summarizing : The so-called EMC effect can be roughly understood in the framework of a statistical parton model. We suggest that the experimenters check the saturation law (6), very characteristic to the picture where the whole nucleus is regarded as one bag of partons.

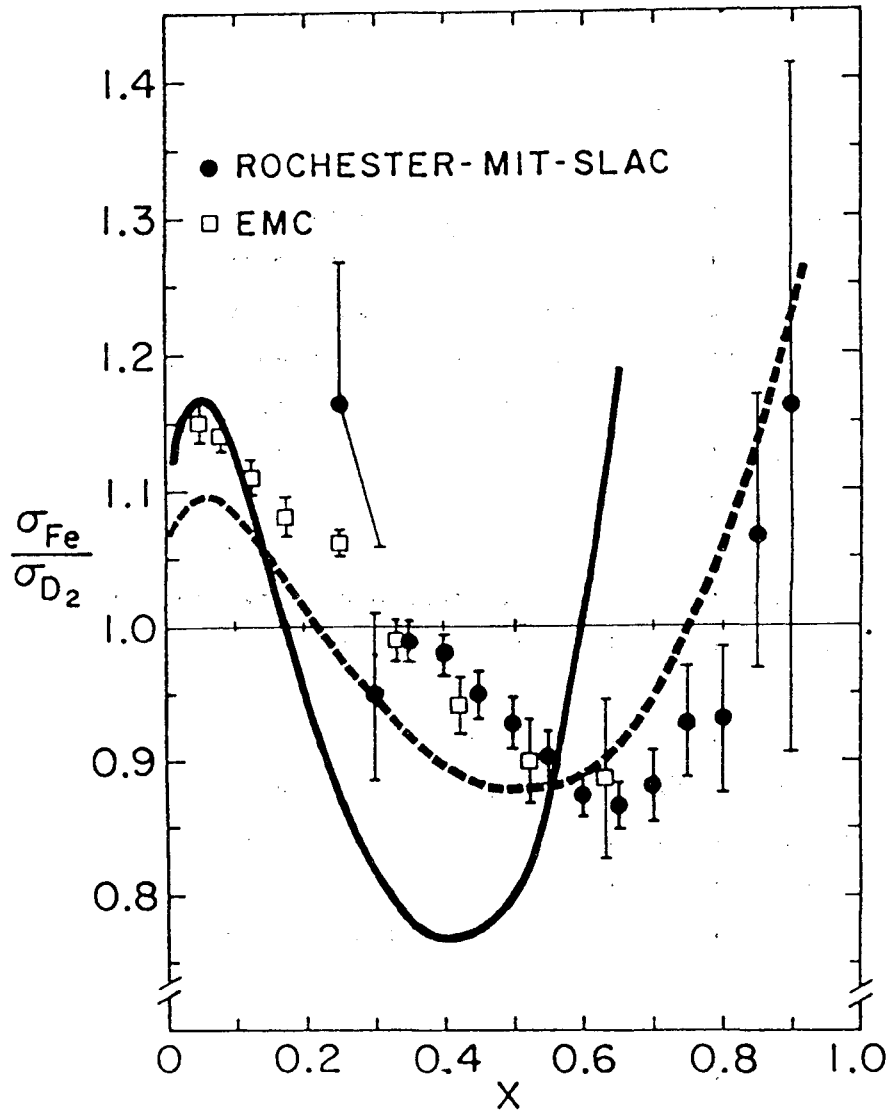

Fig. 1

References:

1. A. Krzywicki, Phys. Rev. D14 (1976) 152.
2. J.J. Aubert et al., Phys. Lett. 123B (1983) 275; A.Bodek et al., Phys. Rev. Lett., 50 (1983) 1431.
3. J. Kuti and V. Weisskopf, Phys. Rev. D4 (1971) 3418.
4. W. Furmanski and A. Krzywicki, forthcoming Orsay preprint.
5. H. Abramowicz et al. , Zeits. f.Phys. C17 (1983) 283.

Stopping Process of GeV Particles in Target Nuclei

K. Nakai

Department of Physics, University of Tokyo, Hongo, Bunkyo-ku, Tokyo 113, Japan

§1. Introduction

The issue whether and how we can produce high energy densities in nuclear matter is one of central subjects in high energy nuclear reaction studies. Theoretical speculations for possible phenomena associated with nuclear matter at high baryon densities or high energy densities stimulated experimental efforts to study high-energy heavy-ion reactions at Bevalac. However, we don't know yet what would be the best energy for generation of high energy densities. Obviously, one needs nucleus-nucleus collisions at high energies, but at higher energies nuclei would become transparent, so that there must be an optimum energy for this purpose. It is, therefore, very important to study the nuclear stopping process and mechanisms of energy deposition of GeV particles in target nuclei.

In order to survey the energy region above the Bevalac, we started experimental programs at KEK to study hadron-nucleus interactions in a few GeV region. In the following I would like to discuss about the stopping process of GeV particles based mainly on our experimental results and combining with information from other experiments. Let me first summarize our experimental observations.

§2. Summary of the KEK experiment*.

Experimental setup

The experimental setup is shown in Fig. 1. Unseparated proton and pion beams of 1 to 4 GeV/c from the KEK $\pi 2$ channel were used on nuclear targets. Beam particles were identified with two Cherenkov counters C_1 and C_2.

---

* The KEK experiment E71 were carried out by T.-A. Shibata, H. En'yo, I. Arai S. Saski, M. Sekimoto, K. Nakayama, K. Ichimaru, H. Nakamura-Yokota, R. Chiba and K.N[1].

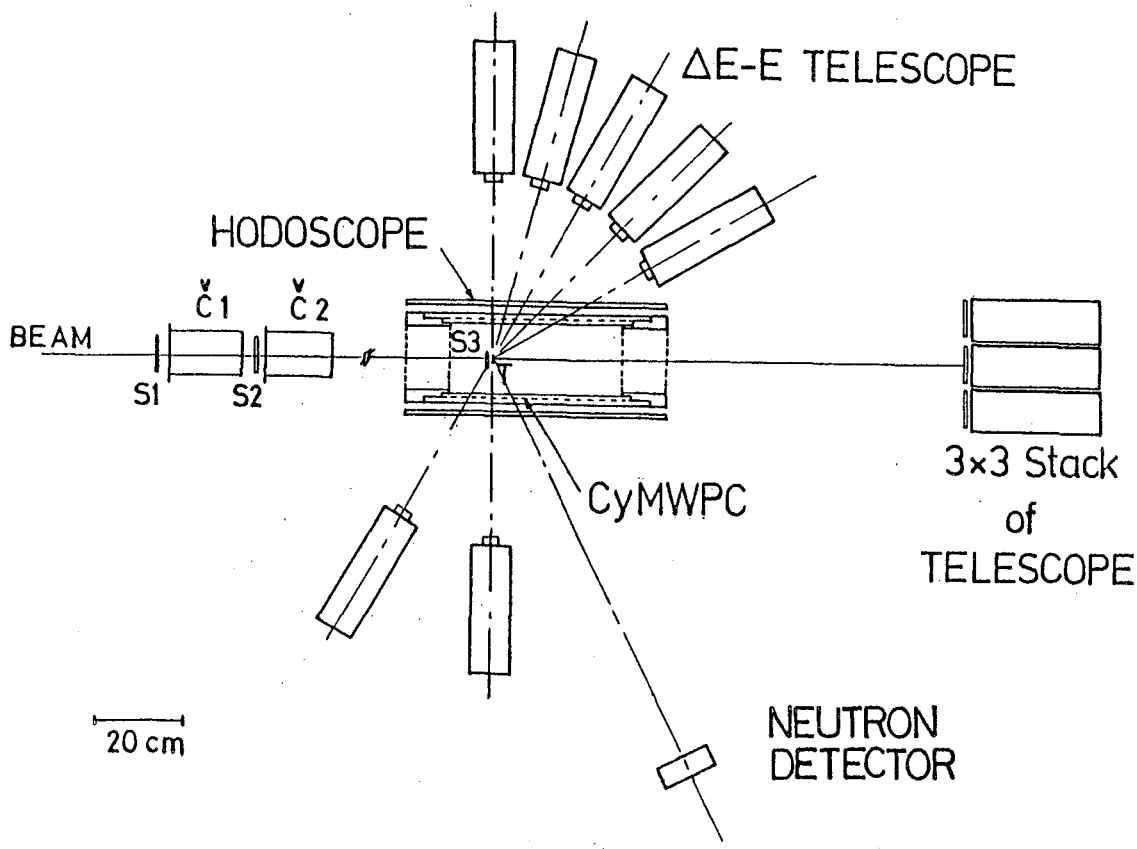

Fig. 1 Experimental layout.

A cylindrical MWPC was placed sorrounding the nuclear target for detection of charged particles emitted in an angular range of θ = 30° to 120° and ϕ = 0° to 330°. Seven ΔE-E scintillation telescopes were placed at 40 cm from the target at angles from 30° to 120° for measurements of emitted proton spectra. For measurement of neutron spectra a liquid scintillation counter was used at 1 m from the target and at angle of 60°. These detectors were for observation of particles emitted in the target-rapidity region. For detection of forward particles, a stack of ΔE-E counters was put on the beam line at 1 m from the target to cover an angular range of $\theta \lesssim 10°$.

Inclusive proton spectra

Energy and angular distributions of protons measured by the ΔE-E telescopes are shown in Fig. 2. The distributions were well reproduced with a model assuming the isotropic emission of protons from a source moving with a velocity β_s. The energy spectrum of protons in the moving frame was given as, $(1/p)(d^2\sigma/dEd\Omega) = N\exp(-E/E_o)$.

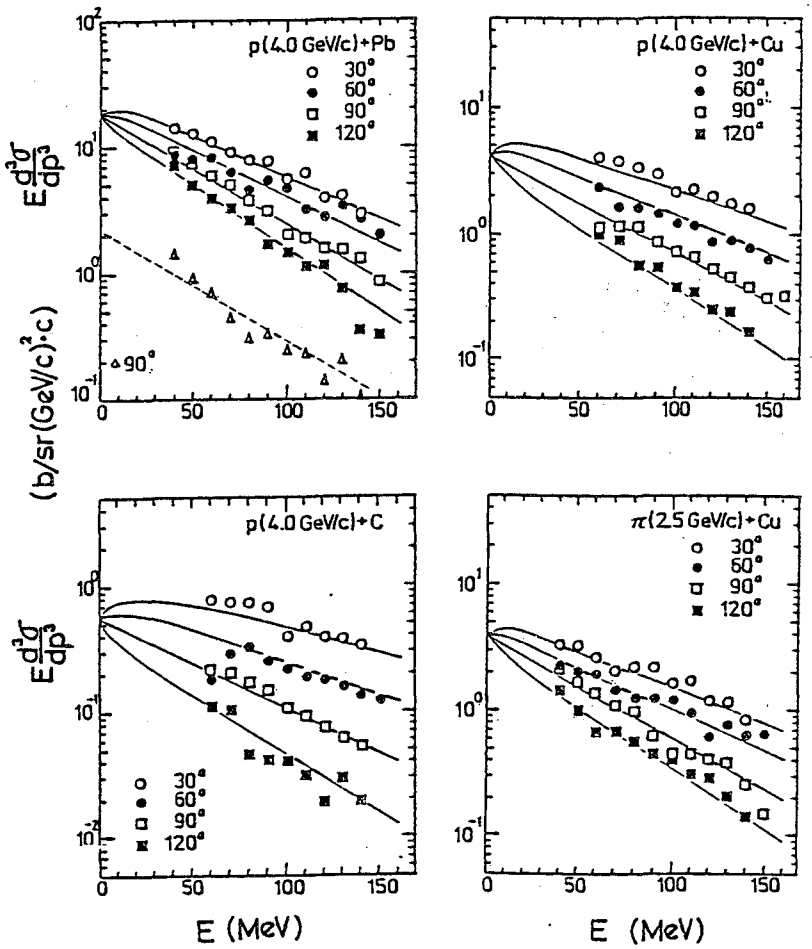

Fig. 2 Examples of inclusive proton spectra and results of the single-moving-source fit (solid curves).

The parameters β_s, E_o and N were determind by the least-square fitting to data. Examples of the single-moving-source fit to data are shown Fig. 2.

Cross sections and multiplicities of protons

The cross sections for formation of the single moving source, σ_{HI} (in a highly inelastic process), and multiplicities of emitted protons, $\langle m_p \rangle$, were determind from the single(Y1) and two-fold-coincidence(Y2) counting rates of the ΔE-E telescopes.

Those are given as;

$$(Y1(\theta_j)) = \sigma_{HI}\langle m_p\rangle IRN\Omega_j F_j$$

$$(Y2(\theta_j,\theta_k) = \sigma_{HI}\langle m_p(m_p-1)\rangle IRN\Omega_j\Omega_k F_j F_k$$

$$F_j(\theta) = \int_\Omega d\Omega \int_E dE\ f(\theta_j,E_j).$$

The angular and energy distribution $f(\theta_j,E_j)$ was calculated with the single-moving-source model. The cross sections σ_{HI} are plotted versus target mass number in Fig. 3 (open and closed circles). The cross sections were about 1/3 of the geometrical ones.

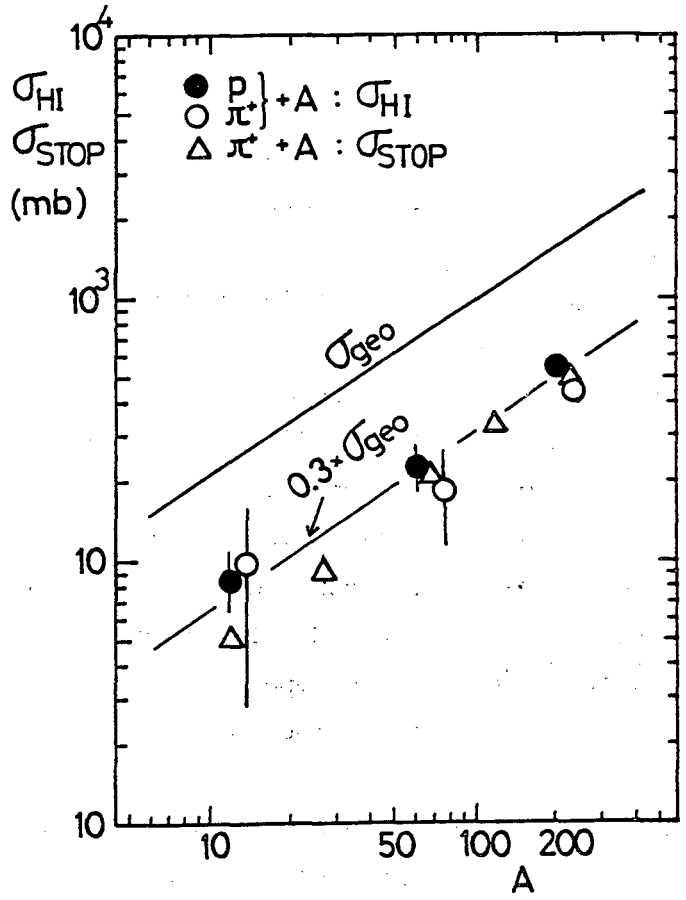

Fig. 3 Cross sections σ_{HI} (● and o) and σ_{stop} (Δ) versus target mass number.

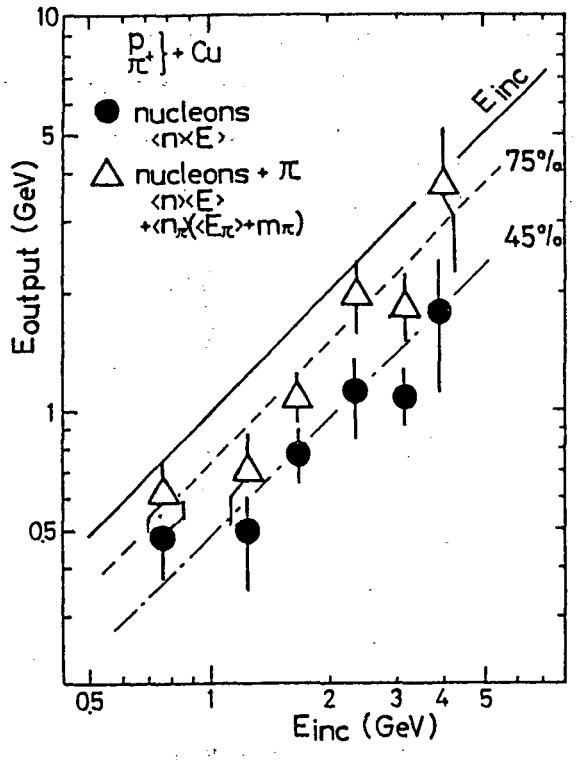

Fig. 4 Energies carried away by nucleons and pions.

Energy deposition

With use of the temperature parameter E_o and the mean multiplicity of protons $\langle m_p \rangle$, we estimated average energies carried away by the emitted nucleons. As shown in Fig. 4, it was about a half of the incident projectile energy. Estimation of energies carried away in pion production was remote, because our measurements were not sufficient to determine the angular and energy distribution of pions. We obtained, however, an estimate of lower limit by calculating the energy from pion data at 90° and 120° assuming isotropic distributions. Then, the estimate of energy carried away by both nucleons and pions came up to 70 to 80% of the projectile energy. In addition, non negligible contributions of deuterons and other composite particle emissions have to be included. Hence, we concluded that in these highly-inelastic processes most of the projectile energy was deposited in target nuclei to form the moving source, and then carried away by the emitted particles.

Stopping process

In the multiplicity distribution measured by the cylindrical MWPC, we observed two components which were strongly correlated with the forward particle emission (Fig. 5a). Among the two components, events in the high-multiplicity component were mostly associated with no forward particle, while those with low multiplicity were with forward particle(s) (Fig. 5b). The strong correlation between the high-multiplicity and the no-forward-particle conditions seemed to imply that in those events the leading particle

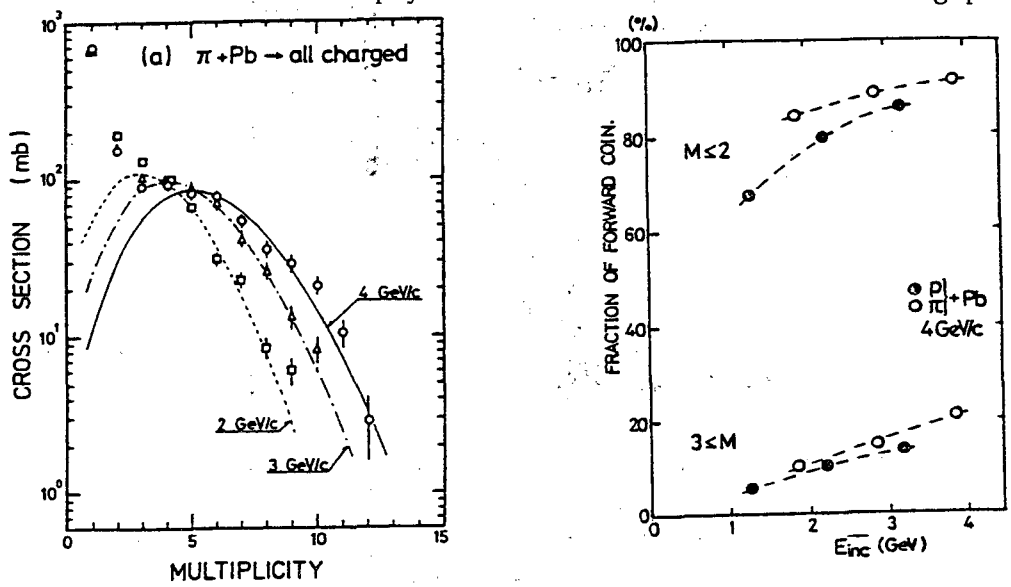

Fig.5 (a) Charged-particle multiplicity distributions. (b) Fraction of events with forward particle vs. multiplicity

was stopped. We proposed to call such events as the 'stopped' events. The 'stopping' cross sections, σ_{stop} were determind by integrating the multiplicity distributions and plotted with triangles in Fig. 3.

We noted that the events which form the moving source have also correlation with the forward particle emission. Shown in Fig. 2 with triangles was a proton spectrum at 90° taken with a trigger condition requiring at least one particle in the forward direction ($\theta \lesssim 10°$). The yield of proton was reduced by a factor of 10, and will be reduced further if we make a correction for a contribution of the randomly emitted multiparticles which hit the forward counter. This result indicated the good correspondence between the event with high multiplicity and the event forming the moving source. Indeed, as shown in Fig. 3, the cross sections, σ_{HI} and σ_{stop}, deduced in totally different ways are in good agreement.

Dependence of the cross sections on incident projectile energy are plotted in Fig. 6. The cross sections are nearly constant over the energy range from 1 to 4 GeV.

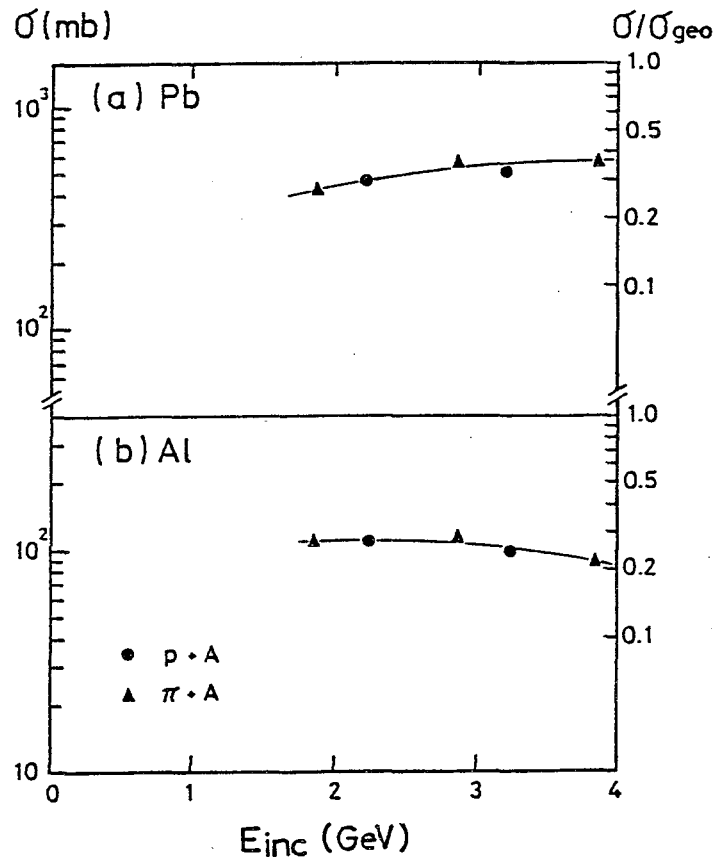

Fig. 6 The 'stpping' cross sections versus incident projectile energy.

Size of the moving source

The number of nucleons involved in the moving source, ν, was deduced from the source velocity, β_s, with the relation; $\beta_s = p_{inc}/(E_{inc} + \nu M)$. In Fig. 7 the numbers ν are plotted against the target mass number. This number, ν, gives an upper limit because the above relation assumes full energy deposition of projectile into the moving source. An alternative estimate of the number can be obtained from the proton multiplicity, $\langle m_p \rangle$, as $\nu' = (Z/A)\langle m_p \rangle$. The number ν' gives a lower limit. Thus, we concluded $\nu = (3 - 5)A^{1/3}$. The dependence of ν on incident energy is shown in Fig. 8.

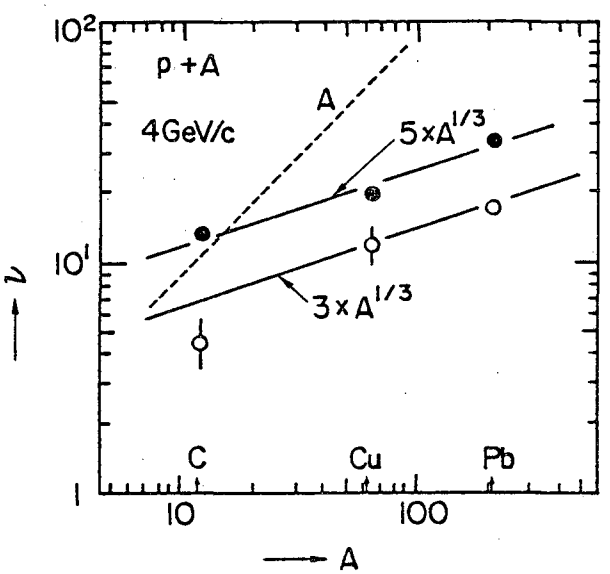

Fig. 7 Number of nucleons involved in the moving source ν vs. target mass.

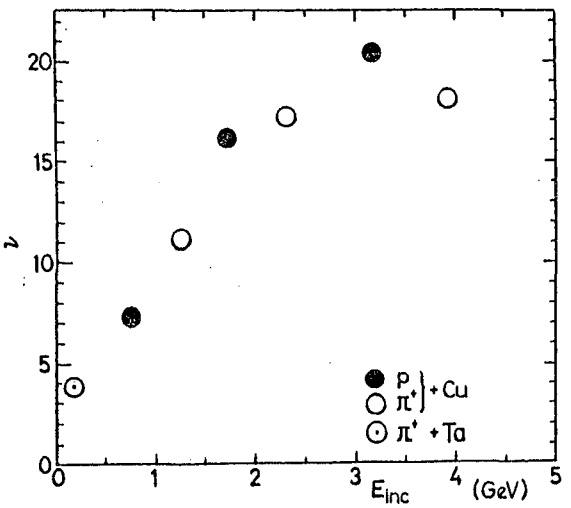

Fig. 8 Number of nucleons involved in the moving source ν vs. incident energy

Three components in nucleon spectra

In the neutron spectra, we observed three components as shown in Fig. 9. The nucleon spectra may be decomposed as; $(1/p)(d^2\sigma/dEd\Omega) = A^i \exp(-E/E_o^i)$. For the case of data shown in Fig. 9, E_o's were; $E_o^I = 40$ MeV, $E_o^{II} = 8$ MeV, $E_o^{III} = 1.6$ MeV. Such decomposition is generally applicable for nucleons emitted in medium- and high-energy reactions, and the E_o parameters are; $E_o^I = 30 - 60$ MeV, $E_o^{II} = 6 - 8$ MeV, $E_o^{III} = 1 - 2$ MeV. The three components seem to be nucleons emitted in three different stages; I. primary, II. pre-equilibrium and III. equilibrium stages. The protons shown in Fig. 2 and discussed in the previous sections must be from the stage I. The component with $E_o^{II} = 6 - 8$ MeV are observed in the low-energy nuclear reactions, in the pion capture reactions as well as in the high-energy reactions. In our study of composite particle production we have noted the difference in time scales of emitting particles in stages I and II. The component III is obviously the evaporated nucleons.

In the case of peripheral collisions with large impact parmeters, there will be no multiparticle emission in the first stage, but the nucleons from the stages II and III must be emitted. The inclusive neutron spectrum in Fig. 9 must include such components.

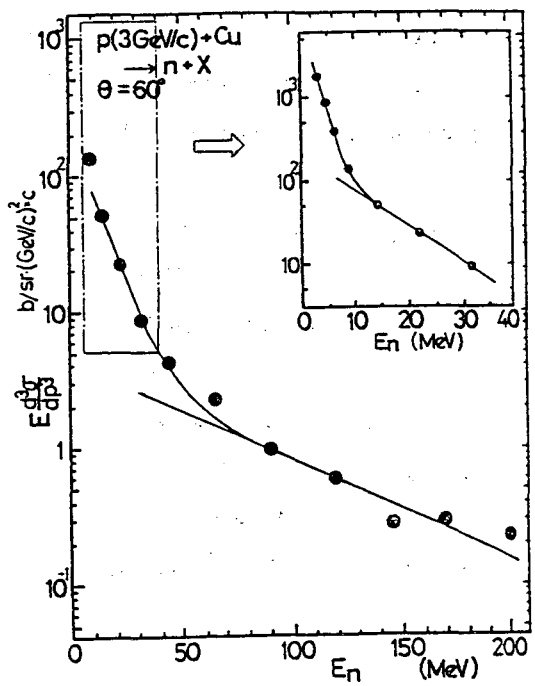

Fig. 9 Neutron spectrum at 60° from 3-GeV/c protons on Cu.

A picture of the reaction process

Summarizing these experimental results, we may draw the following picture of the reaction process: When a hadron with energy of several GeV was incident on a nucleus, in one third of the reaction processes the incident particle was stopped in the nucleus depositing most of its energy to form a local moving source which decays immediately emitting nucleons and pions. After emission of those fast particles in the stage I, the target nucleus is left 'wounded'. The 'wounded' nucleus is then repaired by emitting the nucleons with E_o^{II} = 6 - 8 MeV in the second stage. Finally, in the stage III, the residual excitation energy is released by evaporating nucleons.

§3. General aspects at higher energies.

It is very encouraging that the 'stopping' cross sections are nearly constant up to 4 GeV even for the nucleus as small as Al (Fig. 6). In the earlier stage of Bevalac research it was generally believed that nuclei would become transparent at high energies such as 2 GeV and nuclear interactins would become less collective than the low-energy region. This is not correct at least up to the energies we studied. Below 2 GeV, mechanisms for energy dissipation of projectile in a nucleus are multiple scatterings and the single Δ formation. Above 2 GeV, however, many channels open such as double Δ formation and excitation of higher-mass resonances (excited baryons). The stopping power of nuclear matter must, therefore, increases with incident energy.

Then, what would be the energy at which point projectile particles would penetrate through nuclei. The data shown in Fig. 10 may be indicating the break point. In the figures various observables are plotted against incident hadron energy. Those are:

a) The E_o parameter, or the temperature parameter, of invariant proton energy distributions deduced from spectra at 90°. Data were taken not only from our KEK experiment but also from LAMPF[2], AGS[3] and FNAL-ps[4].

b) The mean multiplicity of heavily ionizing tracks from emulsion experiments[5].

c)-e) Cross sections for the fragment production in deep spallation processes measured in radiochemical reaction studies[6].

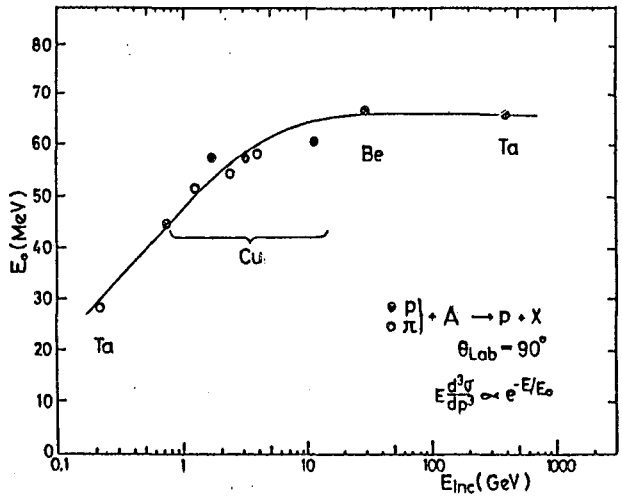

(a) The E_o parameters of proton spectra at 90°.

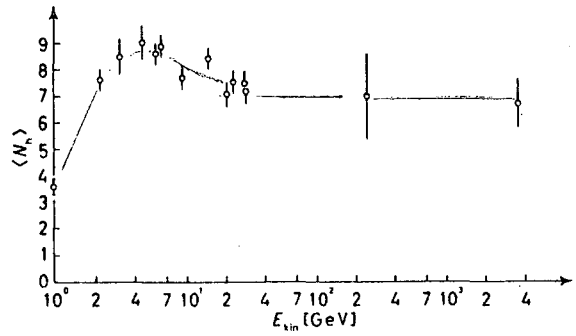

(b) Multiplicity of heavily ionizing tracks in nuclear emulsion.

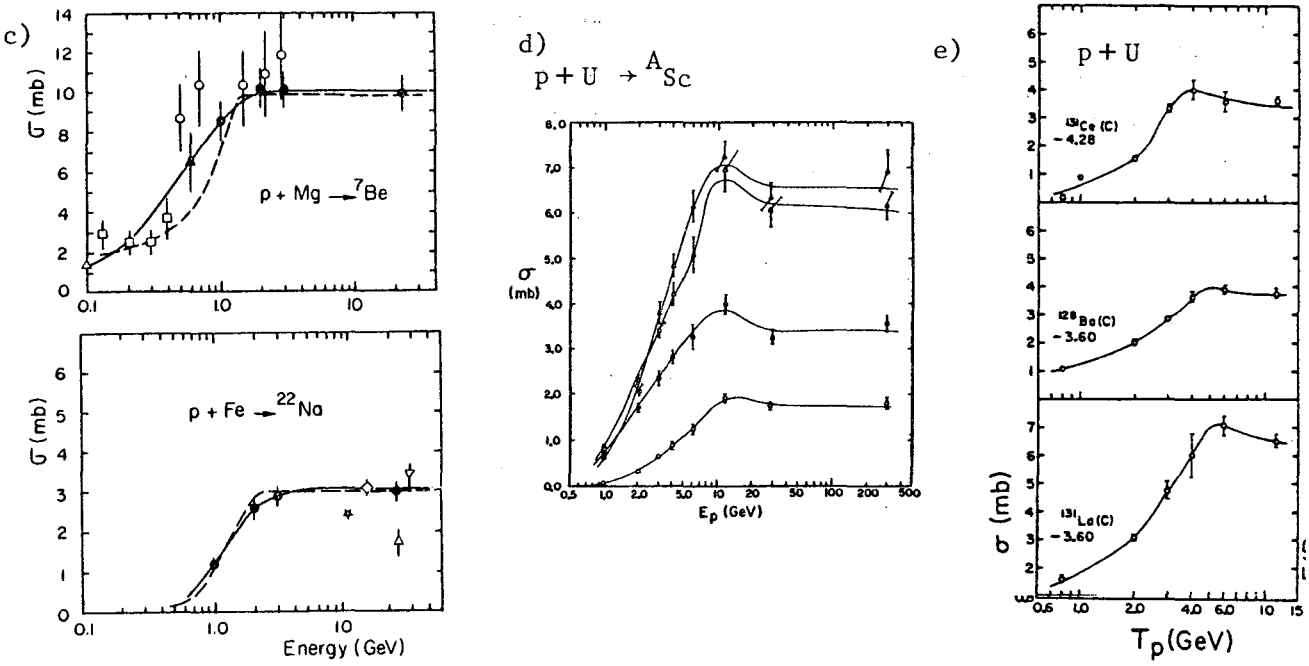

(c)(d)(e) Cross sections for the deep spallation process.

Fig. 10 Incident energy dependences of various observables in p+A reactions.

All these data seem to indicate a change in target excitation mechanisms at energies between 5 and 10 GeV. The results imply to conclude that at those energies the nuclei would become transparent. At higher energies, the leading particle(s) would carry away most of the incident energy, leaving a certain amount of energy in the fireball-like object in the target region. As seen in Fig. 10(a) and Figs. 8 and 10(b), the E_o parameter and the size of fireball ν, which reflect the degree of nuclear excitation, reach to saturation values. The independence of target excitation on incident energy is understood as an example of the limiting-fragmentation phenomena.

It was noted, however, that E_o parameters for pion spectra at 90° behaves differently as shown in Fig. 11. In contrast to the data in Fig. 10 the E_o parameter for pions increases with incident energy up to the 100-GeV region. This might mean that the pion spectra reflect an earlier hot stage (Stage-0) than protons which are emitted at a later stage (Stage-I) after formation of the local fireball.

The processes discussed here are stopping in the laboratory frame and production of excited nuclear matter in the target-rapidity region. The 'stopping' is, however, a frame-dependent concept. In nucleus-nucleus collisions stopping in the center-of-mass (CM) frame would be more important for generation of higher energy densities in the central region. Theoretical estimates[7] as well as an empirical estimate[8] have been made for the stopping in CM frame. More experimental studies are highly required with available proton beams in the energy range from 10 to 30 GeV.

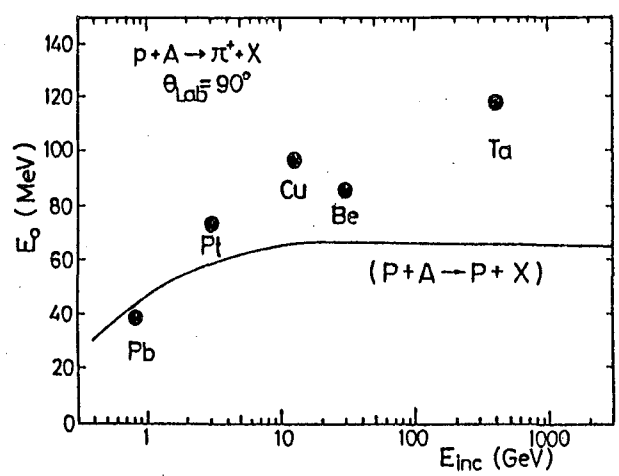

Fig. 11 The E_o parameters of pion spectra at 90° versus incident energy.

Theoretically, a phase transition of nuclear matter to a quark-gluon plasma phase (deconfinement phase transition) has been predicted to occur with a critical temperature in a range from 150 MeV to 200 MeV.
In the fragmentation region, even with heavier projectiles, it is questionable whether we can heat up nuclear matter so high enough to observe the deconfinement phase transition. However, we should note that the theoretical estimates for the critical temperature were made assuming thermal equilibrium which is essential for the phase transition phenomena. Experimentally, the equilibrium may not be realized anyway, and in a non-equilibrium phase there would be a good chance to observe deconfined states even at lower reaction energies. We should, therefore, prepare for studies of such possibilities both experimentally and theoretically.

On the other hand, I would like to stress that the fireball-like object produced in the target region is already a very interesting object. In order to stop the GeV particle in a nucleus, the projectile energy must be dissipated by producing many Δ's and N*'s in a localized part of the nucleus. Studies of interactions among the excited nucleons and nucleons are of great interest. We may expect to observe multi-Δ correlations in nuclear matter. Studies of such collective phenomena in hadronic phase involving the excited hadrons would be more practical than, and as important as, those in the quark-gluon phase.

(References)

1) K. Nakai, T.-A. Shibata, H. En'yo, S. Sasaki, M. Sekimoto, I Arai, K. Nakayama, K. Ichimaru, H. Nakamura-Yokota and R. Chiba, Phys. Lett. 121B (1983) 373.
T.-A. Shibata et al., to be published in Nucl. Phys. (1983).

2) R.D. McKeon, S.J. Sanders, J.P. Schiffer, H.E. Jackson, M. Paul, J.R. Speckt, E.J. Stephenson, P.R. Redwine and R.E. Segel, Phys. Rev. Lett. 44 (1980) 1033.

3) V.L. Fitch, S.L. Meyer and P.A. Piroue, Phys. Rev. 126 (1962) 1849.

4) Y.D. Bayukov, V.I. Efremenko, S. Frankel, W. Frati, M. Gazzaly, G.A. Leksin, N.A. Nikiforov, C.F. Pardisat, V.I. Tchistilin and Y.M. Zaitsev, Phys. Rev. Lett. 85B (1979) 315.

5) H. Meyer, M.W. Teucher and E. Lohrmann, Nuovo Cimento 28 (1963) 1399.

6) G.M. Raisbeck and F. Yiou, Phys. Rev. C12 (1975) 915.
O. Scheidemann and N.T. Porile, Phys. Rev. C14 (1976) 1534.
S. Biswas and N.T. Porile, Phys. Rev. C20 (1979) 1467.

7) A.S. Goldhaber, Nature 275 (1978) 114.
M. Gyulassý, Proc. of Conference on Quark Matter and Heavy Ion Collisions, Bielefeld, 1982 (World Scientific Publ. Co., Singapore).

8) W. Busza and A.S. Goldhaber, SUNY preprint ITB-SB-82-22 (1982)

FIRST PERFORMANCE TESTS OF THE DIOGENE DETECTOR, WITH ALPHA PARTICLES

Jean GOSSET
DPh-N/ME, CEN Saclay, 91191 Gif-sur-Yvette Cedex, France

The Saturne synchrotron at Saclay will soon deliver beams of heavy ions up to mass 40 at energies up to 1.2 GeV per nucleon. The first generation of experiments on central collisions of relativistic heavy ions, performed mainly at the Berkeley Bevalac with the aim to study the behaviour of nuclear matter at high density and high degree of internal excitation, has shown that inclusive measurements are too sensitive to trivial aspects such a geometry and kinematics, and not enough to the dynamics of the reactions. Only exclusive measurements can lead to some information about the dynamics and possibly on the equation of state of nucler matter at high density and high temperature.

In order to make useful exclusive measurements with beams from the Saturne synchrotron, a detector should have the following characteristics : a very large solid angle, as close as possible to 4π sr ; the possibility of handling multiplicities of light particles as high as 40 ; the momentum of all particles whatever their type, energy and direction should be measured within an accuracy of 10 to 20 % up to momentum values of 1.5 GeV/c ; the different types of charged particles ($\pi^{\pm}$, p, d, t ...) should be clearly identified ; it should be possible to trigger the data acquisition on central collision events.

In principle all these requirements are met by streamer chambers. However the full tridimensional analysis of the events from the stereoscopic photographs is a huge problem especially for high multiplicity events. This problem is not yet solved satisfactorily in an automatic way. Hence the number of events which can be fully analyzed with this kind of detector is strongly limited.

Another possibility would have been to build an absorption detector, like the plastic ball[1], where the particles are identified by the combination of an energy loss and their total energy. We rejected this solution because of its limited energy range, and the quasi impossibility to measure π^-.

Another type of detector can be used for high multiplicity event measurements, and has already been developed for high energy physics experiments : based upon drift chambers located in a magnetic field, it is called a pictorial drift chamber and allows full three-dimensional recording of points along the trajectories. The particles are identified by their energy loss and the curvature of their trajectories which is a measure of their transverse rigidity. Diogène is an adaptation of these huge high energy physics detectors to the mass and energy range of the species to be detected at Saturne. In particular its internal detector is derived from the "jet chamber" of the JADE detector[2] installed at Petra.

The "Diogène" detector has been developed by a collaboration[3] between physicists from Saclay, Strasbourg and Clermont-Ferrand. Its configuration is shown on fig. 1. A solenoid made with aluminium coils and surrounded on top and bottom by an iron yoke provides a magnetic field of 1 tesla. This field is homogeneous within 1 % in the whole active volume, 80 cm in length and 70 cm in diameter. Both left and right hand sides of the coil are left available for future detection of neutral particles.

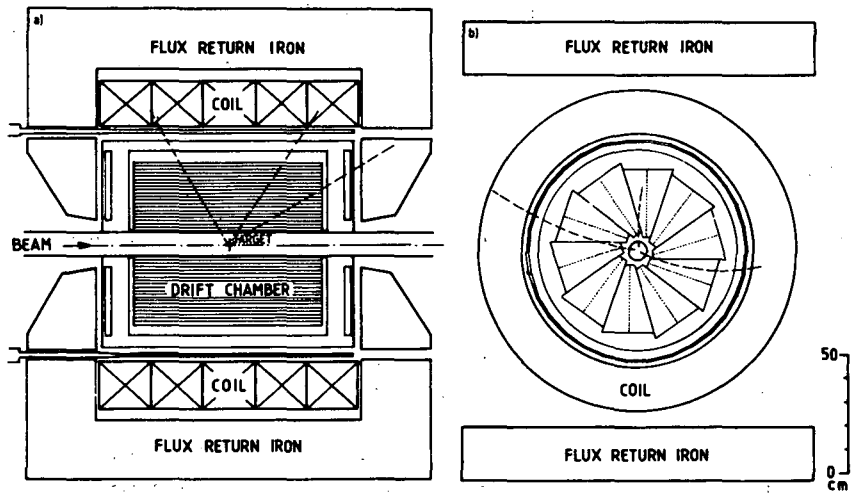

Fig. 1 - Two views of the Diogène detector : a) radial cut in the vertical plane ; b) cut through the target perpendicular to the beam axis.

The drift chamber consists of ten sectors, each of them subtending 36 degrees of azimuthal angle around the beam. In each sector there are 16 sense wires regularly spaced along 26 cm. These wires are made of Ni-Cr, 30 μm in diameter. The chamber is filled with an argon (86 %) and propane (14 %) mixture at a pressure that can be varied between 1 and 4 atmospheres depending upon the incident beam energy. This enables us to make a compromise between a good momentum resolution which requires low pressure in order to minimize multiple scattering and a good energy loss resolution which requires high pressure. The argon propane mixture was chosen to fulfil the following requirements : the drift angle should be kept to a reasonably small value ; this implies a small enough value of the drift velocity, which should saturate at the used electric field ; finally the electric field should not be too high in order to avoid high voltage problems. With our argon-propane mixture, the drift velocity saturates at about 40 mm/μs for an electric field of around 1.5 kV/cm leading to a drift angle slightly below 25 degrees. The electric field is fixed by the potential wires, printed circuits at the top and bottom of each sector and strips of coppered kapton between the sectors. In order to stand the 4-atmosphere pressure, the chamber is put in a stainless steel vessel, 4 mm thick. The gas is separated from the beam by a 1.3 mm thick stainless steel pipe 10 cm in diameter which gives at 90° a lower cut-off of 26 MeV for protons, 12 MeV for pions and 120 MeV for α particles. This pipe might be replaced in near future by a carbon fiber one of the same thickness reducing thus the cut-off to 12 MeV, 5 MeV and 60 MeV for protons, pions and α particles respectively.

In order to help in solving the left-right ambiguity between tracks on the right hand side or the left hand side of the wire plane, two different solutions are used in Diogène. Like in many other similar drift chambers the sense wires are alternately staggered by ± 200 μm from the average wire plane. If one takes this into account, the χ^2 of the fit of the true track should be significantly smaller than the χ^2 of the wrong track, provided that the number of points is large enough since there is always an uncertainty on the measured coordinates. This usual way can be used wherever the particles come from. However Diogène will be used with a target so that we know where a trajectory

is to come from. We decided to shift all the wire planes by about 2 cm from the axis of the chamber. The wrong track symmetric with respect to the wire plane of the true trajectory can then not originate from the target, which makes the solution of the leftright ambiguity very easy.

The electronics has been copied from the jet chamber one[4], just adding a ninth bit to the time digitization : it is a multiple-hit electronics, allowing the time and pulse height digitization of up to 8 hits per wire for each event.

The drift chamber is triggered by a majority coincidence requirement among 30 scintillators surrounding it. This multiplicity of laterally emitted particles should be sensitive enough to the centrality of the events.

The Diogène characteristics can be summarized as follows. It can handle charged particle multiplicities up to at least 40. The maximum of counts which can be recorded per wire is 8, limiting theoretically the possible multiplicity to 80. The actual limit is certainly smaller due to double track resolution and the difficulty to reconstruct the pattern, which increases exponentially with the density of tracks. The drift chamber covers about 85 % of the full 4π solid angle, with polar angles ranging from 20° to 155°. However the momentum resolution becomes poor at very forward and backward angles when the number of hitted wires becomes small. The measured resolutions (full width at half maximum) are 400 μm for the drift distance and 1.5 cm for the coordinate along the wires. These figures lead to 10-15 % for the momentum resolution of protons hitting 16 wires (fig. 2), 1 to 2 degrees for the polar angle and less than 1 degree for the azimuth. The various particles, $\pi^{\pm}$, p, d, t ... can be easily identified, as shown on fig. 3.

A comparison with the plastic ball detector[1] can be made. The maximum multiplicity that can be handled by the plastic ball is higher. The angular range covered by the plastic ball is also wider, with no hole between roughly 10 and 15 degrees like in Diogène. The momentum resolution of the plastic ball is also better. On the other hand the momentum range for which particles can be completely identified is larger for Diogène. Moreover both π^+ and π^- can be analysed with Diogène, as opposed to the plastic ball which can only handle π^+, with at most 80 % efficiency.

A very important task for our Diogène project has been the track reconstruction. The program which has been developed[5] decouples the treatment in the (r,Z) plane, looking for straight lines, and in the (X,Y) plane, looking for circles coming from the target point. The left-right ambiguity is easily solved by the fact that the ghost track cannot stand the tests of coming from the target, due to the shift of the wire planes with respect to the beam axis. An example of track reconstruction is shown on fig. 4 for an α on lead collision at 800 MeV per nucleon with eleven tracks.

The whole detector, that is the ten sectors of the drift chamber, the pressure vessel and the magnet, is now completed and installed at Saturne. It has already been used to take data with α beams at 800 MeV per nucleon on carbon and lead targets. A total of 300,000 events has been accumulated on tape, last november. The complete processing of these data is in progress. Before starting data taking with heavy ions when they become available at Saturne at the beginning of next year, we intend to complete an experimental program with

α beams at four energies (200, 400, 600 and 800 MeV per nucleon) on three targets (carbon, copper and lead).

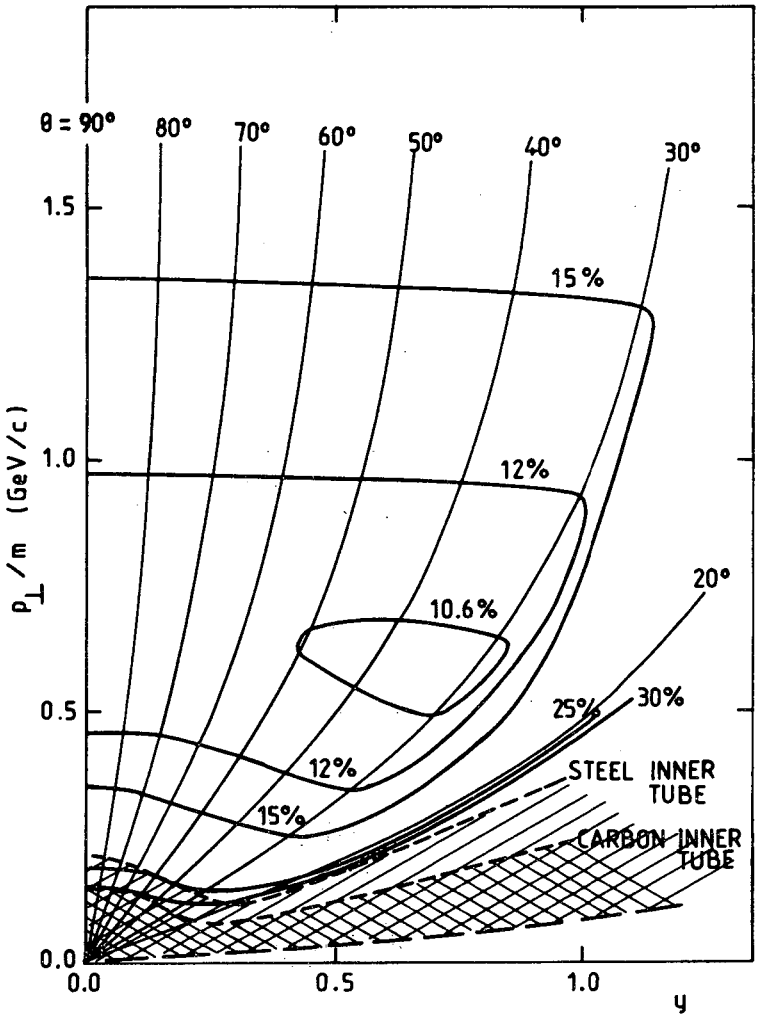

Fig. 2 - Contour diagrams of Diogène momentum resolution (in percent and full width at half maximum) for protons detected in the forward hemisphere, calculated with the resolutions measured with a prototype sector, in the rapidity-transverse momentum plane. The target is located 20 cm upstream of the geometrical center of Diogène. The cuts due to the inner tube are shown for the current steel tube and the future carbone fiber one. The shaded area is a dead one for Diogène. The region below the shaded area is to be detected with the plastic wall.

Fig. 3 - Truncated mean energy loss versus *rigidity scatter plot for α (3.2 GeV) on lead. Starting from the left side lower corner, pions, protons and deuterons are clearly resolved.*

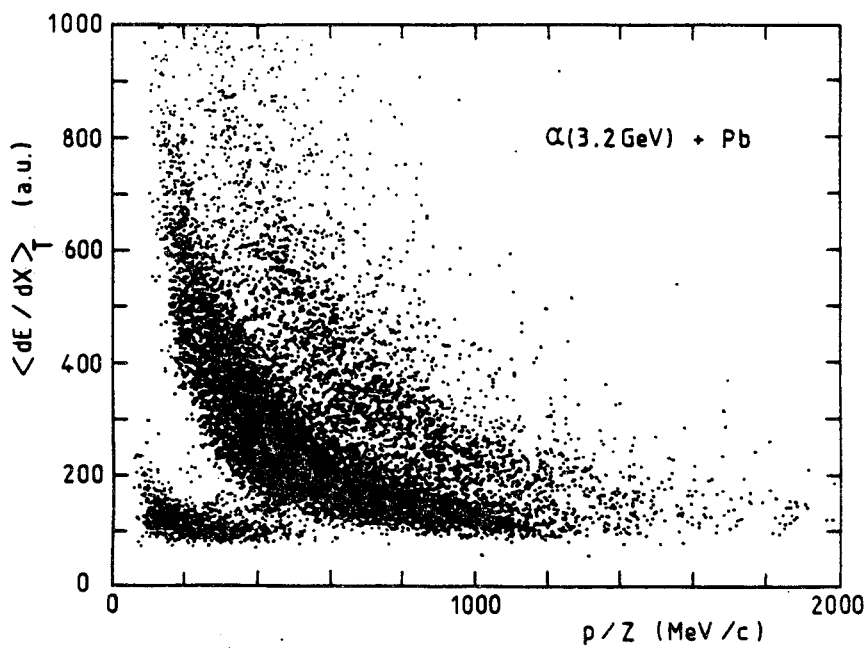

In addition to the complete processing of our first data, with track reconstruction, we have started some analysis based on the raw data. In particular our attention was drawn to the fact that the frequency of events similar to the one shown

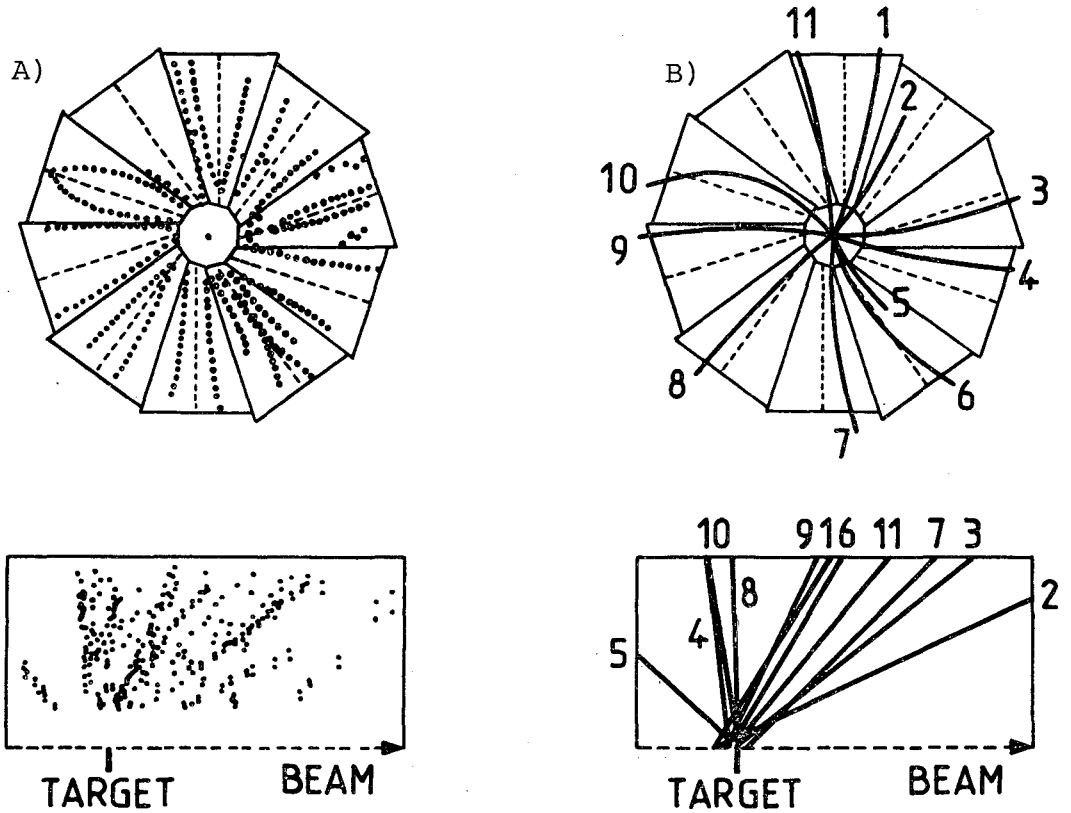

Fig. 4 - a) An event from the reaction of 3.2 GeV α with ^{208}*Pb. Top : projection on a plane perpendicular to the beam axis. Bottom : projection on the r,Z plane, r is the distance to the beam axis, Z is the coordinate along the beam axis. For each hit the two* a priori *possible points (due to left-right ambiguity) are plotted. b) Result of the analysis of this event by our track reconstruction progam.*

in fig. 5 seems rather high. The characteristics of such events is that most of the particles are emitted at about the same polar angle with respect to the beam axis, within a total width of less than 20 degrees. Since this kind of conical emission seemed rather frequent from on-line event displays, we decided to check whether it is significant or not, compared to what can be expected from the inclusive angular distribution. By comparing the angular groupings obtained respectively from our data and from a Monte-Carlo simulation using our measured inclusive angular distribution, we can now draw the conclusion that the observed conical particle emission is compatible with statistical fluctuations on random sampling from the inclusive angular distribution. This kind of analysis could be performed on raw data, before track reconstruction, since the polar angle information can be simply derived for each hit on a wire, and the same wire number was selected in all ten sectors in order to count each track only once.

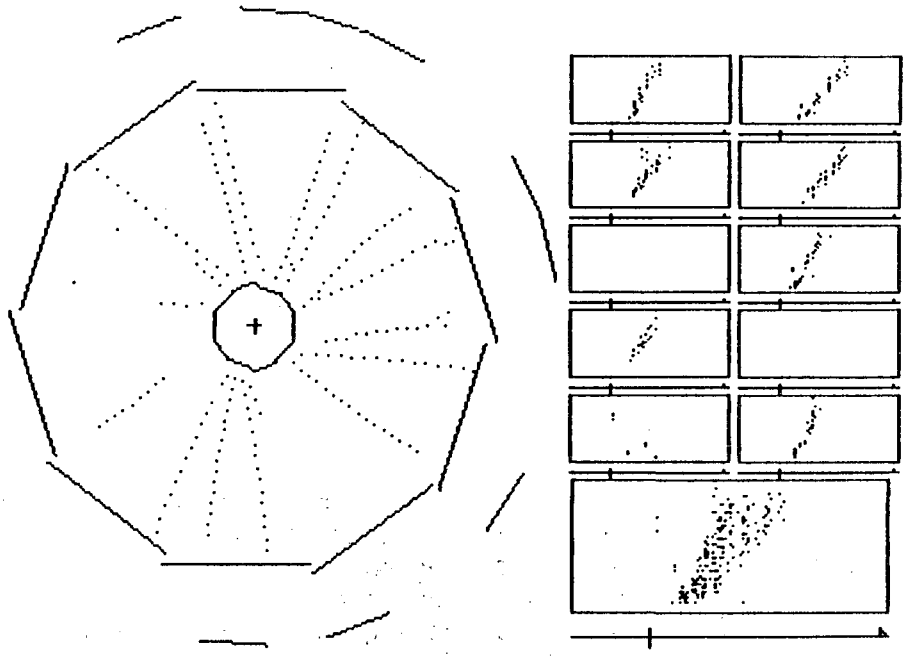

Fig. 5 - On-line display of one event from α (3.2 GeV) on lead, with both transverse and longitudinal views in cylindrical coordinates with respect to the beam axis. One longitudinal view is also shown for each sector, which helps giving the third dimension from this kind of display.

References

1. A. Baden, H.H. Gutbrod, H. Löhner, M.R. Maier, A.M. Poskanzer, T. Renner, H. Riedesel, H.G. Ritter, H. Spieler, A. Warwick, F. Weik and H. Wieman, Nucl. Instr. Meth. 203 (1982) 189.

2. J. Heintze, Nucl. Instr. Meth. 156 (1978) 227.

3. J.P. Alard, J. Augerat, R. Babinet, F. Brochard, Y. Cassagnou, J.P. Costilhes, L. Fraysse, J. Girard, P. Gorodetzky, J. Gosset, J. Julien, C. Laspalles, M.C. Lemaire, D. L'Hôte, B. Lucas, G. Montarou, A. Papineau, M.J. Parizet, J. Poitou, C. Racca, J.C. Tamain and Y. Terrien, Letter of intent n°8 and proposal n°43, Laboratoire National Saturne, Saclay ; J. Gosset, Nucl. Instr. Meth. 196 (1982) 299.

4. W. Farr and J. Heintze, Nucl. Instr. Meth. 156 (1978) 301.

5. J. Poitou, International Wire Chamber Conference, Vienna (1983), to be published in Nucl. Instr. Meth.

HYDRODYNAMICAL ASPECTS OF ULTRARELATIVISTIC HEAVY ION COLLISIONS

P. V. Ruuskanen
Department of Physics, Univ. of Jyväskylä
Seminaarinkatu 15, 40100 Jyväskylä 10
FINLAND

ABSTRACT

Hydrodynamics with source terms is used to describe the space-time behaviour of hadronic matter produced in ultrarelativistic heavy ion collisions. Resulting energy density in the Central Region (CR) appears to be high enough for the formation of quark-gluon plasma, but the life-time of the plasma (if produced) is very short. In Fragmentation Regions (FR) the energy densities are probably too low for the formation of QCD-plasma.

1. Introduction

There is a widely held hope among physicists working on heavy ion reactions, that quark-gluon plasma[1] will be produced in central collisions (impact parameter $b \approx 0$) of two heavy nuclei when the collision energy is high enough ($E_{CM} \gtrsim 10$ GeV/nucleon). It has been argued theoretically[2] and the arguments have been supported by the Monte Carlo results[3] on the lattice QCD that the confinement-deconfinement phase transition is of the first order[4]. Let me remind you of the relevant energy densities: In the nucleus $\varepsilon \approx 0.2$ GeV/fm^2, in the nucleon $\varepsilon \approx 0.5$ GeV/fm^2 and recent Monte Carlo estimates[5] for the latent phase transition energy in the case of pure SU(3) Yang-Mills theory give $\Delta\varepsilon \lesssim 1$ GeV/fm^3. Thus a reasonable guess would be that the phase transition starts at $\varepsilon \sim 0.5$ GeV/fm^3 and is completed at $\varepsilon \sim 2$ GeV/fm^3.

Several signals for observing the plasma have been proposed[6]. The estimates of most of the signals are extremely sensitive to the space-time history of the plasma. Thus in order to assess realistically the possibilities of actually producing the plasma as well as observing it, we need a reliable description of the space-time behaviour of the hadronic matter which is produced in the collision of heavy ions.

We envisage the high energy central A + A collision to proceed through three different stages: (1) the formation of the dense final state hadronic matter in the collision proper, (2) its subsequent hydrodynamic expansion and (3) finally the freezout to (separate) hadrons after the energy density (or temperature) has become small enough.

The hydrodynamic treatment of stage (2) is based on the fact that for heavy nuclei the size of the system $\sim R_A = r_0 A^{1/3}$ is much larger than the mean free path, ℓ_{free}, of the hadronic particles. Actually we are assuming more since we treat the hadronic matter as a perfect fluid locally in thermal equilibrium. For this to hold, we should have $\ell_{free} \ll L$ = the distance over

which any of the hydrodynamic quantities change appreciable. The numerical results imply, that this condition is not well satisfied, but on the other hand the estimates of the viscous effects indicate that they are small[8] during the expansion.

One should notice that the three stages do not constitute a clear-cut temporal sequence. Since our description of the formation of the matter is based on the inside-outside cascade[9] picture, it follows that in any fixed frame the slow particles are formed first and they will be already in the stage (3), when the fastest moving matter is produced.

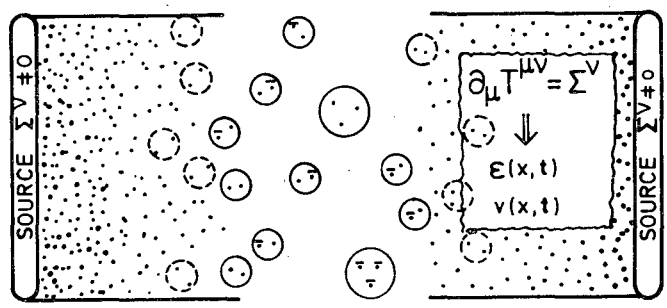

Fig. 1. A snapshot of the A + A collision in CM frame at t $\sim$ 10 fm/c after the collision. The energy density is highest immediately behind the Lorentz contracted nuclei. As the expansion dilutes ε, the hadrons start to decouple in the center.

This is schematically shown in Fig. 1 in the CM frame. Even more important is the fact that the final state matter moving with certain velocity, is not produced instantaneously but during a finite period of time. It turns out that in FR's this production time is essentially independent of energy and it is a large fraction of the total hydrodynamic expansion time. To treat properly this simultaneous production and expansion, we must construct source terms[10] for the hydrodynamic equations.

I will next specify the hydrodynamic problem to be solved and argue for the importance of the source terms in more details. Then I will describe the construction of the source terms before discussing the main numerical results and their implications.

2. Hydrodynamics with source terms.

Hydrodynamic equations

$$\partial_\mu T^{\mu\nu} = \Sigma^\nu \tag{1}$$

$$\partial_\mu J^\mu_B = \sigma \tag{2}$$

specify the evolution of the final state matter in terms of energy density $\varepsilon(x,t)$, baryon number density $n_B(x,t)$ (both defined in local rest frames) and the flow velocity field $v(x,t)$. The energy-momentum tensor $T^{\mu\nu}$ and baryon number current are defined as

$$T^{\mu\nu} = -pg^{\mu\nu} + (\varepsilon+p)u^{\mu}u^{\nu} \tag{3}$$

$$J_B^{\mu} = n_B u^{\mu} \tag{4}$$

where $u^{\mu} = \gamma(1,v)$ ($\gamma = 1/\sqrt{1-v^2}$) is the two-velocity and p is the local pressure. The three densities p, ε and n_B are connected through the equation of state $p = p(\varepsilon,n_B)$.

Since at high energies longitudinal velocities dominate, we have neglected the transverse variables and we will neglect the transverse flow completely. It turns out that the time scale due to longitudinal expansion is shorter than the time for the transverse rarefaction wave to reach the collision axis[11]. Thus our 1 + 1 dimensional treatment[7] should be adequate for the region around collision axis not too close to the nuclear surface.

The source terms Σ^{ν} and σ in Eq.'s (1) and (2) describe how the hadronic particles, which are produced in the primary collisions, enter the hydrodynamic system. The use of them allows a consistent treatment of the system during that time interval when part of the matter is already formed and is expanding but simultaneously the later collisions (due to the finite size of the nuclei) still produce new matter into the same domain. When source terms are used, they express the properties of the particle production in the collision. In this case initial conditions are very simple. This should be contrasted with a treatment, when Σ^{ν} and σ are taken to be zero. Then the initial conditions on ε, n_B and v contain both the properties of the production and the effects of expansion during the production period.

In the CR the production (proper) time $\Delta\tau_{CR}$ is short for high energy collisions and the use of source terms is not essential. However, the inside-outside dascade picture with an intrinsic proper time τ_0 for the formation of the produced particles leads in the FR's to an overall production time $\Delta\tau_{FR} \sim \sqrt{4\tau_0 R_A}$ independent of the collision energy. Since τ_0 is expected to be $\sim$ 1 fm, $\Delta\tau_{FR} \approx$ 5 fm for heavy nuclei; roughly half of the whole expansion period! Thus the use of the source terms is essential in the evaluation of the FR's.

3. Formation of the final state matter

Since the details of the construction of the source terms can be found in Refs. 7 and 12, I will here concentrate on the underlying assumptions and the resulting main features. Our starting point is nuclear transparancy, the fact that in the high energy h + A collisions the spectrum in the FR of hadron h depends only weakly on the size of the nucleus A[13]: We have assumed that this feature persists also in the A + A collisions. As a result the produced hadronic matter enters the hydrodynamic stage in fast longitudinal expansion. This has two important consequences: (1) Large part of the collision energy remains as kinetic energy and is not available for the heating of the matter and (2) the energy and baryon number densities are rapidly diluded. One should notice, that the longitudinal gradient of the initial flow velocity also exists in the FR's. This together with long production time there prohibits the formation of high density (energy and baryon number) target and beam fireballs.

Initial conditions which are appropriate in the case of nuclear transparancy at high energies, are quite different from the initial conditions in the original Landau model[14], which describe a situation for a completely opaque colliding matter. Then all the matter is stopped in a small Lorentz contracted volume and all the collision energy is used to heating up the matter. At lower energies the situation may well be approaching the Landau type initial conditions[15].

We implement the nuclear transparancy through a condition that the hadronic particles, which are produced in the primary N+N collisions, do not interact before a proper time τ_0 ($\approx$ 1 fm/c) is elapsed from the collision. Up to that time the produced particles stream freely from the collision point. At $\tau = \tau_0$ they are assumed to enter the hydrodynamic system depositing their energy and momentum into the system and being thermalized with the previously produced matter. If the rapidity distributions of particles produced in a primary N+N collision are given, their contribution along the hyperbola $\tau = \tau_0$ to the source terms Σ^ν and σ are easily calculated[12].

At high enough energies all primary collisions are between the incoming nucleons since the secondaries have not had time to materialize before the nuclei have passed through each others. In the simplest version of the model we assume that nucleons collide pairwise like free nucleons each one suffering only one collision. Since the mean free path of a nucleon in nuclear matter is $\lesssim$ 2 fm, we assume that in the CM frame the collisions take place at x = 0 and within time interval

$$0 \leq t \leq d_t = \frac{2R_A}{\mathrm{sh}\, y_B^*} \quad , R_A = r_0 A^{1/3}, \quad r_0 = 1.1 \text{ fm} \qquad (5)$$

as depicted in Fig. 2. y_B^* is the CM rapidity of the incoming beam nucleus.

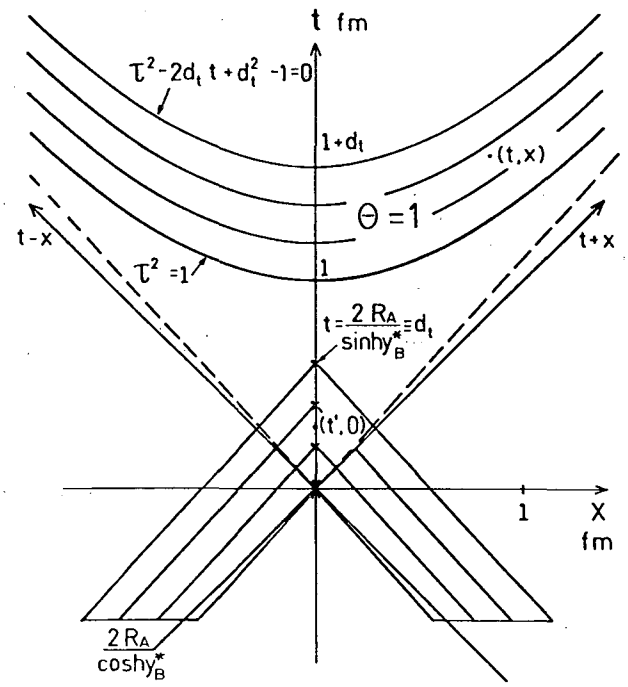

Fig. 2. Space-time illustration of a central A+A collision. Particles from a collision at (0,t') are produced on the hyperbola $\tau' = [(t-t')^2 - x^2]^{\frac{1}{2}} = \tau_0$. Thus the source region is bound by the hyperbolas $[t^2 - x^2]^{\frac{1}{2}} = \tau_0$ and $[(t-d_t)^2 - x^2]^{\frac{1}{2}} = \tau_0$. Multiple scattering between the incoming nucleons are ignored in this picture.

When we turn the sum over hyperbolas from discrete collisions into an integral by assuming continuous distribution of nuclear matter inside nuclei, we get

$$\Sigma^0(x,t) = \frac{n_0}{\tau_0} \sinh y_B^* \sum_i \bar{m}_i \rho_i\left(\log \frac{x+\sqrt{x^2+\tau_0^2}}{\tau_0}\right) \theta(x,t) \tag{6}$$

$$\Sigma^1(x,t) = \frac{x}{\sqrt{x^2+\tau_0^2}} \Sigma^0(x,t)$$

$$\sigma(x,t) = \frac{n_0}{\sqrt{x^2+\tau_0^2}} \sinh y_B^* \; \rho_N\left(\log \frac{x+\sqrt{x^2+\tau_0^2}}{\tau_0}\right) \theta(x,t). \tag{7}$$

$\rho_i(y)$ are the measured distributions of produced particles ($i = \pi, K, N, \ldots$) and $\theta = 1$ in the source region and 0 elsewhere. For our purposes it is sufficient to include into $\rho_\pi(y)$ all particles except nucleons which are the source of baryon number current and contribut significantly to energy density in FR's.

The source region, where $\Sigma^\nu \neq 0$ and $\sigma \neq 0$, lies between the hyperbolas $t^2-x^2 = \tau_0 = 1$ and $(t-d_t)^2 - x^2 = \tau_0 = 1$ where the particles from the first and last collisions materialize. Thus the width of the source region in time direction is d_t. In x the source extends to $|x| = x_{max} = \tau_0 \sinh y_{max}$ with y_{max} = maximum rapidity of the produced particles. For nucleons $y_{max} = y_B^*$. In Fig. 3a the source region is shown for $y_B^* = 3.4$.

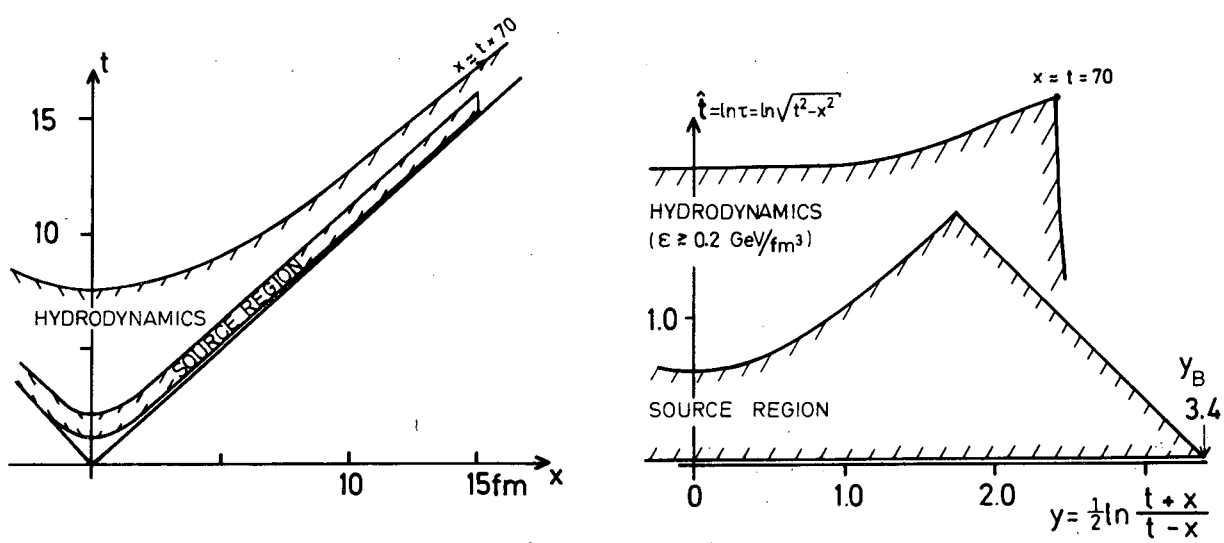

Fig. 3. Source region for central uranium-uranium collision (a) in (x,t)-plane and (b) in $(y,\hat{t})$-plane. The extend of the hydrodynamic region (defined by $\varepsilon \gtrsim 0.2$ GeV/fm^3) is also indicated.

Instead of x and t, we have used variables

$$\hat{t} = \tfrac{1}{2}\ln\frac{t^2-x^2}{\tau_0^2} = \ln\frac{\tau}{\tau_0} \quad \text{and} \quad y = \tfrac{1}{2}\ln\frac{t+x}{t-x}\,. \tag{8}$$

These are convenient in several ways. The source region and the whole region of hydrodynamic expansion become compact and regular (see Fig. 3b) simplifying the numerical integration of hydrodynamic equations and the presentation of results. Moreover the interpretation of results is facilitated by the fact that y does not deviate much from the rapidity field

$$\theta(x,t) = \tfrac{1}{2}\ln\frac{1+v(x,t)}{1-v(x,t)} \tag{9}$$

of the flow.

The plot of the source region in terms of y and $\hat{t}$, Fig. 3b, shows also clearly the difference in production time between the CR and FR's. The shape of the source region (especially the height in $\hat{t}$) for a fixed distance from the endpoints $|y| = y_B^*$ is essentially independent of energy; the increase of energy just streches the central region and makes it narrower around y = 0.

So far we have neglected the multiple interactions between the colliding nucleons. If the above model is applied to h+A scattering, the incoming hadron would interact once and in addition the slow secondaries, which have time to materialize within the nucleus, would cascade. This cascading is not enough to reproduce the observed enhancement in the central rapidity region and the colliding hadron is known to suffer several interactions when traversing the nucleus. E.g. in the context of the multi-chain dual parton model this corresponds to an excitation of extra hadron chains between the slow colored fragments of colliding nucleons[16]. For central collisions the resulting rapidity distribution in the CR behaves as $\rho_{AA}^{\pi}(y) \propto A^{3/4}$.

To see the effect of enhanced central production on the expansion, we use the following modification for the input pion distribution:

$$\rho_\pi(y) \to [\tfrac{1}{2}+\tfrac{1}{2}A^{\alpha(y)}]\rho_\pi(y) \quad , \quad \alpha(y) = \tfrac{1}{2}\exp\{-(y/1.5)^2\} \tag{10}$$

At $y \approx 0$, the multiplicative factor is $\tfrac{1}{2}+\tfrac{1}{2}A^{1/3}$ and it goes to 1 in FR's. This factor does not take into account the smearing of the collision region from the line $x = 0$ as shown in Fig. 4, which may somewhat slow down the expansion in the CR[17].

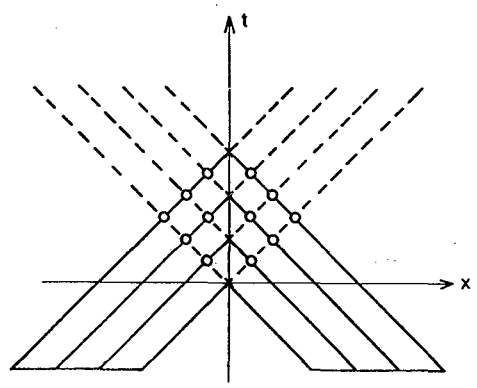

Fig. 4. Collision region in A+A reaction with multiple scatterings.

4. Results.

The numerical methods which we have employed, are explained in details in Ref. 7. The parameters which enter the calculations are:

E_{CM} = 14 GeV/nucleon corresponding to $y_B = 2y_B^* = 6.8$
nuclear radius $R_A = r_0 A^{1/3}$, $r_0 = 1.1$ fm
nuclear density $n_0 = A/V_A = 0.18$ 1/fm^3
pion transverse mass $\bar{m}_\pi = 0.5$ GeV
pion plateau height (all charges) $\rho_0 = 2.4$

The results refer to the region close to the collision axis in a central uranium-uranium collision. This means that even in such collisions all of the produced matter (at given y), will not reach as high energy densities as shown below; a fact that should be kept in mind when estimating signals.

For the case of A independent N+N collisions (case (A)) the contour plots of the resulting energy density ε, baryon number density n_B and the difference of flow rapidity field θ and the variable y are shown in Fig. 5a, b and c, respectively. The energy density for enhanced central production (case (B)) is shown in Fig. 6. The baryon number density in case (B) is similar to that of case (A) since we modified the pion distribution only. If the conservation of energy were imposed in case (B), it would slow somewhat the baryon number distribution. Flow rapidities are qualitatively similar in both cases[7].

The results of Fig.'s 4 and 5 are calculated with the simple equation of state $p = 1/3\ \varepsilon$. We have done the calculation[7] also with a naive bag model equation of state, $p = 1/3\ \varepsilon$ for $T < T_c$ and $p = 1/3(\varepsilon - 4B)$ for $T > T_c$, where B is the bag constant and T_c the critical temperature. The expansion in the first case is a little faster than in the second but the differences are certainly smaller than uncertainties due to the lack of knowledge of the details of production mechanism. The insensitivity of the rate of expansion to the equation of state is a consequence of the fast initial expansion.

Let me summarize the main features of the results in the high energy uranium-uranium collision:

(1) In the source region the energy (baryon number) density grows as the produced particles enter the hydrodynamic stage. The growth is fastest in CR and slows down towards the FR's as the total production time increases from $\Delta\tau_{CR} \sim 0.9$ fm/c to $\Delta\tau_{FR} \sim 5$ fm/c in FR's (cf. Fig. 3b). From the time dependence in the CR we see that at $\tau \sim 5$fm/c ($t \sim 1.6$) the energy density has been diluted to $\sim 1/4$ of the maximum value, $\varepsilon_{max} \sim 1.8$ GeV/fm^3 at $\tau \sim 1.9$ fm/c. A comparable dilution of the previously produced matter in FR's is going on at the same time as new matter is produced there, offsetting to a large extent the growth of the energy density. As a result the maximum energy density which is achieved in FR's is much smaller than that in the CR and also much smaller than originally estimated by Anishetty et al.[18].

(2) The baryon number density peaks in theFR's reflecting the leading particle character of the input spectrum $\rho_N(y) \propto$ chy (in CM frame). Its maximum value 0.36 corresponds to a compression factor 0.36/0.18 = 2 to be compared with 3.6 from the fireball analysis[18].

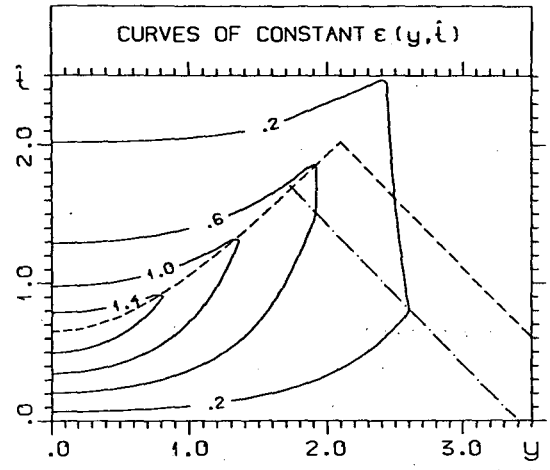

(a)

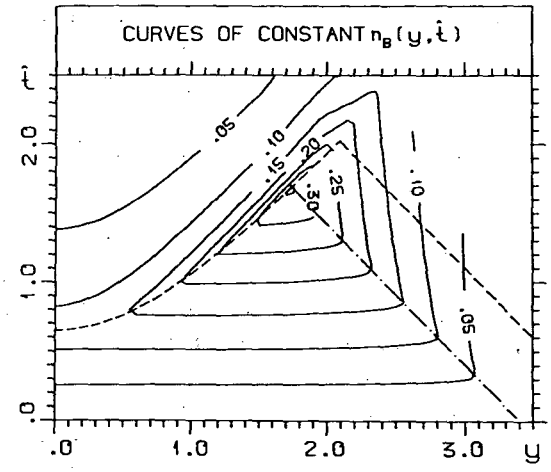

(b)

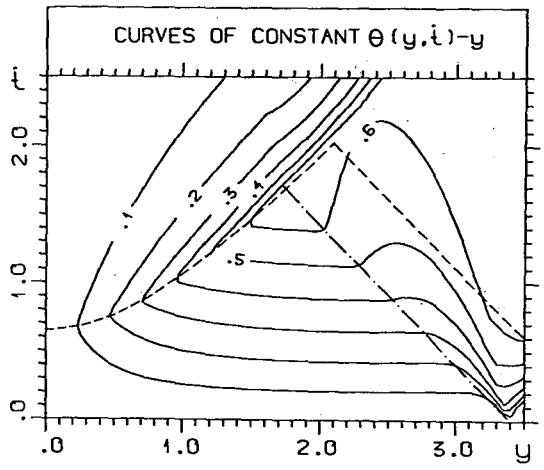

(c)

Fig. 5. Contour plots of ε, n_B and θ-y (a, b and c, respectively) in the case of A independent N+N collision, case (A). The maximum value of ε at y = 0 and $\hat{t} \approx 0.6$ ($\tau \approx 1.9$ fm/c) is $\varepsilon_{max} \approx 1.8$ GeV/fm^3.

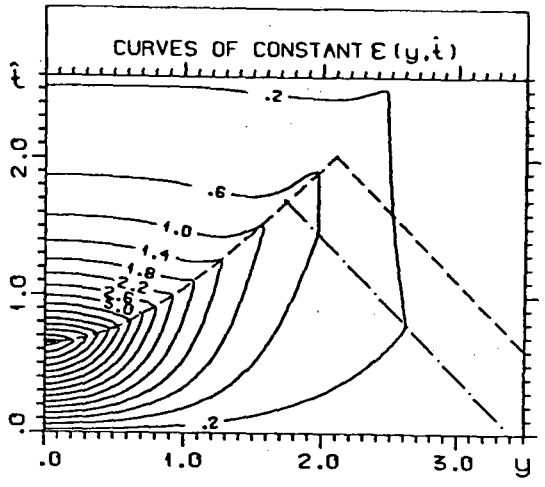

Fig. 6. Contour plot of ε in the case of enhanced central production, case (B). Now $\varepsilon_{max} \approx 6.0$ GeV/fm^3.

(3) For the case (B) the solution at $y \approx 0$ is roughly three times the solution of case (A). In FR's, $|\theta| \geq 2.0$, the maximum energy densities are essentially the same. One should notice that the final rapidity distribution of the emerging particles is not the same as the rapidity distribution in the production. The effect of the hydrodynamics is to accelerate the expansion and thus to broaden the distribution.

(4) On the basis of h+A data it seems reasonable to argue that the case (A) gives a lower bound for the maximum energy density in the CR. We then conclude that the energy density will be high enough for the formation of the QCD-plasma. However, the duration of high energy densities, $\varepsilon \gtrsim 2$ GeV/fm^3, is very short and may not be longer than the timescale of the phase transition. It appears, that the lifetime of the pure QCD-plasma will be extremely short.

(5) In FR's ($\theta \gtrsim 2$), the energy densities are not high enough for the formation of QCD-plasma. The results on baryon number density should be considered as giving the upper bound for the maximum value. This is due to the fact, that as the baryon distribution slows down due to the enhanced central production, it will most probably also spread more in rapidity.

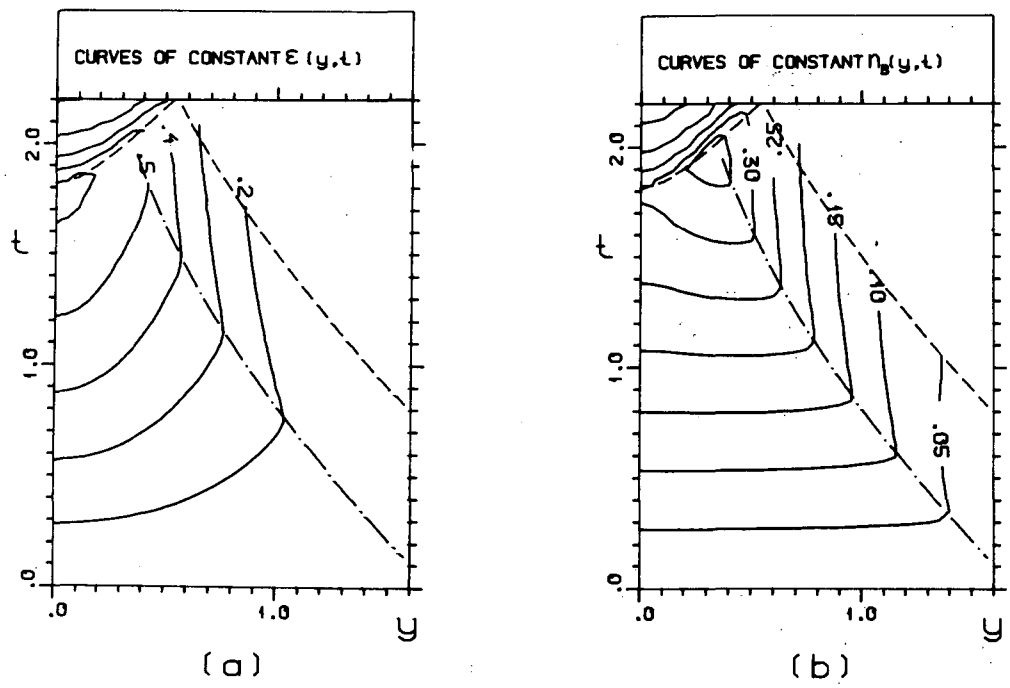

Fig. 7. Contour plots of energy density (a) and baryon number density (b) at E = 14 GeV/nucleon on fixed taget in case (A).

In Fig. 7a and b the results on ε and n_B are shown for a calculation in case (A) except that $y_B = 2y_B^* = 3.4$, corresponding to a collision energy E = 14 GeV/nucleon on fixed target. The model is not really applicable in this situation, but I want to emphasize the importance of the energy range $E \sim 10$ GeV/nucleon on fixed target, if we want to study hadronic matter at high baryon number densities. Fig. 7b shows that the fragmentation regions are fusing to-

gether even though we have assumed the case of extreme transparancy. However, in addition to the multiple scattering between the incoming nucleons, they will collide also with the produced particles. This is illustrated in Fig. 8.

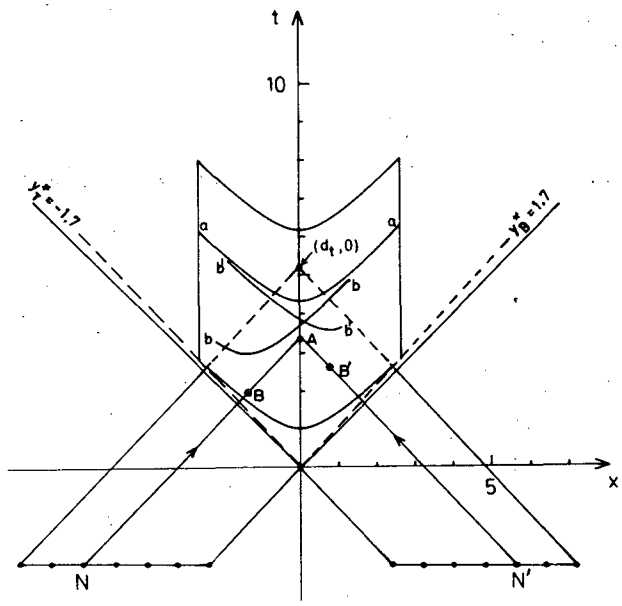

Fig. 8. Space-time illustration of a medium energy uranium-uranium collision showing the overlap of collision region and source region. This indicates that collisions between primary nucleons and produced secondary particles can not be neglected as is done at ultrarelativistic energies (cf. Figs. 2 and 4).

The incoming nucleons N and N', instead of colliding with each other at the point A and producing particles on the hyperbola aa, may collide at points B and B' with particles which have materialized from earlier collisions. Particles from these collisions are produced along the hyperbola bb and bb'. As a result particles are produced within smaller volume and earlier in time; the fragmentation regions will fuse together leading to larger baryon number densities than those attainable at high collision energies.

On the basis of these (non)results it is not possible to say if the energy density will be high enough for the phase transition, but it seems that it is higher than that at n_B^{max} in the high energy collisions (cf. Fig. 5). The cascading of the secondaries may also slow down the initial velocity of the expansion and lead to a longer overall expansion time. Anyway, it seems that medium energies are the only chance we have to achieve high baryon number densities together with reasonably high energy densities and they certainly merit further studies[15].

4. Conclusions and comments

I have argued for the use of the source terms instead of just the initial boundary conditions when hydrodynamics is used to describe the evolution of the final state matter in heavy ion collisions. This is essential in FR's in order to account properly for the initial velocity gradient and for the expansion during the long production period.

According to our results energy densities well above 2 GeV/fm^3 are quite plausible in the CR but in the FR's energy densities will not reach high enough values for the phase transition to QCD-plasma to occur. The expansion time scale is dominated by the initial expansion and is short enough that the neglect of the transverse flow seems justified. In estimating different singnals from the plasma it is not justified to use $R_A/c_s \sim \sqrt{3}\, R_A$ = time for the transverse rarefaction wave to reach the collision axis as the lifetime of the plasma.

In high energy collisions the baryon number is spread in rapidity and high baryon number densities are not reached ($n_B \gtrsim 0.4/\mathrm{fm}^3$). The only region to study high baryon number densities are the medium energies ($\sim$ 10 GeV/nucleon on fixed target) where energy densities still are high enough for the formation of mixed phase.

I do not have much to say about the signals but I should like to divide them into two groups; signals directly related to the existence of the quark-gluon plasma and signals related to the phase transition if it is of the first order.

Examples of the signals in the first group are the thermal production of l^+l^--pairs and photons in the plasma and enhancement of strange particles. First of all, according to our results these signals are confined to the CR whereas several estimates are based on the fireball analysis and predict them in the FR's. Their strength is difficult to estimate because they depend strongly on the achieved temperature which we do not know very well due to the uncertainties in the production. They all have backgrounds and the ratios of signals to their backgrounds depend in addition to the achieved temperature also on the lifetime of the plasma and on the fraction of matter which can experience the phase transition. Our results refer to the situation close to the collision axis in a central collision. Off the axis the densities will be smaller. E.g. in the case (A) the maximum energy density for a large fraction of produced matter even at $y \sim 0$ would be well below 2 GeV/fm^3. From the point of view of these signals the difference between the cases (A) and (B) is large. Even though the production of quark-guon plasma may not be possible in an A'+A collision, with A' a light nucleus, the results would tell us what to expect in the CR when both nuclei are heavy.

Signals in the second group are based on the properties of the first order phase transition. In the mixed phase temperature T = critical temperature T_c and this might be reflected in the behaviour $p_\perp$-spectrum of produced particles[19] or in the spectrum of radiated photons[20] as the maximum energy density increases. The first order phase transition may proceed through the formation of shock waves[21,22] which might lead e.g. to large fluctuations in rapidity spectra. The plus side of these signals is that they do not depend

critically on the plasma lifetime or the maximum temperature which is achieved but on the other hand it is difficult to judge how conclusive they are.

I should like to thank the organisers of this Workshop for a most stimulating meeting and the LBL Nuclear Science Division for the hospitality. In addition to my collaborators K. Kajantie and R. Raitio, I have benefited much from discussions with A. Capella, M. Guylassy, H. Satz and H. Sumiyoshi.

References

1. For a general reference see M. Jacob and H. Satz (editors) "Quark Matter Formation and Heavy Ion Collisions", Proceedings of the Bielefeld Workshop, May 1982, World Scientific.

2. B. Svetitsky and L. G. Yaffe, Nucl. Phys. B210 [FS6] (1982) 423.

3. T. Çelik, J. Engels and H. Satz, Univ. of Bielefeld preprint BI-TP 83/04, March 1983.

4. See, however, T. A. DeGrand and C. E. DeTar, Contribution to this Workshop.

5. T. Çelik, J. Engels and H. Satz, Univ. of Bielefeld preprint, May 1983; J. Kogut et al., University of Illinois preprint, ILL-(TH)-83-9, April 1983.

6. G. Domokos and J. Goldman, Phys. Rev. D23 (1981) 203;
K. Kajantie and H. I. Miettinen, Z. Phys. C9 (1981) 341 and C14 (1982) 357:
E. Shuryak, Yad. Fiz, 28 (1978) 796;
F. Halzen and H. C. Liu, Phys. Rev. D25 (1982) 1842;
J. Cleymans, M. Dechantsreiter and F. Halzen, Z. Phys. C17 (1983) 341;
J. Rafelski and B. Müller, Phys. Rev. Lett. 48 (1982) 1066;
T. Biro and J. Zimanyi, Phys. Lett. 113B (1982) 6.

7. K. Kajantie, R. Raitio and P. V. Ruuskanen, Nucl. Phys. B222 (1983) 152.

8. G. Baym, these proceedings.

9. J. D. Bjorken, in "Current-Induced Reactions", Proceedings of the DESY International Summer Institute on Theoretical Physics, Hamburg 1975, edited by J. G. Körner, G. Kramer, and D. Schildknecht;
L. McLerran in Ref. 1;
J. D. Bjorken, Phys. Rev. D27 (1983) 140.

10. K. Kajantie and L. McLerran, Phys. Lett. 119B (1982) 203; Nucl. Phys. B214 (1983) 261.

11. G. Baym, B. L. Friman, J.-P. Blaizot, M. Soyer, and W. Czyż, Nucl. Phys. A, in press.

12. P. V. Ruuskanen, Invited talk at the XIV International Multiparticle Symposium, Lake Tahoe , June 1983, Univ. of Bielefeld preprint NI-TP 83/09.

13. M. A. Faessler, Ann. of Phys. 137 (1981) 44;
C. De Marzo et al., Phys. Rev. D26 (1982) 1019;
W. D. Shephard, contribution to the XIV International Multiparticle Symposium, Lake Tahoe , June 1983.

14. L. Landau, Izv. Akad. Nauk SSSR 17 (1953) 51.

15. M. Guylassy, Invited talk at the XIV International Multiparticle Symposium, Lake Tahoe, June 1983.

16. A. Capella, C. Pajares, and A. V. Ramallo, contribution to this Workshop.

17. H. Sumiyoshi, contribution to this Workshop;
T. Ochiai, S. Date, N. Suzuki, O. Miyamura, and H. Sumiyoshi, Univ. of Tokyo preprint, INS-Rep.-471, May 1983.

18. R. Anishetty, P. Koehler, and L. McLerran, Phys. Rev. D22 (1980) 2793.

19. L. Van Hove, Phys. Lett. B118 (1982) 138.

20. V. V. Dixit, H. Satz, E. Suhonen, Z. Phys. C14 (1982) 275.

21. M. Guylassy in Ref. 1;
L. Van Hove, CERN preprint TH-3592;
M. Guylassy, K. Kajantie, H. Kurki-Suonio, and L. McLerran, Deflagration and Detonation as Mechanisms of Hadron Bubble Growth in Supercooled Quark-Gluon Plasmas, to appear.

TRANSVERSE EXPANSION AT CENTRAL RAPIDITIES IN ULTRA-RELATIVISTIC HEAVY ION COLLISIONS*

Gordon Baym

Department of Physics
University of Illinois at Urbana-Champaign
Urbana, Illinois 61801 U.S.A.

Abstract

This talk describes the transverse hydrodynamic expansion of the central rapidity regime in a central ultra-relativistic heavy ion collision. The hydrodynamic equations, and numerical and analytic solutions for the expansion are presented. The formation of a "condensation discontinuity" in the dynamical phase transition from a quark-gluon plasma to hadronic matter, and the final freezeout to free-streaming hadrons, are also briefly discussed.

1. Introduction

Central collisions of heavy ions at ultra-relativistic energies ($\sqrt{s} \gtrsim$ 25-50 GeV per nucleon) are expected,[1] as described by Ruuskanen in his talk,[2] to develop a regime at central rapidities having small net baryon number, between two baryon-rich nuclear fragmentation regions (Fig. 1), a structure similar to that observed in pp scattering at the ISR.[3] Following the collision the central rapidity region will undergo longitudinal expansion along the collision (z) axis, with accompanying transverse rarefaction. In this talk I would like to review work carried out with J.-P. Blaizot, W. Czyż, B. Friman, and M. Soyeur[4] to understand, within the framework of hydrodynamics, the nature of the transverse expansion of the central rapidity regime.

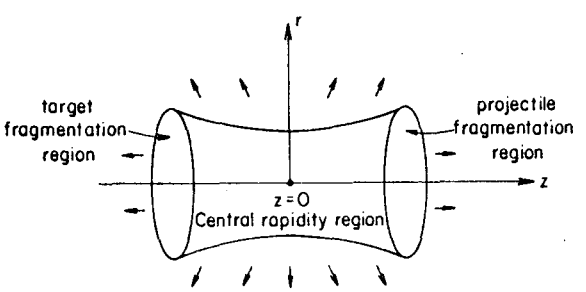

Fig. 1

In the central regime one can, to a first approximation, neglect the finite thickness of the fragmentation regions, and assume, with Bjorken,[1] approximate Lorentz invariance at small rapidities, which is the statement that conditions at a given point z depend only on the local proper time

$$\tau = (t^2 - z^2)^{1/2} \tag{1}$$

* Research supported in part by NSF Grant DMR81-17182.

at that point. While not crucial, this latter assumption, related to the existence of a central plateau in the final multiplicity versus rapidity, greatly simplifies the analysis of the problem. We also assume that local thermalization of the excitations produced in the collision takes place by a proper time $\tau_o \sim 1$ fm, after which a hydrodynamic description becomes valid. Thus the initial conditions on the hydrodynamics are constant energy density $\varepsilon = \varepsilon_o$ and initial flow velocity $v_z = z/t$ at $\tau = \tau_o$. A space-time diagram of the collision, Fig. 2, illustrates the hydrodynamic regime after proper time $\tau = \tau_o$, together with the subsequent hadronization transistion and eventual "freezeout" of the system from collision-dominated to free-streaming hadrons.

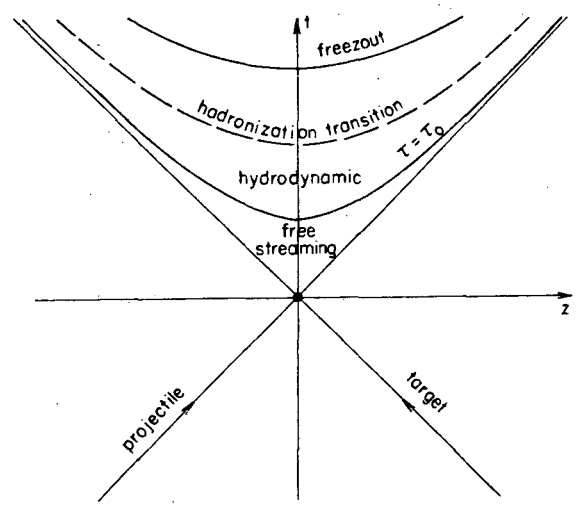

Fig.2

For proper times short compared with the sound travel time, R_A/c_s, across a nuclear radius R_A, where c_s is the sound velocity of the matter, the dominant motion of the central regime is its longitudinal expansion. Since the hydrodynamic equations preserve the Lorentz-invariant character of the initial boundary conditions, the longitudinal expansion obeys a simple scaling solution[1]

$$s(\tau) = s_o \tau_o/\tau \ , \quad v_z = z/t \ , \tag{2}$$

where s is the local entropy density, and $s_o = s(\tau_o)$.

2. Hydrodynamic equations

In the central regime, where the net baryon density vanishes to a first approximation, the hydrodynamic equations are the conservation laws for energy and momentum

$$\partial_\mu T^{\mu\nu}(x) = 0, \tag{3}$$

where, in the absence of dissipation, the stress tensor is given by

$$T^{\mu\nu} = (\varepsilon + P)u^\mu u^\nu + Pg^{\mu\nu} \ ; \tag{4}$$

P is the pressure, $g^{oo} = -1$, and the four-velocity $u^\mu = \gamma(1,\underset{\sim}{v})$, with $\underset{\sim}{v}(x)$ the local flow velocity, and $\gamma = (1 - v^2)^{-1/2}$.

For simple one dimensional motion, Eqs. (3) assume the form

$$\frac{\partial}{\partial t}(s \cosh y) + \frac{\partial}{\partial z}(s \sinh y) = 0$$
$$\frac{\partial}{\partial t}(T \sinh y) + \frac{\partial}{\partial z}(T \cosh y) = 0 \ , \tag{5}$$

where T is the temperature and $y = \tanh^{-1} v_z$ is the hydrodynamic rapidity; when Lorentz invariant boundary conditions are imposed, these equations have the scaling solution (2).

The underlying Lorentz invariance greatly simplifies the problem of the coupling of the longitudinal and transverse expansions, since the transverse motion for any z in the central rapidity regime can be found from that at z = 0, the "central slice," by a Lorentz boost along z. Using $v_z = z/t$, one finds from (3) that at z = 0, with cylindrically symmetric transverse geometry, the hydrodynamic equations (in cylindrical coordinates) are:[4]

$$\frac{\partial}{\partial t}(rts \cosh \alpha) + \frac{\partial}{\partial r}(rts \sinh \alpha) = 0$$

$$\frac{\partial}{\partial t}(T \sinh \alpha) + \frac{\partial}{\partial r}(T \cosh \alpha) = 0, \qquad (6)$$

where $\alpha = \tanh^{-1} v_r$ is the transverse rapidity variable. The "rt" is just the phase space factor for cylindrical coordinates with longitudinal expansion of the scaling form.

Equations (6) can also be cast into characteristic form, useful for numerical solution, as

$$\frac{\partial}{\partial t} a_\pm(r,t) + \frac{v_r \pm c_s}{1 \pm v_r c_s} \frac{\partial}{\partial r} a_\pm(r,t) + \frac{c_s}{1 \pm v_r c_s}\left(\frac{v_r}{r} + \frac{1}{t}\right) a_\pm(r,t) = 0, \qquad (7)$$

where

$$a_\pm = e^{\Phi \pm \alpha}, \qquad (8)$$

and the potential $\Phi(T)$ is defined by

$$d\Phi = \frac{d\ell nT}{c_s} = c_s d\ell ns. \qquad (9)$$

3. Transverse expansion

Full numerical solutions of Eqs. (7) for the transverse motion are described in detail in Ref. 4. For an ideal gas equation of state, $P \propto T^4$, the temperature distributions at z = 0, in terms of the initial temperature T_o, evolve as shown in Fig. 3 (where τ_o = 1 fm and R_A are assumed); the curves are labelled by the time. The corresponding transverse velocities are shown in Fig. 4. As we see in Fig. 3, the radial expansion causes an inwardly propagating rarefaction wave (the corners at small r on the curves at 4, 7 and 10 fm). A primary conclusion to be drawn from these calculations is that the accompanying longitudinal expansion leads to an overall rapid cooling of the matter; interior to the rarefaction front the cooling is uniform. A quark-gluon plasma, if produced, will last a relatively short time. In addition, the final transition from collision-dominated to free-streaming hadronic matter will take place fairly close to the collision volume, before the matter undergoes appreciable transverse acceleration. Thus one expects relatively small effects of the transverse expansion on the final observed momentum distributions.

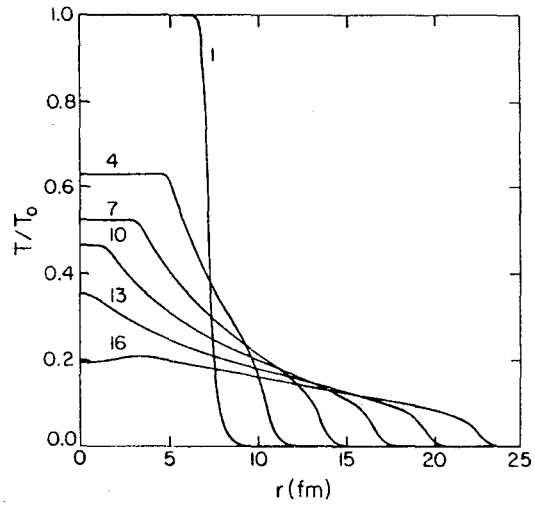

Fig. 3

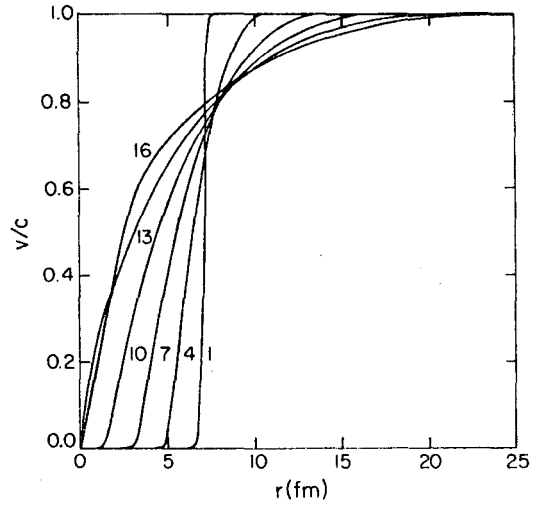

Fig. 4

While the calculations described above were done numerically, one can, in fact, construct a useful analytic solution to the transverse motion by noting that the general behavior of the temperature and velocity is that of a scaled Riemann expansion:

$$T(r,t) = T_R(r,t)\left(\frac{t_o}{t}\right)^{c_s^2} , \qquad v(r,t) = v_R(r,t) \quad , \tag{10}$$

where

$$\begin{aligned} T_R &= T_o\left(\frac{t-r+R_A}{t+r-R_A}\,\frac{1-c_s}{1+c_s}\right)^{c_s/2} && : \quad r > R_A - c_s t \\ &= T_o && : \quad r < R_A - c_s t \end{aligned} \tag{11}$$

is the simple one-dimensional Riemann expansion solution, R_A is the initial nuclear radius, and T_o the initial temperature; in Eqs. (10) and (11) the sound speed c_s is assumed constant. The flow velocity in the Riemann wave is

$$\begin{aligned} v_R(r,t) &= \tanh^{-1}\alpha_R = \frac{r-R_A + c_s t}{t+c_s(r-R_A)} && : r > R_A - c_s t \\ &= 0 && : r < R_A - c_s t. \end{aligned} \tag{12}$$

The scaling factor $(t_o/t)^{c_s^2}$ in the temperature (10) reflects the entropy density falloff described by the scaling solution (2). Using (10) as a first approximation in an iteration of the characteristic equations (7), one finds that the transverse expansion is given quite accurately, over the times of interest, by the approximate analytic solutions:

$$T(r,t) = T_R(r,t)\left(\frac{t_o}{t}\right)^{c_s^2\left[1+(1-v_R(r,t)c_s)^{-1}\right]/2} \tag{13}$$

and

$$\alpha(r,t) = \alpha_R(r,t) + \frac{c_s^2}{2}\,\frac{v_R(r,t)}{1-v_R(r,t)c_s}\,\ln\frac{t}{t_o} \; . \tag{14}$$

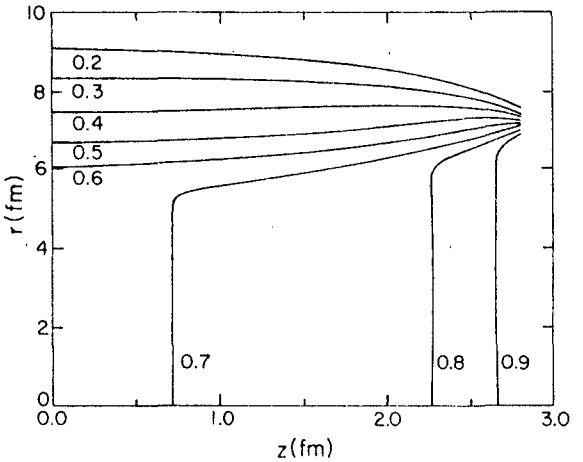

Fig. 5

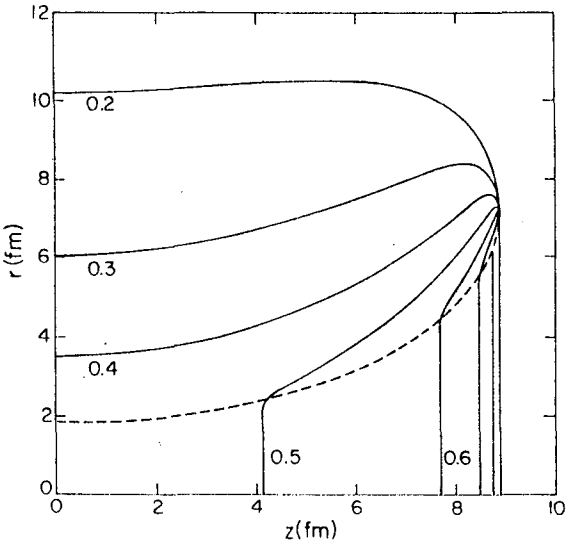

Fig. 6

4. Hadronization transition in the transverse expansion

The calculations discussed above describe the behavior of the central slice, z = 0. An overall picture of the thermal evolution of the central region is given in Figs. 5 and 6, which show, in the z,r plane, isotherms (labelled by T/T_o) at t = 3 fm (Fig. 5) and t = 9 fm (Fig. 6). The dashed curve in Fig. 6 represents the inwardly propagating rarefaction wave. We see from these curves the geometry in the collision volume of the (de)confinement transition from a quark-gluon plasma to hadronic matter. If, for the sake of illustration, we assume the transition to occur at $T_c = 0.6T_o$, then in Fig. 5 the outer regions beyond r = 6 fm have undergone the transition, while the interior regions remain in the deconfined phase; on the other hand, at the later time shown in Fig. 6, the entire central regime to z ~ 7.5 fm has undergone the transition. At earlier times the transition occurs as a consequence of the transverse expansion, while at later times it is driven by the longitudinal cooling, as illustrated by the vertical segment of the $T/T_o = 0.6$ isotherm.

If the deconfinement transition is first order. then as matter goes through the transition in transverse expansion, the flow will develop a shock-like entropy-producing discontinuity across the transition.[5*] By contrast the one-dimensional scaling solution is stable against small perturbations and

---

* Entropy production across the deconfinement phase transition is discussed from a general point of view by Csernai,[6] while Gyulassy et al.[7] have presented a classification of the possible subsonic and supersonic flows when the phase transition occurs dynamically. Estimates of the entropy production and acceleration across the transition similar to those of Ref. 5 (described below) have been given independently by Van Hove.[8]

exhibits no instability against formation of growing infinitesimal discontinuities across the transition.[4]

Let us assume that the equation of state has a jump in entropy at the phase transition temperature T_c, from s_h in the hadronic phase to s_q in the quark phase. To see how a discontinuity develops in the transverse expansion, we note that in a Riemann-like expansion the pattern velocity moves at sound speed inward, in the frame in which the matter is at rest. However, across the two phase region of a first order phase transition, between s_h and s_q, the sound velocity $c_s = (\partial \ln T/\partial \ln s)^{1/2}$ vanishes. Hence as shown in Fig. 7a, a plot of entropy versus transverse coordinate (x or r), a Riemann-like flow (see particularly the curves labelled t = 4 and 7 fm in Fig. 3) will develop a flat portion at the purely quark end (entropy density s_q) of the two phase region, and will "crest" and thus form a discontinuity across the purely hadronic end (entropy density s_h) of the two phase region. A fully developed discontinuity, shown in Fig. 7b, extends from the pure quark phase, at entropy s_q, to a point cooler than the hadronic phase at the static transition; at this point the flow velocity of the hadronic matter with respect to the discontinuity must be the sound speed of the hadronic matter there (the Jouget point), in order that the discontinuity no longer gains on the pattern in the hadronic matter. [If the quark phase supercools then s_q becomes the entropy of the quark phase at the point where it makes a transition.]

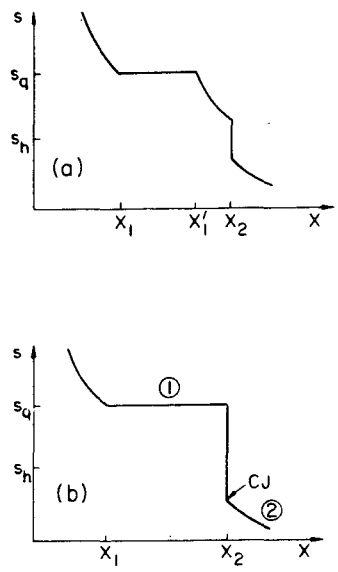

Fig. 7

To determine the entropy production and acceleration of the matter across the transition, which we assume to be a fully developed discontinuity, we apply the conditions that the stress tensor components T^{or} and T^{rr} be continuous across the discontinuity, in its rest frame, denoted by primes. Using (4) we have

$$T_c s_q \gamma_1'^2 v_1' = \frac{T_2 s_2 c_{s2}}{1 - c_{s2}^2} \tag{15}$$

$$P_c + T_c s_q \gamma_1'^2 v_1'^2 = P_2 + \frac{T_2 s_2 c_{s2}^2}{1 - c_{s2}^2} , \tag{16}$$

where 1 and 2 denote the upper and lower phases, $P_1 = P_c$ is the critical pressure at T_c, continuous across the discontinuity in the equation of state, and $v_2' = c_{s2}$, the sound speed. For the special case that below T_c the matter is an ideal massless gas, then the solution of (15) and (16) with non-negative entropy generation, $s_q \gamma_1' v_1' \leq s_2 \gamma_2' v_2'$, is

$$v_1' = \frac{\sqrt{3} - \left(3 - 16\xi + 16\xi^2\right)^{1/2}}{4(1 - \xi)} , \tag{17}$$

$$\left(\frac{T_2}{T_c}\right)^4 = \frac{\gamma_1'^2 v_1'}{2\sqrt{3}\,\xi} = \frac{1}{3 - 2\sqrt{3}\,v_1'} , \tag{18}$$

where $\xi = P_c/T_c s_q$. The entropy generation, measured by

$$R = \frac{s_2\gamma_2' v_2'}{s_q\gamma_1' v_1'} = \left(\frac{4}{3}\right)^{1/4}\left(1 - 2v_1'/\sqrt{3}\right)^{1/4}\gamma_1' , \tag{18}$$

decreases from 1.075 to 1 as v_1' increases from 0 to $1/\sqrt{3}$. The entropy generated in the shock is at most 7.5% of the incident entropy, and is closer to 6% for a transition with T_c = 200 MeV and latent heat[9] $\Delta\varepsilon$ = 1.5 GeV/fm^3 (corresponding to $\xi \sim 0.04$).

The matter, in passing through the discontinuity, is accelerated by the release of latent heat, and one finds from (15) and (16) that for small ξ the increase in transverse rapidity α is

$$\alpha_2 - \alpha_1 = 0.66 - 2\xi/\sqrt{3}, \tag{19}$$

on the order of 0.6 units.

5. Freezeout

As the matter expands in the hadronic phase the collision rates fall to the point where the matter can no longer maintain itself in thermal equilibrium, and it undergoes "freezeout" to a free-streaming gas. Even while evolving in the collision-dominated phase the matter cannot maintain perfect "chemical" equilibrium. To see this, assume that the hadronic matter emerging from the deconfinement transition is a purely pion gas with zero chemical potential. Then as the gas expands and cools, elementary thermodynamics implies that, as a consequence of the non-zero pion rest mass, the entropy per pion, $s/\left(n_{\pi^0} + n_{\pi^-} + n_{\pi^+}\right)$, must increase if zero chemical potential is to be maintained. This requires the number of pions in a co-moving volume to decrease. However, the most rapid process that can destroy pions is $4\pi \to 2\pi$, which by phase space considerations must be negligibly slow on expansion time scales. The total number of pions in a co-moving volume, and hence the entropy per pion, remains fixed, and the distribution shifts in the expansion to one with positive chemical potential for all three pion components.

The freezeout process is itself a possibly important source of entropy in the final distribution. As the system begins to decouple and mean free paths λ grow compared to the system scale size, R, the rate of entropy production increases, $\sim \lambda$, reaching a maximum when $\lambda \sim R$, then falling off as λ^{-1} for $\lambda \gg R$. The net increase in entropy appears, from preliminary estimates, to be a non-negligible fraction of the initial entropy. Quantitative estimates will be published shortly.[9]

References

1. J. D. Bjorken, Phys. Rev. D27 (1983) 140.
2. P. V. Ruuskanen, this volume.
3. Reviewed in L. Van Hove and M. Jacob, Phys. Reports 62 (1980) 1.
4. G. Baym, B. L. Friman, J.-P. Blaizot, M. Soyeur and W. Czyż, Nucl. Phys. A (1983) in press.
5. B. L. Friman, G. Baym and J.-P. Blaizot, Phys. Letters B (1983) in press.
6. L. P. Csernai, this volume.
7. M. Gyulassy, K. Kajantie, H. Kurki-Suonio and L. McLerran, preprint LBL-16277 (1983).
8. L. Van Hove, CERN preprint TH.3592 (1983).
9. J. Kogut, H. Matsuoka, M. Stone, H. W. Wyld, S. Shenker, J. Shigemitsu and D. K. Sinclair, Phys. Rev. Letters 51 (1983) 869.
10. G. Baym, G. Bertsch, B. L. Friman and S. Gavin, to be published.

Shock fronts without thermalization in ultrarelativistic heavy-ion reactions

L.P. Csernai
Central Research Institute for Physics, Budapest, Hungary

If we study a heavy-ion reaction at ultrarelativistic energies $E > 10$ GeV/nucleon, in lab. frame the collision proceeds as follows 1): The Lorentz contracted projectile passes through the target with almost the speed of light. Since the free N-N cross section is very much forward peaked, we assume that the two heavy-ions penetrate through each other with only a small momentum loss and only a minor part of the initial kinetic energy will be thermalized inside the projectile or target remnants. Our aim is to describe the target and projectile fragmentation regions in a simple model. It is assumed that the Lorentz contracted projectile in the target frame can be represented as a shock front which, however, contrary to the ordinary compression shock (CS) transmits energy and momentum to the target matter. (Fig. 1)

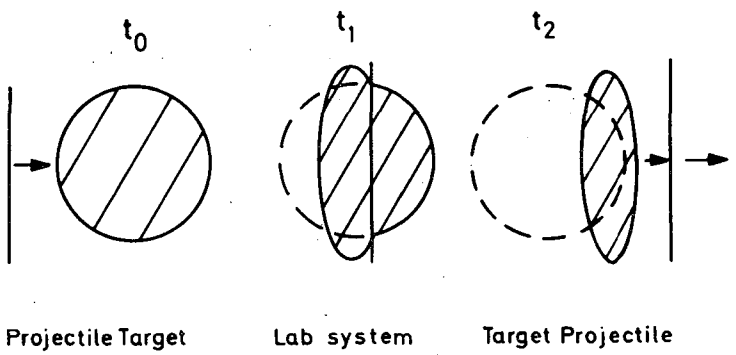

Fig. 1

Now the conservation laws across the shock front for energy, momentum and baryon charge can be formulated as:

$$-c\,[T_{0x}] = c\,[w\beta\gamma^2] = \alpha\, w_0 \gamma_0 \sqrt{\gamma_0^2 - 1}$$

$$[T_{xx}] = [w\beta^2\gamma^2 + p] = -\delta' \left(w_0 (\gamma_0^2 - 1) + p_0\right)$$

$$[j_{Bx}] = [n\beta\gamma] = 0$$

where the square bracket denotes the difference of a quantity a before and behind the shock in its frame, $[a] = a_1 - a_0$, w is the enthalpy density, p is the pressure, and α and δ' are the parameters expressing how much part of the initial projectile energy and momentum is absorbed by the target ($0 < \alpha, \delta' \ll 1$). For this type of passing shock (PS) the relativistic shock adiabat can be derived 2):

$$\left\{ p_1 - p_0 (1-\delta') \right\} \left\{ \frac{w_1}{n_1^2} + \frac{w_0}{n_0^2}(1+\alpha) \right\} \left\{ \frac{w_1}{n_1^2} - \frac{w_0}{n_0^2}(1+\alpha) \right\} =$$

$$= \left\{ \frac{w_1^2}{n_1^2} - \frac{w_0^2}{n_0^2}(1+\alpha)^2 \right\} \left\{ \frac{w_1}{n_1^2} - \frac{w_0}{n_0^2}(1-\delta') \right\}$$

having the same or similar properties as the shock or Rankine-Hugoniot adiabat. Plotting this shock adiabat on the pressure p, generalized specific volume w/n^2 plane we obserwe that the shock adiabat of the nuclear matter goes through the point $(p_o, w_o/n_o^2)$ representing the initial state, and the final state is given by the intersection with the $j_B^2 = n_o^2 \, sh^2 y_o = (p_1 - p_o)(1-\delta')/(w_1/n_1^2 - w_o(1-\delta')/n_o^2)$ straight line.

In the case of a phase transition, detonation or condensation the shock adiabat does not go through the initial point, and so, one might need a stronger incoming flux in order to end up in the second phase. However, this is not the case for passing shocks.

Let us assume that our second phase is a quark-gluon plasma with the equation of state:

$$-\frac{\Omega}{V} = p = \left(\frac{37}{90}\pi^2 T^4 + \frac{1}{9}\mu_B^2 T^2 + \frac{1}{162\pi^2}\mu_B^4 - \Lambda_B^4 \right) / (\hbar c)^3$$

Now the shock adiabat can be solved directly for an incoming flux giving the enthalpy density of the final state as:

$$w_1 = \frac{4}{3} w_o \left[(1-\delta)(\gamma_o^2 + s - 1) \pm \sqrt{4(1-\delta)^2(\gamma_o^2 - 1 + s)^2 - 3(1+\alpha)^2 \gamma_o^2 (\gamma_o^2 - 1)} \right.$$

where $s = \Lambda_B^4/(w_o(\hbar c)^3)$ and $\delta = \delta'(\gamma_o^2 - 1)/(\gamma_o^2 - 1 + s)$. The "-" sign corresponds to the PS mechanism, while the sign "+" with $\alpha = \delta = 0$ to the conventional CS 3). For very high projectile energies $\gamma_o \to \infty$ the generalized specific volume tends asymptotically to

$$\frac{w_o}{3n_o^2}\left\{ 2(1-\delta) \mp \sqrt{4(1-\delta)^2 - 3(1+\alpha)^2} \right\} = \begin{cases} \xrightarrow{CS} \frac{1}{3}\frac{w_o}{n_o^2} \\ \xrightarrow{PS} \frac{w_o}{n_o^2} \end{cases} \quad \alpha = \delta = 0$$

So we see that the compression shock provides a higher compression which is asymptotically 3 times larger than that of the passing shock.

In fig. 2 the shock adiabats a,b,c,d,e are plotted for different α and δ parameters. a is belonging to CS with $\alpha = \delta = 0$, and d and e are the PSs. Dashed lines correspond to constant baryon current through the shock front (j_B =const.). The most interesting feature of the PS solution is that the pressure can be very small or even negative, i.e. by this mechanism low density, low pressure, but highly excited quark-gluon plasma can be formed.

Fig. 3 shows that for a given set of parameters $\gamma_o = 5$, s=3, which is the range where physical PS solutions exist with real positive enthalpy and temperature. Note that PS solutions exist only for very small α and δ values. This result is consistent with the basic assumptions of our model (i.e. that the projectile looses only a very small part of its energy and momentum and so it can be considered as a sharp

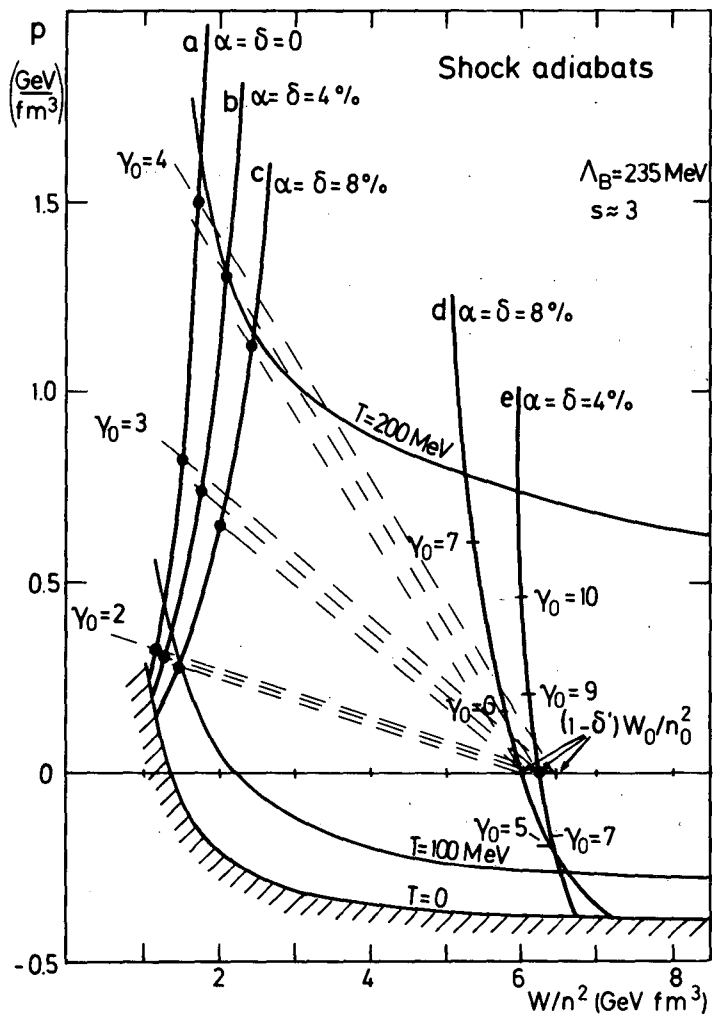

shock front during the whole reaction process).

The passing shock mechanism which describes the interpenetration of two nuclei is distinctively different from the conventional shock. The final state reached in the PS is not too much compressed and has a small pressure while its temperature is high. This PS mechanism may lead to the formation of quark - gluon plasma at similar energies like the compression shock, and it does not even require a partial thermalization between the projectile and the target.

Fig. 2.

Fig. 3.

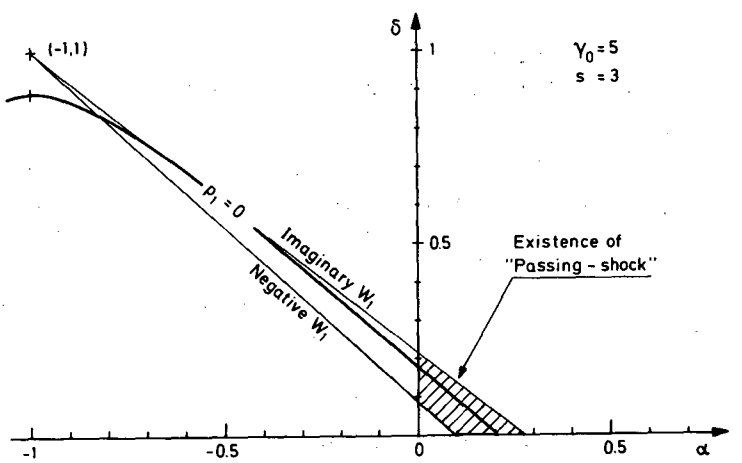

1) L. McLerran, Phys.Rep. 88 (1982) 379.
2) L.P. Csernai, UFTP rep. Frankfurt, 110/1983
3) E. Shuryak, Phys.Rep. 61 (1980) 71.

ENTROPY PRODUCTION BY NONQUASISTATIC PHASE TRANSITIONS IN HIGH-ENERGY HEAVY-ION REACTIONS

L.P. Csernai and B. Lukács
Central Research Institute for Physics, Budapest Hungary

There are different views of which are the most essential entropy-producing mechanisms: shock waves, viscosity, chemical reactions far from equilibrium, or the initial thermalization of the transparent nuclear matter as described in cascade models. However, it is important to note that quasistatic phase transitions (PTs) alone do not lead to entropy generation. Usually the produced entropy is estimated by a shock wave approximation [1] with a given equation of state. If the shock wave approximation is applicable the generated entropy is determined completely, irrespective of the other irreversible processes within the shock front, so also when a PT is present. But in this latter case the extra entropy generation is due to the softening of the equation of state only and not directly connected with the PT. On the other hand, there are doubts about the applicability of the stationary shock wave approximation in the presence of a PT [2]. The conventional shock wave approximation is also not applicable at ultrarelativistic energies, where the matter is expected to become transparent [3].

In these latter cases the amount of generated entropy can only be evaluated by considering each irreversible process individually. The contribution of viscosity [4], nonequilibrium chemical reactions and initial thermalization has already been discussed. The PT may also contribute to entropy generation in itself provided that the transition is not quasistatic. Our aim is to estimate this kind of entropy production.

In complete equilibrium in a quasistatic transition of two phases 1 and 2, the Gibbs conditions

$$T_1 = T_2 \tag{1}$$
$$p_1 = p_2 \tag{2}$$
$$\mu_1 = \mu_2 \tag{3}$$

have to be fulfilled. There is a hierarchy among the Gibbs criteria, because the different equilibrating processes have different relaxation times. In kinetic theory it can be shown that first thermal equilibrium is established ($T_1=T_2$), then the

pressure balance ($p_1=p_2$) follows, and chemical equilibrium is last, because it requires not only elastic collisions but reactions leading to the new structure of the 2nd phase.

Here we discuss an irreversible PT where only the first Gibbs criterion holds. Consider a two phase mixture of domains $\alpha=1,2$. Each domain posesses a local energy-momentum tensor

$$T_\alpha^{ik} = e_\alpha u^i u^k + p_\alpha (g^{ik}+u^i u^k) , \qquad (4)$$

For a larger volume containing many domains, there is an average energy-momentum tensor

$$T^{ik} = \frac{1}{V} \{V_1 T_1^{ik} + V_2 T_2^{ik}\} . \qquad (5)$$

$V_1/V=(n_2-n)/(n_2-n_1)$ and $V_2/V=(n-n_1)/(n_2-n_1)$, where n is the volume average of the baryon charge density while n_α is the density of the αth phase. Eq.(5) is correct up to surface terms, neglected in the thermodynamical limit. The energy-momentum tensor of a closed system always fullfils the balance equation $T^{ir}{}_{,r}=0$. The equation describing the baryon charge conservation takes the form: $(nu^r)_{,r}=0$. In order to separate the information for the thermodynamic quantities one must contract the balance eq. by u_i: $T^{ir}{}_{,r}u_i = 0$. Then, using cond. (1) and the thermodynamical relations of the two individual phases the result is

$$S = \frac{\mu_1-\mu_2}{T} N_2 . \qquad (6)$$

where S is the total entropy of the system, and the operator $\dot{}$ denotes the comoving derivative

$\dot{} \equiv u^r \partial_r$.

Hence there is no entropy production for quasistatic transitions, when the Maxwell-Rule, eqs. (1-3) is valid. For irreversible processes $\mu_1 \neq \mu_2$ is possible, thus entropy may be generated during the transition.

To show the mechanism of entropy generation let us consider a rapid PT, where the pressure and temperature balance are

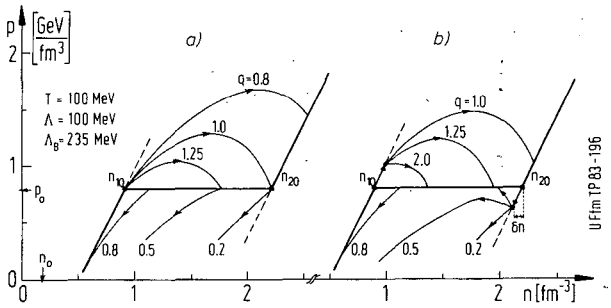

Fig. 1.

established, but not the chemical one. In order to define completely the dynamics of the PT we have to instead of using eq.(3), determine how the second phase builds up. Let us assume that

$$\frac{1}{N}\frac{dN_2}{dt} = q\,\frac{1}{\Delta n_0}\,\frac{dn}{dt} \qquad (7)$$

where $\Delta n = n_{20} - n_{10}$ is the difference of the densities of the two phases in equilibrium with each other at the same temperature T, and q is the ratio of the PT and compression speeds.

Eq. (7) gives us the upper limit of the PT speed. If the equality of the chemical potentials can be reached by slower transition, the system stays in phase equilibrium. We have to define also, when (at which density) the construction of the second phase starts. In a quasistatic PT this is usually the density where the two phases can balance each other at first $n = n_{10}(T)$, but as we know the matter can be supercompressed before the start of the PT, and so the second phase may appear first at $n = n_{10}(T) + \delta\eta$. On the other hand in the expansion the new phase appears first at $n = n_{20}(T)$ or at $n = n_{20}(T) - \delta n$ if there is some delay.

Let us consider the nuclear matter - quark matter PT as an example and take the equation of state as calculated in ref.[5]. In the vicinity of the PT the equation of state of the two phases (j=1,2) can be approximated and consequently the difference of the chemical potentials is given by

$$\mu_1 - \mu_2 = B_1(T)\,\ln\frac{n_1}{n_{10}} - B_2(T)\ln\frac{n_2}{n_{20}}\,. \qquad (8)$$

Now the dynamics of a rapid PT can be displayed as follows: The matter is in the first phase up to a starting value n_{1s} which can be n_{10} or larger. Then according to eq.(8) the build-up of the second phase starts and the equilibrium pressure can be calculated. Using eqs. (6-8)the entropy change can be integrated. This PT lasts till the matter reaches the phase equilibrium or until it is completely in the second phase (Fig.1a). If the PT speed is relatively high ($q>>1$) the deviation from the quasistatic path on the [p,n] plane is small. This deviation increases with increasing compression speed (compared to PT speed) and with increasing supercompression (Fig.1b). In a heavy-ion collision the compression stage is followed by an expansion similarly to a cyclic thermodinamical process. Now the pressure deviates from the equilibrium pressure but contrary to the previous compression, the pressure is now smaller than it would be in complete phase equilibrium. Thus the path of the system on the [p,n] plane shows a hysteresis, which leads to he appearance of a latent heat, i.e. in a rapid PT more kinetic energy is converted into heat than in a quasistatic process. The amount of extra entropy generated in the irreversible PT-s of Fig.1 is $\Delta\sigma=0-6$. The produced entropy is already essential $\Delta\sigma=1-2$ for q values around $q=1$. To estimate the q value is a difficult task. Up to now no theoretical extimates exist about the dynamics of the quark-gluon PT.

1)P.J. Siemens, J. Kapusta,
Phys.Rev.Lett. 43 (1979)1486.
2)J. Hofmann et al.,
Phys. Lett. 82B (1979) 195.
3)L.McLerran,Phys.Rep.88(1982)379.
4)L.P.Csernai, H.W. Barz,
Z. Phys. A296 (1980) 173
5)J. Kuti et al.,
Phys. Lett. 95B (1980) 75.

PARTONS IN NUCLEAR COLLISIONS BEFORE RECOMBINATION

Rudolph C. Hwa

Institute of Theoretical Science and Department of Physics
University of Oregon, Eugene, Oregon 97403, USA

ABSTRACT

Nucleus-nucleus collisions at asymptotic energies are considered in the parton basis. Using parton distributions in hadronic processes as input, we calculate, in the context of a simple thermalization model, the parton number density and energy density in the nucleus fragmentation region.

1. Introduction

A central problem in the study of highly relativistic nucleus-nucleus collisions is the determination of some basic parameters of the hadronic or partonic matter, such as its energy density, whether or not phase transition can occur. We address that problem here in the nucleus fragmentation region by using the parton basis from the very beginning. Two important aspects of this problem are (1) the nucleon structure as an essential input and (2) the development of a description of the physics of A+A collisions in the parton basis. The two are linked by the parton distributions in nucleon scattering before hadronization, which are precisely what the valon-recombination model can readily provide. Thus our study of A+A collisions is a very natural extension of our previous work on the multiparticle

dynamics of p+p collisions with emphasis on the time interval just before recombination takes place.

The subject of plasma formation in ultra-relativistic A+A collisions has been studied in various ways,[1] the most recent attempts being in the frameworks of hydrodynamics[2] and thermodynamics.[3] The success of any such macroscopic theory must ultimately be understood in the context of an underlying microscopic theory. What is needed is a kinetic theory of quark-gluon plasma, which has not yet been developed. The work that I shall discuss represents an initial step in the direction of describing A+A collisions in terms of partons.

2. Particle Correlations in the Fragmentation Region

In the pioneering work of Anishetty et al,[4] the single-particle inclusive cross sections for $p+p \to h+X$, where $h = p, \pi$, and K, have been used as inputs to account for the nucleon recoil and inelastic effects in a crude estimate of the energy deposited in the nucleus fragmentation region. The result obtained is that the energy density ε is about 2 GeV/fm^3. While the procedure is reasonable as a first try on a complicated problem, it ignores the dynamical and kinematical correlations among the produced particles, all of which must be in the same fragmentation region so as to contribute to the enhancement in energy deposition. Such correlations mean that the contributions from all the produced particles should not be simply added. In any given event the detection of any hadron at momentum fraction x restricts all other fragments of the initial nucleon to 1-x. Dynamically there are also contraints on the hadronization of valence quarks; e.g., a valence u quark cannot simultaneously contribute to the formation of a proton and a π^+. The neglect of such correlations is likely to lead to an over-estimate of ε.

To take the correlations into account at the hadronic level is difficult. We circumvent the problem by going directly to the quark-gluon basis, which must automatically account for hadron correla-

tions[5] in a parton model that is reliable for low-p_T hadronic reactions.[6] Indeed, partons (referring generically to quarks and gluons) form the proper basis for an investigation of the present problem since hadronization is an irrelevant and unnecessary complication insofar as energy density is concerned -- especially if a plasma is to be formed. To that end the valon-recombination model[7] is ideally suited for the purpose. Though the recombination part is not explicitly needed for the problem considered here, it is because of that hadronization mechanism that the parton distributions determined in the model have any phenomenological significance for hadronic reactions.

3. Parton Distribution in a Nucleon Before Recombination

For nucleon-nucleon collisions at high energies, the parton distributions in the fragmentation region just before recombination are known in the valon-recombination model. Based on those distributions, the inclusive cross sections of produced pions in $p+p \to \pi^{\pm}+X$ reactions have been calculated.[7,8] The agreement with data gives a measure of credibility to the physical relevance of the parton distributions. Since the pion recombination function applies only to quarks and antiquarks and not to gluons directly, the correct normalization for pionization obtains when all the gluons are first converted into $q\bar{q}$ pairs, giving rise to the so-called "saturated sea." The result may be summarized by giving here the total single-parton distribution function of a nucleon

$$F(x) = \int_x^1 dx' \; G(x') \; [K_{NS}(x/x') + L(x/x')] \tag{1}$$

where

$$G(x) = 16\, x^{0.65}\, (1-x)^2 + 6\, x^{0.35}\, (1-x)^{2.3} \tag{2}$$

$$K_{NS}(z) = z, \; L(z) = 3(1-z)^5 \tag{3}$$

$K_{NS}(z)$ is the non-singlet quark distribution in a valon, and specifies the valence-quark component in $F(x)$. The simple form given for it in (3) is a fair approximation of earlier, more complicated results,[7,8] subject to the sum rules

$$\int_0^1 dz K_{NS}/z = 1 \quad \text{and} \quad \int_0^1 dz K_{NS} = 1/2 \tag{4}$$

the latter being only a phenomenological constraint. $L(z)$ gives the sea quark distribution for all types;[9] it carries the balance of momentum in a valon, i.e. $\int_0^1 dz\, L = 1/2$. For some hadronic data, the exponent of $(1-z)$ may be as low as 3, in which case $L(z)$ would be $2(1-z)^3$. We do not believe that the difference would affect the final result very much. It should be noted that $G(x')$ is the valon distribution in a nucleon satisfying $\int_0^1 dx'\, G(x') = 3$ and that $F(x)$ satisfies the momentum sum rule $\int_0^1 dx\, F(x) = 1$. For A+A collisions, the precision of the parameters in (2) and (3) are not crucial.

$F(x)$ is the parton distribution just before hadronization, after the nucleon bag is broken by collision. The distribution does not depend on the nature of the other colliding particle because the two fragmentation regions are well separated in rapidity at high incident energy. Since for hadronic collisions hadronization takes place at proper time $\tau \approx 1$ fm (the hadronic size), we regard $F(x)$ to be meaningful for each nucleon in an A+A collision only for $\tau \gtrsim 1$ fm. For $\tau < 1$ fm, parton interaction is complicated and unknown; indeed, even the meaning of a parton distribution is questionable when at small momentum transfer the time resolution is not much better than 1 fm. We may, however, at $\tau = 0$ regard the nucleon as a bound state of three valons whose momentum distribution is given in (2).[7,10] The breaking of the nucleon bag beginning at $\tau = 0$ leads to a parton cluster distribution $P(z) = K_{NS}(z) + L(z)$ for each valon at $\tau \gtrsim 1$ fm. We may interpolate the interval $0 \leqslant \tau \lesssim 1$ fm by a smooth transition from $\delta(z-1)$ to $P(z)$, so that $F(x)$ attains the meaning of valon distribution $x\,G(x)$ as $\tau \to 0$.

Although our result will be for $\tau \gtrsim 1$ fm, we do want our energy density ε to satisfy the initial condition that at $\tau = 0$, $\varepsilon = \varepsilon_o = n_N M$ where n_N is the nucleon number density in the nucleus and M the nucleon mass.

The momentum distribution $F(x)$ of the partons in a nucleon is our basic input in the present problem of A+A collisions. It represents an aspect of the nucleon structure studied in the valon model. A more elaborate description of it can specify multiparton distributions, which would be needed for the calculation of hadronization[7] and correlations,[5] but they are not needed in the following since the parton number density and energy density that we shall calculate depend only on the single-parton distribution. That is the advantage of working at the parton level.

4. Nuclear Fragmentation

In applying $F(x)$ to the nuclear problem we shall determine the parton distribution in the nuclear fragmentation region by ignoring the cooperative effects of the nucleons in the nucleus. This approximation therefore neglects not only the partons in the cummulative region $(x>1)$, but also the effect seen by EMC[11] on the ratio of the structure functions of Fe to D. These effects are attributable to the Fermi motion of the nucleus and to multiquark clusterings.[12] Though interesting in their own right, they represent, however, only a less-than-10% effect on what we shall calculate and are consequently negligible compared to other uncertainties involved in the nucleus-nucleus collision problem. Those complications, when fully understood, can easily be incorporated in our formalism. Neglecting them now facilitates a clearer description of our treatment of the problem.

We shall sum the parton contributions from the different nucleons in the struck nucleus with time delay carefully taken into account. We shall, however, assume that each struck nucleon contributes the same parton distribution $F(x)$ at its own proper time $\tau \gtrsim 1$ fm. This approximation ignores the possibility that the down-

stream nucleons might fragment somewhat differently from those near the front of the nucleus. But our result will be independent of this detailed aspect of the nuclear collision problem because the maximum energy density, as we shall show, depends largely on the partons originated from the upstream nucleons.

Consider now in the rest frame of the target nucleus a longitudinal tube of length L through the center. We assume that the impact parameter is zero and regard the tube as the optimal place to achieve the highest energy density. In the 1+1 space(z)-time(t) the tube at rest extends from z=0 to L. The projectile nucleus at infinite energy cuts across the z-t space along the light cone. Define $z_\pm = t \pm z$. Thus the nucleons along z_+ at $z_- = 0$ between $z_+ = 0$ and 2L are struck by the projectile at local proper time $\tau = 0$. The variable z_+ measures the "spatial" locations of the nucleus whose partons are liberated, and τ measures the age of the partons since liberation. If the struck nucleon is located at $z_+ = \zeta$, and $z_- = 0$, then the associated τ-hyperbola is determined by $(z_+ - \zeta)z_- = \tau^2$. Thus for every ζ between 0 and 2L, the nucleon there contributes to a spatial spread of partons along the τ-hyperbola with apex at ζ.

The partons at every space-time point (z,t), or alternatively (z_+, z_-), in the forward light cone, come from nucleons at various locations ζ and have various proper times τ. Thus in order to calculate the number density there, it is necessary to assume first that F(x) is the parton distribution per nucleon for all $\tau > 1$ fm if there is no interaction and no hadronization. We shall not investigate any region requiring $\tau < 1$ fm, thus $z_- < 1$ fm is off limits. Since the density falls off with increasing z_-, the region of greatest interest will be at $z_- \sim 1$ fm. The problem of interaction and thermalization will be addressed later after we set up the problem in which the partons arising from different nucleons are assumed not to interact.

5. Kinematics

The translation from the momentum-fraction distribution of the

partons to their space-time distribution will be done by means of free-particle kinematics. Defining x as the ratio of light-cone momenta of the parton and nucleon, we have

$$x = \frac{k_+}{p_+} = \frac{m_T}{M} \exp(y-y_N) \tag{5}$$

where m_T and y are the transverse mass $(m^2 + k_T^2)^{\frac{1}{2}}$ and rapidity of the parton, while M and y_N are the mass and rapidity of the nucleon. For brevity, we write $\alpha = m_T/M$, but in the calculation we shall take it to be 1/3 numerically, which not only is reasonable phenomenologically, but also permits (5) to be evaluated in the nucleon rest frame without losing the physical interpretation of x. Converting (5) from the projectile to the target variables, and evaluating in the target rest frame for which $y_N = 0$, we have

$$x = -\alpha\, e^{-y} \tag{6}$$

Next, in going from y to $z_\pm$ and τ, we adopt the usual definition of rapidity on a hyperbola and write

$$z_+ = \zeta + \tau\, e^{y}, \quad z_- = \tau\, e^{-y} \tag{7}$$

Thus we have

$$|x| = \frac{\alpha z_-}{\tau} = \frac{\alpha\, \tau}{z_+ - \zeta} \tag{8}$$

The absolute sign of $|x|$ will be omitted in the following and $F(x)$ will be used for its distribution at every ζ. We shall assume that the nucleons are distributed uniformly along z_+ for $0 \leq \zeta \leq 2L$ with a density $n_N/2$ where n_N is the nucleon density in the rest frame of the target nucleus.

At fixed (z_+, z_-) the maximum rapidity y_2 is for a parton from the nucleon at $\zeta = 0$; hence, $y_2 = \frac{1}{2} \ln(z_+/z_-)$. The minimum rapidity y_1 corresponds either to $x = 1$, i.e $\ln \alpha$, or to

$\zeta = 2L$, i.e. $\frac{1}{2}\ln(z_+ - 2L)/z_-$, whichever is larger.

6. Energy Momentum Tensor and Current Density

At the space-time point (z,t) the energy-momentum tensor $T^{\mu\nu}$ is

$$T^{\mu\nu} = \sum_n \frac{k_n^\mu k_n^\nu}{k_n^o} \delta[z - z(t)] \tag{9}$$

where k_ν^μ is the momentum two-vector of nth parton and where the summation is over all partons at (z,t). In a manifestly covariant form it is[13]

$$T^{\mu\nu} = \sum_n \int d\tau\, k_n^\mu \frac{d}{d\tau} Z_n^\nu \delta^2 [Z-Z_n(\tau)] \tag{10}$$

where Z^ν is the space-time two-vector (t,z). In accordance with our foregoing discussion, we write $\sum_n = \frac{1}{2}n_N \int d\zeta\, dy\, F(y)$ where $F(y) \equiv F[x(y)]$. Eq. (10) can then be reduced to the form

$$T^{\mu\nu} = n_N m_T \int_{y_1}^{y_2} dy\, F(y)\, e^y\, v^\mu(y)\, v^\nu(y) \tag{11}$$

where we have used $k^\mu = m_T v^\mu(y)$ with

$$v^\mu(y) = (\cosh y, \sinh y) \tag{12}$$

The exponential e^y is the local compression factor that emerges from the integration over the δ-function. $F(y)$ is now the rapidity distribution of the partons contributing to $T^{\mu\nu}$ at (z,t).

Similar considerations lead to the following expression for the parton current density

$$J^\mu = n_N \int_{y_1}^{y_2} dy\, F(y)\, e^y v^\mu(y) \tag{13}$$

From our expression for $F(x)$ in (1)-(3), it is clear that $F(y)$

is a monotomically increasing function of y from y_1 to y_2. Being nonisotropic, it describes an imperfect fluid. Indeed, since we have not put in parton interaction, the system is far from thermal equilibrium. One manifestation of this is that there is no unique comoving frame. The two definitions according to $T^{30} = 0$ and $J^3 = 0$ yield two different fluid velocities, $\tilde{u}^\mu$ and $\bar{u}^\mu$, respectively. It can be shown that the corresponding rapidities, $\tilde{y}$ and $\bar{y}$, are

$$\tilde{y} = \tfrac{1}{4}\ln \frac{\langle e^{2y}\rangle}{\langle e^{-2y}\rangle} \quad , \qquad \bar{y} = \tfrac{1}{2}\ln \frac{\langle e^{y}\rangle}{\langle e^{-y}\rangle} \tag{14}$$

where

$$\langle g(y)\rangle = \int_{y_1}^{y_2} dy\ F(y)e^{y}\ g(y)$$

Moreover, one can show that in terms of $\tilde{u}^\mu$ and $\bar{u}^\mu$, the canonical forms

$$T^{\mu\nu} = (\varepsilon+p)\ \tilde{u}^\mu\tilde{u}^\nu - pg^{\mu\nu} \tag{15}$$

$$J^\mu = n\ \bar{u}^\mu \tag{16}$$

follow. For a perfect fluid for which $F(y)$ is symmetric, then $\tilde{y} = \bar{y}$. Since the fluid we have at hand is not in thermal equilibrium, in fact far from it, ε and p do not have the usual interpretation of energy density and pressure.

7. Thermalization

The partons from the different nucleons do interact and should result in local thermalization. It is unreasonable to expect all the partons in the entire rapidity range from y_1 to y_2 (which can spread to as much as 3 units of y for z_- near 1fm) to interact effectively enough to give rise to an overall thermal equilibrium in a small spatial cell at (z,t). We can, however, expect partons in a

rapidity range of $\Delta y \sim 1$ to thermalize. In that case, an overall fluid velocity would be meaningless; instead, there would be a spectrum of local fluid velocities. We are familiar with this kind of phenomenon in hadron-hadron collisions except that here it is for each spatial cell.

What we need at this point is a kinetic theory of quarks and gluons so that we can calculate the effect of parton interaction on the randomization of their momentum distribution. In the absence of such a theory now, we make the reasonable ansatz that the effect of local thermalization is to cause the following change in the rapidity distribution

$$F(y)e^{y} \rightarrow \int dy' \; F'(y') \; e^{y'} \; f(y-y') \tag{17}$$

where y' is the local fluid rapidity and $f(y-y')$ is a symmetric distribution function characterizing a local parton subsystem in thermal equilibrium. $F'(y')$ is the distribution of such local subsystems. Consider two extreme cases. If the partons do not interact at all, then $f(y-y')$ would be $\delta(y-y')$ and (17) renders no change on the original distribution. On the other hand, if there is total thermalization, $F'(y')$ would become proportional to $\delta(y'-\bar{y})$ corresponding to having one unique fluid velocity, and apart from a constant factor (17) gives $e^{\bar{y}} f(y-\bar{y})$ a symmetric thermal distribution in the comoving frame of the fluid. Thus $f(y-y')$ describes the effect of thermalization and should be parametrized by a temperature. We normalize $f(y-y')$ by $\int_{-\infty}^{\infty} dy \; f(y-y') = 1$.

If u^{μ} denotes the local fluid velocity $(\cosh y', \sinh y')$ and k^{μ} the parton momentum, the relativistically-invariant description of the parton meomentum distribution requires that f be a function of $k_{\mu}u^{\mu}$, which is $m_T \cosh(y-y')$. For illustrative purposes below, we shall take f to be a simple Boltzmannian distribution

$$f(k_{\mu}u^{\mu}) = f_o \exp[-\beta \cosh (y-y')] \tag{18}$$

where $\beta = m_T/T$. This can be improved with statistics and chemical potential taken into account. But in view of our ignorance about the thermalization process, more sophistication in the parametrization of f seems unwarranted at this stage. According to (18) the full widths Δy at half maximum corresponding to $T = 50$, 100, and 200 MeV are $\Delta y = 0.9$, 1.3, and 1.8, respectively. They span a reasonable range of values which will be considered for numerical estimates below. In the following we shall work out the case of the minimal model, namely, $F'(y') = F(y')$, and T in the range 50-200 MeV. Thus (17) effects a local smearing of the original distribution.

8. Energy and Number Densities

According to our thermalization model, we have from (11) and (13)

$$T^{\mu\nu} = \alpha\varepsilon_o \int dy\, dy'\, F(y')e^{y'}\, f(y-y')\, v^{\mu}(y)\, v^{\nu}(y) \tag{19}$$

$$J^{\mu} = n_N \int dy\, dy'\, F(y')e^{y'}\, f(y-y')\, v^{\mu}(y) \tag{20}$$

where $\varepsilon_o = n_N M$, the energy density of the nucleus. Define

$$T^{\mu\nu} = \int_{y_1}^{y_2} dy'\, \Lambda^{\mu}_{\mu'}(y')\, \Lambda^{\nu}_{\nu'}(y')\, T'^{\mu'\nu'} \tag{21}$$

$$J^{\mu} = \int_{y_1}^{y_2} dy'\, \Lambda^{\mu}_{\mu'}(y')\, J'^{\mu'} \tag{22}$$

where $$\Lambda^{\mu}_{\mu'}(y') = \begin{pmatrix} \cosh y' & \sinh y' \\ \sinh y' & \cosh y' \end{pmatrix}$$

Then we get

$$T'^{\mu\nu} = \alpha\varepsilon_o\, F(y')\, e^{y'} \int dy\, f(y-y')\, v^{\mu}(y-y')\, v^{\nu}(y-y') \tag{23}$$

$$J'^{\mu} = n_N\, F(y')\, e^{y'} \int dy\, f(y-y')\, v^{\mu}(y-y') \tag{24}$$

where

$$v^{\mu}(y-y') = \Lambda^{-1\mu}{}_{\nu}(y')\, v^{\nu}(y) = \begin{pmatrix} \cosh\,(y-y') \\ \sinh\,(y-y') \end{pmatrix} \tag{25}$$

Obviously, $T'^{\mu\nu}$ and J'^{μ} are the energy-momentum tensor and current vector in the comoving frame at rapidity y'. Since $f(y-y')$ is symmetric, it is clear from (23) and (24) that both T'^{30} and J'^{3} vanish, thereby defining the unique, local fluid velocity $u = \tanh y'$.

The integrals in (23) and (24) are independent of u. If we denote them by $\langle v^{\mu}v^{\nu}\rangle$ and $\langle v^{\mu}\rangle$, we obtain from (18)

$$\langle v^{o}\rangle = K_1(\beta) \,/\, K_o(\beta) \tag{26}$$

$$\langle v^{o}v^{o}\rangle = 1 + K_1(\beta) \,/\, \beta K_o(\beta) \tag{27}$$

where $K_n(\beta)$ is the modified Bessel function.

The energy and number densities for fixed z_+, z_-, and y', are

$$\varepsilon(y') = T'^{00} = \alpha\varepsilon_o\, F(y')\, e^{y'} \langle v^{o}v^{o}\rangle \tag{28}$$

$$n(y') = J'^{0} = n_N\, F(y')\, e^{y'} \langle v^{o}\rangle \tag{29}$$

Note that the ratio ε/n is independent of y' and is a function of β only. For a numerical estimate of ε and n separately, we consider the space-time point where they are likely to be largest, i.e. $z_+ = 2L$ and $z_- = 1$ (in units of fm). For uranium, $L \simeq 15$, we have $y_1 = -1.1$ and $y_2 = 1.7$. For y' at its highest value, i.e. y_2, we obtain

T(MeV)	$\varepsilon(y_2)/\varepsilon_o$	$n(y_2)/n_N$
50	7.5	20.7
100	8.8	22.0
200	11.6	24.5

These are likely to be the maximum values for $z_- \geq 1$. As y'

decreases from y_2, $\varepsilon(y')$ and $n(y')$ decrease rapidly, so the average ε and n would be much lower. Even if we focus only on the maximum values at y_2, the energy density given above corresponds to the range

$$\varepsilon_{max} \approx 1.0 - 1.6 \text{ GeV/fm}^3 \tag{30}$$

while the number density of all partons (valence and sea quarks) is in the range

$$n_{max} \approx 3.1 - 3.7 \text{ fm}^{-3} \tag{31}$$

9. Conclusion

The approach that we have taken is to study the energy-momentum tensor and current density in the parton basis. We have assumed that after a proper time of 1 fm no new partons are created so those quantities are conserved. However, those partons can interact and redistribute themselves. In the absence of a kinetic theory of partons which is very much needed, we have proceeded with a crude model for thermalization. We relate the rapidity range of interaction ($\Delta y \sim 1$-2) to the temperature of a subsystem in thermal equilibrium ($T \sim 50$-200 MeV). Since the overall rapidity spread of partons at certain space-time points is nearly 3 units, we cannot expect all the partons at every space-time point to be totally thermalized. We therefore allow the superposition of a collection of separately thermalized subsystems, each having its own fluid velocity. The energy and number densities, by definition, refer to those subsystems in their comoving frames. The numerical estimates that we have made for those quantities turn out to be low compared to previous estimates,[4] even when we consider the most favorable condition for high densities. They seem to be compatible with the results of Kajantie et al[2] who treated the hydrodynamics of the problem with hadron production regarded as source.

In view of the crudeness of our way in handling the thermalization problem, the numerical implications of our result should not be taken seriously. While further attention will be given to the problem of parton interactions and thermalization, it is the approach adopted for this investigation that we want to emphasize here. We have seen in our formalism that ε and n depend on the fluid-rapidity distribution $F'(y')$ and the compression factor $e^{y'}$ in addition to the temperature-dependent quantities $\langle (v^o)^2 \rangle$ and $\langle v^o \rangle$. Since the parton distribution $F(y)$ without interaction gives a strong hint for the behavior of $F'(y')$, we learn that ε and n are large where $F(y)$ is large; thus it is the front side of the nucleus that makes the dominant contribution to the densities.

It is straightforward to calculate ε and n as functions of z_+ and z_-. The details of those results will be presented elsewhere.

Acknowledgements

I have benefitted greatly from discussions with K. Kajantie, C. S. Lam, L. McLerran, and L. VanHove, to all of whom I am very grateful. The work was supported in part by the U. S. Department of Energy under contract number DE-AT06-76ER70004.

References

1. Proc. of Bielefeld Workshop "Quark Matter Formation and Heavy Ion Collisions," ed. M. Jacob and H. Satz (World Scientific, Singapore, 1982).

2. J. D. Bjorken, Phys. Rev. D27, 140 (1983); G. Baym et al, Illinois preprint (1983); K. Kajantie, R. Raitio, and P. V. Runskanen, Nucl. Phys. B222, 152 (1983).

3. R. Hagedorn and J. Rafelski, Phys. Lett. 97B, 136(1980); for a recent review see J. Rafelski and M. Danos, NBSIR-83-2725 (1983).

4. R. Anishetty, P. Koehler, and L. McLerran, Phys. Rev. D22, 2793 (1980).

5. E. Takasugi and X. Tata, Phys. Rev. D21, 1838 (1980); R. C. Hwa and M. S. Zahir, Zeit. f. Physik C19, No. 3 (1983).

6. R. C. Hwa in "Partons in Soft-Hadronic Processes" ed. R. T. Van de Walle (World Scientific, Singapore, 1981).

7. R. C. Hwa, Phys. Rev. D22, 759, 1593 (1980).

8. L. Gatignon et al, Zeit. f. Physik C16, 229 (1983).

9. L. Gatignon (private communication); R. C. Hwa and M. S. Zahir, Ref. 5.

10. R. C. Hwa and M. S. Zahir, Phys. Rev. D23, 2539 (1981).

11. J. J. Aubert et al, Phys. Lett. 123B, 275 (1983); A. Bodek et al, Rochester report COO-3065-348 (1983).

12. R. L. Jaffe, Phys. Rev. Lett. 50, 228 (1983); C. E. Carlson and T. J. Havens, Phys. Rev. Lett. 51, 261 (1983); H. J. Pirner and J. P. Vary, Heidelberg preprint UNI-HD-83-02; F. E. Close, R. G. Roberts, and G. G. Ross, Rutherford preprint RL-83-051; S. Date, Waseda preprint WU-HEP-83-4.

13. S. Weinberg, "Gravitation and Cosmology" (Wiley, N.Y., 1972).

CENTRAL COLLISIONS OF HEAVY IONS IN THE DUAL PARTON MODEL

by

A. Capella*, C. Pajares+, A. V. Ramallo+

ABSTRACT

Average multiplicities and rapidity densities in high energy nucleus-nucleus collisions are computed in the framework of the dual parton model. Particular attention is given to the case of central collisions.

* Laboratoire de Physique Théorique et Hautes Energies, Université de Paris-Sud, Orsay, France.

+ University of Santiago de Compostela, Spain.

The multi-chain dual parton introduced by the Orsay group (1) has been able to describe with considerable success the multi-particle production in hadron-hadron collisions. (The density of 3.5 charged particles per unit rapidity at $y^* \sim 0$ at the colliders was in fact predicted (1c) before the first data taking at the colliders). The model can be extended in a straightforward way to describe hadron-nucleus (1b) and nucleus-nucleus interactions (1e) at high energies. The α-α data at $\sqrt{s}$ = 31 GeV per nucleon-nucleon collision have been described with great success (1e).

Here we present calculations of average multiplicities and rapidity densities at $y^* \sim 0$ for nucleus-nucleus interactions. Particular attention is devoted to the case of central nucleus-nucleus collisions - where one might observe the transient production of a quark-gluon plasma.

Let us recall that in the dual parton model particle production in a nucleon-nucleon collision takes place in the form of chains of hadrons stretched between colored fragments of the colliding hadrons with compatible quantum numbers. The nucleon splits into a valence quark and diquark and two chains of hadrons are formed $q_1^v - qq_2$ and $qq_2 - q_1^v$. This corresponds to a single inelastic collision. The rapidity densities $N^{q_1^v - qq_2}(y)$ and $N^{qq_2 - q_1^v}(y)$ of the chains are obtained by a convolution of momentum distribution functions and fragmentation functions of the hadron constituents.

The genralization to nucleus-nucleus collisions in ref. (1e) neglects the difference between valence and sea quarks. This is quite harmless for α-α collisions but it could be too rough in the case of a collision involving heavy nuclei. Thus we propose here a somewhat improved version of the model.

Let us consider the particular situation in which $n_A(n_B)$ nucleons of nucleus A(B) are wounded (i.e. interact inelastically), with a total number of n inelastic collisions taking place. Let $\sigma_{n_A,n_B,n}$ be the corresponding cross-section. Since each inelastic collision produces two chains of hadrons,

2n chains will be produced. The valence fragments available are : $n_A(n_B)$ valence quarks and diquarks in nucleus A(B). In the case $n_A < n_B$ the only chains one can form involving these valence constituents are n_A chains of type $qq_A - q^v_B$, n_A chains of type $q^v_A - qq_B$, $n_B - n_A$ chains of type $\bar{q}^s_A - q^v_B$ and $n_B - n_A$ chains of type $q^s_A - qq_B$, i.e. $2n_B$ chains.(Here q^s and $\bar{q}^s$ are sea quarks and antiquarks). Since this takes care of all the valence constituents, the remaining $2n - 2n_B$ chains have to be of the type $\bar{q}^s_A - q^s_B$(or $q^s_A - \bar{q}^s_B$). The rapidity density in a nucleus A-nucleus B collision is therefore given by

$$N^{A-B}(y) = \frac{1}{\sigma_{A-B}} \sum_{n_A,n_B,n} \sigma_{n_A,n_B,n}\, \theta(n_B - n_A)$$

$$[\, n_A(N^{qq_A - q^v_B}(y) + N^{q^v_A - qq_B}(y)) + (n_B - n_A)(N^{\bar{q}^s_A - q^v_B}(y) + N^{q^s_A - qq_B}(y)) \qquad (1)$$

$$+ (n - n_B)(N^{\bar{q}^s_A - q^s_B}(y) + N^{q^s_A - \bar{q}^s_B}(y)) + \text{symmetric } A \leftrightarrow B]$$

For A << B a good approximation to eq.(1) is obviously to take

$$N^{A-B}(y) = \langle n_A \rangle\, (N^{qq_A - q^v_B}(y) + N^{q^A_v - qq^B}(y) + \qquad (2)$$

$$+ (\langle n_B \rangle - \langle n_A \rangle)(N^{\bar{q}^s_A - q^v_B}(y) + N^{q^s_A - qq_B}(y)) + (\langle n \rangle - \langle n_B \rangle)(N^{\bar{q}^s_A - q^s_B}(y) + N^{q^s_A - \bar{q}^s_B}(y))$$

In fact this formula gives results remarkably close to those obtained from the exact expression (1) for $A \lesssim B$.

Let us consider next the case of a central nucleus A-nucleus B collision. There are many definitions in the literature about what is a central collision. Usually is referred to a collision at zero impact parameter. However, this definition is not suitable to compare with experimental data. We adopt here an experimental definition (2) : central collision is the collision in which there is not any fragment of the projectile inside a small veto angle. This definition corresponds to the cross section of having A wounded nucleons in the projectile and all of them giving rise to a slow baryon in the final state which therefore is not seen in the veto angle.

According to this definition we have to replace in eq.(1), $\langle n_A \rangle$, $\langle n_B \rangle$ and $\langle n \rangle$ by A, $\langle n_B \rangle^C$ and $\langle n \rangle^C$ respectively. The last two values are computed following the method described in ref.(3). We use the optical approximation. The results for different beam and target nuclei at $\sqrt{s}$ = 31 GeV per nucleon-nucleon collision are given in Table I. The numbers refer to produced negative particles. The contribution to the average multiplicity of particles produced via intra-nuclear cascade is not considered. We have also computed the dispersion of the multiplicity distribution, assuming that the particles produced in different chains are uncorrelated and those produced in a single chain have a Poisson distribution. The results and the details of our calculations will be reported elsewhere (4).

In order to test our results with cosmic ray data, we have computed dN/dy for a S_i-A_g collision at $\sqrt{s} \sim 80$ GeV. We obtain about 250 particles per unit of rapidity, which is quite close to observed value (5).

In the case of A_g-P_b central collision we obtain a density of about 620 particles per unit rapidity. Assuming that the nuclei are compressed to a longitudinal thickness of about one fermi (6) and taking 0.5 GeV per charged particle, one obtains an energy deposition of

$$\frac{0.5 \times 620}{\pi R^2_{P_b}} \sim 3 \text{ GeV/fermi}^3$$

Such an energy density is believed (7) to be sufficient to observe the phase transition to a quark-gluon plasma.

REFERENCES

1. a) A. Capella, U. Sukhatme, C. I. Tan and J. Tran Thanh Van, Phys. Lett. 81B, 68 (1979) ; A. Capella, U. Sukhatme and J. Tran Thanh Van, Z. Phys. 3, 329 (1980).
   b) A. Capella and J. Tran Thanh Van, Z. Phys. 10, 249 (1981) ; Phys. Lett. 93B, 946 (1980).
   c) A. Capella, Partons in Soft Hadronic Physics, Proc. Europhys. Study Conf., Erice (1981), ed. R. Van de Walle.
   d) A. Capella and J. Tran Thanh Van, Z. Phys. 18, 85 (1983) ; See also Phys. Lett. 114B, 450 (1982).
   e) A. Capella, J. Kwiecinski and J. Tran Thanh Van, Phys. Lett. 108B, 347 (1982).
2. R. Swed, in Proc. of the 5th High Energy Heavy Ion Study, LBL, Berkeley.
3. C. Pajares and A. V. Ramallo, preprint US-FT 11, Santiago de Compostela (Spain).
4. A. Capella, C. Pajares and V. A. Ramallo Univ. of Santiago preprint (in preparation)
5. JACEE collaboration AIP Conf. Proc. n° 26 (1981) ed. V. Barger, D. Cline and F. Halzen.
6. J.D. Bjorken in Current-Induced Reactions, J. Körner et al (Ed), Springer-Verlag, Berlin, 1976.
7. H. Satz preprint BI-TP 82/29.

CAPTION

The average multiplicities and central densities of negative particles produced in a collision nucleus A-nucleus B at $\sqrt{s}$ = 31 GeV per nucleon-nucleon collision. The last two columns are the corresponding values for central (head-on) collisions.

TABLE I

A	B	dN^-/dy	$< N^- >$	$(\frac{dN^-}{dy})^c$	$< N^- >^c$
12	27	4.9	22.6	15.5	69.6
12	108	8.2	37.4	24.1	108
12	208	10.3	46.8	29.5	132
27	208	18.3	82.7	64.7	286
64	208	33.4	149	139	598
108	208	45.5	203	207	877

Thermalization of Central Products in Ultra-Relativistic Heavy Ion Collisions

S.Date[a)], O.Miyamura[b)], T.Ochiai[c)], H.Sumiyoshi[d)] and N.Suzuki[a)]

a) Department of Physics, Waseda University, Tokyo 160
b) Faculty of Engineering Science, Osaka University, Toyonaka, Osaka 560
c) Department of Physics, Rikkyo University, Tokyo 171
d) Institute for Nuclear Study, University of Tokyo, Tanashi, Tokyo 188

ABSTRACT

Average number of collisions per particle and the energy density are calculated for the central products in ultra-relativistic heavy ion collisions based on the multi-chain model. Within rather short time after the collision, enough collisions per particle take place in the system keeping sufficient energy density for the phase transition to quark-gluon matter(QGM) when the incident energy and the mass number are appropriately high and large.

Whether the QGM can be created in high energy heavy ion collisions, is widely investigated both for fragmentation and for central regions. In almost all of these works /1~4/, the attention is paid to the energy density achieved in the heavy ion collisions while the thermal equilibrium of the produced high energy density matter is presupposed. Certainly, the Monte-Carlo lattice gauge theory calculation /5/ have shown the existence of the quark-gluon plasma phase, under the condition that the treated system is in a thermal equilibrium. Therefore, it becomes now very important to address whether the thermal equilibrium of the system produced through the heavy ion collision is realized or not, especially keeping sufficiently high energy density. In the present work, we calculate the average collision number per particle, C_π, and the energy density, ε, of the central products in the ultra- relativistic A-A′ collisions by the use of the knowledge of the soft h-N and h-A interactions at high energies. Both ε and C_π are obtained as a function of the proper time $\hat{t}$ of the system.

We assume that the whole processes of A-A′ interaction are divided into three stages. (i) Beam nucleons successively collide with target nucleons. (ii) The secondary hadrons are produced at a proper time τ_0=1fm/c (formation time) after each N-N collision. (iii) The third step is the final state interaction among the produced particles which are relevant for their thermalization. In addition, we will pay particular attention to the facts on N-N collisions that (a) the rapidity density and the inelastic cross section, σ_{in}^{NN}, markedly increase with the energy above TeV region and (b) the correlation length of produced particles in rapidity space is 1~2 /6/.

Let us consider the system composed of $N(y_1,y_2)$ hadrons that are produced in an A-A′ central collision between rapidities y_1 and y_2, (y_1,y_2). Rapidity variables are defined in the center of mass frame of N-N collisions. At time $\hat{t}$, $N(y_1,y_2)$ hadrons occupy the space volume $V(\hat{t})$ in the co-moving frame (COMF) of the system with velocity v_c;

$$v_c = \mathrm{th}\eta = \int_{y_1}^{y_2} dy\ \mathrm{sh}\ y\ \frac{dN}{dy} \Big/ \int_{y_1}^{y_2} dy\ \mathrm{ch}\ y\ \frac{dN}{dy} \qquad (1)$$

where dN/dy is the rapidity density of the A-A′ collision. We define $\hat{t}$=0 when all the particles in (y_1,y_2) hadronize within the system. The energy density of the system at $\hat{t}$ is given by

$$\varepsilon(y_1,y_2;\hat{t}) = \varepsilon_0 N(y_1,y_2)/V(\hat{t}) \qquad (2)$$

where $\mathcal{E}_0$ is the mean energy of a secondary hadron within (y_1,y_2) and is taken to be 0.4 GeV. Here,

$$V(\hat{t}) = \hat{z}^{AA}(y_1,y_2;\hat{t})\ \pi R_A^{\ 2} \tag{3}$$

where R_A is the radius of the smaller nucleus A and $\hat{z}^{AA}$ is the longitudinal extension of the system at $\hat{t}$.

Let us consider, firstly, the N-N collision. According to the assumption (ii), a hadron of rapidity y appears after $\tau_0 ch(y-\eta)$ and away $\tau_0 sh(y-\eta)$ from the N-N interaction point O in Fig.1(a). Taking the frame independent hadron size S_h(=1.0fm) /7/, the system has already extended at $\hat{t}$=0 by

$$\hat{z}_0^{NN}(y_1,y_2) = \tau_0 ch(y_2-\eta)\{th(y_2-\eta)-th(y_1-\eta)\}+S_h \tag{4}$$

The system continues to expand and the longitudinal extension of the system at $\hat{t}$ is given by

$$\hat{z}^{NN}(y_1,y_2;\hat{t}) = \hat{z}_0^{NN}(y_1,y_2)+\{th(y_2-\eta)-th(y_1-\eta)\}\hat{t} \tag{5}$$

In the A-A collision, reflecting the finite nuclear size, the interaction points of the successive collisions spread in $\hat{t}$-$\hat{z}$ space over a parallerogram OPQR as is in Fig.1(b). Accordingly, the longitudinal extension of the system is given by

$$\hat{z}^{AA}(y_1,y_2;\hat{t}) = \hat{z}^{NN}(y_1,y_2;\hat{t}+\hat{t}_A+\hat{t}_A')+\hat{L}_A+\hat{L}_A' \tag{6}$$

where

$$\hat{L}_A=\{th(y_{in}+\eta)+th(y_1-\eta)\}\hat{t}_A \tag{7a}$$

$$\hat{L}_A'=\{th(y_{in}-\eta)-th(y_2-\eta)\}\hat{t}_A' \tag{7b}$$

and

$$\hat{t}_A=\hat{t}_Q-\hat{t}_P=\{2R_A+S_h ch(y_{in}+\eta)\}ch(y_{in}-\eta)/sh(2y_{in}) \tag{8a}$$

$$\hat{t}_A'=\hat{t}_Q-\hat{t}_R=\{2R_A'+S_h ch(y_{in}-\eta)\}ch(y_{in}+\eta)/sh(2y_{in}) \tag{8b}$$

The factor S_h in Eqs. (8a) and (8b) comes from the size of nucleons. During the expansion, the particles in the system interact with each other (assumption (iii)) and the system is expected to tend gradually towards a thermalized state.

If we assume that all the hadrons in the system are pions, the mean free path of a pion is given as

$$\lambda(y_1,y_2;\hat{t})=\{\sigma_{in}^{\pi\pi}N(y_1,y_2)/V(\hat{t})\}^{-1} \tag{9}$$

We take $\sigma_{in}^{\pi\pi}$=20mb. The mean collision number $C_\pi(y_1,y_2;\hat{t})$ per pion, during the time of $0\leq\hat{t}'\leq\hat{t}$ can be obtained as follows;

$$\begin{aligned} C_\pi(y_1,y_2;\hat{t}) &= \int_0^{\hat{t}} d\hat{t}'\ \bar{v}(y_1,y_2)\ /\ \lambda(y_1,y_2;\hat{t}') \\ &= \frac{\sigma_{in}^{\pi\pi}\ \bar{v}(y_1,y_2)\ N(y_1,y_2)}{\pi R_A^2\{th(y_2-\eta)-th(y_1-\eta)\}}\ \ln\{\hat{z}^{AA}(y_1,y_2;\hat{t})/\hat{z}^{AA}(y_1,y_2;\hat{t}=0)\} \end{aligned} \tag{10}$$

The mean relative velocity $v(y_1,y_2)$ among the pions in the COMF used in eq.(10) is taken to be $(\overline{v^2})^{1/2}$, where

$$\overline{v^2}=\int_{y_1}^{y_2} dy\ th^2(y-\eta).dN/dy\ /\ N(y_1,y_2) \tag{11}$$

The remaining point for the numerical calculation of $\mathcal{E}$ and C_π is to obtain $N(y_1,y_2)$ in A-A' collisions. As the energy momentum conservation in the successive collision is very important, we employ the multi-chain model (MCM)/8/ to obtain $N(y_1,y_2)$. Only numerical results of $N(y_1,y_2)$ from MCM are tabulated in table I.

The results on the energy density, $\mathcal{E}$, of the system and the average collision number per pion, C_π, are shown in Fig. 2. (I) Incident energy dependence: Owing to the increase of $N(y_1,y_2)$, the energy density and the average collision number per pion, as

shown in Figs. 2(a)-(f), become larger as the incident energy increases. (II) Mass number dependence: As the nuclear mass number becomes larger, the total collision number in the A-A′ interaction increases. This leads to the increase of $N(y_1,y_2)$. We can confirm that ε and C_π increase with the nuclear mass number. The results on the collisions of $A < A'$, which is the case of the cosmic ray experiments /9,10/, are also shown in Fig.2(g) /9/, (h) /10/ and (i). (III) Dependence on rapidity region of the system: The difference of ε and C_π among various rapidity regions comes mainly from the change in values of $N(y_1, y_2)$, thus, both ε and C_π decrease as the system deviates from the central rapidity region. (IV) Finite size effect of hadrons: We have taken the frame-independent hadron size S_h (=1.0 fm) into account in $\hat{Z}^{AA}$. Of course, this acts to reduce the values of ε and C_π. Moreover, due to this finite size effect, ε and C_π decrease as Δy decreases.

From Figs.2(a)~(c) and (i) we can safely conclude that the thermalized QGM of life time 10^{-23} sec is realized in the central rapidity regions in A-A′ collisions of large enough nuclei at high enough incident energy. The spatial volume of the QGM is estimated as $V(\hat{t}) \sim 5\text{fm}\cdot\pi R_A^2$ even at $\hat{t}$ corresponding to $C_\pi = 3$. We have to notice that there exist the cases (Figs.2 (e),(f) and (h)) where the energy densities are above the critical value, for example, 0.6 GeV/fm , but the average collision number per pion are not sufficient to get a thermalized QGM, say $C_\pi \lesssim 3$.

Hereafter, we discuss several points on our formalism. In the MCM, leading nucleons are excluded from the application of the formation zone and repeatedly interact with nucleons in the colliding nucleus. Therefore, in the present formalism we cannot treat the fragmentation region in a consistent manner with the central region. It can be said if its application to leading nucleons is abandoned in Ref./4/, the predicted energy density of the fragmentation region may be shifted to higher values. If we include the possible cascade interaction of A-A collisions, ε and C_π in the central rapidity region may be larger than the value obtained here. To the contrary resonance or cluster production, in place of the direct pion, certainly reduce the number density of the system. Moreover, if emission of particles from a hit nucleon takes place at points which spread within the hadron size S_h, the maximum value of ε may somewhat decrease from our results. In our calculation, C_π is considered only within the longitudinal direction. Collisions are possible also in the transverse direction. Therefore, we may take rather smaller values of C_π as a criterion of the thermalization. On the other hand, the expansion of the system to the transverse direction acts to decrease the ε and C_π. At any rate quantitative investigation on the degree of freedom of the transverse direction is very important.

References

1) R.Anishetty, P.Koehler and L.McLerran, Phys.Rev.D22 (1980),2793.
2) J.D.Bjorken, Phys.Rev.D27 (1983),140.
3) M.Gyulassy, Preprint LBL-15175, Oct. 1982.
4) K.Kajantie, R.Raitio and P.V.Ruuskanen, TFT Preprint HU-TFT-83-9, Feb. 1983.
5) J.Engels et al., Phys.Lett.101B (1981),89; J.Kuti, J.Polonyi and K.Szlachanyi, Phys.Lett.98B (1981), 199; L.McLerran and B.Svetitsky, Phys.Lett.98B (1981), 195.
6) C.Ezell et al., Phys.Rev.Lett.16 (1977),873.
7) J.D.Bjorken Proceedings of the Summer Institute on Theoretical Particle Physics in Hamburg 1975, J.G.Korner , G.Kramer and Schildknecht(Editors), Springer-Verlag, Berlin, Heidelberg, New York 1976.
8) K.Kinoshita, A.Minaka and H.Sumiyoshi, Z.Phys.C8 (1981),205
9) S.Tasaka et al., Phys.Rev.D25 (1982),1765.
10) JACEE collabolation, AIP Conf.Proc.,No.85 Particles and Fields Subseries,No.26,p.552 ed. by V.Berger, D.Cline and F.Halzen AIP,New York 1982.

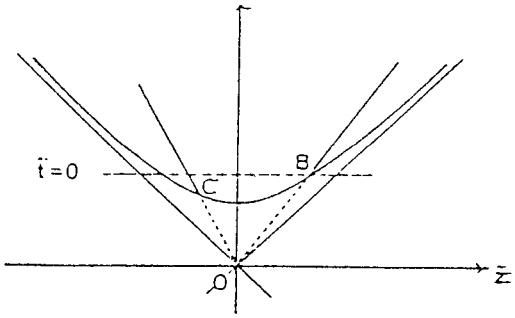

Fig.1a

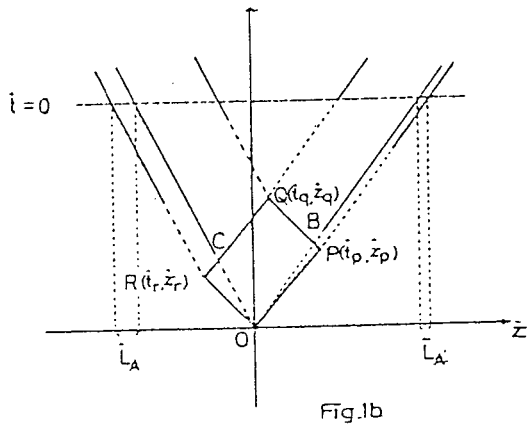

Fig.1b

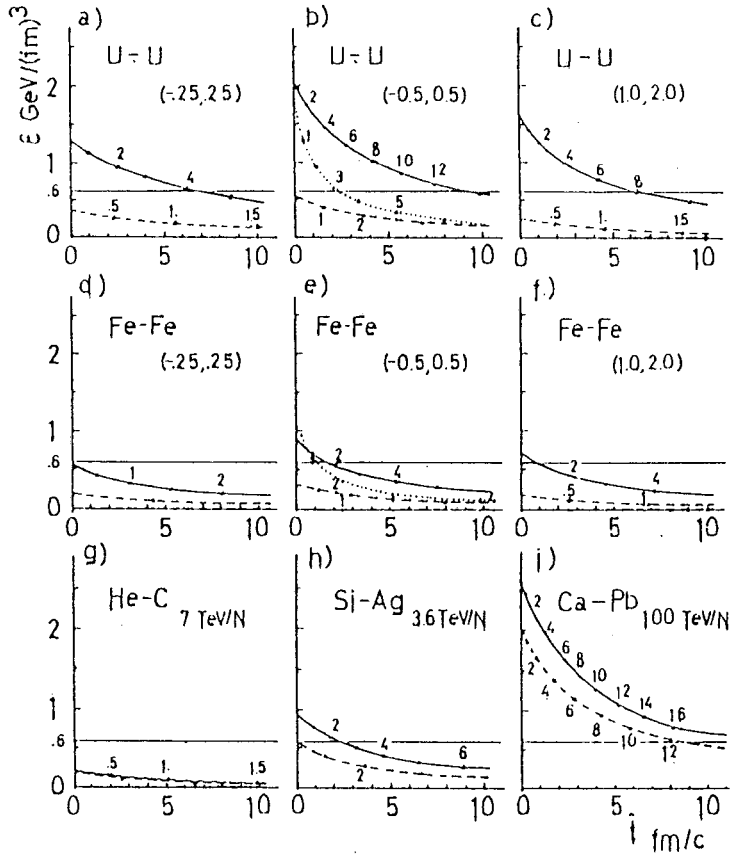

Fig.2

Fig.1: (a) The longitudinal extension of the hadronic system in a N-N collision. Secondary particles hadronize on the hyperbola in the COMF. (b), The same as (a) but of A-A collisions. Within the parallelogram, multiple N-N collisions take place.

Table I

A + A'	E(TeV/N)	N (-.5,.5)	N (1.,2.)	N (-.25,.25)
U + U	0.4	867	403	445
	10.0	3202	2440	1616
Fe+Fe	0.4	199	114	102
	10.0	508	420	256
He+C	7.0	23	19	11
Si+Ag	3.6	350	213	177
Ca+Pb	100.0	1224	942	614

Table I: Numerical results of $N(y_1,y_2)$ from MCM at incident energy, E (TeV/N) for various A-A collisions.

Fig.2: Energy density as a function of t for U-U collision ((a) (c)) and Fe-Fe collision ((d) (f)) at 0.4 TeV/N (broken lines) and 10 TeV/N (solid lines). The cases of different combination of nuclei are shown in (g) He-C, (h) Si-Ag and (i) Ca-Pb at rapidity interval (-0.5,0.5) (solid lines) and (1.0,2.0) (broken lines). The average collision number, C, per pion are indicated on each line. Dotted lines in (b) and (e) are the same as broken lines except they are calculated for the case of $S_h=0$ and $L_A=L_A'=0$. The maximum values of the result in this case is very close to that of Ref./4/.

SESSION VII: MORE OR LESS EXOTICA

STRANGENESS AND PHASE CHANGES IN HOT HADRONIC MATTER

J. Rafelski

CERN, Geneva, Switzerland
and
Institut für Theoretische Physik der Universität Frankfurt

1. PHASE TRANSITION OR PERHAPS TRANSFORMATION HADRONIC GAS AND THE QUARK GLUON PLASMA

I explore here consequences of the hypothesis that the energy available in the collision of two relativistic heavy nuclei, at least in part of the system, is equally divided among the accessible degrees of freedom. This means that there exists a domain in space in which, in a suitable Lorentz frame, the energy of the longitudinal motion has been largely transformed to transverse degrees of freedom. The physical variables characterizing such a "fireball" are: energy density, baryon number density, and total volume. The basic question concerns the internal structure of the fireball. It can consist either of individual hadrons, or instead, of quarks and gluons in a new physical phase, the plasma, in which they are deconfined and can move freely over the volume of the fireball. It appears that the phase transition from the hadronic gas phase to the quark-gluon plasma is controlled mainly by the energy density of the fireball. Several estimates[1] lead to 0.6-1 GeV/fm^3 for the critical energy density, to be compared with 0.16 GeV/fm^3 in nuclear matter.

We first recall that the unhandy extensive variables, viz., energy, baryon number, etc., are replaced by intensive quantities. To wit, the temperature T is a measure of energy per degree of freedom; the baryon chemical potential μ controls the mean baryon density. The statistical quantities such as entropy (= measure of the number available states), pressure, heat capacity, etc., also will be functions of T and μ, and will have to be determined. The theoretical techniques required for the description of the two quite different phases, viz., the hadronic gas and the quark-gluon plasma, must allow for the formulation of numerous hadronic resonances on the one side[2], which then at sufficiently high energy density dissolve into the state consisting of their constituents. At this point we must appreciate the importance and help by a finite, i.e., non-zero temperature in reaching the transition to the quark-gluon plasma: to obtain a high particle density, instead of only compressing the matter (which as it turns out is quite difficult), we also heat it up; many pions are generated in a collision, allowing the transition to occur at moderate, even vanishing baryon density[3].

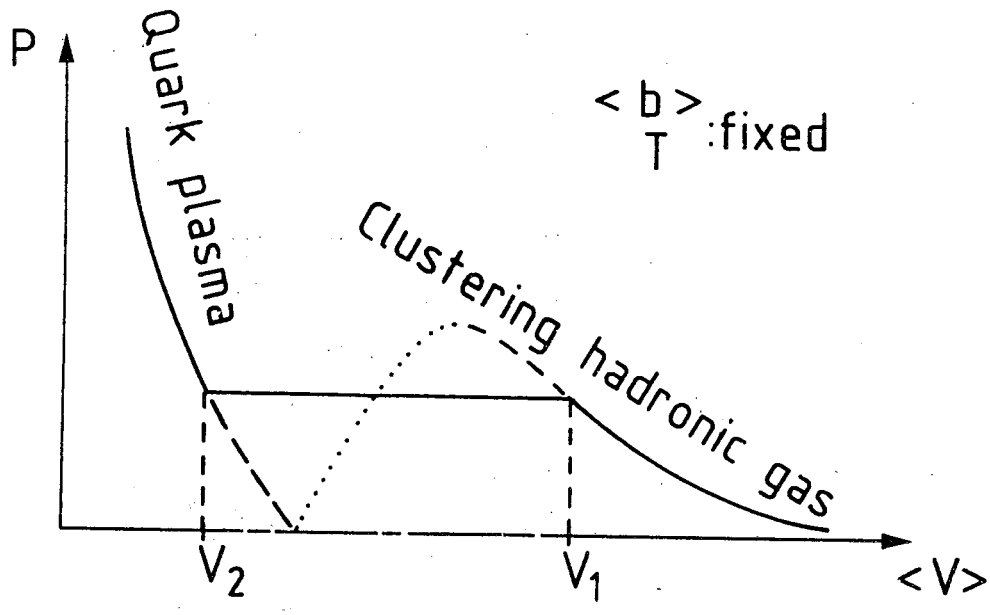

Fig. 1: p-V diagram for the gas-plasma first order transition, with the dots indicating a model-dependent, unstable domain between overheated and undercooled phases.

Consider, as an illustration of what is happening, the p-V diagram shown in Fig. 1. Here we distinguish three domains. The hadronic gas region is approximately a Boltzmann gas where the pressure rises with reduction of the volume. When the internal excitation rises, the individual hadrons begin to cluster. This reduces the increase in the Boltzmann pressure, since a smaller number of particles exercises a smaller pressure. In a complete description of the different phases we have to allow for a co-existence of hadrons with the plasma state in the sense that the internal degrees of freedom of each cluster, i.e., quarks and gluons, contribute to the total pressure even before the dissolution of individual hadrons. This indeed becomes necessary when the clustering overtakes the compressive effects and the hadronic gas pressure falls to zero as V reaches the proper volume of hadronic matter. At this point the pressure rises again very quickly, since in the absence of individual hadrons we now compress only the hadronic constituents. By performing the Maxwell construction between volumes V_1 and V_2, we can in part account for the complex process of hadronic compressibility alluded to above.

As this discussion shows, and detailed investigations confirm[4)], we cannot escape the conjecture of a first order phase transition in our approach. This conjecture of Ref. 1g) has been criticized, and only more recent lattice gauge theory calculations have led to the widespread acceptance of this phenomenon provided an internal SU(3) (colour) symmetry is used - SU(2) internal symmetry leads to a second order phase transition[1i)]. It is difficult to assess how such hypothetical changes in actual internal particle symmetry would influence phenomenological descriptions based on an observed picture of nature;

for example, it is difficult to argue that, were the colour symmetry SU(2) and not SU(3), we would still observe the resonance dominance of hadronic spectra and could therefore use the bootstrap model. All present understanding of phases of hadronic matter is based on approximate models, which requires that the table below be read from left to right.

Object →	Observational hypothesis→	Theoretical consequence
Nature →	Internal SU(3) symmetry →	1st order phase transition (on a lattice)
Nature →	Bootstrap ≙ Resonance dominance of hadronic interactions →	1st order phase transition (in a phenomenological bootstrap approach)
? →	Internal SU(2) symmetry →	2nd order phase transition (on a lattice)

Phase transition of hot hadronic matter in theoretical physics

I believe that the description of hadrons in terms of bound quark states on the one hand, and the statistical bootstrap for hadrons on the other hand, have many common properties and are quite complementary. Both the statistical bootstrap and the bag model of quarks are based on quite equivalent phenomenological observations. While it would be most interesting to derive the phenomenological models quantitatively from the accepted fundamental basis - the Lagrangian quantum field theory of a non-Abelian SU(3) "glue" gauge field coupled to coloured quarks - we will have to content ourselves in this report with a qualitative understanding only. Already this will allow us to study the properties of hadronic matter in both aggregate states: the hadronic gas and the state in which individual hadrons have dissolved into the plasma consisting of quarks and of the gauge field quanta, the gluons.

It is interesting to follow the path taken by an isolated quark-gluon plasma fireball in the μ-T plane, or equivalently in the ν-T plane. Several cases are depicted in Fig. 2. In the Big Bang expansion, the cooling shown by the dashed line occurs in a Universe in which most of the energy is in the radiation. Hence, the baryon density ν is quite small. In normal stellar collapse leading to cold neutron stars, we follow the dash-dotted line parallel to the ν-axis. The compression is accompanied by little heating.

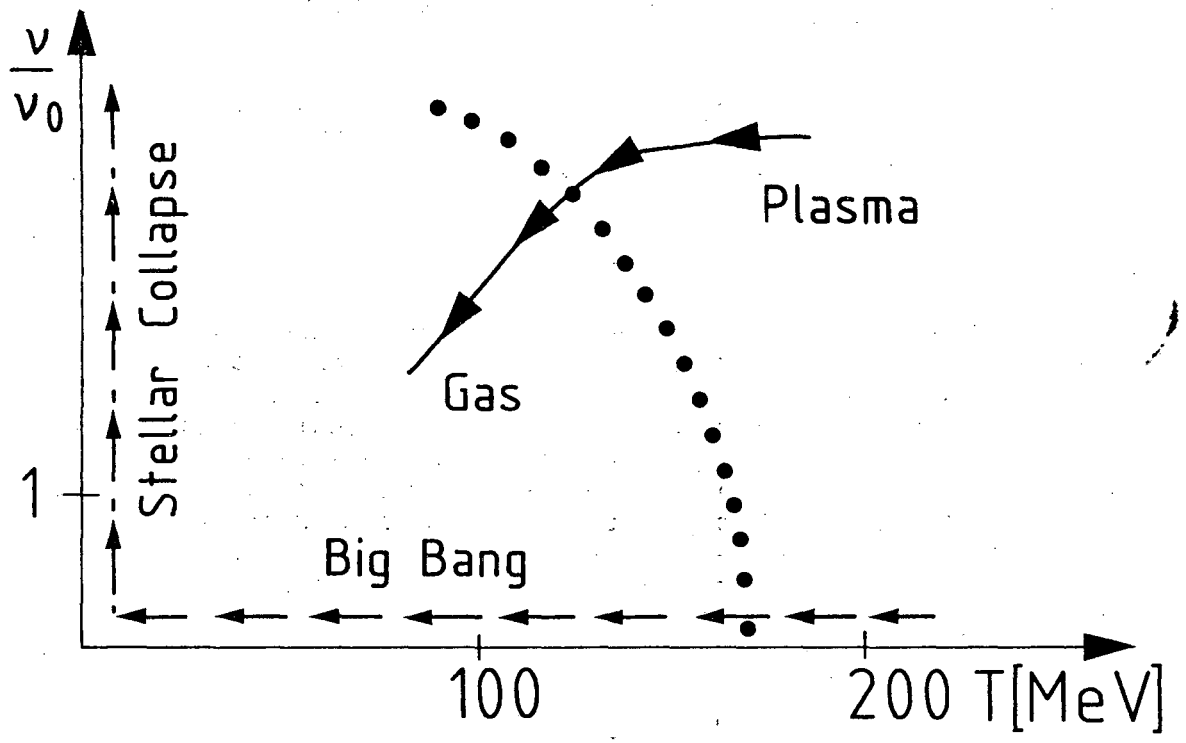

Fig. 2: Paths taken in the ν-T plane by different physical events.

In contrast, in nuclear collisions almost the entire ν-T plane can be explored by varying the parameters of the colliding nuclei. We show an example by the full line, and we show only the path corresponding to the cooling of the plasma, i.e., the part of the time evolution after the termination of the nuclear collision, assuming a plasma formation. The figure reflects the circumstance that in the beginning of the cooling phase, i.e., for $1 - 1.5 \times 10^{-23}$ sec., the cooling happens almost exclusively by the mechanism of pion radiation[5]. In typical circumstances, about half of the available energy has been radiated away before the expansion, which brings the surface temperature close to the temperature of the transition to the hadronic phase. Hence a possible, perhaps even likely, scenario is that in which the freezing-out and the expansion happen simultaneously. These highly speculative remarks are obviously made in the absence of experimental guidance. A careful study of the hadronization process most certainly remains to be performed.

In closing this section let me emphasize that the question whether the transition hadronic gas ↔ quark-gluon plasma is a phase transition (i.e., discontinuous) or continuous phase transformation will probably only be answered in actual experimental work, as all theoretical approaches suffer from approximations unknown in their effect. For

example, in lattice gauge computer calculations, we establish the properties of the lattice and not of the continuous space in which we live.

The remainder of this report is therefore devoted to the study of strange particles in different nuclear phases and their relevance to the observation of the quark-gluon plasma.

2. STRANGE PARTICLES IN HOT NUCLEAR GAS

My intention in this section is to establish quantitatively the different channels in which the strangeness, however created in nuclear collisions, will be found. In our following analysis a tacit assumption is made that the hadronic gas phase is practically a superposition of an infinity of different hadronic gases, and all information about the interaction is hidden in the mass spectrum $\tau(m^2,b)$ which describes the number of hadrons of baryon number b in a mass interval dm^2 and volume $V \sim m$. When considering strangeness-carrying particles, all we then need to include is the influence of the non-strange hadrons on the baryon chemical potential established by the non-strange particles. The total partition function is approximately multiplicative in these degrees of freedom:

$$\ln Z = \ln Z^{\text{nonstrange}} + \ln Z^{\text{strange}} . \tag{2.1}$$

For our purposes, i.e., in order to determine the particle abundances, it is sufficient to list the strange particles separately and we find

$$\ln Z^{\text{strange}}(T,V,\lambda_s,\lambda_q) = C\{2W(x_k)[\lambda_s\lambda_q^{-1} + \lambda_s^{-1}\lambda_q] + 2[W(x_\Lambda) + 3W(x_\Sigma)][\lambda_s\lambda_q^2 + \lambda_s^{-1}\lambda_q^{-2}]\} \tag{2.2}$$

where

$$W(x_i) = \left(\frac{m_i}{T}\right)^2 K_2\left(\frac{m_i}{T}\right) . \tag{2.3}$$

We have $C = VT^3/2\pi^2$ for a fully equilibrated state. However, strangeness-creating $(x \to s+\bar{s})$ processes in hot hadronic gas may be too slow (see below) and the total abundance of strange particles may fall short of this value of C expected in absolute strangeness chemical equilibrium. On the other hand, strangeness-exchange cross-sections are very large (e.g., K^-p cross-section is $\sim$100mb in the momentum range of interest), and therefore any momentarily available strangeness will always be distributed among all particles in (2.2) according to the values of the fugacities $\lambda_q = \lambda_B^{1/3}$ and λ_s. Hence we can speak of relative strangeness chemical equilibrium.

We neglected to write down quantum statistics corrections as well as the multistrange particles, Ξ and Ω^-, as our considerations remain valid in this simple approximation[6]. Interactions are effectively included through explicit reference to the baryon number content of the strange particles as just discussed. Non-strange hadrons influence the strange fraction by establishing the value of λ_q at the given temperature and baryon density.

The fugacities λ_s and λ_q as introduced here control the strangeness and the baryon number respectively. While λ_s counts the strange quark content, the up- and down-quark content is counted by $\lambda_q = \lambda_B^{1/3}$.

Using the partition function Eq. (2.2) we calculate for given μ_B, T, and V the mean strangeness by evaluating

$$\langle n_s - n_{\bar{s}} \rangle = \lambda_s \frac{\partial}{\partial \lambda_s} \ln Z^{strange} (T, V, \lambda_s, \lambda_q), \tag{2.4}$$

which is the difference between strange and antistrange components. This expression must be equal to zero due to the fact that the strangeness is a conserved quantum number with respect to strong interactions. From this condition we get:

$$\lambda_s = \lambda_q \left| \frac{W(x_k) + \lambda_B^{-1} [W(x_\Lambda) + 3W(x_\Sigma)]}{W(x_k) + \lambda_B [W(x_\Lambda) + 3W(x_\Sigma)]} \right|^{1/2} \equiv \lambda_q \gamma, \tag{2.5}$$

a result contrary to intuition: $\lambda_s \neq 1$ for a gas with total $\langle s \rangle = 0$. We notice a strong dependence of γ on the baryon number. For large μ_B the term with λ_B^{-1} will tend to zero and the term with λ_B will dominate the expression for λ_s and γ. As a consequence the particles with fugacity λ_s and strangeness s = -1 (note that by convention strange quarks s carry s = -1, while strange antiquarks $\bar{s}$ carry s = 1) are suppressed by a factor γ which is always smaller than unity. Conversely, the production of particles which carry the strangeness s = +1 will be favoured by γ^{-1}. This is the consequence of the presence of nuclear matter; for $\mu = 0$ we find $\gamma = 1$.

In nuclear collisions the mutual chemical equilibrium, that is, a proper distribution of strangeness among the strange hadrons, will most likely be thus achieved. By studying the relative yields, we can exploit this fact and eliminate the absolute normalization, C, cf., Eq. (2.2), from our considerations. We recall that the value of C is uncertain for several reasons: (i) V is unknown, (ii) C is (through space-time dependence of temperature) strongly (t,r)-dependent, and (iii) most importantly, the absolute normalization $C = VT^3/2\pi^2$ which

assumes absolute chemical equilibrium, is not achieved owing to the shortness of the collision. Indeed we have [cf., Eq. (4.3) for further details and solutions]

$$\frac{dC}{dt} = A_H \left(1 - C(t)^2 / C^2(\infty)\right) . \tag{2.6}$$

and the time constant $\tau_H = C(\infty)/A_H$ for strangeness production in nuclear matter can be estimated to be 10^{-21}sec.[7]. Thus C does not reach $C(\infty)$ in plasmaless nuclear collisions. If the plasma state is formed, then the relevant $C > C(\infty)$ (see below).

Now, why should we expect relative strangeness equilibrium to be reached faster than absolute strangeness equilibrium[2]? Consider the strangeness exchange reaction

$K^- p \to \Lambda \pi^0$

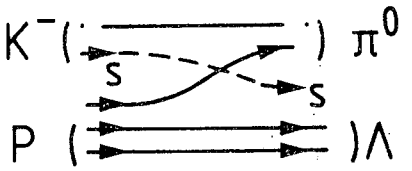

(2.7)

which has a cross-section of about 10mb at low energies while the $s\bar{s}$ "strangeness-creating" associate production

$pp \to p\Lambda K^+$

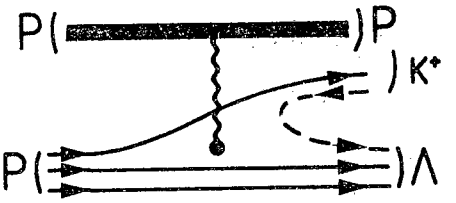

(2.8)

has a cross-section of less than 0.06mb, i.e., 150 times smaller. Since the latter reaction is somewhat disfavoured by phase space, consider further the reaction (Y is any hyperon = strange baryon)

$\pi p \to Y K$

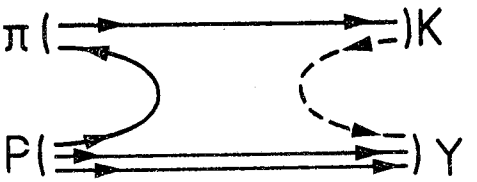

(2.9)

which has a cross-section of less than 1mb, still 10 times weaker than one of the s exchange channels (2.7). Consequently, I expect the relative strangeness equilibration time to be about ten times shorter than the absolute strangeness equilibration time, namely 10^{-23}sec., in hadronic matter of about twice nuclear density.

We now compute the relative strangeness abundances expected from nuclear collisions. Using Eq. (2.5) we find from Eq. (2.2) the grand canonical partition sum for zero average strangeness:

$$\ln Z_0^{strange} = C\{2W(x_K)[\gamma\lambda_K + \gamma^{-1}\lambda_{\bar{K}}] + 2W(x_\Lambda)[\gamma\lambda_B\lambda_\Lambda + \gamma^{-1}\lambda_B^{-1}\lambda_{\bar{\Lambda}}] + 6W(x_\Sigma)[\gamma\lambda_B\lambda_\Sigma + \gamma^{-1}\lambda_B^{-1}\lambda_{\bar{\Sigma}}]\}, \tag{2.10}$$

where, in order to distinguish different hadrons, dummy fugacities λ_i, $i = K, \bar{K}, \Lambda, \bar{\Lambda}, \Sigma, \bar{\Sigma}$ have been written: the strange particle multiplicities follow then from

$$\langle n_i \rangle = \lambda_i \frac{\partial}{\partial \lambda_i} \ln Z_0^{strange} \Big|_{\lambda_i = 1} . \tag{2.11}$$

Explicitly we find (notice that the power of γ follows the s-quark content):

$$\langle n_{K^\pm} \rangle = C\gamma^{\mp 1} W(x_K) \tag{2.12}$$

$$\langle n_{\Lambda/\Sigma^0} \rangle = C\gamma^{+1} W(x_{\Lambda/\Sigma^0}) e^{+\mu_B/T} \tag{2.13}$$

$$\langle n_{\bar{\Lambda}/\bar{\Sigma}^0} \rangle = C\gamma^{-1} W(x_{\bar{\Lambda}/\bar{\Sigma}^0}) e^{-\mu_B/T} . \tag{2.14}$$

In Eq. (2.14) we have indicated that the multiplicity of antihyperons can only be built up if antibaryons are present according to their (small) phase-space. This still seems an unlikely proposition and the statistical approach may be viewed to provide an upper limit on their multiplicity.

From the above equations we can derive several very instructive conclusions[8]. In Fig. 3 we show the ratio $\langle n_{K^+}\rangle/\langle n_{K^-}\rangle = \gamma^{-2}$ as a function of the baryo-chemical potential μ_B for several temperatures that can be expected and which are seen experimentally.

We note that this particular ratio is a good measure of the baryon chemical potential in the hadronic gas phase, provided that the temperatures are approximately known. The mechanism for this process is: the strangeness exchange reaction [Eq. (2.7)] tilts to the left (K^-) or to the right (abundance $\gamma \sim K^+$), depending on the value of the baryo-chemical potential.

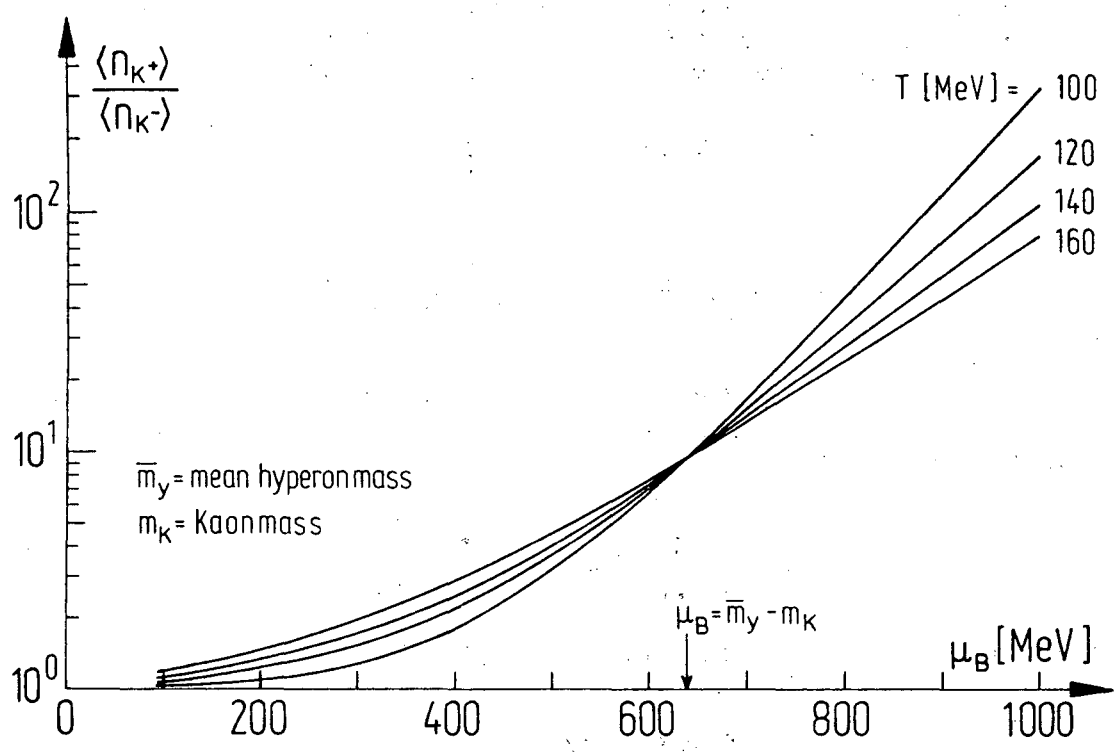

Fig. 3: The ratio $\langle n_{K^+}\rangle/\langle n_{K^-}\rangle = \gamma^{-2}$ as function of the baryo-chemical potential for several temperatures.

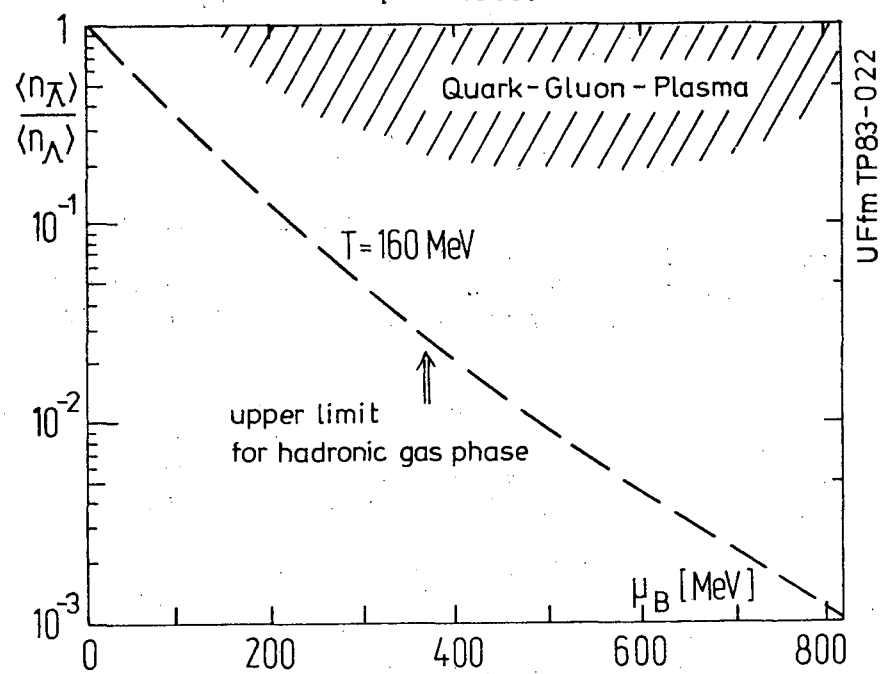

Fig. 4: Relative abundance of antilambdas: the actual yield from the hadronic gas limit may be still 10-100 times smaller than the statistical value shown.

In Fig. 4 the upper limit for the abundance of $\bar{\Lambda}$ as measured in terms of Λ-abundances is shown. Clearly visible is the substantial relative suppression of $\bar{\Lambda}$, in part caused by the baryo-chemical potential factor, Eq. (2.14), but also by the strangeness chemistry (factor γ^2) as in K^+K^- above. Indeed, the actual relative number of $\bar{\Lambda}$ will be even smaller, since Λ are in relative chemical equilibrium and $\bar{\Lambda}$ are not: the reaction $K^+\bar{p} \to \bar{\Lambda}\pi^0$, analogue to (2.7), will be suppressed by low $\bar{p}$ abundance. Also indicated in the Fig. 4 is a rough estimate for the $\bar{\Lambda}$ production in the plasma phase, which suggests that anomalous $\bar{\Lambda}$ abundances may be an interesting feature of highly energetic nuclear collisions[6] (cf. Section 5).

3. QUARK-GLUON PLASMA

From the study of hadronic spectra, as well as from hadron-hadron and hadron-lepton interactions, there has emerged convincing evidence for the description of hadronic structure in terms of quarks[9]. For many purposes it is entirely satisfactory to consider baryons as bound states of three fractionally charged particles, while mesons are quark-antiquark bound states. The Lagrangian of quarks and gluons is very similar to that of electrons and photons except for the required summations over flavour and colour:

$$L = \bar{\Psi}(\gamma\cdot(p-gA)-m)\Psi - \frac{1}{4}F_{\mu\nu}F^{\mu\nu}. \tag{3.1}$$

The flavour-dependent masses m of the quarks are small. For u, d flavours, one estimates $m_{u,d} \sim 5$-20 MeV. The strange quark mass is usually chosen at about 150 MeV[10]. The essential new feature of QCD, not easily visible in Eq. (3.1), is the non-linearity of the field strength F in terms of the potentials A. This leads to an attractive glue-glue interaction in select channels and, as is believed, requires an improved (non-perturbative) vacuum state in which this interaction is partially diagonalized, providing for a possible perturbative approach.

The energy density of the perturbative vacuum state, defined with respect to the true vacuum state, is by definition a positive quantity, denoted by B. This notion has been introduced originally in the MIT bag model[11], logically, e.g., from a fit to the hadronic spectrum[11], which gives

$$B = [(140-210)\,\mathrm{MeV}]^4 = (50-250)\,\mathrm{MeV/fm}^3. \tag{3.2}$$

The central assumption of the quark-bag approach is that inside a hadron where quarks are found, the true vacuum structure is displaced or destroyed. One can turn this point around: quarks can only propagate in domains of space in which the true vacuum is absent. This statement is a reformulation of the quark confinement problem. Now the remaining difficult problem is to show the incompatibility of quarks with the true vacuum structure. Examples of such behaviour in ordinary physics

are easily found: e.g., a light wave is reflected from a mirror surface; magnetic field lines are expelled from superconductors; etc. In this picture of hadronic structure and quark confinement all colourless assemblies of quarks, antiquarks, and gluons can form stationary states, called a quark bag. In particular all higher combinations of the three-quark baryons (qqq) and quark-antiquark mesons ($q\bar{q}$) form a permitted state.

As the u and d quarks are almost massless inside a bag, they can be produced in pairs, and at moderate internal excitations, i.e., temperatures, many $q\bar{q}$ pairs will be present. Similarly, $s\bar{s}$ pairs will also be produced. We will return to this point at length below. Furthermore, real gluons can be excited and will be included here in our considerations.

Thus, what we are considering here is a large quark bag with substantial, equilibrated internal excitation, in which the interactions can be handled (hopefully) perturbatively. In the large volume limit, which, as can be shown, is valid for baryon number $b \gtrsim 10$, we simply have for the light quarks the partition function of a Fermi gas which, for practically massless u and d quarks can be given analytically[12),1b)] even including the effects of interactions through first order in $\alpha_s = g^2/4\pi$:

$$\ln Z_q(\beta,\mu) = \frac{gV}{6\pi^2}\beta^{-3}\left[\left(1-\frac{2\alpha_s}{\pi}\right)\left(\frac{1}{4}(\mu\beta)^4+\frac{\pi^2}{2}(\mu\beta)^2\right)+\left(1-\frac{50}{21}\frac{\alpha_s}{\pi}\right)\frac{7\pi^4}{60}\right]. \tag{3.3}$$

Similarly, the glue is a Bose gas

$$\ln Z_g(\beta,\lambda) = V\,\frac{8\pi^2}{45}\,\beta^{-3}\left(1-\frac{15}{4}\frac{\alpha_s}{\pi}\right), \tag{3.4}$$

while the term associated with the difference to the true vacuum, the bag term, is

$$\ln Z_{bag} = -BV\beta. \tag{3.5}$$

It leads to the required positive energy density B within the volume occupied by the coloured quarks and gluons and to a negative pressure on the surface of this region. At this stage, this term is entirely phenomenological as discussed above. The equations of state for the quark-gluon plasma are easily obtained by differentiating

$$\ln Z = \ln Z_q + \ln Z_g + \ln Z_{vac}, \tag{3.6}$$

with respect to β, μ, and V.

An assembly of quarks in a bag will assume a geometric shape and size such as to make the total energy E(V,b,S) as small as possible at fixed given baryon number and fixed total entropy S. Instead of just considering one bag we may, in order to be able to use the methods of statistical physics, use the microcanonical ensemble. We find from the first law of thermodynamics

$$dE = -PdV + TdS + \mu db \tag{3.7}$$

that

$$P = -\frac{\partial E(V,b,S)}{\partial V} \tag{3.8}$$

We observe that stable configuration of a single bag, $\partial E/\partial V = 0$, corresponds also to the configuration with vanishing pressure P in the microcanonical ensemble. Rather than work in the microcanonical ensemble with fixed b and S, we exploit the advantages of the grand canonical ensemble and consider P as a function of μ and T:

$$P = -\frac{\partial}{\partial V}\left(T \ln Z(\mu, T, V)\right) \tag{3.9}$$

with the result

$$P = \frac{1}{3}(\varepsilon - 4B), \tag{3.10}$$

where ε is the energy density:

$$\varepsilon = \frac{6}{\pi^2}\left[\left(1-\frac{2\alpha_s}{\pi}\right)\left(\frac{1}{4}\left(\frac{\mu}{3}\right)^4 + \frac{1}{2}\left(\frac{\mu}{3}\right)^2(\pi T)^2\right) + \left(1-\frac{50}{21}\frac{\alpha_s}{\pi}\right)\frac{7}{60}(\pi T)^4\right] + \frac{8}{15\pi^2}(\pi T)^4\left(1-\frac{15}{4}\frac{\alpha_s}{\pi}\right) + B \tag{3.11}$$

In Eq. (3.10) we have used the relativistic relation between the quark and gluon energy density and pressure:

$$P_q = \frac{1}{3}\varepsilon_q, \qquad P_g = \frac{1}{3}\varepsilon_g. \tag{3.12}$$

From Eq. (3.10), it follows that when the pressure vanishes in a static configuration, the energy density is 4B, independent of the values of μ and T which fix the line P = 0. We note that in both quarks and gluons the interaction conspires to reduce the effective available number of degrees of freedom. At $\alpha_s = 0$, $\mu = 0$, we find the handy relation

$$\varepsilon_q + \varepsilon_g = \left(\frac{T}{160\,\mathrm{MeV}}\right)^4 \left[\frac{\mathrm{GeV}}{\mathrm{fm}^3}\right]. \tag{3.13}$$

It is important to appreciate how much entropy must be created to reach the plasma state. From Eq. (3.6), we find for the baryon density ν and entropy density $\mathcal{S}$:

$$\mathcal{S} = \frac{2}{\pi}\left(1-\frac{2\alpha_s}{\pi}\right)\left(\frac{\mu}{3}\right)^2(\pi T) + \frac{14}{15\pi}\left(1-\frac{50}{21}\frac{\alpha_s}{\pi}\right)(\pi T)^3 + \frac{32}{45\pi}\left(1-\frac{15}{4}\frac{\alpha_s}{\pi}\right)(\pi T)^3. \tag{3.14}$$

$$\nu = \frac{2}{3\pi^2}\left[\left(1-\frac{2\alpha_s}{\pi}\right)\left(\left(\frac{\mu}{3}\right)^3 + \frac{\mu}{3}(\pi T)^2\right)\right], \tag{3.15}$$

which leads for $\mu/3 = \mu_q < (\pi T)$ to the following expression for the entropy per baryon [including the gluonic entropy second T^3 term in Eq. (3.14)]

$$S/V \approx 37/15\,\pi^2\,(T/\mu_q) \xrightarrow{T\sim\mu_q} 25\ ! \tag{3.16}$$

As this simple estimate shows, plasma events are extremely entropy-rich, i.e., they contain very high particle multiplicity. In order to estimate the particle multiplicity, one may simply divide the total entropy created in the collision by the entropy per particle for massless black body radiation, which is $S/n = 4$. This suggests that at $T \sim \mu_q$ there are $\sim$ six pions per baryon

4. STRANGE QUARKS IN PLASMA

In lowest order in perturbative QCD, $s\bar{s}$-quark pairs can be created by annihilation of light quark-antiquark pairs (Fig. 5a) and in collisions of two gluons (Fig. 5b). The averaged total cross-sections for these processes were calculated by Combridge[13].

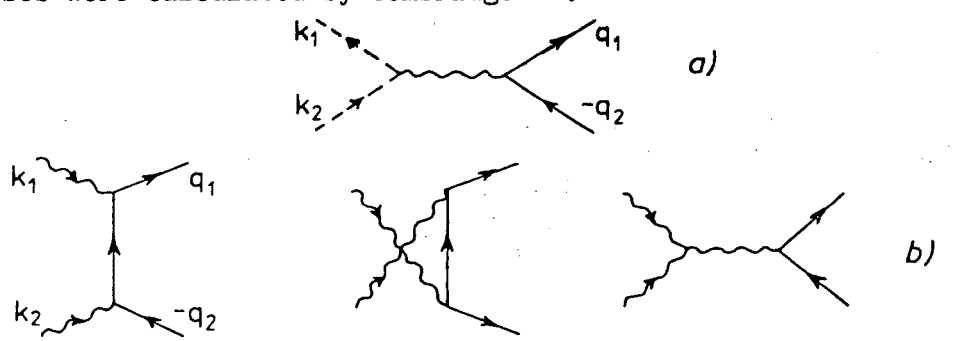

Fig. 5: Lowest order QCD diagrams for ss production: a) $qq \to s\bar{s}$; b) $gg \to s\bar{s}$.

Given the averaged cross-sections, it is easy to calculate the rate of events per unit time, summed over all final and averaged over initial states:

$$\frac{dN}{dt} = \int d^3x \int \frac{d^3k_1}{(2\pi)^3|k_1|} \sum_i \rho_i(k_1,x)$$

$$\int \frac{d^3k_2}{(2\pi)^3|k_2|} \sum_i \rho_i(k_2,x) \int_{4M^2}^{\infty} ds\, \delta(s-(k_1+k_2)^2)\, k_1^{\mu} k_{2\mu}\, \bar{\sigma}(s). \tag{4.1}$$

The factor $k_1 \cdot k_2/|k_1||k_2|$ is the relative velocity for massless gluons or light quarks, and we have introduced a dummy integration over s in order to facilitate the calculations. The phase-space densities $\rho_i(k,x)$ can be approximated by assuming the x-independence of temperature T(x) and the chemical potential $\mu(x)$, in the so-called local statistical equilibrium. Since ρ then only depends on the absolute value of $\vec{k}$ in the rest frame of the equilibrated plasma, we can easily carry out the relevant integrals and obtain for the dominant process of the gluon reaction (Fig. 5b) the invariant rate per unit time and volume[14)]

$$A = \frac{d^4N}{d^3x\,dt} \approx A_g = \frac{7}{3\pi^2}\alpha_s^2 M T^3 e^{-2M/T}\left(1+\frac{51}{14}\frac{T}{M}+\ldots\right), \tag{4.2}$$

where M is the strange quark mass.

The abundance of $s\bar{s}$-pairs cannot grow forever; at some point the $s\bar{s}$-annihilation reaction will restrict the strange quark population. It is important to appreciate that the $s\bar{s}$-pair annihilations may not proceed via the two-gluon channel, but instead occasionally through γG final states[15)]. The noteworthy feature of such a reaction is the production of relatively highly energetic γ's at an energy of about 700-900 MeV (T = 160 MeV) stimulated by coherent glue emission. These γ's will leave the plasma without further interactions and provide an independent confirmation of the s-abundance in the plasma.

The loss term of the strangeness population is proportional to the square of the density n_s of strange and antistrange quarks. With $n_s(\infty)$ being the saturation density at large times, the following differential equation determines n_s as a function of time[2b)]:

$$\frac{dn_s}{dt} \approx A\left[1-(n_s(t)/n_s(\infty))^2\right]. \tag{4.3}$$

Thus we find

$$n_s(t) = n_s(\infty)\,\frac{\tanh(t/\tau) + n_s(0)/n_s(\infty)}{1 + n_s(0)/n_s(\infty)\,\tanh(t/\tau)}\,, \tag{4.4}$$

where

$$\tau = n_s(\infty)/A\,. \tag{4.5}$$

The relaxation time, τ, Eq. (4.5) of the strange quark density is easily obtained using the saturated phase-space in Eq. (4.5). We have[14)]

$$\tau \approx \tau_g = \frac{9}{7}\left(\frac{\pi}{2}\right)^{1/2} \alpha_s^{-2} M^{1/2} T^{-3/2} e^{M/T}\left(1 + \frac{99}{56}\frac{T}{M} + \ldots\right)^{-1}. \tag{4.6}$$

For $\alpha_s \sim 0.6$ and $M \sim T$, we find from Eq. (4.6) that $\tau \sim 4\cdot 10^{-23}$sec. τ falls rapidly with increasing temperature; in Fig. 6, I show the approach to the fully saturated phase-space as a function of time, Eq. (4.4). For $M \lesssim T = 160$ MeV, the saturation requires $4\cdot 10^{-23}$sec., while for $T = 200$ MeV we need $2\cdot 10^{-23}$sec., corresponding to the anticipated lifetime of the plasma. But it is important to observe that even at $T = 120$ MeV, the phase-space is half-saturated in $2\cdot 10^{-23}$sec., a point to which we will return below. Another remarkable fact is the high abundance of strangeness relative to baryon number in Fig. 6 - here, baryon number was computed assuming $T \sim \mu_q = \frac{1}{3}\mu$, c.f., Eq. (3.15).

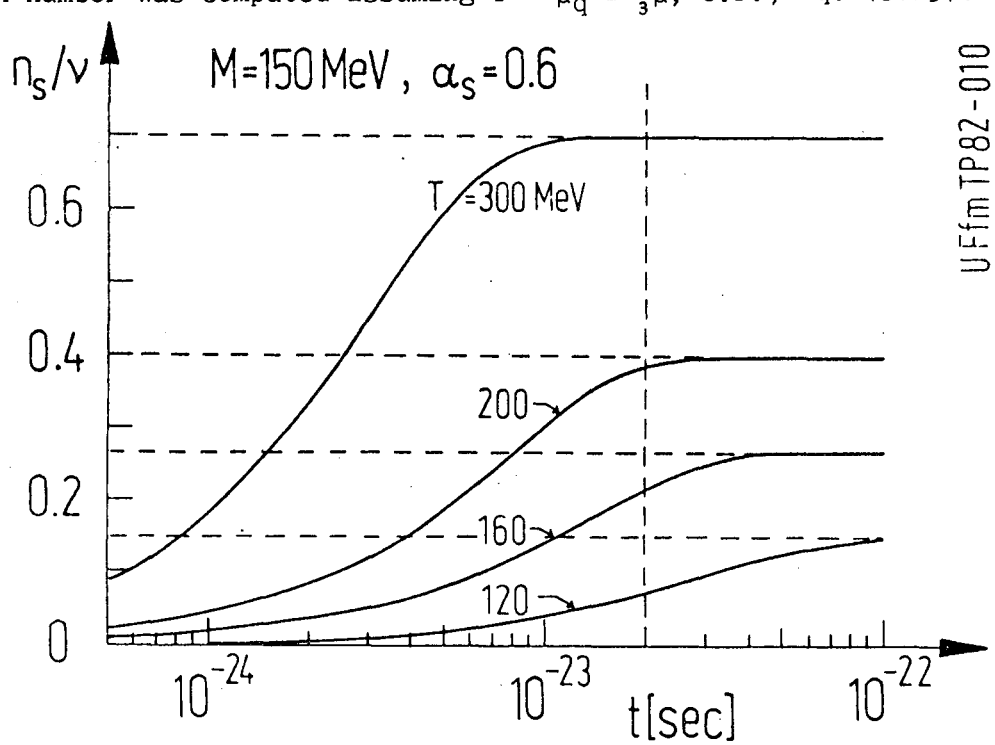

Fig. 6: Time evolution of the relative strange quark to baryon number abundance in the plasma for various temperatures T. M = 150 MeV, α_s = 0.6.

These two facts, namely

1) high relative strangeness abundance in plasma;
2) practical saturation of available phase space, as demonstrated above

have led me to suggest the observation of strangeness as a possible signal of quark-gluon plasma[16]. There are two elements in point 1) above: firstly, strangeness in the quark-gluon phase is practically as abundant as the antilight quarks, $\bar{u} = \bar{d} = \bar{q}$, since both phase spaces have similar suppression factors: for $\bar{u}$, $\bar{d}$ it is the baryo-chemical potential, for $s, \bar{s}$ the mass ($M \approx \mu_q$):

$$s/V = \bar{s}/V = 6\int \frac{d^3p}{(2\pi)^3} \frac{1}{\left(e^{\sqrt{p^2+M^2}/T} + 1\right)} \tag{4.7a}$$

$$\bar{q}/V = 6\int \frac{d^3p}{(2\pi)^3} \frac{1}{\left(e^{|p|/T+\mu_q/T} + 1\right)} \tag{4.7b}$$

Note that the chemical potential of quarks suppresses the $\bar{q}$ density. This phenomenon reflects on the chemical equilibrium between q-$\bar{q}$ and the presence of a light quark density associated with the net baryon number. Secondly, strangeness in the plasma phase is more abundant than in the hadronic gas phase (even if the latter phase space is saturated) when compared at the <u>same</u> temperature and baryo-chemical potential in the phase transition region. The rationale for the comparison at fixed thermodynamic variables, rather than at fixed values of microcanonical variables such as energy density and baryon density, is outlined in the next section. I record here only that the abundance of strangeness in the plasma is well above that in the hadronic gas phase space (by factors 1-6) and the two become equal only when the baryo-chemical potential μ is so large that abundant production of hyperons becomes possible. This requires a hadronic phase at an energy density of 5-10 GeV/fm^3.

5. HOW TO DISCOVER THE QUARK-GLUON PLASMA

Here only the role of the strange particles in the anticipated discovery will be discussed. My intention is to show that under different possible transition scenarios, characteristic anomalous strange particle patterns emerge. Examples presented are intended to provide some guidance to future experiments and are not presented here in order to imply any particular preference for a reaction channel. I begin with a discussion of the observable quantities.

Temperature and chemical potential associated with the hot and dense phase of nuclear collision can be connected with the observed particle spectra, and, as discussed here, particle abundances. The last grand canonical variable - the volume - can be estimated from particle interferences. Thus, it is possible to use these measured variables - even if their precise values are dependent on a particular interpretational model - to uncover possible rapid changes in a particular observable. In other words, instead of considering a particular particle multiplicity as a function of the collision energy, $\sqrt{s}$, I would consider it as a function of, e.g., mean transverse momentum $\langle p_\perp \rangle$, which is a continuous function of the temperature (which is continuous across any phase transition boundary).

To avoid possible misunderstanding of what I want to say, here I consider the (difficult) observation of the width of the K^+ two-particle correlation function in momentum space as a function of the average K^+ transverse momentum obtained at given $\sqrt{s}$. Most of K^+ would originate from the plasma region, which, when it is created, is relatively small, leading to a comparatively large width. (Here I have assumed a first order phase transition with substantial increase in volume as matter changes from plasma to gas.) If, however, the plasma state were not formed, K^+ originating from the entire hot hadronic gas domain would contribute a relatively large volume which would be seen; thus the width of the two-particle correlation function would be small. Thus, first order phase transition implies a jump in the K^+ correlation width as a function of increasing $\langle p_\perp \rangle_{K^+}$, as determined in the same experiment, varying $\sqrt{s}$.

From this example emerges the general strategy of my approach: search for possible discontinuities in observables derived from discontinuous quantities (such as volume, particle abundances, etc.) as a function of quantities measured experimentally and related to thermodynamic variables always continuous at the phase transition: temperature, chemical potentials and pressure. This strategy, of course, can only be followed if, as stated in the first sentence of this report, approximate local thermodynamic equilibrium is also established.

Strangeness seems to be particularly useful for plasma diagnosis, because its characteristic time for chemical equilibration is of the same order of magnitude as the expected lifetime of the plasma: $\tau \sim 1-3 \cdot 10^{-23}$ sec. This means that we are dominantly creating strangeness in the zone where the plasma reaches its hottest stage - freezing over the abundance somewhat as the plasma cools down. However, the essential effect is that the strangeness abundance in the plasma is greater, by a factor of ~ 30, than that expected in the hadronic gas phase at the same values of (μ, T). Before carrying this further, let us note that in order for strangeness to disappear partially during the phase transition we must have a <u>slow</u> evolution, with time constants of $\sim 10^{-22}$ sec. But even so, we would end up with strangeness-saturated phase space in the hadronic gas phase, i.e., $\sim$ ten times more strangeness than otherwise expected. For similar reasons, i.e., in view of

the rather long strangeness production time constants in the hadronic gas phase, strangeness abundance survives practically unscathed in this final part of the hadronization as well. Facit:

> if a phase transition to the plasma state has occurred, then on return to the hadron phase there will be most likely significantly more strange particles around than there would be (at this T and μ) if the hadron gas phase had never been left.

In my opinion, the simplest observable proportional to the strange particle multiplicity is the rate of V-events from the decay of strange neutral baryons (e.g., Λ) and mesons (e.g., K_S) into two charged particles. Observations of this rate require a visual detector, e.g., a streamer chamber. To estimate the multiplicity of V-events, I reduce the total strangeness created in the collision by a factor 1/3 to select only neutral hadrons and another factor 1/2 for charged decay channels. We thus have

$$\langle n_V \rangle \approx 1/6 \; \frac{\langle s \rangle + \langle \bar{s} \rangle}{\langle b \rangle} \; \langle b \rangle \sim \langle b \rangle / 15, \qquad (5.1)$$

where I have taken $\langle s \rangle / \langle b \rangle \sim 0.2$, cf. Fig. 6. Thus for events with a large baryon number participation, we can expect to have several V's per collision, which is 100-1000 times above current observation for Ar -KCl collision at 1.8 GeV/Nuc kinetic energy[17].

Due to the high $\bar{s}$ abundance, we may further expect an enrichment of strange antibaryon abundances[16]. I would like to emphasize here $\bar{s}\bar{s}\bar{q}$ states (anticascades) created by the accidental coagulation of two $\bar{s}$ quarks helped by a gluon $\to \bar{q}$ reaction. Ultimately, the $\bar{s}\bar{s}\bar{q}$ states become $\bar{s}\bar{q}\bar{q}$, either through an $\bar{s}$ exchange reaction in the gas phase or via a weak interaction much, much later. However, half of the $\bar{s}\bar{q}\bar{q}$ states are then visible as $\bar{\Lambda}$ decays in a visual detector. This anomaly in the apparent $\bar{\Lambda}$ abundance is further enhanced by relating it to the decreased abundance of antiprotons as described above.

Unexpected behaviour of the plasma-gas phase transition can greatly influence the channels in which strangeness is found. For example, in an extremely particle-dense plasma, the produced $s\bar{s}$ pairs may stay near to each other - if a transition occurs without any dilution of the density then I would expect a large abundance of $\phi(1020)$ $s\bar{s}$ mesons, easily detected through their partial decay mode (1/4%) to a $\mu^+\mu^-$ pair.

Contrary behaviour will be recorded if the plasma is cool at the phase transition, and the transition proceeds slowly - major coagulation of strange quarks can then be expected with the formation of sss and $\bar{s}\bar{s}\bar{s}$ baryons and in general $(s)^{3n}$ clusters. Carrying this even further, supercooled plasma may become "strange" nuclear (quark) matter[18]. Again, visual detectors will be extremely successful here, showing substantial decay cascades of the same heavy fragment.

In closing this discussion I would like to give warning about the pions. From the equations of state of the plasma, we have deduced in Section 3 very high specific entropy per baryon. This entropy can only increase in the phase transition and it leads to very high pion multiplicity in nuclear collisions, probably created through pion radiation from the plasma[5] and sequential decays. Hence by relating anything to the pion multiplicity, e.g., considering K/π ratios, we dilute the signal from the plasma. Furthermore, pions are not at all characteristic for the plasma; they are simply indicating high entropy created in the collision. However, we note that the K/π ratio can show substantial deviations from values known in pp collisions - but the interpretations of this phenomenon will be difficult.

It is important to appreciate that the experiments discussed above would certainly be quite complementary to the measurements utilizing electromagnetically interacting probes, e.g., dileptons, direct photons. Strangeness based measurements have the advantage that they have much higher counting rates than those recording electromagnetic particles.

I would like to thank R. Hagedorn, B. Müller and P. Koch for fruitful and stimulating discussions, and R. Hagedorn for a thorough criticism of this manuscript.

REFERENCES

1) An incomplete list of quark-gluon plasma papers includes:
   a. B.A. Freedman and L.C. McLerran, Phys. Rev. D16 (1977) 1169;
   b. S.A. Chin, Phys. Lett. 78B (1978) 552;
   c. P.D. Morley and M.B. Kislinger, Phys. Rep. 51 (1979) 63;
   d. J.I. Kapusta, Nucl. Phys. B148 (1979) 461;
   e. O.K. Kalashnikov and V.V. Kilmov, Phys. Lett. 88B (1979) 328;
   f. E.V. Shuryak, Phys. Lett. 81B (1979) 65; also Phys. Rep. 61 (1980) 71;
   g. J. Rafelski and R. Hagedorn, "From Hadron Gas to Quark Matter II", in Thermodynamics of Quarks and Hadrons, ed. H. Satz, North Holland, Amsterdam 1981.
   h. J. Rafelski and M. Danos, "Perspectives in High Energy Nuclear Collisions", NBS-IR-83-2725 (1983) and GSI -xx-83 (1983).
   i. H. Satz, Phys. Rep. 88 (1982) 321.

2) These ideas originate in Hagedorn's statistical bootstrap theory, see:
   a. R. Hagedorn, Suppl. Nuovo Cimento 3 (1964) 147; and Nuovo Cimento 6 (1968) 311, also
   b. R. Hagedorn, "How to Deal with Relativistic Heavy Ion Collisions", in the proceedings of the Workshop at GSI, October 1980: "Future Relativistic Heavy Ion Experiments", GSI-81-6 report, eds. R. Stock and R. Bock, p. 236.

3) R. Hagedorn and J. Rafelski, Phys. Lett. 97B (1980) 136; see also Ref. 1g).

4) a. R. Hagedorn, Z. Phys. C17 (1983) 265 [CERN preprint TH.3392 (1982)];
   b. R. Hagedorn, I. Montvay and J. Rafelski, "Hadronic Matter at Extreme Energy Density", Plenum Press, NY (1980), ed. N. Cabibbo.

5) J. Rafelski and M. Danos, "Pion Radiation by Hot Quark-Gluon Plasma", CERN preprint TH.3607 (1983);
   M. Danos and J. Rafelski, Phys. Rev. D27 (1983) 671.

6) P. Koch, Diploma Thesis, Universität Frankfurt (1983).

7) A.Z. Mekjian, Nucl. Phys. B384 (1982) 492.

8) P. Koch, J. Rafelski and W. Greiner, Phys. Lett. 123B (1983) 151.

9) See, e.g.,
   S. Gasiorowicz and J.L. Rosner, "Hadron Spectra and Quarks", Am. J. Phys. 49 (1981) 954.

10) a. P. Langacker and H. Pagels, Phys. Rev. D19 (1979) 2070, and references therein;
    b. S. Narison, N. Paver, E. de Rafael and D. Treleani, Nucl. Phys. B212 (1983) 365.

11) a. A. Chodos, R.L. Jaffe, K. Johnson, C.B. Thorn and V.F. Weisskopf, Phys. Rev. D9 (1974) 3471;
b. K. Johnson, Acta Phys. Polon. B6 (1975) 865; and
c. T. De Grand, R.L. Jaffe, K. Johnson and J. Kiskis, Phys. Rev. D12 (1975) 2060.

12) H.-Th. Elze, W. Greiner and J. Rafelski, J. Phys. G6 (1980) L149;
J. Rafelski, H.-Th. Elze and R. Hagedorn, "Hot Hadronic and Quark Matter in $\bar{p}$-Annihilation on Nuclei", CERN preprint TH.2912 (1980), in Proceedings of 5th European Symposium on Nucleon-Antinucleon Interactions, Bressanone 1980, CLEUP, Padua, 1980.

13) B.L. Combridge, Nucl. Phys. B151 (1979) 429.

14) J. Rafelski and B. Müller, Phys. Rev. Lett. 48 (1982) 1066.

15) G. Staadt, Diploma Thesis, Universität Frankfurt (1983), and to be published.

16) J. Rafelski, "Extreme States of Nuclear Matter", Universität Frankfurt preprint UFTP 52/1981 (1981), in the proceedings of the Workshop at GSI (1980) "Future Relativistic Heavy Ion Experiments", GSI-81-6 Report, eds. R. Stock and R. Bock.

17) J.W. Harris, A. Sandoval, R. Stock et al., Phys. Rev. Lett. 47 (1981) 229.

18) S.A. Chin and A.K. Kerman, Phys. Rev. Lett. 43 (1979) 1292.

Meson Emissions from Quark-Gluon Plasma through Formation and Fission of Chromoelectric Flux Tubes

T. Matsui, B. Banerjee,* and N.K. Glendenning
Nuclear Science Division, Lawrence Berkeley Laboratory
University of California, Berkeley, CA 94720

In the recent theoretical development of hadron physics based on QCD,[1-4] it has appeared very likely that the matter that consists of hadrons dissolves into an almost ideal gas of quark-gluon plasma at a sufficiently high energy density, which was once realized in the early universe and perhaps will be reproduced again in the future program of ultrarelativistic heavy ion collisions. Several estimations of the expected energy deposition in the energetic central collision ($\sqrt{s} \geq 20$ GeV/nucleon) confirmed that the energy density will certainly exceed the critical value, ~2 GeV/fm^3, which is required to complete the phase transition, both in the fragmentation (nuclear fireball) region[5] and in the central rapidity region.[6,7] Once a quark-gluon plasma is formed in such a process, the high internal pressure and temperature will cause its rapid disassembly into hadrons, leptons, and photons. Thus, to make a reliable prediction for possible signals of plasma formation a dynamical description of the plasma evolution is of crucial importance.

One facet of the time evolution of quark-gluon plasma has been studied by several authors[6,8,9] who use Landau's relativistic hydrodynamics to describe the plasma expansion. In the present work we study another facet of the plasma evolution, the formation and radiation of mesons at the surface of hot plasma. The surface meson radiation would play two important roles. First, it may carry some information about the pre-freezeout stage of the plasma evolution.[10] Second, it causes a pressure decrease at the surface that works against the expansion. In the extreme, the plasma may extinct very rapidly by the surface meson radiation without collective expansion. Such an extreme scenario was proposed recently by Danos and Rafelski with a two-parameter model of surface radiation.[11] However, in their model there is no dynamical description of meson formation at the plasma surface. Thus, it is very unclear how the incident quark degrees of freedom is converted into mesonic degrees of freedom and how the color confinement works in such a process. Quite independently we have studied the same problem by fully employing the chromoelectric flux tube model. We found that their parametrization is quite unsatisfactory and is actually incompatible with such a dynamical description of color confinement. In the following we shall briefly recapitulate our treatments and findings. Some details of our calculation can be found in ref. 12 and more in the forthcoming paper.

Our scenario of the surface meson radiation is threefold. First, we assume the presence of smooth and sharp surface of quark-gluon plasma. The plasma may be viewed as a big MIT bag occupied by the gas of almost free quarks and gluons. The surface of the plasma is identified with the bag surface, which separates the perturbative vacuum in the plasma from the true nonperturbative QCD vacuum outside of the plasma. Then we assume that the meson radiation is initiated by the emission of a single quark from the plasma surface. This is caused by the thermal motion of quarks, and the flux of the quark is therefore characterized by the surface temperature. This leading quark cannot escape from the plasma alone because of the color confinement. Next stage of our scenario is the formation of chromoelectric flux tube that connects the leading quark to the plasma surface. Now the leading quark suffers a very strong attractive interaction with the plasma, which is characterized by the string tension of the flux tube. It is decelerated and will eventually be reabsorbed by the plasma unless the flux tube breaks. The fission of the flux tube can occur through the quantum tunneling of a virtual $q\bar{q}$ pair, formed in the uniform color electric field inside the tube, into a real state. The piece of flux tube disconnected from the plasma forms a meson and is emitted from the plasma. This is the last stage of meson radiation. The energy and momentum of the mesons formed by this process are determined by the initial energy and momentum of the leading quark and the space-time positon where $q\bar{q}$ pair creation occurs. This mechanism of hadronization has been commonly used to describe particle production in high-energy e^+e^- annihilation. Although in our problem the average momentum of the quarks is not so high ($k_0 \sim T \sim$ 200 MeV), we expect that this picture will qualitatively describe the fate of the high momentum component of quarks (antiquarks) in the thermal distribution. The contribution of the low-momentum quarks to this hadronization process is suppressed. This supports our idealization of a smooth plasma surface. One may consider another mechanism for the hadronization at the plasma surface, i.e., the coalescence of a quark-antiquark pair that already

exists in the plasma. We do not deal with this process here, because at the expected plasma temperature the thermal flux of quarks and antiquarks with specified color charge is small.

As a quark coming out of the plasma, its kinetic energy is gradually converted into the field energy of the chromoelectric field, causing the deceleration of the quark. The energy stored in the flux tube per unit length is given by the string tension $\sigma = \epsilon^2 A/2$ where the field strength ϵ and the cross section of the flux tube A can be also related to the QCD coupling constant, g/2, by the Gauss' law $\epsilon A = g/2$, yielding $\sigma = g\epsilon/4$. The classical trajectory of the leading quark is shown in Fig. 1. The motion of the quark normal to the surface is decelerated until it stops at time $t_c = (E_0/E_{z0})(k_{z0}/\sigma)$ characterized by initial quark energy and momentum. Thereafter it is accelerated back into the plasma. During this period the normal component of the quark momentum decreases linearly as a function of time t. The field energy stored in the flux tube can be further converted into a new $q\bar{q}$ pair through the quantum tunneling, causing the fission of the flux tube. If such a pair is created at a distance z' from the surface and at a time t, a meson consisting of the original quark together with the antiquark of the new created pair is formed with energy $E^M = E_0 - (E_0/E_{z0})\sigma z'$ and normal momentum $k_z^M = k_{z0} - (E_{z0}/E_0)\sigma t$.

The $q\bar{q}$ pair creation in the constant color electric field is quite analogous to the problem considered by Schwinger relating to the vacuum persistency against e^+e^- pair creation in the constant electric field.[13] This old rather academic problem has been recently rediscovered by several authors[14,15] to be of practical importance in the context of QCD. We derived a new result for the $q\bar{q}$ pair creation rate using an improved energy balance relation in the intermediate virtual state, which includes the effect of the mutual interaction of new $q\bar{q}$ pair.[16] Our result for the probability of making a $q\bar{q}$ pair per unit four volume is given by

$$p = \sum_{\text{Flavor}} \frac{(g\epsilon)^2}{64\pi^3} \sum_{n=1}^{\infty} \frac{1}{n^2} \exp\left(-\frac{4\pi^2 m_f^2 n}{g\epsilon}\right) \tag{1}$$

If we use current quark masses as in ref. 15, then this probability is well approximated by $p = (g\epsilon)^2/(192\pi) = \sigma^2/(12\pi)$.

The fission probability of the flux tube at time t and at position z' with infinitesimal space-time interval is now given by $d^2P = pA\,R(t)dz'dt$ where $R(t) = 1 - P(t)$ is the attenuation factor, which selects out the unwounded flux tube. Noting the previous relation between the space-time position of the fission and the energy momentum of the created meson, we can rewrite this fission probability as a function of meson coordinates, k_z^M, E^M. In the massless quark limit, we have a very simple result

$$d^2P = \exp\left(-\frac{k_0(k_z^M - k_{z0})^2}{2k_{z0}k_c^2}\right) d\left(\frac{k_z^M}{k_c}\right) d\left(\frac{E^M}{k_c}\right) \tag{2}$$

where $k_c = \sqrt{\sigma^2/(pA)} = \sqrt{24\sigma/\alpha_c}$ is a parameter that scales the energy momentum involved in this process. Physical meaning of this parameter is obtained if one computes dP/dk_z^M from eq. (2). The result is plotted in Fig. 2, which shows that the most probable momentum k_m of created meson is smaller than the incident quark momentum k_{z0} by the amount k_c. Thus k_c characterizes the effect of confinement that suppresses the contribution of the low momentum quark (antiquark) to this process and also prohibits the large momentum transfer to the meson. For $\sigma = 0.177\ (\text{GeV})^2$ and for $\alpha_c = g^2/4\pi = 2\ (0.55)$, corresponding to the value used by Casher, et al.[14] (MIT bag model[17]), we have $k_c = 1.45\ (2.78)$ GeV, which is very large compared to the relevant temperature that we consider.

The meson flux is given by the thermal flux of the quark and antiquark multiplied by the fission probability of the flux tube. Because the fission probability has been computed as a function of meson momentum and energy, we can derive the spectrum of the radiated mesons by integrating over the quark coordinates.

$$\frac{d^2(\text{Meson Flux})}{dk_z^M dE^M} = \frac{\gamma}{(2\pi)^3} \int d^3k_o \, e^{-E_o/T} \frac{k_{zo}}{E_o} R(k_z^M, k_o) \frac{1}{k_c^2} \theta(k_z^M < k_{zo}) \theta(k_z^M > 0)$$
$$\times \, \theta\left(\sqrt{k_z^{M2} + m^2} < (E_{zo}/E_o) E^M\right) \theta(E^M < E_o) \quad . \tag{3}$$

where the step functions make several constraints for the kinematically allowed processes. Here we simply use the Boltzmann distribution with zero chemical potential and $\gamma = \gamma_c \cdot \gamma_s \cdot \gamma_f \cdot 2 = 24$ is the degeneracy factor including quark-antiquark degrees of freedom.

We first apply this result to estimate the influence of the meson radiation on the hydroexpansion. Because the radiated mesons carry away certain amount of momentum of quarks that otherwise contribute to generate the quark pressure acting on the plasma surface, there is a pressure decrease at the surface. Figure 3 shows the numerical result of the ratio of radiation pressure to the quark pressure. Since this ratio is less than 20% up to T = 500 MeV, we may conclude that the meson radiation due to this process is a minor perturbation on the hydrodynamical expansion of the plasma. Our result also shows that the parametrization of Danos and Rafelski[11] is not adequate to describe this process, leading to the opposite conclusion.

Because the emitted mesons have continuous invariant mass M_s that is greater than the pion mass, they will eventually decay into pions, photons, and so on. If we take the flux tube model seriously, we have to compute the cascade decay of long flux tube until we get only pions or other stable particles. Instead of doing this, we compute the dominant decay mode by assuming the statistical distribution in the phase space. This is done analytically up to three pion decay. For large M_s, we use empirical inclusive cross section of $e^+e^- \to q\bar{q} \to \pi + X$, which exhibits very simple scaling nature for high energy.[18] Besides the initial electromagnetic process, this process is identified as a decay of high energy strings. Once the rapidity distribution of pions, dN_π/dy, is given on the rest frame of the string (= heavy meson), the rapidity distribution of pion flux on the rest frame of the plasma surface can be obtained by folding this by the rapidity-invariant mass distribution of the emitted string flux.

The numerical result of the rapidity distribution of pion flux at T = 300 MeV is shown in Fig. 4 where the rapidity distributions of the thermal quark-antiquark flux and the broken string flux are also plotted. Although the quark confinement reduces the number of strings and pions from that of quark-antiquark, we see that a large number of pions are still produced compared to the black body radiation of pions at the same temperature in the case of large coupling constant $\alpha_c = 2$. The peak of the rapidity distribution is also shifted downward showing a characteristic nature of the pion spectrum produced in this particular process. This result may be used to extract some information on the early stage of plasma evolution by holding with a solution of hydrodynamics.

This work was supported by the Director, Office of Energy Research, Division of Nuclear Physics of the Office of High Energy and Nuclear Physics of the U.S. Department of Energy under Contract DE-AC03-76SF00098.

References

*Permanent address: Tata Institute for Fundamental Research, Bombay, India
1. J.C. Collins and M.J. Perry, Phys. Rev. Lett. 34 (1975) 1353
2. E.V. Shuryak, Phys. Rep. 61 (1980) 72
3. D.J. Gross, R.D. Pisarski, and L.G. Yaffe, Rev. Mod. Phys. 53 (1981) 43
4. A complete up-to-date survey of this field is contained in "Quark Matter Formation and Heavy Ion Collisions", Proceedings of the Bielefeld Workshop, Ed. M. Jacob and H. Satz, World Scientific (1982)
5. R. Anishetty, P. Koehler, and L. McLerran, Phys. Rev. D22 (1980) 2793
6. J.D. Bjorken, Phys. Rev. D27 (1983) 140
7. M. Gyulassy and T. Matsui, Lawrence Berkeley Laboratory report LBL-15947
8. K. Kajantie, R. Raitio, and P.V. Ruuskanen, preprint (Helsinki, 1983)
9. G. Baym, J.-P. Blaizat, W. Czyz, B.L. Friman, and M. Soyeur, preprint (Illinois, 1983)

10. N.K. Glendenning and Y. Karant, Phys. Rev. C21 (1980) 1501
11. M. Danos and J. Rafelski, Phys. Rev. D27 (1983) 671
12. B. Banerjee, N.K. Glendenning, and T. Matsui, Lawrence Berkeley Laboratory report LBL-15949
13. J. Schwinger, Phys. Rev. 82 (1951) 664
14. A. Casher, H. Neuberger, and S. Nussinov, Phys. Rev. D20 (1979) 179
15. E.G. Gurvich, Phys. Lett. 87B (1979) 386
16. N.K. Glendenning and T. Matsui, Lawrence Berkeley Laboratory preprint LBL-15957
17. K. Johnson, Act. Phys. Pol. B6 (1975) 865
18. R. Brandelik, et al., Phys. Lett. 67B (1977) 358; 89B (1980) 418

Figure Captions

Fig. 1. Classical trajectory of the leading quark on the rest frame of plasma surface.
Fig. 2. Momentum distribution of radiated mesons for initial quark momentum $k_{zo} > k_c$.
Fig. 3. Backward radiation pressure as a function of plasma temperature.
Fig. 4. Rapidity distribution of radiated pions is compared with that of incident quark flux, broken string, and black body pion radiation.

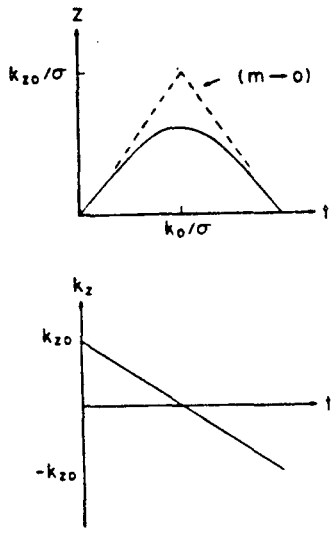

Fig. 1

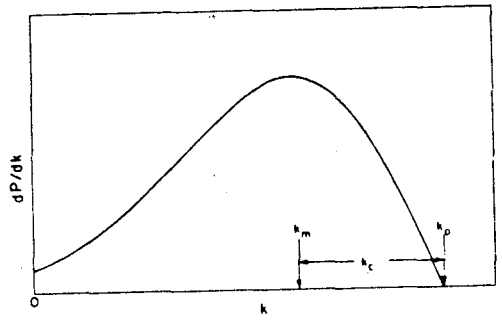

Fig. 2

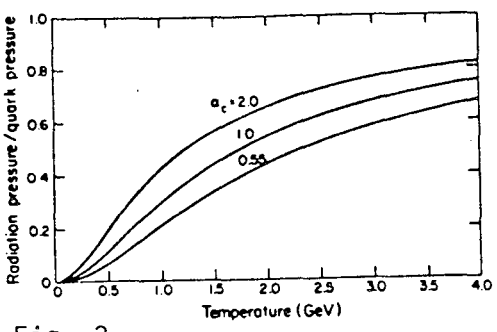

Fig. 3

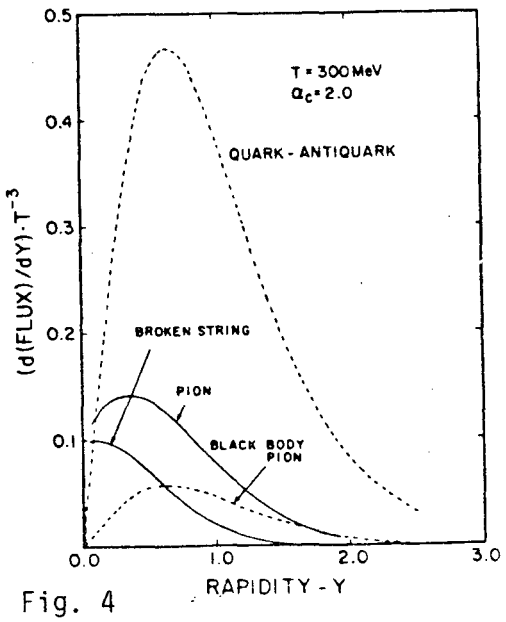

Fig. 4

PION RADIATION BY HOT QUARK-GLUON PLASMA

Johann Rafelski

CERN, Geneva
and
Universität Frankfurt

and

Michael Danos

National Bureau of Standards, Washington

We consider here an approximately spherical region of the perturbative QCD vacuum, filled with quarks, antiquarks and gluons. The particle densities are assumed to be reasonably well described by local thermal and chemical equilibrium distributions. The basis for these assumptions is the point that the mean free path of a colour-charged particle in the plasma is of the order of 1/3 - 1/2 fm. Outside the perturbation region, coloured particles cannot exist and hence any matter found there is in the form of colourless hadrons. Even though indirect evidence supports the picture of the true and perturbative QCD states, we must remember that no direct evidence is available as of now. We regard the observation of the quark-gluon plasma state as the most direct confirmation of the ideas about the nature of strong interactions and quark confinement.

For an impenetrable surface between the perturbative and true vacuum states, the inside thermal and degeneracy pressure would lead to an expansion until either pressure equilibrium or a phase transition into individual hadrons is reached. However, if the surface is penetrable, i.e., if it allows transmission of momentum and energy (but not colour) from the inside, then this can lead to a substantial internal energy and pressure loss by radiation -- the pressure acting on the surface is reduced, as not all the momentum impinging on the surface has to be reflected. On first thought, the microscopic mechanism for this transmission arises in the following manner: when a fast quark or antiquark hits the boundary, a jet-like structure filled with colour field flux, i.e., a fluxtube might be formed. For sufficiently high quark momentum, this tube, instead of retracting, splits by $q\bar{q}$ pair creation. The leading particle associates with the antiparticle of the pair to form a meson, while the remaining pair particle may retract into the plasma. This microscopic picture[1),2)] suffers from several difficulties, in particular as far as pion radiation is concerned.

Before turning to the results of Ref. 1), we wish to discuss here the reasons for these difficulties. We first note that a pion is not an average $q\bar{q}$ bag with a mass of several hundred MeV like, e.g., the ρ meson. Any proposed microscopic mechanism for pion production must take into account the small mass of the produced final state, i.e., the strong $q\bar{q}$ binding effects and the rôle of the pion as Goldstone meson. These complex pionic structure effects have not been included in the presently available microscopic calculation[2)]. Therefore, the results of Ref. 2) should be applied at best to the production of the heavy mesons. However, we see a further difficulty of principle when generalizing results of Ref. 3) to the particle

radiation problem. This has to do with the necessity of conservation of the energy and the momentum during the string evolution. In particular, part of the energy used to extend the string (with the vacuum) does not require a momentum transfer. This excess momentum must be carried by additional degrees of freedom, which are not included in the present models.

Therefore, in the present qualitative context, we prefer to develop a quantitative model suitable for surface temperatures of 160 - 220 MeV and moderate baryon densities, so that the particle density is less than ~ 10 particles/fm^3. Under these circumstances, surface collisions involving more than one particle per fm^2 are rare. Hence we can limit ourselves to consider sequential one-particle events. We assume[1] that in order for the surface collision to lead to pion emission, the particle momentum normal to the surface must exceed a certain threshold. This momentum has to be larger than the normal momentum of the emitted pion. We take this quark threshold momentum p_M to be of the order of 1/4 GeV/c and observe that the results are quite insensitive to this choice, as well as to the actual shape of the threshold function θ describing the probability of pion emission. However, we note that the string breaking calculations of Ref. 2) would be reproduced only if the choice of $p_M \sim 700$ MeV is made.

The energy per unit surface and unit time that leaves the quark-gluon plasma is therefore simply given by

$$\frac{d^3E}{d^2Adt} = g \int \frac{d^3p}{(2\pi)^3} \rho(p) f(E)\, E(p) \theta(p) \frac{d^3V}{d^2Adt} \tag{1}$$

where $g = 12$ is the degeneracy of the light quarks. The differential is the normal velocity of particles impinging on the surface. The energy leaving the plasma region is not the total energy contained in the leading particle and we include in (1) the efficiency factor f. A naïve degree of freedom counting leads to $f \approx 2/3$. $\rho(p)$ is the phase space quark and antiquark particle density. We observe here that the presence of a net baryon number in the plasma enhances ρ and therefore the particle radiation. In view of the uncertainties it is sufficient to expand the Fermi distributions and to retain only the Boltzman term

$$\rho(p) \approx 2\cosh(\mu/T)\; e^{-\sqrt{p_\parallel^2 + p_\perp^2}/T} \quad . \tag{2}$$

For $\mu/T \simeq 1.5$ the effect of radiation is enhanced by a factor 2.4 as compared with a baryonless plasma. Combining Eqs. (1) and (2), we obtain the generalized Stefan-Bolztman (SB) law:

$$\frac{d^3E}{d^2Adt} = \bar{f}\, \frac{g}{2\pi^2} \cosh(\mu/T)\; T^4\; 3e^{-p_M/T} \left(\frac{1}{3} \left(\frac{p_M}{T}\right)^2 + \left(\frac{p_M}{T}\right) + 1 \right) . \tag{3}$$

the SB limit is recovered for $p_M \to 0$. The deviation of Eq. (3) from SB is significant for the evolution of the plasma, but nonetheless both quantities are of the same order of magnitude. In Fig. 1 we show the cooling rate calculated from Eq. (3) for two choices of p_M as a function of the surface temperature T, choosing $\mu/T = 1$.

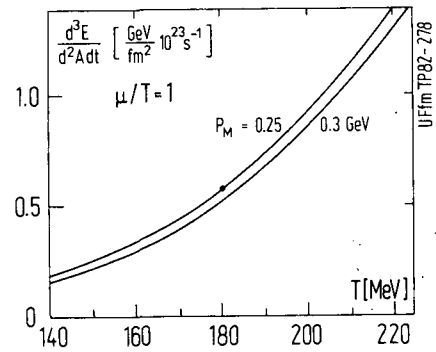

Fig. 1: Surface brightness of a quark-gluon plasma as function of the temperature for several cut-offs p_M at fixed $\mu/T = 1$. The dot indicates the parameters of our numerical example.

To appreciate the physical importance of these results, we now discuss the rate of energy loss through a surface A, assuming T = 180 MeV, $\mu = T$. First we find

$$\frac{dE}{dt} = A\ 0.58\ \frac{GeV}{fm^2}\ 10^{+23}\ sec^{-1} \quad .$$

This is a very large energy loss rate ! For example, through the surface of a sphere with a radius of 4 fm, the energy loss per $\Delta t = 2 \times 10^{-23}$ sec is 260 GeV. The available energy contained in such a sphere at 2.1 GeV/fm^3 (1.4 GeV/fm^3 available energy density) is 380 GeV. This shows that during the minimum estimated lifetime of the plasma, a substantial part of plasma energy can be radiated by the surface. We have added here the word "available" since at the chosen $\mu - T$ values the actual energy density is higher by 0.7 GeV/fm^3, in order to allow for the 150 baryons ($\mu \neq 0$) present.

To conclude we note that those particles which penetrate the surface do not exert their full force on it. In particular one can show[1)] that the quark pressure is substantially reduced and is given by

$$\bar{P}_q = P_q \left(1 - f\ \frac{P_q(p_\perp > p_M)}{P_q}\right) \cong 0.4\ P_q \quad . \tag{4}$$

Since the quark pressure is about twice as large as the glue pressure, only about 60% of the internal pressure is felt by the surface.

The physical distinction between the cooling by pion radiation and by expansion resides in the reduction of the temperature without a significant increase of the plasma volume. Here we have demonstrated that the pion

radiation is an essential feature controlling the evolution of a hot baryon-rich quark-gluon plasma droplet.

We would like to thank L. Van Hove for stimulating discussions and careful reading of the manuscript.

REFERENCES

1) M. Danos and J. Rafelski, Phys. Rev. D27 (1983) 671; in this work, though reference is made to the tube breaking mechanism, the actual calculations are performed in an effective manner avoiding reference to the details of microscopic processes.

2) B. Banerjee, N.K. Glendenning and T. Matsui, "Fission of a chromo-electric flux tube and meson radiation from a quark-gluon plasma", LBL preprint LBL-15349; in this reference the consequence of the Casher-Neuberger and Nussinov[3)] mechanism of string breaking for meson production is explored.

3) A. Casher, H. Neuberger and S. Nussinov, Phys. Rev. 20 (1979) 179.

DO LIGHT FERMIONS DESTROY THE CONFINEMENT/DECONFINEMENT PHASE TRANSITION?

T.A. DeGrand, Department of Physics,
University of Colorado, Boulder, CO 80309
C.E. DeTar, Department of Physics,
University of Utah, Salt Lake City, Utah 84112

1. Introduction and Conclusions

Two phenomena may give rise to a phase transition in nuclear matter at high temperatures or high densities. One is associated with the restoration of SU(2) $\underline{X}$ SU(2) chiral symmetry, the order parameter for which is the scalar density $\langle\bar{\psi}\psi\rangle$; the other is the confinement/deconfinement phase transition (CDPT), the order parameter for which is the "Wilson line" $L = e^{-F/T}$ where F is the free energy of an isolated test quark.

Let us review what is known theoretically about these phenomena. It has been shown in lattice gauge theories both in numerical calculations[1] and in the strong coupling high temperature approximation[2] that the SU(2) Yang-Mills theory, i.e. a theory with <u>only gluons</u>, undergoes a CDPT at a temperature of the order of the strong interaction confinement scale Λ. In SU(3) the pure gluon theory evidently has a first order CDPT.[3] Because of the numerical complexities of introducing fermions into lattice gauge theories and particularly because of difficulties in formulating a chirally invariant lattice version of QCD, much less is known about the chiral symmetry breaking phase transition. It has been suggested that the latter phase transition is connected with the former, but numerical evidence[4] has been based upon such a drastic approximation (the "quenched" approximation) that one cannot make definitive statements at present. Indeed, it is not even known what effect, if any, fermions have on the CDPT.

It is the purpose of the study reported upon here to address this question in a model lattice gauge theory constructed to imitate the characteristics of the CDPT of SU(3), and including a chemical potential coupled to baryon number density. We do not consider the chiral symmetry transition. We conclude, at least within the confines of our approximation, (a) that the CDPT, although of first order, is unstable against the introduction of light fermions, i.e. if the bare fermion mass is less than a few times the putative deconfinement temperature, there is a smooth transition from matter with confining characteristics to a plasma with screening characteristics, and (b) that at temperatures somewhat below the deconfinement temperature, as the chemical potential or baryon number density in increased, there is again a smooth transition.

Conclusions (a) and (b) are supported in the mean field approximation to the model at high temperatures and conclusion (a) is supported in our numerical Monte Carlo studies. These conclusions are summarized in the three dimensional phase diagram of Fig. 1. It should be emphasized that these results are found in a simple model that is chosen to imitate the phase structure of QCD. Thus the terms "bare mass", "temperature", and chemical potential" do not have a precise physical meaning. However, our results offer a concrete example that may represent the qualitative phase structure for QCD itself. Indeed, it is possible that with massless or nearly massless quarks the only phase transition is one associated with chiral symmetry breaking. Such a situation could have important phenomenological consequences in heavy ion collisions and in dense stars.

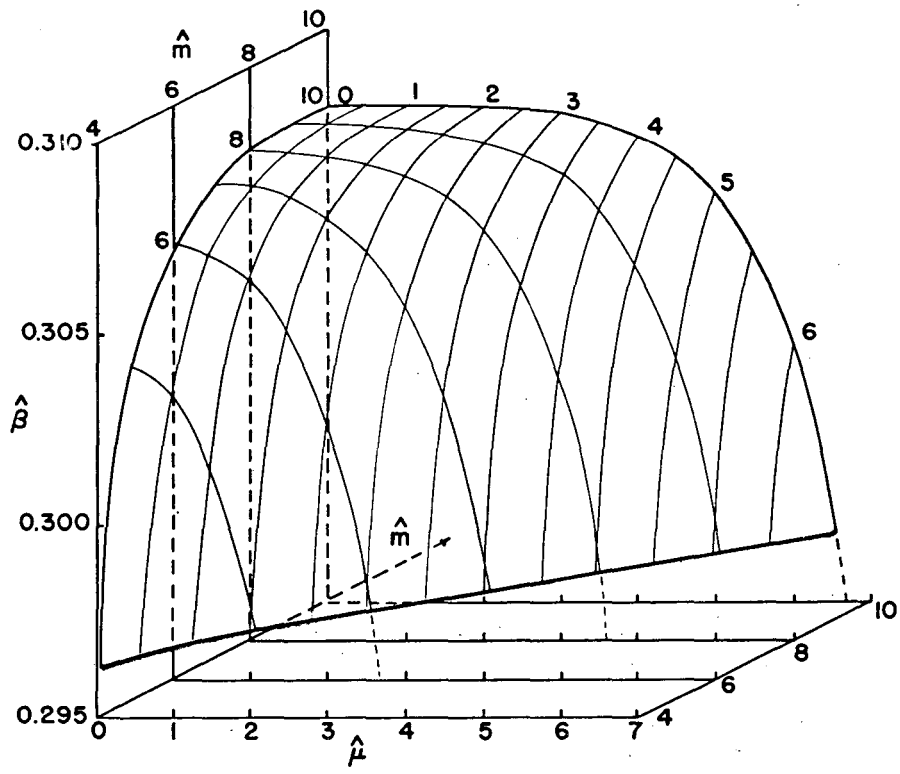

Fig. 1. Mean field phase diagram for the Potts model corresponding to the high temperature strong coupling limit of QCD. Three dimensions are plotted: $\hat{\beta}$ increases with temperature; $\hat{\mu}$ and $\hat{m}$ correspond to chemical potential and quark mass in units of the deconfinement temperature. The surface is the locus of a first order phase transition. The heavy line denotes a second order transition.

2. Synopsis of the Analysis

We proceed to give a sketch of our analysis. Details are given elsewhere[5]. Working with the Wilson form for QCD lattice gauge theory,[6] modified for an anisotropic lattice and chemical potential, we write the partition function at finite temperature

$$Z = \int [dU\, d\eta^* d\eta] \exp\, [S_G(U) + S_F\, (\eta^*, \eta, U)]\ , \tag{1}$$

where the integration is over the Haar measure for the gauge links $U_{n\mu} \varepsilon\, SU(3)$ and over the Berezin measure for the fermion Grassmann variables η^* and η. The pure gauge action is

$$S_G = \frac{\beta}{6} \sum_n [a/\tau \sum_{i=1}^{3} \mathrm{ReTr}(U_{n4i}) + \tau/a \sum_{i<j} \mathrm{ReTr}(U_{n,ij})]. \tag{2}$$

The first term refers to the time-like plaquettes and the second to space-like plaquettes. The lattice has dimensions $N_t \times N_s^3$. The lattice spacing is a in spatial directions and τ in the Euclidian time direction. The fermion action is

$$S_F = \sum_n \bar{\eta}_n \eta_n - \frac{\kappa\tau}{a} \sum_{n,i} [\bar{\eta}_{n+\hat{i}} (1 + \gamma_i) U^\dagger_{ni} \eta_n$$

$$+ \bar{\eta}_n U_{ni} (1 - \gamma_i) \eta_{n+\hat{i}} - \kappa \sum_n [\bar{\eta}_{n+\hat{4}} (1 + \gamma_4) U^\dagger_{n4} e^{-\tau\mu} \eta_n$$

$$+ \bar{\eta}_n U_{n4} (1 - \gamma_4) e^{\tau\mu} \eta_{n+\hat{4}}] \ . \tag{3}$$

The coefficient κ is the "hopping parameter", which is related to the "bare mass". For large masses

$$\kappa \approx \frac{1}{2} e^{-m\tau} \ . \tag{4}$$

The chemical potential is μ. The temperature of the lattice is:

$$T = (N_t \tau)^{-1} \ . \tag{5}$$

Thus high temperatures can be obtained by making N_t and τ/a small. Here we discuss the case $N_t = 1$. Because of the renormalization properties of SU(3), as the lattice spacing is taken to zero at fixed τ/a, the coupling β must be increased so as to keep physical quantities (hadron masses, the string tension, etc.) fixed. Therefore, increasing T corresponds to decreasing τ, decreasing a, and increasing β.

We now replace the sum over SU(3) by a sum over Z(3), the center of SU(3). This approximation is justified for the following reasons: (a) The CDPT with fermions absent reflects a breakdown of a part of the gauge symmetry associated with the center of SU(3). The same is true of a lattice gauge theory based on Z(3). (b) The order parameter for the SU(3) transition is the same as the order parameter for the Z(3) transition. Thus we do not expect a qualitative difference between Z(3) and SU(3) in this regard.[7] Finally we assume that $\tau/a \ll 1$. This approximation allows us to drop the space-like plaquettes in (2) and space-like links in (3). The time-like plaquettes in (2) take on a simple form when $N_t = 1$, because of the periodic boundary conditions on the gauge-like variables:

$$U_{n,4i} = z_{\vec{n}} z^*_{\vec{n}+i} \tag{6}$$

where $n=(\vec{n}, 0)$ is the coordinate of a three dimensional lattice and $z_{\vec{n}} \varepsilon Z(3)$ is the time-like gauge link associated with the spatial coordinate $\vec{n}$. The integration over the Grassmann variables can be carried out with the final result that

$$Z \sim \sum_{z_{\vec{n}} \varepsilon Z(3)} \exp \Big(\beta a/2\tau \sum_{\vec{n},i} \mathrm{Re}\, z^*_{\vec{n}} z_{\vec{n}+i}$$

$$+ 24\kappa \cosh \tau\mu \sum_{\vec{n}} \mathrm{Re} z_{\vec{n}} + 24\kappa\, i \sinh \tau\mu \sum_{\vec{n}} \mathrm{Im} z_{\vec{n}}\Big) \tag{7}$$

The model of Eq. (7) is known in statistical mechanics as the three-state, three-dimensional Potts model.[8] In the present version both real and purely imaginary external fields occur. At zero chemical potential the imaginary field vanishes, and at infinite mass, both external fields vanish. The model has been studied widely for $\kappa=0$. Here a first order phase transition occurs as β is varied. The order parameter is the Wilson line

$$L = \langle z_n^{\rightarrow} \rangle$$

averaged over the lattice. At low β, $L=0$; at high β, $L\neq 0$. Less is known numerically for $\kappa>0$ and $\mu=0$. Qualitatively, it is evident that for large κ, no phase transition occurs.[9] Therefore, introducing a sufficiently light fermion may destroy the phase transition. As far as we can determine, the model has never been studied with the imaginary term of (7).

We have analyzed the Potts model (7) in mean field theory and found the phase diagram shown in Fig. 1. For purposes of this figure $\hat{\beta}=\beta a/\tau$, $\exp(-\hat{m})=24\kappa$ and $\mu=\mu\tau$. A first order surface is shown corresponding to the coexistence of two phases, one with large L and one with small L. The surface terminates on a second order line. The critical "mass" below which no phase transition occurs is $m \approx 4$. Lowering the fermion mass or raising the chemical potential lowers the temperature of the phase transition slightly.

We have also studied the Potts model numerically with a Monte Carlo simulation for the case $\mu=0$. Here we find a first order phase transition at $\kappa=0$ in agreement with other work.[10] We also find that the phase transition persists at small κ, but has evidently gone away when $24\kappa>0.01$ corresponding to $\hat{m}<4.6$. All masses are expressed in units of $1/\tau$, the lattice temperature. These results form the basis for our conclusions stated with the introduction above.

References

1. L. McLerran and B. Svetitsky, Phys. Lett. 98B, 195 (1981); J. Kuti, J. Polónyi, and K. Szlachányi, Phys. Lett. 98B, 199 (1981).
2. A.M. Polyakov, Phys. Lett. 72B, 447 (1978); L. Susskind, Phys. Rev. D20, 2610 (1979).
3. J. Engels, F. Karsch, I. Montvay, and H. Satz, Phys. Lett. 101B, 89 (1981); T. Celik, J. Engels, and H. Satz, Univ. Bielefeld report BI-TP 83/04 (1983).
4. J. Kogut et al., Phys. Rev. Lett. 50, 393 (1983).
5. T.A. DeGrand and C.E. DeTar (in preparation).
6. K.G. Wilson, Phys. Rev. D10, 2445 (1976); K.G. Wilson in New Phenomena in Subnuclear Physics, ed. A. Zichichi (Erice 1975) (Plenum, N.Y., 1977).
7. B. Svetitsky and L.G. Yaffe, Nucl. Phys. B210 [FS6], 423 (1982).
8. F.Y. Wu, Rev. Mod. Phys. 54, 235 (1982).
9. J.P. Straley and M.E. Fisher, J. Phys. A 6, 310 (1973).
10. S.J. Knak Jensen and O.G. Mouritsen, Phys. Rev. Lett. 43, 1736 (1979).

Normalons, Anomalons and Anomalies in High Energy Cosmic Rays

Arnon Dar†
Department of Physics, McGill University, Montreal, Canada

Abstract

We summarize the major anomalies that were reported by cosmic ray experiments and discuss possible origins of some of these anomalies.

† On leave from the Technion-Israel Institute of Technology Haifa, Israel.

Introduction

Very high energy cosmic rays are a unique source of information on interactions of high energy particles and nuclei at energies well above those available at man-made accelerators. Moreover, the unknown sources that produce cosmic rays with enormous energies (energies in excess of 10^{20} eV) may also produce new species of particles (and matter) that are difficult or impossible to produce under terrestial conditions (e.g. GUT monopoles with mass $\sim 10^{16}$GeV/c^2). Is there any evidence for new species of particles among the primary cosmic rays? Is there any evidence for new forms of interactions at extremely high energies?

In this lecture I will summarize the major anomalies that were reported by high energy cosmic ray experiments and I will discuss their possible origin. Following H. Primakoff I will use the following classification of particles:

Normalons - Particles that have been observed at man made accelerators (and are listed e.g. in the Particle Data Booklet[1]) including the recently discovered $W^{\pm}$ and Z^{0}.

Exotics - Particles that are expected to exist, but their existence has not been confirmed yet (e.g. quarks, gluons, Higgs, leptoquark bosons, monopoles, gravitons, ..., and their supersymmetric partners).

Anomalons - Unexpected particles that have been claimed to be observed. (e.g. nuclear fragments with anomalously large nuclear cross sections).

Note in particular that the term "anomalon" will be used to denote any unexpected or unusual particle while nuclear fragments with anomalously large hadronic cross sections, will be called "nuclear anomalons". The plan of the talk is as follows: First I will summarize briefly some basic properties of high

energy cosmic rays and experimental techniques used for their study. Then I will list and discuss the major anomalies which were reported by cosmic ray experiments and which may be related to the presence of anomalons or exotics, either among the primary cosmic rays or among the products of their collisions with atomic nuclei. Conclusions will be drawn after a short discussion of each of the individual anomalies. Special attention will be given to cosmic ray anomalies that may be related to the formation of quark-gluon plasma droplets or to the formation of nuclear anomalons, because the question whether such phases of finite nuclear matter do exist has been the focus of this conference.

II. Some Background Material

The atmospheric thickness at sea level is $\sim$ 1030 gm/cm^2. The mean interaction length of protons in the atmosphere is $\sim$ 86 gm/cm^2 at $\sim$ 400 GeV and it decreases with increasing energy. The interaction lengths of atomic nuclei in the atmosphere are even shorter and the radiation length of photons in the atmosphere is 36±1 gm/cm^2. Consequently, the atmosphere is highly opaque to normal cosmic rays (atomic nuclei, protons, electrons and photons), and their study requires to fly detecting equipment above, or at the top of the atmosphere. However, the flux of the primary cosmic rays drops fastly with their energy (approximately, $dF/dE \sim 1.6E^{-2.67\pm0.05}$ particles/cm^2·sr·sec·GeV for $E \lesssim 10^6$ GeV). Above about 10^6 GeV their flux becomes so low that the high altitude flown equipment with its rather limited detecting area and exposure time run out of statistics and their study must rely on measurements of atmospheric cascades with ground or space based equipment. (The space shuttle and the prposed space platform probably will make possible direct observations up to 10^7 GeV).

Fig. 1 which is adapted from ref. 2, shows the integral spectrum of the primary cosmic rays at the top of the atmosphere. Below 10^6 GeV it was determined from detection equipment flown at high altitudes. Above 10^6 GeV it was determined from ground based measurements of atmospheric cascades. Also indicated there are the equivalent lab energies of the CERN SPS and Fermilab Tevatron $\bar{p}p$ colliders.

The composition of the primary cosmic rays is known only up to energies of about 10^5 GeV. Fig. 2 shows the differential energy spectra of the major cosmic ray species, adapted from ref. 2.

The major techniques that were used for studying high energy cosmic rays are listed in Table I.

Table 1 : Observation Techniques

1. High Altitude Emulsion Exposures:
   Mountain Labs, Balloons, Planes,
   Rockets, Satellites, Space Shuttle
   $E/A \lesssim 10^3$ TeV
   * Space Shuttle, Space Platform $E/A \lesssim 10^4$ TeV ?

2. Extensive Air Showers:
   Ground Based Measurements
   * Space Based Measurements
   $E \gtrsim 10^3$ TeV

3. Deep Underground Massive Detectors
   (Proton Decay Detectors)
   $1 \text{ TeV} \lesssim E_\mu \lesssim 10^3 \text{ TeV}$
   $100 \text{ MeV} \lesssim E_\nu \lesssim 10 \text{ GeV}$

* DUMAND = Deep Underground Muon and Neutrino Detector

* proposed

We shall now discuss the major anomalies that have been observed by these techniques.

III. Anomalies Observed With Emulsion Chambers (10^3 GeV $\lesssim E \lesssim 10^6$ GeV)

Table II summarizes the major emulsion chamber experiments at mountain altitudes that have been investigating cosmic ray interactions in the energy range 10^3 GeV $\lesssim E \lesssim 10^6$ GeV.

Table II : Major Mountain Chambers

Mountain	Alt. (m)	Atm. Depth (gm/cm^2)	Detectors	
			Area (m^2)	Pb(Tons)
Mt. Chacaltaya (Bolivia)	5220	540	150	100
Mt. Pamir	4370	596	500	1000
Mt. Fuji (Japan)	3780	650	100	100
Mt. Kanbara* (Tibet)	5500	520	>1000	?

Atmospheric depth at sea level : ~ 1030 gm/cm^2

Mean free path of protons at 100 TeV : ~ 50 gm/cm^2

* Under Construction

Table III summarizes the major anomalies that have been reported by these experiments. They are divided there into three categories: (i) anomalous multiplicities (ii) anomalous transverse momenta (iii) anomalous cross sections. In Table III we also include anomalies that have been observed in balloon born emulsion chambers.

Table III : Anomalies Observed in Emulsion Chambers
(Balloons, Rockets, Planes, Sattelites, Mountain Tops)

COLLISION			ANOMALY			
Projectile	Target	E or E/A	Property	Obser.	Expec.	Name
?	Air	> 350 TeV	n_c, n_γ	$n_c \sim 100$ $n_\gamma \sim 0$	$n_\gamma \sim n_c$	Centauro
?	Air	> 350 TeV	n_c, n_γ	$n_c \sim 15$ $n_\gamma \sim 0$	$n_\gamma \sim n_c$	Mini Centauro
S_i	Emulsion	~ 3.6 TeV/n	n_c	1010	< 500	Plasmon
?	Air	> 350 TeV	$\langle p_t \rangle_h$	1.5GeV/c	.5 GeV/c	Centauro
?	Air	~ 100 TeV	$\langle p_t \rangle_h$	15GeV/c	.4 GeV/c	Geminion
Ar	Pb	~ 1 TeV/n	$\langle p_t \rangle_{\pi^0}$	1.2GeV/c	.36GeV/c	Plasmon
Ca	C	~ 83 TeV/n	$\langle p_t \rangle_{\pi^0}$	0.7GeV/c	.42GeV/c	Plasmon
Nuclear fragment	Emulsion	> 1 GeV/n	σ_{in}	$\gg \pi R_A^2$	$\sim \pi R_A^2$	Anomalon
?	Air	3000 TeV	σ_{in}	$\ll \sigma_{\pi N}$	$> \sigma_{\pi N}$	Penetron

1. Anomalous Multiplicities

Centauros-

Experiments with accelerator beams show that up to energies of at least 150 TeV the number of photons, n_γ, and of charged hadrons, n_c, that are produced in hadron collisions are approximately equal. This result is expected if most of the produced particles are pions (as indeed observed), if $n_{\pi^0} \sim (n_{\pi^+} + n_{\pi^-})/2$ as implied by charge symmetry, and if most of the γ's result from $\pi^0 \to 2\gamma$ decays.

However, a Brazil-Japan Collaboration that studied cosmic ray interactions with emulsion chambers at the top of Mount Chacaltaya in Bolivia reported the observation of several high energy (E > 350 TeV) cosmic ray interactions with air nuclei above their chamber (see fig. 3) which had a high charged multiplicity, $n_c \sim 75 \pm 15$, but a seeming absence of accompanying photons from $\pi^0 \to 2\gamma$ and $\eta^0 \to 2\gamma$ decays[3]. These events had also unuaual high average transverse momenta, $\langle p_T \rangle \sim 1.5$ GeV/c, and a large production probability (rising from $\sim 10\%$ around 350 TeV to $\sim 40\%$ around 3000 TeV). They called these unusual events "centauros". They also reported the observation of many more similar events but with much less hadron multiplicity, $n_c \sim 15 \pm 2$, which they called "Mini Centauros". A detailed description of these events can be found in ref. 3. Therefore I will limit my discussion to a few comments:

Centauro events have not been reported by the Pamir and Mount Fuji experiments. However, the Brazil-Japan Collaboration claim[3] that the results from these experiments are not inconsistent with theirs. The reason is that even if the primary interaction produces only charged hadrons (in a collision well above the chamber) these charged hadrons will produce π^0's (and η^0's) in secondary collisions with air nuclei and the chamber will record both hadron and photon jets. They claim that some of the Pamir events may be "centauros". The UA5 search of Centauro events in $\bar{p}p$ collisions at ~ 150 TeV has yielded negative results[4]. However the Centauro events have been observed at somewhat higher energies. The multi-TeV $\bar{p}p$ colliders under construction will have c.m. energies well above the "threshold" energy for Centauro production and will provide a clear answer to the question whether Centauros are produced in $\bar{p}p$ collisions.

It is of course possible that Centauros are produced only in high energy nuclear collisions and not in $\bar{p}p$ (or pp) collisions. A Japanese-American Cooperative Emulsion Experiment (JACEE) have recently investigated interactions of cosmic ray nuclei with energies up to 100 TeV per incident nucleon, using a balloon borne emulsion chamber[5]. For medium weight nuclei such energies per nucleus extend well into the energy region where the Centauro events have been observed. (The JACEE highest energy event was a Ca+C collision at $\sim$ 100 TeV/nucleon, i.e. at a total incident energy of 4000 TeV). The JACEE studied primary interactions inside their chamber but did not see any Centauro events in a total exposure of 100 $m^2 \cdot hr \cdot sr$ at an atmospheric depth of 3.5-5 gm/cm^2.

The total exposure which led to the discovery of a few centauro events on Mount Chacaltaya was of the order of $100 m^2 \cdot$ year, i.e. much higher than the JACEE exposure. However, the flux of high energy protons is strongly degraded at atmospheric depth of $\sim$ 540 gm/cm^2 compared to the primary cosmic ray flux at the top of the atmosphere, where the balloon-borne emulsion chamber of the JACEE was flown. (The mean free path for energy loss of $\sim$ 1000 TeV protons in the upper atmosphere, estimated from Glauber's theory with cross sections extrapolated from measurements at the SPS $\bar{p}p$ collider, is approximately 50 gm/cm^2). Consequently the total number of high energy interactions in the balloon-borne emulsion chamber of the JACEE and in the Mount Chacaltaya chambers are not very much different.

It is possible that Centauros are produced by very penetrating hadrons either present among the primary cosmic rays (collapsed nuclei[6], superdense nuclear droplets[7]..) or produced in cosmic ray collisions with air nuclei (glue balls[8], quark-glue droplets[9]...). It is however not clear: (i) why such systems produce only charged hadrons but no π^0's, η^0's, etc., (ii) why they are so abundant?

Plasmons- Quark Gluon Plasma Droplets?

The Japanese-American Cooperative Emulsion Experiment has recently investigated the interactions of cosmic ray nuclei with energy > 1 TeV per incident nucleon. From a total exposure of $\sim 100\ m^2 \cdot sr \cdot h$ in the stratosphere they have observed 100 events, two of which had extremely high multiplicities:[10] The highest multiplicity event was of the form:

$$Si(\sim 4\ TeV/nucleon) + AgBr \rightarrow 5N_h + (1010 \pm 30)N_{ch} + > 170\gamma \quad , \qquad (1)$$

while the second highest multiplicity event, which is also the most energetic nucleus ever directly observed, was of the form:

$$Ca(\sim 100\ TeV/nucleon) + C(or\ O) \rightarrow He + (760 \pm 30)N_{ch} + > 300\gamma \quad , \qquad (2)$$

where N_h and N_{ch} stand for heavily ionizing tracks and singly charged relativistic tracks, respectively. Such high multiplicities are not predicted by models which describe nucleus-nucleus collisions as a simple superposition of independent collisions between their nucleons[11]. Moreover, the average transverse momenta of the π^0's in these events were estimated from the p_T's of the γ's to be 550 ± 100 and 700 ± 50 MeV/c, respectively, which are much higher than those observed at the CERN ISR and SPS $\bar{p}p$ collider at the same energies. (~ 340 MeV/c at ~ 2 TeV[12] and 424 MeV/c at ~ 150 TeV[13]. Are these high multiplicities and high transverse momenta due to the formation of plasmons (droplets of quark-gluon plasma) in these events?

It has been suggested a long time ago[14] that the study of high energy central collisions between complex nuclei may yield information on the equation of state of nuclear matter at high density and temperature such as those encountered in astrophysical phenomena (e.g. gravitational collapse of massive stars) and at the early stage of the universe (the Big Bang). A clear proof of the formation of high density - high temperature nuclear matter

in high energy nucleus-nucleus collisions requires detecting a signature which is unique to such matter and cannot be predicted by models which describe nucleus-nucleus collisions as a simple superposition of independent collisions between their constituents[15]. Until recently no such signature has been discovered, neither in high energy interactions of cosmic ray nuclei[16], nor in α-α collisions at ISR[17], nor in interaction of relativistic heavy ions at the Bevalac.

Recently, however, new interest has been focused on high energy nucleus-nucleus interactions due to claims by some authors that quantum chromodynamics leads at sufficiently high density and temperature to a phase transition of normal nuclear matter into unconfined quark-gluon plasma[18a] and because of speculations that such quark-gluon plasma will be formed in high energy central nucleus-nucleus collisions[18b]. When the results of the JACEE became known they led a few authors[18c] to suggest that the high multiplicities and transverse momenta observed in events (1) and (2) are due to the formation of a quark-gluon plasma in these events. Unfortunately, the high multiplicities and average p_T observed in events (1) and (2) are in fact predicted also by a simple superposition model - a "Wounded Quarks Model" of nucleus-nucleus collisions[15,26], without invoking the formation of a quark-gluon plasma.

The "Wounded Quarks Model" is based on five main assumptions:

A1) The Constituent Quark Model - Each nucleon in a nucleus is made of three constituent quarks (which consist of a valence quark and a sea of gluons and $q\bar{q}$ pairs).

A2) The Additivity Assumption - In a collision the constituent quarks of the beam particle interact independently with the constituent quarks of the target (via gluons and/or quark exchanges) and with a small interaction probability.

A3) The Fragmentation Hypothesis - The fragmentation/recombination of wounded quarks (quarks that have suffered collisions) populate the central rapidity region while the fragmentation/recombination of spectator quarks from wounded nucleons (nucleons that have suffered collisions) populate the beam and target fragmentation regions.

A4) The "Wounding Approximation" - Multiple collisions of a quark do not change the multiplicity of hadrons that it fragments/recombines into.

A5) The Glauber Approximation - The multiple scattering of quarks within a nucleus can be described by the Glauber Approximation[19], (straight line trajectories, neglecting off shell effects).

Assumptions A1-A4 yield direct and simple relations between proton-proton (pp), proton-nucleus (pA) and nucleus-nucleus (BA) collisions : If one denotes by $\bar{W}_N^B$ and $\bar{W}_q^B$ the number of wounded nucleons and wounded quarks, respectively, in nucleus B then the inclusive distributions of hadrons produced in pp, pA and BA collisions, at the same energy per incident nucleon, are related as follows : In the beam fragmentation region

$$\frac{dn_f}{dx}(BA\to hX) \cong \bar{W}_N^B \frac{dn_f}{dx}(pA\to hX) \quad , \tag{3a}$$

where[20]

$$\frac{dn_f}{dx}(pA\to hX) \cong \bar{s}_q^p \frac{dn_f}{dx}(pp\to hX) \quad . \tag{3b}$$

In eqs. (3) the subscript f denotes the fragmentation region, i.e. $x\to 1$ where x is the fraction of the nucleon momentum in the nucleon-nucleon c.m. system that is carried by the produced hadron h, and $\bar{s}_q^p = 3 - \bar{W}_q^p$ is the average number of spectator quarks in the incident proton (assuming that h is mainly produced by the fragmentation/recombination of a single quark[20]).

$$\frac{dn_c}{dx}(BA\to hX) \cong \frac{\overline{W}_q^{\,B} + \overline{W}_q^{A}}{2} \frac{dn_c}{dx}(pp\to hX) \ , \tag{4}$$

where the subscript c denotes the central region, i.e. $x \sim 0$. One can combine eqs. (3) and (4) in a single interpolating formula of the form

$$R_{BA}(x) \equiv \frac{(dn/dx)_{BA}}{(dn/dx)_{pp}} \cong (1-|x|)\frac{\overline{W}_q^{\,B} + \overline{W}_q^{\,A}}{2} + \frac{|x|}{2}\begin{cases}\bar{s}_q^{\,B}, & x > 0\\ \bar{s}_q^{A}, & x < 0\end{cases} \ , \tag{5}$$

where $\bar{s}_q^{\,B} = 3\overline{W}_N^B - \overline{W}_q^B$ and $\bar{s}_q^A = 3\overline{W}_N^A - \overline{W}_q^B$ are the total numbers of spectator quarks in wounded nucleons in nuclei B and A, respectively. Since most of the produced particles in high energy pp collisions are produced in the central rapidity region we obtain from eq. (4) a simple relation also between the integrated multiplicities in BA and pp collisions at the same nucleon-nucleon c.m. energy :

$$\langle n\rangle_{BA} = (\overline{W}_q^B + \overline{W}_q^A)\ \langle n\rangle_{pp}/2 \ . \tag{6}$$

Assumptions A1 and A2 are the underlying assumptions of the Additive Quark Model[21]. They yield its well known relation $\sigma_{qN} = (1/3)\sigma_{pN}$. The average number of wounded constituents in a nucleus B that collides with a nucleus A at impact parameter b can then be shown, using standard nuclear optics techniques[22] or Glauber's multiple scattering theory[19] to be given by

$$\overline{W}_N^B(b) = \int (1-\exp(-\sigma_{pp}T_A(b')))T_B(\vec{b}-\vec{b}')d^2b' \ , \tag{7}$$

$$\overline{W}_q^B(b) = 3\int(1-\exp(-(1/3)\sigma_{pp}T_A(b')))T_B(\vec{b}-\vec{b}')d^2b' \ . \tag{8}$$

where $T_i(b') \equiv \int_{-\infty}^{\infty} \rho_i(b')dz$, $i = A,B$, ($T_i(b')$ is the nuclear thickness at transverse coordinate b') and the nuclear density function ρ_i is normalized such that $\int\rho_i\, d^3r = i$. Eq. (8) is valid also for B = 1 provided that $T_1(\vec{b}-\vec{b}') = \delta(\vec{b}-\vec{b}')$.

Eqs. (7), (8) can be averaged over any desired range of impact parameters. Table IV summarizes the resulting expressions for $\overline{W}_N$ and $\overline{W}_q$ in three typical ranges of impact parameters. The total inelastic quark-nucleus, nucleon-nucleus and nucleus-nucleus cross sections, σ_{qA}, σ_{pA} and σ_{BA}, respectively, can be calculated from Glauber's multiple scattering theory[19] employing nuclear density functions that were determined from electron scattering, $\sigma_{qp} = \frac{1}{3}\sigma_{pp}$ and σ_{pp} ($= \sigma_{p\bar{p}}$) values that were measured at the CERN ISR and $\bar{p}p$ collider.

Table IV

Model →	Wounded Nucleons		Wounded Quarks	
Collision ↓	$\overline{W}_N^{\,B}$	$\overline{W}_N^{\,A}$	$W_q^{\,B}$	$W_q^{\,A}$
All Impacts ($0 < b < \infty$)	$\frac{B\sigma_{pA}}{\sigma_{BA}}$	$\frac{A\sigma_{pB}}{\sigma_{BA}}$	$\frac{3B\sigma_{qA}}{\sigma_{BA}}$	$\frac{3A\sigma_{qB}}{\sigma_{BA}}$
Central ($b < \lvert R_A - R_B \rvert$)	B	$\frac{A\sigma_{pB}}{\sigma_{pA}}$	$\frac{3B\sigma_{qA}}{\sigma_{pA}}$	$\frac{3A\sigma_{qB}}{\sigma_{pA}}$
Head On ($b = 0$)	$\sim B$	$\sim A[1-(1-\frac{\sigma_{pB}}{\sigma_{pA}})^{3/2}]$	$\sim 3B$	$\sim \frac{3A\sigma_{qB}}{\sigma_{pB}}[1-(1-\frac{\sigma_{pB}}{\sigma_{pA}})^{3/2}]$

Table IV : Analytic estimates of the average number of wounded constituents in nucleus-nucleus collisions as deduced from eqs. (6) and (7) and assuming B<<A for central and head-on collisions.

In Table V we list the numerical values of $\overline{W}_N$ and $\overline{W}_q$ obtained by applying Table V to Si+Ag and Ca+C collisions at incident energies of 4 TeV/nucleon and 100 TeV/nucleon, respectively, and the resulting values of $\langle n_c \rangle_{BA}$ and of $R(x \sim 0)$ (i.e. R around zero c.m. pseudorapidity, $\eta \sim 0$) for these reactions.

Table V

	Theory			JACEE
	All Impacts $0 < b < \infty$	Central $b < \lvert R_A - R_B \rvert$	Head On $b = 0$	
	Si + Ag ; E/A = 4 TeV			
$\overline{W}_N^{Si}$	10.4	28	28	
$\overline{W}_N^{Ag}$	16.4	42	60	
R_c	13.4	35	44	
$\langle n_c \rangle$	161	420	522	
W_q^{Si}	20.8	55	84	
W_q^{Ag}	27.4	72	108	
R_c	24.1	63.5	96	100±20
$\langle n_c \rangle$	289	762	1152	1010±30
	Ca+C ; E/A = 100 TeV			
W_N^{Ca}	6.4	19	24.8	
W_N^{C}	4.3	12	12	
R_c	5.4	15.5	18.4	
$\langle n_c \rangle$	128	372	441	
W_q^{Ca}	7.9	19.6	35.1	
W_q^{c}	8.9	26.2	36	
R_c	8.4	22.9	35.5	30±6
$\langle n_c \rangle$	202	550	853	760±30

Table V : Comparison between the predictions of the Wounded Nucleons Model, the Wounded Quarks Model and the JACEE events (1) and (2).

In the calculations we used the experimental values[12] $\sigma_{pp} \equiv \sigma_{pp}^{in} \cong 0.83\ \sigma_{pp}^{t} \cong 40$ mb, $\frac{dn_c}{d\eta}(pp) \cong 2$ around $\eta_{c.m.} \sim 0$ and $\langle n_c \rangle_{pp} \cong 12$ at $P_{LAB} \sim 4$ TeV/c, and[13] $\sigma_{pp} \cong 0.81\sigma_{pp}^{t} \cong 50$ mb, $\frac{dn_c}{d\eta}(pp) \simeq 3$ and $\langle n_c \rangle_{pp} \cong 24$ at $P_{LAB} \sim 100$ TeV/c, obtained from measurements at the CERN ISR and $\bar{p}p$ Collider. As can be seen from Table V the Wounded Nucleons Model [11] underestimates the total multiplicity and the density of particles in the central rapidity region. (Note that the dispersion of the multiplicity at a fixed and small impact parameter is expected to satisfy $D \equiv \sqrt{\langle n_c^2 \rangle - \langle n_c \rangle^2} = \sqrt{\langle n_c \rangle}$, i.e. $D \ll \langle n_c \rangle$, because the multiplicity distribution is expected to approach there a Gaussian distribution[23]. This is due to the Central Limit Theorem in the theory of probability that applies here to the total multiplicity which is a sum of multiplicities from many independent constituent-constituent collisions). However, Table V also shows that the predictions of the Wounded Quark Model are consistent with events (1) and (2) assuming they are due to very central collisions. Support for the assumption that events (1) and (2) are indeed due to central collisions is provided by the absence of "spectator" protons in the beam fragmentation region (spectator protons are expected to retain their original momentum, i.e. the average momentum per nucleon in the beam modified only by internal Fermi motion). Moreover, from impact parameter considerations one expects a few percent of central collisions events in an unbiased sample of nucleus-nucleus collisions. This is consistent with the observations of events (1) and (2) in a sample of $\sim$ 100 nucleus-nucleus collisions[10]

In Fig. 4 we compare our predictions for the rapidity distribution in events (1) and (2) as given by eq. (5) (assuming that the relativistic charged tracks are due to $\pi^{\pm}$) and the experimental distributions. Fig. 4

shows good agreement between the predictions and the observations, within the present statistics. Refinements of the Wounded Quarks Model[20] probably will be required only when high statistics experiments on high energy nucleus-nucleus collisions will become available.

The nuclear enhancement of the production of large p_T's in hadron-nucleus collisions is a well known effect[24]. It results from multiple scattering of the constituent quarks of the projectile on target constituents[25] and from the internal (Fermi) motion of the constituents in the target. In nucleus-nucleus collisions the internal motion of the constituents in the incident nucleus, and their scattering among themselves after scattering off target constituents, further enhances the production of large p_T's. A detailed evaluation of the effect and its dependence on A and B, on impact parameter, on incident energy and on longitudinal momentum and quantum numbers of the produced particles, requires the construction of a complicated Monte Carlo code, which is beyond the scope of this research. However the magnitude of the effect is expected to be given approximately by

$$\langle p_T \rangle_{BA} \simeq [B\sigma_{pp}/3\sigma_{pB} + A\sigma_{pp}/3\sigma_{pA} + 1/3\,]^{1/2} \langle p_T \rangle_{pp} \,, \tag{9}$$

where the square brackets stand for the average number of collisions that a wounded quark suffers (both in A and B) in central collisions, and where we neglected the transverse momenta of the quarks that it collides with. Eq. (9) yields $\langle p_T \rangle_{SiAg} = 1.5 \langle p_T \rangle_{pp} = 540$ MeV/c using $\langle p_T \rangle_{pp} = 360$ MeV/c[12], at 4 TeV per incident nucleon, and $\langle p_T \rangle_{CaC} = 1.45 \langle p_T \rangle_{pp} = 635$ MeV/c using $\langle p_T \rangle_{pp} = 424$ MeV/c at 100 TeV per incident nucleon,[13] in good agreement with the experimental estimates of 550±50 MeV/c and 700±50 MeV/c in events (1) and (2), respectively.

In conclusion, the high multiplicities and average transverse momenta observed in events (1) and (2) are consistent with the predictions of a simple Wounded Quarks Model and do not necessarily indicate the formation of quark-gluon plasma. Moreover the agreement between experiment and theory is achieved without the use of free parameters and without even specifying, either the nature of the colour forces between constituents, or the detailed mechanism of particle formation postulated in references 15d-15f.

(ii) High Transverse Momenta

For many years cosmic ray data have suggested the existence of a high transverse momentum tail in the interactions of very high energy particles[27]. This has been observed directly in interactions inside emulsion chambers[28,10,3] and has also been deduced from the lateral distribution of normal air cascades[29], from underground muon observations[30] and from multi-core structure air cascades[29].

It has already been mentioned in the discussion of "plasmons" that an enhancement of the tail of the p_T distribution in particle-nucleus and nucleus-nucleus collisions compared to pp or $\bar{p}p$ collisions is a well known[24] and well understood phenomenon. It results from the multiple scattering of projectile constituents off target constituents and from the Fermi motion inside the nuclei. Cosmic ray collisions with emulsion layers, or with target layers, or with air nuclei are either proton-nucleus or nucleus-nucleus collisions where such an enhancement compared to pp or $\bar{p}p$ collisions is indeed expected.

The large p_T deduced from multicore structure air cascades, such as "Geminions", which are discussed in detail in ref. 3, are probably of completely different origin. It can be due to the production and decay of a pair of massive mesons that contain a new heavy flavour (top or higher flavour).

(iii) Anomalous Cross Sections

Nuclear Anomalons:

Since 1954 there have been sporadic reports from studies of interactions of high energy cosmic rays with atomic nuclei, that some of the fragments of the incident cosmic ray nuclei have anomalously large cross sections for secondary nuclear collisions[31]. These observations have been claimed to be confirmed a few years ago by emulsion experiments[32], and more recently by new emulsion experiments, by experiments employing plastic track detectors and by experiments employing heavy liquid bubble chambers (although there are few experiments that failed to see the effect). This proceeding includes a detailed discussion of the evidence on nuclear anomalons from these experiments, and of their possible origin. Therefore, I will limit my discussion to few remarks:

1. Counter experiments are still badly needed in order to establish the existence of anomalons and to determine their basic properties. Simple schemes for such experiments are described in reference 33.
2. The anamalon search should be extended to elementary particles (using bubble chambers and electronic counters) because there is a gap in our knowledge of the behaviour of elementary particles in the proper time range 10^{-10} sec $< \tau < 10^{-20}$ sec after their formation, and because the situation is reminiscent of the need to introduce strangeness conservation in the 1950's to explain the fact that new particles that were strongly produced in pion-nucleon collisions were living thirteen orders of magnitude too long (for particles that decay into other strongly interacting particles).
3. At this conference evidence was presented that nuclear anomalons are produced mainly in peripheral collisions[34]. This is probably consistent with earlier reports from emulsion experiments that anomalons tend to retain their "anomaly" in successive collisions. These highly suggest that

if the anomalon phenomenon is real, it involves the excitation of only a single nucleon i.e. that it probably exists also at the elementary particle level! It is then natural to speculate that it is due to associated production of a new quantum number, which we suggest to call "Anomaly", associated with a medium-range strong interaction.

Penetrons

The Moscow group[35] and the Pamir collaboration[36] reported the observation of collimated bundles of very energetic hadrons with seemingly anomalously long mean free paths (anomalously small cross sections). Fig. illustrates the Pamir event[36]. It consisted of a highly collimated bundle of particles which penetrated through the whole hadron block and every x-ray film at the different depths recorded a big spot with a halo of about 1 cm^2. Neither attenuation nor variation of the core throughout the chamber have been observed. It was interpreted as a bundle of hundred hadrons or more, with a total energy of more than $3x10^6$ GeV and with anomalously small cross sections. We suggest to name these penetrating anomalon "penetrons". No theoretical scheme has been suggested so far to accommodate them.

IV. Anomalies Seen By Deep Underground Detectors

Underground detectors have been used for quite some time for the study of penetrating cosmic ray components. They detected both single muons and multimuon events that were associated with the decay of pions and kaons in air cascades generated by cosmic ray particles[37]. Searches of prompt muon sources (particles that decay into μ's with a very short life time), based on different dependence on zenith angle of muon yields from prompt and "delayed" sources, were not conclusive[37].

The construction of deep underground proton decay detectors has renewed interest in penetrating cosmic ray components (high energy muons, neutrinos, monopoles, ...,). At present most of the attention in deep underground experiments is focused on:

1) Search of proton decays.
2) Search of magnetic monopoles.
3) Search of baryon-antibaryon oscillations.
4) Search of neutrino oscillations.

However, since the 10 kiloton Irvine-Michigan-Brookhaven (IMB) Water Cherenkov Detector located in the Morton Salt Mine near Cleveland, Ohio, which is the largest among the present generation proton decay detectors, did not see any of these effects[38], it is natural to expect that attention will soon be shifted to the study of penetrating cosmic ray components.

Preliminary results from the operating deep underground detectors (Kolar Gold Field, Homestake, Soudan, Silver King, Mont Blanc, IMB and Kamioka) are consistent with previous observations on single and multimuon events. In particular they also see high energy "muon bundles" - very collimated jets of highly parallel and energetic muons. The origin of these muon bundles is not clear. It has been speculated[39] that these muon bundles may result from the production and decay of a pair of massive mesons that contain heavy flavour (such as b,t,...,). The cascade decay of such heavy flavours can yield many μ's e.g.

$$t \to b(e\nu, \mu\nu, \tau\nu, c\bar{s}, u\bar{d})$$
$$\hookrightarrow c(e\nu, \mu\nu, u\bar{d})$$
$$\hookrightarrow s(e\nu, \mu\nu, u\bar{d})$$

with:

$$\tau \to \nu(e\nu, \mu\nu, u\bar{d})$$

If they are produced at very high energies they may be collimated enough to look like a μ-bundle in a deep underground detector. It is not clear however whether their production cross section is sufficiently large to explain the observed rate of μ-bundles in the underground detectors.

V. Anomalies in Extensive Air Showers (10^6 GeV < E < 10^{11} GeV)

The study of very high energy cosmic rays with high altitude flown equipment is hampered by their low intensities ($\sim 10^{-2}$ particles$\cdot m^{-2} \cdot hr^{-1} \cdot sr^{-1}$ above 10^6 GeV and ~ 1 particle$\cdot km^{-2} \cdot year^{-1} \cdot sr^{-1}$ above 10^{10} GeV). The only practical method for studying very high energy cosmic ray interactions has been to use the atmosphere as a calorimeter and to extract the information on the primaries and their interactions from ground based measurements of the various components of the extensive air showers which they produce in the atmosphere[41]. When the primary cosmic ray particle interacts with air nuclei in the upper atmosphere it produces fast fragments which further collide with air nuclei and produce new fragments. Most of the produced particles are mesons, and at each collision a fraction of the energy is carried off by π^0's (and η^0's) which decay into photons initiating electron-photon cascades. These electromagnetic cascades dissipate most of the primary energy leaving only a small fraction to be carried away by neutrinos and muons (mainly from $\pi^\pm$ and $K^\pm$ decays) and by hadrons stooping in the earth. (The interaction mean free paths of energetic $\pi^\pm$ and K mesons is much shorter than their mean decay lengths in the atmosphere). The electron and muon components of extensive air showers are relatively well understood, as well as the visible photons, whether produced by the Cherenkov process or by atmospheric fluorescence. Their measurements have been used to determine the energy spectrum of the primary cosmic rays. Fig. 5 shows a summary of

cosmic ray energy spectra adapted from ref. 40. One observes three major "anomalies" in these spectra:

1. A break in the spectrum around $E \sim 10^6$ GeV.
2. A break in the spectrum around $E \sim 10^{10}$ GeV.
3. An enhancement of the spectrum beyond $E \sim 10^{10}$ GeV.

Are these "anomalies" due to astrophysics or are they due to high energy particle physics?

Cosmic Rays With 10^6 GeV < E < 10^{10} GeV

It is interesting to note that 10^6 GeV is also the energy where the emulsion chamber experiments reported[41] the set-in of "new physics". Is there any evidence for such "new physics" from extensive air shower?

Linsley[42], Hillas and others[43-48] have suggested, on the basis of very general particle physics arguments that a simple test whether particle physics extrapolates smoothly from the energies of man-made accelerators to the energy range beyond 10^6 GeV is provided by comparing calculations and measurements of the average depth of maximum energy deposition in the atmosphere, t_{max}, in extensive air showers. A simple analytic treatment of air shower development yields the approximate prediction[49]

$$t_{max} = \lambda_N + L\ \ell n(2.3X_m E/\varepsilon) \tag{10}$$

where λ_p is the mean free path (gm/cm^2) of nucleons in the atmosphere, $L \sim 36\pm1$ gm/cm^2 is the radiation length in the atmosphere, $\varepsilon = 0.077$ GeV is the critical energy in air, $x_m E$ is the most probable energy of the π^o's emerging from the primary collision and E is the primary energy per nucleon. Eq. (10) is in good agreement with the results of the detailed Monte Carlo calculations of Hillas[43] and Gaisser[50]. Fig. 6 compares the experimental results compiled by Watson[48] and eq. (10) for pure proton and iron primary CR. (The solid lines refer to Eq. (10) while the dashed lines refer to Monte Carlo

calculations of Hillas[43] and Gaisser[50]). Although the experimental points lie between the pedicted proton and iron curves the slope of the data points is clearly steeper than that of the theoretical lines, suggesting[46] a transition from a heavy nucleus dominated composition near 10^7 GeV to a light element dominated composition by 10^9 GeV.

It has also been suggested[51] that the steepening of the data may be explained by a change in the interaction characteristics above accelerator energies. e.g. if x_m in eq. (10) increases with energy (violation of Feynman scaling) then the maximum possible increase in t_{max} at energies beyond those achieved by man-made accelerators would be ~ 70 gm/cm^2. Such a change could produce the desired steepening; however, although such a possibility cannot be ruled out at present, no such extreme behaviour have been suggested by experimental data from Fermilab, ISR or CERN $\bar{p}p$ collider.

In addition to speculating about possible changes in the interaction characteristics, one can also use eq. (10) to predict the contributions of various possible exotic components in the high energy cosmic ray flux. In Table VI we list some possible exotic particles, together with their corresponding values of x_m and λ_p, and the increase or decrease of t_{max} from the proton value (based on Eq. 10).

Table VI

The mean depths of primary interaction and shower maximum of primary cosmic ray particles.

Particle	λ	x_m	$\langle t_m \rangle - \langle t_m \rangle_p$
Proton	λ_p	1/8	-
Photon	0	1	$2.75L - \lambda_p$
Nucleus	$\sim \lambda_p(E/A)$	1/8A	$-L \ln A + \lambda_p(E/A) - \lambda_p(E)$
Quark	~ 0	1/5	$L - \lambda_p$
	$3\lambda_p$	1/5	$L + 2\lambda_p$
Anomalon	~ 0	1/8A	$-\lambda_p - L \ln A$
Centauro	λ ?	$1/8\langle n_c \rangle$	$\lambda - \lambda_p - L \ln \langle n_c \rangle$

1) Photons: Several authors[52)] have suggested the possibility that a part of the very high energy cosmic ray flux might be due to primary gamma rays. In this case the cascade[53)] begins at a depth $t \cong 0$ rather than λ_p, the factor 2.3 in the logarithm increases to 4.5, and $x_m = 1$, so that photon-induced cascades would mimic the observed high energy behavior by lowering the shower maximum into the atmosphere by an amount $2.75L - \lambda_p$. In fact the 3^oK cosmological microwave radiation becomes opaque[52)] to extragatactic photons around $E_\gamma \sim 10^6$ GeV which is the effective threshold for the reaction $\gamma + \gamma_{3^oK} \rightarrow e^+e^-$. Beyond $E_\gamma \sim 10^6$ GeV the opacity decreases like $\ln E_\gamma / E_\gamma$ because $\sigma_{\gamma\gamma' \rightarrow e^+e^-} \sim \frac{4\pi\alpha^2}{s} [\ln\left(\frac{s}{m_e^2}\right) - 1]$ where $s \sim 4E_\gamma E_{\gamma'}(1-\cos\theta)$. A significant

component of photons among the primary cosmic rays thus may give rise to the break in the CR spectrum around 10^6 GeV and to the steep rise in the depth of shower maximum beyond this energy.

2) Free quarks: The study of quark jets in e^+e^- annihilations, in deep inelastic lepton-nucleon collisions, and in high energy hadron-hadron collisions shows that the π^0 spectrum due to the fragmentation of a quark is somewhat harder than the π^0 spectrum in the fragmentation region of a nucleon. For quark fragmentation, $f(x) \sim (1-x)^2/\sqrt{x}$; then $x_m \sim 1/5$ compared with $x_m \sim 1/8$ for primary protons. From Eq. (9), this increase in x_m induces a small increase in t_{max} (less than a radiation length). However, if free quarks have a large cross section due to unconfined colour, then $\lambda \sim 0$ and their primary interactions take place higher in the atmosphere. Since at high energies $\lambda_p \sim L$, this decrease in the depth of maximum offsets the increase due to the change in x_m, so the net effect on t_{max} is rather small. This is not the case if free quarks have a small cross section (i.e., if they act like bound quarks, for which $\sigma_{up} \sim \sigma_{dp} \sim \sigma_{pp}/3$, $\sigma_{sp} \sim \sigma_{Kp} - \sigma_{\pi p}/2$, etc.). In this case quarks penetrate deeper in the atmosphere and produce harder π^0's than in proton-induced showers. A proper admixture of such quarks in the primary cosmic ray beam could explain the behaviour of t_{max} at energies above 10^7 GeV.

3) Nuclear anomalons: If unstable, they occur only in the hadronic cascade and not in the primary radiation; their net effect on t_{max} is then negligible. However, if stable, they might be present among the primary cosmic rays. Although, compared with normal nuclei, their primary interactions will be higher in the atmosphere, their energy is shared by A nucleons; the main effect, like that of ordinary nuclei, will be to decrease t_{max} by $L\ell nA$.

4) Centauros: If a significant fraction of primary cosmic ray interactions are Centauro events then the π^0's will be produced mostly by second- and later-generation particles with degraded energies; this by itself will decrease t_{max}. However, the mean depth of interaction λ is unknown and might be much larger than λ_p, so that a definite conclusion about t_{max} for Centauros cannot be drawn.

In summary, an increase in the flux of light nuclei, photons, and/or Centauros, quarks, or some other exotic particles with long interaction length would reproduce the observed increase in elongation rate above 10^{17} eV.[54]

Ultrahigh Energy Cosmic Rays ($E > 10^{10}$ GeV)

Greisen, Kuzmin and Zatsepin were the first to point out[55] that if the ultra high energy cosmic rays are protons of extragalactic origin, they must be cutoff at energies exceeding $\sim 3\times10^{10}$ GeV, because their mean free path for undergoing the photoproduction reaction $p+\gamma\rightarrow\pi+N$ in collisions with the 3^oK cosmological background photons becomes shorter than the distances they travel before reaching earth (The photoproduction cross section peaks at the N^*_{1236} resonance. The peak value is $\sim$500 μb which corresponds to a mean free path of $\sim$ 1.6 Mpc in a 3^oK black body radiation of $400\gamma/cm^3$, compared for instance to the distance to the Virgo Cluster which is $\sim$ 20 Mpc). The observations[56] seem to be at odds with this prediction: Cosmic rays have been observed with energies extending up to 10^{11} GeV and with intensities much larger than those expected from a smooth extrapolation from energies below 10^{10} GeV.

One possible solution to this anomaly is that the ultrahigh energy cosmic rays are produced by near-by sources and do not travel cosmological distances before reaching earth. Such a solution implies that ultrahigh energy cosmic rays are highly unisotropic since they are not confined by the galactic magnetic fields.

Another solution is that the ultrahigh energy cosmic rays consist mainly of photons[53], either produced directly by astrophysical point sources, or in collisions of cosmic ray protons with the $3^{o}K$ cosmological photons (through the reaction $p+\gamma\rightarrow\pi^{o}+p$ and the prompt decay $\pi^{o}\rightarrow 2\gamma$). Since the $3^{o}K$ microwave radiation is more transparent to ultrahigh energy photons than to ultrahigh energy protons, photons can arrive from much larger distances and therefore perhaps with accumulated intensities, much larger than those of the primary protons.

It is of course possible, that the energy deposition into the various components of the extensive air showers is different from what is anticipated from extrapolating our knowledge on particle production at accelerator energies to the ultrahigh energies of the most energetic cosmic rays. It then may lead to a wrong determination of the energy of the primary cosmic ray particles and may fake an "anomalous" behaviour and perhaps fake an enhancement of the spectrum at cosmic ray energies above 10^{10} GeV. In this connection it is important to notice that the probability of π^{o}'s produced in extensive air showers to decay before they suffer inelastic collisions with air nuclei, is given by[57] $\sim 1/(1+\gamma E)$ with $\gamma^{-1} \equiv mch_{o}\sec\theta/\tau = 3.6\times10^{10}\cdot\sec\theta\cdot$GeV, where m, τ and E are the mass, proper lifetime and energy, respectively, of the π^{o}, $h_{o} \cong 6.5$ km is the scale parameter of the upper atmosphere and θ is the zenith angle of the incident cosmic ray particle. Therefore, when the energy of the primary cosmic ray protons increases beyond 10^{10} GeV an increasing fraction of the π^{o}'s that are produced in the primary collisions are absorbed in secondary collisions before they decay into 2γ. This tends to supress the increase of the average depth of shower maximum for primary energies beyond 10^{10} GeV.

Acknowledgements

The author would like to thank R. Amado, S. Bludman, M. L. Cherry, K. Lande, P. Langacker, B. Margolis and R. I. Steinberg for many useful discussions, suggestions and ideas.

References and Footnotes

1. Particle Data Group, "Review of Particle Properties" Phys. Lett. 111B, 1 (1982).
2. D. Müller, Proceedings of the Workshop on Very High Energy Cosmic Ray Interactions, University of Pennsylvania, Philadelphia April 22-24, 1982 p. 448 (Editors M. L. Cherry, K. Lande and R. I. Steinberg).
3. C. M. G. Lattes et. al., Phys. Rep. C65, 151 (1980), and references therein.
4. K. Alpgard et al., Phys. Lett. B115 (1982) 65.
5. T. H. Burnett et. al. Reference 2 p. 221.
6. T. D. Lee and G. C. Wick, Phys. Rev. D9, 2291 (1974); H. Primakoff.
7. J. D. Bjorken and L. McLerran, Phys. Rev. D20, 2353 (1979). D. Sutherland, Cosmic Rays and Particle Physics, AIP Proceedings p. 49 (Ed. T. K. Gaisser) 1978.
8. See for instance J. Cleymans et al., Z. Phys. 17, 341 (1983).
9. J. Cleymans et al., Ref. 2. p. 136.
10. T. H. Burnett et al., Phys. Rev. Lett. 50, 2062 (1983).
11. (a) A. Bialas et al., Nucl. Phys. B111, 461 (1976). (b) S. J. Brodsky et al., Phys. Rev. Lett., 39 1120 (1977). (c) I. Otterlund and E. Stenlund, Physica Scripta 22, 15 (1980).
12. B. Alper et al., Nucl. Phys. B100, 237 (1975); W. Thome, NP B129, 365 (1977).
13. G. Arnisoni et al., Phys. Lett., 118B, 167 (1982).
14. A. Dar, Proceedings Topical Meeting on High Energy Collisions Involving Nuclei (Eds. G. Bellini, L. Bertocchi and P. G. Rancoita) Trieste 1974; p. 231.

15. (a) A. Bialas et al., Acta Phys. Pol. 88, 585 (1977).
(b) A. Bialas, Proceedings 1st Workshop On Ultra-Relativistic Nuclear Collisions, Berkeley 1979 (LBL Report 8957) (c) A. Dar, Proceedings Europhysics Conference On Partons In Soft Hadronic Physics, Erice 1981 (Editor R. Van de Walle p.). (d) K. Kinoshita et al., Z. Phys. C8, 205 (1981). (e) A. Bialas et al., Z. Phys. C13, 147 (1982). (f) A. Capella et al., Phys. Lett. 108B, 347 (1982).

16. S. Tokunaga, J. Phys. Soc. Japan 12, 454 (1957); K. Rybicki, Nuovo Cim. 28, 1437 (1963); D. Abraham et al., Phys. Rev. 159, 1100 (1967); S. Tasaka et al., Phys. Rev. D25, 1765 (1982).

17. W. Bell et al., CERN Preprint EP/83-64 (May 1983).

18. (a) See e.g. H. Satz, Phys. Rep. 88, 349 (1982) and references therein.
(b) See e.g. R. Anishetty et al., Phys. Rev. D22, 2793 (1980);
(c) L. McLerran, Phys. Rep. 88, 380 (1982), J. Cleymans et al., Z. Phys. 17, 341 (1983), J. D. Bjorken, Phys. Rev. D27, 140 (1983), and references therein.

19. R. J. Glauber, Boulder "Lectures in Theoretical Physics", Vol. 1 (1958) [Interscience Publishers, Inc., New York 1959) and in "High Energy Physics and Nuclear Structure" p. 311 (North Holland Publ. Amsterdam 1967).
K. S. Kolbig and B. Margolis, Nucl. Phys. B6, 85 (1968).

20. See e.g. N. N. Nikolaev, Phys. Lett. 70B, 95 (1977); A. Dar and F. Takagi, Phys. Rev. Lett. 44, 768 (1980), A. Bialas and E. Bialas, Phys. Rev. D20, 2854 (1979); G. Berlad et al., Phys. Rev. D22, 1547 (1980), and references therein.

21. E. M. Levin and L. L. Frankfurt, Pis'ma Zh. Eksp. Teor. Fiz. 2, 105 (1965).
H. J. Lipkin and F. Scheck, Phys. Rev. Lett. 16, 71 (1966).

22. See e.g. A. Dar and J. Vary, Phys. Rev. D6, 2412 (1972); G. Berlad et al., Phys. Rev. Lett. D13, 161 (1976); Phys. Rev. D22, 1547 (1980); Phys. Lett. 102B, 385 (1981).

23. Y. Afek et al., Phys. Rev. Lett. 41, 849 (1978).

24. J. Cronin et al., Phys. Rev. D11, 3105 (1975); L. Kluberg et al., Phys. Rev. Lett. 38, 670 (1977); D. Antreasyan et al., Phys. Rev. D19, 764 (1979); C. Bromberg et al., Phys. Rev. Lett. 42, 1202 (1979); Nucl. Phys. B171, 38 (1980); B. Brown et al., Phys. Rev. Lett.

25. J. Pumplin and E. Yen, Phys. Rev. D11, 1812 (1975); P. M. Fishbane et al., Phys. Rev. D12, 2133 (1976); D16, 122 (1977); J. H. Kühn, Phys. Rev. D13, 2948 (1976); A. Krzywicki, Phys. Rev. D14, 152 (1976); F. Takagi, Phys. Rev. Lett. 43, 1296 (1979). M. Lev and B. Peterson, Preprint BI-TP 83/08, (University of Bielefeld, May 1983).

26. A. Dar and B. Margolis "Extremely High Multiplicities in High Energy Nucleus Nucleus Collisions From Wounded Quarks", McGill Preprint July 1983.

27. S. Hayakawa, Cosmic Ray Physics - Nuclear and Astrophysical Aspects, Wiley-Interscience, New York 1969.

28. Y. Sato et al., J. Phys. Soc. Japan 41, 1821 (1976).

29. C. B. A. McCusker, Phys. Rep. 20C, 229 (1975).

30. M. L. Cherry et al., in ref. 2 p. 278.

31. A. Milone, Nuovo Cim. Suppl. 12, 354 (1954); H. Yagoda, Bull. Am. Phys. Soc. 2, 64 (1956); S. Tokunaga et al., Nuov. Cim. 5, 517 (1957); B. Judek, Can. J. Phys. 35, 343 (1968); 50, 2082 (1972) and references therein.

32. E. M. Friedlander et al., Phys. Rev. Lett. 45, 1084 (1980); P. L. Jain and G. Das, Phys. Rev. Lett. 48, 305 (1982); H. B. Barber et al., Phys. Rev. Lett. 48, 856 (1982).

33. R. Amado and A. Dar, Phys. Rev. C27, 1325 (1983).

34. M. El Badaway et al., Cairo University Preprint (1983).

35. V. I. Yakovlev et al., Proc. 16th Int. Cosmic Ray Conf. 6, 59 (1979).

36. S. G. Bayburina et al., Proc. 16th Int. Cosmic Ray Conf. 6, 249 (1979).

37. See e.g. M. L. Cherry et al., ref. 2 p. 278; M. L. Marshak, ref. 2, p. 333; J. W. Elbert, ref. 2. p 312,and references therein.

38. R. M. Bionta et al., Phys. Rev. Lett. 51, 27 (1983).
S. Errede et al., Phys. Rev. Lett. 51, 245 (1983).

39. Y. Muraki, ref. 2, p. 261; B. Margolis, private communication.

40. J. Linsley, Proc. IUPAP/IAU Symp. "Origin of Cosmic Rays", Bologna (1980).

41. See e.g. H. Terazawa, Proc. 21st Int. Conf. on HEP, p. 191 (Eds. Petiau, Porneuf,Paris 1982).

42. J. Linsley, Proc. 15th Intl. Cosmic Ray Conf., Plovdiv 12, 89 (1977).

43. A. M. Hillas, in "Cosmic Rays and Particle Physics 1978 (Bartol Conf.)", ed. by T. K. Gaisser, Newark, p. 373 (1979).

44. T. Shibata, Proc. 15th Intl. Cosmic Ray Conf., Plovdiv 8, 358 (1977).

45. T. K. Gaisser, T. J. L. McComb, K. E. Turver, Proc. 16th Intl. Cosmic Ray Conf., Kyoto 9, 275 (1979); T. K. Gaisser and G. B. Yodh, Ann. Revs. Nucl. Part. Sci. 30, 475 (1980); T. K. Gaisser, R. J. Protheroe, K. E. Turver, and T. J. L McComb, Revs. Mod. Phys. 50, 859 (1978).

46. G. Thornton and R. W. Clay, Phys. Rev. Lett. 43, 1622(1979).

47. J. Linsley and A. A. Watson, Phys. Rev. Lett. 46, 459 (1981).

48. A. A. Watson, Proc. Workshop on Very High Energy Cosmic Ray Interactions, ed. by M. L. Cherry, K. Lande, and R. I. Steinberg, Philadelphia, p. 105 (1982).

49. M. L. Cherry, A. Dar and S. Bludman "Analytic Treatment Development" Submitted to Physical Review.

50. T. K. Gaisser, Private Communication (1983).

51. J. Wdowczyk and A. Wolfendale, Nature 236, 29 (1979).

52. J. Wdowczyk, W. Tkaczyk, and A. W. Wolfendale, J. Phys. A5, 1419
R. Amado, A. Dar, and P. Langacker, to be published (1983).

53. B. Rossi and K. Greisen, Revs. Mod. Phys. 13, 240 (1941).

54. A. Dar, M.L. Cherry, S.A. Bludman and R.D. Amado, "Exotic Cosmic Rays and their Extensive Air Showers", University of Penn. Preprint, March 1983.

55. K. Greisen, Phys. Rev. Lett. 16, 748 (1966).
V. A. Kuzmin and G. T. Zatsepin, Zh. Eksp. Teor. Fiz. 4, 78 (1966).

56. See e.g. J. Linsley, in "Origin of Cosmic Rays" pp. 53-68 (Eds. Setti, Spada and Wolfendale, 1981) and references therein.

57. A. Dar, B. Margolis and M. Cherry "Cosmic Ray Muons - Analytic Treatment" to be published (1983).

Figure Captions

Fig. 1. The integral flux (particles with energy larger than E_0) of the primary cosmic rays at the top of the atmosphere.

Fig. 2. Differential energy spectra of the major cosmic ray species:protons, helium, carbon, iron, and electrons. This compilation of data summarizes the results of a number of different measurements (except for electrons where only the Chicago data are shown).

Fig. 3. Schematic description of the first centauro event in the Mt. Chacaltaya emulsion chamber.

Fig. 4. Pseudo rapidity distributions of charded hadrons produced in two of the JACEE events.

Fig. 5. The integral flux of the primary cosmic rays at the top of the atmosphere multiplied by $E^{1.5}$.

Fig. 6. Comparison between experimental results compiled by Watson[48)] and theoretical predictions of the mean depth of shower maximum t_{max} as a function of primary energy. The solid lines represent formula (10) while the dashed lines refer to Monte Carlo results of Hillas[43)] and Gaisser[50)] for pure iron and proton primaries.

Integrated Flux of Primary CR

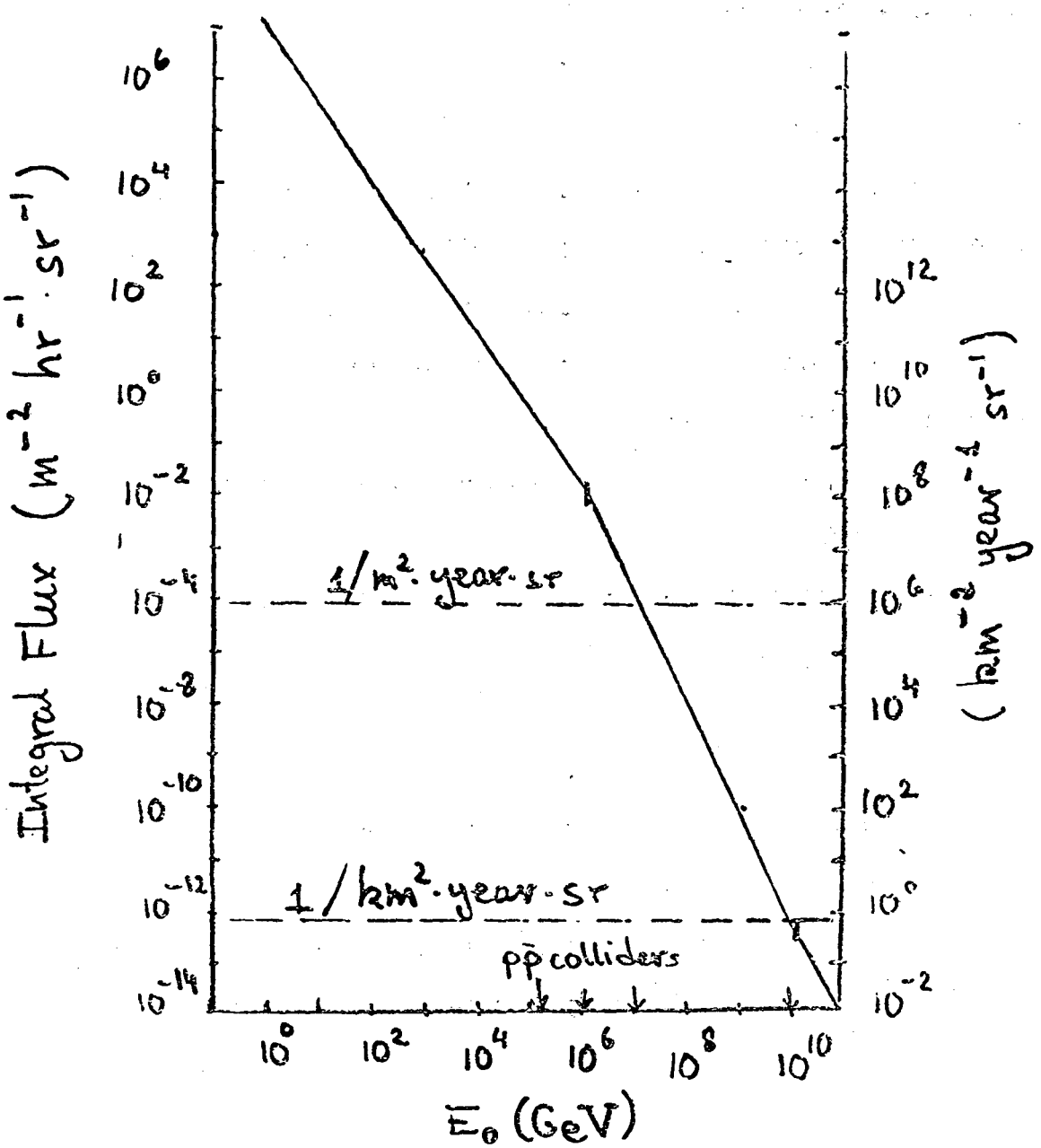

1 particle/ $m^2\cdot year\cdot sr$ for $E \geq 10^7$ GeV

1 particle/ $km^2\cdot year\cdot sr$ for $E \geq 10^{10}$ GeV

Fig. 1.

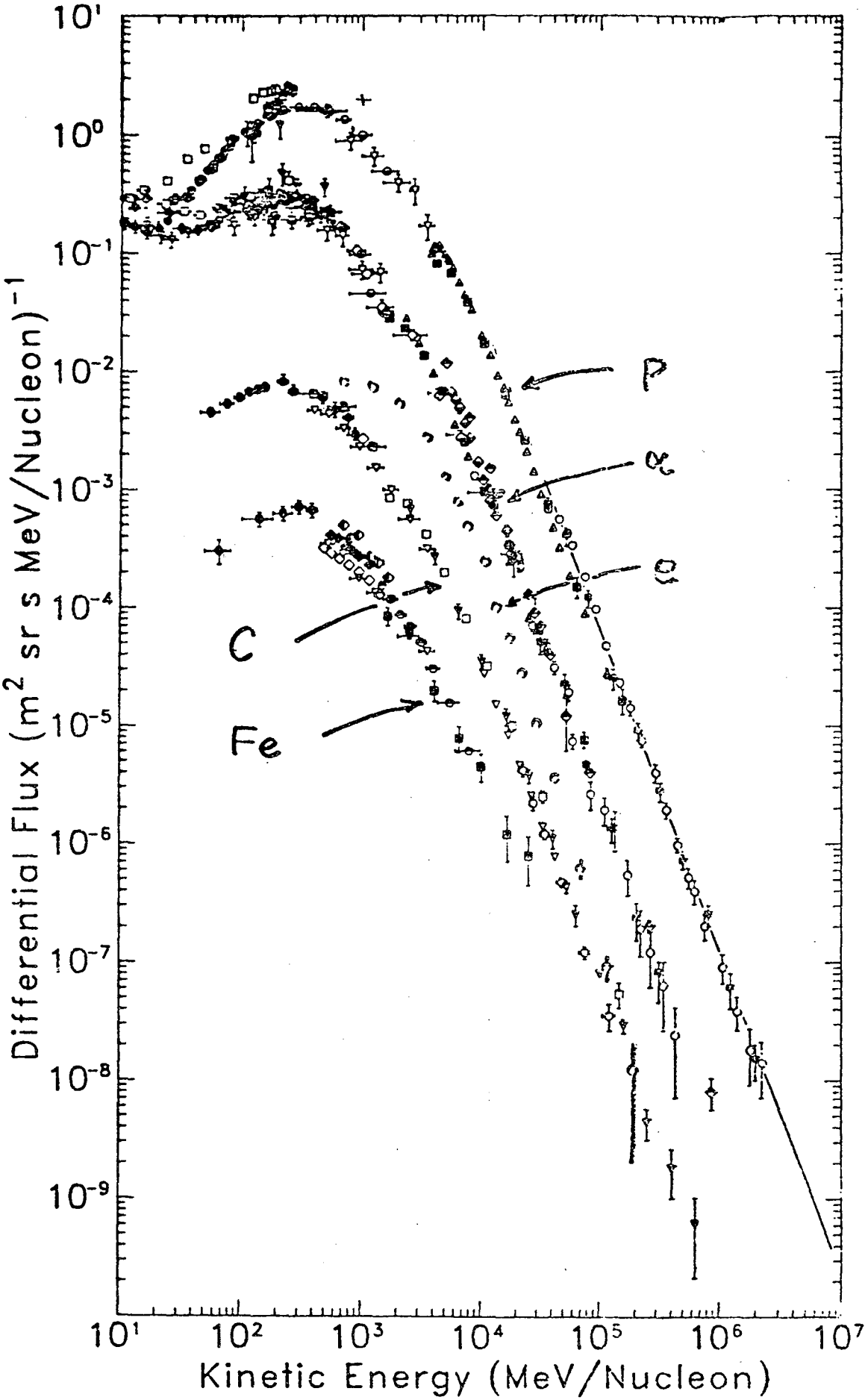
Differential Flux (m^2 sr s MeV/Nucleon)$^{-1}$
Kinetic Energy (MeV/Nucleon)
P
α
C
Fe

Fig 2.

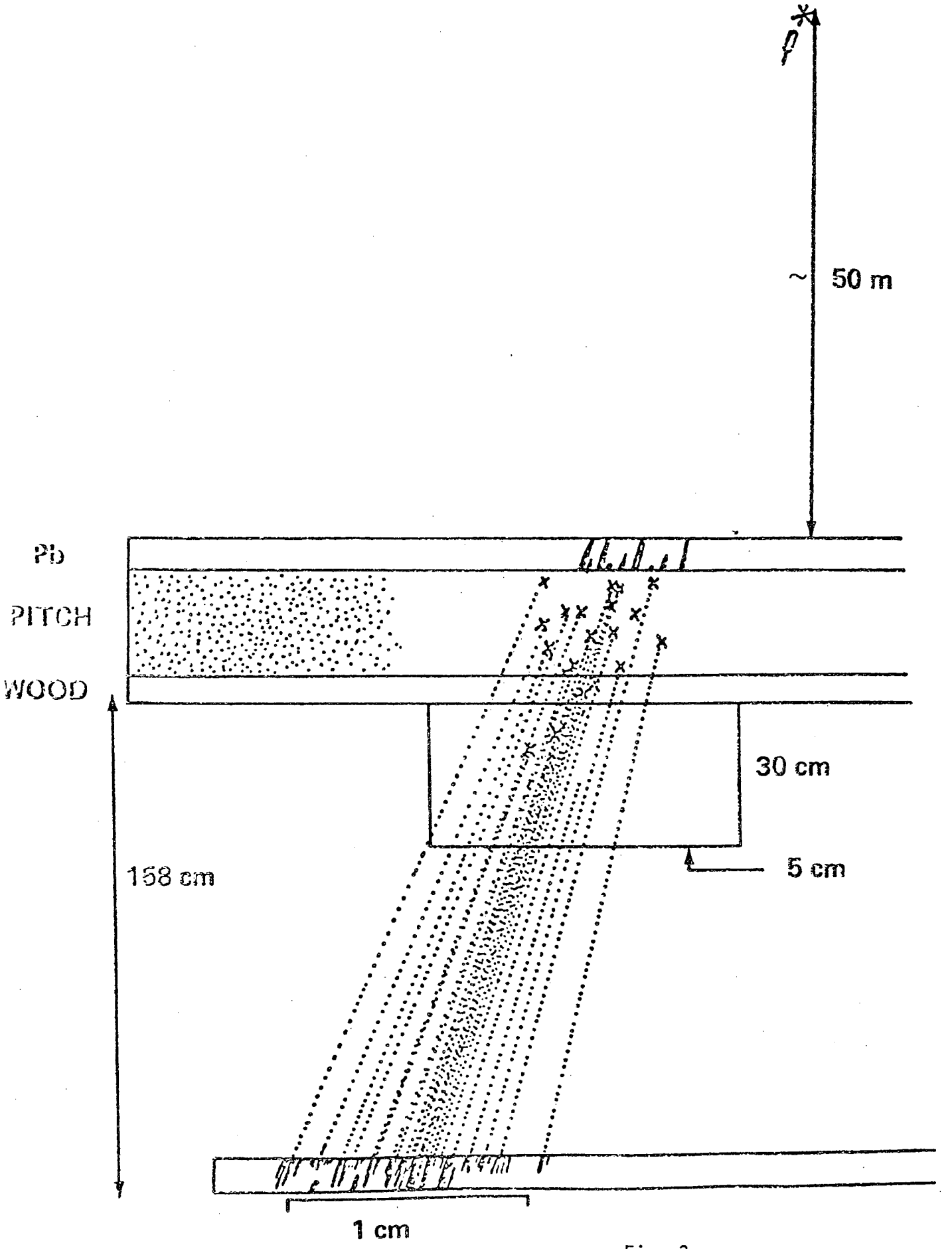

Fig. 3.

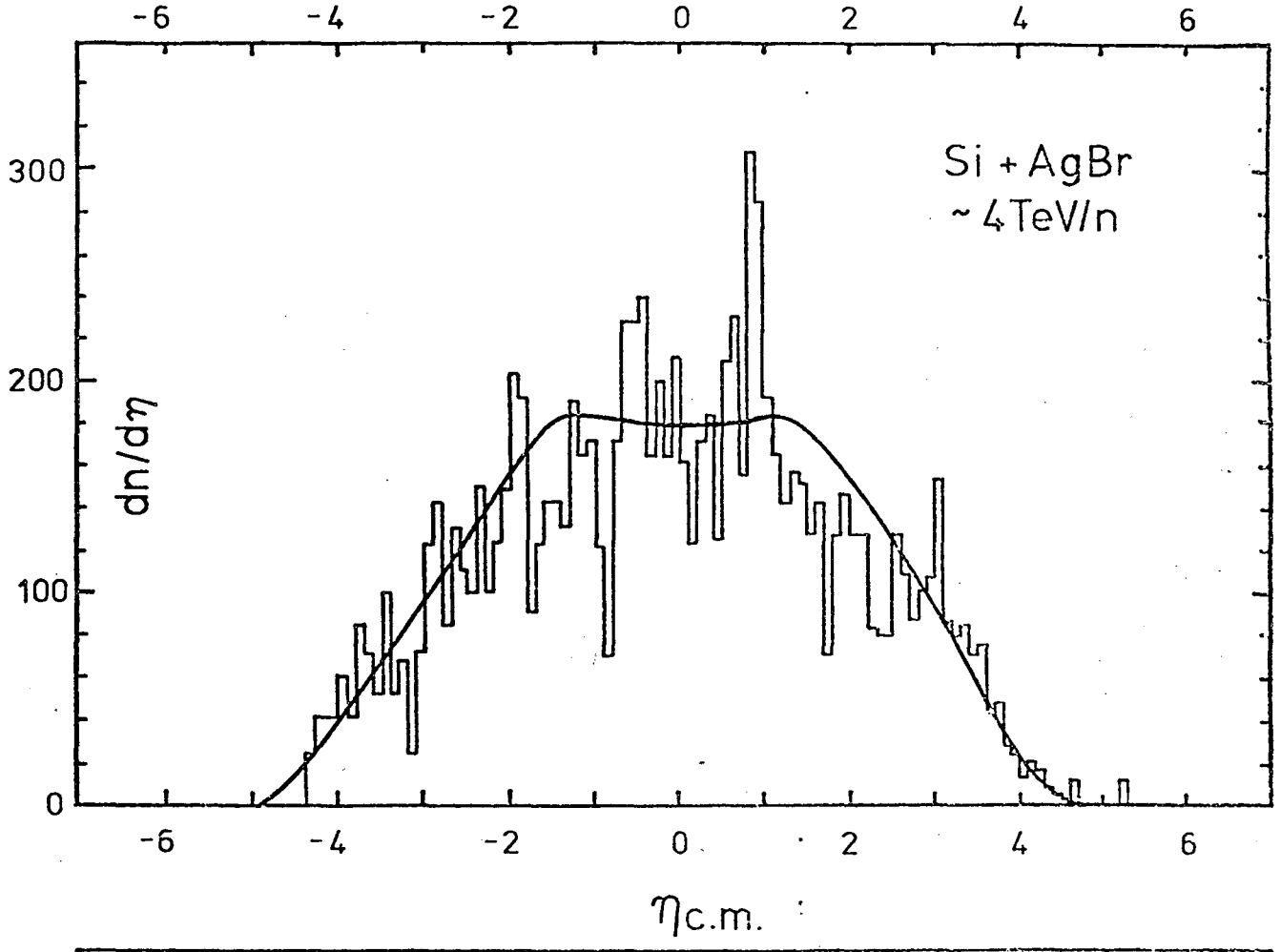

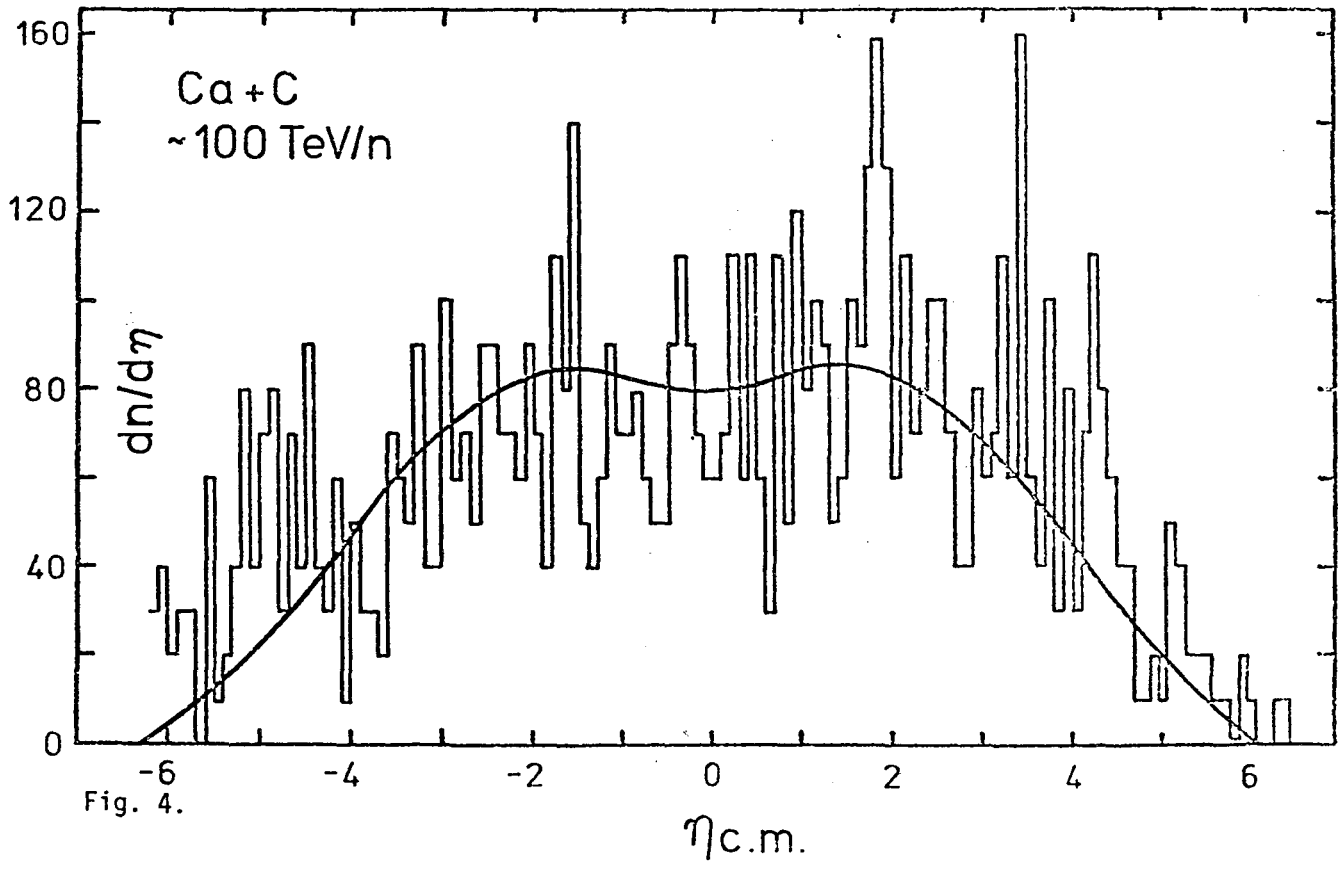

Fig. 4.

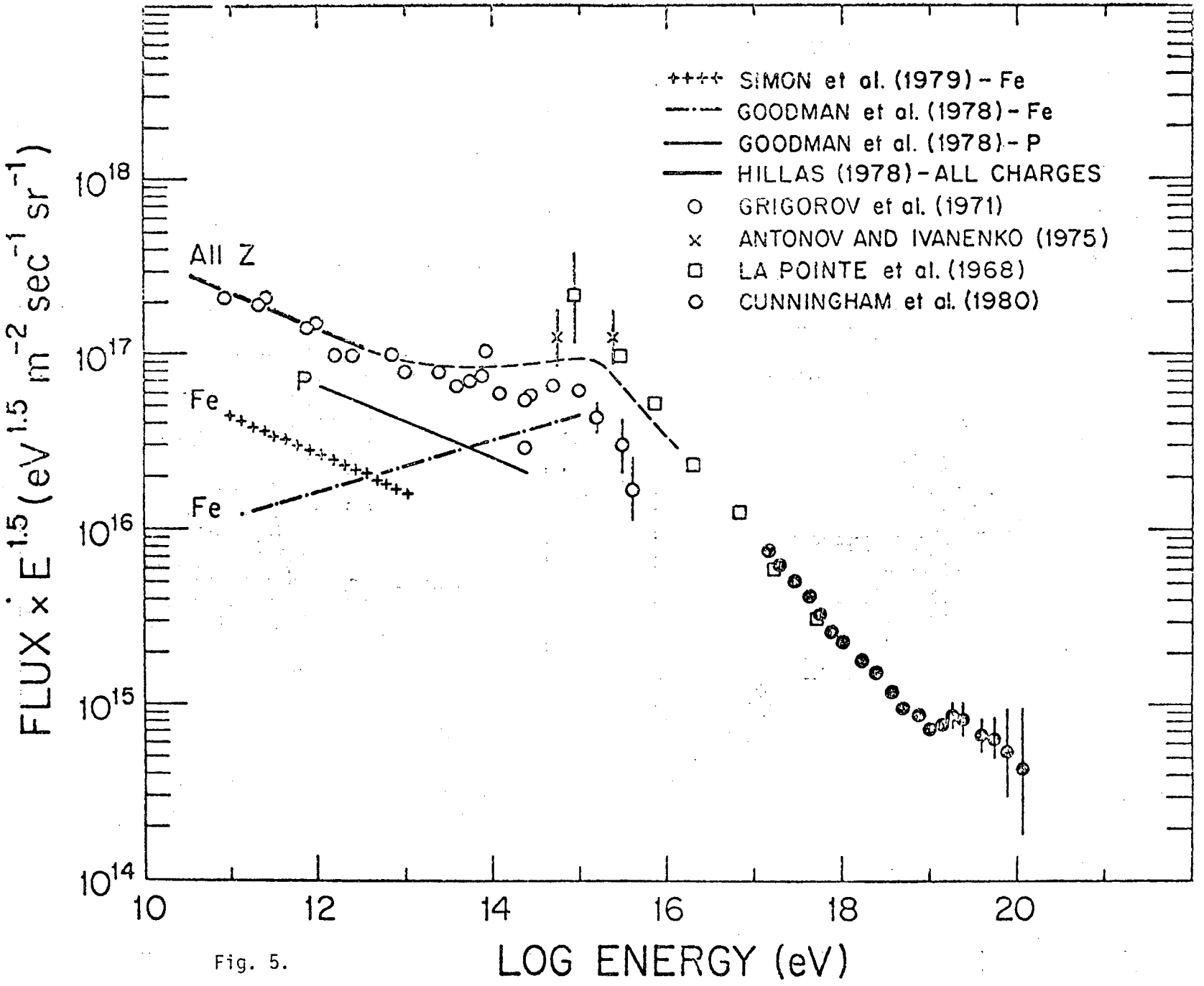
SIMON et al. (1979) - Fe
GOODMAN et al. (1978) - Fe
GOODMAN et al. (1978) - P
HILLAS (1978) - ALL CHARGES
GRIGOROV et al. (1971)
ANTONOV AND IVANENKO (1975)
LA POINTE et al. (1968)
CUNNINGHAM et al. (1980)
All Z
P
Fe
Fe
FLUX × E^1.5 (eV^1.5 m^-2 sec^-1 sr^-1)
10^18
10^17
10^16
10^15
10^14
10
12
14
16
18
20
LOG ENERGY (eV)

Fig. 5.

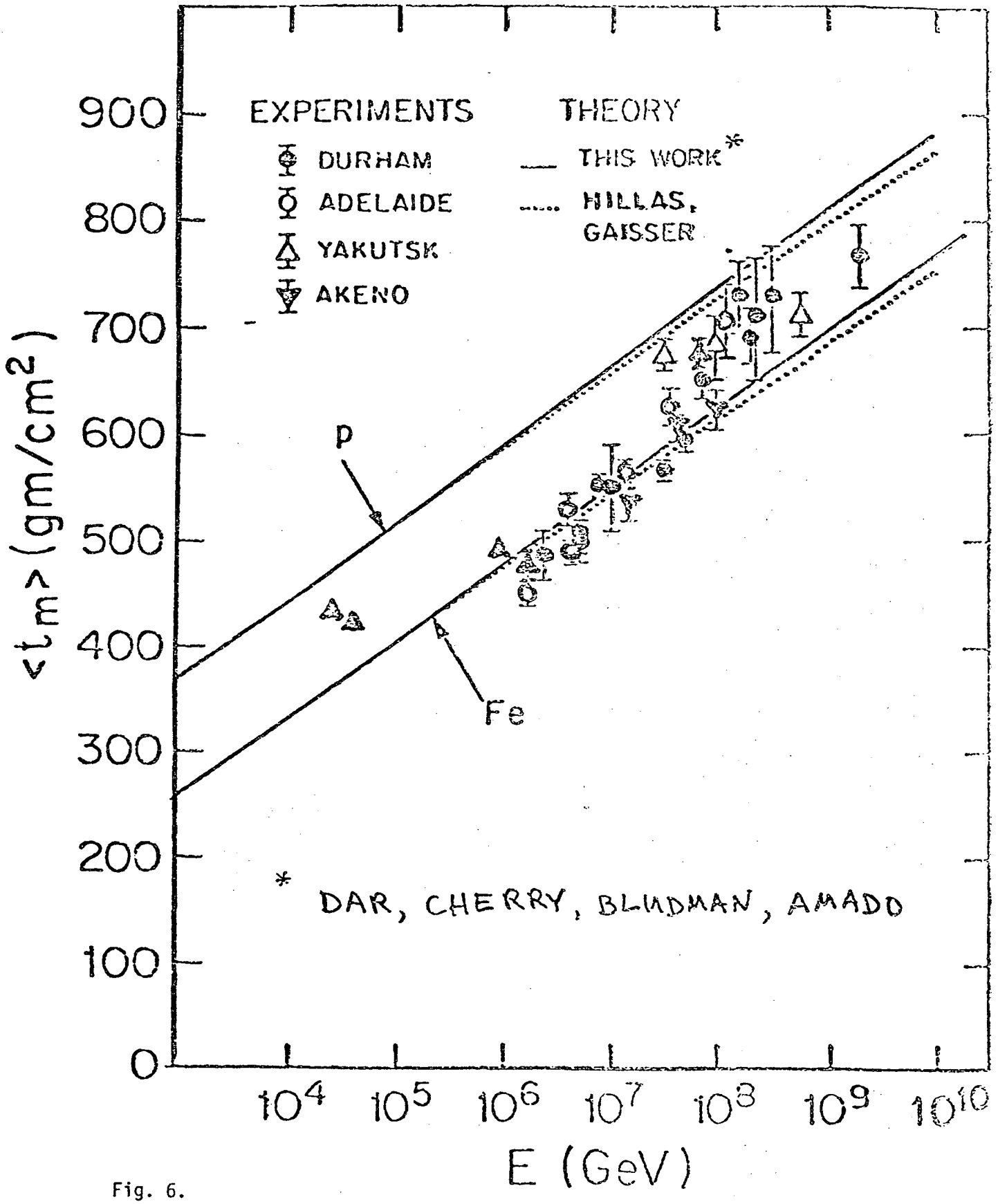
EXPERIMENTS
DURHAM
ADELAIDE
YAKUTSK
AKENO
THEORY
THIS WORK*
HILLAS, GAISSER
p
Fe
* DAR, CHERRY, BLUDMAN, AMADO
<t_m> (gm/cm²)
E (GeV)
900
800
700
600
500
400
300
200
100
0
10⁴
10⁵
10⁶
10⁷
10⁸
10⁹
10¹⁰

Fig. 6.

POSSIBLE CANDIDATES FOR QUARK-GLUON PLASMA IN THE JACEE EMULSION CHAMBER*

The JACEE Collaboration+

T. H. Burnett[h], S. Dake[b], M. Fuki[b], J. C. Gregory[g], T. Hayashi[d], R. Holynski[i], J. Iwai[h], W. V. Jones[e], A. Jurak[i], J. J. Lord[h], O. Miyamura[c], H. Oda[b,f], T. Ogata[a], T. A. Parnell[f], T. Saito[a], T. Tabuki[a], Y. Takahashi[e], T. Tominaga[c], B. Wilczynska[i], R. J. Wilkes[h], W. Wolter[i], and B. Wosiek[i].

ABSTRACT

Cosmic ray nucleus-nucleus interactions have been analyzed at energies exceeding 1 TeV/nucleon. A high P_T tail ($\langle P_T \rangle \gg$ 1 - 1.2 GeV/c) has been observed in C + C interactions, and three anomalous central collision events (Ar + Pb, Ca + C, and Si + AgBr) each imply energy densities $\geq$4.0 - 4.6 GeV/fm^3, for an expansion time of 1 fm/c, which exceed the predicted critical value for quark-gluon deconfinement. The average P_T for these anomalous events is significantly above normal (400 MeV/c).

1. INTRODUCTION:

The Japanese-American Cooperative Emulsion Experiment (JACEE) has been investigating high energy interactions of cosmic ray nuclei with balloon-borne emulsion chambers (Burnett, et al., 1981). About 100 nucleus-nucleus (A-A) events with energy $\geq$ 1 TeV/n ($\sqrt{s} \geq$ 45 GeV/n) have been observed from a total exposure of ~100 m^2-sr-hr in the stratosphere (3.5 - 5 g/cm^2). Distributions of rapidity and transverse momentum (P_T) are measured for individual events, providing data for both event-by-event studies and quasi-inclusive analysis. This report focuses on the high energy events. Low energy interactions (20 - 80 GeV/n; ~100 Fe and $\geq$100 events for 14 $\leq Z \leq$25; all in targets of C, AgBr and Pb) are being investigated with a hybrid emulsion chamber-electronic counter system and will be reported elsewhere.

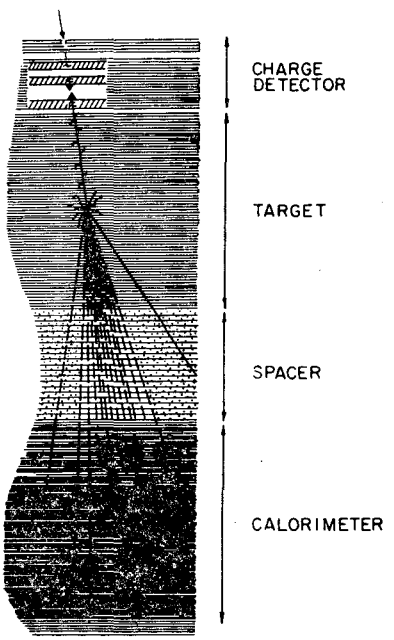

Fig. 1

2. METHOD:

The JACEE instrument (Fig. 1) employs thin

* Work supported in part in Japan by the ICR, the JSPS, and the Kashima Foundation; in part in the USA by the DOE, NASA, and NSF.

+ Mailing address: Dept. of Physics and Astronomy, Louisiana State Univ., Baton Rouge, LA 70803, or Institute for Cosmic Ray Research, Univ. of Tokyo, Tanashi-shi, Tokyo 188, Japan.

[a] Institute for Cosmic Ray Research, Univ. of Tokyo; [b] Dept. of Physics, Kobe University, Kobe; [c] Dept. of Applied Mathematics, Osaka Univ., Osaka; [d] Science & Engineering Research Lab., Waseda Univ., Tokyo; [e] Dept. of Physics & Astronomy, Louisiana State Univ.; [f] NASA/Marshall Space Flight Center, Huntsville, AL; [g] Dept. of Chemistry, Univ. of Alabama, Huntsville, AL; [h] Dept. of Physics, Univ. of Washington, Seattle, WA; [i] Institute for Nuclear Physics, Krakow.

double-sided emulsion plates, x-ray films and plastic detectors throughout the chamber to (a) define the incident particle, (b) observe the interaction in a target, (c) follow the secondary particles, and (d) measure the energy in a calorimeter section. Chambers are sensitive to all secondary particles except low energy photons (E_γ < 30 GeV). With the incident particles ~perpendicular to the emulsion plates, the interaction cores can be resolved satisfactorily even in extremely high multiplicity events. Emulsion plates in the calorimeter measure individual photon energies to ±20-30%.

3. RESULTS:

By scanning x-ray films for cascades with $\Sigma E_\gamma \geq 2$ TeV, about 400 interactions have been obtained, for which analysis of the inclusive parameters is partially complete (Table 1).

Table 1

Number	Z:1	2	3-5	6-8	>9
Detected	223	92	12	44	21
Measured	122	40	7	19	16
Analyzed	38	28	2	13	9

The pseudo-rapidity distributions for protons, helium, and iron nuclei are shown in Fig. 2. The central rapidity densities for all five charge groups are plotted in Fig. 3, where the normalization at 1 TeV/n has been made assuming an energy dependence similar to the proton-carbon data (Burnett et al., 1981): $dn(E)/dn = [dn(E = 1\ \text{TeV/n})/dn]\ (E/\text{TeV/n})^{0.15}$. The central rapidity density can be roughly described by $A^{0.4}$ up to A = 20 for a carbon target. The predictions of the wounded nucleon model (WNM) by Bialas et al. (1976) and multi-chain model (MCM) by Kinoshita et al. (1981) are also shown in Fig. 3.

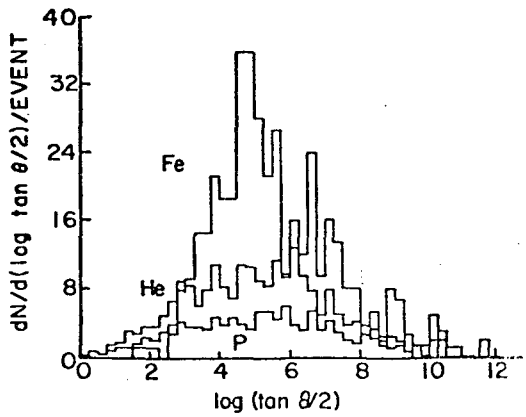

Fig. 2

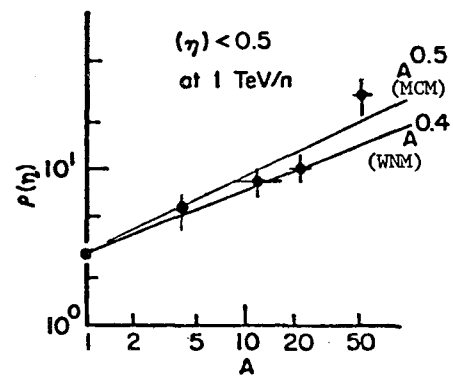

Fig. 3

The inclusive P_T distribution of photons in C + C reactions (Fig. 4b) is compared with that in p + C reactions (Fig. 4a), where the solid line represents the normal exponential distribution with average value of $\langle P_{T\gamma}\rangle = 1/2 \langle P_{T\pi}\rangle = 200$ MeV/c. The proton events are consistent with this curve, while the C + C events show deviations at high P_T values ($P_{T\gamma} \geq 500$ MeV/c).

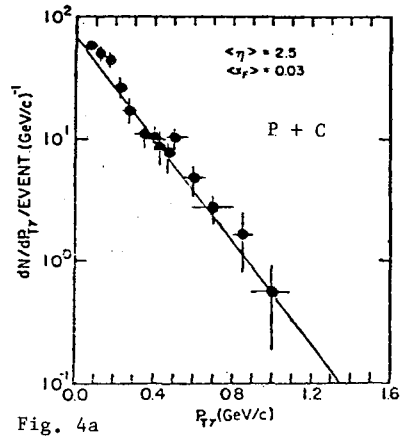

Fig. 4a

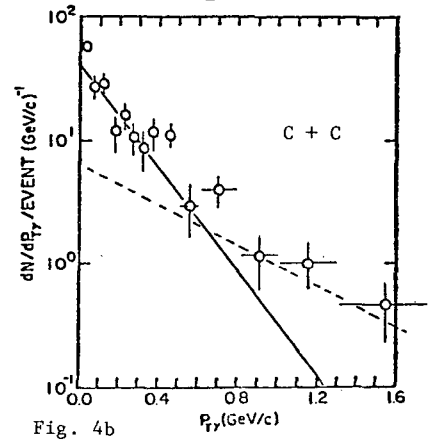

Fig. 4b

The high P_T tail in the C + C events is consistent with previously reported high P_T tails shown in Fig. 5 (from Burnett et al., 1981), which correspond to $\langle P_{T\pi} \rangle = 1 - 1.2$ GeV/c, about three times the normal value (400 MeV/c). It has been shown recently by the CERN $\bar{p}p$ collider at $E_{lab} = 150$ TeV that elementary nucleon-nucleon interactions do not produce such high values of $\langle P_{T\pi} \rangle$ in the region 1 - 4 GeV/c.

Anomalously high $\langle P_T \rangle$ is also observed in the three highest multiplicity events in this experiment. Among the 40 analyzed (A-A) events with primary charge Z > 6, two events have been found with a charged multiplicity (1010 for Si + AgBr, and 760 for Ca + C) far exceeding any other directly observed interactions (Figs. 6 and 7). The $\langle P_{T\pi^0} \rangle$ for these events was noticeably high (600 - 700 MeV/c), as displayed in Fig. 8 for the Ca + C event, also the highest energy event (~100 TeV/n). A third event of slightly smaller multiplicity (416 for Ar + Pb) shows an even larger $\langle P_{T\pi^0} \rangle \approx 1.2$ GeV/c and $\langle P_T \rangle$ for protons ≈ 850 MeV/c. All three events are apparently central collision events.

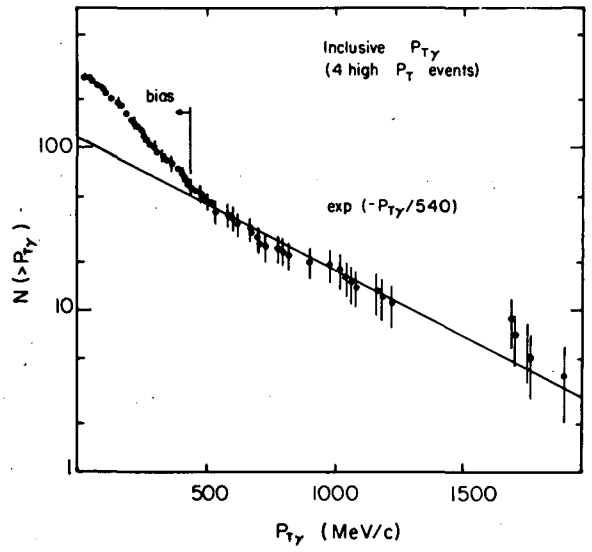

Fig. 5

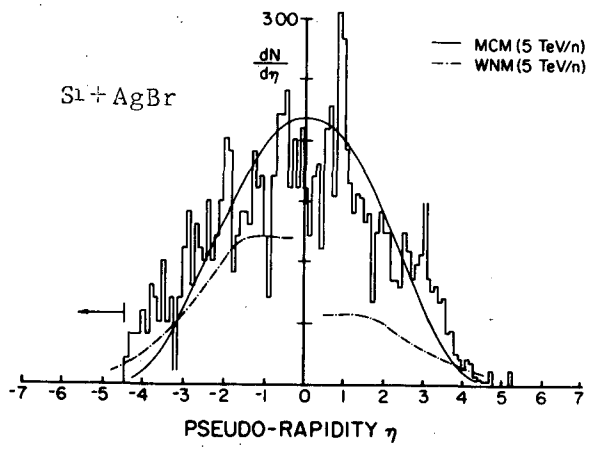

Fig. 6

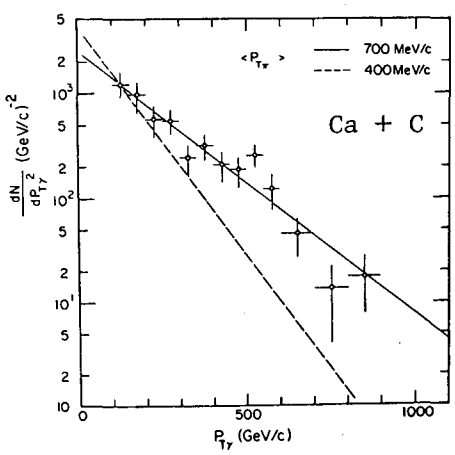

Fig. 8

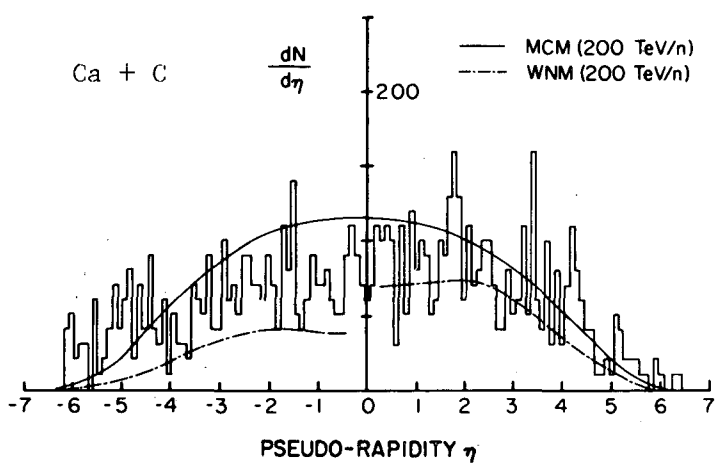

Fig. 7

Table 2 compares the observed multiplicities of the three anomalous central collision events with the corresponding calculations by the WNM and MCM models. The Ar event seems to have a multiplicity (N_{ch}) less than either model predicts, even considering the dispersion, D. The Si and Ca events are in reasonably good agreement with the MCM model (both multiplicities and rapidity distributions) and are far from the WNM prediction. It should be noted, however, that if we consider the observed high P_T values of 600 - 700 MeV/c for these events, even the MCM model cannot reproduce the data.

Table 2

Event Type	Energy (TeV/n)	Observed Nch	WNM Nch	WNM D	MCM Nch	MCM D	Observed $\langle P_{T\pi^0} \rangle$
Si + AgBr	5	1010	589	68	1020	110	550 ± 100 MeV/c
Ca + C	100	760	399	70	779	166	700 ± 50 MeV/c
Ar + Pb	1	416	710	67	1070	145	1200 ± 150 MeV/c

These three heavy nucleus events differ from each other in many aspects, e.g., primary energy (1 - 100 TeV/n), primary and target charge (hence the size of the colliding volume), and the final state characteristics. Yet, they show more or less similar energy densities (4.0 - 4.6 GeV/fm^3) deposited in the central region at the expansion time of 1 fm/c, exceeding the theoretically predicted critical values (0.6 - 1.5 GeV/fm^3) for quark-gluon deconfinement.

It is also interesting to note that these events seem to hold an inverse-linear relationship between $\langle P_T \rangle$ and the particle density per unit rapidity and unit space-time. These nucleus-nucleus events do not agree, in this correlation, with the $\bar{p}p$ collider data (Arnison et al., 1982). Van Hove (1982) has suggested that the saturation of the increase in $\langle P_T \rangle$ with increasing rapidity density, observed in $\bar{p}p$ interactions, might be an indication of a phase transition. However, the $\bar{p}p$ maximum $\langle P_T \rangle$ of 480 MeV/c does not seem to be valid for the (A-A) events in Table 2.

4. CONCLUSIONS:

During the analysis of high energy cosmic ray interactions, the following new characteristics have been observed: (i) A high P_T component with an average value of 1.0 - 1.2 GeV/c for mesons seems to exist in high energy nucleus-nucelus interactions; (ii) For central collisons, a very high energy density is achieved, providing candidate events for observing quark-gluon plasma. The correleation of temperature-equivalent average P_T and entropy-equivalent rapidity density in (A-A) interactions does not follow the form observed in recent $\bar{p}p$ measurements.

5. REFERENCES:

Alper, B., et al., Nucl. Phys. B100, 237(1975).
Arnison, G., et al., Phys. Lett. 118B, 167(1982).
Bialas, A., et al., Nucl. Phys. B111, 461(1976).
Burnett, T. H., et al., AIP Conf. Proc. No. 85, p. 552(1981).
Kinoshita, K., et al., Zeit. fur Physik C8, 205(1981).
van Hove, L., Phys. Lett. 118B, 138(1982).

Fractional Charge Search at the Bevalac

Gordon L. Shaw
Physics Department
University of California
Irvine, California 92717

Abstract

The glow model of broken QCD allows for free, low-mass, fractionally charged, glow-singlet, color $\underline{6}$, diquarks Q. Although these composite Q's may be difficult to produce at present e^+e^- and hadronic energies, the situation could be much more favorable in heavy-ion collisions. In contrast to other models, the glow model allows for parameters which could lead to the production of fractional charge at Bevalac energies. A two stage experiment is in progress: The first step consisted of an (initial) exposure of a heavy target configuration to a total of 3×10^{10} Fe ions of 1.9 GeV/nucleon kinetic energy. Fractional charge which escaped the target was stopped in five gallon tanks of CCl_4 and collected (and thus concentrated) on thin central wires. The target materials and collection wires were distributed to a number of laboratories conducting experiments designed to look for free fractional charge in bulk matter. The first results from the SFSU automated Millikan droplet experiment found less than one fractional charge produced per 10^4 Fe-Pb collisions (and with further assumptions, less than one for 2×10^6 collisions).

In order to account for the reported observation of free fractional charge,[1] the glow model[2] of broken QCD was proposed. $SU(3)^c$ color is spontaneously broken to $SO(3)^g$ glow and five of the eight gluons acquire a mass μ that can be somewhat less than the QCD scale parameter Λ. Just as unbroken QCD would perfectly confine color, glow is perfectly confined. Thus for $\mu > 0$, there can exist free, fractionally charged quark-quark composites Q that are $\underline{1}^g$ of glow and $\underline{6}^c$ of color. It is not possible to determine from present theory or experiment whether the "exact" local symmetry in nature is $SU(3)^c \times U(1)^{em}$ or $SO(3)^g \times U(1)^{em}$ (or some smaller group). In a previous model (DGJ)[3] of completely broken QCD, the experimental limit on fractional charge produced in elementary particle collisions required that (all eight gluons have a common mass) $\mu_o \lesssim 15$ MeV and a corresponding quark mass $\gtrsim 10$ GeV. Shaw and Slansky[4] argued that the Q's, as a result of their composite nature, are much harder to form and free than the quarks in the DGJ model (see discussion following Fig. 1 in Ref. 4). Thus μ may be nearly as large as Λ, giving a Q mass as small as 1 GeV and still be surpressed in elementary particle collisions. They proposed[4] that Q production be searched for in heavy-ion collisons since the environment of a quark-gluon sea[5] should enhance both the formation and freeing of the Q's.

Although the present Bevalac energies are clearly marginal for producing the "optimum" conditions for the sea,[5] a very sensitive experiment should be of great interest. It was stressed that the mass of the Q must be $\lesssim 1.5$ GeV and the QCD breaking range $1/\mu \lesssim$ the radii of the projectile and target nuclei (both of which are allowed by experiment and the glow model) for the Bevelac experiment to be worthwhile. The proposed experiment[4,6] is a production, collection (and thus concentration) scheme combined with the existing conventional searches[1,7,8,9] for fractional charge in bulk matter. In principle, it could be sensitive to the production of 10^{-11} diquark/collision.

The first version[6] of Bevalac experiment 669H, the production and concentration stage, was run on May 21. The target materials and collection wires (see Fig. 1) were distributed to a number of groups which either have or will shortly have operating experiments designed to detect fractional charge in bulk matter. They consist of (a) magnetic levitation experiments[1,7]; (b) automated Millikan type droplet experiments[8]; (c) tandem Van de Graaff charge-spectrometer experiments[9] which involve vaporizing a source by sputtering off ions and measuring charge/(kinetic energy) and kinetic energy, with the use of charge-exchange filters to reject background. The amounts of material that these experiments can or expect to process vary from $\sim 10^{-4}$ to ~ 1 g/day with a "typical" efficiency of $\sim 10\%$ for detecting fractional charge. The first limits (of Q production in this run) from the San Francisco State University Automated Millikan apparatus (which processes material at a low rate with very high efficiency) are now available.[10]

A total of $3x10^{10}$ Fe ions of 1.9 GeV/nucleon kinetic energy in this initial run were incident on a target configuration. The Fe beam was 1.5 cm in diameter and was accurately maintained in the center of the target. The target consisted of ~ 1 interaction length of heavy materials: 22 Pb and 9 In (interspersed) wafers 1/8" thick and 3 cm in diameter. Near the middle were some Cu plates, 10g of Hg and some steel balls suitable for the magnetic levitation experiments. Within a 30° cone behind the target were 26 five-gallon tanks of CCl_4 (a non-polar liquid) as shown in Fig. 1. Each tank had a thin central wire maintained at a potential either of +90 or -90 volts with respect to its inside wall. Fractionally charged particles that stop in the tank form fractionally charged atoms or molecules (not necessarily of the same sign) which drift to the wire[11] (if it has the appropriate sign of its voltage) and are permanently trapped there by their image charge since no subsequent reaction can neutralize them. Thus 50% of fractional charge stopping in the tanks are concentrated on the thin central (Au, In, Cu, Nb or W) wires.

The choice of a mainly Pb target was made to optimize the probability of a central collision with the incident Fe ions. The remaining materials in the target configuration and the choice of materials for the collection wires were done in consultation with the groups who will analyze these materials for fractional charge. (For example, In mixed with 3 parts Ga is liquid at room temperature and can be analyzed in the Millikan type apparatus of Hendricks.[12] This experiment when operational is expected to process grams of matter per day.) We selected fully ionized Fe for the beam since we wanted the largest nucleus and highest energy having a reasonable intensity. Following the nuclear collision, fractional charge may be part of a nuclear fragment. The total collection configuration (of target plus tanks) was designed to stop both low and high charge fragments. Most high-charge fragments ($Z > 6$) are expected to stop in the target, whereas most low-charge fragments pass through the target plates into the tanks (the preparation of the Pb and In into separated wafers was done to enhance this escape of the low-charge fragments from the target). The stopping efficiency of the tanks was estimated using Monte-Carlo techniques and the Bethe-Block relation. For a large range of mass (.5 - 1.5 GeV) and reasonable momentum distribution for the produced particles, roughly 1% of all particles with charge e/3 and ~ 8% of those with charge 4e/3 are stopped in each of the front tanks. The stopping efficiencies of the other tanks decrease with production angle and distance from the target.

The SFSU Millikan type experiment using Hg drops has now completed an analysis[10] of some target and collection wire materials. We[6] prepared two samples for them: Sample A was prepared from the 36μ diameter gold wires from two tanks, one of each polarity. Each wire was passed twenty times through a small drop of Hg in a capillary tube in order to remove the surface layer of the wire. The two drops were combined to form Sample A. Since the fractional charge is transferred to the Hg

Figure 1. Schematic top view of the setup for experiment 669H at the Bevalac[6] showing the target configuration and stopping tanks of CCl_4. Some of the five-gallon tanks are arranged in a double layer as denoted by the 2. The 26 central collection wires included Au, In, Cu, Nb and W wires, each maintained at +90 V or -90 V with respect to the inside wall of its tank. The target configuration consisted of 22 Pb and 9 In (interspersed) wafers 1/8" thick and 3 cm in diameter. Near the middle were some Cu plates, 10 g of Hg and some steel balls suitable for the magnetic levitation experiments. The Fe beam was 1.5 cm in diameter and was accurately maintained in the center of the target.

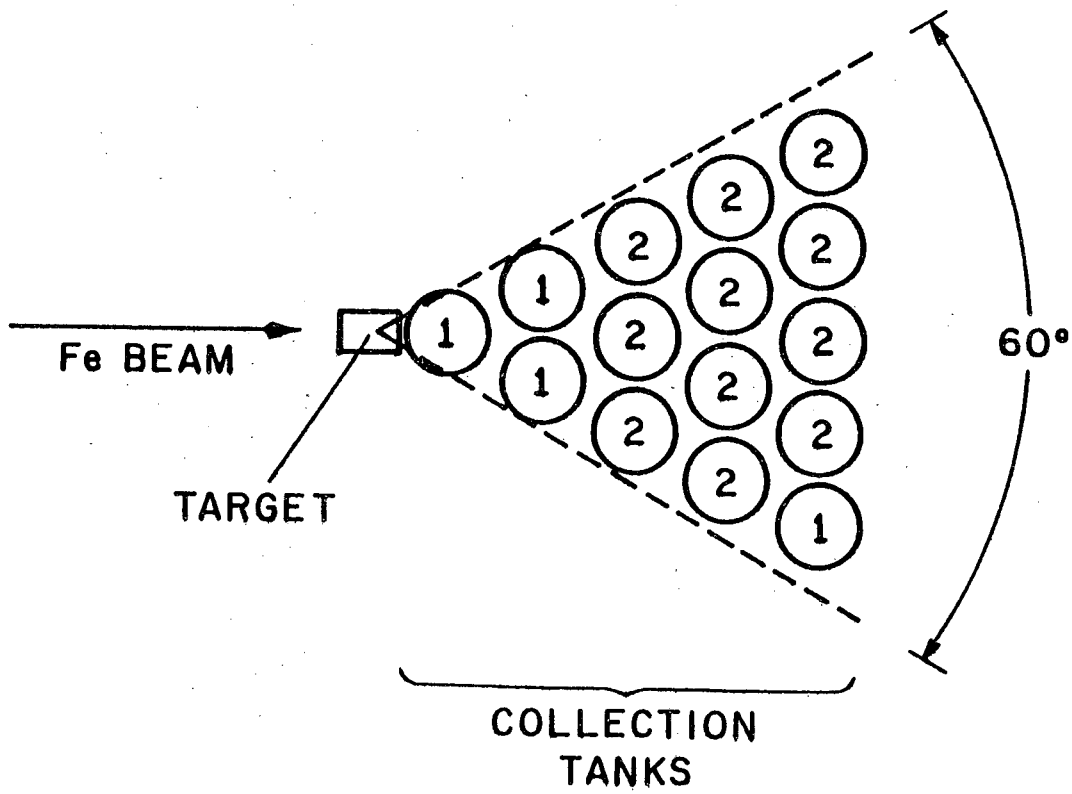

in Sample A with an unknown efficiency, perhaps small, the two Au wires were then dissolved in a larger amount of Hg from the target configuration to form Sample B. They have measured a total of ~ 250,000 drops or a total of .5 mg of Hg roughly half from each sample. After making appropriate analysis and cuts on certain distributions, no drops with fractional charge were found.[13] A limit[10] of less than one fractional charge produced per 10^4 Fe-PB collisions (at the 95% confidence level) was obtained from Sample B; with the further assumption that all of the possible fractional charge collected on the wires is transferred to Sample A, the limit is less than one per 2×10^6 collisions.

In conclusion, these first results from SFSU are already of interest, in particular, if the limit from Sample A is relevant. We can look forward during the coming year to other analysis of the 669H materials by groups which can, in principle, measure substantially more material. It is further hoped that the Bevalac intensity will be increased by a factor of 10^2 in the next year.[14] Further improvements in concentration techniques are being considered. Thus we expect that if fractional charge can be produced in 1.9 GeV/nucleon Fe-Pb collisions at the level of one part in 10^{11}, it will be seen by the end of 1984.

Clearly, the advent of higher energy, very intense heavy ion beams would be of enormous interest in a future version of this experiment. If a true quark-gluon phase transition is produced in the collision, then color confinement will really be tested by the search for fractional charge. Higher center of mass energies will also allow for heavier fractional charge to be produced and thus test models other than glow. It is not clear what the optimum energy would be. Highly relativistic heavy-ion colliders might not be as useful as perhaps a 10 GeV/nucleon fixed target machine. Finally, we note an analogous experiment at the Fermilab Tevatron fixed target proton machine could set much better limits on fractional charge production than by direct electronic detection means.

We thank J. Carroll and collaborators, of Bevalac experiment 671H, for permitting a test of parts of this experiment, and the staff of the Bevalac, especially Fred Lothrop and Bob Miller, for their enthusiastic help. We also thank George Basile for assistance in the construction of the collection tanks, and George Chapline and Cherrill Spencer for useful discussions. This work was supported in part by the U.S. Department of Energy and by the National Science Foundation.

References

1. G. S. LaRue, J. D. Phillips, and W. M. Fairbank, Phys.Rev. Lett.46, 967 (1981).

2. R. Slanksy, T. Goldman, and G. L. Shaw, Phys. Rev. Lett 47, 887 (1981).

3. A. De Rujula, R. C. Giles, and R. L. Jaffe, Phys. Rev. D17, 286 (1978). Similar bounds hold for the mass of fractional charged leptons.

4. G. L. Shaw and R. Slansky, Phys. Rev. Lett. 50, 1967 (1983).

5. The transition from nuclear matter to a quark-gluon nonconfining phase has been discussed by many authors. See, e.g., the Proceedings of this Conference and the papers listed in footnote 4 of Ref. 4. Although the present Bevalac ion kinetic energies of ~ 2 GeV/nucleon seem marginal to accomplish the quark-gluon nonconfining phase, it is not far outside the range of estimates. Since there are many hundreds of quarks in a heavy ion-nucleus collision and since nonequilibrium dynamics (including shock phenomena) may be involved, a phase transition may not be necessary to have the color screening required for the validity of Fig. 1 of Ref. 4.

6. The present experiment consisting of the production and concentration stage is Bevalac experiment 669H. The group members are A. A. Hahn, K. S. Lackner, H. G. Pugh, G. L. Shaw and R. Slansky.

7. M. Marinelli and G. Morpurgo, Phys. Rep. 85, 161 (1982); D. Liebowitz, M. Binder, and K. O. H. Ziock, Phys. Rev. Letter 50, 1640 (1983).

8. C. L. Hodges et al., Phys. Rev. Lett 47, 1651 (1981); G. Hirsch, R. Hagstrom, and C. D. Hendricks, Lawrence Berkeley Laboratory Report No. LBL-13636, 1981 (unpublished).

9. K. H. Chang et al., to be published; D. Elmore, private communication; R. McKeown, private communication.

10. M. A. Lindgren et al., San Francisco State University preprint, Aug. 1983.

11. For an estimate of drift times see the measurements of A. O. Allen, M. P. de Haas and A. Hummel, J. Chem. Phys. 64, 2587 (1976).

12. C. D. Hendricks, private communication.

13. A number of cuts for each drop are placed on a number of determined quantities (see Ref. 10) such as charge change, χ^2 of the fit of the velocities and the drop radius. In particular, although the determination of the charge on the drop is not dependent on the drop radius, this quantity is extremely constant (to .1%) over long running time. Thus a particularly large or small drop size could really reflect some fluctuation in the applied field (or switched field) or brief air current in the tube and thus influence the charge determination. Four drops (with non-integer charge) were rejected solely for the radius cut. It is interesting to note that assuming that their radii were not different from the mean but that there was an error in the first velocity (see Fig. 2 of Ref.10) for each drop corrected its charge to integer.

14. H. G. Pugh, private communication.

Recent Atomic Physics Experiments at the Bevalac

Harvey Gould

Materials and Molecular Research Division,
71-259 Lawrence Berkeley Laboratory,
Berkeley, California 94720.

Recent atomic physics experiments at the Bevalac have concentrated on atomic collisions of very heavy particles, and three of these experiments are outlined here. energy loss by very heavy relativistic nuclei; radiative electron capture; and charge capture and loss by highly stripped uranium. The selection while incomplete is chosen to give an overall view of the atomic physics being studied at the Bevalac. These experiments point the way toward more ambitious experiments as more intense beams become available and experimenters gain experience.

The energy loss of a (relativistic) nucleus in matter is usually calculated from the Bethe theory.[1] A number of corrections have been applied to the theory[2] as measurements became more precise and as heavier and higher energy nuclei have been studied. Two recent experiments, one by Ahlen and Tarle[3] and a second by Waddington, Freier, and Fixsen,[4] have examined the energy loss of 955 MeV/nucleon uranium in Cu, and the stopping of 1.0 GeV/nucleon gold in nuclear emulsions, respectively. Two corrections to the Bethe theory are found to be very important for very heavy nuclei at relativistic energies. The Mott correction is a correction to the use of an approximation to the exact cross section for scattering of a charged particle in a Coulomb field.[5] The correction is small for $Z/137 << 1$ and low velocities, which is to say that it is large for relativistic gold and uranium. The second correction is the Bloch correction[6] which arises because the wave functions of the target electrons can not be properly treated as having infinite extent. An extension of the Bloch correction to relativistic energies has been calculated by Ahlen[7].

Both experiments find that without the Mott and the Bloch corrections, theory and experiments are in serious disagreement. In these experiments the Mott correction increases the rate of energy loss by about 10.5% and the Bloch correction decreases it by 5%. Including these terms brings theory and the experiments into agreement. There is a small difference in conclusions of the experimenters in that Ahlen and Tarlé[3] find the relativistic from of the Bloch correction gives better agreement, where as Waddington, Freier, and Fixsen,[4] find that it does not.

The study of radiative electron capture, is carried out by a collaboration[8] from Stanford, LBL and Shanghai. In this experiment, a beam of heavy ions pass through a target at sufficient energy to ionize most (or all) of the projectile L and K shell electrons. Electrons are recaptured into these states by nonradiative charge exchange, and by radiative electron capture (the inverse of photoionization). In radiative electron capture, the emitted photon has an energy which is equal to the binding energy of the state into which the electron is captured (minus its binding energy in the target) plus the kinetic energy of an electron at rest in the laboratory as seen in the rest frame of the projectile.

Fig. 1 shows the spectra from 190 MeV/nucleon Xe atoms passing through a beryllium target.[9] The peak near channel 550 is due to the $\approx$ 143 keV x ray from radiative electron capture into the K shell of the Xe projectile. A much weaker peak at channel 300 corresponds to radiative electron capture into the L shell. The height of the peaks normalized to the solid angle of

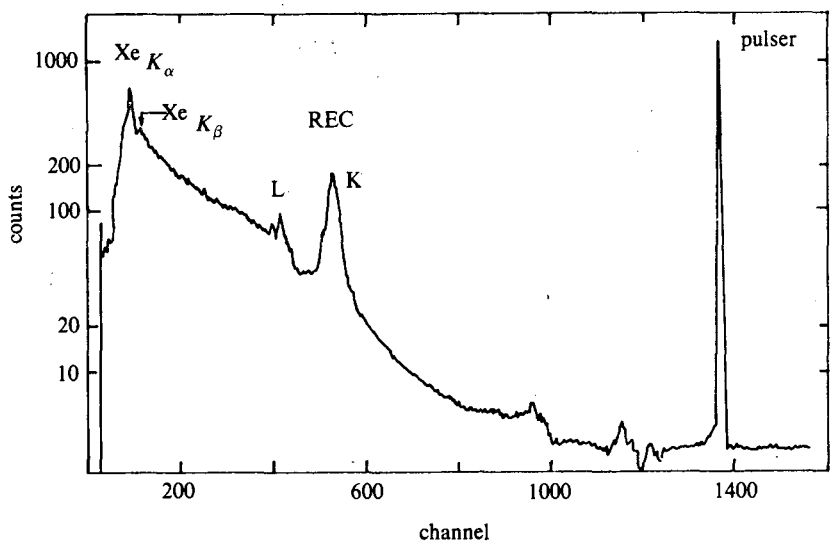

Figure 1. - Pulse height spectra of x rays from 190 MeV/nucleon Xe (Z=54) in a Be target. Peaks from radiative electron capture into the Xe K- and L- shells and K_α and K_β lines are visible. The detector is an intrinsic Ge x-ray detector.

the detectors, the beam intensity, and the average number of K- and L- shell vacancies determines the absolute cross sections. The natural width of the radiative electron capture peak in Fig. 1 is dominated by the Doppler width due to the large acceptance angle of the detector. With the more intense beams now obtainable, tighter collimation may be used to reduce the Doppler line width. At that point, the radiative electron capture peak for capture from heavy targets is expected to show structure reflecting the momentum of electrons captured from different target subshells.

Figure 1 also shows peaks near channel 100 corresponding to Xe K_α and K_β transitions. Since a fraction of the Xe ions have been stripped of all but their last one- or two- electrons, these peaks contain contributions from the 2p - 1s transitions in hydrogenlike and heliumlike Xe.

An LBL - University of California Space Science Laboratory collaboration, is a studying[10] electron capture by U^{91+} and U^{92+} and ionization of U^{90+} and U^{91+}. In this experiment U^{68+} ions are passed through targets, analyzed in a magnetic spectrometer and then detected in a position-sensitive ionization chamber. At 962 MeV/nucleon, beams containing more than 85% bare U^{92+} are obtained by stripping U^{68+} in Cu and Ta targets of $\geq$ 150 mg/cm^2 and $\geq$ 85 mg/cm^2 respectively. The charge state fractions as a function of the thickness of a Cu target are shown in Fig. 2. At the target thickness necessary to produce fully-stripped uranium, the deterioration in the beam emittance is small, and injecting beams of bare uranium nuclei into an ultrarelativistic accelerator is entirely feasible.

The equilibrium charge state distributions for several materials are shown in Fig. 3. In the interstellar medium 65% of the 962 MeV/nucleon uranium will contain bound electrons, and almost 90% of the 437 MeV/nucleon uranium will contain bound electrons, including $\approx$ 9% which contain two- K shell and one- L shell electrons. Entering the atmosphere results in a net ionization of the cosmic ray and a copper target increases the charge state still further.

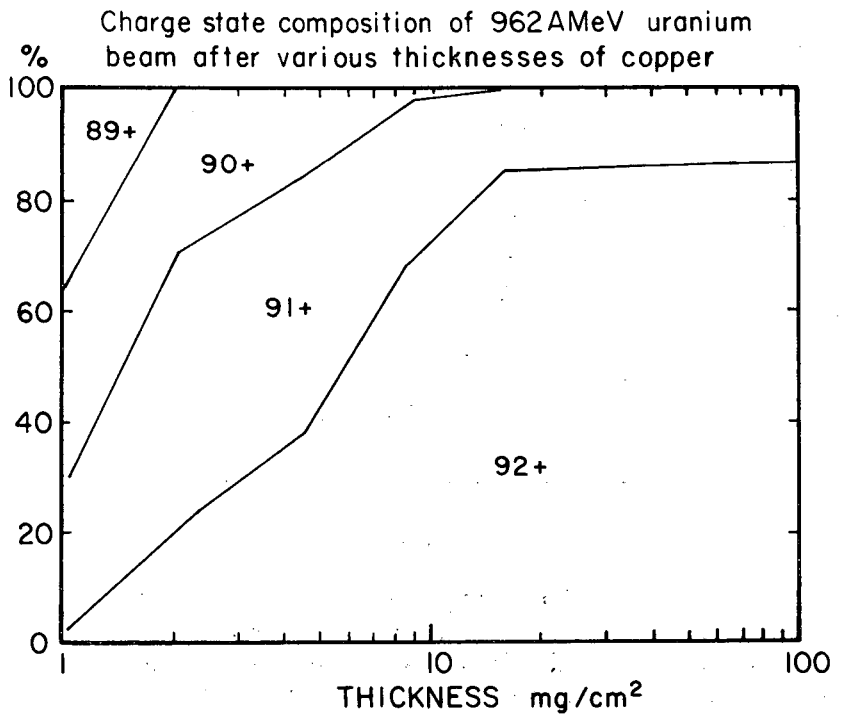

Figure 2.

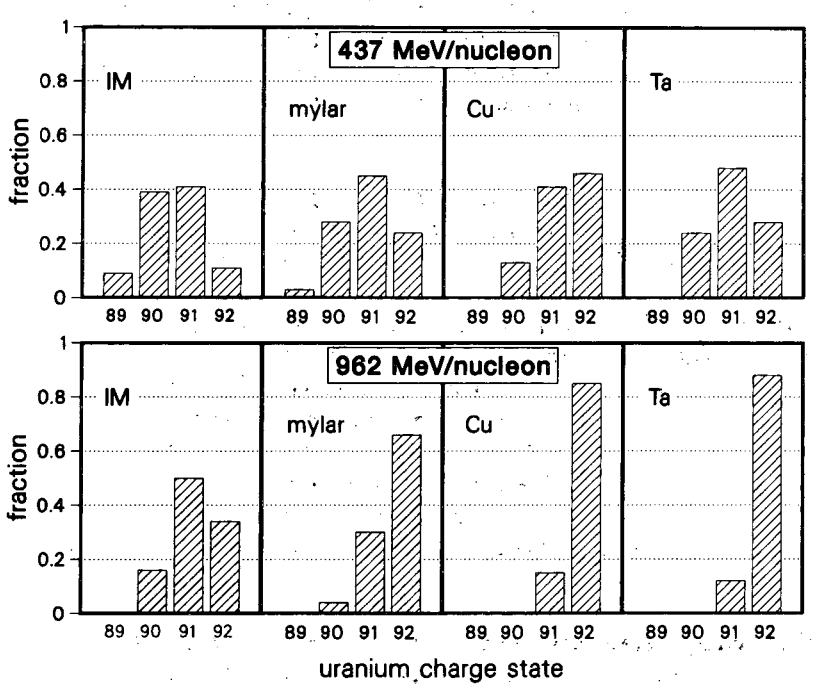

Figure 3. - Charge state distributions of uranium at 962 MeV/nucleon and 437 MeV/nucleon for equilibrium thickness targets of interstellar medium (IM), mylar ($Z \approx 6.6$), Cu ($Z = 29$), and Ta ($Z = 73$).

This work was supported by the Director, Office of Energy Research, Office of Basic Energy Sciences Chemical Sciences Division, of U.S. D.O.E. under Contract No. DE-AC-03-76SF00098.

Footnotes

[1]H. A. Bethe, Ann Phys. (Leipzig) 5 ,325 (1930); C. Møller, Ann. Phys. (Leipzig) 14 ,531 (1932).
[2]See, for example, S.P. Ahlen, Rev. Mod. Phys. 52 ,121 (1980), and references contained therein.
[3]Ahlen and Tarlé, Phys. Rev. Lett. 50 , 1100 (1983).
[4]C.J. Waddington, P.S. Freier, and D.J. Fixsen, Phys. Rev. A 28 , 464 (1983).
[5]See, for example, N.F. Mott and H.S.W. Massey, *The Theory of Atomic Collisions,* (published, Oxford University Press, London, 1965) 3rd edition, pp. 233 - 237.
[6]F. Bloch, Ann. Phys. (Leipzig) 16 ,285 (1933).
[7]S.P. Ahlen, Phys. Rev. A 25 ,1856 (1982).
[8]S. Andriamonje, R. Anholt, O.R. Baker, H. Bowman, K. Crowe, K. Fraenkel, W.E. Meyerhof, J.D. Molitoris, E. Morenzoni, D. Murphy, J. Rasmussen, and J.-S. Xu.
[9]W.E. Meyerhof, *et.al.* , unpublished.
[10]H. Crawford, H. Gould, D. Greiner, P. Lindstrom, and T. Symons, in Preprints of Contributed Papers of the Sixth High Energy Heavy Ion Study and Second Workshop on Anomalons, Lawrence Berkeley Laboratory, June 28 - July 1, 1983, p. 207 (Lawrence Berkeley Laboratory Report No. LBL-16281); H. Gould, D. Greiner, P. Lindstrom, T.J.M. Symons, and H. Crawford, *Electron capture by* U^{91+} *and* U^{92+} *and ionization of* U^{90+} *and* U^{91+}, Lawrence Berkeley Laboratory Report No. 16467.

Evidence for the Non-existence of Anomalous Projectile Fragments with Z* = 1.33, 1.67, 2.33 and 2.67

M.A. Bloomer, E.M. Friedlander, H.H. Heckman, and Y.J. Karant

Lawrence Berkeley Laboratory, University of California
Berkeley, California 94720

Recent speculation on the cause of the anomalously short reaction mean free paths of projectile fragmentation products (PF's) produced from relativistic heavy-ion (RHI) collisions with emulsion nuclei[1-5] has led to the suggestion that "anomalons" (i.e., the fraction of PF's exhibiting this anomaly) are nuclei with bound third-integral charges.[6-9] In an earlier paper[10] we described in detail how to measure the nuclear charge of $1 \leqslant Z \leqslant 3$ PF's of RHI collisions in nuclear emulsion: specifically, measurements based on the lacunarity, i.e., fractional transparency, of the linear track structure of such ionization tracks will easily yield a precision of $\sigma = 0.05$ charge units for Z=1 and Z=2, and about $\sigma = 0.07$ charge units for Z=3. We now present the results of 1179 measurements carried out by 3 observers on $1 \leqslant Z \leqslant 3$ PF's produced by the extra-nuclear cascade of interactions initiated by a 1.88 AGeV ^{56}Fe beam incident upon a stack of Ilford G-5 emulsion pellicles.

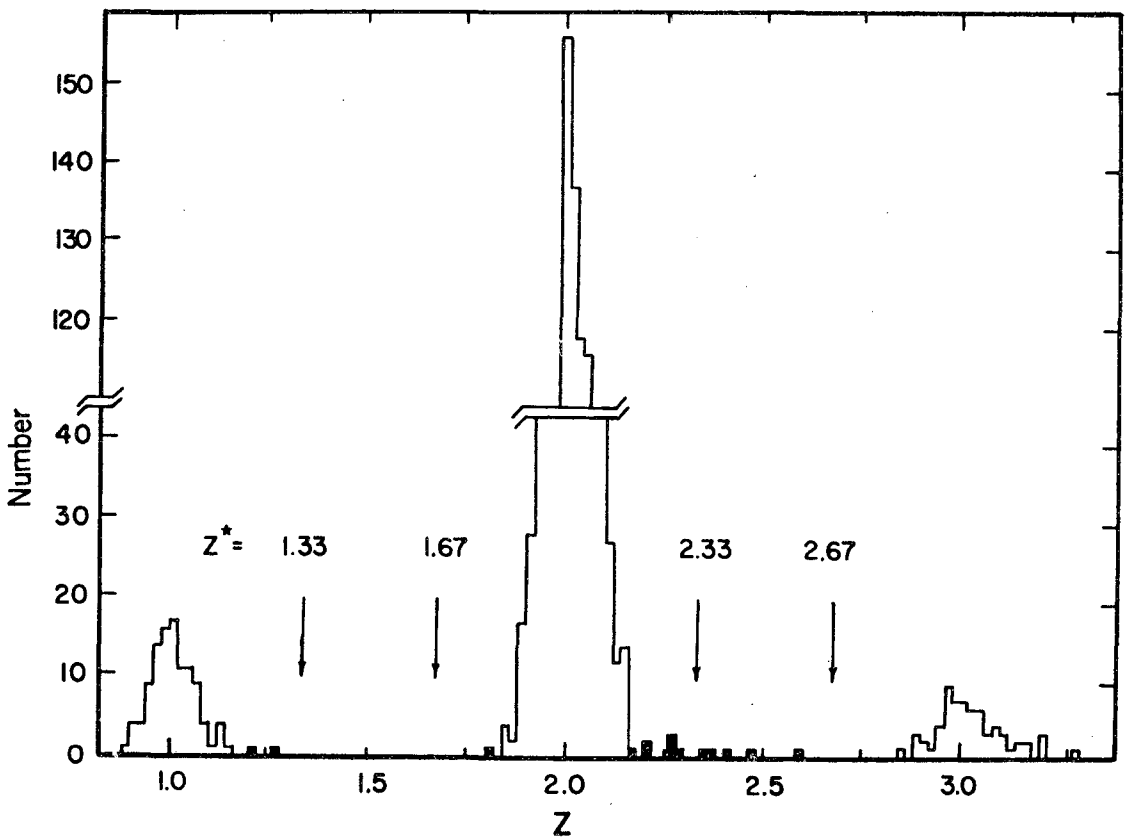

FIG. 1. Charge distribution of $1 \leqslant Z \leqslant 3$ projectile fragments from the extra-nuclear cascade of interactions from a ^{56}Fe beam, all generations and all observers. The blackened squares are those measurements which lie outside intervals of $\pm 3\sigma_Z$ centered around the integer means Z = 1.0, 2.0 and 3.0. Not shown are the charge measurements of $4 \leqslant Z \leqslant 6$ PF's.

We show in Fig. 1 a plot of the charge distribution for $1 \leqslant Z \leqslant 3$ PF's of all generations and all observers. No corrections of any kind described in the earlier paper have been made to these data. Each charge distribution was separately normalized to the $\bar{\rho}$ of its sub-sample of "secondary" (i.e., produced from the "primary" ^{56}Fe beam) PF charge measurements. Recall that $Z = k_0\rho$, where

$$\rho = \sqrt{-\ln L}\ , \quad L = \text{lacunarity, i.e., fractional transparency}$$

The values of $k_0(Z)$ and σ_Z derived therefrom are shown below in Table 1. Not displayed are the charge measurements for $4 \leqslant Z \leqslant 6$, since the saturation of the grain density beyond Z=3 makes measurement insufficiently precise to resolve third-integral charges. The salient feature of Fig. 1 is that all charge measurements for each PF are narrowly distributed around their integer means, and, with the possible exception of the set of measurements scattered around Z = 2.33, there is no indication that PF's of third-integral charge are produced with the same relative abundance as reported for anomalons to date ($\gtrsim$6% for $3 \leqslant Z \leqslant 26$).[1-4] Since a relativistic track of Z = 0.67 would have a grain density of only 7 grains per 100 microns, it is improbable that any observer could have detected such a lightly ionizing track in our emulsion stack. Hence we limit the test of non-integral charged PF's to Z* = 1.33, 1.67, 2.33 and 2.67 (from henceforth Z* will be used to denote these hypothetical fractional charges).

We can rigorously test for the existence of fractional charge by first asking how many charge measurements lie outside intervals of $\pm 3\sigma_Z$ centered

	N (# of measurements)	$k_0(=Z/\bar{\rho})$ and σ_Z for secondary PF's	$N \geqslant \pm 3\sigma_Z$ from integer mean Z before/after remeasurement and energy loss corrections, etc.	Improved charge estimates (deviation from mean Z* in units of σ_{Z*}) of remaining candidates
Z = 1	108	k_0 = 3.096 σ_Z = 0.055	2 / 2	1.160 ± 0.035 ($-5.4\sigma_{Z*}$, Z* = 1.33) 1.203 ± 0.029 ($-4.1\sigma_{Z*}$, ")
Z = 2	1006	k_0 = 3.137 σ_Z = 0.052	13 / 3	2.199 ± 0.036 ($-4.1\sigma_{Z*}$, Z* = 2.33) 2.131 ± 0.019 ($-6.1\sigma_{Z*}$, ") 2.319 ± 0.035 ($-0.5\sigma_{Z*}$, ")
Z = 3	65	k_0 = 3.116 σ_Z = 0.068	0 / 0	-----

TABLE 1. Results of charge measurements on $1 \leqslant Z \leqslant 3$ projectile fragments. $k_0 = Z/\rho$, where $\rho = \sqrt{-\ln L}$, L = lacunarity, i.e. fractional transparency of track structure (see ref. 10). For Z*= 1.33 and 2.33, σ_{Z*} = 0.055 and 0.057, respectively.

around means of Z = 1.00, 2.00 and 3.00, where σ_Z for each charge is that displayed in Table 1. Of the total 1179 measurements, 15 meet this criterion (seen as the black squares in Fig. 1). One observer subsequently remeasured several times the charge of each candidate, making a correction for apparent charge increase due to energy losses by ionization of its ancestor nuclei. We rejected candidates whose improved charge estimate was compatible with an integer mean, as well as Z=1 PF candidates with emission space angle $\theta_{sp} > 10°$ and Z=2 PF candidates with $\theta_{sp} > 6°$, since such large angles would imply large momentum transfers, and one can then no longer assume that the projectile fragments have the same velocity as their parent projectile.[11] Five candidates remain: two are $-5.4\sigma_{Z*}$ and $-4.1\sigma_{Z*}$ from $Z^* = 1.33$ (where $\sigma_{Z*} = 0.055$), and three are $-4.1\sigma_{Z*}$, $-6.1\sigma_{Z*}$, and $-0.5\sigma_{Z*}$ from $Z^* = 2.33$ (where $\sigma_{Z*} = 0.057$, a precision interpolated from $\sigma_{Z=2} = 0.052$ of Z=2 and $\sigma_{Z=3} = 0.067$ of Z=3). Of these five, only the charge measurement at $-0.5\sigma_{Z*}$ from $Z^* = 2.33$ ($Z_{meas} = 2.32 \pm 0.04$) presents any difficulty. This 3rd generation PF travelled a distance of 4.04 cm before interacting, emitting two light tracks of $Z_{meas} = 1.78 \pm 0.03$ and 1.66 ± 0.05, and $\theta_{sp} = 36°$ and 13°, respectively. The track signatures from this interaction are consistent with those of low energy (120-140 AMeV) projectile fragmentation products: thus, this was most likely a low energy fragment (~490 AMeV if we use the charge to estimate the energy). Therefore, we conclude that we observed from 1179 charge measurements none with $Z^* = 1.33$, 1.67, 2.33 or 2.67. This puts an upper limit of 8×10^{-4} at a confidence level in excess of 99.9% on the relative number of such PF's with a charge differing from an integer by 0.33 charge units. This result is in agreement with a similar fractional charge search recently carried out by Price et. al.[12] on $10 \leqslant Z \leqslant 18$ PF's from the cascade of interactions produced by a ^{40}Ar beam incident on CR-39 plastic track detector.

To date no one has reported conclusive evidence for a short mean free path effect for Z=1 and Z=2 PF's (see however Judek's, El-Nadi's et. al., and Karant's et. al. contributions to this conference). If such an effect does become firmly established for these PF's, bound fractional charges cannot explain it. If we assume that, in every generation of PF's with $1 \leqslant Z \leqslant 3$, there is a 6% admixture of anomalons having third-integral charge (ignoring the possibility of "memory" effects in subsequent generations[5]), we would expect on the average to see ~66 such fractional charge candidates, when in fact we see none. Even if the admixture were as small as 1%, we would still expect ~11 candidates. The explanation for anomalons in the PF's from relativistic nucleus-nucleus collisions must lie elsewhere.

This work was supported by the Director, Office of Energy Research, Division of Nuclear Physics of the Office of High Energy and Nuclear Physics of the U.S. Department of Energy under Contract DE-AC03-76SF00098.

References:

[1]B. Judek, Can. J. Phys. 46, 343 (1968); 50, 2082 (1972).

[2]E.M. Friedlander, R.W. Gimpel, H.H. Heckman, Y.J. Karant, B. Judek, and E. Ganssauge, Phys. Rev. Lett. 45, 1084 (1980).

[3]P.L. Jain and G. Das, Phys. Rev. Lett. 48, 305 (1982).

[4]H.B. Barber, P.S. Freier, and C.J. Waddington, Phys. Rev. Lett. 48, 856 (1982).

[5]E.M. Friedlander, R.W. Gimpel, H.H. Heckman, Y.J. Karant, B. Judek, and E. Ganssauge, Phys. Rev. C 27, 1489 (1983).

[6]G.F. Chapline, Phys. Rev. D 25, 911 (1982).

[7]G. Baym, Prog. Part. Nucl. Phys. 8, 73 (1982).

[8]R. Saly, M.K. Sundaresan, and P.J.S. Watson, Phys. Lett. 115B, 239 (1982)

[9]G.N. Fowler, S. Raha, and R.M. Weiner, to be published (submitted to the Anomalon Workshop, Lawrence Berkeley Laboratory, Berkeley, California, February 8-10, 1982).

[10]M.A. Bloomer, H.H. Heckman, and Y.J. Karant, Lawrence Berkeley Laboratory Report LBL-15246 (to be published in Nuclear Instruments and Methods).

[11]D.E. Greiner, P.J. Lindstrom, H.H. Heckman, Bruce Cork, and F.S. Beiser, Phys. Rev. Lett. 35, 152 (1975).

[12]P.B. Price, M.L. Tincknell, G. Tarlé, S.P. Ahlen, K.A. Frankel, and S. Perlmutter, Phys. Rev. Lett. 50, 566 (1983).

Equilibrium charge states of uranium
at relativistic energies

Henry Crawford[a], *Harvey Gould, Douglas Greiner,*
Peter Lindstrom, and James Symons

Lawrence Berkeley Laboratory,
Berkeley, California 94720

We have measured the charge fractions of uranium ions at energies of 962 MeV/amu and 430 MeV/amu passing through various thickness targets of mylar ($Z \approx 6.6$), Cu ($Z=29$) and Ta ($Z=73$). From these we determine the equilibrium charge state distributions.

Uranium 68+ ions from the LBL Bevalac are transported in vacuum through a windowless beam line and pass through targets located upstream of the beam 40 magnetic spectrometer (Fig. 1). The charge states produced by collisions in the targets are spatially separated in the magnets and are detected by a position sensitive ionization chamber located approximately 10 meters downstream from the magnets. At the detector the charge states are separated by roughly 1 cm. The convolution of the instrumental resolution and the beam width is about 0.2 cm (Fig. 2).

The equilibrium charge state distributions are shown in Fig. 3. These distributions were obtained from the data as follows: Charge capture and loss cross sections were fit[1] to the curves of charge state population verses target thickness. The fitted capture and loss cross sections were then used to construct the equilibrium distributions.

Fig 3 shows that at 962 MeV/amu the average charge state of the uranium ions is monotonic with target Z. However, at 430 MeV/amu the average charge state first rises and then falls with increasing target Z. The qualitative behavior of the charge state distributions can be understood in terms of the different energy and target Z dependence of the ionization cross section and of the charge exchange, and radiative electron capture cross sections[2]. These will discussed in detail in a future paper.

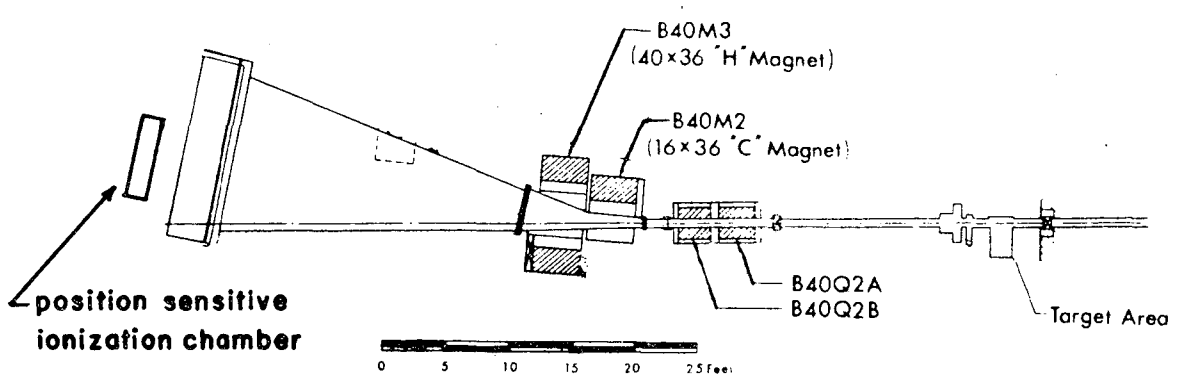

Figure 1. - Schematic diagram of the experimental apparatus

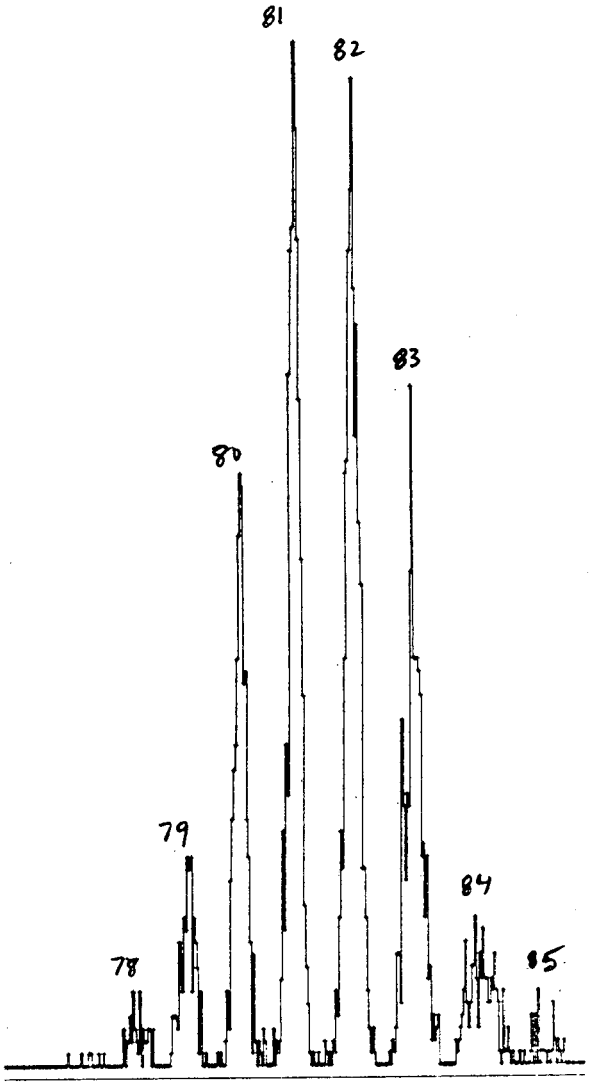

Figure 2. - Charge state fractions of 962 MeV/amu uranium (incident charge state 68+) after passing through 7.1 mg/cm^2 of mylar.

We thank Dr. Jose Alonso, Mr. Ismael Flores and Mr. Douglas MacDonald for their assistance in analyzing the data and in setting up the experiment. We are especially grateful to the operators and staff of the Bevalac and the Super-HILAC whose skill and dedication made this experiment possible. This work was supported by the Director, Office of Energy Research: Office of Basic Energy Sciences, Chemical Sciences Division, and Office of High Energy and Nuclear Physics, Nuclear Science Division, of U.S. Department of Energy, under Contract No. DE-AC-03-76SF00098.

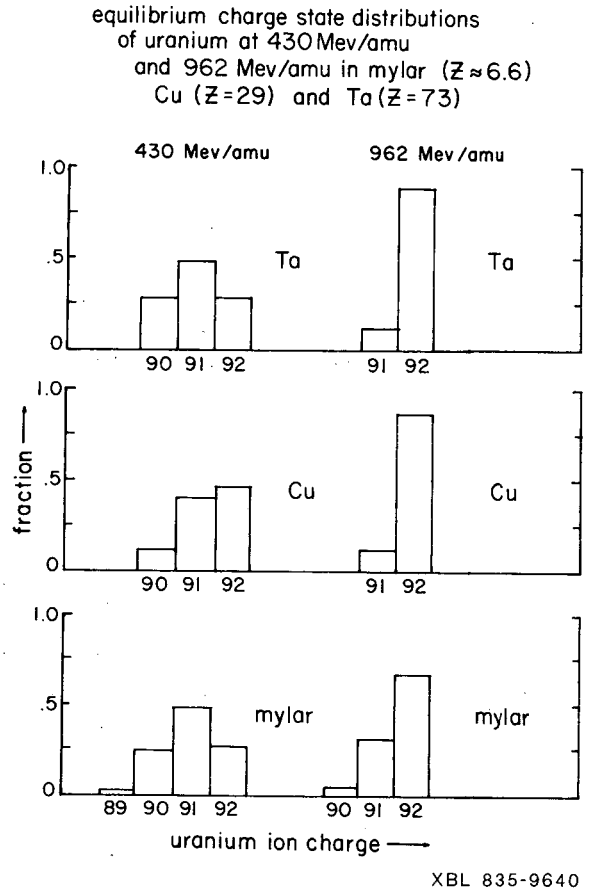

Figure 3. - Equilibrium charge state distributions

References

(a) also University of California Space Sciences Laboratory, Berkeley Ca. 94720.

(1) The method used to fit the cross sections to the data is described in S. Datz, H.O. Lutz, L.B. Bridwell, C. D. Moak, H.D. Betz, and L.D. Ellsworth, Phys. Rev. A2, 430 (1970).

(2) see for example, H. Bethe, Ann. Phys. (Leipsig) 5, 325 (1930); P.H. Fowler, V.M. Clapham, V.G. Cowen, J.M. Kidd, and R.T. Moses, Proc. Roy. Soc. (London) A318, 1 (1970); C. Raisbeck and F. Yiou, Phys. Rev. A4, 1858 (1971); C.M. Lee, Phys. Rev. A17, 566 (1978); L. Wilson, Lawrence Berkeley Laboratory report No LBL-7723; H. Crawford, Lawrence Berkeley Laboratory report No LBL-8807; R. Shakeshaft, Phys. Rev. A20, 779 (1979); B.L. Moiseiwitsch and S.G. Stockman, J. Phys. B13, 2975 (1980). D.H. Jakubaβa-Amundsen and P.A. Amundsen, Z. Physik A298, 13 (1980).

The Stopping of 200 GeV Gold Nuclei in Nuclear Emulsions

C.J. Waddington, P.S. Freier, and D.J. Fixsen
School of Physics and Astronomy, University of Minnesota,
Minneapolis, Minnesota 55455

Abstract. The residual ranges of $^{197}_{79}$ Au-nuclei stopping in nuclear emulsions has been measured for nuclei with an incident energy of 991 MeV per amu. The mean ranges observed are appreciably less than those predicted from measurements made on energetic particles of lower charge. However, by considering higher order correction terms to the rate of energy loss, good agreement can be obtained between the predicted and observed ranges.

Two small and identical stacks of Ilford G5 nuclear emulsion pellicles have been exposed to a beam of gold nuclei, $^{197}_{79}$ Au, accelerated by the LBL Bevalac. This report describes a determination of the residual ranges of these nuclei as they are brought to rest in these stacks, and relates the residual range observed for those nuclei that come to rest without making a visible interaction to that predicted from measurements made on particles of lower charge. In particular, we are interested in whether there is evidence for non Z^2 terms in the energy loss similar to those reported for Fe and U nuclei.[1,2]

The emulsions were exposed during a calibration of the HEAO-3 UH-nuclei cosmic ray detector[3] to a beam of Au nuclei having a nominal energy of 1063.8 MeV per amu and an intensity of about 1000 nuclei per dump, spread over an area of some 100 cm^2. The energy of the beam was measured by a bending magnet after extraction from the Bevalac and after passage through a thin foil to ensure that the nuclei were fully stripped, since they were accelerated to a rigidity of about 5.7 GV as Z = 61 particles, i.e., with 18 electrons still attached. This measurement of the energy is stated to be accurate to 1 MeV per amu.[4] The beam then passed through a thin scintillator before leaving the vacuum through a sailcloth window, traversing a gas-filled MWPC, air and the light-tight paper wrapping of the emulsions. A proton with an initial energy of 1063.8 MeV would have lost 2.077 MeV while traversing these various materials. Hence a $^{197}_{79}$ Au-nucleus, if its energy loss were purely Z^2 dependent, would have lost (65.8 ± 2.0) MeV per amu and the energy on entry into the emulsions would have been (998 ± 2) per amu.

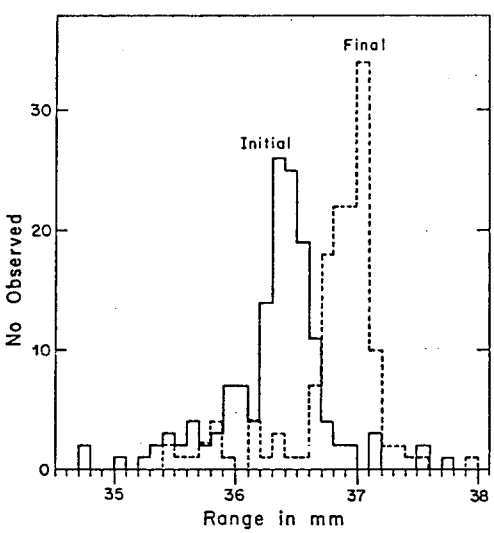

Fig. 1. The distribution of range in emulsion for ending Au-nuclei; as observed in the initial exposure made shortly after the beam energy determination and in the final exposure made at the end of the run.

The tracks of Au nuclei were found by scanning 1 mm below the top edges of the pellicles and then traced back to the top edge and down into the emulsions until the nuclei either interacted or came to rest. Residual ranges, R, were measured on only those tracks that remained in a single pellicle. Figure 1 shows the distribution between the two mean values, as well as wide tails on the distributions. This latter "straggling" we attribute mainly to unobserved interactions causing relatively small changes in Z and/or A. Proton and/or

neutron stripping of Au-nuclei could lead to quite large range differences without necessarily producing an observable interaction. The observed FWHM of the two distributions of 0.4 mm of emulsion, gives standard deviations of 0.17 mm, corresponding to an energy spread of ±3 MeV per amu (assuming only Z effects), which is thus an upper limit to the energy dispersion in the beam. However, the difference between the two exposures, which is about 0.5 mm, i.e., some 10 MeV per amu, is too small to be due to the imposition of additional detector elements in the beam, since it represents an imposition of only 0.16 g cm^{-2} of low Z absorber. It is possible, but not verifiable, that this difference represents a slow drift in the beam energy over the six hours between the energy determination, which was closely followed by the initial exposure, and the second exposure. We will therefore take the lower value of R, which is from the initial exposure, as the value appropriate to the measured energy.

If we combine the various forms of energy loss that have been described in the literature, we can write the rate of energy loss, following Ahlen,[5] as

$$\frac{dE}{dx} = \frac{4\pi\ NZ_m e^4}{mc} \cdot \frac{Z_p^{\,2}}{\beta^2} \left[n \frac{2mc^2}{I_m} \frac{\beta^2}{(1-\beta^2)} - \beta^2 - S - D + M - B + BR \right] \cdot J \qquad \text{(eq. 1)}$$

where N is the number of atoms per unit volume in the medium with mean atomic number Z_m and adjusted ionization potential I_m. Z_p is the effective charge of the projectile of velocity βc and m is the mass of the electron. Z_p differs from the true atomic number of the projectile, Z_o, due to the effects of electron pickup and stripping. We have used the semiempirical expression of Pierce and Blauer[6] to estimate Z_p from $Z_p = Z_o[1 - \exp(-130\beta/Z_o^{2/3})]$. This expression has been found to be a reasonable fit to a wide range of experimental results.[5] In this experiment changing the exponential constant to 150 alters Z_p by 10% at a β where $Z_p = Z_o/2$ and changes the residual range of a 1000 MeV per amu Au-nucleus by 0.3 mm (see Fig. 2).

$M = G/2\ (Z_p, \beta, I_m)$ is the correction for Mott scattering which accounts for the finite size of the charge distribution on the projectile. It has been approximated by Ahlen[5] who included terms in Z_p and β up to Z_p^5 and β^{-3}. Consequently, this approximation is invalid at low velocity. Conventionally it has been customary to "turn-off" this correction at a velocity where the uncertainties equal the magnitude of the correction.[1] This approach introduces a somewhat arbitrary discontinuity into the calculation, which, however, does not sensitively affect the range. Thus varying the turn-off energy by 10% only changes R by 0.06 mm. In our calculations we have chosen to set the Mott correction to a constant when the energy fell to a value where the estimated error in the approximation equals the correction itself, E $\simeq$ 200 MeV per amu. Since the Mott correction term varies slowly with energy, $\sim$ 3%/100 MeV per amu, fixing its value at the turn-off point seems more physically plausible than turning it off. The reduction in calculated range from this approach compared with turning off the correction

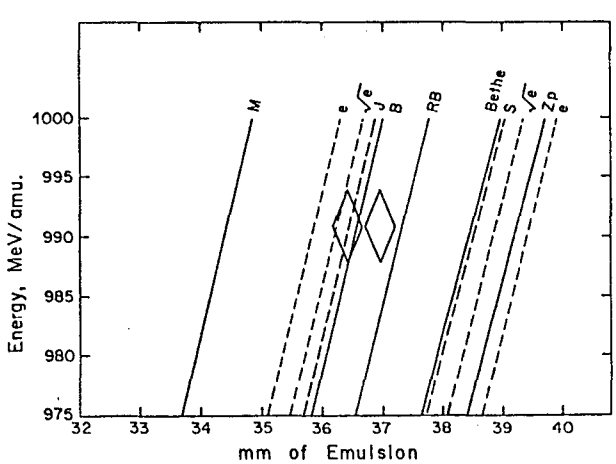

Fig. 2. The observed mean ranges as a function of energy of the incident nuclei. Also shown are the predictions from successive terms of eq. 1 (see text).

is 0.33 mm.

$B = f(Z_p\alpha/\beta)$ is a correction derived by Bloch[8] for the electron binding during close collisions. The validity of this correction in the relativistic limit is not clear, and Ahlen[9] has introduced a further term: $BR = C(Z_p,\beta,\theta,\lambda)$, the relativistic Bloch correction, where θ and λ are adjustable parameters of the theory, and λ is of the order of unity and has been set equal to 1 in what follows.

$J = F(\beta,Z_m)$ is the so-called low velocity correction introduced by Jackson and McCarthy.[10]

The residual range, R(E) is then given by $R_i(E) = \int dE/(dE/dx)$ where (dE/dx) is evaluated including each of the above terms in turn. Values of $R_i(E)$ between 975 and 1000 MeV/amu for $^{197}_{79}$Au-nuclei are shown in Fig. 2, under the following assumptions.

The Bethe terms are straightforward apart from the selection of the correct value for I_m in the nuclear emulsion. A range of values appear in the literature. The majority of these have been calculated from the adjusted ionization potentials derived for each element and the assumed composition of nuclear emulsions. Depending on the quantities selected, values of I_m between 286 eV and 323 eV can be obtained.[11,12] However, Barkas et al.[13] have used direct range measurements of pions and protons with $E \lesssim 800$ MeV to derive a value for I_m of 323 eV. We have used this value in what follows, but it may be noted that the effect on the range of a 1000 MeV per amu Au-nucleus is quite small, making R change by 0.62 mm from 38.99 mm to 38.37 mm as I_m is varied from 323 eV to 286 eV. A further small source of uncertainty comes from the precise value of the relative humidity, and thus the density, appropriate to this particular exposure. In this case the emulsions were allowed to equilibrate with a 50% relative humidity atmosphere before being sealed. The effect on the density is to increase it from the nominal 3.828 g/cm^3 by 0.45%, thus decreasing the range by 0.3%, or $\sim$ 0.11 mm on the 1000 MeV per amu Au-nucleus. Since the standard deviation of batch density variations is of the order of 0.5%,[14] we have neglected this effect, but note that density uncertainties could produce an error similar to the statistical spread.

Figure 2 shows that the Bethe range is significantly greater than the measured range, and that the addition of the Shell and Z_p corrections merely reduce the rate of energy loss, dE/dx, over at least some part of the trajectory, and hence extend the range, increasing the discrepancy. However, including the Mott correction greatly increases dE/dx and leads to a range significantly less than that measured. Adding the Bloch correction and the minor multiplication of the Jackson term, leads to a range in good agreement with the value from the initial exposure.

The remaining correction is the relativistic Bloch correction. The form suggested by Ahlen[9] leads to too high a range. However, the parameter θ has a major influence on the result. Some plausible values even change the sign of the correction. The values of θ must lie between $\alpha\gamma/\beta$ and 1, where α is the fine structure constant and $\gamma = (1-\beta^2)^{-\frac{1}{2}}$. Ahlen selects the energy independent value of 0.1 as it is the geometric mean of $\alpha\gamma/\beta$ and 1 over the energy interval 100 MeV/amu to 750 MeV/amu. In our initial calculation θ was taken to be the energy dependent geometric mean of $\alpha\gamma/\beta$ and 1. The difference between these two approaches is only 0.16 mms of range. If θ is arbitrarily increased or decreased from this geometric mean value by a factor of $\sqrt{e}$ or e, the resulting calculated ranges over a wide band of values which includes

both of the measurements (see Fig. 2).

If the energy loss experienced by the beam before entering the emulsion is now re-evaluated using the dE/dx expression up to and including the J term, but neglecting BR, the primary energy of the Au-nuclei is reduced by a further 7.1 MeV/amu to 990.9 ± 3.0 MeV/amu, where the error includes allowance for uncertainties in the thickness of the matter. Both experimental mean range values are then in reasonable agreement with the predictions of this energy loss expression. It appears unnecessary to invoke any relativistic Bloch correction, although such a term, with θ reduced by approximately $\sqrt{e}$, could be included.

We conclude that the range-energy relation of highly charged nuclei with $\beta \lesssim 0.9$ can be adequately derived from eq. 1, neglecting the BR term, unlike Ahlen and Tarle,[2] who do include the BR term.

Acknowledgments. We are grateful to the staff of the LBL Bevalac for their dedicated efforts in achieving the first beam of relativistic gold nuclei, and in particular to Hank Crawford for all his interest and guidance. We are also grateful to the other members of the HEAO C-3 team for the opportunity to make the emulsion exposure. This work was supported by NASA under Contract No. NAS8-27977 and by NSF under Grant No. Phy 8119421.

---

[1] M.H. Salamon, S.P. Ahlen, G. Tarlé and K.C. Crebbin, Phys. Rev. A, 23, 73 (1981).

[2] S.P. Ahlen and G. Tarlé, Phys. Rev. Lett. 50, 1110 (1983).

[3] W.R. Binns, M.H. Israel, J. Klarmann, W.R. Scarlett, E.C. Stone, and C.J. Waddington, Nucl. Inst. Meth. 185, 415 (1981).

[4] H. Crawford (private communication).

[5] S.P. Ahlen, Rev. Mod. Physics, 52, 121 (1980).

[6] T.E. Pierce and M. Blann, Phys. Rev. 173, 390 (1968).

[7] W.H. Barkas and M.J. Berger, Nat. Acad. of Sci. Pub. 1133 (1964).

[8] F. Bloch, Ann. Phys. Leipzig 16, 285 (1933).

[9] S.P. Ahlen, Phys. Rev. A, 125, 1856 (1982).

[10] J.D. Jackson and R.L. McCarthy, Phys. Rev. B, 6, 4131 (1972).

[11] J.F. Janni, Tech. Rep. No. AFWL-TR-65-150 (1966).

[12] V. Fans, Ann. Rev. Nucl. Sci. 13, 1 (1963).

[13] W.H. Barkas and S. von Friesen, Nuovo Cimento 19, 41 (1960).

[14] M.M. Shapiro, Handbuch der Physik, XLV, 342 (1958).

Search for Unstable Superdense Nuclei at the Dubna Synchrophasotron

A.A. Kuznetsov

Joint Institute for Nuclear Research, Dubna

The existence of superdense nuclei has been first predicted in papers[1]. During the ensuing years attempts have been made to observe this effect. A more complete review of experimental results obtained until 1977 can be found in [2].

One of the fields of a search for radioactive superdense nuclei has been proposed and implemented by A.V. Kulikov and B.M. Pontecorvo[3]. Using the setup with parameters $\tau \geq 5\ 10^{-3}$ s and $E_e > 45$ MeV, they have obtained the upper limit of the production cross section for radioactive superdense nuclei in pPb interactions.

Later on the energy threshold of electron detection was decreased in the experiments [4], in which bubble chambers were used under special conditions and targets were exposed to relativistic nuclei. This technique allowed one to detect decay particles of practically any energy, but it did not allow one to obtain data in the region $\tau \leq 10^{-3}$ s.

As shown[5], the production of metastable superdense nuclei in nuclear reactions can be observed by delayed nucleon radiation. An experimental search in this field for the lifetime of metastable states $\tau \geq 1$ s has been performed in the experiment[6].

Below we discuss experimental results[7] on a search for superdense nuclei unstable to β-decay for a lifetime of $10^{-8} \leq \tau \leq 10^{-6}$ s and metastable superdense nuclei decaying with π°-meson emission for a lifetime of 10^{-7}–10^{-1} s. These experiments have been recently carried out at the synchrophasotron on beams of carbon relativistic nuclei. The momenta of the beam of ^{12}C nuclei extracted from the synchrophasotron were 1.68 and 4.5 GeV/c per nucleon. A layout of the experiment and a trigger system are presented in fig. 1. Curve 4 in fig. 2 gives the upper limit (with a confidence level of 90%) of the production cross section for superdense nuclei having lifetime and decaying with the emission of electron or positron with $E \geq 45$ MeV in ^{12}CPb interactions at 4.5 GeV/c per nucleon. Curve 5 shows the upper limit (with a confidence level of 90%) of the production cross sections for nuclei, unstable to the emission of π°-mesons with a kinetic energy of ~50 MeV, in ^{12}CPb interactions for a momentum of 1.68 GeV/c per nucleon.

As seen from the figures, the probability of nucleus production having a lifetime of 10^{-8}–10^{-6} s with the emission of electron/positron with $E_e \geq 45$ MeV is no larger than $3 \cdot 10^{-4}$ in inelastic CPb interactions, and the probability of nucleus production having a lifetime of 10^{-7}–10^{-1} s with the emission of π°-meson does not exceed $6 \cdot 10^{-4}$ in inelastic CPb collisions.

The data on the observation of superdense nuclei are summarized in the table.

An account of other experiments in the program of the Dubna Synchrophasotron is given in Dubna preprint E1-83-334, from which this report is an extract.

	NATURE	P(10-100)GeV	n,f	Heavy ions $E \geq 1$ GeV/A
$E_s/E_0 \gg 1$	R. Holtet et al.[1] $(Rn)_s \leq 10^{-29}$ Si $Rn_s(n,\gamma)$ $E > 30$ MeV S. Frankel et al.[2] (P,P') C-Ta, 10^{-7}	B.M. Pontekorvo et al.[3] $E_\beta > 45$ MeV $> 5\cdot10^{-3}$ s $\sigma \leq 10^{-33}$ cm^2	G. Samosvat et al.[4] E_γ,En 40 MeV $<10^{-7}$/act	P.B. Price et al.[5] $Ar + Pb \rightarrow (fr)_s$ $<10^{-31}$ cm^2 A. Abdivaliev et al.[6] $C + A \rightarrow A^*_s$ $A^*_s \rightarrow \beta$, $E^\beta > 20$ MeV 10^{-29} cm^2 M.Kh.Anikina et al.[7] $C + Pb \rightarrow A^*_s$ $A^*_s \rightarrow \pi^\circ, \beta$ $E_\beta > 45$ MeV $\tau > 10^{-6}$ s $\sigma < 10^{-29}$ cm^2 $E_{\pi^\circ} \approx 50$ MeV $\tau > 10^{-7}$ s $\sigma < 10^{-29}$ cm^2
$E_s/E_0 \ll 1$	V.Aleshin et al.[8] a)C-W, $\tau \geq 10^{+21}$ years b)E_γ(Cf) 100 MeV $5\cdot10^{-8}$/act A.A.Borovoi et al.[9] E_β(Cf) > 20 MeV $< 2\cdot10^{-8}$/act	V.A. Karnaukhov et al.[10] Ta,Th + p,d,$\alpha \rightarrow$ $\rightarrow$ Rb, Cs, Fr $T_\beta > 1$ hour, $\sigma < 10^{-32}$ cm^2 A.G. Bugorsky et al.[11] $P(70\ GeV) + A \rightarrow X_s$ $X_s \rightarrow Y + n + \gamma$ $T_{1/2} \approx 1$ year $\sigma < 3\cdot10^{-34}$ cm^2		S.P.Avdeev et al.[12] $C + Fe,Sn,Pb \rightarrow X_s$ $X_s \rightarrow 3n + Y$ $\sigma < 10^{-29}$ cm^2 $T_{1/2} > 1$ s

1. Phys. Rev. Lett. 36 (1976) 183
2. Phys. Rev. 13C (1976) 737
3. Phys. Lett. 66B (1977) 136
4. Phys. Rev. Lett. 34 (1975) 409
5. Ya.F. 30 (1979) 313
6. JETP 81 (1981) 1153
7. JINR, Dubna, preprint 1-83-275 (1983)
8. Letters to JETP 24 (1976) 114
9. J. of Phys. G5 (1980) 723
10. Ya.F. 31 (198) 289
    Nucl. Phys. A381 (1982) 419
11. Letters to JETP 32 (1980) 487
12. JINR, Dubna, preprint P1-81-590 (1981)

References

1. A.B. Migdal, Fermions and bosons in strong fields, Nauka (1978), Moscow.
2. V.A. Karnaukhov, USSRAS Izvestiya 41 (1977) 1538.
3. A.V. Kulikov, B.M. Pontekorvo, JINR, Dubna, Preprint P1-10202 (1976).
4. A. Abdivaliev, et al., JETP 77 (1979) 20; 81 (1981) 1153.
5. I.N. Mishustin, A.V. Karnyukhin, YaF 32 (1980) 945.
6. S.P. Avdeev, et al., YaF 36 (1982) 315.
7. M.Kh. Anikina, et al., JINR, Dubna, Preprint 1-83-275 (1983).

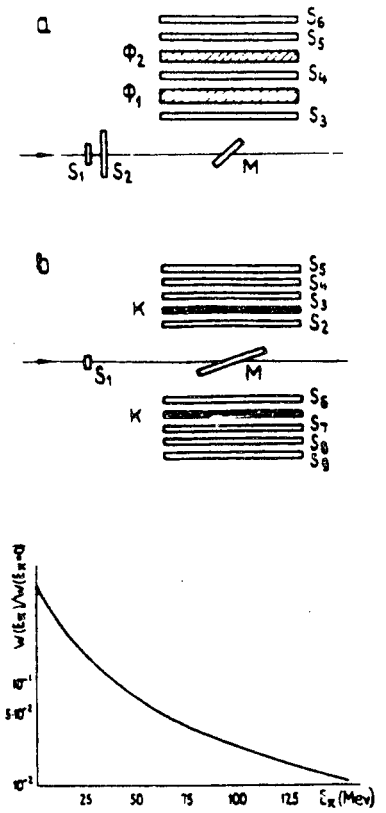

Fig. 1

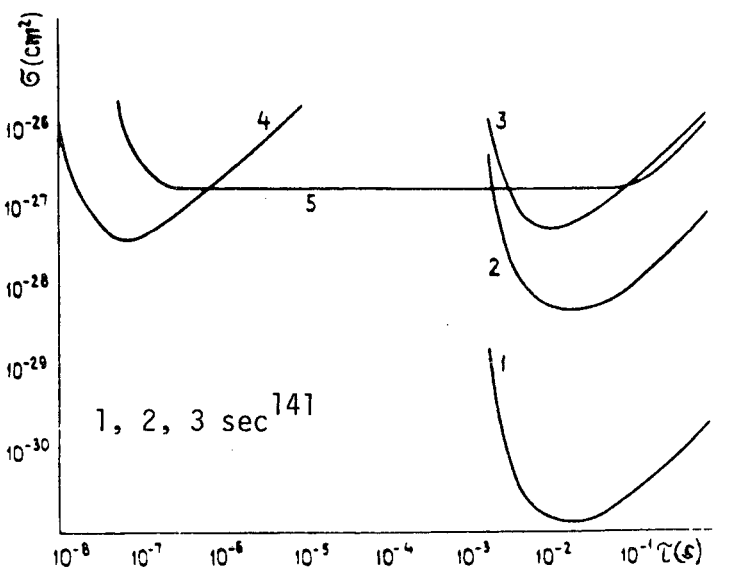

Fig. 2

SESSION VIII: FINAL SESSION

Multiquark Exotics

Harry J. Lipkin

Weizmann Institute of Science, Rehovot, Israel*

and

Argonne National Laboratory, Argonne, IL 60439†

and

Fermi National Accelerator Laboratory, Batavia, IL

I. Introduction - Constituent Quarks, Current Quarks and Partons
II. Why Bag Models Fail to Describe Multiquark Exotics
III. Why Multiquark States are Not Bound by Color-Electric Forces
IV. Color-Magnetic Forces and Color-Spin Exotics
V. Conclusions - Are Anomalons Multiquark Exotics?

*Supported in part by the Israel Commission for Basic Research.
This work supported in part by the U. S. Department of Energy under contract number W-31-109-ENG-38.

I. Introduction - Constituent Quarks, Current Quarks and Partons

Experimenters have been working very hard on anomalons by studying secondary interaction in emulsions. However it is still an open question whether this work constitutes convincing evidence that anomalons have any connection to the real world. Similarly we can note that theorists have been working very hard on supersymmetry, supergravity, technicolor, grand unification, solitons, bags, and composite models for quarks and leptons. Here again one can ask where is the convincing evidence that these have any connection to the real world? So far there is not a single piece of such evidence!!!

Unfortunately the history of the search for multiquark exotics has been full of theories which have shown no connection with the real world. A wild goose chase by experimentalists for objects predicted by these theories reached its peak in the baryonium fiasco. We therefore begin this discussion of multiquark exotics by returning to the real world and seeing what real experiments have taught us about hadron structure. We choose models which have proved themselves by giving a reasonable description of these experimental results and by demonstrating predictive power that can be used to investigate the possible existence of multiquark exotics.

There is now overwhelming experimental evidence that hadrons are made of colored quarks bound by interactions with colored gluons. We have every reason to believe that the correct theory for these interactions is QCD. However, we do not know how to calculate the structure and spectrum of hadrons with QCD starting from first principles. We therefore have to use phenomenological models.

The first indications that hadrons were composed of quarks came from the Constituent-Quark model[1] in which the hadron spectrum was calculated by the assumption that hadrons contained constituent quarks in the same way that atoms and nuclei contain constituent electrons and constituent nucleons. The deep inelastic lepton scattering data interpreted with the Quark-Parton model[2] provided completely independent evidence for the existence of quarks. In this picture hadrons consist of elementary point-like "current" quarks which behave like free point particles in deep inelastic scattering. But in addition to the valence quarks which give the hadron its spin and flavor quantum numbers, each hadron also contains an ocean of quark-antiquark pairs and gluon constituents.

The Constituent-Quark model and the Quark-Parton model provide complementary descriptions of hadrons in different domains of hadron physics. In the Quark-Parton model, the properties of quarks are well defined. They are point-like current quarks whose electroweak couplings are described exactly by the Glashow-Weinberg-Salam standard model. However, the way in which these quarks are bound together to make hadrons is completely unknown and the model gives no way of determining the hadron wave functions. These are determined by experiment and expressed in terms of the conventional structure constants, F_1, F_2 and F_3.

In the Constituent-Quark model, on the other hand, the hadron wave function is described completely in terms of the constituent quarks. The baryons consist of three quarks and nothing else, the mesons consist of a

single quark-antiquark pair and nothing else, and the wavefunctions are described by various models such as the potential models used in the description of charmonium. However, the properties of the quarks themselves are completely unknown and not specified by the theory. All that is known are the valence quantum numbers which correspond to quantities like electric charge and strangeness. These are conserved in strong interactions and must add up to give the correct total value for each hadron. But other properties such as the quark masses, the quark form factors, and the axial vector couplings are unknown and cannot be predicted in the framework of this model.

The magnetic moment of a hadron in the Constituent-Quark model is completely given in terms of the magnetic moments of the quarks.[3] However these quark magnetic moments are not known from first principles. If they are assumed to be proportional to the electric charges of the quarks, one can write then as Dirac magnetic moments

$$\mu_q = \frac{e\hbar}{M_q C} \tag{1a}$$

where M_q is the quark mass. However the quark mass is not known

$$M_q = ? \tag{1b}$$

This is the characteristic dilemma of the Constituent Quark model. Experimentally measured quantities like hadron magnetic moments are expressed in terms of parameters like the quark masses which are unknown from first principles. These properties, like the structure functions of the Quark-Parton model, are determined from experiment and relations between different experimental quantities are obtained when these unknown quantities can be eliminated.

There are then two approaches to the problem of baryon magnetic moments. One is simply to get relations between baryon moments like the ratio of the neutron moment to the proton moment by eliminating the unknown quark mass parameters.[4] The other approach is to attempt to determine the quark mass parameters from other data on hadrons, namely hadron mass splittings.[5,6,7] This approach has been surprisingly successful in calculating the magnetic moments of the nucleon and the lambda. It has had moderate success in the calculation of other hyperon moments, while leaving some discrepancies and some open questions.[8,9]

The complementary nature of the two models is illustrated by the calculation of G_A/G_V in the two models. The Constituent-Quark model gives the value of G_A/G_V for the nucleon in terms of unknown quark properties

$$(G_A/G_V)_{\text{nucleon}} = \frac{5}{3}\,(G_A/G_V)_{\text{quark}} = ? \tag{2a}$$

The best that can be done with this expression is to invert it to give the value of G_A/G_V for the quark in terms of the measured data for the nucleon.

$$(G_A/G_V)_{\text{quark}} = \frac{3}{5}\,(G_A/G_V)_{\text{nucleon}} \tag{2b}$$

In a sense, this relation (2) is complementary to the determination of the structure functions F_1, F_2 and F_3 in the Quark-Parton model. In both models

the experimental data are used to determine the properties of quarks or of hadron wave functions which are not given by the model.

In the Quark-Parton model, the value of G_A/G_V for the quark is given as unity by the Glashow-Weinberg-Salam standard model

$$(G_A/G_V)_{quark} = 1 \ . \tag{3a}$$

However there is no relation analogous to (2a) because we do not have any hadron wavefunctions from first principles. The value of G_A/G_V for the nucleon is not given in the Quark-Parton model

$$(G_A/G_V)_{hadron} = ? \tag{3b}$$

Adler and Weisberger obtained G_A/G_V for the nucleon by using PCAC and pion-nucleon scattering data. They took from experiment the information about hadron wave functions needed to calculate the value G_A/G_V. In some sense, this is analogous to the calculation of baryon magnetic moments in the Constituent-Quark model using unknown quark parameters whose values are determined from other hadron data, in that case the quark masses determined from hadron masses.

The Quark-Parton model and the Constitutent-Quark model must arise as complementary aspects of the same basic theory which hopefully will come from QCD. But so far no one has succeeded in obtaining either model from first principles using QCD. Gell-Mann has suggested that constituent quarks and current quarks are two different descriptions which should be related by some kind of unitary transformation. However the search for such a transformation has not been very fruitful and it has been very difficult to translate the results from one model into the language of the other.

II. Why Bag Models Fail to Describe Multiquark Exotics

An intermediate approach between the two models has been provided by the various bag models which consider the hadron as consisting of point-like zero-mass current quarks with valence quantum numbers and a bag. In this approach, the complications of the ocean of quark-antiquark pairs, gluons, etc. are all swept under the rug and into the bag. One might say that in the Constituent-Quark model, these complications are swept into the definition of the constituent quarks, with each constituent quark carrying its share of the ocean gluons, etc. whereas in the bag model the valence quarks are kept as bare current quarks and the additional constituents are all described by the degrees of freedom of the bag. Intuitively this seems to be a very attractive approach. In practice, however, it has not led to any new insight into hadron structure.

The spectroscopy of the low-lying hadrons seems to be adequately described by the degrees of freedom of the Constituent-Quark model in which each valence quark is "dressed" by its share of gluons and pairs and moves as a unit in a manner described by a simple Schrödinger equation and shows no signs of excitation of its internal structure.[10] We know that there must be other degrees of freedom present in baryons and mesons beyond the three quarks and the quark-antiquark pair. In the Constituent-Quark model, these would show up as excitations of the constituent quarks. In the Bag model, these

would show up as excitations of the bag or as motion of the valence quarks relative to the bag. So far no experimental evidence has been found for the existence of any of these additional degrees of freedom. All new effects predicted by the Bag Model have led to unsuccessful experimental searches with negative results, the most striking being the baryonium catastrophe.

Many years ago, Yoshio Yamaguchi visited the Weizmann Institute from CERN and gave a seminar summarizing recent developments there. When he was asked whether there had been any thought about the breakdown of QED at small distances, he hesitated for a moment then said "No. Many calculations, no thought." Unfortunately this seems to characterize most of the work with bag models. The main success of the Bag Model is that it has obtained similar results to those of the nonrelativistic quark model in a formulation which is manifestly relativistic. This perhaps shows that the relativistic corrections to the nonrelativistic Quark model are small or are somehow renormalized away by the procedure of adjusting phenomenological parameters like constituent quark masses to fit experimental data. Such renormalization effects have been demonstrated in some simple models.[7] But one would have hoped to get much more from the Bag Model. It has taught us no new physics and has not succeeded in providing any new predictions to be tested by experiment which show the presence of the bag.

In the case of multiquark exotics, the Bag Model has actually led us astray as shown in the case of baryonium. In fact there are two important aspects of the physics of multiquark systems which are left out in the Bag Model.

1. Correlations. One can expect clustering to occur in multiquark systems. It is difficult in the bag framework to describe a system of quarks which separates into two or more localized clusters.

2. The wave nature of hadrons. The bag is semiclassical. A model of a neutron with three quarks and a bag cannot describe neutron diffraction or a two slit experiment. The constraints on the motion of a bag due to the uncertainty principle are not easily included since the bag itself does not carry momentum.

The importance of these two features for multiquark systems is easily seen in the case of the description of the deuteron. The phenomenological picture of the deuteron in nuclear physics is a state of two nucleons interacting with a short range potential and with a tail on the wave function in which the nucleons spend a large part of the time outside the range of interactions. The wave nature of the nucleon is essential for the description of such a state with the tail of the wave function in the classically forbidden region. The question of whether a bound state exists depends upon the delicate balance between the potential energy obtained from the short range interaction and the kinetic energy required by the uncertainty principle when the nucleons are close enough together to feel the effects of the potential. In a Bag Model, where the nucleons are three quarks in a bag, it is very difficult to describe this kind of physics. One part of the wave function has the two bags outside their interaction range. Another part of the wave function must have two overlapping bags. A third part of the wave function must have all six quarks in the same bag. All these parts of the wave function are coherent and quantum effects with relative phases are important.

III. Why Multiquark States are Not Bound by Color-Electric Forces

The simple Constituent-Quark model, with all its difficulties, does include a proper treatment of the wave nature of the quarks and of the uncertainty principle as well as the possibility of describing states consisting of several separated clusters. These seem to be crucial for the description of multiquark bound states. We therefore use the Constituent-Quark model with two body potentials as the basis for our further analysis of multiquark systems.

Why are multiquark states considered exotic? If the forces between quarks and antiquarks are attractive shouldn't there be bound states with larger numbers of quarks than three quarks and a single quark-antiquark pair? The first answer to this question can be found in Nambu's old mass formula for color singlets.[11] Nambu noted long before QCD that a crude mass formula could be obtained for a system of n-particles, quarks or antiquarks in a color singlet state interacting via the exchange of colored gauge gluons

$$M(n) = n\, m_0 \tag{4}$$

where m_0 is a parameter.

Although Nambu simply called this result a linear mass formula for multiquark states, it already suggests that only the quark-antiquark and three quark states are stable. For the color singlet states with n=2, and 3, we obtain

$$M(q\bar{q}) = 2m_0 \tag{5a}$$

$$M(qqq) = 3m_0 \tag{5b}$$

For the exotic four and five body systems we obtain

$$M(qq\bar{q}\bar{q}) = 4m_0 = 2M(q\bar{q}) \tag{6a}$$

$$M(qqqq\bar{q}) = 5m_0 = M(qqq) + M(q\bar{q}) \tag{6b}$$

All larger states are seen to have sufficient mass to break up into two smaller color singlet clusters having the same mass. They will therefore be unstable against such breakup in this crude approximation.

Nambu did not consider the kinetic energies of the quarks nor the spatial variation of the potential in deriving his mass formula. He simply took the quark masses and a constant value for the two body quark potential independent of the spatial wave functions.

A generalization of Nambu's formula is obtained by taking into account the spatial variation of the potential and including kinetic energies.[12] For an n-particle system containing both quarks and antiquarks,

$$V(n) = \frac{1}{8} \sum_{i \neq j} V_{ij} \sum_{\sigma} \lambda_{i\sigma}\lambda_{j\sigma} \tag{7a}$$

where V_{ij} depends on all the noncolor variables of particles i and j and $\lambda_{i\sigma}(\sigma = 1, \ldots, 8)$ denote the eight generators of $SU(3)_{color}$ acting on a

single quark or antiquark i. This is directly analogous to the "isospin exchange interaction" for nucleons of isospin $1/2$ interacting by exchanging ρ mesons,

$$V(n) = \frac{1}{2} \sum_{i \neq j} V_{ij} \vec{t}_i \cdot \vec{t}_j \tag{7b}$$

where $\vec{t}_i$ is the isospin of particle i and V_{ij} contains the dependence on all other degrees of freedom except isospin. If we assume factorization of isospin from these other degrees of freedom we can write for any n-particle system containing antinucleons and nucleons,

$$V(n) = \frac{V}{2} \left[\sum_{\substack{all \\ ij}} \vec{t}_i \cdot \vec{t}_j - \sum_i \vec{t}_i \cdot \vec{t}_i \right] = \frac{V}{2} [I(I+1) - nt(t+1)] \tag{8a}$$

where V is the expectation value of V_{ij} integrated over all variables except isospin, I is the total isospin of the system and t is the isospin of one particle; i.e., $1/2$ for a nucleon.

For the colored quark interaction (7a) the interaction energy of an n-particle system can be calculated by the same trick used in Eq. (8a) to give

$$V(n) = \frac{V}{2} (C - nc) \tag{8b}$$

where V is the expectation of V_{ij}, integrated over the noncolor variables, C is the eigenvalue of the Casimir operator for $SU(3)_{color}$ for the n-particle system and $c = 4/3$ is the eigenvalue for a single quark or antiquark. These eigenvalues are directly analogous to the SU(2) Casimir operator eigenvalues $I(I + 1)$ and $t(t + 1)$ in Eq. (8a).

The mass of the n-particle state is given by the sum of n times the quark mass, the interaction (8b) and the kinetic energy T. For a color singlet state, $C = 0$ and

$$M(n) = nM_q + V(n) + T = n(M_q - \frac{cV}{2}) + T \tag{9}$$

This is just the Nambu formula (4) with an additional kinetic energy term. Again we see that there are no bound multiquark states. When two color singlet hadrons are brought together eq. (9) shows that their potential energy is unchanged. Their kinetic energy must be increased by the localization of the two particles as a result of the uncertainty principle. Thus any color singlet state of more than four particles will have a larger mass than the two color singlet clusters into which it can decay by breakup.

The factorization of color from the other degrees of freedom assumed in deriving eqs. (8) and (9) is automatic for the quark-antiquark and three quark systems where the color coupling is unique for a color singlet state. This no longer holds for multiquark systems and the possibility exists that states of lower mass than that given by eq. (9) could be obtained by introducing correlations between color and the other degrees of freedom. These effects were first investigated for the $(qq\bar{q}\bar{q})$ system where there are two independent couplings to make an overall color singlet.[12] For this system, the interaction (7a) is a nontrivial 2 x 2 matrix in color space. It was shown by diagonalizing this matrix that there were no exotic bound states for well-behaved spin-independent potentials where the criterion for well-behaved included all the commonly used potentials like Coulomb, harmonic oscillator, Yukawa, etc.

The conclusion from this treatment was that color singlet hadrons are color-electric neutral objects and behave like neutral atoms. There are no strong color-electric forces between color-singlet hadrons.

IV. Color Magnetic Forces and Color-Spin Exotics

The color-magnetic forces introduce the possibility of bound states produced by color-spin correlations.[13] A simple picture of a such a bound state is seen by examining what happens when two kaons are brought together so that the quarks in one kaon can feel the interactions due to the quark-antiquark pair in the other kaon. Our results (8) and (9) show that there is essentially no effect from the color-electric forces. This is confirmed by the experimental observation that the binding energy of the deuteron is very small and there is no evidence for any larger color-electric effects. However energies of several hundred MeV are seen to be available from the hyperfine interaction since flipping a spin in either kaon to make a K^* instead of a kaon costs an energy of 400 MeV.

In the system of two kaons where each kaon is in a spin-zero color singlet state, the hyperfine energy within each kaon is minimized while the hyperfine interactions between the quark or antiquark in one kaon and the quark or antiquark in the other average to zero. However recoupling color and spin can gain binding energy from the hyperfine interaction between pairs in the two different hadrons at the price of losing energy in the interaction between the quark and antiquark in the same kaon. It has been shown that there is a net gain in hyperfine energy by recoupling in certain cases and that therefore there is a possibility of having bound multiquark states.[13,14,15,16]

Jaffe first showed that the lowest multiquark states in the light quark sector are "crypto-exotic" and do not have exotic quantum numbers.[13] This makes it difficult to prove experimentally that they are indeed four-quark states rather than ordinary mesons. However, Jaffe's result was shown to break down when there are more than three flavors.[14] In the charm sector the lowest-lying four quark state can have exotic quantum numbers if all four constituents have different flavors; e.g. $(cs\bar{u}\bar{d})$. Such exotics would provide striking and convincing signatures for multiquark states, but so far none have been found.

For more detailed calculations we use the potential model with the interaction (7a) including the spin dependent forces. As discussed above, bag model calculations are useless because they cannot treat the effects of correlations and of the uncertainty principle applied to the motion of bags in any simple way.

A phenomenological approach was tried in which the parameters of the interaction (7a) could all be determined from experiment with a minimum of model dependence.[15] Consider the case of two mesons (e.g. $K\bar{K}$) brought together to make a four particle wave function like an α-particle. We assume that the change in color-electric energy is negligible and investigate the optimum coupling of color and spin to minimize the color magnetic energy. We choose a wave function in which the spatial wave function for any pair in the four body system is the same as in a meson. The matrix elements of the hyperfine interaction are obtained directly from the experimental hyperfine

splittings observed in the meson spectrum.

If such an α-particle-like wave function were shown to have a lower mass than two mesons, this would prove the existence of a bound state by the variational principle even though the α-particle-like wave function chosen may not be the best or the correct wave function. However the results showed that the gain in hyperfine potential energy by recoupling spins was not quite enough to overcome the kinetic energy required to bring two mesons together, thus indicating that the α-particle wave function is not bound.

V. Can These be Bound Multiquark Clusters?

The question then arises whether a slightly better wave function might give a bound state. However there is no way of getting matrix elements of the interaction directly from experimental data for spatial wave functions different from those in the mesons. Some model must be assumed to make definite predictions. But it is already clear at this stage that any bound state will be barely bound and therefore very close to threshold. The δ and S^* scalar mesons are candidates for such bound states of the $K\bar{K}$ system since they are both very close to $K\bar{K}$ threshold and the S^* does not couple strongly to two pions. The degeneracy of the isovector state with the isoscalar state decoupled from pions arises naturally in the four-quark state of one strange and one nonstrange pair. In the quark-antiquark system the degenerate isoscalar and isovector states are both nonstrange, like ρ-ω and f-A2 and the even -G state couples strongly to two pions.

Weinstein and Isgur tested this idea using a harmonic-oscillator potential model because of its ease of calculation.[16] Although this potential has peculiar unphysical long range effects,[17] they concluded that their calculation was insensitive to these long range properties. They found by using a variational calculation with a large space of trial wave functions that the $K\bar{K}$ system was the only four-quark system where binding occurred and that the wave function resembled the deuteron; i.e. it consisted mainly of two quark-antiquark clusters separated by a distance which was larger than the size of each cluster. Although their variational trial wave functions included a continuum between α-particle-like states and such cluster states, the variational principle picked out the states having this clustering property.

Their results can also be expressed in terms of a simple phenomenological model for a two meson bound state.[18] Consider a meson-meson scattering problem with the hyperfine interaction replaced by a short range effective interaction in the two-meson space with a strength inversely proportional to the product of the quark masses as indicated by the hyperfine interaction. For a square well potential with a range a, the condition for the existence of a bound state is

$$\frac{MV}{m_1 m_2} > \frac{\pi^2 \hbar^2}{4a^2} \qquad (10)$$

where M is the mass of the meson, m_1 and m_2 are the masses of the constituent quarks in the meson, and U is a parameter specifying the strength of the potential. Substituting constituent quark masses and experimental meson masses into the left hand side of eq. (10) shows a maximum for the case of the kaon where the two quarks are an up quark and a strange quark.

The physics of this maximum is easily seen. For low-mass mesons like pions, the hadron mass in the numerator of the left hand side of eq. (10) is too small; i.e. the kinetic energy required to localize a low mass pion in a bound state is too large. At high masses like those of charm or bottom quarks, the quark masses in the denominator are too large; i.e. the hyperfine interaction is too weak to produce a bound state. Without a model to give the values of the parameters U and a, we cannot say whether there will be bound states. However eq. (10) shows us that the best place to look for them is in the $K\bar{K}$ system and supports the idea that the δ and S^* scalar mesons are indeed four quark states. In this case their binding energy is so low that eq. (10) shows that there are no other bound four quark states.

How can we test experimentally whether the S^* and δ are indeed four quark states? Unfortunately, the $(s\bar{s}u\bar{u})$ system can decay by annihilation of the $(s\bar{s})$ pair into the open $\pi\pi$ and $\delta\pi$ channels, even if the state is below the $K\bar{K}$ threshold and cannot decay by breakup. For this reason the charmed-strange exotic configurations $(cs\bar{u}\bar{d})$ and $(cu\bar{s}\bar{d})$ were suggested[14] as better candidates for unambiguous evidence of a four quark structure. These cannot decay by annihilation and must be stable against strong decays if the breakup channels are closed. However, the Weinstein-Isgur calculation[16] with the result (10) shows that if the $K\bar{K}$ system is barely bound, the the DK system is unbound and might be observed as an exotic resonance but not as a bound state.

The S^* and δ might be "mini-anomalons" with a shorter mean free path in nuclear matter than $q\bar{q}$ mesons. If they are indeed larger structures looking like two mesons separated by a distance large compared to the size of an individual meson one would expect that they would be absorbed much more quickly in nuclear matter than ordinary $q\bar{q}$ mesons and that this might be detected in experiments on complex nuclei.[18] For example, these mesons going through a nucleus could produce a hypernucleus and a kaon

$$(\delta, S^*) + (Z,A) \rightarrow {}_{\Lambda}(Z,A) + K^0 \qquad (11a)$$

$$(\delta, S^*) + (Z,A) \rightarrow {}_{\Lambda}(Z-1,A) + K^+ \qquad (11b)$$

The structure of these mesons might be tested experimentally by comparing the A-dependence of their production in nuclei with the production of conventional quark-antiquark mesons having the same decay modes. Consider for example, the reactions

$$K^- + p \rightarrow \Lambda + S^* \rightarrow \Lambda + \pi + \pi \qquad (12a)$$

$$K^- + p \rightarrow \Lambda + (\rho, f) \rightarrow \Lambda + \pi + \pi \qquad (12b)$$

$$K^- + p \rightarrow \Lambda + \delta \rightarrow \Lambda + \eta + \pi \qquad (13a)$$

$$K^- + p \rightarrow \Lambda + A2 \rightarrow \Lambda + \eta + \pi \qquad (13b)$$

In the reaction (12) the $\pi\pi$ spectrum should show peaks at masses of the ρ, S^* and f. A shorter mean free path in nuclear matter for the S^* implies a qualitatively different behavior in the A-dependence of the S^* peak as compared with the ρ and the f. Similarly the A-dependence of the δ and A2 peaks in the η,π spectra of the reactions (13) can be compared.

VI. Conclusions - Are Anomalons Multiquark Exotics?

So far there is no convincing experimental evidence for any multiquark exotic bound state nor for any exotic resonance. Except for the δ and S^* there are no candidates for bound states and no firm theoretical predictions waiting to be tested. Exotic resonances may exist in the 1.5-2.0 GeV region and in the charmed sector, e.g. the charmed-strange exotics. The experimental search for multiquark resonances is still open and active.

All this brings us back to the topic of anomalons and the question of whether some kind of multiquark exotic could be responsible for the experimental observations reported here. Could a meson bind to a nucleus in this kind of deuteron-like state to make an exotic anomalon? One might envision a binding of a meson to several nucleons with very short range interactions giving additional binding not present in the meson-nucleon system. However carrying this point of view further encounters difficulties. The long lifetime of anomalons is a serious problem because pions bound to a nucleus should be absorbed much too quickly. Similarly the K^- bound to a nucleus should react to form a hyperon and a pion in a time shorter than the observed anomalon lifetime. A K^+ bound to a nucleus would be stable against decays by strong interactions and would have a reasonable lifetime comparable to the kaon lifetime. However there does not seem to be any simple mechanism for producing such a bound state. The s-wave K^+-nucleon interaction is known to be repulsive. However perhaps there are other possibilities.

References

[1]Harry J. Lipkin in Common Problems in Low and Medium Energy Nuclear Physics, (NATO ASI Series B, Physics, vol. 45) Proceedings of NATO Advanced Study Institute/1978 Banff Summer Institute on nuclear theory held at Banff, Canada, August 21 to September 2, 1978, ed. B. Castel, B. Goulard and F. C. Khanna (Plenum, New York) p. 175; R. H. Dalitz, Prog. Part. Nucl. Phys. 8 (1982) 7; H. J. Lipkin, Physics Reports 8C (1973) 173.

[2]A Bodek, These proceedings.

[3]O. W. Greenberg, Phys. Rev. Lett. 13 (1964) 598.

[4]H. Rubinstein, F. Scheck and R. H. Socolow, Phys. Rev. 154 (1967) 1608; J. Franklin, Phys. Rev. 172 (1968) 1807; 182 (1969) 1607.

[5]A. De Rujula, H. Georgi and S. L. Glashow, Phys. Rev. D12 (1975) 147.

[6]H. J. Lipkin, Phys. Lett. 74B (1978) 399.

[7]Isaac Cohen and Harry J. Lipkin, Phys. Lett. 93B (1980) 56.

[8]J. L. Rosner, in High Energy Physics -- 1980, Proceedings of XX International Conference, Madison, Wisconsin, edited by Loyal Durand and Lee G. Pondrom (AIP, New York, 1981) p. 540.

[9]H. J. Lipkin, Nucl. Phys. B214 (1983) 136.

[10]H. J. Lipkin, Phys. Lett. 113B (1982) 490.

[11]Y. Nambu, in Preludes in Theoretical Physics, ed. A. de Shalit, H. Feshbach and L. Van Hove (North-Holland, Amsterdam, 1966) p. 133.

[12]Harry J. Lipkin, Phys. Lett. 45B (1973) 267.

[13]R. L. Jaffe, Phys. Rev. D15 (1977) 267 and 281.

[14]Harry J. Lipkin, Phys. Lett. 70B (1977) 113.

[15]Nathan Isgur and H. J. Lipkin, Phys. Lett. 99B (1981) 151.

[16]John Weinstein and Nathan Isgur, Phys. Rev. Lett. 48 (1982) 659.

[17]O. W. Greenberg and H. J. Lipkin, Nucl. Phys. A179 (1981) 349.

[18]H. J. Lipkin, Phys. Lett. 124B (1983) 509.

ARE ANOMALONS STILL PROVOCATIVE?

- A SUMMARY OF THE PRESENT EXPERIMENTAL SITUATION -

Ingvar Otterlund
Division of Cosmic and Subatomic Physics
University of Lund
Sölvegatan 14; S-223 62 LUND, Sweden.

Abstract: A number of experiments have shown that enlarged cross sections exist for projectile fragments which are emitted in relavistic heavy ion collisions. The present status of these investigations is reviewed and new detector techniques for anomalon search are discussed. Most experiments are compatible with an assumption that the anomalon effect is smaller than 3% and appears within distances shorter than about 2 cm from the parent reaction.

Introduction.

High energy heavy ion reactions are normally described in the spectator-participant picture, Fig. 1. Spectators are comparatively cold fragments, while the participants may form a fireball of hot hadronic matter. During resent years it has been widely speculated if two different exotic channels are available via relativistic heavy ion reactions. One speculation has its origin from theoretical studies which suggest that nuclear matter can be heated up or compressed to such an extent that the participant system passes a phase transition to quark-gluon matter [1,2]. The other speculation has its origin from early experimental observations that a few fragments have a mean free path considerably shorter than the value expected from simple geometrical considerations [3-7]. Here theoretical speculations [8-10] came first when the effect was more systematically studied in accelerator based experiments [11-13]. The explanation for this anomaly was searched among quark-gluon effects [8], nuclear physics effects [9] and effects originating from quasi-molecular states of projectile fragments [10]. The name "anomalons" has been given to fragments exhibiting anomalously short mfp's [14].

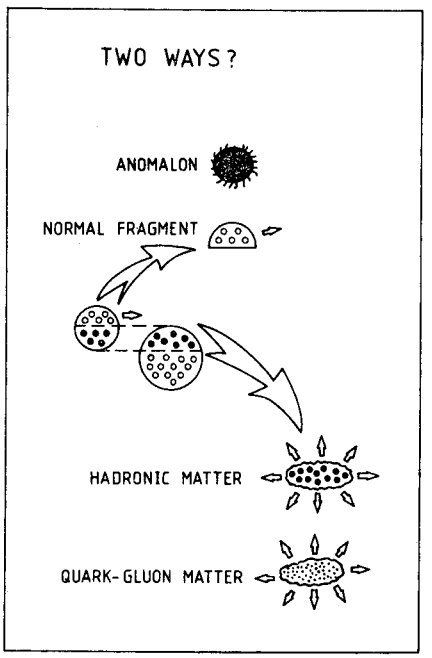

Fig. 1. Two different exotic channels (quark-gluon matter and anomalons) may be available via relativistic heavy ion reactions.

Since the first anomalon workshop in February 1982 many new experiments have taken data [15-28]. The new results presented during the workshop, gave however a somewhat confusing picture of the magnitude of the anomalon effect.

In this summary I will first review different experimental techniques used for anomalon search and thereafter I will

approach the experimental data from a new point of view in order to present an answer to the question raised above.

Solid state nuclear track detectors (SSNTDs) for anomalon search.

Data from experiments using two different techniques (emulsion nuclear track detectors and plastic nuclear track detectors) and with different systematic errors and methodology were presented at the workshop. Before the presentation of the results obtained from SSNTDs I give below a short description of the two types of experiments.

Emulsion nuclear track detectors.

In the anomalon experiments emulsions are exposed parallel to the surface. Scanning of the emulsion pellicles involves picking up the entering beam nuclei within a few mm from the entrance edge and following along each individual track until it either interacts or leaves the stack. The followed track length of the beam nuclei are measured. Different beam nuclei are in general used to determine Λ^*_{beam} and b in the relationship, eq. (1), between the mean free path (mfp), λ, and the charge of the nuclei, Z:

$$\lambda = \Lambda^*_{beam} Z^{-b} \qquad (1)$$

Relativistic projectile fragments (PF's) emitted in the first, second, third etc. generation of events are followed until they either interact or leave the stack. For each fragment the charge and the potential path available for interaction in the detector or the distance to the interaction, if it interacts, are measured. The reduced mfp, Λ^*, in each individual path is used for the analysis.

$$\Lambda^* = (\sum_z x_z Z^b) N^{-1} \qquad (2)$$

x is the total distance followed for fragments with charge Z and N is the total number of events observed for all charges. Observations of $\Lambda^* < \Lambda^*_{beam}$ at small distances from the parent interactions have been interpreted as signals of anomalons [29]. Λ^*_{beam} varies substantially from one experiment to another. Values from $\Lambda^*_{beam} = 25.1 \pm 1.7$ cm [13] to $\Lambda^*_{beam} = 32.4 \pm 1.7$ cm [12] have been obtained. The large fluctuations may depend on different sensitivities of the emulsions used and on different scanning efficiencies. A normalized mfp R^*, where

$$R^* = \frac{\Lambda^*}{\Lambda^*_{beam}} , \qquad (3)$$

is therefore more convenient than Λ^* for comparisons between different emulsion experiments.

Scanning efficiency, ε.

The probability density for an interaction distance x is given by

$$f(x)dx = \lambda^{-1} \exp(-x/\lambda) dx \quad (\varepsilon=1) \qquad (4)$$

In nuclear track detectors the mfp, λ, has a simple physical interpretation in terms of number densities of target nuclei and cross sections, namely:

$$\lambda = \left[\sum_{i=1}^{k} n_i \sigma_i\right]^{-1} \tag{5}$$

k is the number of different nuclides in the nuclear track detector, n_i is the number of nuclei per unit volume of nuclei i and σ_i is the total reaction cross section [30].

Scanning in emulsion is not perfect. A reduced efficiency, $\varepsilon < 1$, results in a longer mfp, i.e.

$$\lambda_\varepsilon = \lambda/\varepsilon \tag{6}$$

This may introduce a bias in the results e.g. if primary nuclei and fragments are scanned with different efficiencies a small "anomalon effect" will be observed in the density of interactions for small distances x, from the starting points of the scanning. I illustrate this effect in the following unrealistic example.

There are two scanners A and B. B is scanning primaries and unhappy because he (she) does not expect any surprises like anomalons to appear in his (her) work. Scanner B has been chosen to scan tracks of multiply charged fragments because he (she) is known to be an excellent scanner (in fact perfect $\varepsilon=1$) and he (she) is happy to do something else than boring primary scanning.

The two scanners follow the same number of tracks of primary nuclei respectively fragments with the same charge. Because of different efficiencies there will be an important difference in the registration of reactions. At long distances scanner B does not have many tracks to follow because he (she) has already found the events. Scanner A on the other hand still has tracks to follow because he (she) is missing interactions (c.f. Fig. 2). The ratio of the probability densities to find interactions depends on x and is given by

$$\frac{f(x)}{f_\varepsilon(x)} = \varepsilon^{-1} \exp\left[(\varepsilon-1)x/\lambda\right] \tag{7}$$

When $x \approx \lambda$ scanner A and B find the same number of events.

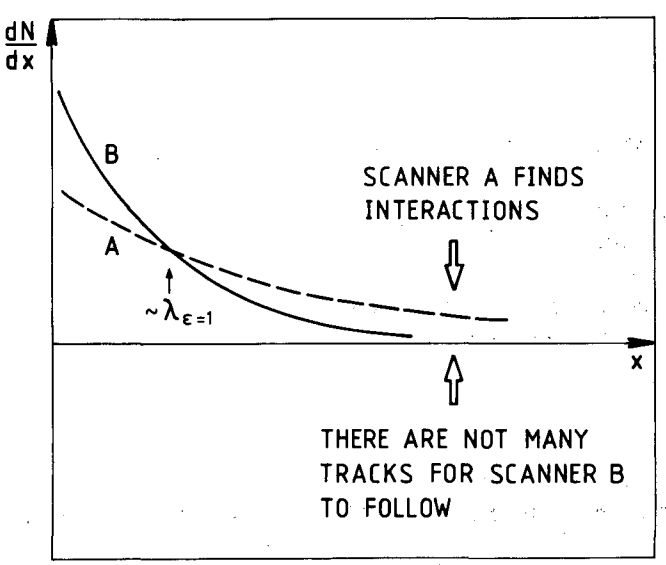

Fig. 2. There will be an important difference in the registration of interactions for scanner A and scanner B. At long distances scanner B finds more interactions than scanner A.

After the data aquisition they compare the number of found events as a function of the distance, x, followed from the starting points. The result, exhibited in Fig. 3,

is that scanner B observes an enhancement of interactions when $x \lesssim \lambda$.

In the following I intend to examine the emulsion data presented at this and the previous workshop in such a way that neither do I have to normalize to the primaries nor do I have to worry about scanning efficiencies.

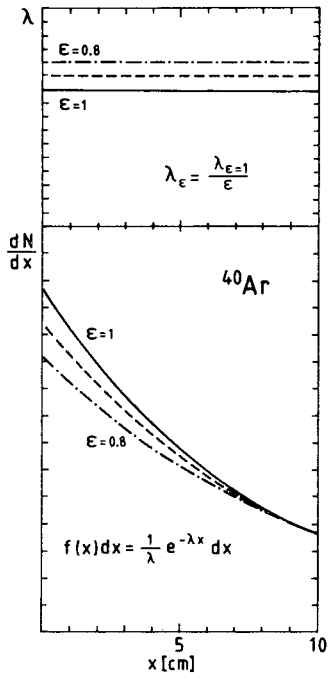

Fig. 3.
a. λ_ε increases with decreasing efficiency, ε.
b. Distribution of interaction distances x for different values of ε calculated for ^{40}Ar nuclei.

Plastic nuclear track detectors.

In plastic experiments ~ 600 μm thick foils of CR-39 are radiated perpendicular to the ion beam. After etching particle tracks can be observed in the foils and the charge can be measured with high resolution at about 600 μm intervals along the path of incident and emitted fragments. Due to the threshold for detection of relativistic particles only nuclei with charges ≥ 7 can be observed [15]. The mean free paths in plastic for relativistic beams of ^{20}Ne, ^{40}Ar, ^{56}Fe and ^{238}U producing charge changing interactions are shown in Fig. 4. The data are well represented by the relationships $\lambda = \Lambda^*_{beam} Z^{-b}$ and $\lambda = \Lambda^*_{beam} A^{-c}$, where b and c are constants.

Only a charge change ($\Delta Z \geq 1$) can be measured and the foil where the charge change tooks place can be identified. No other information about the reaction is obtainable. The accuracy in determining the vertex position of an event is limited by the sheet thickness. Tracks shorter than 600 μm (1 foil thickness) can therefore not be detected.

Two plastic experiments were presented by W. Heinrich [15] and M. Tincknell [16] respectively. The Siegen-group [15] uses an automatic

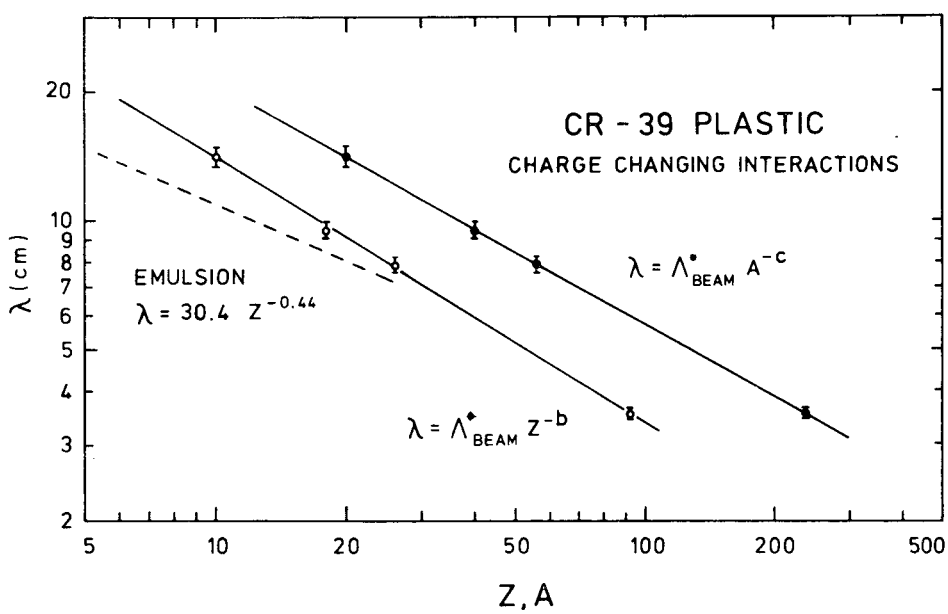

Fig. 4. The mean free path for charge-changing interactions of relativistic ^{20}Ne, ^{40}Ar, ^{56}Fe and ^{238}U beam nuclei in plastic CR-39 as a function of the charge, Z, and the mass A. Emulsion ($\lambda = 30.4\ Z^{-0.44}$ [29]) is shown for comparison.

track measuring system and has therefore access to a comparatively fast data aquisition experiment. The UC-group [16] has slow data taking (like emulsion experiments) thus limited statistics but comparatively small systematic errors.

Two extreme hypothesis for the anomalon effect.

To obtain some insight as to the nature of the excess of interactions of PF's at short distances two different approaches have been presented. One is the anomalon decay hypothesis (ADH) suggested by Barber et al. [13]. The other is the stable anomalon hypothesis (SAH) suggested by Friedlander et al. [11,29]. In both models the probability density for an interaction distance x can be written as:

$$f(x)dx = [A \exp(-\alpha x) + B \exp(-\beta x)]\, dx \qquad (8)$$

with values of A, B, α and β depending on the model. The mfp, λ, as a function of the distance x from the parent interaction is in Fig. 5 shown for the different hypothesis.

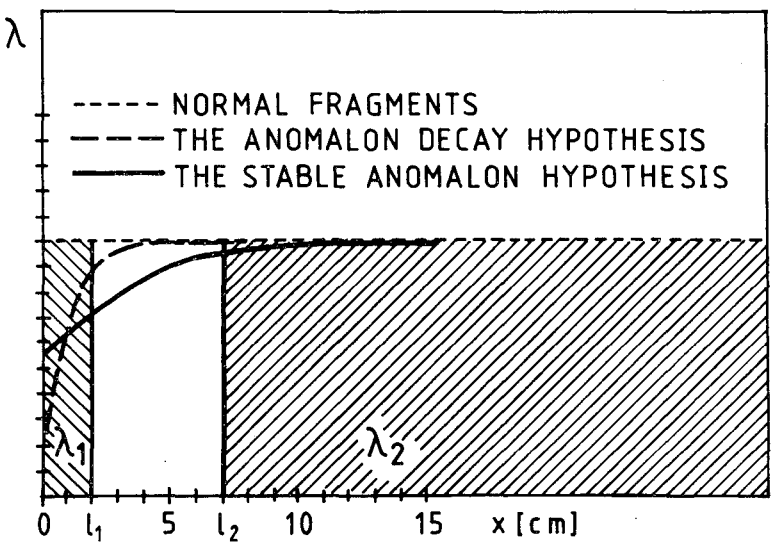

Fig. 5. λ as a function of the distance x from the parent interactions shown for normal fragments and for fragments produced in accordance with the ADH and the SAH. It is convenient to study correlations between $\lambda_1 = \lambda(\leq \ell_1)$ and $\lambda_2 = \lambda(> \ell_2)$ where λ_1 and λ_2 are the mean free path in the shaded regions respectively.

The anomalon decay hypothesis (ADH).

In this hypothesis it is assumed that a fraction f of the fragments are anomalons with enhanced cross section, $\sigma_a = m\,\sigma_n$, c.f. Fig. 6. σ_a and σ_n are the interaction cross sections for anomalons and normal fragments respectively and m is the enhancement factor. A decay time is introduced which determines when the transition from the anomalon state to the normal state takes place. This decay time corresponds to a decay length of t cm. The probability density, eq. (8), when f=1, has the coefficients:

$$A = \frac{(m-1)\lambda_n + m(m-1)t}{\lambda_n(\lambda_n + (m-1)t)};\quad B = \frac{1}{\lambda_n + (m-1)t};\quad \alpha = \frac{\lambda_n + mt}{\lambda_n t};\quad \beta = \frac{1}{\lambda_n} \qquad (9)$$

In a recent experiment [23] where the production of projectile fragments were detected when the beam hit a solid target and a diluted target respectively ruled out the anomalon decay hypothesis with the values of m = 1.54 and t = 0.85 cm given by Barber et al. [13]

The stable anomalon hypothesis (SAH)

This hypothesis is built on the assumtion that a fraction, a, of the projectile fragments are anomalons with a mfp λ_a (c.f. Fig. 6). The probability density, eq. (8), has then the coefficients:

$$A = \frac{a}{\lambda_a};\ \alpha = \frac{1}{\lambda_a};\ B = \frac{1-a}{\lambda_a};\ B = \frac{1}{\lambda_n} \qquad (10)$$

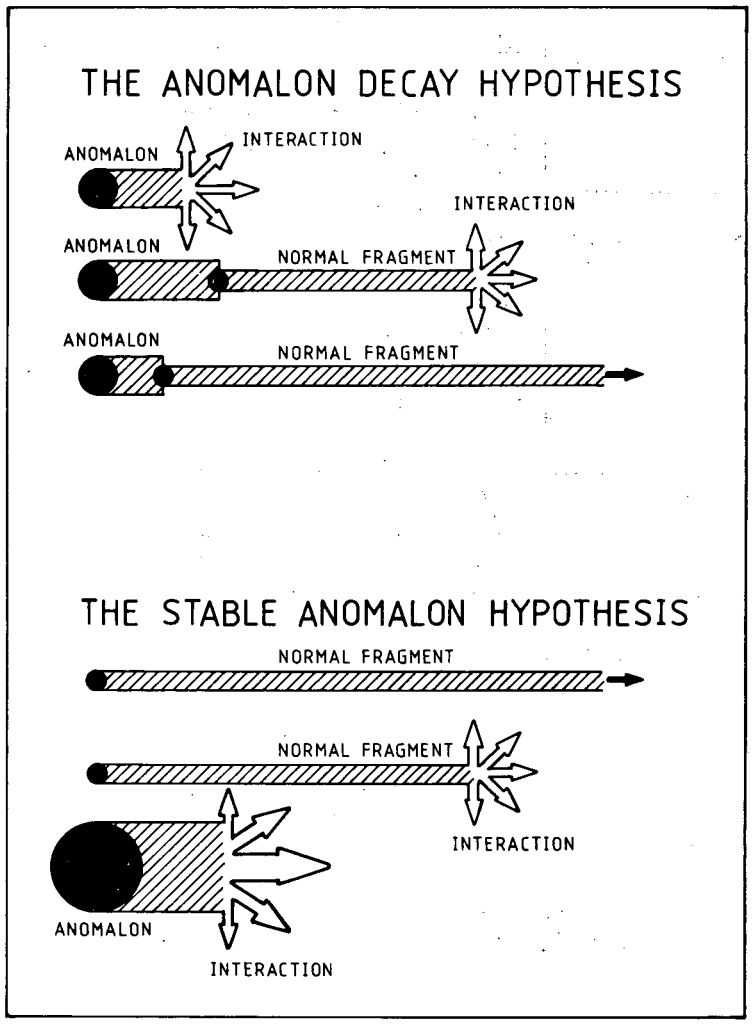

Fig. 6. An artist drawing of the two hypothesis for anomalon production; the ADH and the SAH.

When analysing the data Friedlander et al. [11] tentatively assumed that the anomalons have a mfp λ_a independent of charge. The best fit to the correlation between Λ^* and followed distance, x, in the LBL - NRC experiment [11] gives a = 6% and λ_a = = 2.5 cm.

The F-parameter.

If the anomalon effect has such a large magnitude as a = 6% and λ_a = 2.5 cm a simple strategy would be first to hunt a significant enhancement of fragments with mfp's shorter than normal using only a very rough charge classification and to analyse the results in a way which is comparatively independent on the scanning efficiency. I illustrate this using the F-parameter defined as

$$F(Z) = \frac{\lambda(x>\ell_2)}{\lambda(x\leq\ell_1)} = \frac{\lambda_2}{\lambda_1} \qquad (11)$$

$\lambda_2 = \lambda(x>\ell_2)$ is the mfp of PF's beyond $x = \ell_2$ and $\lambda_1 = \lambda(x \leq \ell_1)$ is the corresponding value in the first $x \leq \ell_1$ cm. The F-parameter has the merit of being rather insensitive to scanning efficiency why fluctuations from one experiment to another is expected to be small. The reason is that λ_1 and λ_2 are normally measured by the same scanner.

The dependence of F on the fragment charge, Z, estimated from the ADH and the SAH are shown in Fig. 7 with $\ell_1 = \ell_2 = 2.5$ cm. In the calculations I have used λ_n estimated from Bradt and Peters cross section formula [31,32].

$$\sigma_{BT} = \pi r_o^2 (A_B^{1/3} + A_T^{1/3} - b_o)^2 \qquad (12)$$

where A_B and A_T are the mass numbers of the beam (B) and the target (T) nuclei, respectively. b_o is the overlap parameter and r_o is the constant of proportionality in the expression for the geometrical nuclear radius $r = r_o A^{1/3}$. The b_o and r_o values given in Fig. 1 ref. [32] are used. The estimates for f=1, m=1.54 and t=0.85 cm (c.f. Barber et al. [13]) in the ADH are shown by the solid curve in Fig. 7. This model gives essentially Z-independent F-values $F \approx 1.18$). The dotted curve shows the values expected from the SAH using a = 6% and λ_a = 2.5 cm. Because of the assumption that λ_a is independent on Z this model always predicts a decrease of F with increasing Z. F is ~ 1.3 for He-fragments but only ~ 1.06 for Ar-fragments.

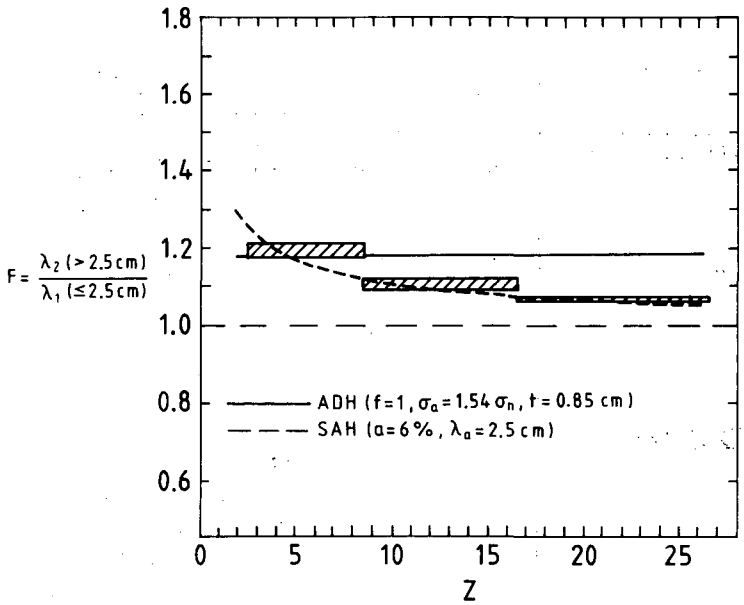

Fig. 7. $F = \lambda_2/\lambda_1$ as a function of Z estimated for the ADH (f=1, m=1.54, t=0.85 cm) and the SAH (a=6% and λ_a = 2.5 cm). The hatched boxes exemplify the uncertainties if the sample of followed fragments is divided into charge groups without identification within the subsample (see the text).

However, to pool information for fixed charge $Z \geq 3$ is difficult in emulsion experments. One may thus consider F when the sample is divided into charge intervals $Z_i \leq Z \leq Z_j$.

$$F(Z_i \leq Z \leq Z_j) = S_2N_1/S_1N_2 = \frac{\lambda(x > \ell_2)}{\lambda(x \leq \ell_1)} = \frac{\lambda_2}{\lambda_1} \qquad (13)$$

$S_2(S_1)$ is the total followed distance of fragments with charge $Z_i \leq Z \leq Z_j$ and with observed track paths $x > \ell_2$ ($\leq \ell_1$). N_2 respectively N_1 are the number of reactions observed.

Using the parametrization $\lambda = \Lambda Z^{-b}$ we obtaine the approximative relation

$$F(Z_i \leq Z \leq Z_j) = \frac{\lambda_2}{\lambda_1} \approx \frac{\langle Z_*^{-b}(> \ell_2)\rangle}{\langle Z_*^{-b}(\leq \ell_1)\rangle} \qquad (14)$$

where Z_* is the charge of the interacting fragments. Observe that $F > 1$ if $i \neq j$ because the charge spectrum of interacting fragments is changing with x resulting in decreasing mean values of Z_* with increasing x-values. This effect is however small and can be calculated if we know the charge spectrum of interacting fragments. The magnitude of this effect is shown in Fig. 7 by the hatched boxes for three different charge groups $3 \leq Z \leq 8$, $9 \leq Z \leq 16$ and

$16 \leq Z \leq 26$. The lower limits of the boxes are calculated from the SAH ($a = 6\%$, $\lambda_a = 2.5$ cm) assuming a flat charge spectrum in the charge bin considered. The upper limit is the corresponding value assuming a linear decrease of the charge spectrum with the constraint that the number of fragments with charge Z_i is twice the number of fragments with charge Z_j.

Another alternative is to study the correlation between $\lambda_1 (\leq \ell_1)$ and λ_2 $(> \ell_2)$.

Correlations between λ_1 $(\leq \ell_1)$ and λ_2 $(> \ell_2)$.

Figure 8 shows λ_1 $(\leq \ell_1)$ versus λ_2 $(> \ell_2)$. In this diagram the diagonal $\lambda_1 = \lambda_2$ is of course available if no anomalons exist. A reduced scanning efficiency ($\varepsilon < 1$) results in a movement upwards along the diagonal in comparison with the value obtained when $\varepsilon = 1$. The triangle to the right of the diagonal can be reached if anomalons exist. This diagram will be further discussed below.

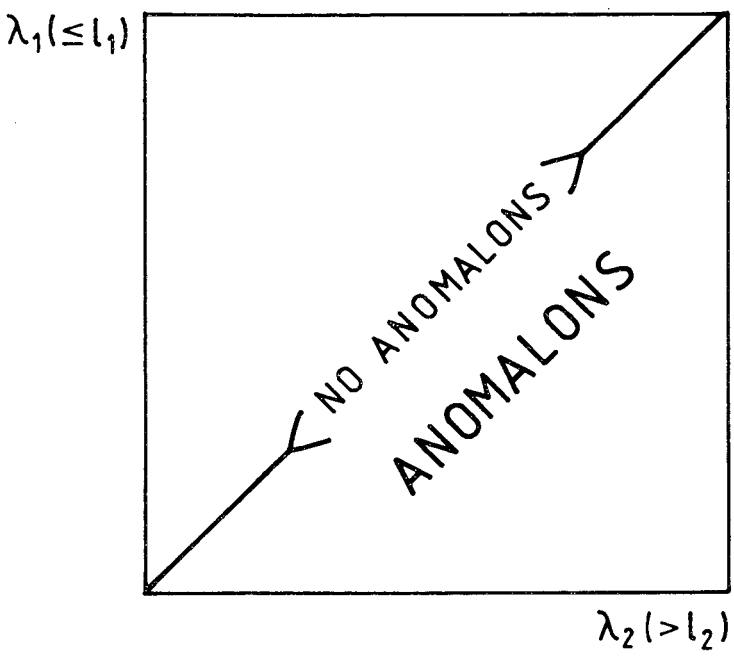

Fig. 8. Correlations between λ_1 $(\leq \ell_1)$ and λ_2 $(> \ell_2)$.

Results.

Mean free paths of projectile fragments.

In the two plastic experiments presented at this workshop [15,16] beams of 1.85 A GeV ^{40}Ar were used. The results are shown in Table 1 and Fig. 9. Both experiments observe a depression of the mean free path in the first cm from the parent interaction. Tincknell and Price [16] found a fraction $a = 5\%$ of anomalons with a mfp $\lambda_a \approx 1$ cm (in plastic) and that both even and odd charged secondaries exhibited anomalon behaviour. In a plastic experiment the UC-group reached a charge resolution of $\sigma_Z = 0.06$ and they could rule out explanations of anomalons based on models in which anomalons have nonintegral charge in the charge range $10 \leq Z \leq 18$ [26]. Heinrich et al. [15] obtained $a = 1.2$ % and $\lambda_a = 0.65$ cm (in plastic). These values are smaller than the corresponding values reported from emulsion experiments at the first anomalon workshop [11-13].

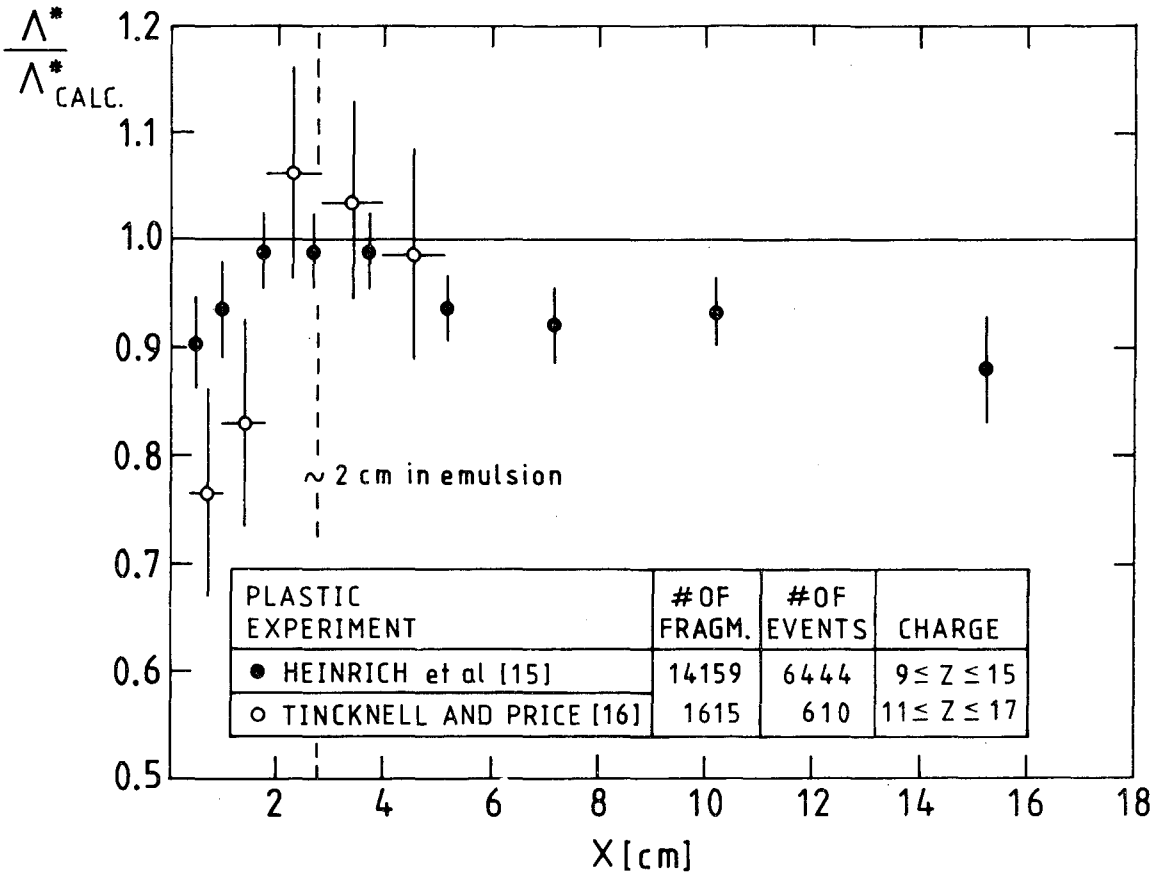

Fig. 9. A plot of $R^* = \Lambda^*/\Lambda^*_{calc}$ versus x for data from two plastic experiments [15,16].

Table I.
Observations in plastic experiments.

EXPERIMENT	DEPRESSION RANGE CM	a	λ_a [CM] PLASTIC	λ_a [CM] EMULSION*)
Heinrich et al. ref. [15]	0.2 - 1.4 (2.6SD)	1.2%	0.65	0.89
Tincknell and Price ref. [16]	0.38-1.54 (2.6SD)	~ 5%	~ 1	~ 1.4

*) When estimating the emulsion values we assume that a mfp of 1 cm in CR-39 corresponds to 1.37 cm in emulsion [15].

Table II
Emulsion data presented at the first anomalon workshop 1982.

EXPERIMENT	FRAGMENT CHARGE INTERVAL	# OF FRAGMENTS	# ON INTERACTIONS	REF
LBL	$3 \leq Z \leq 26$	2621	730	11
NRC	$3 \leq Z \leq 8$	1797	730	11
BUFFALO	$4 \leq Z \leq 26$	2100	865	12
MINNESOTA[1)]	$3 \leq Z \leq 28$	2424	634	13
TOTAL	$3 \leq Z \leq 28$	8942	2882	

1) Cosmic ray interactions. The median energy is somewhat over 2 A GeV [13].

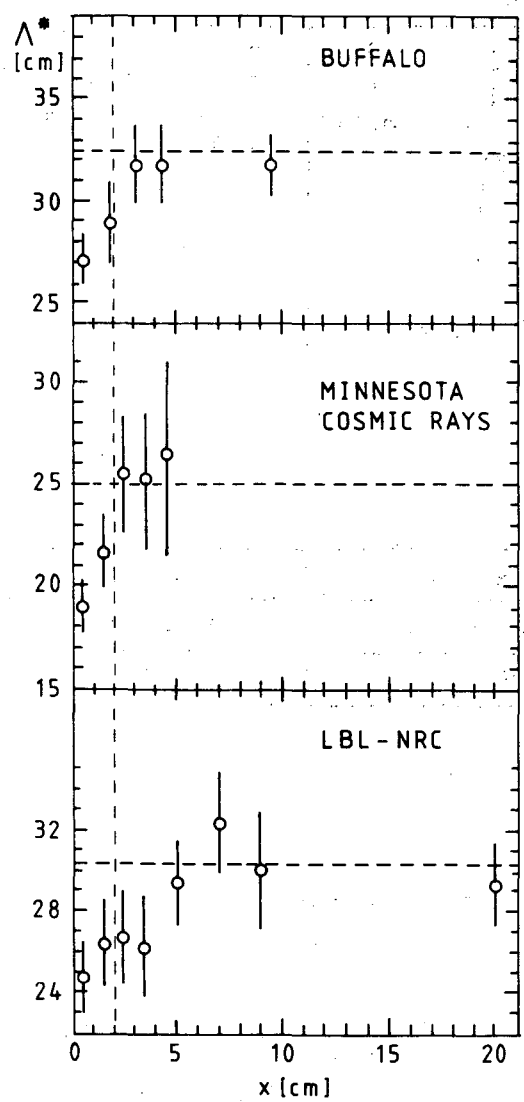

Fig. 10. Plots of Λ^* versus x for the three emulsion experiments; Buffalo [12], Minnesota [13] and LBL-NRC [11].

The early emulsion experiments (Table II and Fig. 10 [11-13]) registrated a depression of the PF mfp within distances $x \lesssim 2$ cm. For $x \gtrsim 2$ cm the Buffalo [12] and Minnesota [13] experiments did not detect different Λ^*-values for projectile fragments and beam nuclei. Only the LBL--NRC [11] experiment exhibits data points below Λ^*_{beam} (dotted line in Fig. 10) when $x > 2$ and such a deviation can well have its origin in statistical fluctuations. Thus both observations from early emulsion experiments [11-13] and from new plastic experiments [15,16] point towards an anomalon effect which mainly appears within distances shorter than about 2 cm from the parent interaction. Having this in mind we look back to the three cosmic ray heavy nuclear cascades [3-5] which initiated more than 25 years of speculations about the anomalon effect (Fig. 11). There are three facts I like to focus our attention on. Firstly the incident energies are high $\gtrsim$ 10 A GeV [5]. Secondly the parent interactions have no visible target fragmentation ($N_h = 0$). Thirdly the distances between the events in the heavy ion cascades (HIC) are $\lesssim$ 2 cm and most of them even smaller than 1 cm (c.f. Fig. 11). If these distances were deter-

mined by a characteristic decay time for anomalons a complete different picture would appear at 2 A GeV. Depending on the small γ-factor the distances between the events in a HIC would be very small at Bevalac energies. This has not been observed. As an example I show in Fig. 12 a very impressive event observed by Heckman and collaborators [33]. This event exhibits multifragmentation of an Fe nucleus where all multiply charged fragments but one (He) interact.

$$Fe \rightarrow O^* + C^* + 2He^* + He + 6p$$
$$\hookrightarrow 2\,He^* + 2\,p$$

YEAR	1954	1956	1957
INVESTIGATOR	A. MILONE [3].	S. TOKUNAGA et al. [4].	H. YAGODA [5]
ENERGY [5]	~ 9A GeV	~ 500A GeV	~ 18A GeV
PARENT INTERACTION	$N_h = 0$	$N_h = 0$	$N_h = 0$
HEAVY ION CASCADES (HIC)	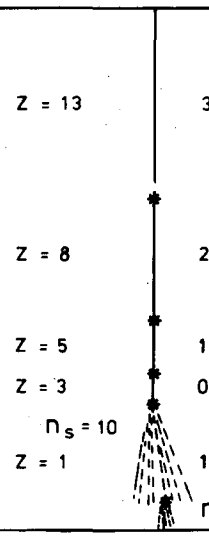	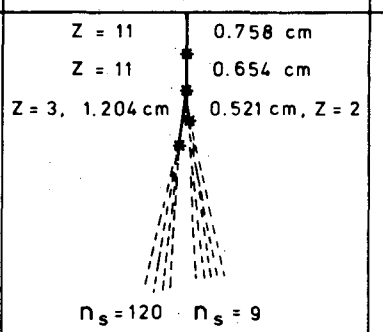	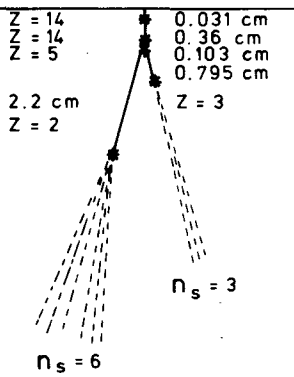
λ^* (WITHIN CASCADE)	1.89 cm	0.791 cm	0.698 cm
λ (GEOMETRY)	13.1 cm [5]	14.3 cm [5]	13.8 cm [5]
PROBABILITY	$3.7 \cdot 10^{-5}$ [5]	$1.9 \cdot 10^{-5}$ [5]	$2 \cdot 10^{-7}$ [5]

Fig. 11. The three first observed cosmic ray heavy ion cascades. N_h = number of charged target fragments; n_s = number of singly charged relativistic particles.

The probability for normal nuclei to give rise to large HIC's within short distances is small. The probabilities estimated by Yagoda [5] for the three cosmic ray events are shown in Fig. 11.

Unfortunately heavy ion beams at energies $\gtrsim$ 10 A GeV are not yet available. The highest energy at present is provided from 3.3 A GeV beams at the JINR Dubna synchrophasotron. At this workshop the Cairo-group (El-Nadi et al. [19])

presented results from an experiment where Z=2 fragments from 3.3 A GeV ^{12}C in-

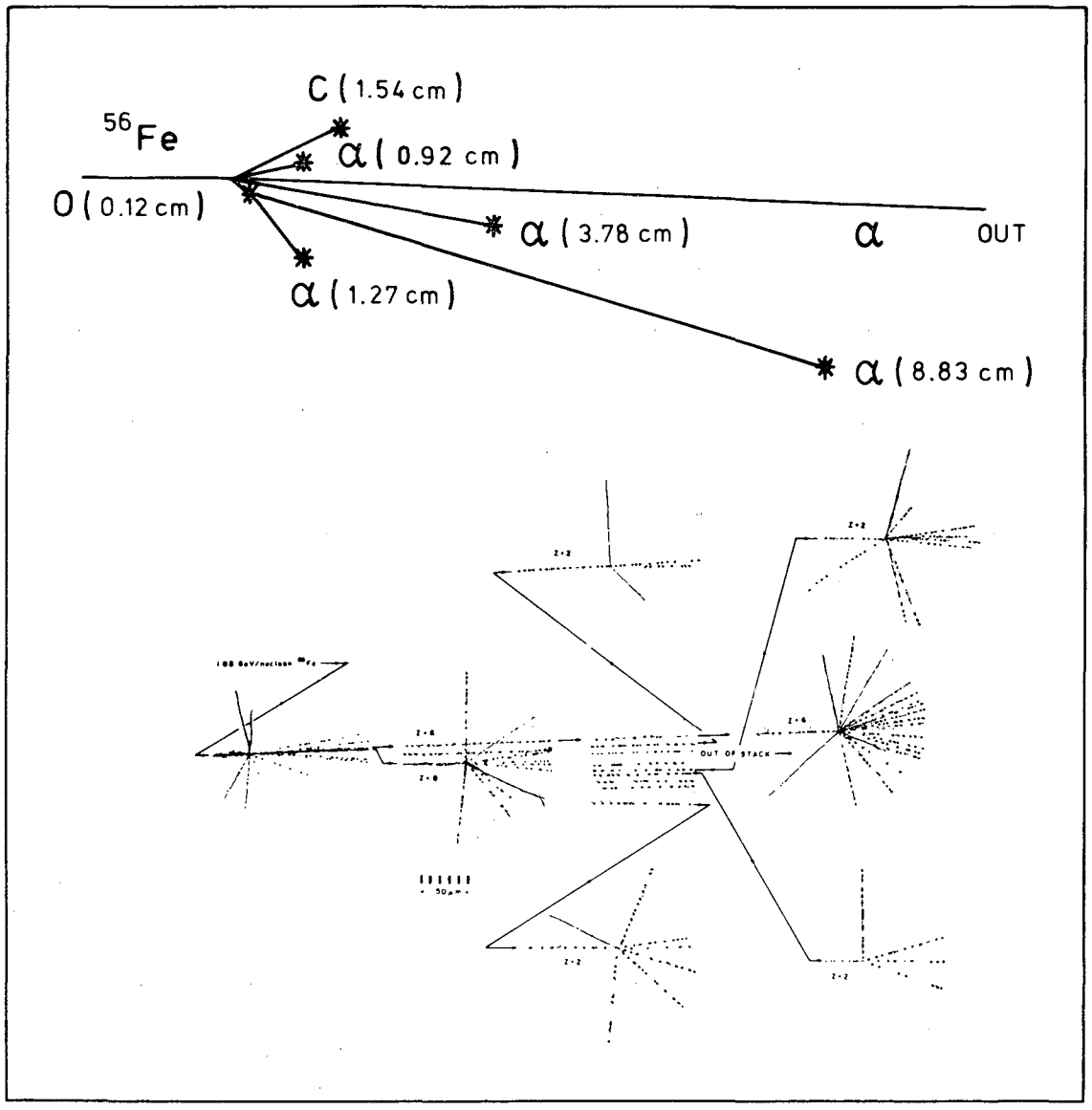

Fig. 12. A multi-interaction event produced by a ^{56}Fe nucleus at 1.9 A GeV [33].

duced reactions are followed. They claim that the He-fragments exhibit an anomalon effect which is strongly dependent on the destruction of the interacting nuclei. However, this experiment still suffers from low statistics and the observations have to be confirmed with higher statistic experiments.

At this workshop results from ~ 8000 scanned fragment reactions in emulsion were presented (Table III). All together data from ~ 11000 reactions excist. When the emulsion data are plotted in a λ_1 ($\leq$ 1 cm) versus λ_2 (> 2.5 cm) diagram

Table III
Emulsion data presented at the second anomalon workshop 1983.

EXPERIMENT	FRAGMENT CHARGE INTERVAL	# OF FRAGMENTS	# OF INTERACTIONS	REF
LBL	$2 \leq Z \leq 26$	5054	1915	17
NRC	$Z = 1$	2385	1087	22
ROME	$3 \leq Z \leq 26$	1426	936	29
BUFFALO	$2 \leq Z \leq 4$	5539	1030	21
BCJJL	$2 \leq Z \leq 18$	10119	2574	18
TOTAL	$1 \leq Z \leq 26$	24523	7542	
CAIRO	$Z = 2$	636	280	19
MARBURG	$Z = 2$		246	24
TOTAL NUMBER OF EMULSION INTERACTIONS AVAILABLE FOR ANOMALON SEARCH			10950	

the different experiments exhibit good agreement between each other and all data points except one fall on the anomalon side of the diagram (Fig. 13).

In order to get some idea about the magnitude of the anomalon effect I show in Fig. 13 calculations using the SAH with $\lambda_a = 1$ cm and a = 1%, 2% and 3% respectively. Because of the assumption that λ_a is independent of Z the deviations of the calculated curves from the diagonal decrease with decreasing λ_2 values i.e. with increasing Z. The experimental data exhibit a slightly different trend with deviations from the diagonal which are more weakly dependent on Z than the calculated curves. This may indicate that eventually existing anomalons produced in accordance with the SAH have a mean free path λ_a which depends on Z. Most (λ_1,λ_2) values are compatible with an assumption that the anomalon effect is smaller than 3%.

Topological correlations.

A natural next step of anomalon studies is to investigate what correlations exist between the characteristics of the events in which anomalons are produced and to compare with corresponding correlations in events without anomalon production. Also correlations between the properties of primary and secondary events as well as correlations between production and interaction events from the heavy ion cascades are of interest. Both the Marburg group [20] and the LBL-group [25] are studying such correlations. Especially they study the forward (F) - backward (B) asymmetry, A, of charged target fragments.

$$A = (F-B)/(F+B) \qquad (16)$$

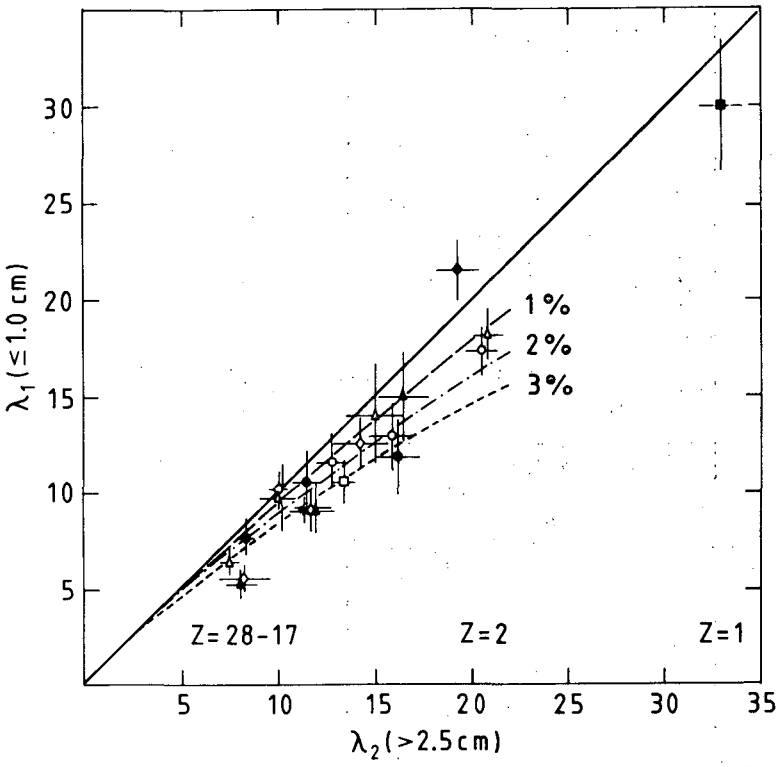

Fig. 13. λ_1 ($\geq$ 1 cm) versus λ_2 (> 2.5 cm for emulsion experiments.

A promising detector technique to study topological correlations is a combined plastic-emulsion detector, Fig. 14 [34]. The incident beam nuclei hit the detector perpendicular to the plastic foils. The charge (Z > 7) of primary nuclei and fragments are determined using the plastic foils. The (Y,Z) coordinates of the tracks of incident and outgoing nuclei when an interaction occurs in an emulsion pellicle are measured in the plastic foils (c.f. Fig. 14 b). With this information the reaction can easily be found in the emulsion, the vertex determined and the characteristics of the event studied. This combined plastic-emulsion detector therefore has comparatively fast data aquision (plastic, Siegen), excellent charge resolution (plastic), excellent vertex localization (emulsion) and provides visible events (emulsion).

▲	LBL	old data	[29]		($3\leq Z\leq 8$),	($9\leq Z\leq 16$),	($17\leq Z\leq 26$)
Δ	LBL	new data	[17]	(Z=2),	($3\leq Z\leq 8$),	($9\leq Z\leq 16$),	($17\leq Z\leq 26$)
□	NRC	old data	[29]		($3\leq Z\leq 8$)		
■	NRC	new data	[22]	(Z=1),			
○	BCJJL		[18]	(Z=2),	($3\leq Z\leq 5$),	($6\leq Z\leq 9$),	($10\leq Z\leq 18$)
●	ROME		[28]		($3\leq Z\leq 5$),	($6\leq Z\leq 8$),	($10\leq Z\leq 26$)
✦	BUFFALO		[21]	(Z=2),			
◇	MINNESOTA		[13]		($2\leq Z\leq 8$),	($9\leq Z\leq 16$),	($17\leq Z\leq 28$)
*	UC (Plastic)		[16]			($11\leq Z\leq 17$)	

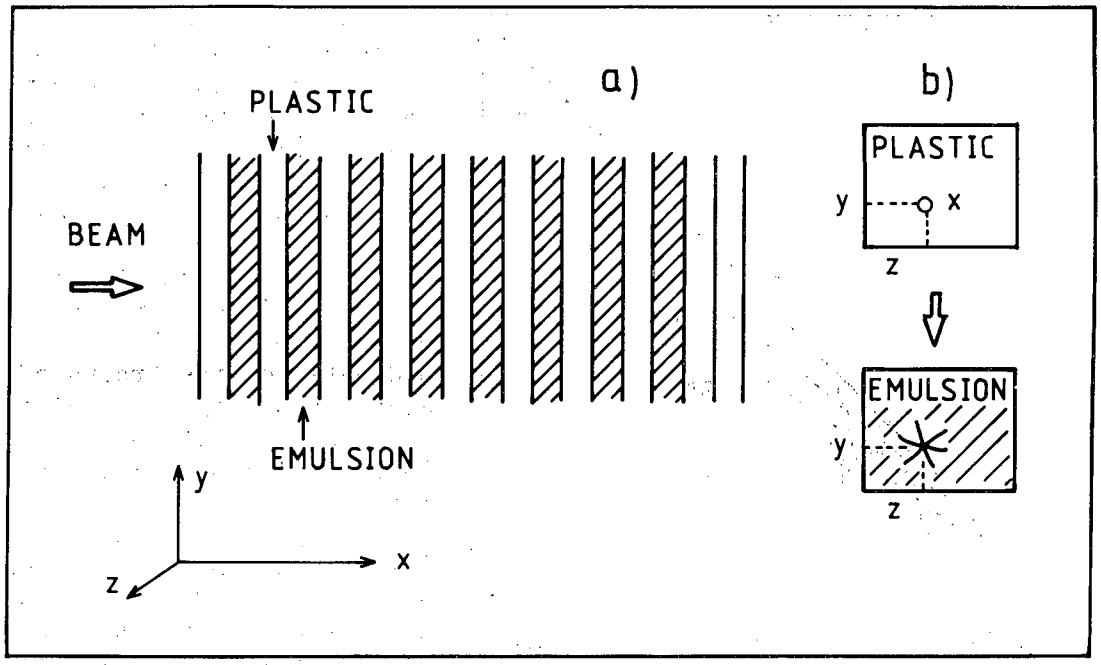

Fig. 14. A combined plastic-emulsion detector has fast data aquisition, excellent charge resolution, excellent vertex localization and provides visible events.

Other metohds for anomalon search.

Radioactive methods.

A method using a radiochemical approach to the investigation of the stability of projectile fragments from relativistic heavy ion collisions were presented by E.M.Friedlander [35]. In this experiment two identical Cu disks, 1 cm thick and 8 cm in diameter are exposed in pairs to heavy ion beams. Two configurations are used:

i) in close contact, and
ii) separated by 10 cm of air.

After exposure, spectra of the induced gamma activities are measured. A special attention to the production of ^{24}Na are made because this isotope is produced with a sizable cross-section only by hadrons and projectile fragments above ~ 1 A GeV which are well collimated forward.

The ratio:

$$Q = R1/R2$$

is studied. R1 and R2 are the ratios of initiated activities (after correction for ^{24}Na decay) in the two geometrical configurations of the Cu disk pairs. The experiment is sensitive in principle, to the presence of stable anomalons but its main aim is to test the ADH.

Segmentad Cerenkov detectors.

A new type of detector which measures charge changing cross sections of fragments produced in relativistic heavy ion collisions has been developed at LBL [36,37]. An artist drawing of such a device is shown in Fig. 15 a-b. Thin (3 mm) Lucite plates are used. Each of these provides an independent measurement of the fragment charge. The Cerenkov light emitted is by multiple internal total reflection at the surface of the plate transported to the photomultiplier tube which then measures the intensity of the signal. At relativistic energies, the intensity of the radiation produced is proportional to Z^2, allowing a direct measurement of the fragment charge. Not many of the nuclear products from the target nucleus contributes to the Cerenkov light intensity because most of these fragments have energies below the Cerenkov threshold of ~ 310 A MeV.

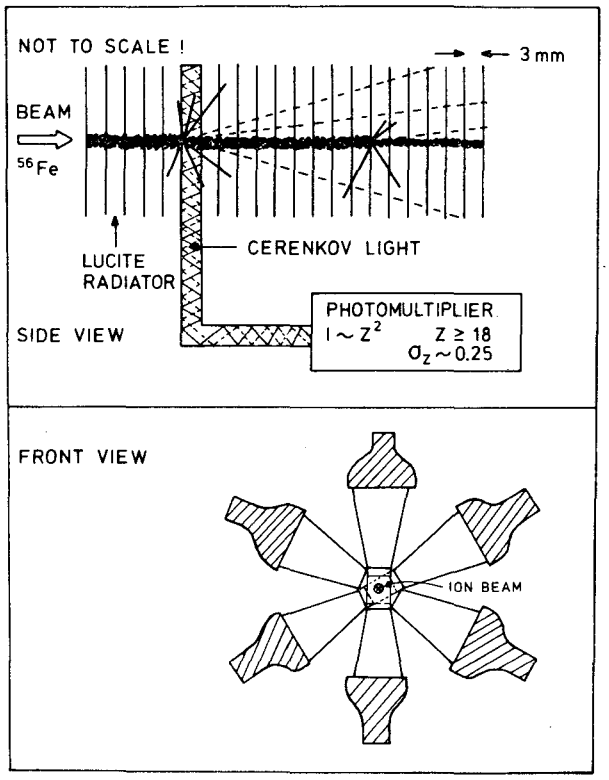

Fig. 15. An artist drawing of a segmented Cerenkov Detector.

In paper 14, J.P. Dufour et al. [36], present a Cerenkov detector for measurement of fragment interaction cross sections. This detector provides excellent directional selection as shown in Fig. 16. Energetic light ions like p and α are emitted with typically a few degree angle relative to the incident ion, why most of the Cerenkov light from them will be strongly suppressed. In this experiment fragments with $Z \geq 18$ will be registrated and the charge resolution is expected to be $\sigma_Z = 0.25$. One intends to use 50 3 mm radiators why the mean free path for secondary fragments in the range interval 1-13 cm can be measured. In a shorter range interval also tertiary fragments are going to be registrated. If the detector is successful and the anomalons present the device will be used as a filter for more specific studies of anomalons with the HISS-spectrometer.

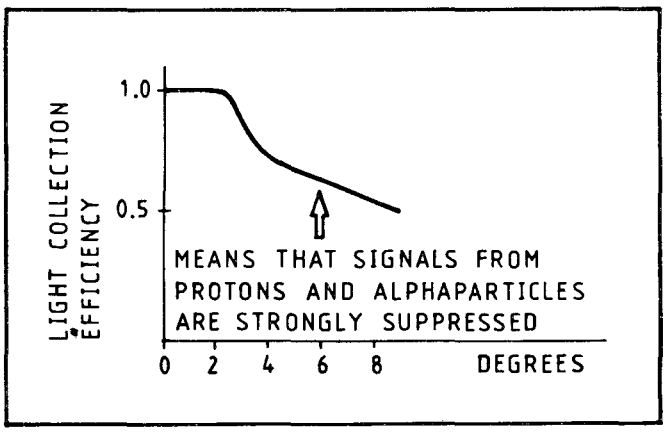

Fig. 16. The intensity of the Cerenkov light as a function of the emission angle. The beam is perpendicular to the surface of the radiation paddle [36].

J.D. Stevenson et al. [37] present in Paper 15 a very si-

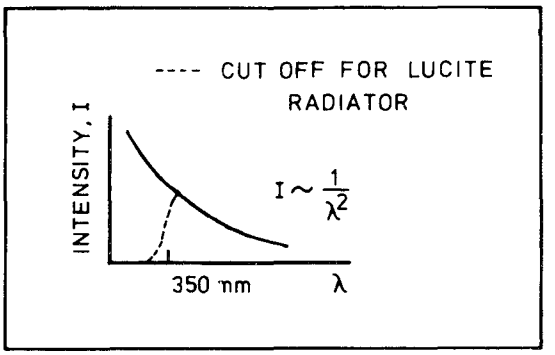

Fig. 17. The intensity of the Cerenkov radiation as a function of the wavelength, λ [37].

milar experiment. The feeble Cerenkov light output has here been increased by using wave lengths shifter paddles. Therefore they can extend intensity measurements to lower wavelength and thereby increase the signal (c.f. Fig. 17) and reach a charge resolution of $\sigma_Z \lesssim 0.15$. Thus this experiment differ from the previous one by better charge resolution but the directional selection of the Cerenkov light has been lost.

Active multitarget detectors.

Great technical developments have made solid state detectors to a major instrument in high energy physics. For example an assembly of thin silicon devices as multitarget has been successfully used in studying charm particle decay (e.g. D-mesons) [38]. In Paper 16 M. Enorini et al [39] suggest to use subsequent active targets in order to trigger on reinteraction of produced fragments. The experimental apparatus is composed by three identical silicon solid state targets, each 2 mm thick. Their relative distance can be continously varied from ~ 1 cm to ~ 15 cm. The sign of an interaction in the first silicon solid state target is performed by comparing the released energy with the expected energy loss of the incident ion. Each target is followed by an assembly of microstrip chambers. They detect the emitted fragments and measure their charges. The presence of anomalons among the fragments give rise to an overproduction of secondary interactions. To trigger on successive interactions of the fragments when an interaction in the first target occurs, would evidenciate the existence of anomalons.

Conclusions.

The experimental data are not yet conclusive enough to finally establish that anomalons exist. The anomalons are still provocative and the effect has not gone away. The anomalon effect appears for distances smaller than 2 cm and the effect is less than 3 %.

Homework for the third anomalon workshop.

Fig. 18 shows charge and x-ranges where different detectors may be the best for anomalon search at the present time. For the emulsion work the following suggestion can be given:

i) Study fragments with $Z \leq 7$.
ii) Study the range interval $x < 2$ cm in detail. In the first mm from the parent reactions corrections must be done for the background of interactions induced by hadrons emitted from the incident nuclei [18].

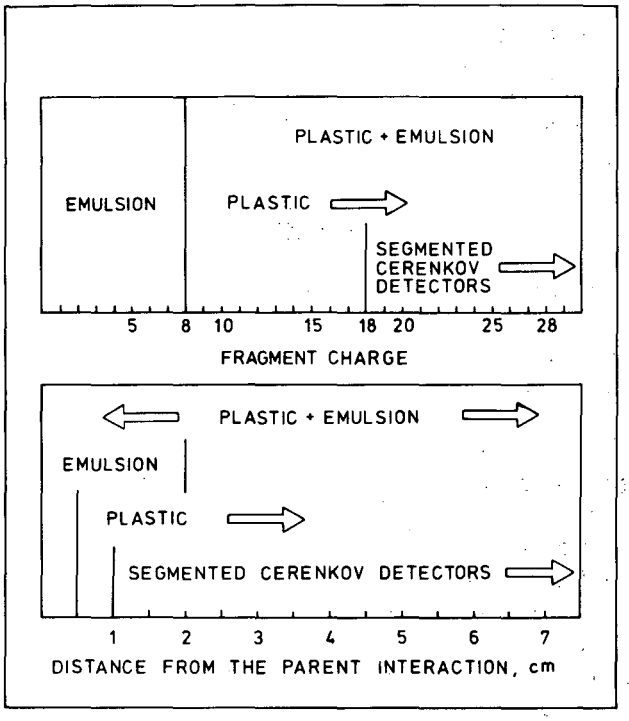

Fig. 18. Z- and x-ranges, where different detectors for anomalon search may be the best at the present time.

iii) Study the topology of interactions in the range 0-2 cm and compare with interactions in range intervals where no anomalons are expected.

iv) Study the anomalon effect in single- and multi-fragment events separately i.e. in events where $N_F = 1$, $N_F = 2$ and $N_F > 2$. N_F is the number of fragments with $Z \geq 2$.

v) Study HIC's and correlations in HIC's.

vi) Beams of O(C) and Fe(Ar) still seems to be the best to use. It is important to compare observations of the anomalon effect at Bevalac energies with observations at Dubna (Synchrophasotron) energies.

vii) Pool all data at LBL (H.H. Heckman's group) for a worldwide evaluation.

Acknowledgements.

Helpful discussions with E. Friedlander, H.H. Heckman, B. Jakobsson, W.Heinrich, S. Lokanathan, Y. Prakash, E. Stenlund and J. Symons are gratefully acknowledged. Special thanks go to G. Baroni, P.B. Freier, P.L. Jain, B. Judec, J. Karant, B. Price, M. Tincknell and C.J. Waddington for providing me with their data.

References.

1. L. van Hove, Proceedings of the Bielefeld Workshop on Quark-Gluon Matter and Very High Energy Heavy Ion Collisions; ed. by M. Jacob and R. Satz, pp. 349-370, World Scientific Publishing Co., Singapore, 1982, and references therein.
2. H. Satz, Proceedings of the International Conference on Nucleus-Nucleus Collisions, Sept. 25 - Oct. 1, 1982, Michigan State University, East Lansing, Michigan, USA, and University of Bielefeld preprint BI-TP 82/29 (1982).
3. A. Milone, Nuovo Cimento Suppl. 12, 353 (1954).
4. S. Tokunaga, T. Ishii, and K. Nishikawa, Nuovo Cimento 5, 517 (1957).
5. H. Yagoda, Bull. Am. Phys. Soc., Series II, 64 (1956), Nuovo Cimento 6, 559 (1957).
6. E.M. Friedlander and M. Spârchez, International Working Meeting on Cosmic Rays (Romanian Academy of Science, Bucharest, Romania, 1959), p.155; Nucl. Sci. Abstr. 15, 347 (1061).
7. B. Judek, Can. J. Phys. 46, 343 (1968); 50, 2082 (1972).

8. Y. Karant, Lawrence Berkeley Laboratory Report No. LBL-9171 (1979). W.J. Romo and P.J. Watson, Phys. Lett. 88B, 354 (1979), S. Fredriksson and M. Jandel, Phys. Rev. Lett. 48, 14 (1982).
9. J. Boguta, Lawrence Berkeley Laboratory Report No. LBL-13885 (1982), W.C. McHarris and J.O. Rasmussen, Lawrence Berkeley Laboratory Report No. LBL-14075 (1982).
10. B.F. Bayman, P.S. Ellis and Y.C. Tang, Phys. Rev. Lett. 49, 532 (1982), Y.C. Tang, these Proceedings.
11. E.M. Friedlander, G.W. Gimpel, H.H. Heckman, Y.J. Karant, B. Judek and E. Ganssauge, Phys. Rev. Lett. 45, 1084 (1980).
12. P.L. Jain and G. Das, Phys. Rev. Lett. 48, 305 (1982).
13. H.B. Barber, P.S. Freier and C.J. Waddington, Phys. Rev. Lett. 48, 856 (1982).
14. See Phys. Today 35, No. 4, 17-19 (1982).
15. W. Heinrich et al., these Proceedings, University of Siegen Preprint SI-83-11 (1983).
16. M.L.Tincknell and P.B. Price. Preprints of Contributed Papers at the Sixth High Energy Heavy Ion Study and Second Workshop on Anomalons, LBL, Berkeley, June 28 - July 1, 1983, Lawrence Berkeley Laboratory Report No. LBL-1628 (1983). Paper 1, p.1.
17. Y.J. Karant, H.H. Heckman and E.M. Friedlander, Lawrence Berkeley Laboratory Report No. LBL-1628 (1983); Paper 2, p.5.
18. O.E. Badaway et al., Lawrence Berkeley Laboratory Report No. LBL-1628 (1983); Paper 3, p.9. S. Bale et al. (BCJJL-collaboration), Lund University Preprint LUIP-8314 (1983).
19. M. El-Nadi et al., Lawrence Berkeley Laboratory Report No. LBL-1628 (1983); Paper 4, p.11.
20. N. Klein et al., Lawrence Berkeley Laboratory Report No. LBL-1628 (1983); Paper 5, p.15.
21. P.L. Jain et al., Lawrence Berkeley Laboratory Report No. LBL-1628 (1983); Paper 6, p.19.
22. B. Judek, Lawrence Berkeley Laboratory Report No. LBL-1628 (1983), Paper 7, p.20.
23. H.H. Gustafsson et al., (GSI-LBL-collaboration), Lawrence Berkeley Laboratory Report No. LBL-1628 (1983); Paper 8, p.24.
24. F. Killinger et al., Lawrence Berkeley Laboratory Report No. LBL-1628 (1983); Paper 10, p.31.
25. E.M. Friedlander, H.H. Heckman, and Y.J. Karant, Lawrence Berkeley Laboratory Report No. LBL-1628 (1983), Paper 11, p.35.
26. T.M. Liss, S.P. Ahlen, P.B. Price and G. Tarlé, Phys. Rev. Lett. 49, 775 (1982).
27. P.B. Price, M.L.Tincknell, G. Tarlé, S.P. Ahlen, K.A. Fraenkel and S. Perlmutter, Phys. Rev. Lett. 50, 566 (1983).
28. G. Baroni, private communication.
29. E.M. Friedlander, R.W. Gimpel, H.H. Heckman, Y.J. Karant, B. Judek and E. Ganssauge, Phys. Rev. C27, 1489 (1983).
30. W.H. Barkas, Nuclear Research Emulsions (Academic, New York, 1963), Vol.1.
31. H. Bradt and B. Peters, Phys. Rev. 77, 54 (1950).
32. H.H. Heckman, D.E. Greiner, P.J. Lindstrom and H. Shwe, Phys. Rev. C17, 1735 (1978).
33. H. Heckman, private communication.
34. H. Heinrich and K. Söderström, LBL-proposal 1982.
35. G. Dersch et al., Lawrence Berkeley Laboratory Report No. LBL-1628 (1983), Paper 9, p.28.

36. J.P. Dufour et al., Lawrence Berkeley Laboratory Report No. LBL-1628 (1983), Paper 14, p.47.
T.J.M. Symons, private communication.
37. J.D. Stevenson, J.A. Mauser and S.W. Barwich, Lawrence Berkeley Laboratory Report No. LBL-1628 (1983), Paper 15, p.49,
38. E. Albini et al., Phys. Rev. Lett. 110B, 339 (1982).
G. Bellini et al., Phys. Reports 83, 1 (1982).
39. M. Enorini, F.I. Fabbri, and A. Zallo, Lawrence Berkeley Laboratory Report No. LBL-1628 (1983), Paper 16, p.52.

IMPRESSIONS OF THE MEETING

Alfred S. Goldhaber
Institute for Theoretical Physics
State University of New York
Stony Brook, New York 11794

I want to touch on some of the pleasant and rewarding aspects as well as some of the lessons and projects suggested by this meeting. Compared with the first workshop I attended ten years ago, the feeling of progress is overwhelmingly satisfying. There is a large, enthusiastic, spontaneously generated and international attendance, while in 1973 the much smaller assembly was just as eager, but mainly local or specially invited. The quality of the lectures has been almost uniformly high, and reflects a striking maturity for a field so new.

It has been delightful to meet and talk with so many interesting people about many different topics. The main thing that has been missing is enough time for these conversations, or for small-group working sessions. This has become a standard disease of meetings, and I would urge organizers of future conclaves to plan no more than 50% of regular meeting time for plenary sessions, e.g., mornings only. It is important to convey to sponsoring agencies the value of this kind of breathing space as a stimulus to new research, especially when the biggest single expense of the occasion is for travel of the participants. The formal lectures have a rightful place, mainly for education, but everyone knows that the real work goes on in the corridors outside the lecture hall.

The experimental reports were notable for physics content, but also for the new level of technical sophistication, which has made possible far more refined analyses than with earlier generations of detectors. We are seeing at Bevalac something very close to the ideal of identifying and measuring the momentum of every particle coming out of a complex nucleus-nucleus interaction. The plastic ball-wall detector may be the newest to come on line, but work with the streamer chamber also shows increased maturity.

Plastic ball results indicate that when a projectile strikes a target, if projectile remnants are knocked to the right, then target remnants are knocked to the left, even though one believes that the two sorts of remnant never touched each other directly. We may still hope to learn from the data already obtained whether this anticorrelation of recoil direction is a purely geometrical effect, or if the fragments are really communicating with each other by some kind of pulse through the nuclear medium which separates them.

The streamer chamber results on pion multiplicities have been applied most ingeniously to deduce how well nuclear matter is able to resist compression, since cascade models imply too many pions. and the observed deficit may be explained by energy stored in compression. This result deserves further examination, but the agreement with the incompressibility coefficient obtained in other ways is surely encouraging.

Both plastic ball and streamer chamber results suggest that, for bombarding energies of 1 AGeV or less, nuclei bigger than calcium stop each other in central collisions. I hope and believe that's true, since stopping at much higher energies would be necessary to attain compressions and energy densities dramatically greater than those of normal nuclei. It would be interesting to know just how closely comparable definitions of stopping can be made with these two different observational techniques, as well as with others. Even at the moment we can congratulate ourselves on being able to take for granted the ability to make reliable triggers for central collisions, something which seemed very much in doubt only a few years ago.

Another area in which there has been remarkable progress is the study of nuclear response to energy deposited in various ways. One needn't be surprised that a large projectile can cause breakup of a target into small pieces, but the same thing can also be accomplished by a single energetic proton. The main wish one could express for future observations of this type would be elaboration from the present, typically inclusive, measurements to ones in which most or all fragments are seen simultaneously. That's the way to pin down otherwise unfettered theoretical speculations, as is already happening with data from the Bevalac facilities. Low-density critical phenomena should manifest themselves unambiguously in such multiparticle observations--or else be ruled out altogether.

The maturity of theoretical discussions is keeping pace with that of experiment, possibly too much so. While attractive and even compelling ideas were advanced about reactions not yet accessible to laboratory study, I missed hearing about comparisons of the new, refined data with equally refined theories. With that one quibble out of the way, let me say how pleasant it was to learn that theorists have a coherent and plausible view of phenomena which may occur in nuclear collisions beyond, even far beyond, the Bevalac range. While these ideas may be utterly wrong, they provide a helpful framework for thinking about future experimental programs. Many of the discussions represent elaborations of thoughts expressed some years ago, and it is comforting to see that these concepts survive the more searching and precise investigations reported here.

There are two parameters which might be changed dramatically

in "macroscopic" volumes of space-time, by high energy collisions between large nuclei. The first is energy density. This could be made very large when two highly Lorentz-contracted nuclei pass through each other in opposite directions, depositing several Gev/fm^3 over a wide range of rapidity. Because spatial dimensions are large in the directions perpendicular to the collision axis, the dominant direction of the ensuing expansion is along the axis, leading to a dynamics (hydro- or otherwise) in one space dimension. The constraints of energy and momentum conservation, and of relativistic invariance, are enough to determine the result very simply. given the equation of state for the expanding excited matter. The big remaining issue has to do with what if any characteristics of the particles we eventually observe will be symptoms of the nature of the matter first produced. So far I haven't seen convincing proposals to resolve this issue.

The second parameter which could be enhanced is baryon density. There seems to be agreement that, while such enhancement could be achieved in super fast collisions, by compression of the target alone, a comparable or even greater enhancement could come from collision at the largest velocity for which projectile and target still stop each other in the center of mass frame. An energy of 10 AGeV for a beam on a stationary target has been suggested for this. I believe that evidence from stopping of fast protons by large nuclei indicates an even higher value, above 50 AGeV. In any case, this region would be important to explore, and the properties of the resulting dense matter are a fascinating subject for further thought.

The first and last word here is ANOMALON, and I want to say a bit about the subject. Assuming there are such objects, the honest theorist's duty is to find the most conservative explanation, going farther afield only if absolutely necessary. Therefore, unusual, long-lived configurations of nucleons are the first choice. I was glad to hear that such configurations are conceivable, and hope to learn in the future of more complete studies which could rule this conservative explanation in or out. Of course, I have a vested interest in the failure of the nucleon picture, but the truth is what really matters, and if nucleons can do such remarkable things, we shall all be glad to know about it.

My other comment here is experimental, and perhaps complementary to Otterlund's beautiful analysis of the current situation and best plan for pinning things down. It could be valuable to re-examine a possibility which appeared to be excluded by the original Berkeley-Ottawa data, namely, that anomalons are longlived but delicate systems, which can break up either by spontaneous decay or from the stimulus of a gentle collision with a target nucleus. This means that secondary interactions of such fragments would include a higher proportion

of unexcited or minimally excited target nuclei than for normal projectiles, but would not involve much larger interaction radii than normal. We need to know if such a description of the anomalon is definitely inconsistent with data which demonstrate the existence of the anomalon. If it were consistent, then the object would still be remarkable, but a bit less so.

In short, my strongest impression is that we have reason to be most impressed by what has been accomplished and what is in prospect for studies of nuclear collisions. I thank the organizers of this meeting for their hospitality, and their extraordinary efficiency in taking care of every practical aspect. This work was supported in part by the National Science Foundation.

LIST OF PARTICIPANTS

Shahriar Abachi
Lawrence Berkeley Laboratory

Kjell Aleklatt
Studsvik Science Research Lab.

Regis P. Babinet
LNS/SACLAY

O. E. Badawi
Cairo University

E. Barasch
UC Davis

Giustina A. Baroni
Universita di Roma

Gordon A. Baym
University of Illinois

Dana Beavis
UC Riverside

James R. Beene
Oak Ridge National Laboratory

Curtis E. Bemis, Jr.
Oak Ridge National Laboratory

Robert W. Birge
Lawrence Berkeley Laboratory

Rudolf M. Bock
GSI, Darmstadt

A. Bodek
University of Rochester

Arnold Bodmer
Argonne/U. of Illinois at Chicago

Harold Britt
Los Alamos National Laboratory

Robert Brockmann
LBL/GSI

Alfons Capella
L.P.T.H.E. ORSAY (France)

Jim B. Carroll
Lawrence Berkeley Laboratory

Arthur S. Cary
California Polytechnic State Univ.

Ronald Cassou
University of San Francisco

Carlos M. Castaneda
UC Davis

Leonardo Castillejo
University College, London

Joseph Cerny
Lawrence Berkeley Laboratory

Aaron Chacon
Lawrence Berkeley Laboratory

George Chapline
Lawrence Livermore Laboratory

Chellis Chasman
Brookhaven National Laboratory

Shu-Yuan Chu
UC Riverside

Hank Crawford
Lawrence Berkeley Laboratory

Laszlo P. Csernai
Central Research Institute
for Physics, Budapest

A. Dacal
Universidad de Mexico

Janis M. Dairiki
Lawrence Berkeley Laboratory

Arnon Dar
Technion-Israel
Institute of Technology

Subal Das Gupta
McGill University

Ferenc Dea'k
Eotvos Loraud University, Budapest

Ivo Derado
Max-Planck-Institut
für Physik, München

Carleton E. Detar
University of Utah

Philip A. Deutchman
University of Idaho

Hartmut Deyda
Bundesministerium für Forschung
und Technologie, W. Germany

Jean-Pierre Dufour
Lawrence Berkeley Laboratory

Mohamed El Sayed El-Nagdy
State Univ. of New York at Buffalo

F. L. Fabbri
INFN, Frascati

Kenneth A. Frankel
Lawrence Berkeley Laboratory

Svarker Fredricksson
Royal Tech., Stockholm

Phillis S. Freier
University of Minnesota

Erwin Friedlander
Lawrence Berkeley Laboratory

Eberhard R. Ganssauge
Philipps-Universität Marburg

Jean-Francios Gilot
Louisiana State University

Norman Glendenning
Lawrence Berkeley Laboratory

A. S. Goldhaber
SUNY, Stony Brook

Jean Gosset
DPhN/ME - CEN de SACLAY

Harvey A. Gould
Lawrence Berkeley Laboratory

Douglas Greiner
Lawrence Berkeley Laboratory

Eckart Grosse
GSI, Darmstadt

Jean-Yves Grossiord
Inst. de Physique Nucleaire
de Lyon

Charles R. Gruhn
Lawrence Berkeley Laboratory

Hermann A. Grunder
Lawrence Berkeley Laboratory

Shi-Lun Guo
Lawrence Berkeley Laboratory

Hans Gustafsson
Lawrence Berkeley Laboratory

Hans Gutbrod
GSI/LBL

Miklos Gyulassy
Lawrence Berkeley Laboratory

Hideki Hamagaki
INS/LBL University of Tokyo

Ole Hansen
Brookhaven National Laboratory

John W. Harris
GSI/LBL

Richard Harris
Tri-Valley Herald, Livermore

Osamu Hashimoto
INS/LBL

Harry Heckman
Lawrence Berkeley Laboratory

Wolfgang Heinrich
University of Siegen

David Hendrie
DOE/LBL

Richard P. Henke
University of San Francisco

Andrew S. Hirsch
Purdue University

Tom Humanic
Lawrence Berkeley Laboratory

John E. Huth
Lawrence Berkeley Laboratory

Rudolph C. Hwa
University of Oregon

George Igo
UC Los Angeles

Junsuke Iwai
University of Washington

P. L. Jain
SUNY, Buffalo

Bo I. Jakobsson
University of Lund

Barbara Judek
National Res. Council of Canada

Joseph I. Kapusta
University of Minnesota

Yasha Karant
Lawrence Berkeley Laboratory

Declan Keane
UC Riverside

Bill Keirstead
LBL/Stanford

Adam Kiss
Eotvos University, Budapest

W. J. Knox
UC Davis

James J. Kolata
University of Notre Dame

Hans-Joachim Korner
Technischen, Universität München

Robert H. Kraus, Jr.
Oregon State University

Gary Krebs
LSU/LBL

Jutta Kunz
Los Alamos National Laboratory

Robert G. Legrain
C.E.N. SACLAY

Michael J. LeVine
Brookhaven National Laboratory

Alan Ling
UC Los Angeles

Harry J. Lipkin
Weizmann Institute

S. Lokanathan
University of Rajasthan

Roselyne Lombard
C.E.N. SACLAY

Bernhard Ludewigt
GSI/LBL

Thomas W. Ludlam
Brookhaven National Laboratory

Uli Lynen
GSI-Darmstadt

Malcolm Mac Gregor
Lawrence Livermore Laboratory

Prof. Richard Madey
Kent State University

Michael Maier
Lawrence Berkeley Laboratory

Howard Matis
Los Alamos National Laboratory

Tetsuo Matsui
Lawrence Berkeley Laboratory

J. B. McGrory
ORNL/DOE

William C. Mc Harris
Michigan State University

Aram Mekjian
Rutgers University

Curtis A. Meyer
UC Berkeley

Donald H. Miller
Northwestern University

Jack Miller
Lawrence Berkeley Laboratory

Don L. Murphy
Lawrence Berkeley Laboratory

Martin J. Murphy
University of Washington

William D. Myers
Lawrence Berkeley Laboratory

Kozi Nakai
University of Tokyo

Cornelius C. Noack
University of Bremen

Grazyna Odyniec
Lawrence Berkeley Laboratory

Shigemi Ohta
University of Tokyo

Douglas Olson
Lawrence Berkeley Laboratory

M. K. Orlowski
Purdue University

Maria-Esther Ortiz
University of Mexico

Ingvar K. N. Otterlund
University of Lund

Marie José Parizet
Clermont-Ferrand

Thomas A. Parnell
Marshall Space Flight Center

Victor Perez-Mendez
Lawrence Berkeley Laboratory

Franz Plasil
Oak Ridge National Laboratory

Norbert T. Porile
Purdue University

Arthur M. Poskanzer
Lawrence Berkeley Laboratory

Yog Prakash
Jammu University

P. Buford Price
UC Berkeley

Howel G. Pugh
Lawrence Berkeley Laboratory

Johann Rafelski
Frankfurt and CERN

Wolfgang Rauch
GSI/LBL

John Rasmussen
Lawrence Berkeley Laboratory

Martin Redlich
Lawrence Berkeley Laboratory

E. A. Remler
College of William and Mary

Tim Renner
Lawrence Berkeley Laboratory

Robert Richard
UC Los Angeles

Hans George Ritter
GSI Darmstadt/LBL

Guy R. Roche
Université de Clermont

William T. Romo
Carleton University

John G. Rushbrooke
Cambridge University

Y. Ruuskanen
University of Jyvaskyla

Michael Salamon
UC Berkeley

Rudolf Saly
Carleton University

Andres Sandoval
GSI/LBL

Rolf Scharenberg
Purdue University

Lee S. Schroeder
Lawrence Berkeley Laboratory

Bernd Schuermann
Technischen, Universität München

David K. Scott
Michigan State University

R. Seki
California State University

Zoltan Seres
Central Research Inst.
for Phys., Budapest

Dan Shapira
Oak Ridge National Laboratory

Gordon Shaw
UC Irvine

Yoshijiro Shida
INS University of Tokyo

Asher Shor
LBL/UCLA

Radhey Shyam
GSI, Darmstadt

Philip J. Siemens
Texas A & M University

Rein Silberberg
Naval Research Laboratory

Helmuth Spieler
Lawrence Berkeley Laboratory

C. Frederick Stanland
Lawrence Berkeley Laboratory

Evert A. Stenlund
CERN

John D. Stevenson
UC Berkeley

Robert Stokstad
Lawrence Berkeley Laboratory

Daniel Strottman
Los Alamos National Laboratory

Uday P. Sukhatme
University of Illinois at Chicago

John Sullivan
Texas A & M University

Hiroyuki Sumiyoshi
University of Tokyo

T. J. M. Symons
Lawrence Berkeley Laboratory

Yoshiyuki Takahashi
Louisiana State University

Y. C. Tang
University of Minnesota

Craig E. Thorn
Brookhaven National Laboratory

Mark L. Tincknell
UC Berkeley

Lawrence W. Townsend
NASA Langley Research Center

C. C. Trail
Brooklyn College

Wolfgang Trautmann
Brookhaven National Laboratory

Jean Girard
Lawrence Berkeley Laboratory

James P. Vary
Iowa State University

C. Jake Waddington
University of Minnesota

Peter J. S. Watson
S.I.N., Switzerland

Harvey E. Wegner
Brookhaven National Laboratory

Gary Westfall
Michigan State University

Gary White
Texas A & M University

Howard Wieman
GSI/LBL

Kevin Wolf
Texas A & M University

Mervyn Wong
Lawrence Berkeley Laboratory

Gordon J. Wozniak
Lawrence Berkeley Laboratory

Craig Wuest
UC Irvine

Glenn R. Young
Oak Ridge National Laboratory

John C. Young
California State University, Chico

Michael S. Zisman
Lawrence Berkeley Laboratory

GPO 787-116/104

This report was done with support from the Department of Energy. Any conclusions or opinions expressed in this report represent solely those of the author(s) and not necessarily those of The Regents of the University of California, the Lawrence Berkeley Laboratory or the Department of Energy.

Reference to a company or product name does not imply approval or recommendation of the product by the University of California or the U.S. Department of Energy to the exclusion of others that may be suitable.

TECHNICAL INFORMATION DEPARTMENT
LAWRENCE BERKELEY LABORATORY
UNIVERSITY OF CALIFORNIA
BERKELEY, CALIFORNIA 94720